NASA SP-116

CONFERENCE ON V/STOL AND STOL AIRCRAFT

AMES RESEARCH CENTER

MOFFETT FIELD, CALIFORNIA

APRIL 4 - 5, 1966

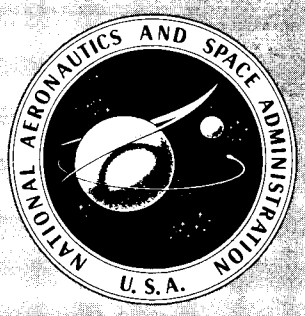

NATIONAL AERONAUTICS AND SPACE ADMINISTRATION

NASA SP-116

CONFERENCE ON V/STOL AND STOL AIRCRAFT

Ames Research Center
Moffett Field, California
April 4-5, 1966

Scientific and Technical Information Division 1966
NATIONAL AERONAUTICS AND SPACE ADMINISTRATION
Washington, D.C.

For sale by the Clearinghouse for Federal Scientific and Technical Information
Springfield, Virginia 22151 – Price $5.25

CONTENTS

Jet-Lift V/STOL

Session Chairman – Richard E. Kuhn

HANDLING QUALITIES

Session Chairman - Seth B. Anderson

V/STOL

STOL

NASA CONTRACTED FEASIBILITY STUDIES OF V/STOL AND STOL CONCEPTS FOR SHORT-HAUL TRANSPORTS

Session Chairman – Wallace H. Deckert

RESEARCH TESTING TECHNIQUES

PREFACE

This compilation contains results of recent NASA research on problems associated with V/STOL and STOL aircraft. The first three sections include papers presented at the NASA Conference on V/STOL and STOL Aircraft held at the Ames Research Center, Moffett Field, California, on April 4 and 5, 1966. The fourth section presents three additional papers on research testing techniques that are particularly pertinent to the subject matter, but were not presented orally at the conference.

Contributors include staff members from the Ames and Langley Research Centers of NASA and industrial representatives from Lockheed Aircraft Corporation; Ling-Temco-Vought, Incorporated; and The Boeing Company.

1. HANDLING QUALITIES AND STRUCTURAL CHARACTERISTICS OF THE HINGELESS-ROTOR HELICOPTER

By Robert J. Huston and John F. Ward

NASA Langley Research Center

SUMMARY

Several advantages and potential problem areas associated with the hingeless-rotor helicopter are discussed. The extent to which two of the advantages - increased control and damping moments - can be obtained with the hingeless-rotor helicopter is established. The upper limit on the available control and damping moments is associated with the excessive gyroscopic coupling that is obtained with heavy rotor blades. The potential problem areas identified include a structural mode of oscillation very similar to that of a pendulum, which causes undesirably large roll accelerations under certain flight conditions, and large cyclic chordwise bending moments that occur during severe maneuvers (the primary structural problem of concern). Solutions are proposed which should eliminate future concern with these problems.

Author

INTRODUCTION

The hingeless rotor is a configuration that will be seriously considered during new rotary-wing-aircraft design studies. Potential design advantages appear to offset the less complete general knowledge and development history that is associated with semiarticulated or fully articulated rotors. Although a possible substantial reduction in hub drag, a reduction in hub complexity, and a reduction in mechanical maintenance are important considerations favorable to utilizing the hingeless-rotor design, the increased control and damping moment capability, as well as good stability characteristics, may become dominant factors in the choice of a rotor configuration.

It is the objective of this paper to take a critical look at some of the characteristics that result from using a hingeless rotor. The Langley Research Center has conducted flight investigations with two hingeless-rotor helicopters to determine these characteristics. The flight investigations have identified several potential problem areas: an undesirable gyroscopic coupling during maneuvers which adversely affects the aircraft handling qualities, a structural mode of oscillation very similar to that of a pendulum which causes undesirably large cyclic roll accelerations to the pilot under certain flight conditions, and, finally, large cyclic chordwise bending moments during severe maneuvers, the primary structural problem of concern.

These problem areas are different from those that have previously been encountered with articulated rotors, but with full awareness of these problem areas, the designer can eliminate them from future aircraft.

SYMBOLS

C factor in blade lock number,

$$\frac{\text{(Slope of lift curve)}}{\left(\dfrac{\text{Cross-sectional area of blade}}{\text{Blade maximum thickness} \times \text{Blade chord}}\right)} \times \frac{\left(\dfrac{\text{Blade aspect ratio}}{\text{Blade thickness ratio}}\right)}{\left(\dfrac{\text{Radius of gyration of blade}}{\text{Blade radius}}\right)^2}$$

r radial distance to blade element

R blade radius

V airspeed, knots

ρ_a mass density of air

ρ_b mass density of blade

ψ blade azimuth angle measured from downwind position in direction of rotation, degrees

FLIGHT INVESTIGATIONS

The Langley Research Center has conducted flight investigations with the two hingeless-rotor helicopters shown in figure 1. The first investigation was with a Bell H-13 helicopter for which the rotor was modified to a rudimentary hingeless-rotor design by cantilevering three nearly standard blades from a massive central hub. The remainder of the aircraft was essentially a production H-13. The second investigation, which is currently in progress, is being conducted with the Lockheed XH-51N, an experimental helicopter designed to demonstrate the potential of the hingeless rotor.

ROTOR MOMENT CHARACTERISTICS

The rotor moment characteristics are discussed first because of some limitations on control and angular-velocity damping moments that occur as a function of blade Lock number. The relative hovering control moment available (sea-level condition) with the three primary classes of rotors is plotted as a function of the blade Lock number in figure 2. The blade Lock number is the

ratio of the air density ρ_a to blade density ρ_b multiplied by a factor C which includes the mass distribution and the blade planform along the blade radius. The control moment of figure 2 was obtained for rotors having the same value of the factor C. Typical values of blade Lock number range from below 4 to over 12, where 4 denotes a heavy blade and 12 denotes a light blade - that is, increasing Lock number indicates decreasing blade weight.

The reference used for comparison of the rotors is the control moment of a rotor with the flapping hinge at the center of rotation and with a rotor height above the aircraft center of gravity equal to 0.3 times the blade radius. The mean blade lift coefficient was assumed to be 0.4. The control moment per unit of cyclic blade pitch is presented for the hingeless rotor and for a rotor with the flapping hinge at 4 percent of the rotor radius, which is typical of offset-hinge rotor design. The rotor height and mean blade lift coefficient were assumed to be constant for all three configurations. The large increase in control moment available due to cantilevering the blade from the rotor hub is apparent throughout the Lock number range. A flapping-hinge offset from 12 to 16 percent would be required to supply the same available control moment.

The effect of density altitude on the hovering control moment of the three configurations is shown in figure 3 for sample values of sea-level blade Lock number. A separate example for the rotor with a 4-percent flapping-hinge offset and a sea-level blade Lock number of 12 is not shown because the effect is almost the same as that of the rotor with the central flapping hinge.

Similar increases in the hovering angular-velocity damping moment are shown in figure 4 through the use of the hingeless-rotor helicopter. The same three classes of rotors are again compared. As was the case with the control moment, a flapping-hinge offset from 12 to 16 percent would be required to supply the same available damping moment.

The effect of density altitude on the hovering angular-velocity damping moment of the three configurations is shown in figure 5 for sample values of sea-level blade Lock number. A separate example for the rotor with a 4-percent flapping-hinge offset and a sea-level blade Lock number of 12 is not shown because the effect is almost the same as that of the rotor with the central flapping hinge.

Since it is presumed that using very high values of control and damping moment will provide a "tight" control system and the tight system will result in superior handling qualities, the information supplied in figures 2 and 4 indicates that designers should attempt to use blades with low Lock numbers based on sea-level conditions. However, this reasoning disregards the effect of the blade Lock number on gyroscopic coupling.

In figure 6 the ratio of the gyroscopic moment to the angular-velocity damping moment is presented as a function of blade Lock number for typical hingeless-rotor designs in hovering. The gyroscopic moment is the moment developed perpendicular to a commanded angular velocity and is divided by the damping moment that would oppose the gyroscopic moment. The solid-line curve indicates the gyroscopic moment for typical hingeless-rotor designs. Calculated

sea-level values of gyroscopic moment for the XH-13N and XH-51N are plotted on this curve. A flight investigation of this type of coupling during rapid rolling maneuvers (refs. 1 and 2) has indicated that values of this ratio in excess of 0.3 in either direction result in unsatisfactory handling qualities and values of this ratio in excess of 0.5 result in unacceptable handling qualities. It is emphasized that the maneuver task that indicated a problem is a rapid rolling maneuver in which excessive longitudinal coupling occurs. The point to be made is that, in order to reduce this coupling to an acceptable magnitude, the blade Lock number should be above 5 for all density altitudes. For a hingeless rotor designed to operate up to a density altitude of 15,000 feet, the blade Lock number at standard sea-level density should be 8 or above. Compromise on this point will depend upon the availability of control devices capable of eliminating gyroscopic coupling.

The extent to which direct control coupling (a pitching control moment accompanying roll control displacement and vice versa) may be used to offset gyroscopic coupling has been briefly investigated with the variable-stability helicopter described in reference 3. It appears from these tests that direct coupling up to about 25° can be used to reduce the effects of the gyroscopic coupling. For a gyroscopic coupling level which was considered to be acceptable only for an emergency condition where gross maneuvering would be restricted, the introduction of direct coupling improved the handling characteristics to a level which was acceptable for maneuvering but still had some unpleasant characteristics. However, for larger angles of direct coupling, the direct coupling becomes a problem in its own right in that lateral control inputs during roll reversals produce an abrupt jerk about the pitch axis. It should be noted that the level of control power and damping used in this investigation was much lower than that typical of hingeless-rotor helicopters. The extent to which higher control power and higher damping would limit the improvement which could be obtained from the application of direct coupling is not known.

The restriction on gyroscopic coupling is not limited to the hingeless rotor. If an articulated rotor with flapping-hinge offset from 12 to 16 percent were used to obtain the same order of magnitude of control and damping moments, undesirable gyroscopic coupling of the same order of magnitude as that shown in figure 6 would again be present.

Unsatisfactory gyroscopic coupling was obtained for the XH-13N as illustrated by the time history of figure 7 showing a lateral step control input and the resulting aircraft response. The calculated response shows reasonable agreement with the measured response, considering that the calculated response is based on a simple first-order two-degree-of-freedom analysis (ref. 2).

Although the coupling illustrated by figure 7 was objectionable, the tight control response, as indicated by rapid attainment of the final velocity, was recognized by pilots as resulting in an improvement in overall handling qualities. In particular, the high damping contribution provides positive maneuver stability throughout the speed range of the hingeless-rotor XH-13N.

As shown in figure 6, gyroscopic coupling would not be expected to be a problem with the XH-51N helicopter because of its relatively high Lock number.

This prediction is verified by the time history shown in figure 8 which indicates nearly a pure roll response to a lateral control input for the XH-51N. In addition, the XH-51N control system does provide some short-term attitude stability which may further reduce any gyroscopic effects (ref. 4).

PENDULUM MODE OF OSCILLATION

The prominent feature of the time history of figure 8, other than the tight response, is the roll velocity oscillation, which indicates that the lateral pendulum mode has been excited. The lateral pendulum mode is frequently excited in the XH-51N by control motions; however, for normal maneuvering, the pilot is not bothered by the oscillation, as he is apparently unable to separate it from normal rotor vibrations. The response of the XH-51N, even with the pendulum mode oscillation, is considered by the pilots to be good and near optimum for hovering. However, the pendulum mode does not always stay below the threshold of the pilot's awareness. A flight condition in which the pendulum mode was excited because of external disturbances is shown in figure 9.

Time histories of the angular velocities and vertical acceleration of the XH-51N while flying in moderately heavy turbulence at 100 knots are shown in figure 9. The lateral pendulum mode shape is illustrated by the highly exaggerated sketches at the top of the figure. The high angular accelerations of the pendulum mode, as indicated by the steep slopes of the rolling velocity trace, provide a very rough ride for the pilot. The roll attitude disturbances, the area under the angular velocity curve, are only about $\pm 1/2^{\circ}$ and are small enough not to be noticeable to the pilot.

Two solutions to this problem are proposed. The first solution is suggested by the sketches at the top of figure 9. Because the oscillation is primarily a rotation of the fuselage against the rotor spring, the addition of a small wing may supply sufficient aerodynamic damping to provide a smoother ride for the pilot. A second solution is to provide vibration isolation of a major part of the fuselage, particularly that portion containing the pilot and passengers. Some limited success along this line was obtained in isolating the pendulum mode of the XH-13N by a random change in the pylon mount stiffness (ref. 2).

STRUCTURAL LOADS

Some of the highlights of the flight investigations in the area of rotor-system structural loads are presented in this section. Because of the basic difference in the aeroelastic characteristics of the hingeless rotor as compared with those of the conventional articulated designs, the objective of the investigations was to identify potential problem areas and to evaluate a simplified analytical treatment that would be useful for preliminary design purposes.

During the flight investigations the rotor and control-system structural loads have been monitored for a wide range of ground and flight operating conditions. Although interesting results have been obtained, the following discussion emphasizes the area of primary concern - that of blade-root structural bending moments developed during rapid maneuvers.

The sensitivity of blade flapwise and chordwise bending-moment amplitudes to maneuvers was indicated in the results of the XH-13N flight investigation. As an example of this situation, a typical time history of a rolling maneuver at 70 knots with the XH-13N is shown in figure 10. The aircraft rolling velocity, blade-root chordwise bending moment, and blade-root flapwise bending moment are plotted over a 6-second interval. The blade response is seen to be primarily one cycle per rotor revolution. The maximum amplitude of the cyclic chordwise bending moment is so large that maintaining this maximum load level would result in a 10-hour fatigue life.

An overall comparison of the results of the flight investigations of the XH-13N and XH-51N to date is shown in figure 11. Nondimensional blade-root cyclic bending moments, flapwise and chordwise, are presented as a function of aircraft velocity. The cyclic moments are nondimensionalized by dividing by the 1 g blade lift moment $\left(\frac{3}{4} R \times \text{Weight of aircraft} \Big/ \text{Number of blades}\right)$. The maximum cyclic moments obtained during maneuvers and the level flight loads are indicated for each of the aircraft. The maneuvers were performed at the maximum angular-velocity capability of the respective aircraft - that is, full available control was used. It can be seen from figure 11 that the maneuver loads are the most critical throughout the speed range shown and that the chordwise cyclic moments are more sensitive to maneuvers.

A parallel goal of the investigation was to determine what analytical method would be adequate to handle the calculation of hingeless-rotor maneuver loads and rotor control-moment and damping-moment capabilities. The approach used was to determine the minimum modification required to extend the simple hinged-rotor analysis to the hingeless-rotor case. The basic objectives were (1) to gain some insight into the parameters that contributed to the buildup of loads in maneuvers and (2) to verify an analytical technique that would be useful in preliminary design studies.

The maneuvers primarily affected the first-mode blade response in both the flapwise and chordwise degrees of freedom. Therefore, the analysis of the hingeless rotor was handled by utilizing the simplified concept of a virtual offset-hinge blade with spring restraint at the hinge. This concept is described in reference 5.

Figure 12 shows the equivalent offset-hinge blade used in the analysis. The normalized displacement of the blade is presented as a function of the radial blade station. The actual first mode shape of a cantilevered blade is shown as the dashed line, and the equivalent hinged-blade mode shape is shown as the solid line. The virtual-hinge offset required for equivalence is approximately 8 to 10 percent of the rotor radius. A virtual spring at this point, the stiffness determined from the structural stiffness of the cantilevered

blade, completes the equivalent system. The equivalent system then provides the correct flapping and lead-lag angles and gives moments at the center of the rotor equivalent to the moments of the cantilevered blade. The moment characteristics shown in figures 2 to 6 were calculated by using this equivalent system to determine the rotor hub moments.

The simplified analysis using the equivalent system was applied to a number of the maneuvers with the XH-13N. Unstalled blade-section aerodynamic characteristics were used, and the main objective was to find out what parameters contributed to the buildup in chordwise moments. In general, it was determined that the particular combinations of blade cyclic flapping and feathering during the maneuver were the primary factors in the buildup of chordwise moments. An example of the results obtained from an analysis of the chordwise moments in a hovering maneuver are shown in figure 13 which is a time history of the amplitude of the cyclic chordwise bending moment and the blade azimuth position where the positive peak moment occurs. The time interval, 5 seconds, covers approximately 30 rotor revolutions. The calculated moment amplitude and blade azimuth position agree quite well with the measured data. The agreement is good because the response of the XH-13N was essentially one cycle per rotor revolution.

The same analysis was applied to a rapid maneuver at 70 knots for the XH-13N and, in general, agreement was obtained. In the XH-51N flight investigation the general behavior of blade structural loads in maneuvers shows the same trends as in the investigation with the XH-13N. However, a large amount of three-cycle-per-rotor-revolution response is present with the XH-51N, which cannot be handled by this simplified approach. The higher mode response of the XH-51N is due to insufficient separation of the second flapwise bending mode and the three-per-rotor-revolution forcing function. This problem, not unusual with rotary-wing aircraft, can be eliminated by a relatively minor change in the blade mass distribution.

Work is continuing in order to evaluate various means of alleviating the tendency for blade-root cyclic-bending-moment buildup in maneuvers. The theoretical analysis suggests three approaches that warrant consideration. They are as follows:

(1) The moments can be reduced by the elimination of gyroscopic coupling by means of light blades.

(2) The moments can be alleviated by rotor unloading (or operating at reduced rotor mean lift coefficients) because of the reduced collective and cyclic feathering trim requirements for compound operation.

(3) A more direct means of reducing the moments in maneuvers is to introduce chordwise flexibility into the blade.

The third approach is verified by the results of a joint NASA-Lockheed-U.S. Army hingeless-rotor dynamic-model investigation, which are shown in figure 14.

The top curve of figure 14 is for a conventional blade similar to that on the XH-51N or the XH-13N. Introducing chordwise flexibility at the blade root equal to the level of flapwise flexibility substantially reduced the moments. A further reduction was obtained by providing chordwise flexibility along the entire blade span. The theoretical analysis indicates that this reduction in cyclic moment will also be obtained for maneuvering. The proper application of this approach is imperative in order to avoid potential problems of ground and air resonance (ref. 6).

CONCLUDING REMARKS

Results of flight investigations with two experimental helicopters have indicated that problem areas different from those encountered with the articulated rotor occurred with the hingeless rotor. Three problem areas associated with the hingeless-rotor helicopter have been identified. These problem areas and proposed solutions are as follows:

1. Undesirably large gyroscopic coupling is found to occur with hingeless-rotor helicopters having low blade Lock numbers. Two solutions are proposed: (a) utilizing blades with high blade Lock numbers (or lighter blades) and/or (b) providing a control feedback device or direct control coupling capable of reducing the adverse effects of gyroscopic coupling.

2. A structural mode of oscillation very similar to that of a pendulum causes undesirably large cyclic roll accelerations to the pilot under certain flight conditions. Two solutions are proposed: (a) providing roll damping with a small wing and/or (b) providing vibration isolation of the pilot and passengers.

3. Large cyclic chordwise bending moments occur during severe maneuvers. Two solutions are proposed: (a) utilizing blades with the level of chordwise stiffness equal to that of the flapwise flexibility and/or (b) designing the rotor to operate at reduced rotor mean lift coefficients.

REFERENCES

1. Garren, John F., Jr.: Effects of Gyroscopic Cross Coupling Between Pitch and Roll on the Handling Qualities of VTOL Aircraft. NASA TN D-812, 1961.

2. Huston, Robert J.: An Exploratory Investigation of Factors Affecting the Handling Qualities of a Rudimentary Hingeless Rotor Helicopter. NASA TN D-3418, 1966.

3. Garren, John F., Jr.; and Kelly, James R.: Description of an Analog Computer Approach to V/STOL Simulation Employing a Variable-Stability Helicopter. NASA TN D-1970, 1964.

4. Foulke, William K.: Exploration of High-Speed Flight With the XH-51A Rigid Rotor Helicopter. USAAML Tech. Rept. 65-25(L. R. 18374), U.S. Army Aviation Materiel Labs. (Fort Eustis, Va.), June 1965. (Available from DDC as AD-617966.)

5. Ward, John F.: A Summary of Hingeless-Rotor Structural Loads and Dynamics Research. NASA paper presented at Symposium on the Noise and Loading Actions on Helicopter V/STOL Aircraft and Ground Effect Machines (Southampton, England), Aug. 31, 1965.

6. Lockheed-California Co.: Wind Tunnel Tests of an Optimized, Matched-Stiffness Rigid Rotor. TRECOM Tech. Rept. 64-56 (Lockheed Rept. No. 17790), U.S. Army Transportation Res. Command (Fort Eustis, Va.), Nov. 1964.

HINGELESS-ROTOR HELICOPTERS

XH-51 N

XH-13 N

L-2647-1

Figure 1

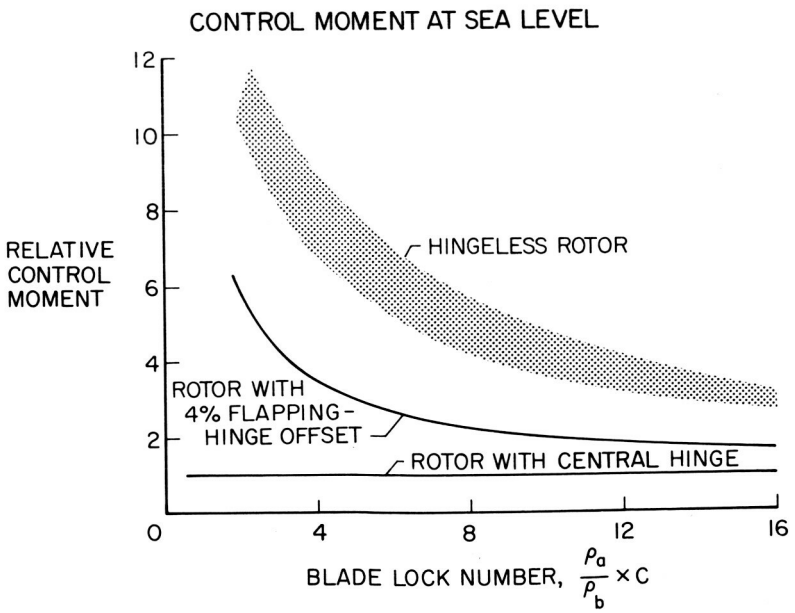

Figure 2

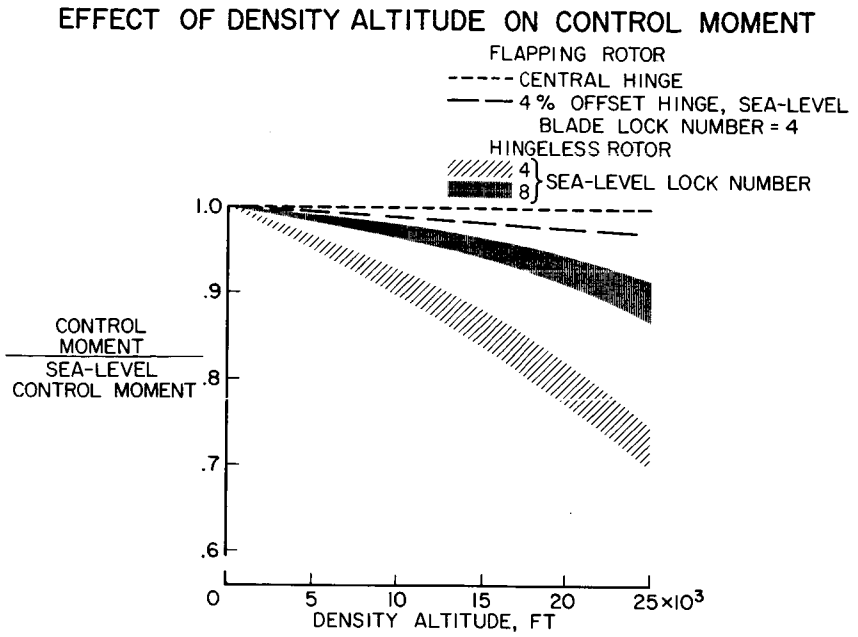

Figure 3

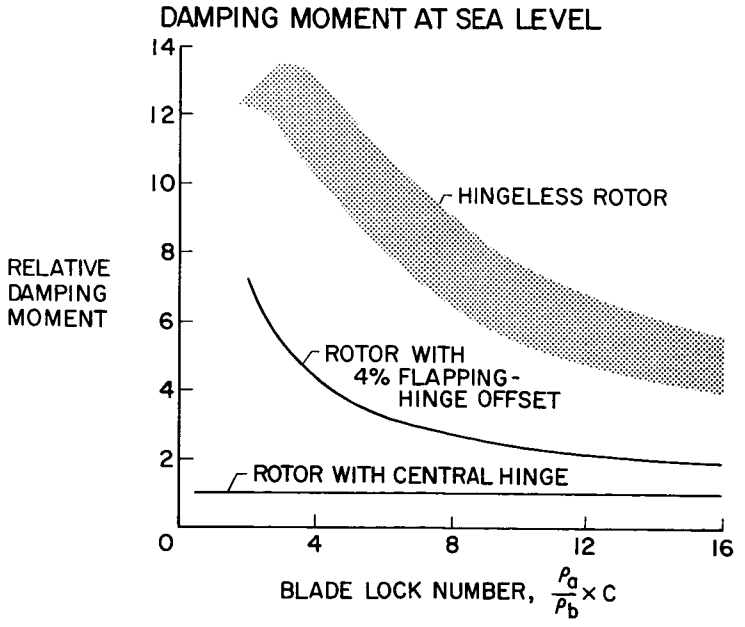

Figure 4

EFFECT OF DENSITY ALTITUDE ON DAMPING MOMENT

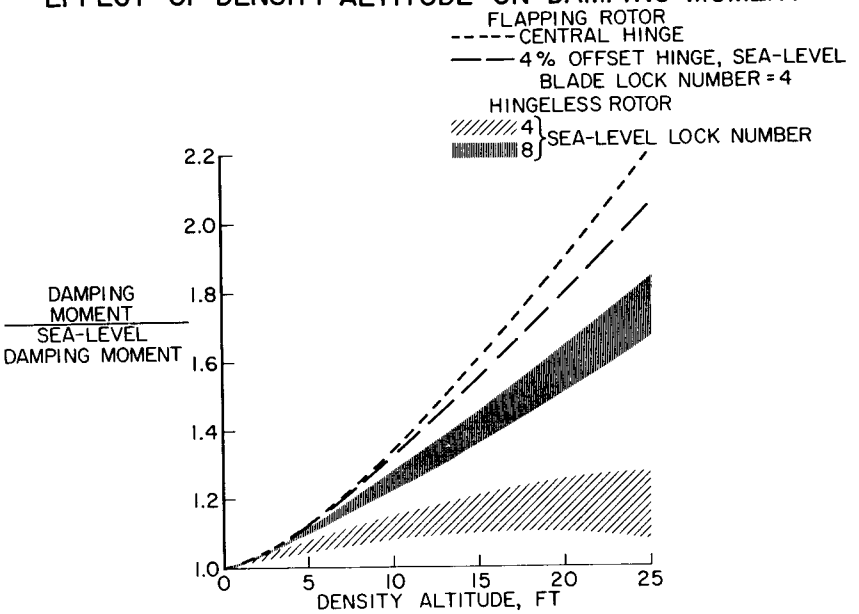

Figure 5

EFFECT OF LOCK NUMBER ON GYROSCOPIC COUPLING FOR HINGELESS ROTORS

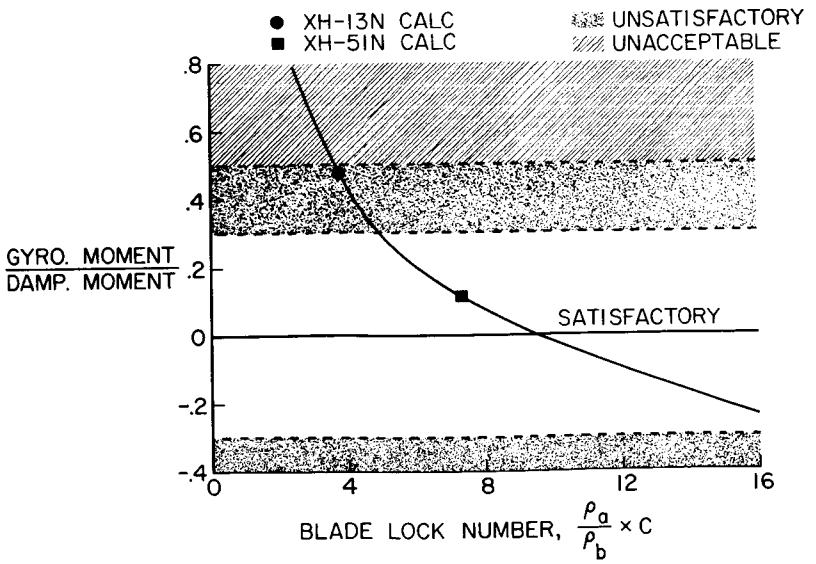

Figure 6

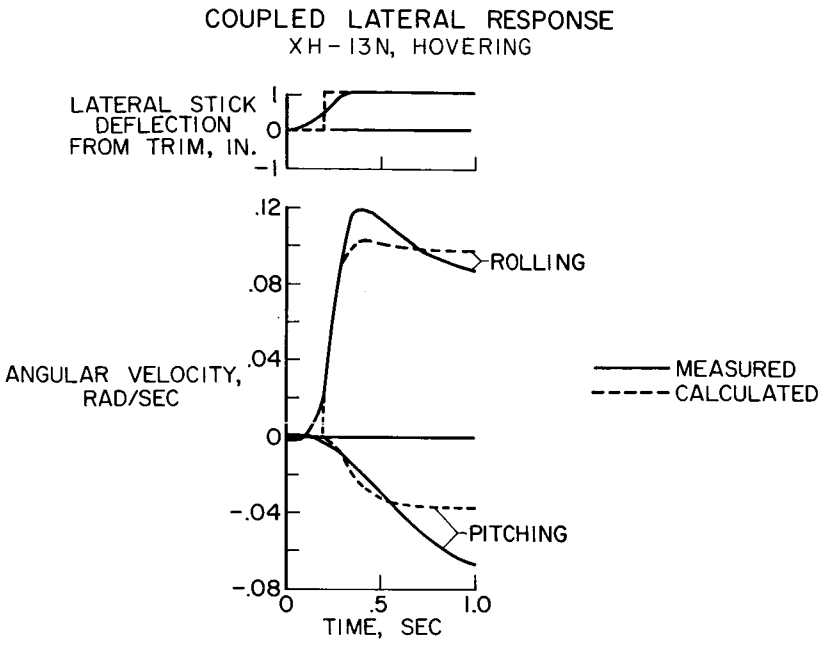

Figure 7

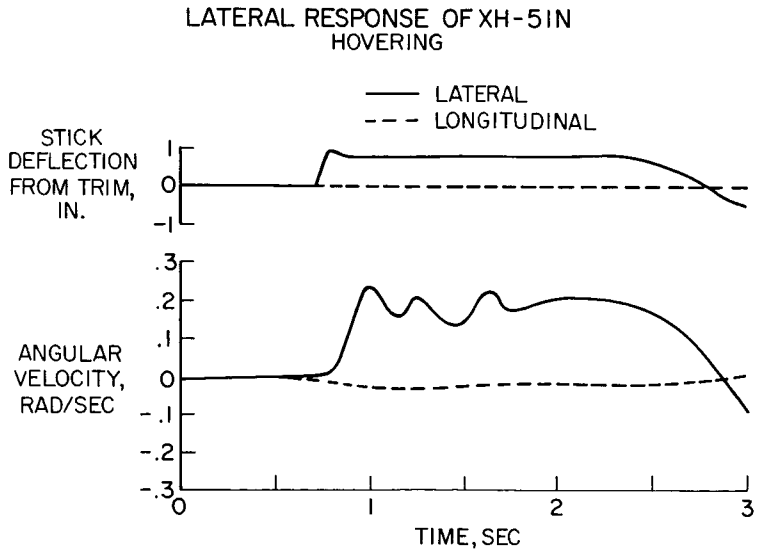

Figure 8

PENDULUM MODE
XH-51N FLIGHT IN GUSTY AIR AT 100 KNOTS

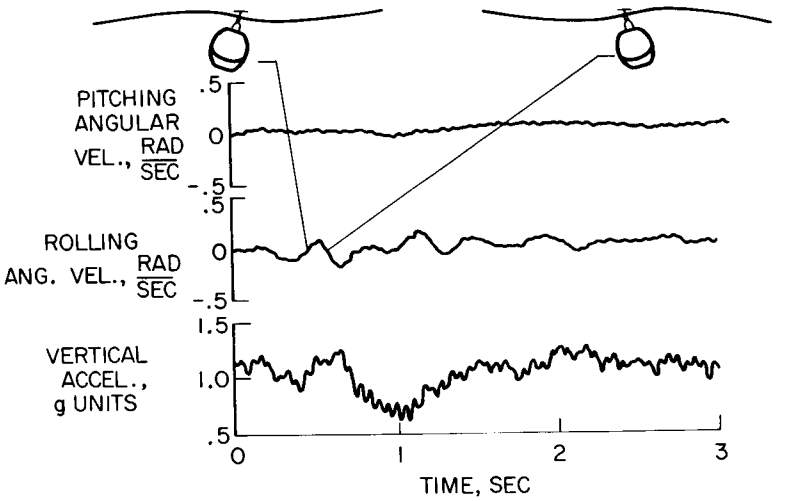

Figure 9

XH-13N STRUCTURAL BENDING MOMENTS
ROLL MANEUVER; V=70 KNOTS

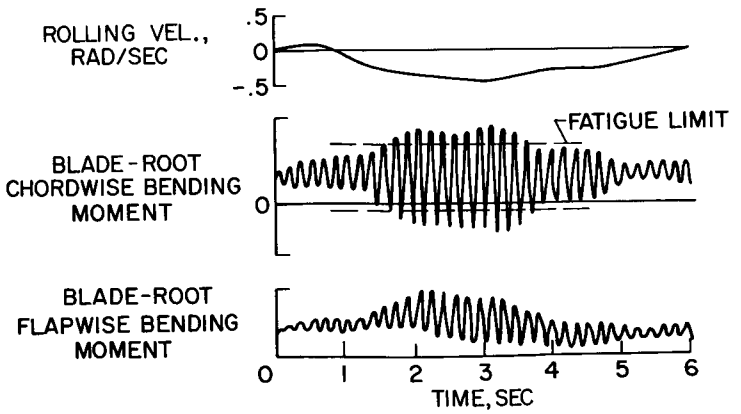

Figure 10

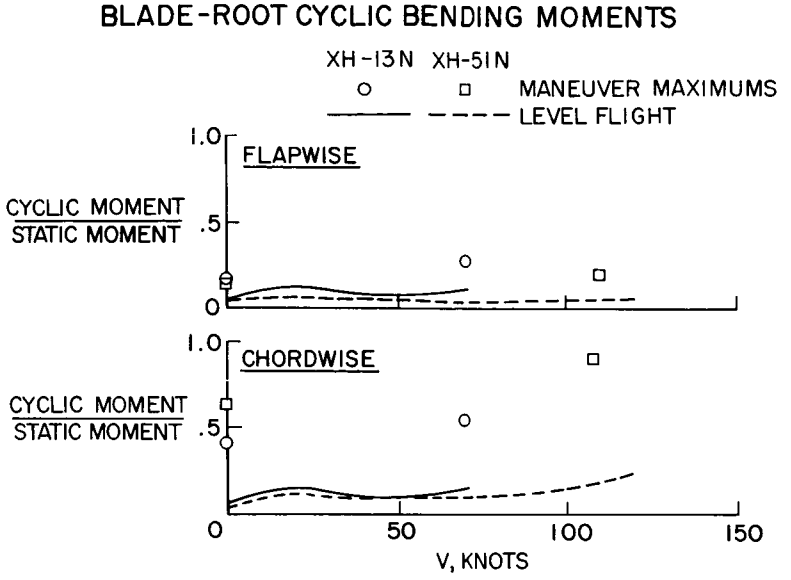

Figure 11

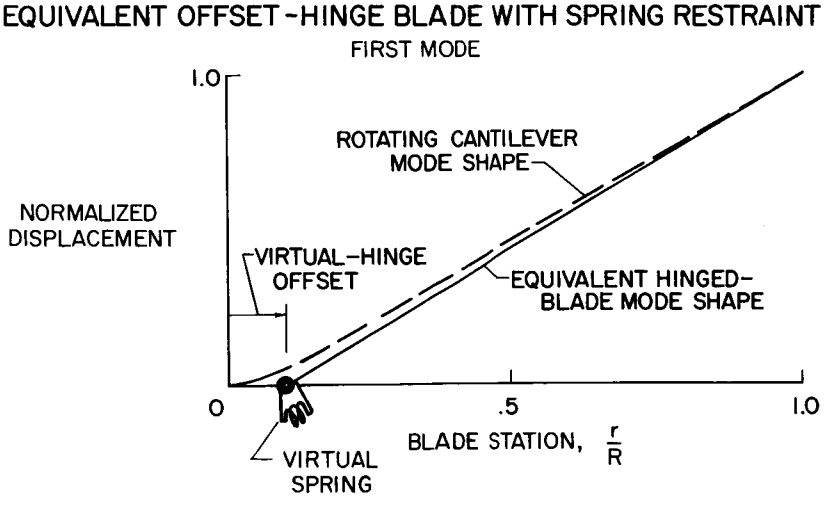

Figure 12

XH-13N MEASURED AND CALCULATED CYCLIC BENDING MOMENTS
PITCH MANEUVER; V=0

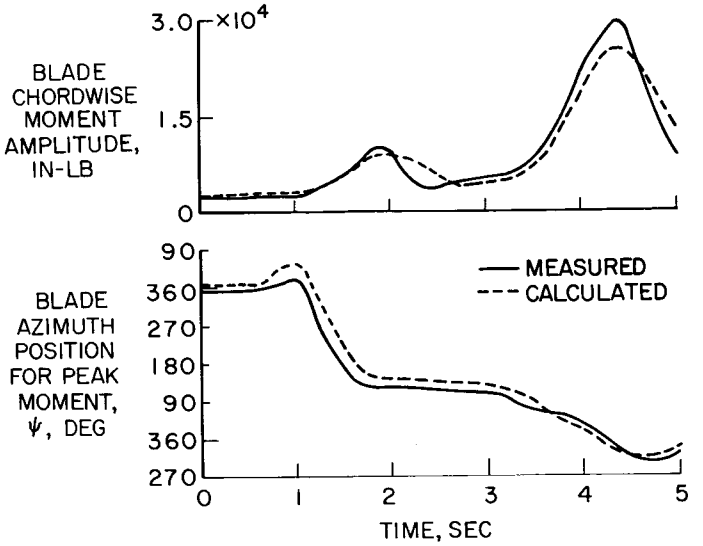

Figure 13

EFFECT OF FLEXIBILITY ON CHORDWISE MOMENTS
DYNAMIC MODEL; LOAD FACTOR = 1

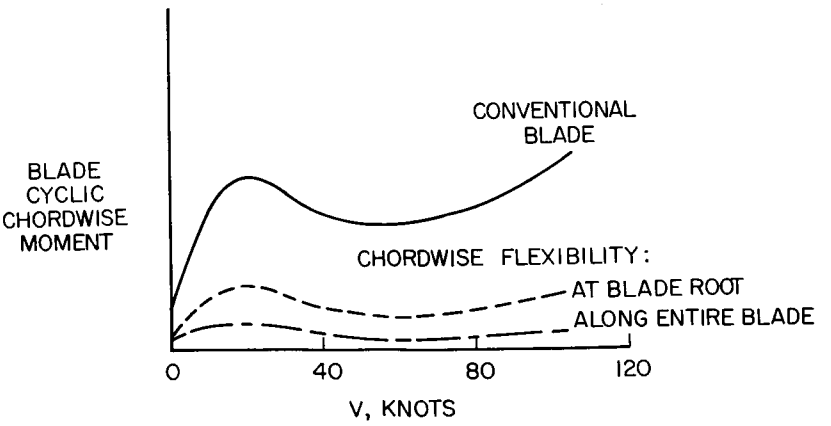

Figure 14

2. CALCULATED BLADE RESPONSE AT HIGH TIP-SPEED RATIOS

By Julian L. Jenkins, Jr.

NASA Langley Research Center

SUMMARY

This paper presents the initial results of a digital computer study of helicopter rotor-blade-motion stability for a broad range of forward speeds encompassing proposed conventional and compound helicopter designs. The analysis treats the general case of nonlinear, coupled flapping and lagging motions of hinged rigid blades. The results of the study to date indicate that blade-motion stability boundaries cannot be specified for a given blade design in terms of a fixed value of rotor tip-speed ratio. The stability boundaries can shift significantly within the desired operational speed range, with the stability limits depending upon the rotor loading, the magnitude of the disturbance encountered by the blade, and the blade position at the instant the external disturbance is encountered. The sample methods suggested for improving blade-motion stability include increasing the effective hinge spring restraint by incorporating pitch-flap coupling or by using hingeless or teetering rotor systems. Reducing rotor loading also has a beneficial effect on the blade-motion stability. The results indicate that methods used to deal with the blade-motion stability problem can be expected to diminish the overall vibration levels of the helicopter rotor system across the entire design speed range.

INTRODUCTION

The rapid advances in helicopter technology in the past few years have considerably expanded the rotor operating envelope. With the introduction of the compound helicopter wherein the low-speed capability of a rotor is coupled with the high-speed performance of a fixed-wing aircraft, this envelope is being further expanded.

The expansion which results from compounding and the more recent interest in stopped rotors have intensified interest in all aspects of the rotor operating environment, including high tip Mach number operation, high tip-speed ratios, and the extreme operating conditions during maneuvers. The purpose of this paper is to discuss some aspects of the blade-motion stability and response characteristics associated with high tip-speed ratio operation as determined from a numerical treatment of the nonlinear, coupled equations of motion of a hinged rotor with flapping and lagging degrees of freedom.

SYMBOLS

R	rotor radius, feet
V	forward velocity, feet per second
$\Delta\alpha$	angle-of-attack increment, degrees
β	blade flapping angle with respect to shaft at particular azimuth position, degrees
δ_3	flap-hinge cant angle, degrees
ζ	blade lead or lag angle at particular azimuth position, degrees
ψ	blade azimuth angle measured from downwind position in direction of rotation, degrees
Ω	rotor angular velocity, radians per second

Subscript:

o	initial

RESULTS AND DISCUSSION

The basic hub geometry of the rotor and the primary angles of interest are illustrated in figure 1. The hub is fully articulated with both flapping and lagging degrees of freedom. The diagram on the left-hand side of the figure simply illustrates the sign convention used to define the azimuth position of the blade.

Variables in the computer program include the blade planform, the blade mass factor, and the offset distance of each hinge point - that is, the distance from the center line of rotation to the respective hinge. The flap-hinge cant angle δ_3 may also be varied, as shown in figure 1. However, the discussion herein is limited to the case of zero δ_3.

Since this discussion is concerned solely with the motions of a blade about the two hinges illustrated in figure 1, it might be well to define the terminology used - in particular, the terms stable and unstable blade motion. As this is a digital computer study, large flapping or lag amplitudes as such are not limiting factors. In other words, the blade-motion amplitudes which may be excessive or intolerable for practical rotor operation are not necessarily unstable; however, in order to place some limit on the amplitudes, transient oscillatory amplitudes which exceed 90° are termed unstable.

Of course, the practical rotor operating limit occurs long before the unstable condition is reached. However, by looking at the extreme condition, it is believed that a better understanding may be gained of the more subtle effects which are present for the conditions at which rotors are currently being operated.

This study indicates that the stability boundaries, as such, are not very rigid in the sense that it is difficult to define a single boundary for the nonlinear system that is valid for all rotor operating conditions, as is illustrated in figure 2. This figure presents regions of stable and unstable blade motion as functions of the blade mass factor and tip-speed ratio for two different initial conditions. Since the mass-factor parameter is inversely proportional to the blade inertia, light blades are at the upper end of the scale and heavy blades are at the lower end. The two boundaries were established by setting an initial flap-angle displacement β_0 of approximately 11° and solving for the transient solution for the unloaded rotor condition. Thus, the stable, steady-state condition expected was one of zero blade flapping and only the forced lead-lag response.

The disturbance was initially introduced at an azimuth angle of 0° - that is, with the blade in the downwind position - and the right-hand boundary shown in figure 2 was developed. The motion is stable or convergent for conditions on the left of this boundary and unstable or divergent for conditions on the right. This boundary is the one generally presented in most studies which use only the nonlinear flapping degree of freedom.

From a study of the various terms in the equations of motion and the blade-motion time histories used to develop this boundary, it became apparent that the unstable moments were developed only in the forward quadrants of an unloaded rotor - primarily in the range of azimuth angles from 90° to 180°. This fact implies that at high tip-speed ratios, the unloaded rotor would be very sensitive to the azimuth position of the blade when it is initially disturbed. As illustrated by the significant shifting of the left-hand boundary shown in figure 2, the unloaded rotor was in fact very sensitive to azimuth position. This boundary was developed by introducing the same initial disturbance at 90° azimuth - that is, on the advancing side of the rotor disk.

The fact that the stability boundary shifts is not unexpected for nonlinear equations; however, the significant shifting which occurs for all but the extremely heavy blade is somewhat surprising. It is significant that there is so much shifting in the boundary for the range of blade mass factors representative of current design practice (i.e., the range from about 1 to 2), for this is the area in which the operating tip-speed ratios are expanding. For example, while pure helicopters operate at tip-speed ratios below 0.5, the experimental compound helicopters have already reached tip-speed ratios slightly in excess of 0.5 and the advanced compounds, such as the advanced aerial fire support system (AAFSS), will operate in the range from 0.5 to about 0.7. Of course, the stopped rotor must go through the entire range of tip-speed ratios.

As mentioned previously, the unstable moments for the unloaded rotor are developed only in the forward quadrants of the rotor disk. Although it is difficult to separate aerodynamic spring and damping forces in a nonlinear analysis, the term which causes the unstable blade motion is what may be considered as the aerodynamic spring term in the equation of flapping motion.

The actual velocity component involved in producing the aerodynamic spring force is illustrated in figure 3. This diagram shows the relative position of the radial component of the forward velocity for a blade in the forward position ($\psi = 180^\circ$) and the rearward position ($\psi = 0^\circ$). It is apparent that the component of this velocity normal to the blade will produce unstable spring forces in the forward quadrants and will produce stabilizing or positive spring forces in the rearward quadrants.

The two stability boundaries shown in figure 2 illustrate the significance of the aerodynamic spring term in the equation of flapping motion. For example, a relatively light blade which is disturbed at an azimuth angle of 0° has both a positive aerodynamic spring force and a positive centrifugal spring force. Thus, the flapping amplitude is reduced considerably by the time the blade reaches an azimuth angle of 90° and the effects of the destabilizing spring forces are minimized. On the other hand, the same blade released at 90° azimuth has a positive centrifugal spring force but encounters a negative or destabilizing aerodynamic spring force and thus becomes unstable at much lower tip-speed ratios.

The boundary for an extremely heavy blade shows very little effect of azimuth angle because of the very low effective damping which is characteristic of a heavy blade. No matter where the blade is disturbed, the motion does not damp out or expand enough in one rotor revolution to alter the boundary significantly.

In order to illustrate the type of response obtained in determining these boundaries and to show the influence of the lagging degree of freedom on the rotor response, blade transient time histories for two flight conditions are shown in figure 4. This figure presents the transient responses of both the flapping and the lagging motion as functions of rotor revolutions for a blade with a mass factor of 1.6. The dashed curves are for a stable condition at a tip-speed ratio of 1.25, which corresponds to a point just to the left of the 90° boundary shown in figure 2. The solid curves are for an unstable condition at a tip-speed ratio of 1.5, which corresponds to a point just to the right of the 90° boundary.

For both β/β_o and ζ/β_o, the time histories for the stable and unstable conditions are very similar during the first two revolutions. The flapping initially increases because of the destabilizing spring moment and then diminishes considerably during the second revolution. The blade initially swings forward or leads because of the Coriolis forces produced by the high flapping velocity. The predominant difference between the curves for stable and unstable conditions is the higher lag angle which exists for the higher tip-speed ratio during the second revolution. It is this large lag amplitude which causes a reduction in the blade flapwise inertia such that even the

relatively small flapping displacement which exists at the end of the second revolution is enough to set off a completely divergent oscillation.

While stability boundaries, as such, may appear to be more of a future problem than one of immediate concern, it should be emphasized that the velocity component, which ultimately causes rotor instability, starts building up when the rotor leaves hovering flight. In fact, linearized equations of motion of a flapping blade can be used to show that the total spring constant can become negative in the forward quadrants at tip-speed ratios well below 1. Another point to consider is the effect of rotor loading on the stability boundary. In general, rotor loading produces a destabilizing moment around the whole azimuth and thus a lifting rotor would be expected to experience instabilities earlier than an unloaded rotor when subjected to a disturbance.

Figure 5 presents regions of stable and unstable blade motion as functions of blade mass factor and tip-speed ratio. The major boundary is simply a repeat of the boundary shown in figure 2. The short boundary indicates the point at which blade-motion instability was encountered when a rotor initially carrying a lifting load was subjected to a disturbance - in this case, a vertical gust. As expected, the lifting rotor became unstable sooner than the nonlifting rotor. Of course, it should be noted that the point at which a lifting rotor encounters unstable blade motion is a function of the initial rotor loading and, also, the magnitude of the disturbance.

There are several methods available for extending the stability boundaries. For example, increasing the effective hinge spring restraint by pitch-flap coupling or by the use of a hingeless or teetering rotor will increase the stability limit. Increased damping will also increase the limit. Of course, flapwise damping will be more effective than in-plane damping; however, an in-plane damper will tend to reduce the lag-angle excursions and thus keep the flapping inertia at its maximum value. Both of these methods, increased spring moment and increased damping, are a matter of detail design for the flight conditions anticipated, because of the root moments introduced by any type of hinge restraint. A third method of extending the boundaries is reduced rotor loading. Rotor unloading decreases the sizable destabilizing moment contributed by rotor thrust.

Practical rotor operating is not necessarily limited by so-called stability boundaries at extreme tip-speed ratios, as mentioned previously, but is more likely to be limited by excessive or intolerable blade-motion amplitudes or vibration problems at more conventional tip-speed ratios. As an example, figure 6 presents the flapwise response characteristics of a rotor which is initially carrying a lifting load and then is subjected to an angle-of-attack step input due to a vertical gust. The maximum peak-to-peak flap amplitude which occurred during the transient is plotted as a function of the angle-of-attack increment caused by the vertical gust.

These data indicate that, at a tip-speed ratio of 0.3, the rotor may be subjected to a sizable disturbance without encountering extreme transient amplitudes; however, at a tip-speed ratio of 0.5, relatively mild disturbances

cause transient amplitudes equal in magnitude to the amplitude reached only for the severe disturbance at the lower tip-speed ratio. At a tip-speed ratio of 1.0, the response is such that even a very modest disturbance causes extreme transient amplitudes. The dashed portion of this curve was extrapolated merely to indicate that a disturbance of approximately 6° caused complete instability. This point at which instability occurred corresponds to the unstable boundary presented in figure 5 for a lifting rotor. It is apparent that the amplitudes which result from a disturbance at the higher tip-speed ratios place a more critical restriction on the acceptable rotor operating condition than does the concern for stability.

Since the stability boundaries shift so much when the disturbances are introduced at different azimuth angles, blade tracking during a transient gives rise to vibration problems associated with tip-path separation during maneuvers or as the result of gusts. Figure 7 shows a time history of tip-path separation for adjacent blades of a four-blade lifting rotor operating at a tip-speed ratio of 0.5 after a step input due to a vertical gust is imposed. The trace represents the difference between the paths of two blades, which are 90° apart. The large separation which initially occurs certainly indicates a source of vibratory input. Although the amplitude is rapidly damped, it is unlikely that the steady gust such as that used in this example will ever exist in practice. In effect, an actual rotor is in a continual transient in gusty air, and consequently the differences in the tip trace are not likely to damp out as rapidly. It is of interest to note that even at this tip-speed ratio of 0.5, there is evidence of a relative difference in the aerodynamic spring moment just past 90° azimuth, as indicated by the change in slope of the curves in each cycle.

Of course, any efforts to extend the stability boundaries by the methods previously discussed are likely to be accompanied by improvements in rotor characteristics at the more conventional tip-speed ratios in terms of vibratory problems. Vibrations associated with tip-path separation and the excessive flapping response, which limits even stable rotor operation, can be expected to decrease across the entire design speed range.

CONCLUDING REMARKS

Although some of the examples presented in this study are not realistic in terms of practical rotor operation, the limited experimental data available indicate that very real problems exist at high tip-speed ratios. These problems, which may be categorized as tip-path separation, blade-motion amplitude response, and blade-motion stability, are all related in some degree to the dissymmetry of the flow conditions around the azimuth as tip-speed ratio increases.

The significant shifting of the rotor stability limits pointed out herein is certainly discomforting, for this shifting makes it impossible to define a so-called stability boundary which must not be exceeded. This study indicates that the predominant destabilizing factor is the aerodynamic

spring force in the flapwise direction and that introduction of the lagging degree of freedom has more of a secondary effect - that is, the lag amplitude tends to reduce the flapwise inertia and this reduction in turn makes the flapping motion more responsive to the driving forces.

The sample methods suggested for improving blade-motion stability include increasing the effective hinge spring moment by incorporating pitch-flap coupling or by using hingeless or teetering rotor systems. Reducing rotor loading also has a beneficial effect on the blade-motion stability. The results indicate that methods used to deal with the blade-motion stability problem can be expected to diminish the overall vibration levels of the helicopter rotor system across the entire design speed range.

BASIC HUB GEOMETRY

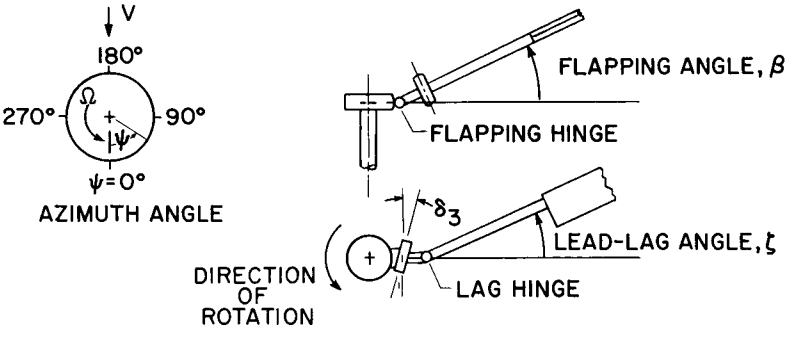

Figure 1

EFFECT OF AZIMUTH ANGLE ON BLADE-MOTION STABILITY BOUNDARY

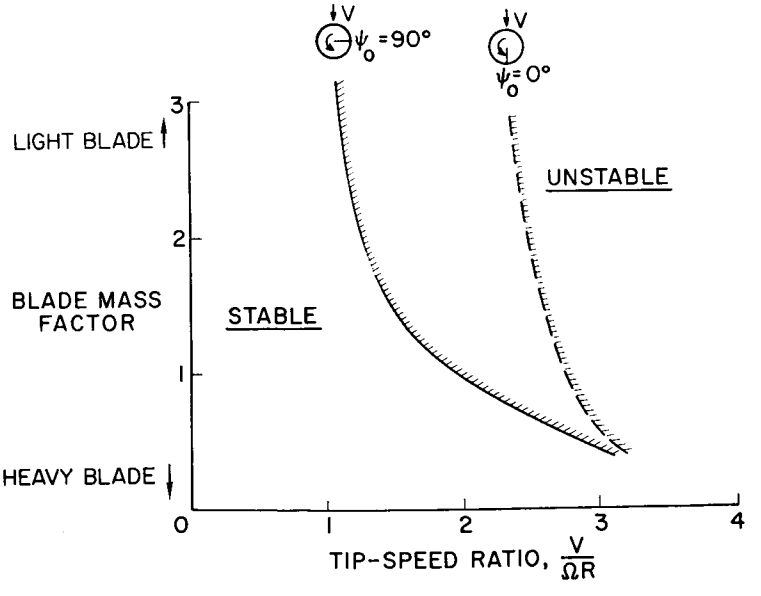

Figure 2

VELOCITY COMPONENT CONTRIBUTING TO
AERODYNAMIC SPRING FORCE

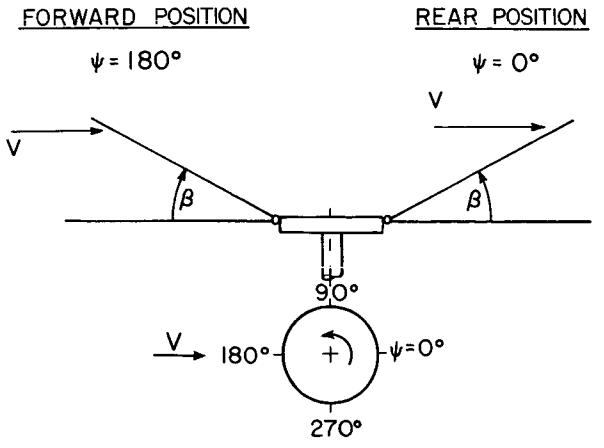

Figure 3

TRANSIENT RESPONSE FOR INITIAL DISPLACEMENT
AT $\psi = 90°$

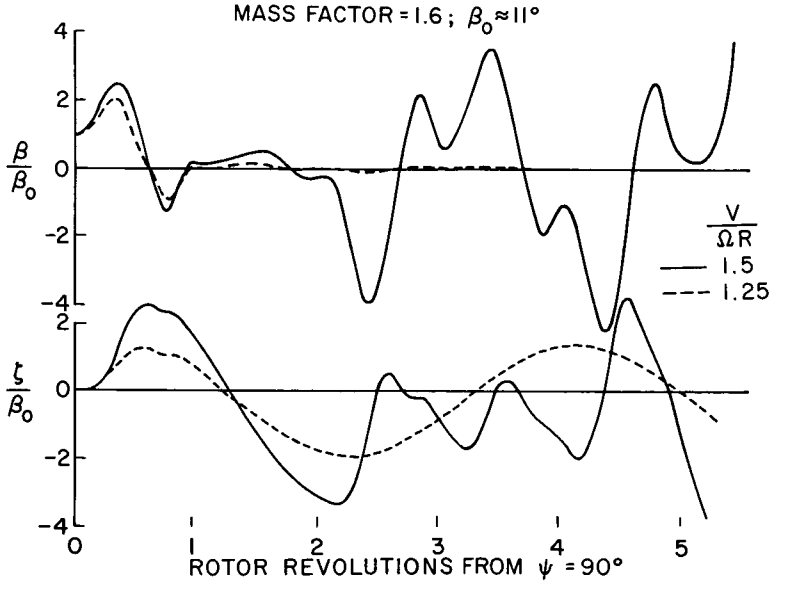

Figure 4

EFFECT OF INITIAL LIFTING LOAD ON BLADE-MOTION STABILITY

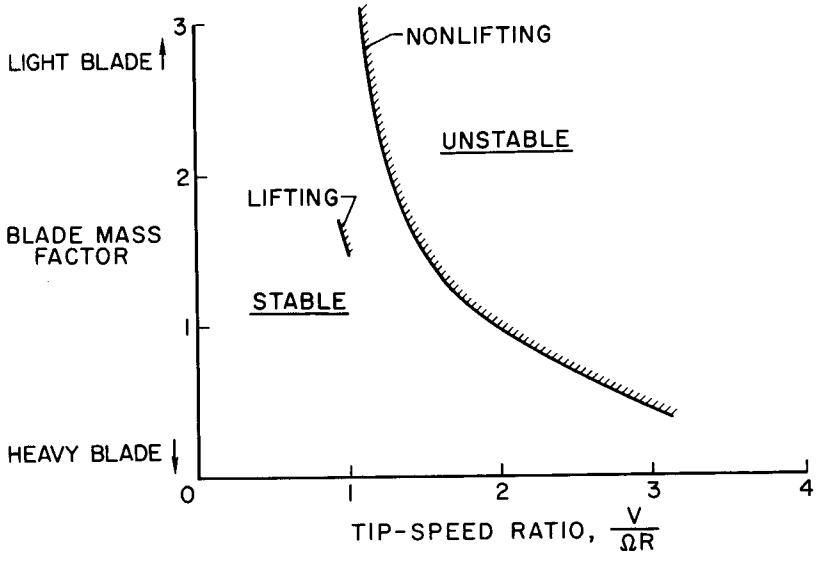

Figure 5

FLAPPING-AMPLITUDE RESPONSE TO A STEP INPUT FOR A LIFTING ROTOR

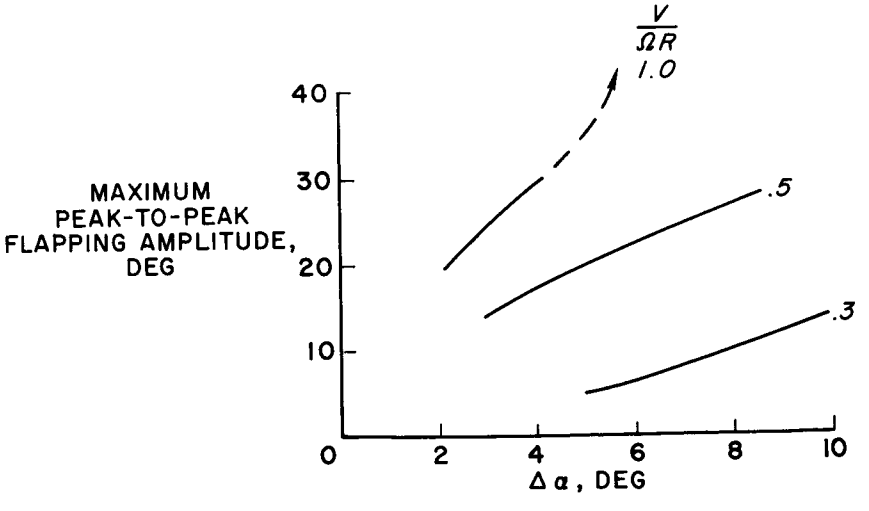

Figure 6

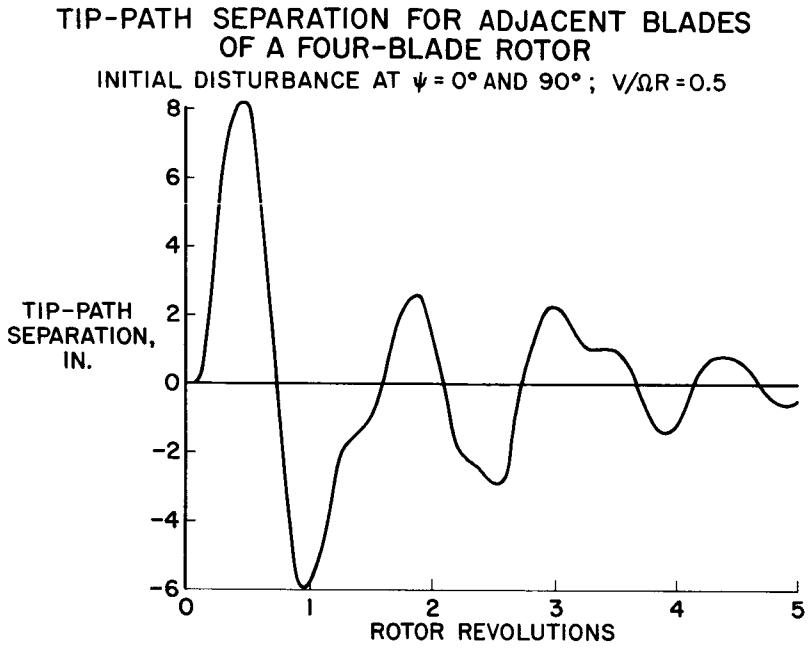
TIP-PATH SEPARATION FOR ADJACENT BLADES
OF A FOUR-BLADE ROTOR
INITIAL DISTURBANCE AT ψ = 0° AND 90° ; V/ΩR = 0.5
TIP-PATH SEPARATION, IN.
8
6
4
2
0
-2
-4
-6
0
1
2
3
4
5
ROTOR REVOLUTIONS

Figure 7

Page intentionally left blank

3. PERFORMANCE CHARACTERISTICS OF A JET-FLAP ROTOR

By John L. McCloud III, William T. Evans,
and James C. Biggers
Ames Research Center

SUMMARY

Results of an experimental investigation of the characteristics of a jet-flap rotor are presented and discussed. Comparisons of the rotor's force-producing capabilities with those of a conventional rotor are made which show the jet-flap rotor to be operable well beyond standard rotor stall boundaries. Correlations are made between measured and calculated results which show generally good agreement.

Author

INTRODUCTION

As a part of NASA's VTOL investigations, various methods of increasing the forward speed capabilities of helicopter rotors are being studied. Rotor forward speeds are aerodynamically limited by retreating blade stall, a decreasing ability to develop propulsive force loads at high advance ratios without extreme rotor tilting, and compressibility effects which occur on the advancing blade tips. One method of avoiding these problems is by application of jet flaps to the helicopter rotor blades. The jet-induced "supercirculation" and BLC effects may delay the stall, permitting large propulsive and lifting loads at high forward speeds.

This type of rotor has been studied analytically and reported in references 1, 2, and 3. The French firm of Giravions Dorand has built such a rotor under contract to the U. S. Army, and this rotor has been tested in the Ames 40- by 80-foot wind tunnel. The jet-flap rotor was driven and controlled by the jet itself. The blades were fixed in pitch and varying the jet-flap deflection angle, both cyclically and noncyclically, controlled the rotor force output.

Data were obtained at hover and forward flight conditions corresponding to advance ratios of 0.3, 0.4, and 0.5 for two blade angle settings. Data presented here compare the jet-flap rotor's force-producing capability with a conventional rotor's stall boundaries. Data showing correlation with calculated performance, obtained by the digital computation methods of reference 1, are also presented.

NOTATION

$\bar{A}_0$ collective jet deflection, deg

$\bar{B}_1$ cyclic jet deflection, deg, $\theta_j = \bar{A}_0 - \bar{B}_1 \sin \psi$

b number of blades

C_{j_R} rotor jet-momentum coefficient, $\frac{M_j V_j}{\rho(\Omega R)^2 \pi R^2}$

C_{L_R} rotor lift coefficient, $\frac{L}{\rho(\Omega R)^2 \pi R^2}$

C_{X_R} rotor propulsive-force coefficient, $\frac{X}{\rho(\Omega R)^2 \pi R^2}$

c blade chord, ft

c_e equivalent blade chord (on thrust basis), $\frac{\int_{0.111R}^{0.99R} cr^2 dr}{\int_{0.111R}^{0.99R} r^2 dr}$, ft

L lift, lb

M_j total mass flow through both blades, slugs/sec

R rotor radius, ft

r radius station, ft

V free-stream velocity, ft/sec

V_j jet velocity, assuming adiabatic expansion from blade duct pressure, ft/sec

$\frac{V}{\Omega R}$ advance ratio

X propulsive force, positive upstream, lb

α_s shaft angle, positive rearward from vertical, deg

θ_j jet deflection, positive downward from chord line, deg

θ blade angle, relative to tip chord line, deg

$\theta_{0.7}$ collective pitch of blade at 0.7R, deg

ρ free-stream air density, slugs/ft^3

σ rotor solidity, $\frac{bc_e}{\pi R}$

ψ blade azimuth angle, measured from downstream in direction of rotation, deg

Ω rotational speed of rotor, rad/sec

MODEL AND APPARATUS

Rotor

Figure 1 shows the rotor and air supply unit installed in the wind tunnel. The rotor was two-bladed, with offset coning hinges and a central teetering hinge. Twist distribution, planform, and airfoil sections of the blades are illustrated in figure 2. A linear twist distribution of -8° is shown for comparison purposes. The blades for these tests had no feather bearings and were fixed in pitch. Tests were made at blade pitch settings of $\theta_{0.7} = 8^\circ$ and 12°. The inboard portion of the blade out to the 0.4R station has elliptical cross sections. The blade has constant chord and thickness from 0.4R to 0.7R and then tapers in both chord and thickness from 0.7R to the tip. The jet flap and nozzle also begin at 0.7R and extend to the blade tip.

The fixed pitch setting of the test rotor is not requisite to the jet-flap principle, but, pending results of application studies, it could be a desirable feature made possible by the jet flap. The other details of the rotor, with the possible exception of thickness, are also not dictated by the jet flap.

The details of the jet flap are shown in figure 3. The compressed air was ducted through the blade spar and then, by a cascade of turning vanes, was exhausted out the trailing portion of the blade over a short mechanical flap. Mechanically deflecting the flap deflects the jet flow as the air follows the upper surface by the Coanda effect. The flow out the nozzle provides the torque for rotor rotation, and deflecting the jet flap cyclically and noncyclically controls the rotor's force output.

The mechanical portion of the flap was deflected by a pneumatic system which was controlled by a swash plate and linkage system. The swash plate, housed in the cylindrical portion of the hub, was positioned by electric actuators (see fig. 4).

Rotor Support System

The rotor suspension shown in figure 4 consisted of a three-legged, spring-loaded parallelogram system. This system provided inplane softness, longitudinal and lateral, without changing the tilt of the rotor shaft. The parallelogram structure was supported in turn by a strain-gage balance platform which

pivoted about point A of figure 4. This pivoting action, which tilts the shaft axis, was controlled by an electric actuator not shown.

The air ducting to the rotor is split to provide two opposing flows to the rotor. This is necessary since the air source is mounted below the balance platform. A universal joint in the ducting accepts these two flows and provides the articulation necessary for shaft-axis tilt.

The rotor suspension system was shielded from air loads by a fairing (see fig. 1) attached to the support system below the strain-gage platform. However, the fairing "cap" was attached to the upper portion of the parallelogram system; hence its air loads were sensed by the strain-gage balance. The drag load of this "cap" and that of the hub, slip rings, etc., have been removed from the data herein as tares.

The compressed air to drive the rotor was supplied by an axial-flow compressor driven by a constant-speed turboshaft engine. The amount of air supplied to the rotor was set by control valves at the compressor outlet (point B of fig. 4).

Instrumentation

All rotor forces and moments were measured by the six-component strain-gage balance system previously discussed. The compressed air-flow rate was measured by an orifice meter in the vertical air-supply line downstream of the flow-control valves. Compressed air temperature was measured at this point. Additional pressures and temperatures and several rotor-blade stresses, hinge motions, and vibration levels were monitored during the investigation.

RESULTS AND DISCUSSION

The basic results of the wind-tunnel tests are shown in figure 5. For the conditions indicated, these plots show the lift and propulsive force coefficients developed by the jet-flap rotor at advance ratios of 0.30 and 0.51. Also indicated on these plots are retreating blade stall limits for a standard rotor. Specifically, these limits correspond to the upper stall boundaries of a rotor having -8° of twist as obtained from the charts of reference 4. Conventional rotors must be operated at force levels below these limits to avoid retreating blade stall. The increased load-carrying capability of the jet-flap rotor is quite substantial, reaching as high as 2 to 2-1/2 times the capability of a conventional rotor. These loads would not have been achieved without the increased lift due to the circulation and BLC effects of the jet flap. The higher force values were limited by the test rotor's mechanical limitation to a maximum jet-flap deflection of approximately 50°. (Note that $\overline{A}_0 + \overline{B}_1 = 46^{\circ}$ for the data of fig. 5.)

The high force capability of the jet-flap rotor is compared in figure 6 to that for a conventional rotor over a range of flight speeds from 0 to 300 knots.

In this instance the highest values of jet-flap rotor lift have been made dimensionless by dividing by the static thrust obtainable from a conventional rotor for the same tip speeds and areas, etc.[1] The upper limit of lift capability for the conventional rotor at forward speeds is based on the retreating blade stall criteria previously stated. The specific value of $V/\Omega R$ for which the conventional rotor can no longer develop any lift at all depends upon its propulsive force requirement (ref. 5).

The jet-flap rotor's experimentally demonstrated capability is indicated by the data points, of which two correspond to the high propulsive force conditions of figure 5. From hover to an advance ratio of 0.5 the increased lift capability is substantial. The data for the jet-flap rotor do not represent flight limits. There were no indications of retreating blade stall, and even higher forces and advance ratios might have been attained with a greater range of flap deflections.

Also indicated on this figure is a region representing lift and forward speed conditions for which performance has been calculated. These calculations are based on the special analyses for jet-flap rotors reported in reference 1. The calculations were made on digital computing machines and include the necessary inputs to account for compressibility and reverse flow effects. Note that calculated performance for the jet-flap rotor indicates a significant rotor force capability at forward speeds up to 300 knots. At this speed conventional rotors must be unloaded by compounding, that is, by the addition of wings and propulsion units to the aircarft.

COMPARISON WITH THEORY

Collective Variation

The large forces developed and the high forward speeds indicated as obtainable by the jet-flap rotor make it desirable to compare measured and calculated performance in more detail. Figure 7 shows such a comparison. Examination of both portions of the figure shows the calculated and measured data to compare very favorably in an overall qualitative sense. There are some slope differences and, hence, the degree of quantitative agreement depends on the conditions chosen for comparison. It may be noted that the data shown in figure 7 are similar to those for a conventional rotor. The variation of C_{L_R} versus C_{X_R} as shaft angle changes (at constant jet collective) is similar to the variation of C_{L_R} versus C_{X_R} as shaft angle (or control axis inclination) changes at a constant collective blade pitch setting for a conventional rotor. The variations of C_{L_R} and C_{X_R} with jet collective changes at constant shaft angles are also similar to those due to blade collective pitch changes on a conventional rotor.

---

[1]Static thrust obtainable is based on a $C_{L_R}/\sigma = 0.16$, which is indicated by reference 4 as a probable upper limit.

Cyclic Variation

The measured and calculated effects of cyclic deflection of the jet flap are shown in figure 8. The data are for various shaft angles of attack and cyclic jet deflections at fixed collective jet deflections.

For a conventional rotor, increasing blade cyclic pitch at constant collective pitch and shaft angle of attack produces C_{L_R} versus C_{X_R} variations similar to those shown for the shaft angle variation. However, increasing jet-flap cyclic deflections increases propulsive force coefficient with little change in lift coefficient.

Again, the calculated variation shows the same general effects as the measured data, and again there are differences in details. For example, the measured data show slight lift increases with increased cyclic jet-flap deflection whereas the calculations show slight decreases.

Data for other blade angles and advance ratios show the same degree of correlation.

Momentum Requirements

Figure 9 shows the momentum requirements for the rotor at the conditions indicated. These data correspond to the data of figure 7. The changes in momentum coefficient C_{j_R} shown in figure 9 reflect the changes in propulsive force coefficient shown in figure 7. The calculated C_{j_R} variations are quite similar to the measured variations although the general level of the measured values is higher. The increment between measured and calculated C_{j_R} values was fairly consistent for all test conditions. For example, figure 10, which shows data obtained for hover conditions, has similar increments. The calculations did not take into account any nozzle losses or thrust losses due to the jet flow over the mechanical portion of the flap, which probably accounts for these differences.

Comparison of equivalent shaft power for the jet-flap rotor with that for a conventional rotor depends upon the conditions chosen. When the conventional rotor is unstalled, the jet-flap rotor requires more power, as discussed in reference 1. When the increased lift capability of the jet-flap rotor is utilized, the extra power required is diminished. At speeds above 200 knots, the conventional rotor can no longer develop lift and propulsive loads; hence shaft power comparisons become meaningless.

CONCLUDING REMARKS

Wind-tunnel tests have been made of a two-bladed rotor, driven and controlled by a jet flap incorporated in the outer 30-percent radius of each blade. The rotor produced very large lift and propulsive forces, indicating that

jet-flap high-lift phenomena can be utilized on a helicopter rotor blade. High advance ratios were reached without indications of retreating blade stall, and the large forces produced per unit blade area exceeded conventional rotor capabilities by factors of 2 and more.

Varying the jet deflection angle, cyclically and noncyclically, was shown to control and direct the rotor's force. Comparisons of measured and calculated characteristics show the calculation method to give generally good correlations. Additional investigations with the test rotor's mechanical limitations removed are needed to evaluate this correlation at even higher advance ratios and at conditions where compressibility effects occur.

The increased lift and propulsive force capabilities shown, which did not represent jet-flap concept limits, indicate the jet-flap rotor to be both feasible and of potential value for high-speed rotors, low or moderate speed rotors where high lift is required, or for helicopters where the high lift per unit area may be utilized to reduce the rotor size.

REFERENCES

1. Evans, William T.; and McCloud, John L., III: Analytical Investigation of a Helicopter Rotor Driven and Controlled by a Jet Flap. NASA TN D-3028, 1965.

2. Dorand, René; and Boehler, Gabriel D.: Application of the Jet-Flap Principle to Helicopters. J. Am. Helicopter Soc., vol. 4, no. 3, July 1959, pp. 26-36.

3. Greenman, R. N.; and Gaffney, M. G.: Application of Circulation Control to Helicopter Rotors. Rep. ARD 158, Hiller Helicopter Co., 1957.

4. Tanner, Watson H.: Charts for Estimating Rotary Wing Performance in Hover and at High Forward Speeds. NASA CR-114, 1964.

5. Fradenburgh, Evan A.; and Segel, Richard M.: Model and Full Scale Compound Helicopter Research. Presented at the American Helicopter Society, Twenty-First Annual National Forum, Washington, D. C., May 12-14, 1965.

JET-FLAP ROTOR IN WIND TUNNEL

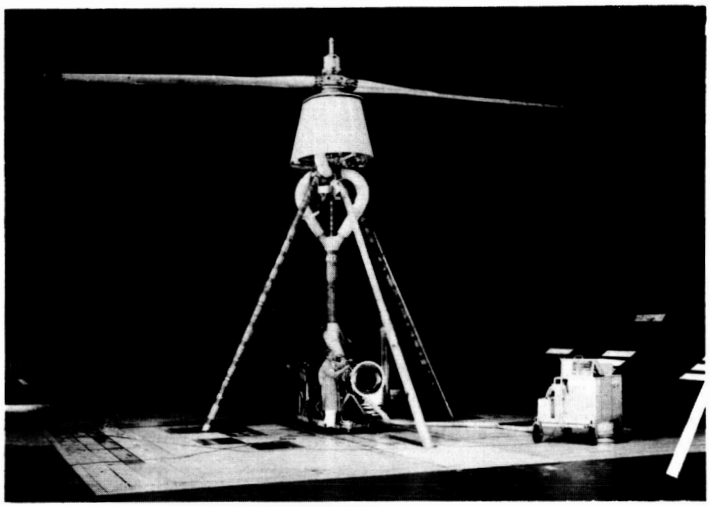

Figure 1 A-34959.1

JET-FLAP ROTOR

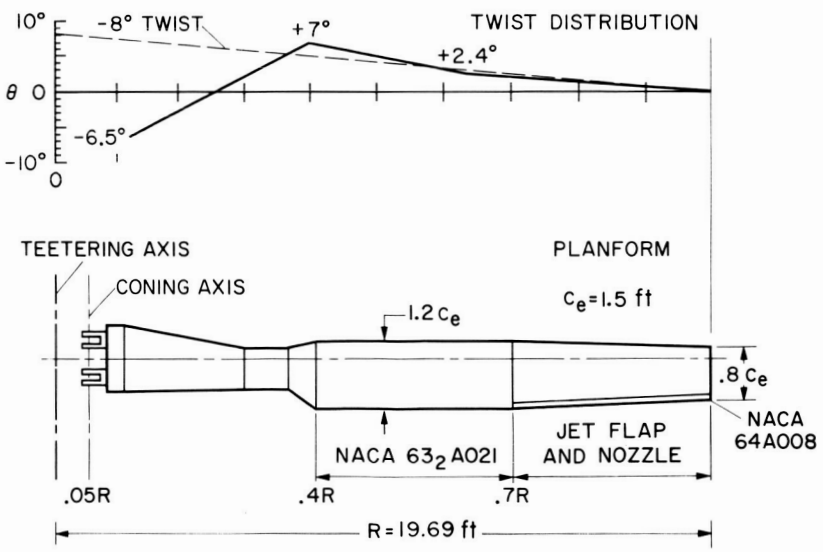

Figure 2

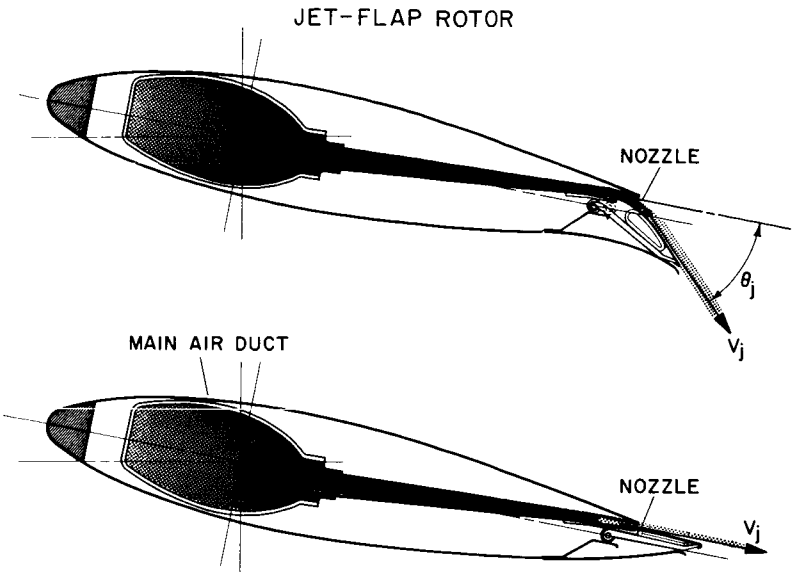

Figure 3

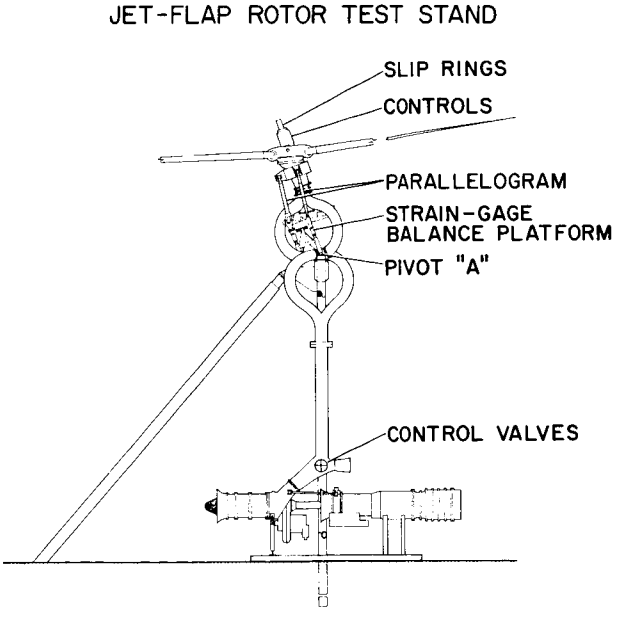

Figure 4

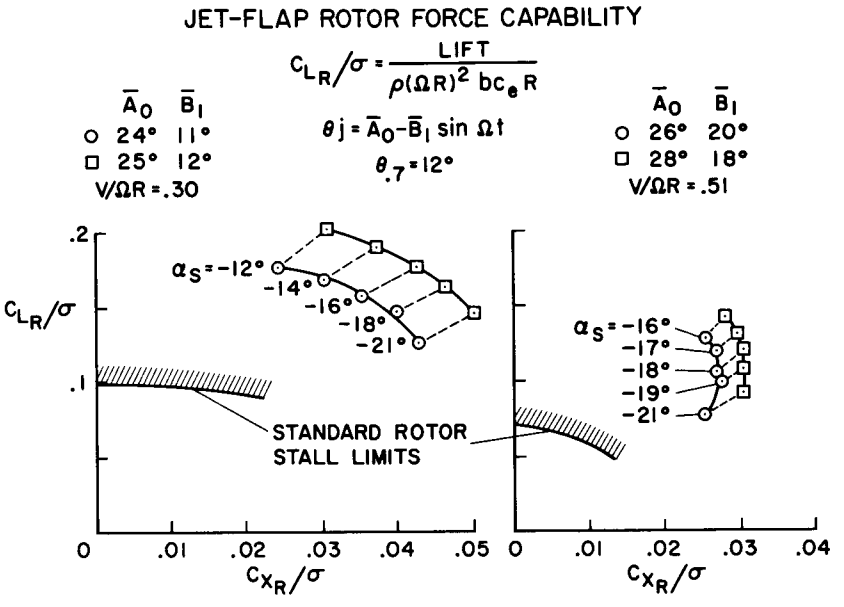

Figure 5

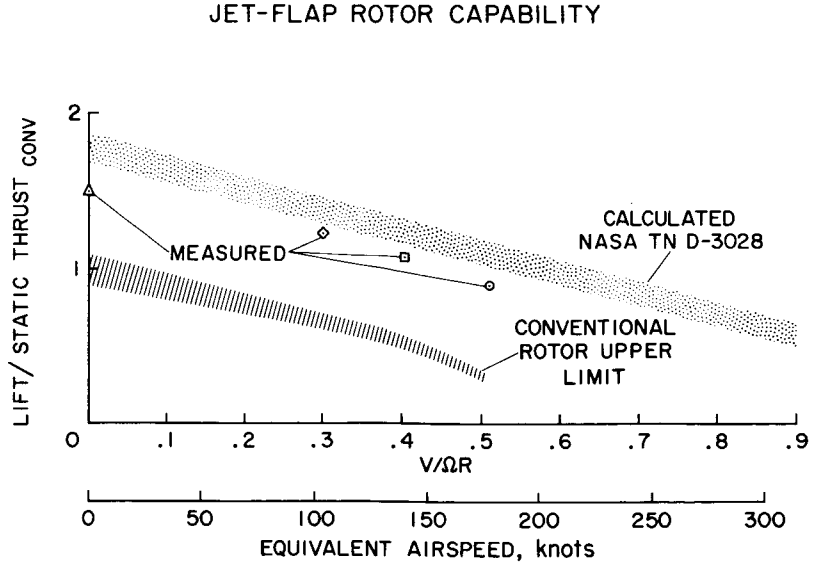

Figure 6

COMPARISON WITH THEORY – COLLECTIVE VARIATION

$\theta_{.7} = 8°$ $V/\Omega R = .30$

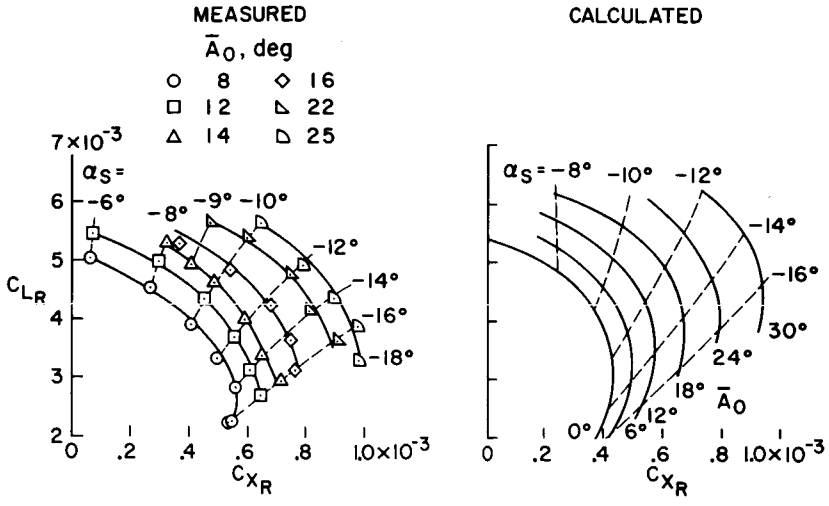

Figure 7

COMPARISON WITH THEORY – CYCLIC VARIATION

$\theta_{.7} = 8°$ $V/\Omega R = .30$

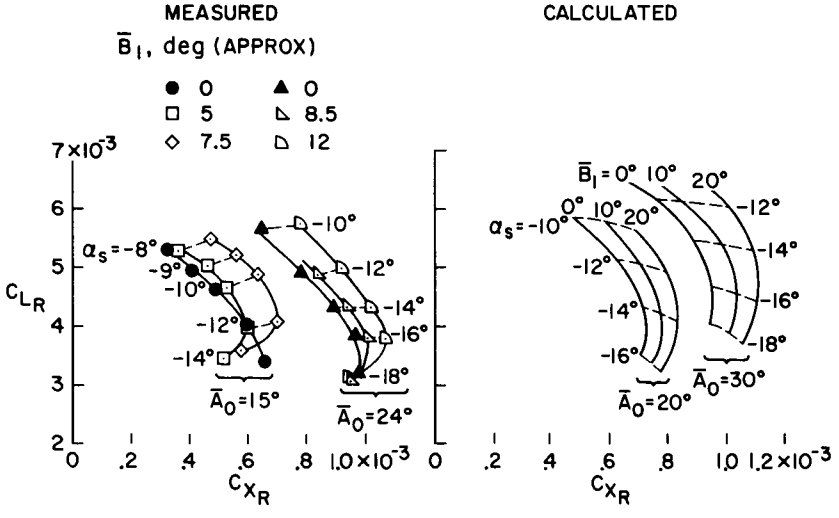

Figure 8

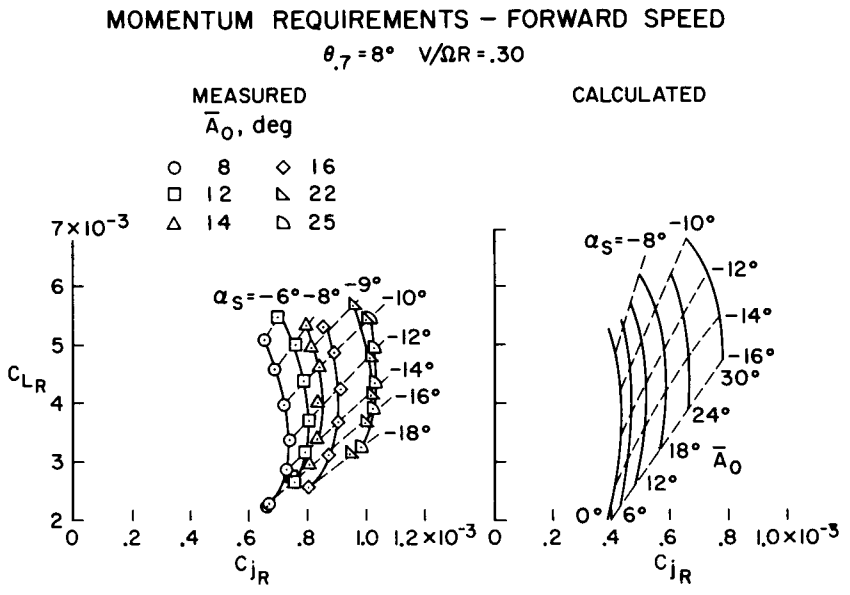

Figure 9

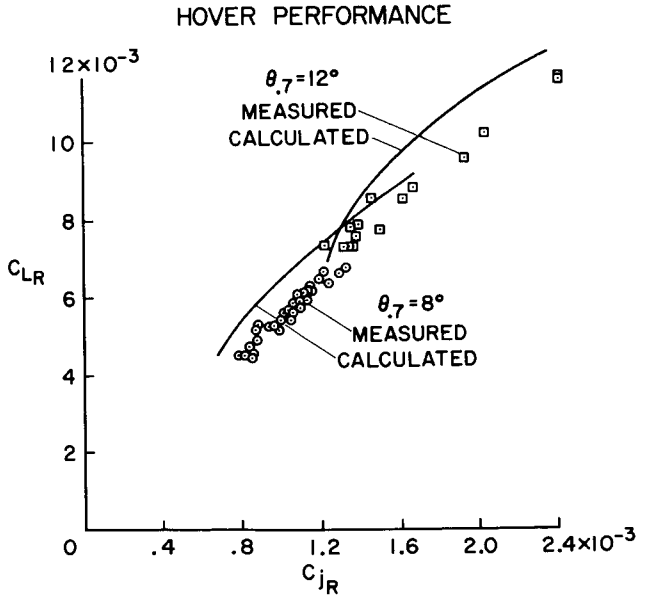

Figure 10

4. DESCENT CAPABILITY OF TWO-PROPELLER TILT-WING CONFIGURATIONS

By James L. Hassell, Jr., and Robert H. Kirby

NASA Langley Research Center

SUMMARY

The wing stall problem encountered with tilt-wing V/STOL designs during low-powered descent flight conditions has led to buffeting which adversely affects both performance and handling qualities. The results of tests conducted in the Langley full-scale wind tunnel with a large semi-span model of a two-propeller tilt-wing configuration have indicated that three important factors provide substantial improvement in the wing stall characteristics with consequent improvement in descent capability: down-at-center propeller rotation resulted in delayed inboard stalling and provided far better descent capability than the up-at-center rotation, moderate lowering of the propeller position relative to the wing chord provided further improvement in descent capability, and some flap deflection was absolutely essential in order to have any descent capability for low-powered flight conditions. Use of all three factors should provide good descent capability even without the complexity of other sophisticated stall control devices.

INTRODUCTION

One of the main problems encountered with tilt-wing V/STOL designs has been wing stall during transition flight. This problem has been particularly true during the low-powered descent conditions. The wing stalling problem is serious because it has adverse effects on both performance and handling qualities as was experienced on the basic VZ-2 aircraft as discussed in references 1 to 4. Improvement of the VZ-2 wing stall characteristics was achieved by various modifications such as leading-edge slats and trailing-edge flaps but further improvement was considered very desirable. Subsequent research by NASA and private industry with small-scale models has defined the problem areas of the wing stalling phenomenon and more clearly indicated the effects of pertinent design variables. (For example, see refs. 5 to 9.)

DISCUSSION

Some of the factors affecting the onset of wing stalling for a two-propeller tilt-wing configuration are illustrated in figure 1. In the course of making a transition from forward flight to hover it is necessary, of course, for wing incidence to be varied from 0° to 90°. Without

the effects of the propeller slipstream over the wing, complete stalling would result for the greater part of the wing incidence range. However, the propeller slipstream produces a chordwise flow component over the wing and, thus, tends to keep it from stalling in that area submerged in the slipstream. Two other areas are involved which are subject to stalling: one is inboard and one is outboard of the contracted propeller slipstream. The crosshatched area inboard of the propeller slipstream stalls at relatively low tilt angles because it is unprotected. The area at the wing tip outboard of the slipstream would also stall at low tilt angles except for the effect of the tip vortex due to lift which has a very strong influence on delaying tip stall. Under descent flight conditions the wing stalling problem is further aggravated because of one additional factor. As power is reduced to set up the descent condition, the propeller slipstream velocity is consequently decreased; therefore, the wing is subjected to substantially higher angles of attack than it would be for a corresponding level-flight case.

A photograph of a large-scale semispan tilt-wing model mounted for testing in the Langley full-scale tunnel is presented as figure 2. This model is being used to study the wing stalling problem on tilt-wing configurations as well as to provide quantitative design-type data on the effect of a number of configuration variables. The model has a boiler plate wing structure to support the propeller, various wing contours, and flap arrangements. Eventually the investigation will provide data for both two- and four-propeller configurations. The tufts which were used to detect local stalling are visible in the photograph.

The problem of predicting the descent capability of full-scale airplanes from wind-tunnel data requires careful interpretation because local stalling which could cause buffeting and adversely affect handling qualities does not always show up in the wind-tunnel force test polars. Therefore tuft photograph studies have to be used to detect such local stalling to correlate descent capability with force test data. For the velocities of interest in the descent flight region, separated flow on the aircraft fuselage or wing center section are unlikely to have appreciable buffeting effects because of the low energies involved, although some work has been directed toward minimizing the effects of these separated flow regions. When separated flow occurs within the propeller slipstream, however, severe buffeting might be expected because these disturbances are being felt at relatively high dynamic pressures. Therefore, the criterion for defining the maximum descent capability in these tests is taken as the largest descent angle that can be achieved without encountering flow separation on the wing anywhere within the propeller slipstream.

A number of wing and flap designs for two-propeller configurations have been investigated at Langley with the large-scale model shown in figure 2 (refs. 10 to 13), and the work accomplished to date is summarized in table I. Experience has shown that tilt-wing designs tend to have more wing area than is required for cruise because of the problem of trying to keep the wing from stalling in the transition range. When the model of the present investigation was designed, it was thought that a ratio of wing chord c to propeller

diameter D of at least 0.6 would be required to obtain adequate descent capability and the program was designed around that ratio. The model was tested first with a ratio of wing chord to propeller diameter of 0.6 with Fowler flaps in one series of tests (ref. 10) and with single-slotted flaps in another series of tests (refs. 11 and 12). The results of these tests were good enough to justify a reduction in wing size so that the next series of tests were conducted with a ratio of wing chord to propeller diameter of 0.5 with both double- and single-slotted flaps. The results of tests with double-slotted flaps are presented in reference 13. These results are also encouraging and therefore the next tests in this continuing series will be made with an even smaller wing having a ratio of wing chord to propeller diameter of only 0.4 with a single-slotted flap. The rest of this paper deals with the low-speed performance that has been achieved in this investigation in terms of descent capability for the $c/D = 0.5$ wing with a single-slotted flap, and the effects of the design variables given at the bottom of table I are illustrated.

The effect of propeller rotation is illustrated in figure 3 where stall boundaries are presented in terms of flight-path angle γ plotted against thrust coefficient $C_{T,S}$ for both modes of rotation, up at center and down at center. These are the stall boundaries that were obtained from the tuft studies according to the criterion previously established. Positive values of γ indicate climb conditions, whereas negative values represent descent conditions. For combinations of $C_{T,S}$ and γ above a boundary the conditions are satisfactory, whereas for combinations below a boundary, local stalling has occurred. A value of $C_{T,S}$ of 1.0 corresponds to the condition of zero velocity or hovering flight, whereas values of 0.6 to 0.9 correspond to flight in the transition range which is the real region of interest for the descent flight conditions. The data show that wing stall can be experienced even in the climb condition for the up-at-center propeller rotation over the transition flight range. The reason for this stalling is illustrated by the sketch in the upper right of figure 3. With up-at-center propeller rotation, the flow from the propeller is such that the area inboard of the nacelle is subjected to higher angle of attack, thereby increasing stall in this region, while at the same time the area at the wing tip (already protected by the tip vortex) gets further protection as a result of the lower angles of attack induced by the slipstream rotation. With down-at-center propeller rotation, a marked improvement in descent capability is achieved in the transition range of thrust coefficients because of delayed inboard stalling. The reason for this reduced stalling is illustrated by the sketch in the lower right of figure 3 where for down-at-center propeller rotation the flow from the propeller is in the proper direction to reduce the stalling tendency inboard of the nacelle, whereas the strong wing-tip vortex still tends to keep the area outboard of the nacelle from stalling. These, and other similar results, indicate that down-at-center propeller rotation should be used unless there are otherwise good reasons for not using it. Direction of propeller rotation might become a trade-off factor when considering cruise performance, for example.

The effect of propeller position in relation to the wing is illustrated in figure 4. Small-scale work by the Vertol Division of the Boeing Company

(refs. 8 and 9) has indicated an important effect of propeller position which led to the study of the propeller positions indicated in this figure, which are referred to as the high, mid, and low positions - 2.5 percent propeller diameter above the wing chord line and 5 and 10 percent below the wing chord line. These positions were all roughly 22 percent propeller diameter ahead of the wing leading edge which approximated the better locations indicated from the small-scale tests. The descent boundaries shown here are for the basic wing with flap deflected 20° and with down-at-center rotation. The descent boundary for the mid propeller position is the same as that for the down-at-center rotation in figure 3. The results show a progressive improvement in descent capability throughout the thrust coefficient range with lowering of the propeller position.

The effect of flap deflection is illustrated in figure 5 where results are presented for various flap deflections δ_f with the propeller position and direction of rotation that were shown to be most favorable - low position and down-at-center rotation. The most notable point is that some flap deflection is absolutely necessary in order to have descent capability for other than the higher thrust coefficients as indicated by the fact that there is no descent capability for much of the thrust coefficient range for the zero-flap-deflection boundary. Flap deflection of 20° provides very good descent capability even without other stall control devices.

The investigation included a number of other stall control devices such as inboard fences and leading-edge slats as illustrated in figure 6. These are the logical "fixes" to try to improve the disturbed flow inboard of the nacelle, especially to prevent the stalled flow on the wing center section from spreading and triggering stall of the area inside the propeller slipstream. Results indicated, however, that these devices gave second-order effects compared to the three major factors discussed previously - that is, propeller rotation, propeller position, and flap deflection. In general, the main effect of this increased sophistication was to provide increased lift capability with only a slight improvement in the descent capability.

CONCLUDING REMARKS

Good descent capability is possible for a wing of relatively low ratio of chord to propeller diameter, even without other stall control devices, providing that a low propeller position in combination with down-at-center propeller rotation is used. Improved lift capability and somewhat improved descent capability may be achieved through the use of leading-edge and other stall control devices. The practicability of further reduction of wing size in combination with relatively simple flaps is indicated.

REFERENCES

1. Reeder, John P.: Handling Qualities Experience With Several VTOL Research Aircraft. NASA TN D-735, 1961.

2. Schade, Robert O.; and Kirby, Robert H.: Effect of Wing Stalling in Transition on a 1/4-Scale Model of the VZ-2 Aircraft. NASA TN D-2381, 1964.

3. Mitchell, Robert G.: Full-Scale Wind-Tunnel Test of the VZ-2 VTOL Airplane With Particular Reference to the Wing Stall Phenomena. NASA TN D-2013, 1963.

4. Pegg, Robert J.: Summary of Flight-Test Results of the VZ-2 Tilt-Wing Aircraft. NASA TN D-989, 1962.

5. Kirby, Robert H.: Aerodynamic Characteristics of Propeller-Driven VTOL Aircraft. NASA TN D-730, 1961.

6. Spreemann, Kenneth P.: Investigation of a Semispan Tilting-Propeller Configuration and Effects of Ratio of Wing Chord to Propeller Diameter on Several Small-Chord Tilting-Wing Configurations at Transition Speeds. NASA TN D-1815, 1963.

7. Newsom, William A., Jr.; and Kirby, Robert H.: Flight Investigation of Stability and Control Characteristics of a 1/9-Scale Model of a Four-Propeller Tilt-Wing V/STOL Transport. NASA TN D-2443, 1964.

8. Fry, Bernard L.: Low-Speed Aerodynamic Flight Boundaries and Control Aspects of Tilt-Wing Aircraft. Proc. Twenty-First Ann. Natl. Forum, Am. Helicopter Soc., Inc., May 1965, pp. 9-26.

9. Carpenter, Bruce; and Matthys, Carl: Wind Tunnel Test Report on a Powered Model of the Boeing-Vertol 147 Tilt-Wing Aircraft in the Langley Full Scale Tunnel. Rept. D8-0255, Vertol Div., Boeing Co., Jan. 15, 1966.

10. Fink, Marvin P.; Mitchell, Robert G.; and White, Lucy C.: Aerodynamic Data on a Large Semispan Tilting Wing With 0.6-Diameter Chord, Fowler Flap, and Single Propeller Rotating up at Tip. NASA TN D-2180, 1964.

11. Fink, Marvin P.; Mitchell, Robert G.; and White, Lucy C.: Aerodynamic Data on Large Semispan Tilting Wing With 0.6-Diameter Chord, Single-Slotted Flap, and Single Propeller Rotating Down at Tip. NASA TN D-2412, 1964.

12. Fink, Marvin P.; Mitchell, Robert G.; and White, Lucy C.: Aerodynamic Data on Large Semispan Tilting Wing With 0.6-Diameter Chord, Single Slotted Flap, and Single Propeller Rotating up at Tip. NASA TN D-1586, 1964.

13. Fink, Marvin P.; Mitchell, Robert G.; and White, Lucy C.: Aerodynamic Data on a Large Semispan Tilting Wing With 0.5-Diameter Chord, Double-Slotted Flap, and Both Left- and Right-Hand Rotation of a Single Propeller. NASA TN D-3375, 1966.

TABLE I

CONFIGURATIONS TESTED

FLAP TYPE	WING CHORD/PROPELLER DIAMETER			
	c/D = 0.7	c/D = 0.6	c/D = 0.5	c/D = 0.4
SINGLE SLOTTED		√	√	
DOUBLE SLOTTED			√	
FOWLER		√		

1. PROPELLER ROTATION
2. PROPELLER POSITION
3. FLAP DEFLECTION
4. LEADING-EDGE SLATS
5. UPPER-SURFACE FENCES

FACTORS AFFECTING WING STALL
TWO-PROPELLER CONFIGURATION

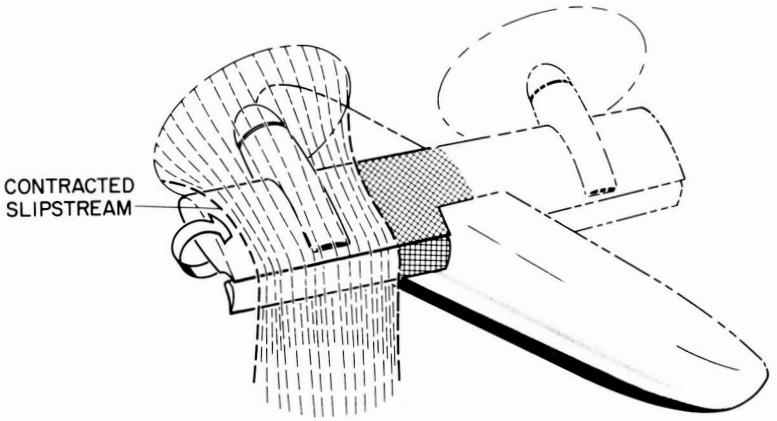

Figure 1

LARGE-SCALE TILT-WING MODEL

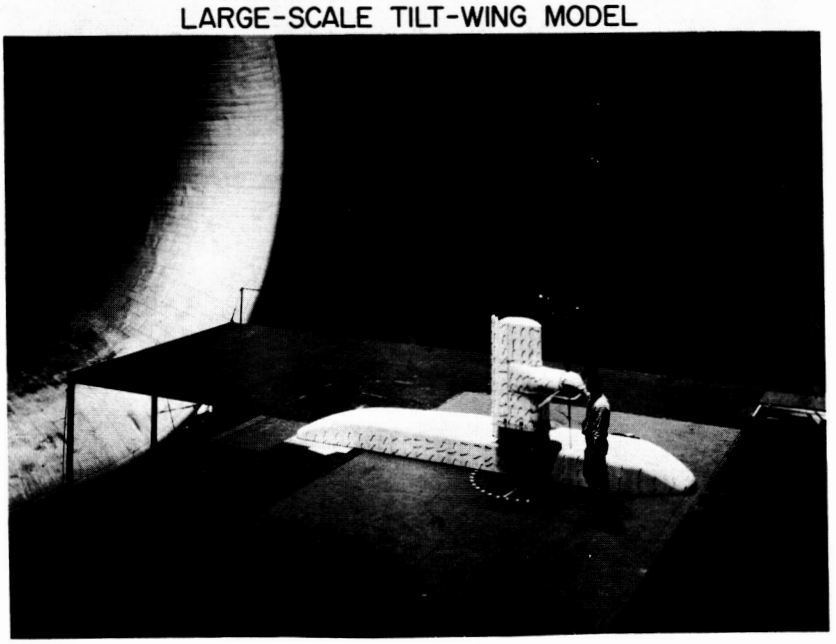

L-2649-2

Figure 2

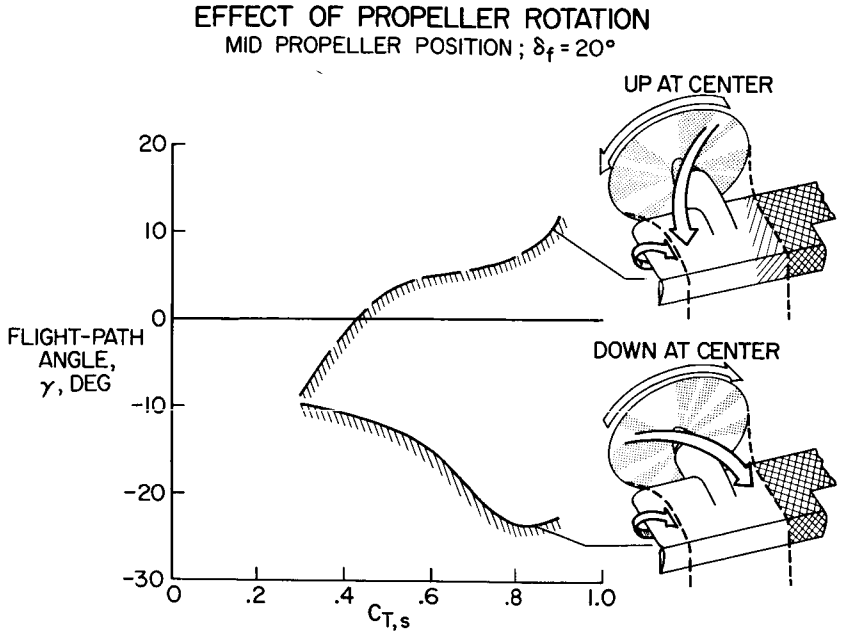

Figure 3

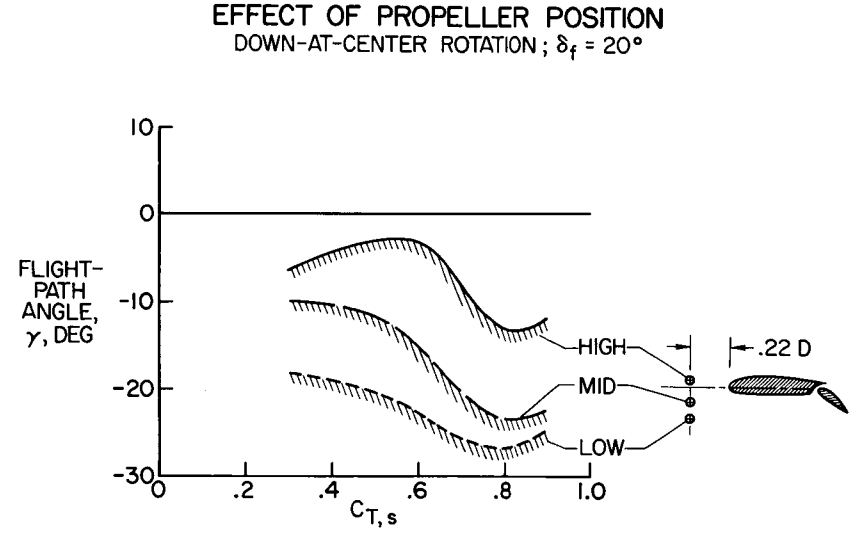

Figure 4

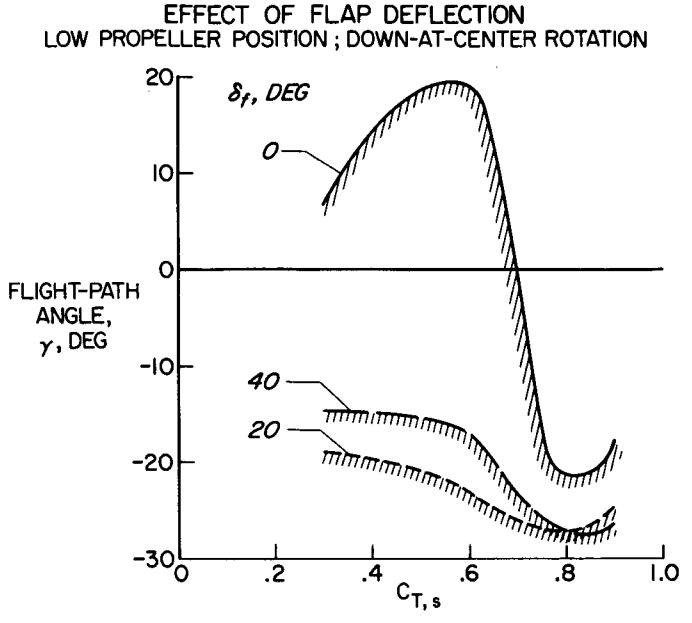

Figure 5

FENCES AND LEADING-EDGE SLATS

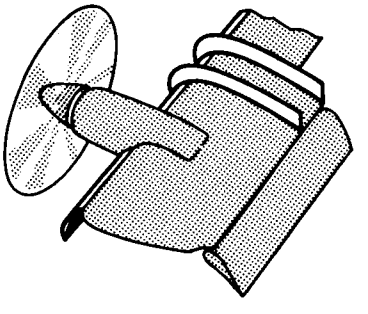

Figure 6

5. COMPARISON OF WIND-TUNNEL AND FLIGHT RESULTS ON A FOUR-PROPELLER TILT-WING CONFIGURATION

By Kenneth W. Goodson

NASA Langley Research Center

SUMMARY

Over the years aerodynamicists have learned to rely heavily on wind-tunnel-model results in predicting the aerodynamic characteristics of conventional aircraft configurations. With the development of V/STOL configurations which have high slipstream deflection angles, such as the four-propeller tilt-wing XC-142A V/STOL aircraft, the reliability of small-scale wind-tunnel-model results in predicting full-scale airplane characteristics needs to be reexamined.

Extensive tests have been made by NASA on several sizes of wind-tunnel models of the XC-142A V/STOL configuration and by Ling-Temco-Vought, Inc., on the airplane. These results show that models predict the slow-speed level-flight characteristics very well but that small models underpredict the descent capability of the airplane. Larger scale wind-tunnel models of approximately half size show better agreement with the airplane descent characteristics.

It was found from smoke flow studies that small models can also predict the region in which self-generated disturbances will be encountered by tilt-wing configurations in ground proximity.

INTRODUCTION

Over the years aerodynamists and designers have learned to rely heavily on model results in predicting the aerodynamic characteristics of conventional aircraft configurations; of course, appropriate corrections had to be applied to account for Reynolds number, Mach number, and tunnel wall effects. With the trend toward powered-lift configurations, the question naturally arises as to how reliable are small-scale-model results in predicting full-scale characteristics. Some early experience with the VZ-2 tilt-wing configuration (refs. 1 to 4) showed that model results predicted the level-flight characteristics reasonably well. (See ref. 5.)

This early work on tilt-wing configurations culminated in the design of the XC-142A V/STOL transport aircraft. NASA has conducted extensive wind-tunnel programs on the XC-142A configuration. (See refs. 6 to 8.) Two of the models used in these programs are shown in figure 1. Figure 1(a)

shows the 0.09-scale model used in the 17-foot test section of the Langley 300-MPH 7- by 10-foot tunnel, and figure 1(b) shows the 0.60-scale model used in the Ames 40- by 80-foot tunnel.

SYMBOLS

A	propeller disk area, ft^2
C_D	drag coefficient
C_L	lift coefficient
D	propeller diameter, ft
h	fuselage-bottom height from ground, ft
h_r	flow recirculation height, ft
h/D	ratio of fuselage height to propeller diameter
i_w	wing incidence angle with respect to fuselage, deg
q	free-stream dynamic pressure
$\dot{r}_{MAX}$	maximum self-generated yaw acceleration, deg/sec^2
S	wing area, ft^2
T	airplane thrust required, lb
T/A	propeller disk loading, lb/ft^2
V	velocity, knots
W	airplane weight, lb
W/S	wing loading, lb/ft^2
x	distance recirculating flow is projected in front of wing pivot, ft
x/D	ratio of forward projection of recirculating flow to propeller diameter
$\beta_{.75R}$	propeller blade angle at 0.75-radius station, deg
γ	flight-path angle, $\tan^{-1}(C_D/C_L)$, deg
δ_f	flap deflection angle, deg

DISCUSSION

Level Flight Transition

The wing tilt angles required in a steady-level flight transition for a wing loading of 70 lb/ft^2 are shown in figure 2. For this comparison the fuselage was held level and the design landing-flap program was used. In general, the model results bracket the scatter band of the flight-test data with the small-scale-model data slightly underpredicting and the large-scale-model data slightly overpredicting the wing incidence angle required. Figure 3 shows the thrust required in transition and indicates good agreement between the models and airplane.

The model data have been limited to velocities above that for which flow breakdown occurs in wind tunnels for models with large wake deflection angles. These limitations have been found by William H. Rae, Jr., of the University of Washington and are discussed in paper no. 24 by Harry H. Heyson and Kalman J. Grunwald.

Figures 2 and 3 show, as did similar previous data on the VZ-2 tilt-wing airplane (ref. 5), that level flight characteristics can be predicted very well from model force data.

Descent Limitations

The problem of determining descent limitations from wind-tunnel tests is one of determining what parameters can be measured in wind-tunnel tests that will make it possible to predict the limiting rate of descent of an airplane. The maximum rate of descent of a tilt-wing V/STOL airplane is limited by flow separation on the wings. The flow separation is manifested to the pilot as buffet and a deterioration in handling qualities. In both the buffet and the handling qualities, a pilot judgment is required in order to determine the airplane descent limitations. Neither of these characteristics, however, can be measured directly in wind-tunnel tests. For free-flight tunnel models, a pilot judgment is also required. Here the pilots, who fly the model remotely, determine the descent conditions and assign ratings to the model handling qualities by using a system similar to the Cooper airplane rating system. With force test models other techniques must be used. For the results reported in this paper tuft studies were used to indicate the angle of attack at which wing stall first occurs, along with the accompanying lift and drag.

Free-flight models.- Figure 4 compares the descent boundaries predicted by observing the flying characteristics of an 0.11-scale free-flight model with those observed on the airplane. The solid curves for the airplane indicate buffet onset at a descent angle of about -10°; as the airplane rate of descent was increased, the buffet increased and the handling qualities deteriorated to the point that flight was limited to a descent angle of about -15°, Now if the airplane boundaries are compared with the free-flight-model boundaries, it can be seen that initial disturbances with the model occurred at a

descent angle of about -6° and the flying characteristics became unacceptable at about -10°. It is believed that this difference between the airplane and the small-model results is primarily due to the lower Reynolds number of the model tests.

Force-test models.- As indicated in paper no. 4 by James L. Hassell and Robert H. Kirby, buffet and deterioration of handling qualities would not be expected to occur until after the breakdown of flow on the wing; therefore, tufts are used on force models to indicate the angle of attack at which local wing stall (see fig. 5) is first encountered. The limiting descent angles are then determined from the lift and drag force data at these angles of attack.

The descent boundaries determined by this technique are shown in figure 6. The descent angles determined from flow studies and force data (corrected for wall effects) of the 0.60-scale model fall between the boundaries obtained with the airplane. For a wing incidence angle of 20°, the model results indicate a descent angle of about -14°. These same results when uncorrected for wall effects gave a descent angle of about -12°. Wall corrections would be greater for larger wing incidence angles and would become inadequate for extremely large wake deflection angles, depending upon tunnel/model size. The data for the small 0.09-scale model (uncorrected for wall effects) considerably underpredict the airplane values. Note that the 0.09-scale-model data give results very similar to those previously shown for the small-scale free-flight model. (Compare figs. 4 and 6.) Again it is believed that this underprediction by the small model is primarily the result of low slipstream Reynolds number.

Recently data have also been obtained which show that propeller blade angle can have considerable effect on the estimated descent angles. (See fig. 7 and ref. 7.) Figure 7 shows that, for both the small 0.09-scale model and the larger 0.60-scale model, reducing the propeller blade angle increases the estimated descent angle. This shows that propeller blade angle and possibly other propeller characteristics should be simulated in model tests if the airplane descent angles are to be simulated.

Self-Induced Turbulence in Ground Proximity

A problem of current interest with many V/STOL configurations is self-generated disturbances encountered in ground effect. In general, an airplane supports itself by deflecting air downward. In the transition speed range, the downward deflection of the air approaches the vertical as the speed approaches zero. When the airplane approaches the ground (see the sketch at the right of fig. 8), the downward flow is stopped by the ground and, at sufficiently low airplane speeds, some of it is deflected forward ahead of the airplane and creates a turbulent region within which the airplane must fly. Within the turbulent region the present tilt-wing airplane experiences large yaw accelerations. At the left of the figure is plotted the yaw acceleration in deg/sec^2 against wing incidence angles in degrees. These results were obtained for the landing-flap program of the airplane. This figure shows that the airplane experiences large disturbances (of the same order as the hovering control available) for wing incidence angles between 30° and 80°. This range

corresponds to velocities from 30 knots down to about 12 knots. For speeds above 30 knots (i_w less than 30°) no disturbances were encountered. At these higher speeds the slipstream was not projected ahead of the airplane.

The recirculating flow which causes these disturbances has also been observed in wind-tunnel tests with the 0.09-scale model. In figure 9 the height, in terms of propeller diameters, at which recirculation is first detected is plotted against a speed parameter which is the ratio of operating disk loading to free-stream dynamic pressure. Increasing values of this parameter represent decreasing speed. These results were obtained for a series of wing incidence angles by lowering the model toward the ground until the beginning of recirculation of the flow was observed. Note the correlation of these data with the faired straight line. These data indicate that the height at which a disturbance is first encountered increases with decreasing speed. It should be mentioned here that, for $i_w = 45°$, the smoke studies showed that out of ground effect the slipstream tended to move outboard toward the wing tip and be swept downstream. As the height was reduced to 1 or 2 diameters, the flow fluctuated from inboard to outboard, being very erratic; as the height was further reduced to about 0.5 diameter, the flow moved inboard and toward the fuselage nose, still being very erratic. At a lower height (approximately landing-gear height) the flow became more steady. These results were obtained by using the moving endless-belt ground plane discussed in paper no. 25 by Thomas R. Turner.

The heights and velocities as predicted from this model curve (fig. 9) are compared in figure 10 with data obtained with the airplane. Here the height in feet is plotted against velocity in knots. The dashed line presents the data from figure 9 for the 0.09-scale model with flaps deflected 60°. The shaded area is based on disturbances observed by the pilot of the airplane. The difference between these curves is that the dashed curve represents the very onset of recirculation (based on smoke flows) whereas the shaded area represents the condition for which recirculation disturbances had developed sufficiently to be noticeable to the pilot.

The development of the disturbed region can also be measured in terms of the forward projection of the flow as shown in figure 11. Here the forward projection of the flow in propeller diameters (as defined by the sketch at the right of the figure) is shown as a function of wing incidence angle. These data are from model tests at a height of 0.5 diameter. The initial indications of recirculation with the model were observed for a wing incidence of about 30° (the end of the solid line). As the wing incidence was increased, the forward projection of the flow disturbance increased and exceeded 3 diameters for the wing incidence of 45°. The extent of the disturbance was also studied recently with the airplane. Airplane flights were made in a smoke flow field generated by ejecting oil into the engine exhaust. Initial indications of recirculation (smoke flow) for the airplane were also observed at a wing incidence of about 30°, which is in good agreement with the model results. The disturbances were not felt by the pilot, however, until the forward edge of the disturbed region reached the fuselage nose - a forward projection of about 1.5 diameters, as indicated by the circular symbol on the curve. This result is also in good agreement with the model results.

CONCLUDING REMARKS

It should be noted that model results obtained on the tilt-wing XC-142A aircraft configuration, as well as results obtained from previous tests of the VZ-2 tilt-wing configuration, have shown that:

Level-flight-transition performance characteristics can be adequately predicted by using scale models. The small-scale-model results, however, are conservative in predicting the descent capability, since the actual airplane could achieve higher descent angles. Larger scale models of approximately half size are in better agreement with airplane descent characteristics.

The flow recirculation results presented show that small-size models can predict the conditions under which self-generated disturbances in ground effect will be encountered.

REFERENCES

1. Pegg, Robert J.: Summary of Flight-Test Results of the VZ-2 Tilt-Wing Aircraft. NASA TN D-989, 1962.

2. Mitchell, Robert G.: Full-Scale Wind-Tunnel Test of the VZ-2 VTOL Airplane With Particular Reference to the Wing Stall Phenomena. NASA TN D-2013, 1963.

3. Schade, Robert O.; and Kirby, Robert H.: Effect of Wing Stalling in Transition on a 1/4-Scale Model of the VZ-2 Aircraft. NASA TN D-2381, 1964.

4. Kirby, Robert H.; Schade, Robert O.; and Tosti, Louis P.: Force-Test Investigation of a 1/4-Scale Model of the Modified VZ-2 Aircraft. NASA TN D-2382, 1964.

5. Staff of Powered-Lift Aerodynamics Section, NASA Langley Res. Center: Wall Effects and Scale Effects in V/STOL Model Testing. AIAA Aerodynamic Testing Conf., Mar. 1964, pp. 8-16.

6. Newsom, William A., Jr.; and Kirby, Robert H.: Flight Investigation of Stability and Control Characteristics of a 1/9-Scale Model of a Four-Propeller Tilt-Wing V/STOL Transport. NASA TN D-2443, 1964.

7. Goodson, Kenneth W.: Longitudinal Aerodynamic Characteristics of a Flapped Tilt-Wing Four-Propeller V/STOL Transport Model. NASA TN D-3217, 1966.

8. Deckert, Wallace H.; Page, V. Robert; and Dickinson, Stanley O.: Large-Scale Wind-Tunnel Tests of Descent Performance of an Airplane Model With a Tilt Wing and Differential Propeller Thrust. NASA TN D-1857, 1964.

0.09 – SCALE MODEL OF XC-142A

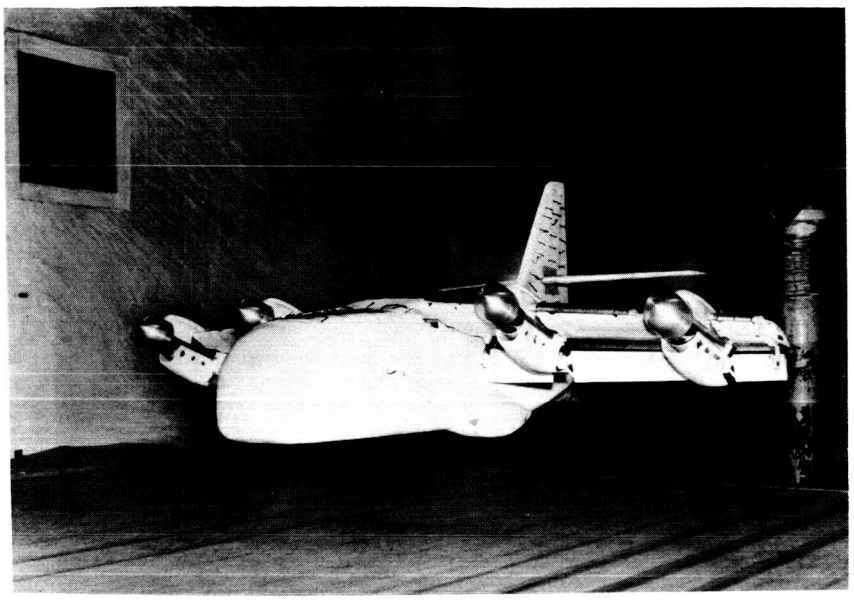

L-2646-1

Figure 1(a)

0.60 - SCALE MODEL OF XC-142A

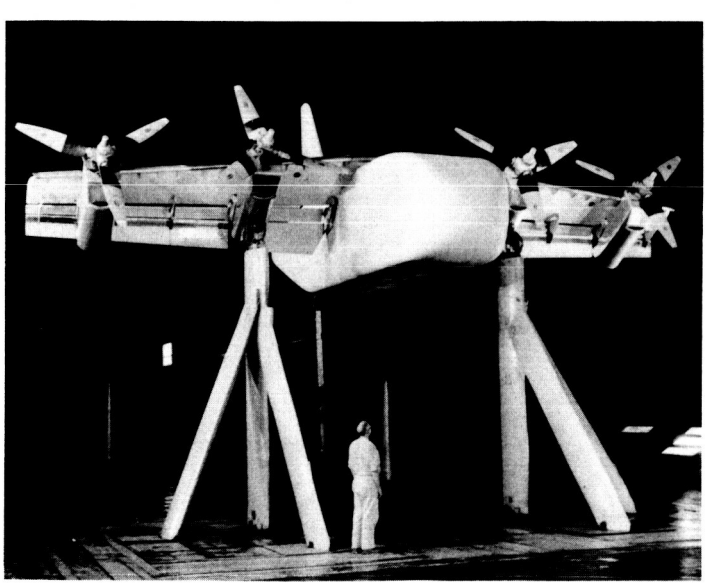

L-2646-2

Figure 1(b)

WING INCIDENCE REQUIRED IN LEVEL FLIGHT

W/S = 70 LB/FT^2

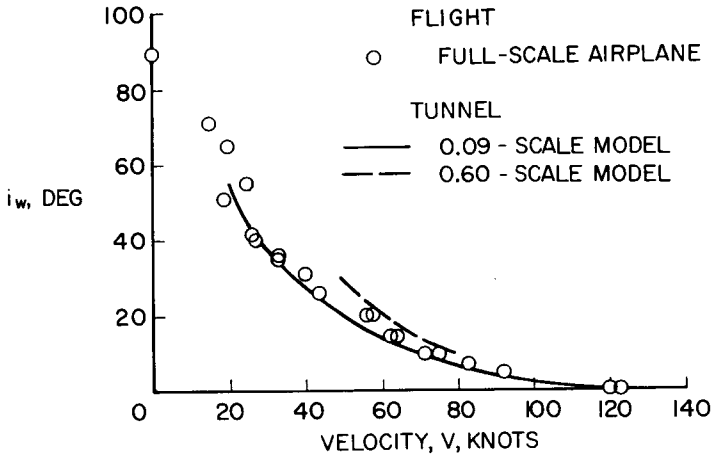

Figure 2

THRUST REQUIRED IN LEVEL FLIGHT

W/S = 70 LB/FT^2

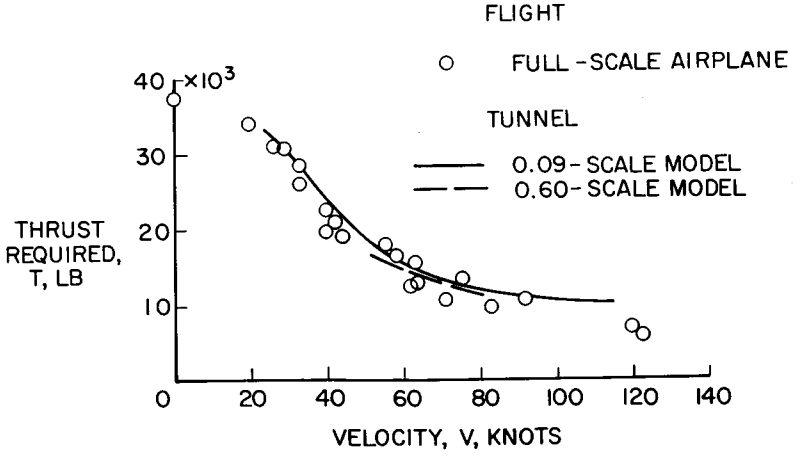

Figure 3

DESCENT BOUNDARIES FOR FREE-FLIGHT MODEL

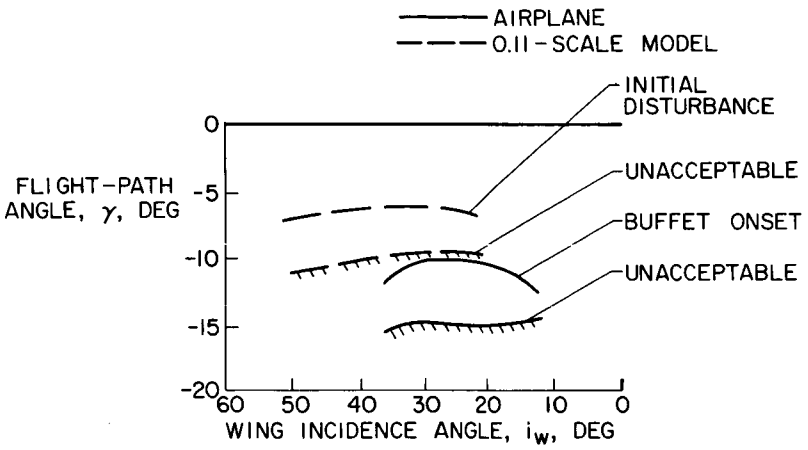

Figure 4

INITIAL WING STALL FROM TUFT STUDIES

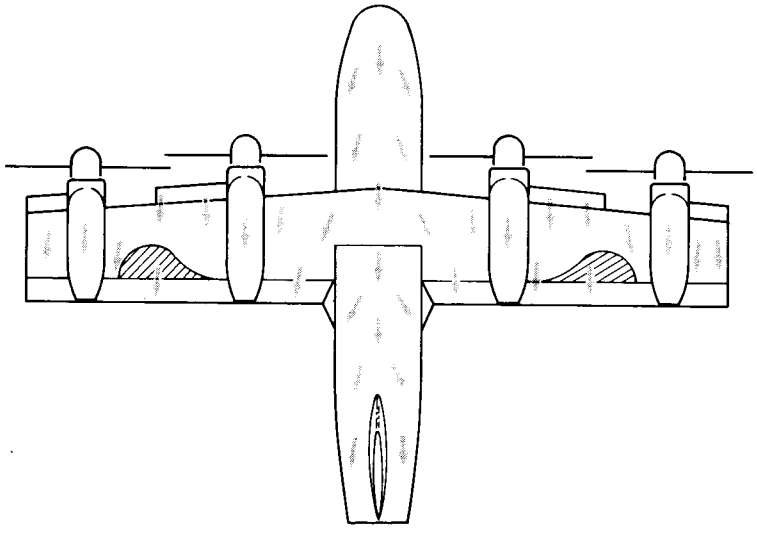

Figure 5

DESCENT BOUNDARIES FROM TUFT STUDIES

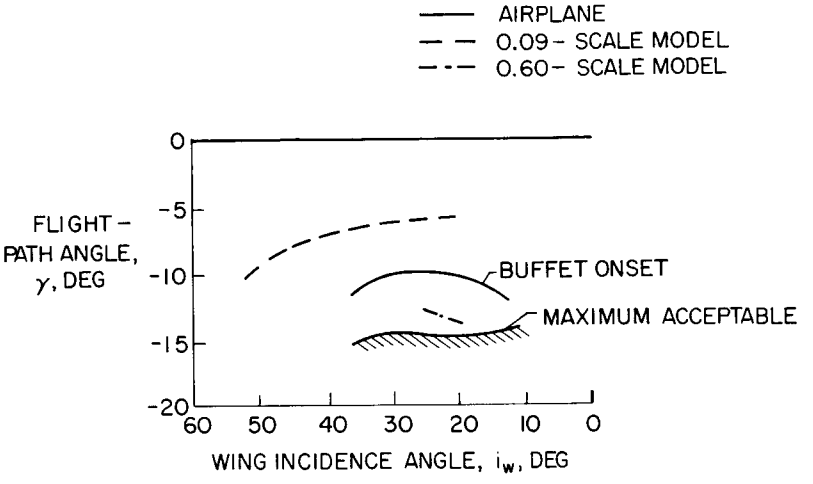

Figure 6

EFFECT OF PROPELLER BLADE ANGLE

$i_w = 20°$; $\delta_f = 60°$; W/S = 70 LB/FT^2

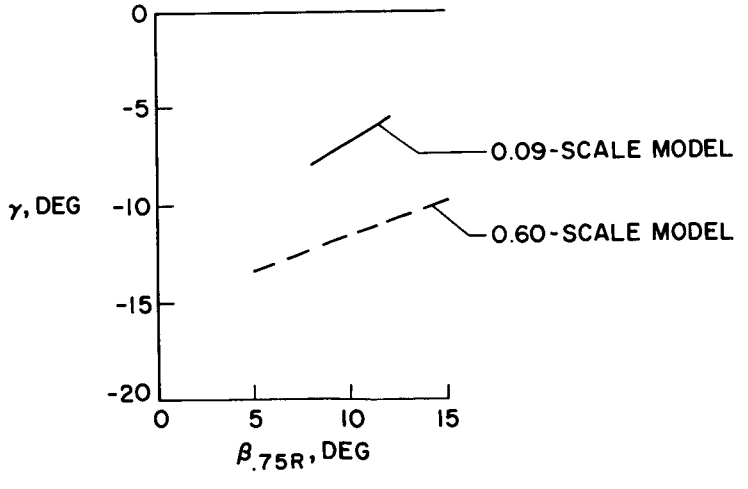

Figure 7

EFFECT OF GROUND ON YAW ACCELERATIONS

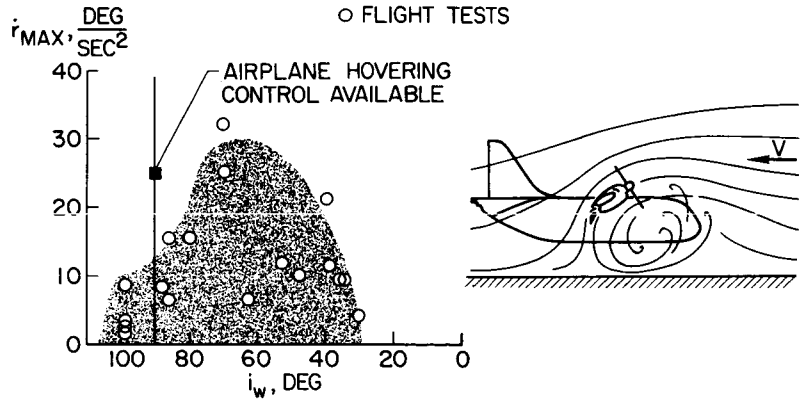

Figure 8

VARIATION OF RECIRCULATION HEIGHT WITH RATIO OF DISK LOADING TO DYNAMIC PRESSURE

$\delta_f = 60°$

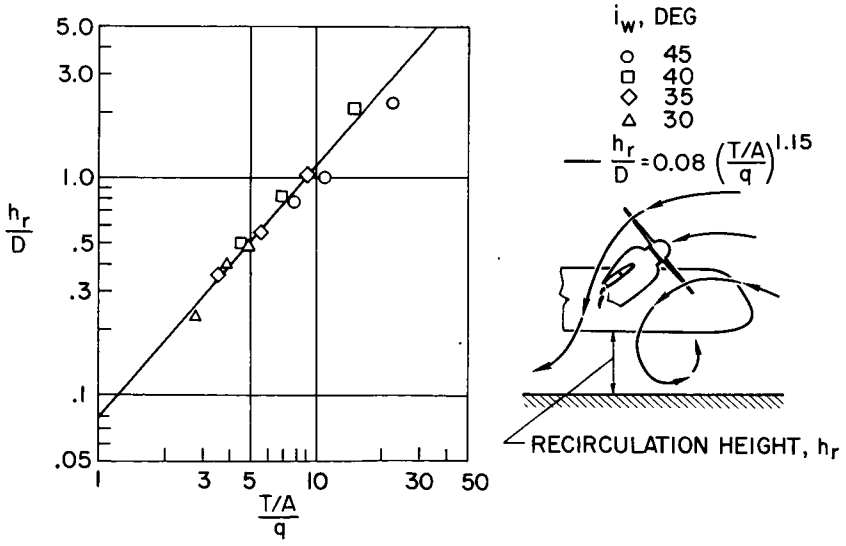

Figure 9

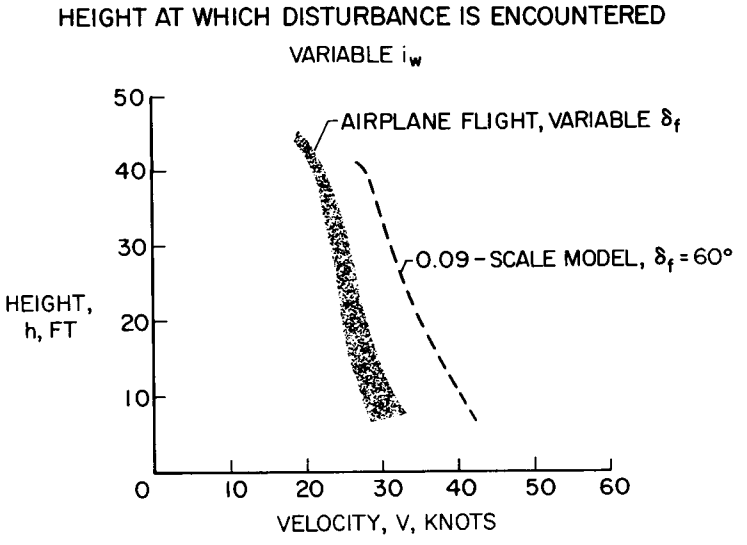

Figure 10

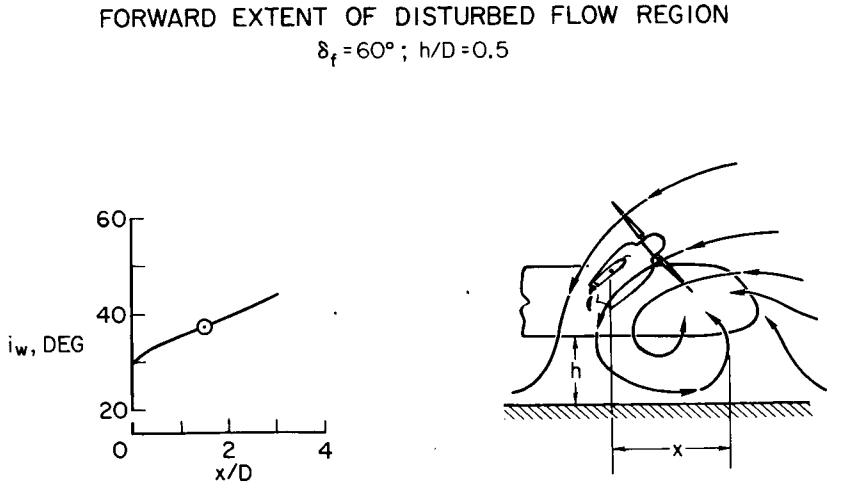

Figure 11

6. A SUMMARY OF RECENT LARGE-SCALE RESEARCH ON HIGH-LIFT DEVICES

By Wallace H. Deckert, David G. Koenig,
and James A. Weiberg
Ames Research Center

SUMMARY

A brief summary of recent 40- by 80-foot wind-tunnel investigations of large-scale models equipped with various high-lift devices is presented. The basic high-lift concepts that were investigated were the externally blown flap, the augmentor wing, and the rotating-cylinder flap. The scope of this paper is limited to a discussion of the wind-tunnel results in terms of maximum lift, descent performance, and pitch trim requirements.

Author

INTRODUCTION

Ames Research Center has a continuing program of developing high-lift devices and determining their effects on aircraft performance, stability, and control characteristics. This paper will summarize three investigations which comprise the most recent work in this area. Two of the high-lift concepts investigated are applicable to jet type STOL aircraft, namely, the externally blown flap and the augmentor wing. The third high-lift concept, the rotating-cylinder flap, may be applicable to any type of aircraft.

The short-field capability of an aircraft is largely a function of the aircraft's ability to fly slowly. For efficient low-speed flight, the requirements are conflicting, that is, to simultaneously provide high lift augmentation and maintain system simplicity. The externally blown flap represents the moderate performance but least complicated approach to the problem. The augmentor wing and the rotating-cylinder flap represent the high performance but relatively complex approach.

Wind-tunnel results of these investigations will be examined from the standpoint of maximum lift, descent performance, and pitch trim requirements. Other performance characteristics peculiar to each of the high-lift devices will be discussed.

NOTATION

b wing span, ft

c wing chord parallel to plane of symmetry, ft

c_{ref}	reference chord, ft
C_D	drag coefficient, $\frac{drag}{q_o S}$
C_J	jet thrust coefficient, $\frac{gross\ thrust}{q_o S}$
C_L	lift coefficient, $\frac{lift}{q_o S}$
ΔC_{L_f}	incremental lift coefficient due to flap deflection at $\alpha = 0^o$, $C_L - (C_L)_{\delta_f=o}$
$(C_m)_{o.25c_{ref}}$	pitching-moment coefficient, $\frac{M}{q_o S c_{ref}}$
ΔC_{m_f}	incremental pitching-moment coefficient due to flap deflection at $\alpha = 0^o$, $C_m - (C_m)_{\delta_f=o}$
C_{μ_f}	flap BLC blowing-momentum coefficient, $\frac{flap\ nozzle\ thrust}{q_o S}$
q_o	free-stream dynamic pressure, lb/sq ft
S	wing area, sq ft
T/W	thrust/gross weight ratio, $\frac{C_J}{C_L}$
T_c'	propeller thrust coefficient, $\frac{thrust}{q_o S}$, where thrust is the total thrust of two propellers
V	free-stream velocity or scaled airspeed as noted, knots
V_s	stall speed, knots
$\frac{U}{V}$	velocity ratio for rotating cylinder, $\frac{cylinder\ surface\ speed}{free\text{-}stream\ velocity}$
W	gross weight, lb
α	geometric angle of attack of fuselage reference line, deg
δ_a	aileron deflection relative to wing chord, deg
δ_f	flap deflection relative to wing chord, deg

$\delta_{f_{AFT}}$ flap deflection of aft segment of a flap relative to chord of forward segment of the flap, deg

$\delta_{f_{AUX}}$ flap deflection of added auxiliary flap relative to chord of basic flap, deg

DESCRIPTION OF THE MODELS

Model With an Externally Blown Flap

A cross section of the externally blown flap configuration that was investigated is shown in figure 1. A J-85 turbojet was installed in the underslung nacelle, with the thrust axis of the J-85 set parallel to the wing chord. A paddle deflector was placed at the exit of the standard round exhaust pipe. The paddle deflector was deflected, trailing edge up, to deflect the hot exhaust gases toward the wing trailing edge and through the flap slot for blowing boundary-layer control. The main or forward flap segment had a chord of 0.22. A small auxiliary flap was added to the main flap. A 0.15 c slat was installed on the wing leading edge.

A photograph of the model installed in the 40- by 80-foot wind-tunnel test section is shown in figure 2. The wing had an aspect ratio of 5.4 and a span of 36.6 feet with the quarter-chord line swept about 35°. The slat was installed full-span across the wing leading edge, except for cutouts for the nacelles. The trailing-edge flaps were installed from 11 to 63 percent of the wing semispan. The horizontal tail was located 1.16 $\bar{c}$ above the wing chord plane, with a tail length of 2.68 $\bar{c}$ and a volume coefficient of about 0.65.

Model With an Augmentor Wing

A cross section of the augmentor wing configuration that was investigated is shown in figure 3.

Primary air was ducted spanwise along the wing and ejected through the primary nozzle. The augmentor wing is essentially an ejector system with the forward wall formed by the wing, fixed vane, and lower door, with the rear wall formed by the upper door and trailing-edge flap. Primary air draws in secondary air from the wing upper surface and the mixed jet is ejected downward between the flap and lower door. A flap BLC system was incorporated. The primary air for flap BLC was also augmented. An inlet for secondary air was provided in the lip of the augmentor upper door. Secondary air flowed through the slot in the upper door and the mixed flow was ejected over the flap knee. The deflection of the upper door lip could also be adjusted as required to maintain attached flow over the outer surface of the upper door. A 15-percent chord slat was installed on the wing leading edge.

Figure 4 is a photograph of the model installed in the 40- by 80-foot test section. The straight wing had an aspect ratio of 8.0 and a span of 42.2 feet. The augmentor extended from 12.5 to 72 percent of the wing

semispan. Blown ailerons extended from 72 percent of the wing semispan to the wing tips. The leading-edge slat extended from the fuselage to the wing tip as shown. The inlet in the nose of the fuselage was for a J-85 gas generator. Hot gases from the J-85 powered the turbines of modified Viper engines and were expelled through the tail pipes located in the aft section of the fuselage as shown in the photograph. The two inlets on the side of the fuselage were for the modified Viper engines. The Viper compressor output was directed to the augmentor primary nozzle and to the aileron BLC system. Primary air for the flap BLC system was supplied by J-85 compressor bleed.

Model With a Rotating-Cylinder Flap

A rotating-cylinder flap was installed on an existing model as shown in figure 5. The cylinder was installed full-span across the trailing edge of the wing. The cylinder on each semispan was composed of two segments with an electric motor driving each. The large diameter disks on the cylinder are end plates for each cylinder segment (the outboard disk is hidden behind the wing tip end plate). The semispan of the cylinder, as viewed in figure 5, was 11 feet. Cylinder diameter was 10.9 inches (0.13 c), and the surface of the cylinder was of smooth aluminum. The insert in figure 5 shows that the cylinder was placed within the leading-edge contour of the flap and that the flap included a slotted aft segment. Flap chord, including the cylinder, was 0.46 c. A full-span slat with a chord of 0.22 c was installed on the leading edge of the wing.

A photograph of the model installed in the wind tunnel is shown in figure 6. The 9.3-foot diameter propellers were driven by electric motors. The straight wing had an aspect ratio of 3.5 and a span of 25 feet.

A 44-percent chord conventional flap was also evaluated on the model shown in figure 6. A cross section of this double-hinged plain flap is shown in figure 7.

TEST AND PROCEDURE

Model With an Externally Blown Flap

The investigation was conducted at Reynolds numbers of 4.3 to 8.2 million based on the wing mean aerodynamic chord of 7.96 feet, which corresponded to free-stream dynamic pressures of 8.5 to 32 psf. The tests were conducted with the horizontal tail set at 0° incidence. The lift and drag coefficients are untrimmed gross coefficients that include the thrust of the J-85 turbojet engines. The engine gross thrust was determined from total pressure probes placed in the exhaust pipe. The mean aerodynamic chord is the reference chord for this model.

The model was mounted on struts as shown in figure 2. Small drag corrections were applied to the data to account for the tail strut which was largely

unfaired (strut forces on all faired portions of the struts were isolated from the model). Standard wind-tunnel wall corrections were applied.

Model With an Augmentor Wing

The investigation was conducted at a free-stream tunnel velocity of about 49 knots (q_o = 8, Reynolds number = 4.9 million based on the wing root chord of 5.67 ft). Test results presented in this paper were conducted with the horizontal tail off. The lift and drag coefficients are untrimmed net aerodynamic coefficients excluding residual thrust in the J-85 exhaust and inlet ram drag. The jet thrust coefficient, C_J, is based on the augmented or "effective" jet thrust of the augmentor measured at q_o = 0 plus the thrust due to BLC on the ailerons. Aileron BLC thrust was about 3 percent of the augmentor thrust. Blowing rates were adjusted by varying J-85 power, with aileron BLC being used continually for all power-on testing, and flap BLC was controlled as desired through a remotely actuated valve controlling J-85 bleed supply. The wing root chord is the reference chord for this model.

The model was mounted on faired struts (fig. 4) in a manner which isolated the strut forces from the model. Standard wind-tunnel wall corrections were applied to the basic power-off, clean configuration.

Model With a Rotating-Cylinder Flap

The investigation was conducted at free-stream tunnel velocities from 30 to 40 knots (q_o = 2.6 to 5.0, Reynolds number = 2.0 to 2.9 million based on the wing mean aerodynamic chord of 7.0 ft). Test results are presented for a wing-body configuration with no empennage. The lift and drag coefficients are untrimmed gross coefficients that include propeller thrust. The propeller thrust characteristics were determined by wind-tunnel tests with the propellers on and off the model. The mean aerodynamic chord is the reference chord for this model.

The model was mounted on faired struts (fig. 6) in a manner which isolated the strut forces from the model. Wind-tunnel wall corrections were not applied.

RESULTS AND DISCUSSION

Model With an Externally Blown Flap

Typical lift-drag polars are presented in figure 8 for thrust coefficients (C_J) of 0, 0.5, and 1.36 which was the highest thrust coefficient evaluated. The polars on the left-hand side of figure 8 are for a flap deflection $\delta_f/\delta_{f_{AUX}}$ of $10^o/20^o$, which was the smallest flap deflection evaluated. For C_J of 1.36, a maximum lift coefficient of 3.4 was obtained at a maximum descent angle of 4^o. For descent, large flap deflections are of interest and

the polars on the right-hand side of figure 8 are for a flap deflection of 40°/40°, which was the largest flap deflection evaluated. For C_J of 1.36, a maximum lift coefficient of 4.3 was obtained at a maximum descent angle of about 13° and an angle of attack of 25°. At 0° angle of attack, a comparison of the data obtained at C_J values of 0 and 1.36 shows that the incremental lift coefficient due to blowing was 1.8. If deflected thrust were used or flap turning efficiency were 100 percent, ΔC_L would be 1.36. Thus of the incremental lift coefficient of 1.8, 75 percent could be provided by the jet reaction. The flap actually converted only 43 percent of the jet reaction to lift so that the circulation and jet lift were nearly equal.

The pitching-moment coefficient for the untrimmed maximum lift coefficient (4.3) was -1.3. This corresponds to a trimmed value of maximum lift coefficient of 3.82 which represents a lift loss of about 11 percent due to trim requirements (static margin was 40 percent). Engine operation and flap deflection did not effect static margin or shift the pitching-moment curve.

Figure 9 illustrates the feasibility of direct flight path control with a rapidly responding small auxiliary flap. Flight path angle, in both climbing and descending flight, is presented against flight speed for an assumed wing loading of 70 pounds per square foot and a constant thrust/weight ratio of 0.4, with flight speed based on a 20-percent margin from trimmed stall speeds. Lines indicate the main flap deflections evaluated 10°, 20°, and 40°; the dashed line is for 30° added by interpolation. Auxiliary flap deflections from 20° to 40° were evaluated, which is the primary variable along any one line as shown. Changes in angle of attack for a given main flap deflection are small. Angle of attack varied from 7° to 11° for a flap deflection change from 40°/40° to 10°/20°. Figure 9 shows that auxiliary flap deflection changes of 20° produced flight path changes of about 4°. Flight path changes of 6° or more appear to be attainable by increasing the deflection range of the auxiliary flap, say from 0° to 50°. For example, for a main flap deflection of 30°, at constant speed and constant thrust, direct flight path control from about a 4° descent angle to a 2° climb angle appears feasible for this configuration.

Model With an Augmentor Wing

Prior to the wind-tunnel investigation, the static performance of the augmentor was measured on the Ames static test stand. Static runs were conducted with the augmentor upper door and trailing-edge flap removed and with these components installed as shown in figure 3. It was found that the primary nozzle thrust was augmented about 40 percent.

Lift coefficient as a function of flap deflection is shown in figure 10 for 0° angle of attack and for an augmented thrust coefficient of 0.81. For all the tests, the upper and lower door positions were adjusted to optimum positions as indicated by the static test results. Figure 10 shows that maximum lift increments due to flap deflection would be obtained at a flap deflection of 80°. The figure also shows that the use of BLC and aileron droop are effective in producing significant lift increments for all the flap settings considered.

Typical lift-drag polars for the augmentor wing configuration are presented in figure 11. The lift and drag coefficients are net aerodynamic coefficients, that is, the combined ram drag of all inlets and small residual thrust of the J-85 exhaust are not included. The polars on the left-hand side of figure 11 are for a flap deflection of 60° with the ailerons drooped 45°. Polars are shown for augmented thrust coefficients of 0, 0.81, and 1.30, which was the highest value investigated, with no blowing at the flap knee. One polar is shown with flap BLC. Figure 11 shows that a maximum lift coefficient of 6 was obtained which, for comparison, is about the same for propeller-driven aircraft with effective large-chord mechanical flaps - such as the Breguet 941 STOL aircraft. At 0° angle of attack, a comparison of the data obtained at C_J values of 0 and 1.30 shows that the lift coefficient increment due to augmentor thrust was 2.4 compared to the vertical component of the augmented thrust of 1.1. Thus over half the lift coefficient increment was due to circulation lift. Blowing over the flap knee with a blowing momentum coefficient of 0.04 increased the lift coefficient by about 0.5 (about a 10-percent increase in maximum lift coefficient). For this configuration, maximum descent angles were 6° to 7°. The effect of increasing the flap and aileron deflections is shown on the right-hand side of figure 11 for a thrust coefficient of 0.81 with flap BLC. The polar for a flap deflection of 60° and aileron deflection of 45° is repeated from the left-hand side of figure 11 for convenience. It is compared to a polar for a flap deflection of 100° and an aileron deflection of 70°. Maximum lift coefficients for both configurations were about the same. The additional drag due to the higher flap and aileron deflections increased the maximum descent angle from about 7° to 12°.

The investigation showed that the pitching moments for the augmentor wing were relatively low. In figure 12, flap lift coefficient is presented against flap lift coefficient divided by flap pitching-moment coefficient for 0° angle of attack. Figure 12 thus shows the lift that was realized for a given pitching moment. Typical jet flap values obtained from references 1 and 2 are shown for comparison. The augmentor wing configuration, compared to the jet flap, produced about twice the lift for a given pitching moment.

Model With a Rotating-Cylinder Flap

Cylinder speed and power requirements are presented in figure 13. On the left-hand side of the figure, lift coefficient is plotted against a velocity ratio. The velocity ratio is the surface speed of the cylinder, made dimensionless by reference to free-stream velocity. Shown, for a flap deflection of 60° with an additional 18° deflection of the aft flap, are curves for propeller thrust coefficients of 0 with an angle of attack of 0°, and a thrust coefficient of 4 with an angle of attack of 16°. The propeller thrust coefficient, T_c', is referenced to free-stream dynamic pressure and wing area. At low velocity ratios, the flow over the surface of the flap was separated. As cylinder speed was increased, the boundary layer was energized to a greater degree, and thus the separated area on the flap was progressively reduced. At the knee of the curves, which corresponds to a velocity ratio of about 5, flow became fully attached. Velocity ratios greater than about 5 increased lift only slightly. As indicated by these two curves, it was found that the velocity ratio required for attached flow was independent of both propeller thrust

coefficient, that is, propeller slipstream effects, and angle of attack. The curve on the right-hand side of figure 13 shows the horsepower required to rotate the cylinder as a function of both velocity ratio and cylinder RPM. The horsepower is the total horsepower required by the cylinder including both frictional horsepower and air horsepower. The curve is for a free-stream velocity of 40 knots. For a velocity ratio of 5, corresponding to about 7000 RPM, 15 horsepower was required. The total length of the cylinder was 22 feet. Thus the power required to energize the boundary layer to achieve fully attached flow was less than 1 hp per foot of cylinder length.

Typical lift-drag polars for the rotating-cylinder flap are presented in figure 14 for a velocity ratio of 6.6. On the left-hand side of figure 14, the solid lines are for the rotating-cylinder flap deflected $60^\circ/18^\circ$ and thrust coefficients of 0 and 4. For comparison, the dashed lines are for the same model, without a rotating cylinder, and with the double-hinged plain flap deflected $60^\circ/30^\circ$. For $T_c' = 0$, and a wing of aspect ratio 3.5, a maximum lift coefficient of 4 was obtained for the rotating-cylinder flap, compared to a value of about 3 for the double-hinged flap. For a thrust coefficient of 4, a maximum lift coefficient of 9.1 was obtained for the rotating-cylinder flap, compared to 7.5 for the double-hinged flap. A maximum lift coefficient of 9.1, for example, corresponds to a 38 knot stall speed at a wing loading of 45 pounds per square foot. The drag value for this maximum lift point corresponds to a maximum descent angle of about 14°. The polars on the right side of figure 14 show that significantly higher drag values, as well as higher lift values, were obtained by increasing the deflection of the main flap to $70^\circ/18^\circ$, with maximum lift occurring at a descent angle of nearly 20°.

The flap lift and moment increments for the model with a rotating-cylinder flap are presented in figure 15 for 0° angle of attack. Incremental flap lift coefficient is plotted against flap lift coefficient divided by flap pitching-moment coefficient. Results for the basic model with the double-hinged flap are shown for reference. Two sets of results are shown for the rotating-cylinder flap, for two different wing-flap configurations. The lower curve is for the flap hinge near the lower surface of the wing, which was the configuration selected for the presentation of results in figures 13 and 14. The upper curve is for a second configuration with the flap hinge located near the wing upper surface. It is seen that the lift obtained for a given pitching moment is significantly higher for the rotating-cylinder flap, compared to the values for the double-hinged flap. And, for the rotating-cylinder flap, lift per unit pitching moment was found to be much greater for the flap hinge located at the upper surface. Lift coefficients for both hinge positions were approximately equal.

CONCLUDING REMARKS

Wind-tunnel investigations of large-scale models equipped with an externally blown flap, an augmentor wing, and a rotating-cylinder flap have been briefly reviewed.

For the model with the externally blown flap, wind-tunnel results show a maximum lift coefficient of 4.3 was obtained for a thrust coefficient of 1.36 and indicate the feasibility of utilizing a small rapidly responding auxiliary flap for direct flight path control.

For the model with an augmentor wing, an augmentation ratio of 1.4 was obtained; for an augmented thrust coefficient of 1.30, a maximum lift coefficient of 6 was obtained which is similar to the maximum lift coefficient achieved by present propeller-driven STOL aircraft; and one problem generally associated with the jet flap concept, namely, the existence of large pitching moments at high lift coefficients, was found to be significantly reduced.

For the model with a rotating-cylinder flap, a maximum lift coefficient of 9.1 was obtained for a thrust coefficient of 4, the power required to energize the boundary layer was found to be low, and pitching moments were found to be significantly less than those for a plain double-hinged flap.

REFERENCES

1. Butler, S. F. J.; Moy, B. A.; and Hutchins, G. D.: Low-Speed Tunnel Tests of an A. R. 9 Jet-Flap Model, With Ground Simulation by Moving-Belt Rig. R.A.E. TN Aero. 2957, 1964.

2. Gainer, Thomas G.: Low-Speed Wind Tunnel Investigation to Determine the Aerodynamic Characteristics of a Rectangular Wing Equipped With a Full-Span and an Inboard Half-Span Jet-Augmented Flap Deflected 55°. NASA MEMO 1-27-59L, 1959.

EXTERNALLY BLOWN FLAP CONFIGURATION

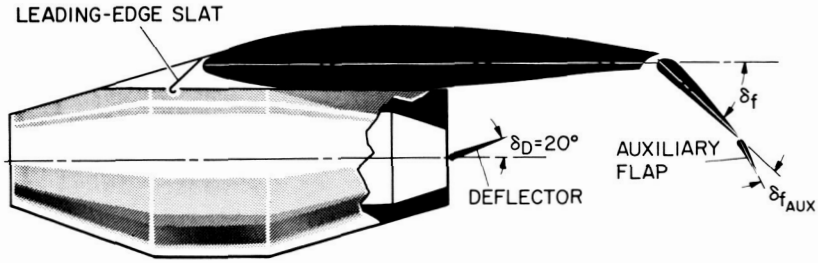

WING ASPECT RATIO = 5.4
HALF-SPAN FLAPS

Figure 1

WIND-TUNNEL MODEL WITH EXTERNALLY BLOWN FLAPS

Figure 2

A-34818.1

AUGMENTOR WING

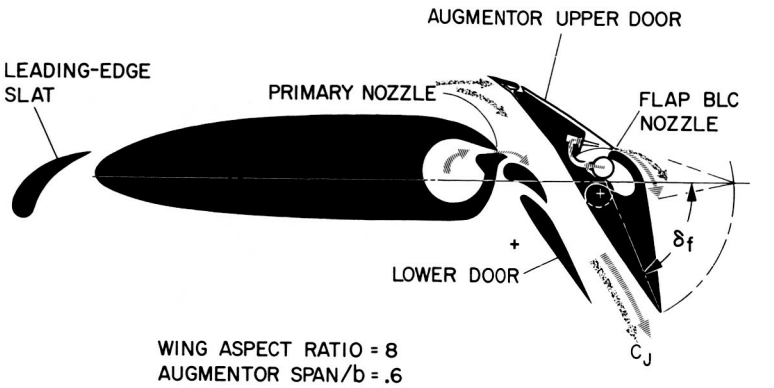

Figure 3

WIND-TUNNEL MODEL WITH AN AUGMENTOR WING

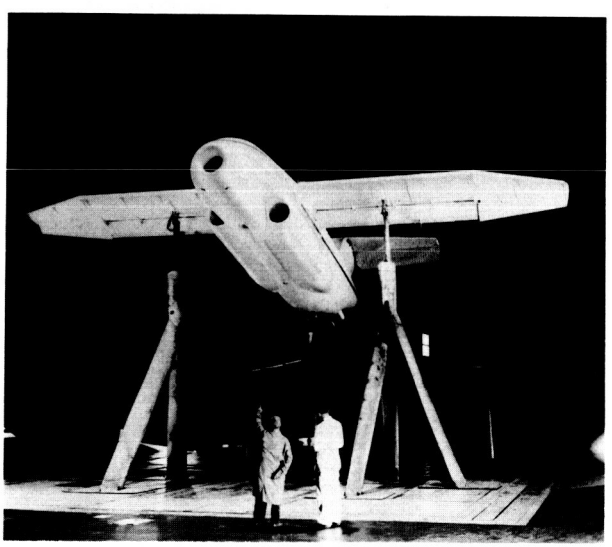

Figure 4 A-35855.1

SIDE VIEW OF ROTATING-CYLINDER FLAP

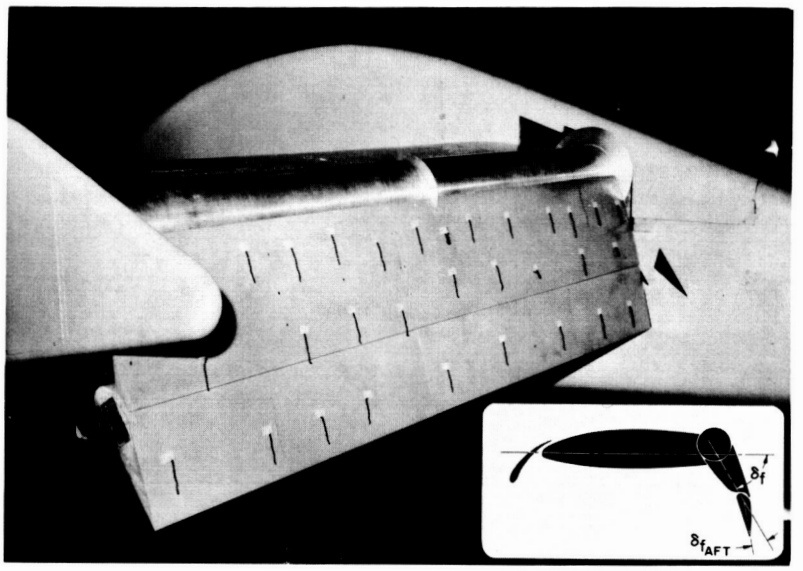

Figure 5 A-35913.1

WIND-TUNNEL MODEL WITH ROTATING-CYLINDER FLAP

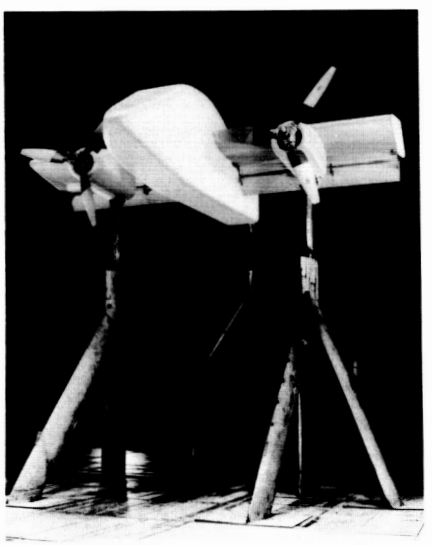

Figure 6 A-35912.1

DOUBLE-HINGE PLAIN FLAP

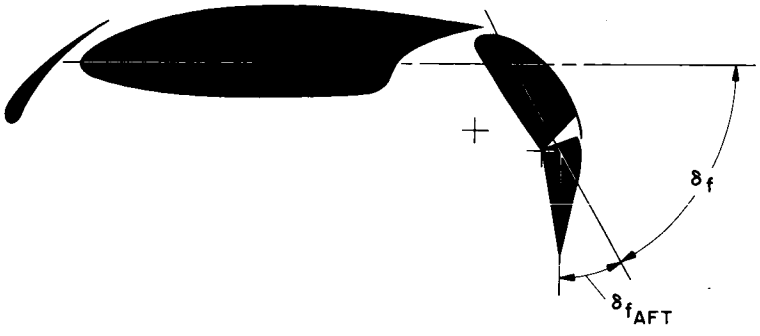

Figure 7

LIFT-DRAG POLARS FOR EXTERNALLY BLOWN FLAP

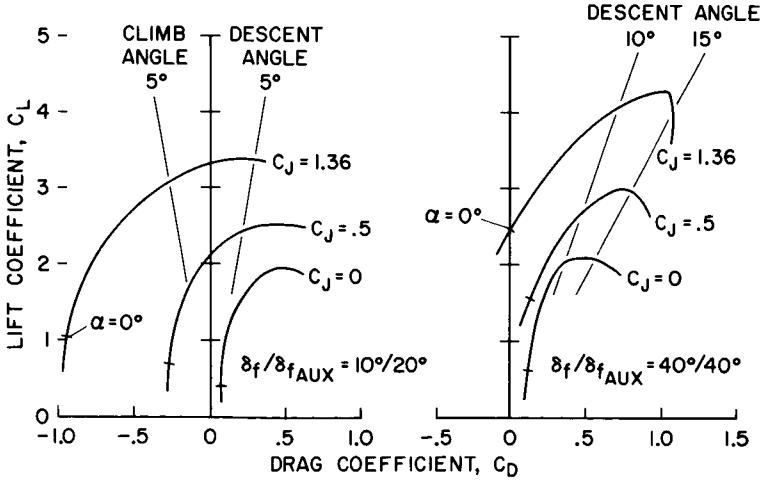

Figure 8

FLIGHT PATH CONTROL WITH AUXILIARY FLAP

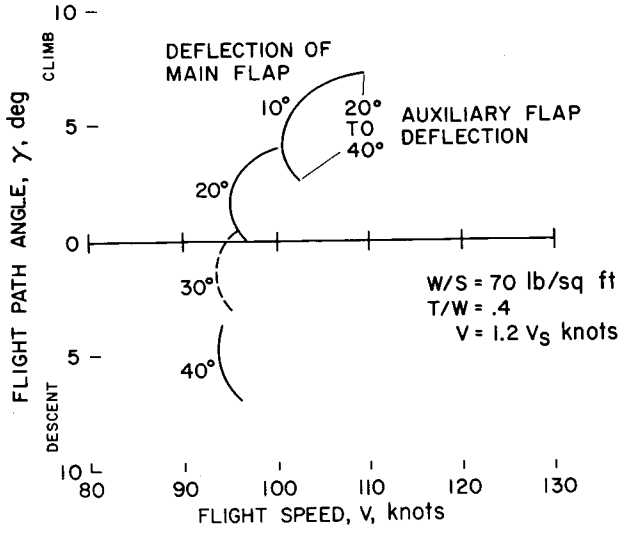

Figure 9

EFFECT OF FLAP AND AILERON DEFLECTION ON LIFT COEFFICIENT

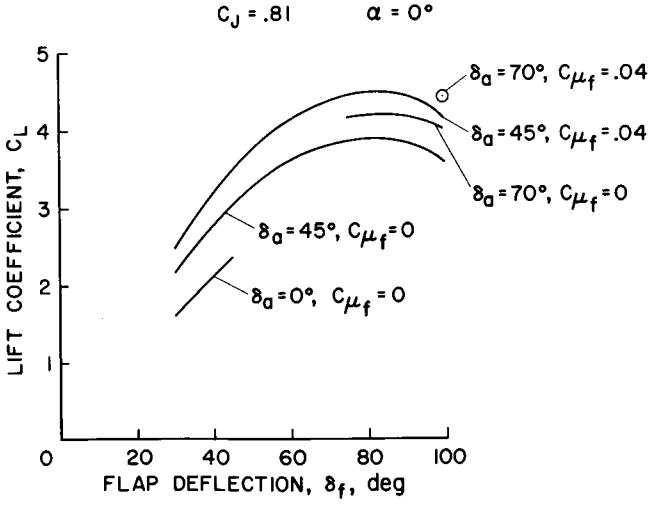

Figure 10

LIFT - DRAG POLARS FOR AUGMENTOR WING

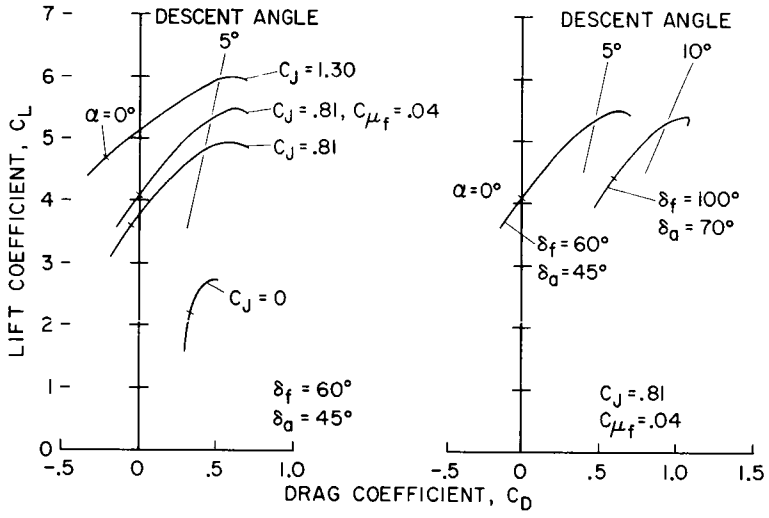

Figure 11

FLAP LIFT AND MOMENT INCREMENTS FOR AUGMENTOR WING

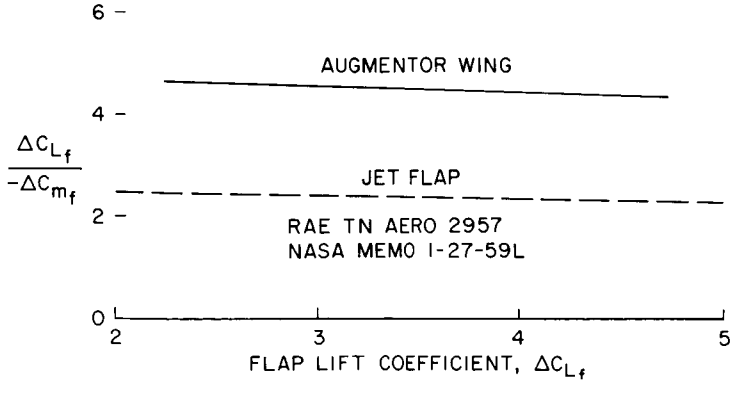

Figure 12

CYLINDER SPEED AND HORSEPOWER REQUIREMENTS

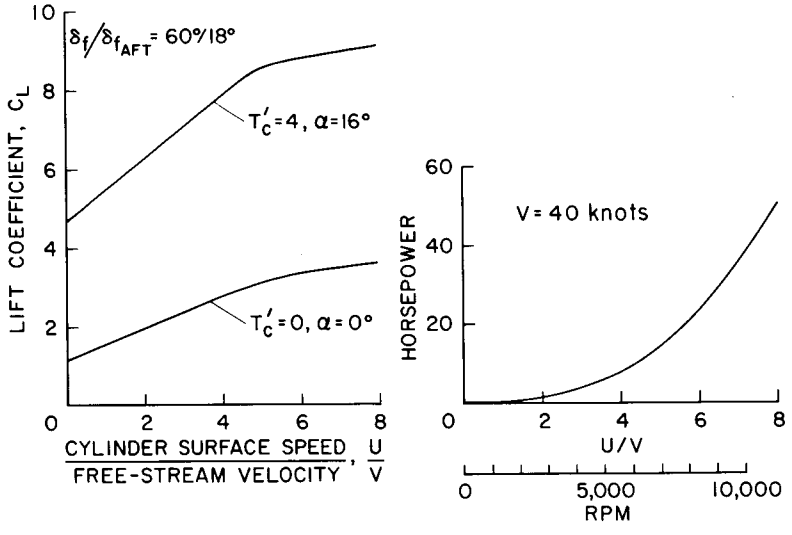

Figure 13

LIFT-DRAG POLARS FOR ROTATING-CYLINDER FLAP
U/V=6.6

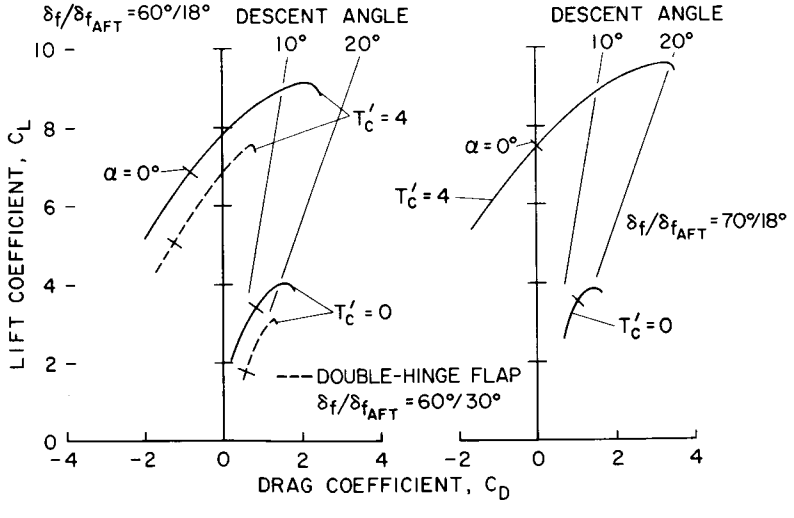

Figure 14

FLAP LIFT AND MOMENT INCREMENTS FOR ROTATING-CYLINDER FLAP

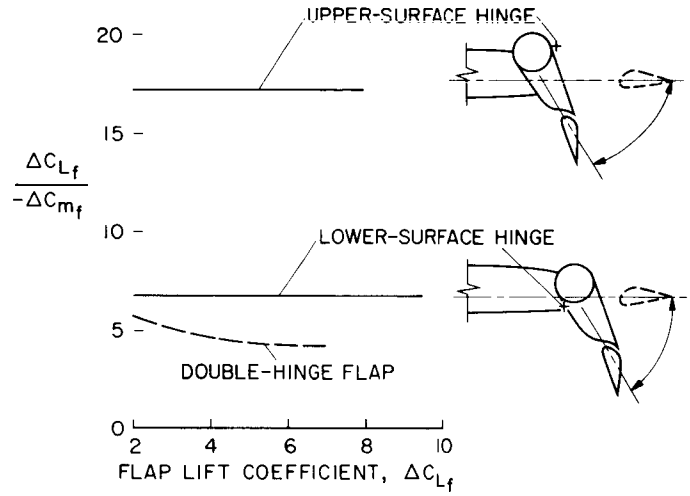

Figure 15

Page intentionally left blank

7. AERODYNAMIC CHARACTERISTICS OF A V/STOL TRANSPORT MODEL WITH LIFT AND LIFT-CRUISE FAN POWER PLANTS

By David H. Hickey, Jerry V. Kirk, and Leo P. Hall
Ames Research Center

SUMMARY

The aerodynamic characteristics of lift fans mounted ahead of the wing, rotating cruise fans, and tandem mounted lift fans faired into the wing have been studied. The tests results indicated that the complete configurations, that is, the lift-cruise fan and tandem lift fan configurations, had generally acceptable aerodynamic characteristics. The positive induced lift due to fan flow interference with the airplane flow field was a small percentage of the installed thrust but was adequate to provide significant increases in payload with STOL operation.

Author

INTRODUCTION

Ames Research Center is conducting a study of the low speed aerodynamic characteristics of V/STOL transport configurations powered by lift fans, cruise fans, or combinations of lift and cruise fans. This paper will present the most recent results from this program, and show the aerodynamic characteristics of configurations having lift fans mounted ahead of the wing, rotating cruise fans, and tandem mounted lift fans faired into the wing. The effect of interference between the fan flow and the airframe flow field on lift and moment will be discussed. Individual lift contributions of the various airplane components will be presented, and the overall characteristics when the components are assembled into a complete configuration will be shown. Limited lateral and directional data from the two complete configurations will also be presented.

NOMENCLATURE

c	local wing chord, ft
C_D	drag coefficient
C_L	lift coefficient
C_{l_β}	variation of rolling-moment coefficient with angle of sideslip
C_m	moment coefficient
C_n	yawing-moment coefficient

CP	center-of-pressure location, x/R
C_{Y_β}	variation of side force with angle of sideslip
D_e	equivalent diameter, $[(n/2)D_f^2]^{1/2}$, ft
D_f	fan diameter, ft
i_D	duct incidence angle, deg
i_t	angle of incidence of the horizontal tail
l	rolling moment, ft-lb
L	lift, lb
L/T_s	ratio of lift-to-fan static thrust
L_w/T_s	ratio of wing-lift-to-fan static thrust
M	pitching moment, ft-lb
n	number of fans
N	yawing moment, ft-lb
P_T/P_o	exhaust pressure ratio of fan
R	fan radius, ft
V	airspeed, knots
V/V_j	ratio of airspeed in free stream to jet exhaust
x	distance from fan axis, positive forward, ft
Y	side force, lb
α	model angle of attack, deg
α_t	angle of attack of the horizontal tail, deg
$\Delta\alpha$	angle-of-attack increment
β	angle of sideslip
β_v	lift fan vector angle from the fan axis, deg
δ_f	flap deflection angle, deg

TEST EQUIPMENT

Model

Figures 1 and 2 are photographs of the model installed in the Ames 40- by 80-foot wind tunnel. The basic wing planform has an aspect ratio of 5.8, sweepback angle of 35°, area of 230 square feet, taper ratio of 0.3, and a 65-412 airfoil section. Two basic configurations were studied; one (shown in fig. 1) was a combination rotating cruise fan and folding lift-fan arrangement with the cruise fan aft and lift fan forward. The other configuration (fig. 2) had tandem lift fans mounted on the fuselage adjacent to the wing leading and trailing edges; fairings covered the gap between the fan and the wing.

For these studies, the four 3-foot-diameter GE X-376 tip turbine driven lift fans were driven by one J-85 engine. The engine exhausted through a diverter valve into a plenum chamber located inside the fuselage. From the plenum chamber, the J-85 exhaust was ducted to the tip turbines of the individual fans. The fan locations and associated ducting arrangements could be varied in order to determine advantageous fan locations. All lift fans were equipped with exit louvers to deflect the flow aft for thrust in fan-powered flight.

Both model configurations were equipped with single-slotted trailing-edge flaps and a horizontal tail mounted high on the vertical fin.

Reduction of Data

Results from tests of V/STOL models in the Ames 40- by 80-foot wind tunnel are usually presented without wind-tunnel wall corrections. Reference 1 presents a correlation of full-scale wind-tunnel data with flight test results for several V/STOL concepts; these results are used to define a preliminary set of model-to-wind-tunnel sizing constraints that have given small wind-tunnel wall effects (as proven by the correlation of flight test and wind-tunnel test data) and therefore acceptable accuracy of the test results. The size of the subject model, referenced to the wind tunnel, and the constraints from reference 1 are presented in figure 3. Lifting-element area ratio is well within the suggested limit, but the momentum area and wing span ratios are slightly larger than the guidelines. The boundaries of reference 1 represent constraints based on limited experience rather than maximum acceptable size boundaries; thus rather than apply wind-tunnel wall corrections of questionable accuracy, the results presented herein are presented without corrections.

RESULTS AND DISCUSSION

Lift-Cruise Fan Configuration

Induced effects of the configuration components.- Unloading of the wing by downwash induced by fan operation has long been of concern for fore and aft

mounted lift-cruise fan configurations. Therefore, before the complete configuration was tested, the lift fans in front of the wing were tested in three locations to assure a location which would produce a near minimum wing download for the tests with the complete configuration. Figure 4 presents the ratio of total lift-to-fan static thrust as a function of flight velocity ratio for these three front lift fan locations (only the two front fans were operating). Power-off wing lift is also shown. The low fan position just forward of the wing leading edge has the largest lift-to-thrust ratio over the whole velocity ratio range. Furthermore, even if power-off wing lift is subtracted from the total, an increase of lift with forward speed is indicated rather than the expected reduction of lift due to fan induced wing download. In order to analyze this result, wing lift was obtained from static pressure distributions and is shown in figure 5(a). The results indicate that in all locations fan operation did cause negative wing lift over part of the velocity ratio range and in the worst fan location caused negative wing lift at all airspeeds. (Wing lift was positive at 0° angle of attack with fan power off because of lift due to camber.) The equivalent average reduction in wing angle of attack is shown in figure 5(b).

Total front fan lift can be calculated from the results in figures 4 and 5 by subtracting the wing lift in figure 5 from the total lift in figure 4; the upper shaded band in figure 6 shows this result as a function of airspeed. The lower band of data represents the fan thrust measured by a pressure survey of the fan wake. The shaded areas indicate the uncertainty of the data. Lift on the fan fairings, induced by fan operation, is indicated by the difference between the two sets of data. This lift was calculated by the method suggested in reference 2, and is shown by the lower line in figure 6. The lift is about the same as indicated by the large-scale experimental results. These results indicate that the lift induced on the front fan fairings by fan operation is large enough to overcome the download on the wing caused by downwash from the fan so that lift increased with airspeed.

The lift of the various individual lift-cruise fan model components is shown in figure 7. The variation of lift with airspeed with only the front fans operating and the exit louvers deflected to make thrust equal to drag is shown in figure 7(a). Balancing drag has a small effect on lift at low speed but at high speed causes a marked reduction in lift. The lift of the model with just the cruise fans operating is shown as a function of airspeed in figure 7(b) for two duct angles. The locus of the thrust equal drag curve is also shown. For values where airplane drag is trimmed the total lift of the duct (wing lift subtracted from the data in figure 7(b)) is greater than static thrust in spite of the trigonometric relationship between lift and thrust. This lift is a significant feature of ducted fan aerodynamics.

The variation of lift-to-thrust ratio with velocity ratio or airspeed (assuming a fan pressure ratio of 1.3) for a complete lift-cruise fan configuration for which the thrust has been vectored to balance the drag is shown in figure 8. The lines in the shaded area represent constant duct angle; the drag was balanced by deflection of the lift fan exit louvers. The shaded area indicates the sensitivity of lift-to-thrust ratio to the combinations of duct and vector angles required to balance drag. These results show a marked increase in the lift ratio with flight velocity ratio which is due to the

trailing-edge flap. At high velocity ratios, the lift-to-static thrust ratio without the wing lift is less than 1.0, indicating that the propulsion system lift has become less than the static value. This, of course, is to be expected at higher transition speeds where the fans or exit louvers are oriented to provide thrust. The airspeed scale for an aircraft with 1.3 pressure ratio fans shows that at 50 knots (the approximate flight airspeed required for about a 1000-foot landing and take-off distance) an overload of 10 to 20 percent of the installed thrust can be carried. Thus payload can be increased sizably with STOL operation of a VTOL machine of this design when suitable runways are available.

Transition characteristics.- The variation of thrust required, cruise-fan duct incidence angle, exit louver deflection angle, and horizontal tail incidence angle, and angle of attack for trim are shown as a function of airspeed in figure 9 for a transition at 0° angle of attack. The thrust required data indicate there was no lift reduction with airspeed for this design. The paper by Kenneth W. Mort discusses the cruise-fan duct stall boundaries using the duct incidence angle required for trim in this figure as an example. Mr. Mort shows that duct inlet stall does not appear to be a problem for this configuration. The tail angle of attack for trim varied from 12° at 60 knots airspeed to 7° at 175 knots airspeed; this variation is not extreme, and the magnitudes are small enough so that tail stall would not be a problem. About one-half of the tail moment capability is available for maneuvering or providing stability. Even less trim would be required of the tail with a hover control contribution to trim.

Figure 10 shows longitudinal characteristics near trim drag and moment at several airspeeds. The model, with its high horizontal tail, has a basic pitch-up problem. Lift-cruise fan operation did not significantly affect this problem.

Figure 11 shows the directional characteristics of the lift-cruise fan configuration at three different duct angles. The variation of side force and rolling moment with sideslip (tabulated on the figure) was linear and stable. The variation of yawing moment with sideslip appears to be neither linear nor stable, and therefore constitutes a possible area of concern for this type of configuration. The available data are not adequate for isolating the cause of the problem.

Tandem Lift-Fan Configuration

The variation of the ratio of lift-to-static thrust with flight velocity ratio for the tandem lift-fan configuration is shown in figure 12. The lift ratio with front fans, rear fans, or all four fans operating is shown on the figure. The rear fans induced a large amount of positive lift, while the front fans induced a negative lift. When all four fans were operating, lift fell approximately midway between that for the other two cases. In figure 13, fan thrust and wing lift have been removed from the basic data so that only induced lift is shown for the three operating conditions. The shaded bands indicate the range of certainty of the data. The positive induced lift noted with the rear fans operating is similar to that described in reference 2; the

flow from the fan induces lift in a fashion similar to a jet flap. An attempt was made to use the method described in reference 2 to estimate lift for both the rear fan and the front fan configurations. However, the estimated lift did not agree well with the experimental value. A more sophisticated three-dimensional approach to this unusual wing planform evidently is required. Since many VTOL designs will consist of multiple lift fans or lift engines, a theory for the induced effects of multiple lifting elements should be developed.

To see whether the fairings between the lift fans and the wing would significantly change induced lift when the four fans were operating, the fairings were removed during the tests of the tandem fan-in-wing configuration. The results (fig. 14) show the effect to be small. When only the front fans were operating, the fairings had a large detrimental effect, as can be seen by a comparison of figures 4 and 12. These results should be viewed with caution, however, because the rear fan was not installed when the data in figure 4 were obtained.

The variation of lift-to-static thrust ratio with airspeed with the drag trimmed and the trailing-edge flaps down is shown in figure 15 for the tandem lift-fan configuration. At 50 knots airspeed (based on a 1.3 P_T/P_O fan) the overload capability is about 12 percent of the installed static thrust. This would provide a significant payload advantage for STOL operation from a 1000-foot field.

Pitching moment of the tandem fan-in-wing configuration.- The large variation of pitching moment with airspeed has been a concern for lift-fan powered aircraft. Reference 2 correlated the results available at that time by presenting the partial derivative of the center-of-pressure location with respect to flight speed ratio evaluated at zero speed as a function of the ratio of diameter-to-local chord. The results from reference 2, along with similar data from the tandem fan-in-wing model, are presented in figure 16. The results with either the front fans or rear fans operating agree well with the data from reference 2. In spite of the large difference in induced lift between fore and aft fans, the variation of pitching moment with airspeed was nearly the same. With four tandem fans running, the variation of moment with airspeed was smaller, and was comparable to single fan-in-wing configurations having twice the ratio of diameter to chord. Figure 17 presents the variation of moment with lift for the tandem lift-fan configuration and for the fan-in-wing configuration (the point on fig. 16 of $D_e/c = 0.425$) from reference 2. The configurations have nearly the same value of $\partial CP/(\partial V_\infty/V_j)$ at $V_\infty/V_j = 0$ but very different effective diameter-to-chord ratios. The variation of moment near zero airspeed is nearly the same. However, the maximum nose-up moment of the tandem lift-fan configuration is about half that of the fan-in-wing configuration because the point of maximum moment occurred at one-half of the velocity ratio of the single fan-in-wing configuration. This peaking of the pitching moment at low flight speeds occurred only with the tandem lift-fan configuration and appears to be a desirable characteristic of this type of configuration.

Lateral-directional stability.- Lateral and directional stability of the tandem fan-in-wing configuration is shown in figure 18 as a function of flight velocity ratio. The variation of side-force gradient and lateral stability with airspeed is large but stable. The directional stability parameter is stable over most of the range, but at low speed becomes unstable. This could prove to be a problem area for this type of aircraft.

CONCLUDING REMARKS

Lift fans and lift-cruise fans have been tested in several different locations and in two different arrangements on a V/STOL transport configuration. The results indicated that these configurations had generally acceptable aerodynamic characteristics. Induced lift due to fan flow interference with the airplane flow field was a small percentage of the installed thrust and was positive. Isolated fan operation could cause either large positive or negative induced lift on the wing. However, the overall induced lift with all fans operating was positive. This positive induced lift was large enough to provide significant STOL capability.

Longitudinal trim requirements of both complete configurations were moderate and easy to provide. However, both configurations were directionally unstable over a portion of the transition speed range, and this may present a problem.

REFERENCES

1. Cook, Woodrow L.; and Hickey, David H.: Comparison of Wind-Tunnel and Flight-Test Aerodynamic Data in the Transition Speed Range for Five V/STOL Aircraft. Presented at NASA V/STOL Conference, Ames Research Center, April 4 and 5, 1966. Paper no. 26.

2. Goldsmith, Robert H.; and Hickey, David H.: Characteristics of Lifting-Fan V/STOL Aircraft. Astronaut. Aerospace Eng., Oct. 1963.

THE LIFT-CRUISE FAN MODEL

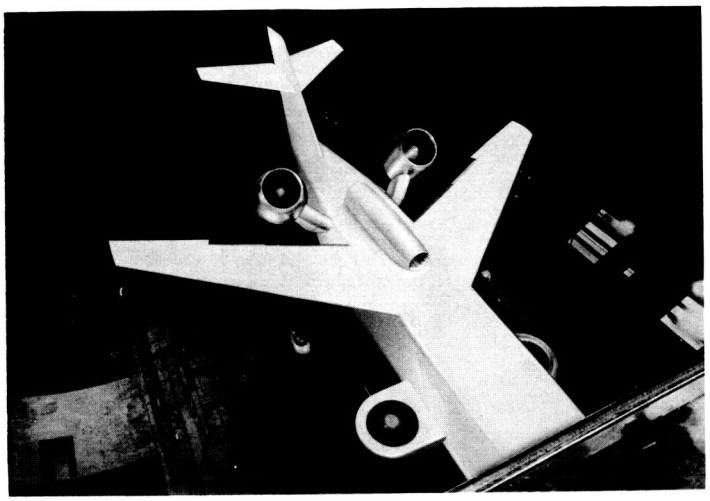

Figure 1 A-35554.1

THE TANDEM LIFT FAN MODEL

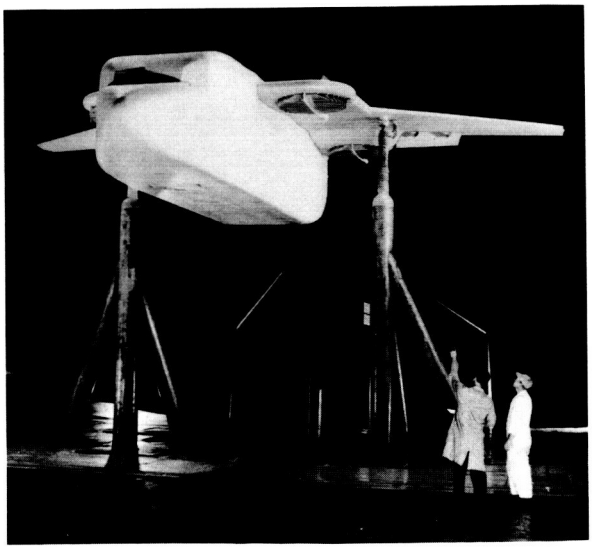

Figure 2 A-35376.1

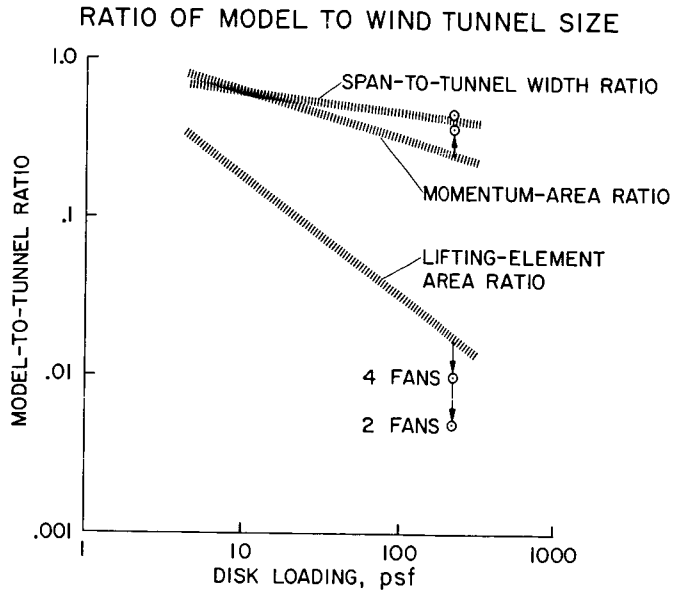

Figure 3

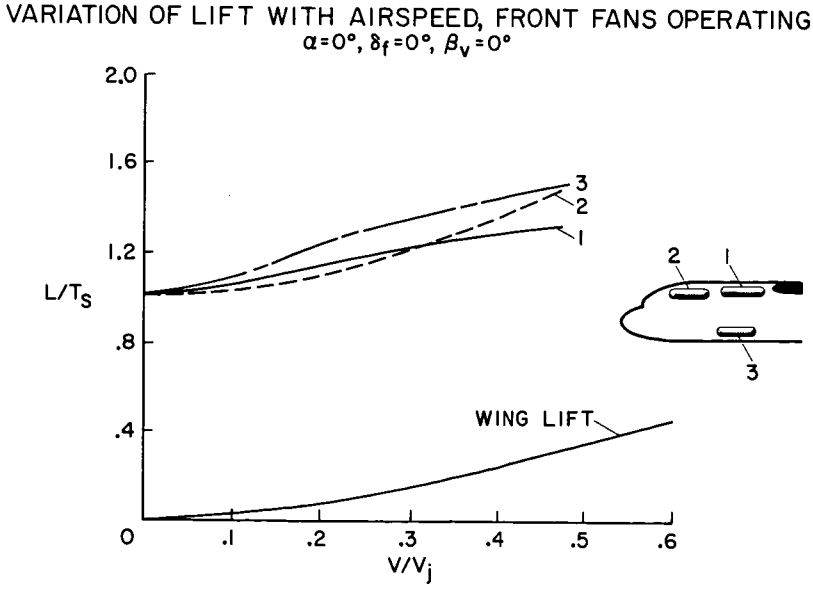

Figure 4

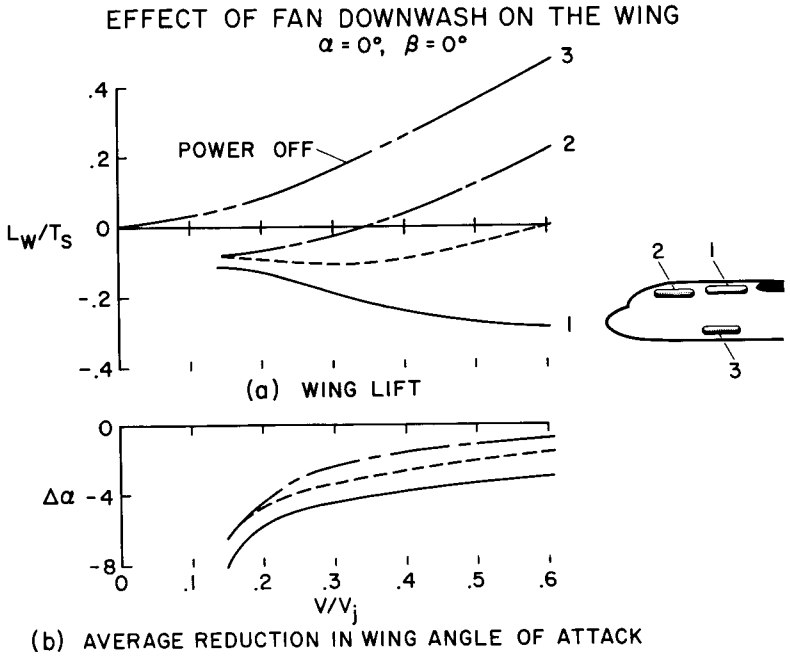

Figure 5

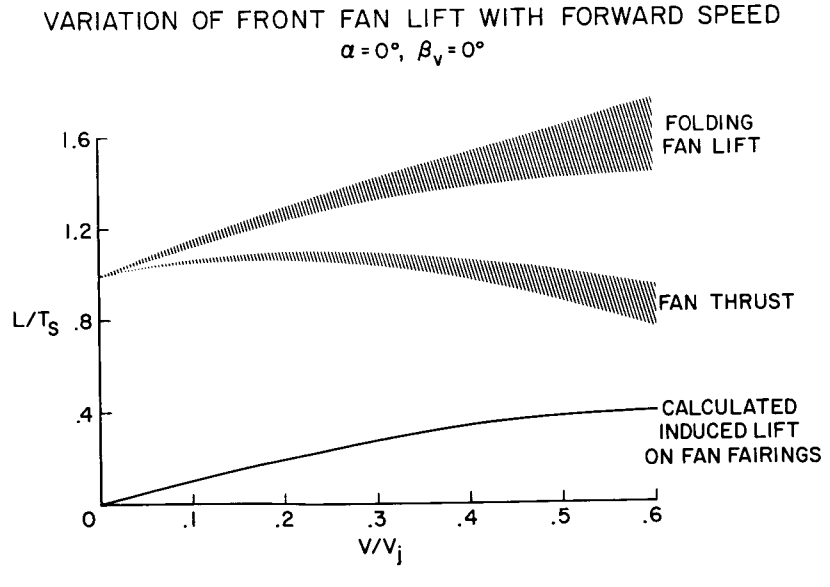

Figure 6

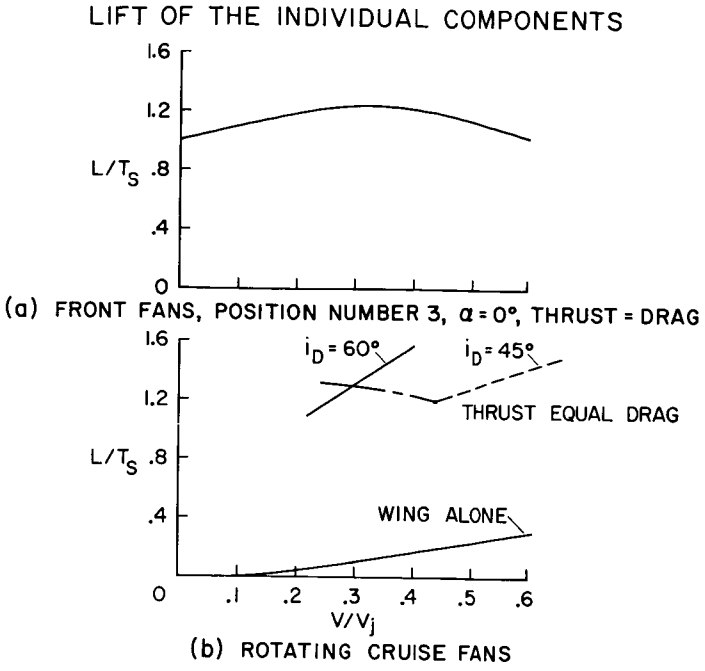

Figure 7

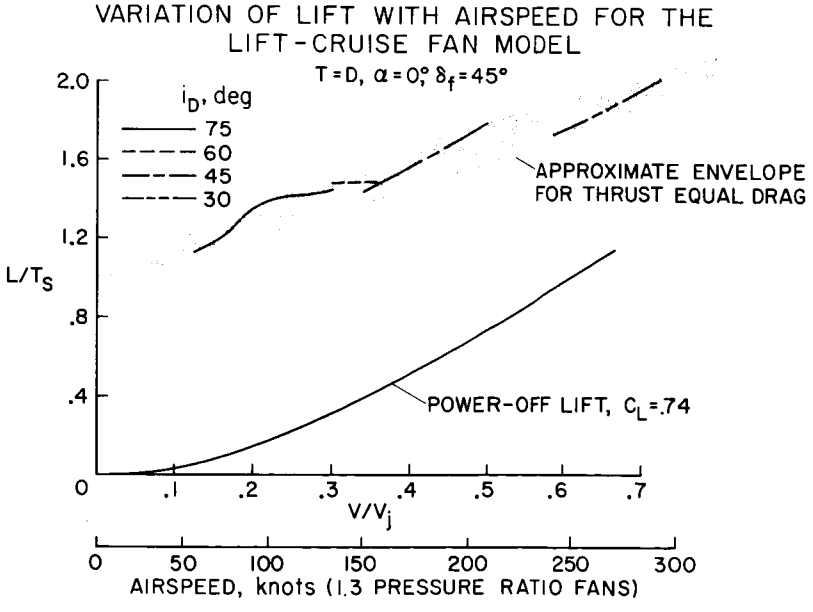

Figure 8

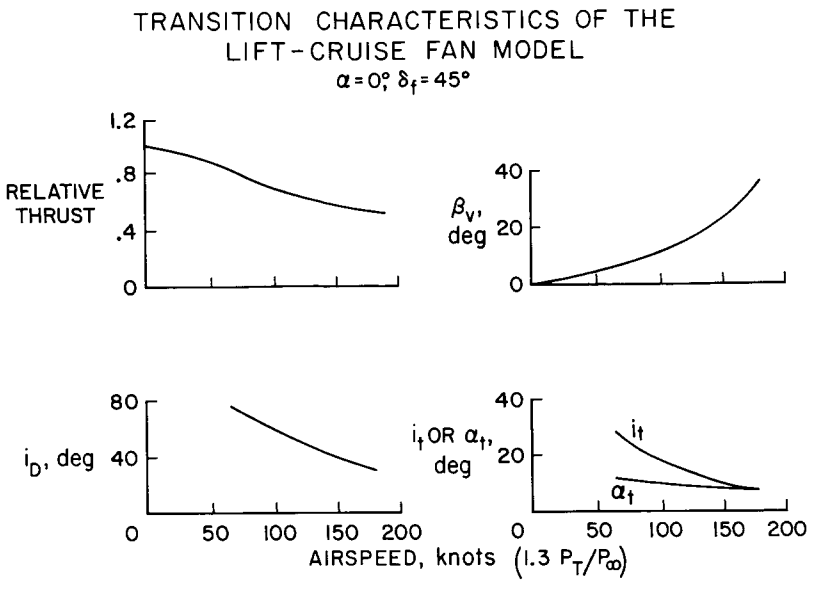

Figure 9

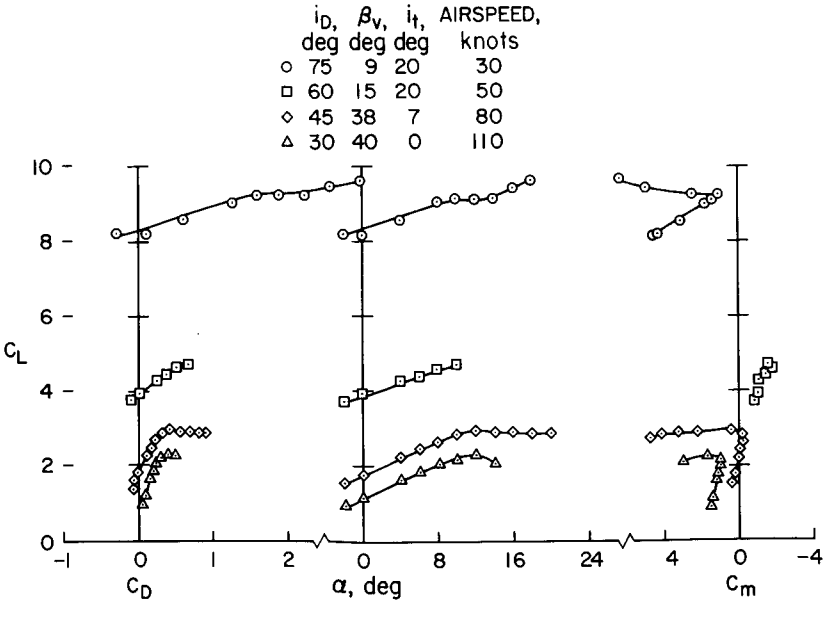

Figure 10

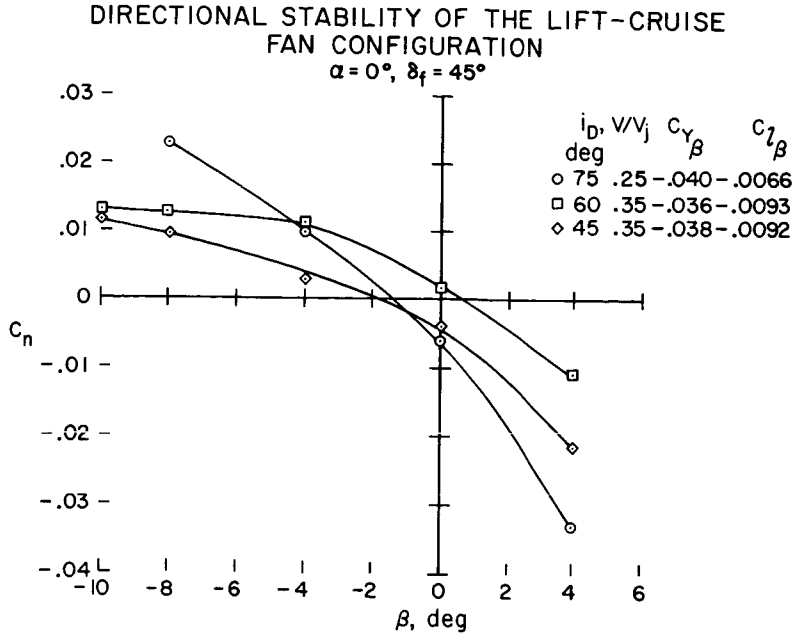

Figure 11

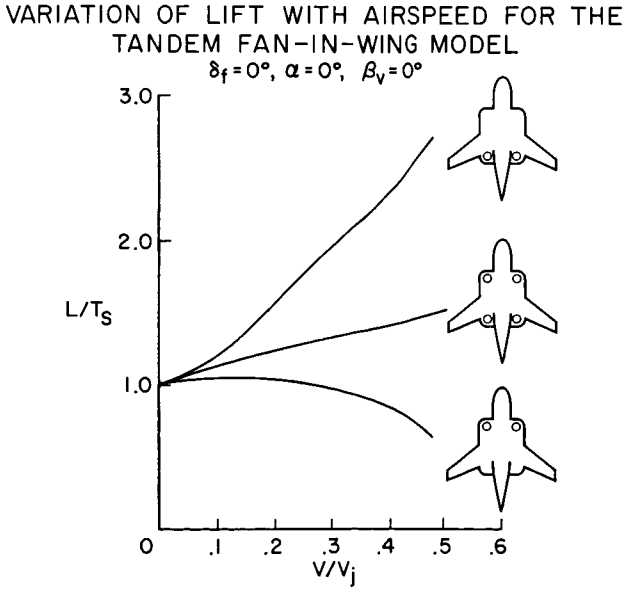

Figure 12

VARIATION OF INDUCED LIFT WITH AIRSPEED

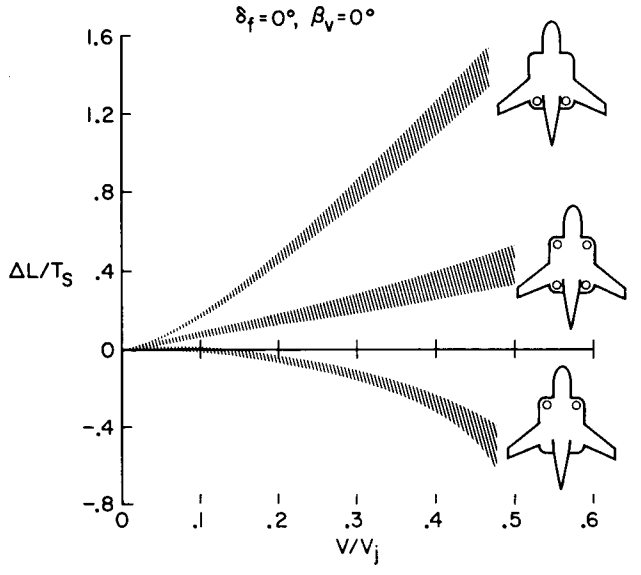

Figure 13

EFFECT OF FAIRINGS ON THE VARIATION OF LIFT WITH AIRSPEED FOR THE TANDEM LIFT-FAN CONFIGURATION

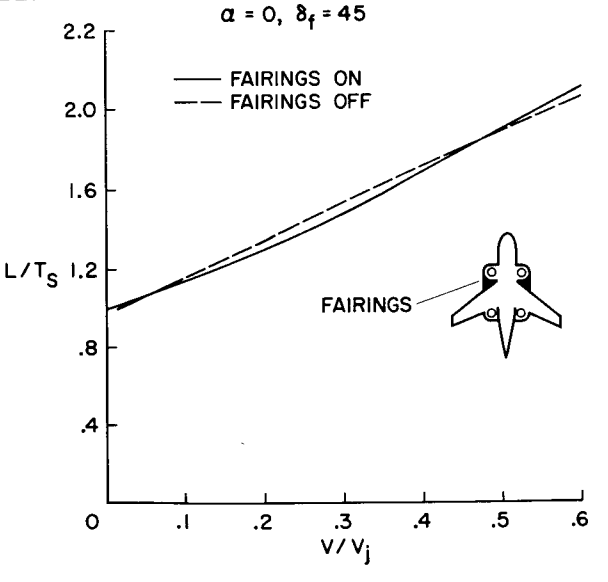

Figure 14

EFFECT OF FLAP DEFLECTION ON THE VARIATION OF LIFT WITH AIRSPEED FOR THE TANDEM LIFT-FAN CONFIGURATION

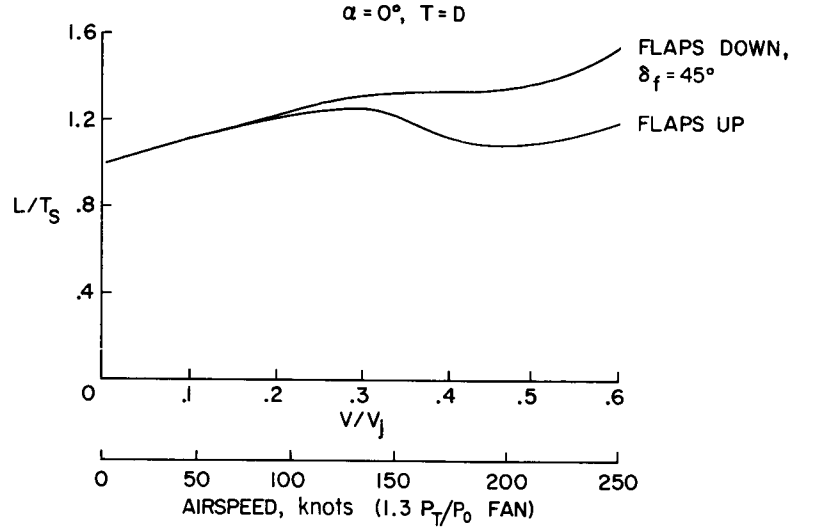

Figure 15

VARIATION OF THE CENTER OF PRESSURE LOCATION WITH AIRSPEED FOR FAN-IN-WING DESIGN

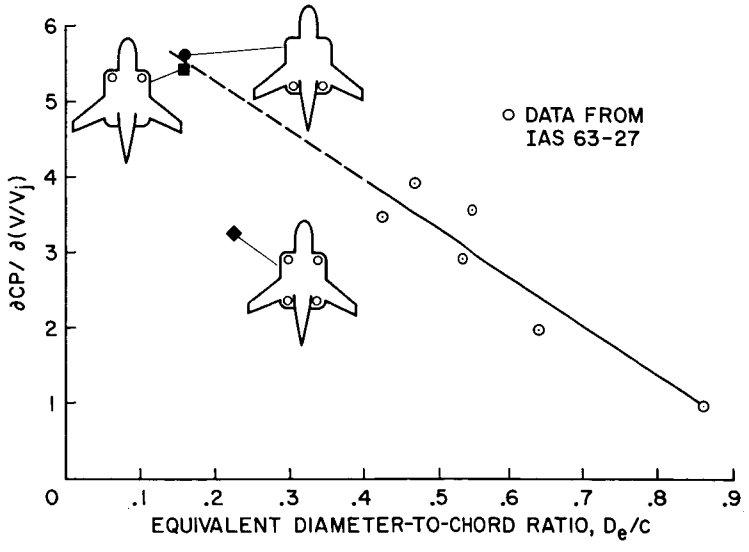

Figure 16

VARIATION OF PITCHING MOMENT WITH AIRSPEED FOR DIFFERENT FAN-IN-WING DESIGNS

$\alpha = 0°, \delta_f = 0°, \beta_v = 0°$

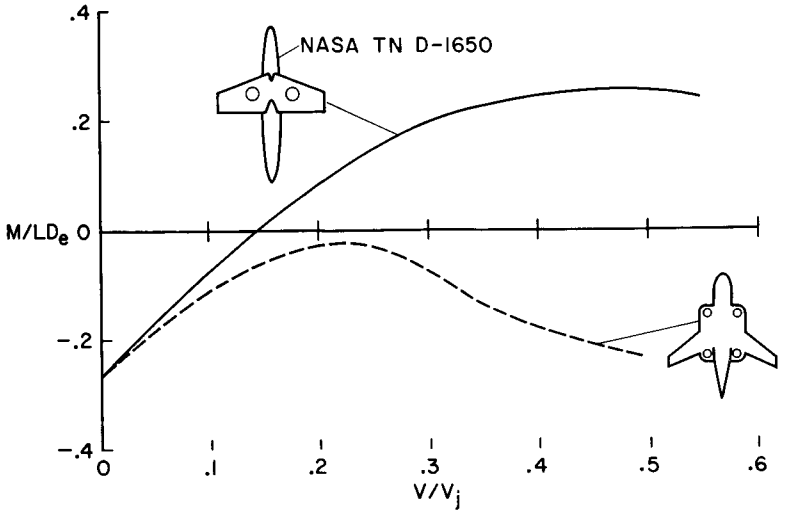

Figure 17

LATERAL-DIRECTIONAL CHARACTERISTICS OF THE TANDEM LIFT-FAN CONFIGURATION

$\alpha = 0°$, T = D, $\delta_f = 45°$

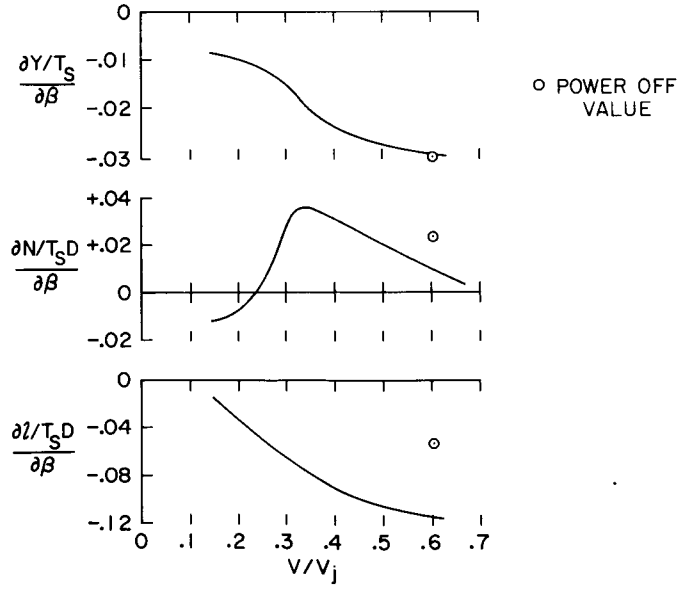

Figure 18

8. SUMMARY OF LARGE-SCALE TESTS OF DUCTED FANS

By Kenneth W. Mort
Ames Research Center

SUMMARY

Several research areas which have been investigated by the NASA on large scale isolated ducted fan models are discussed. Research concerned with performance has indicated that: (1) ducted fan inlet design does not appear to be a major problem, (2) ducted fan nacelles must be very carefully designed, otherwise the drag becomes excessive, and (3) increasing fan tip clearance reduces the shroud thrust and reduces the capability of the fan for absorbing power. Research concerned with the occurrence of duct lip stall due to angle of attack indicates that neither inner nor outer duct lip stall for reasonably sized ducted fans is the problem that it was once considered to be.

Author

INTRODUCTION

Ducted fans have been proposed for many applications, from lifting, thrusting units for VTOL airplanes to propulsive units replacing jet engines for STOL airplanes. In this paper the term ducted fan will be used for all configurations which have a fan or propeller surrounded by a shroud or fairing. Hence configurations which range from ducted propellers (having pressure ratios of 1.03) to high bypass ratio turbofan engines (having pressure ratios of 1.30) will be called ducted fans. In this paper several research areas which have been investigated by the NASA on isolated ducted fan models will be considered. Figure 1 outlines the subjects to be covered. First the ideal performance of ducted fans will be discussed to review the basic performance characteristics of ducted fans. Then several research areas pertinent to performance will be discussed: namely, inlet losses, nacelle drag, and fan tip clearance. Next duct lip stall due to angle of attack will be considered. Both inner and outer lip stall will be covered.

NOTATION

A_j duct exit flow area (see fig. 3)

A_f fan flow area (see fig. 3)

A_o upstream flow area (see fig. 3)

c_D external nacelle section drag coefficient, $\frac{\text{section drag}}{q(\text{overall frontal area})}$

8

C_D overall external nacelle drag coefficient, $\frac{\text{drag}}{q(\text{overall frontal area})}$

C_p power coefficient, $\frac{\text{power}}{\rho n^3 d^5}$

C_{ST} shroud thrust coefficient, $\frac{\text{shroud thrust}}{\rho n^2 d^4}$

C_T total thrust coefficient, $\frac{\text{total thrust}}{\rho n^2 d^4}$

d fan diameter, ft

M free-stream Mach number

n fan rotational speed, rps

P_L local static pressure, psf

P_S free-stream static pressure, psf

P_{T_i} total pressure at fan, psf

P_T free-stream total pressure, psf

q_i dynamic pressure at fan, psf

q free-stream dynamic pressure, psf

T_c total thrust coefficient, $\frac{\text{total thrust at } 0^\circ \alpha}{q\left(\frac{\pi d^2}{4}\right)}$

V forward velocity, fps

V_∞ forward velocity, knots

α angle of attack, deg

ρ mass density of air, slugs/cu ft

RESULTS AND DISCUSSION

Theoretical Considerations

To review the basic reason for studying ducted fans, theoretical ducted fan performance is compared with the actual performance of a turbojet engine.

The results are shown in figure 2. The ratio of ideal thrust-to-static-thrust (computed using compressible, isentropic flow tables assuming a perfect gas) is presented as a function of forward velocity for pressure ratios of 1.03, 1.1, and 1.3. The 1.03 pressure ratio is the approximate value for the ducted fans employed on the X-22A flight vehicle; 1.1 is the value for the models for which experimental results will be discussed later, and 1.3 is a representative value proposed for current V/STOL aircraft designs.

To illustrate the potential of ducted fans, the thrust required curve for a representative VTOL airplane is shown. It is apparent the thrust available curves for the ducted fans generally match the thrust required curve of the VTOL airplane much better than does the curve for the turbojet. For example at the point indicated, the thrust available for the 1.03 pressure ratio matches the thrust required. At this velocity the turbojet has much more thrust available than is required and would have to be operated at partial power to achieve a thrust-drag balance. This is, of course, an inefficient operating condition.

The theoretical curves presented in figure 2 were computed allowing the duct exit area to decrease with forward velocity to maintain a constant fan pressure ratio and flow velocity. The area ratios required will now be discussed briefly to illustrate the effect of pressure ratio. This will be done to allow a broader interpretation of the experimental results which were obtained at only one pressure ratio (1.1).

Figure 3 shows the theoretical inlet flow area variation and the exit area variation required to maintain fan pressure ratio and velocity. The left hand part of figure 3 shows the ratio of upstream-to-fan-flow area as a function of free-stream Mach number. The right hand part of figure 3 shows the ratio of exit-to-fan flow area as a function of free-stream Mach number. As can be seen, the variation in upstream-flow area with Mach number is greater as pressure ratio is reduced. It is also apparent that the variation in exit-flow area with Mach number is greater as pressure ratio is reduced.

This indicates that the problem of designing inlets and nozzles becomes greater as pressure ratio is reduced. Low pressure ratio ducted fans would probably require more inlet diffusion and hence longer inlets. In addition they would probably require longer exhaust nozzles to keep the exhaust flow angularity to an acceptable value.

This analysis has assumed a fixed blade angle fan. If a variable blade angle fan were employed, the large changes in inlet and exhaust area with Mach number would not be required. This is because the variable blade angle fan can tolerate variations in flow velocity and maintain reasonable efficiency as does a free propeller.

Inlet Studies

In practice inlet designs usually involve a compromise between static requirements and cruise requirements to avoid variable inlet geometry. Hence, there is the possibility of large inlet losses at either cruise or static conditions. In view of this, a summary of recent experimental inlet studies will

now be examined. These studies involved testing the two ducted fans shown in figures 4 and 5. Both of these models had pressure ratios of about 1.1 and were quite similar to each other in arrangement. A gas generator was mounted directly to the top of the fan nacelle. The gas generator exhaust was distributed to turbine blades at the tip of the fan blades.

The primary physical differences between the two models were in the method of mounting and size. The model shown in figure 4 was supported by struts and had a 5-foot-diameter fan, while the model shown in figure 5 was sting mounted and had a 3-foot-diameter fan.

The test velocity ranged from 0 to 0.8 Mach number for the 3-foot model and from 0 to 0.2 Mach number for the 5-foot model.

The inlet studies performed on these models are summarized in figure 6. The loss in total pressure divided by the dynamic pressure at the fan is shown as a function of the ratio of free-stream to fan dynamic pressure. Shown at the top of the figure are half section views of the inlets. The 3-foot model was tested with three different inlets.

As can be seen from this figure the 5-foot model had a rather large inlet loss precisely at static conditions.[1] However, at very slight free-stream dynamic pressures, corresponding to about 10 to 20 feet per second, it dropped to below 0.05. As the inlet length was reduced, the inlet loss was reduced, and that of the shortest inlet was negligible.

At static conditions the inlet loss corresponds precisely to the reduction in static thrust. As free-stream dynamic pressure is increased, the loss in thrust becomes a smaller part of the inlet loss divided by dynamic pressure at the fan. In view of this, and because the inlet losses decrease with free-stream dynamic pressure, the magnitude of the inlet losses is not considered serious.

It may be inferred from the theoretical discussion earlier that ducted fans with higher pressure ratios would probably have lower inlet losses than these fans because fewer inlet design compromises are required. (At least for Mach numbers ranging from 0 to 0.8.)

Nacelle Drag

The external nacelle drag of ducted fans is a potential major problem. Figure 7 summarizes the low-speed nacelle drag results obtained from investigations performed on the 5-foot-diameter ducted fan shown before. A sketch of the front view of the ducted fan is shown on the left of the figure. A summary of the drag results obtained at windmill conditions is given on the right. Section drag based on frontal area is shown as a function of azimuth angle. These drag values were obtained from flow momentum surveys at the nacelle trailing edge.

---

[1]See references 1 and 2 for a more detailed discussion of the aerodynamic characteristics of this model.

At 0° azimuth the drag coefficient is about 0.1, at 90° azimuth it reaches a maximum of about 0.5, and at 180°, a minimum of about 0.04. This minimum value is considered representative of the value which could be obtained on an isolated fan nacelle, that is, without the gas generator on top of the nacelle and without support struts. The value of 0.04 is reasonably low, more than half of which can be attributed to friction drag.

Near the 90° azimuth location the drag coefficient is shown as a dashed line because of the influence of the horizontal support struts and the resulting uncertainty of the nacelle drag. It is evident that the strut adversely affects the drag of a considerable area of the nacelle. This suggests that interference drag should be carefully considered on aircraft having strut mounted ducted fans.

At 0° azimuth the drag coefficient is significantly higher than the value at 180° because the flow on the engine fairing was separated.

In figure 8 the nacelle drag obtained from high-speed windmill tests of the 3-foot-diameter ducted fan is summarized. This drag was obtained from balance data and is the overall external nacelle drag. Drag coefficient based on frontal area is shown as a function of Mach numbers for the three inlet configurations. In addition, the minimum section drag coefficient for the 5-foot model is shown along with the estimated friction drag. The friction drag is shown as a band because of the variation in wetted surface area for the different configurations.

Comparison of the low-speed drag coefficients of the 3-foot model with the friction drag and minimum section drag of the 5-foot model suggests that the overall drag of the 3-foot model is high. This is probably because of flow separation on the nacelle fairing around the gas generator.

As shown, the primary difference in drag characteristics between the three inlets is in the value of the drag divergence Mach number. The lowest drag divergence Mach number was only about 0.4, while the highest was 0.6. Both values are about 0.2 lower than the design value. Pressure surveys indicated that this was probably due to the nacelle fairing around the engine.

This is suggested by the results shown in figure 9 for the long inlet. The minimum surface static pressure coefficient is presented as a function of Mach number. The results for three azimuth positions are shown. The divergence Mach number for the 180° station was 0.8. (This is the design value and would be comparable to that for an isolated fan.) For the 30° azimuth station the divergence Mach number is 0.7. No pressure coefficient data were available for the 0° azimuth station. However, the divergence Mach number is probably near 0.6 where the drag divergence shown in figure 8 occurred.

These results suggest that isolated nacelles for low pressure ratio fans can probably be designed with high drag divergence Mach numbers. However, considerable care must be exercised when designing nacelles for configurations which have the engine mounted directly to the fan nacelle.

The significance of the drag coefficient values which have been shown are illustrated in figure 10. Thrust divided by static thrust is shown as a function of forward velocity for 1.1 and 1.3 pressure ratios. The ideal thrust is shown along with the ideal thrust less the external nacelle drag. This drag was computed for drag coefficients of 0.04 and 0.066. (As previously discussed, 0.04 was the minimum section drag coefficient for the 5-foot model and 0.066 was the minimum overall drag coefficient for the 3-foot model.) The drag was computed assuming a ratio of nacelle frontal area-to-fan area of 1.5. As can be seen, increasing the drag coefficient from 0.04 to 0.066 reduces the thrust a significant amount. In addition, the ducted fan with the lower pressure ratio is more sensitive to variations in drag coefficient; that is, the incremental reduction in thrust is much larger for the low pressure ratio fan than it is for the high pressure ratio fan.

Fan Tip Clearance

For shaft-driven ducted fans the minimization of the fan tip clearance is essential for achieving maximum performance. However, this is not compatible with the usual structural requirements, which dictate a reasonable magnitude of tip clearance to prevent fan-shroud interference. Hence it is necessary to precisely define the reduction in performance due to increased tip clearance. In view of this, studies were performed on a 7-foot-diameter, shaft-driven ducted fan. This model is shown in figure 11. It employed a three-bladed propeller with variable pitch and had a static pressure ratio of about 1.03. This ducted fan was a full-scale model of that employed on the X-22A VTOL airplane.

Figure 12 shows representative tip clearance effects on thrust and power coefficient at constant blade angle. Thrust and power coefficients based on fan rotational velocity are presented as functions of advance ratio for two values of tip clearance. Both shroud thrust and total thrust coefficient are shown. As might be expected, the incremental thrust loss due to tip clearance decreased with advance ratio.

The effects of tip clearance on static performance are examined in more detail in figure 13. On the left in figure 13 thrust and power coefficients are presented as functions of the ratio of tip clearance to diameter. Results are shown for the 7-foot-diameter model and for the 4-foot-diameter model of reference 3. Comparison of the shroud thrust with total thrust indicates that, for ratios of tip clearance to diameter up to 0.02, the loss in thrust is primarily due to shroud thrust loss. Hence, the fan thrust, which is the difference between the total and shroud thrust, is essentially unaffected by the increase in tip clearance.

The power results presented on this figure indicate that, not only is the thrust reduced with increased tip clearance, but the power is reduced as well. Hence, increasing the tip clearance reduces the ability of the fan to absorb power.

Comparison of the results for the 7-foot model with the 4-foot model indicates large differences in the power and thrust coefficient variations with tip clearance. The power coefficient variation for the 4-foot model is much flatter than that for the 7-foot model. The shroud thrust is also flatter, although it is not as obvious in the figure. The net effect of the differences are shown in the right hand part of the figure. Here shroud thrust coefficient divided by power coefficient is shown as a function of the tip clearance ratio. The reduction in performance of the 7-foot model as tip clearance is increased is much less than that for the 4-foot model, indicating that the 7-foot model was much less sensitive to increasing tip clearance.

The significance of the results obtained from the 7-foot model may be interpreted in terms of the X-22A flight vehicle. If the power is maintained constant at the maximum of 1250 hp per duct, an increase in tip clearance from 1/4 to 1-1/2 inches would result in a static thrust loss of about 10 percent.

Duct Lip Stall

Ducted fans which are tilted with respect to the airstream during low speed lifting conditions may encounter stall of either the inner or outer duct lip. Previous small scale investigations have indicated this to be a potential major problem area. Stall of the inner lip is of primary concern because it is more heavily loaded and would result in a larger reduction in lift when stalled. In addition, stall of this lip affects the fan loading asymmetrically.

In figure 14 the inner lip stall boundaries are summarized for several ducted fan models. The small sketch shows what is meant by inner lip stall. The angle of attack at which complete stall occurs is shown as a function of the reciprocal of the thrust coefficient based on free-stream dynamic pressure. For angles of attack above these curves the flow is completely separated. For angles less, the flow is either not separated or only partially separated.

The configurations investigated are shown by scale drawings with the respective leading-edge radii indicated. The upper surface is the inside surface of the shroud. As can be seen from the drawings, the two X-22A models and the VZ-4 model are very similar and differ primarily only in scale. Comparison of the lip stall boundaries for the VZ-4[2] and the small scale X-22A model indicates a sizable scale effect. However, the VZ-4 boundary and the full scale X-22A boundary were identical. These results suggest the for a given shape of shroud or duct there is a certain minimum value of lip radius required to achieve the stall angle indicated by the upper boundary. The boundary for the 5-foot model was lower than the boundaries for the other full scale ducts. This was probably because of the lip camber used on the 5-foot model.

Outer lip stall has also been a problem for small scale ducted fan models. In view of this, the outer lip stall boundary for the small scale and full scale X-22A model was examined. The results are shown in figure 15. The sketch shows what is meant by outer lip stall. The angle of attack at which complete

[2]See reference 4 for a more detailed discussion of the inner lip stall boundary for this model.

stall occurs is shown as a function of the reciprocal of the thrust coefficient. These results are similar to those for inner lip stall in that there is a large effect of scale.

As discussed in paper number 9 by Mr. Maki, outer duct lip stall would probably not be encountered by a flight vehicle such as the X-22A. Inner lip stall would only be encountered during flight at high descent rates. The X-22A employs ducted fans having a pressure ratio of 1.03. To investigate the significance of pressure ratio on the lip stall boundaries for flight vehicles, the lip stall boundaries for the vehicle described by Mr. Hickey in the preceding paper were determined.[3] These boundaries were determined assuming the use of 1.3 pressure ratio ducted fans. The results are shown in figure 16.

The level unaccelerated trim curve is shown along with the inner lip stall boundary. The outer lip stall boundary was too far away from the trim curve to appear on this figure. Hence it is not considered to be a problem. In addition, it is apparent from these results that inner lip stall would not be a problem either for this vehicle because of the large duct angle margin between the trim curve and the stall curve. Inner lip stall would not be encountered even at very high rates of descent.

In view of this discussion it is apparent that neither inner nor outer duct lip stall for reasonably sized ducted fans is the problem that it was once considered to be.

CONCLUDING REMARKS

From the discussion contained in this paper the following conclusions can be made.

1. Inlet design does not appear to be a major problem on 1.1 pressure ratio ducted fans as far as inlet losses are concerned. In view of this it would probably not be a problem on higher pressure ratio ducted fans. Hence variable inlet geometry probably would not be required.

2. Nacelle fairings must be carefully designed for ducted fans, especially those for low pressure ratio ducted fans. Otherwise the losses due to drag become excessive. The results also suggest that for isolated nacelles, high drag divergence Mach numbers can be achieved. However, if the engine is mounted on the nacelle, then considerable care is required to achieve high drag divergence Mach numbers.

3. Thrust continues to decrease with increasing fan tip clearance. Hence, the desirability in minimizing fan tip clearance is apparent. In addition, the capability for absorbing power is reduced as fan tip clearance is increased.

---

[3]The boundaries were determined using the results shown in figures 14 and 15 for the full scale X-22A model.

4. For flight vehicles which employ tilting ducted fans, duct lip stall due to angle of attack does not appear to be a major problem. Inner lip stall would only be encountered during high descent rates. This becomes even less of a problem if high pressure ratio ducted fans are employed. Outer lip stall would probably never be encountered during flight.

REFERENCES

1. Giulianett, Demo J.; Biggers, James C.; and Corsiglia, Victor R.: Wind Tunnel Test of a Full-Scale, 1.1 Pressure Ratio, Ducted Lift-Cruise Fan. NASA TN D-2498, 1964.

2. Przedpelski, Z. J.; Heikkinen, A. H.; and Vacek, L.: Aerodynamic Investigation of Low Speed VTOL Transition Characteristics of X353-5B Cruise Fan. General Electric Report Number R63FPD426, Dec. 1963.

3. Hubbard, Harvey H.: Sound Measurements for Five Shrouded Propellers at Static Conditions. NACA TN 2024, 1950.

4. Mort, Kenneth W.; and Yaggy, Paul F.: Aerodynamic Characteristics of a 4-Foot-Diameter Ducted Fan Mounted on the Tip of a Semispan Wing. NASA TN D-1301, 1962.

SUBJECTS TO BE COVERED

- IDEAL PERFORMANCE OF DUCTED FANS
- PERFORMANCE RESEARCH AREAS
  - INLET LOSSES
  - NACELLE DRAG
  - FAN TIP CLEARANCE
- ANGLE-OF-ATTACK RESEARCH AREAS
  - INNER LIP STALL
  - OUTER LIP STALL

Figure 1

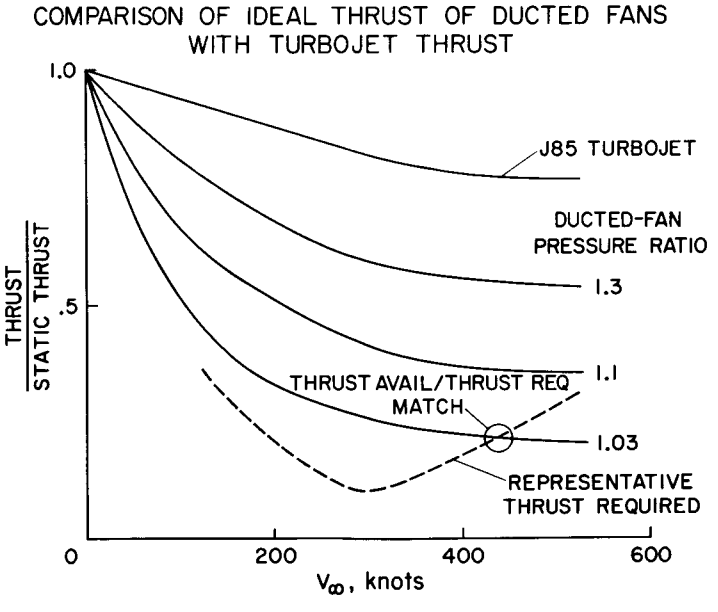

Figure 2

IDEAL FLOW AREA RATIOS OF DUCTED FANS

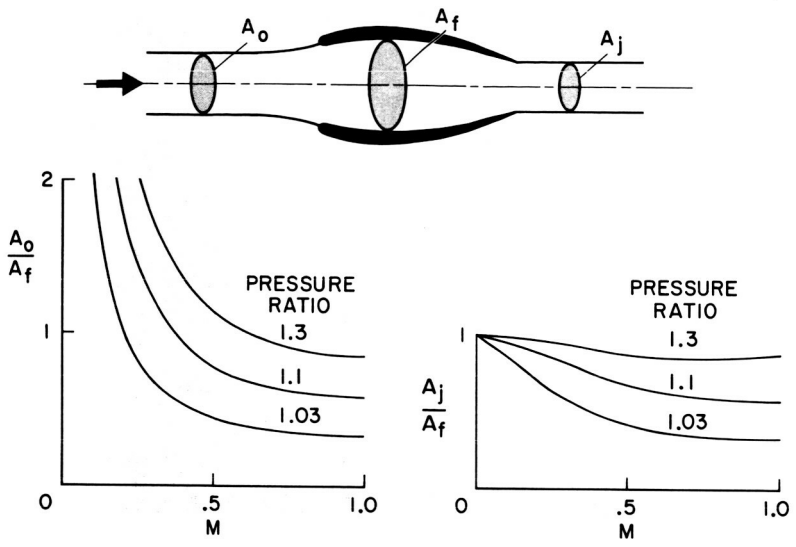

Figure 3

5-FOOT-DIAMETER, 1.1 PRESSURE RATIO DUCTED FAN

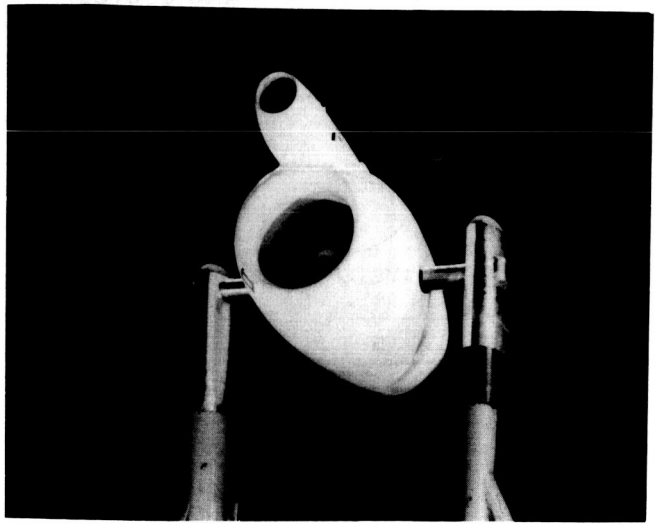

Figure 4 A-31081

3-FOOT-DIAMETER, 1.1 PRESSURE RATIO DUCTED FAN

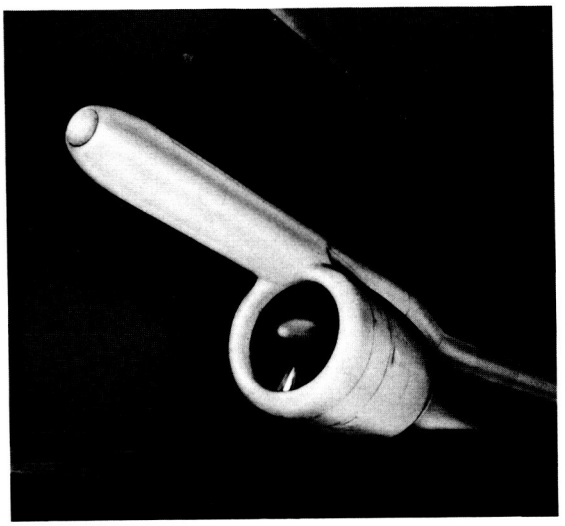

Figure 5 L-65-4553

EFFECT OF INLET GEOMETRY ON INLET TOTAL PRESSURE LOSSES, 1.1 PRESSURE RATIO DUCTED FANS

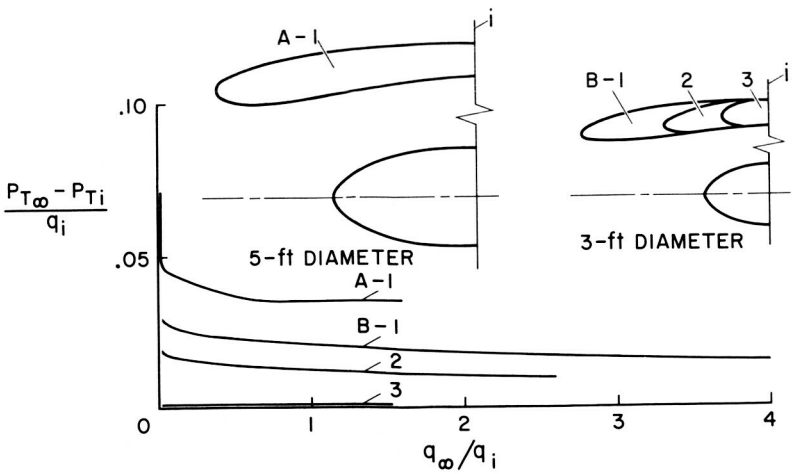

Figure 6

NACELLE DRAG OF 5-FOOT-DIAMETER,
1.1 PRESSURE RATIO DUCTED FAN

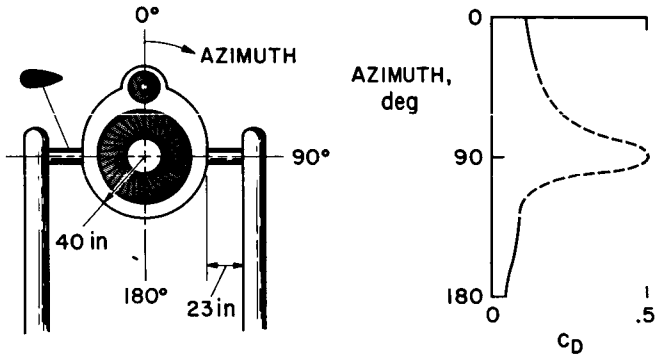

Figure 7

NACELLE DRAG OF 3-FOOT-DIAMETER,
1.1 PRESSURE RATIO DUCTED FAN

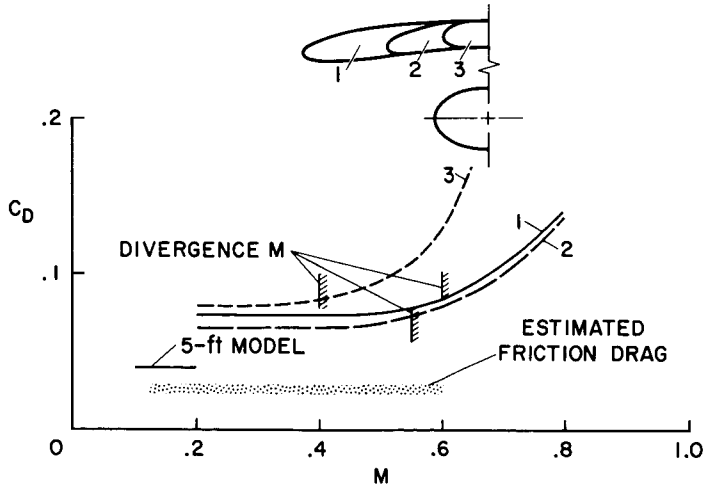

Figure 8

PEAK PRESSURE COEFFICIENT FOR 1.1 PRESSURE RATIO, 3-FOOT-DIAMETER DUCTED FANS

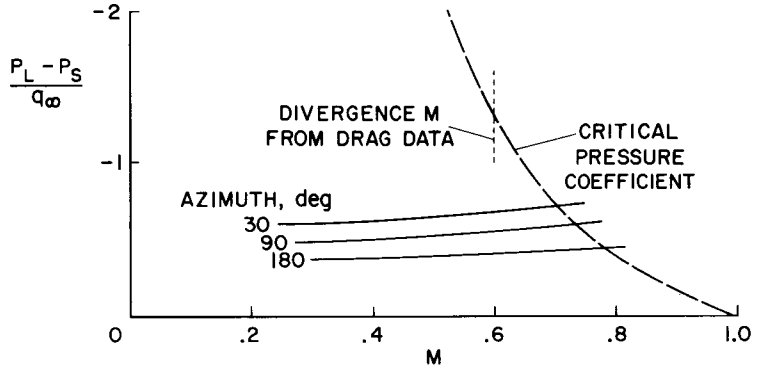

Figure 9

EFFECT OF NACELLE DRAG ON THRUST
FRONTAL AREA/FAN AREA = 1.5

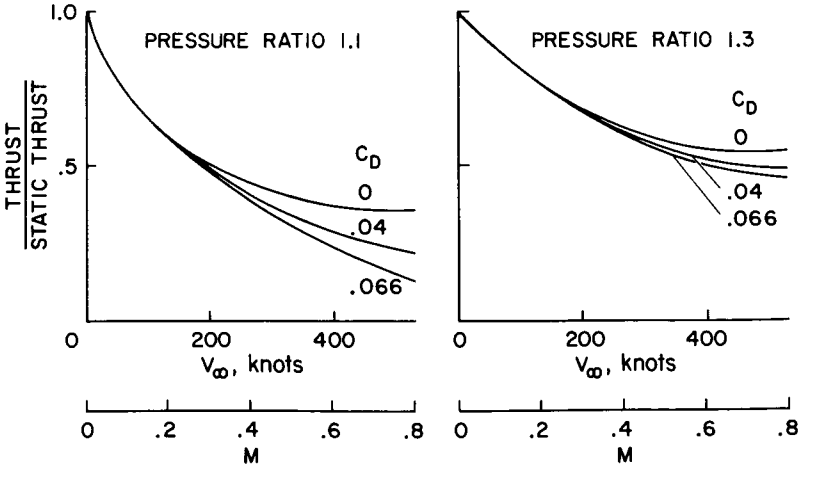

Figure 10

X-22A FULL-SCALE DUCTED FAN, 7-FOOT DIAMETER

Figure 11 A-33770.1

THRUST AND POWER COEFFICIENTS FOR
TWO TIP CLEARANCES

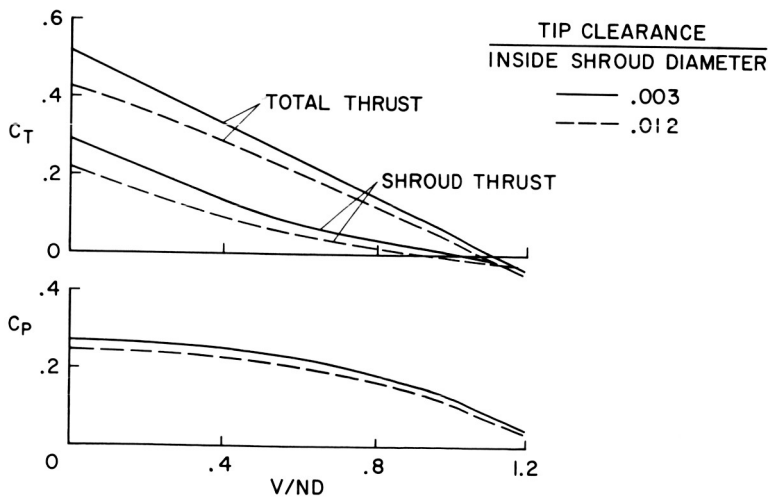

Figure 12

EFFECTS OF TIP CLEARANCE ON STATIC PERFORMANCE

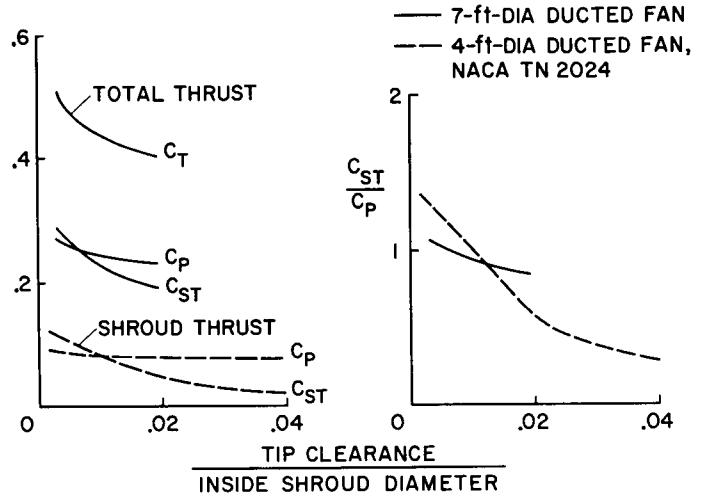

Figure 13

DUCT ANGLE OF ATTACK AT WHICH INNER LIP STALL OCCURS

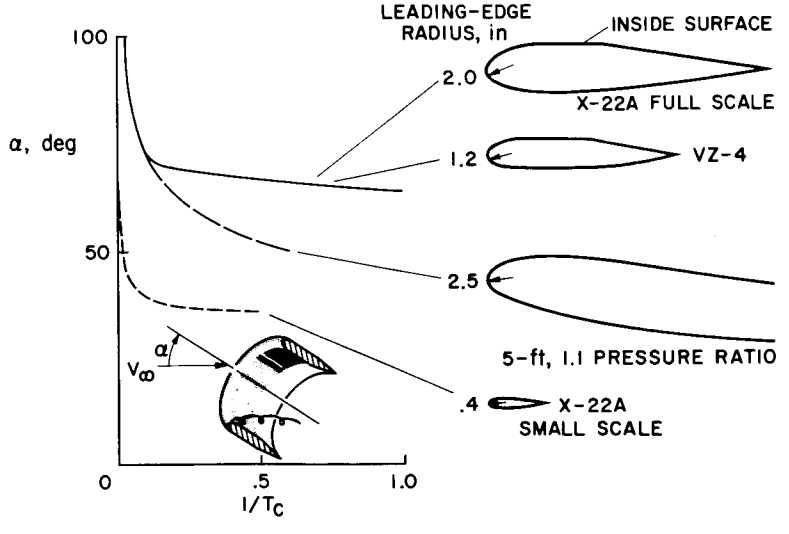

Figure 14

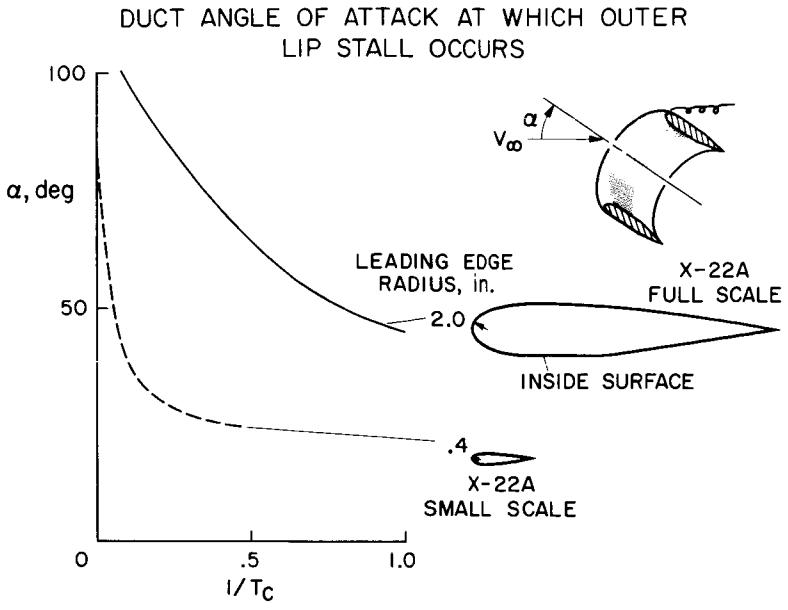

Figure 15

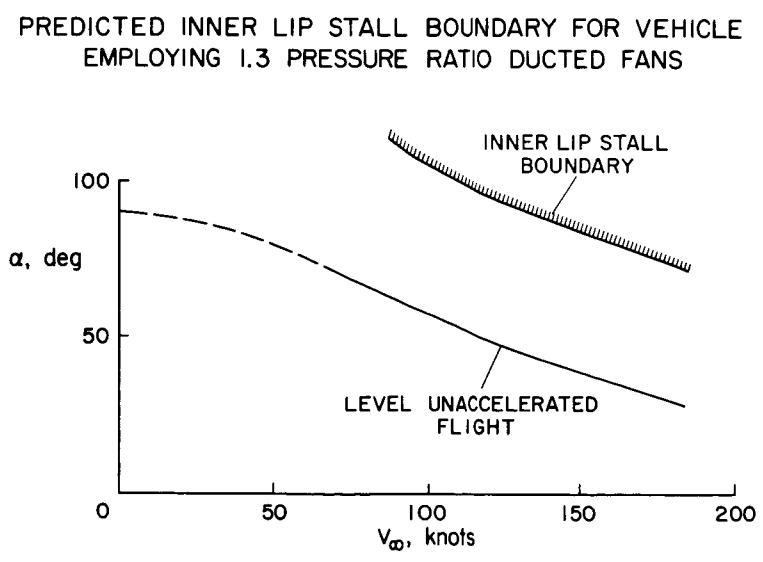

Figure 16

Page intentionally left blank

9. AERODYNAMIC STABILITY AND CONTROL OF DUCTED-PROPELLER AIRCRAFT

By Ralph L. Maki and Demo J. Giulianetti
Ames Research Center

SUMMARY

Test results from studies of small and large powered models of a dual, tandem, ducted-propeller VTOL design are reviewed, with emphasis on stability and control characteristics through the transition speed range. The characteristics are generally satisfactory. Stability augmentation may be required to reduce Dutch roll tendencies. Further study is needed to evaluate the apparently large side-force gradients in sideslip. Reductions in control effectiveness due to ground proximity are similar to those for tilt-wing V/STOL designs.

INTRODUCTION

Author

A VTOL configuration utilizing tilting ducted propellers in an arrangement such as shown in figures 1 and 2, has powerful hovering control available for pitch and roll by direct modulation of individual propeller thrust. Duct exit vanes operating in the duct slipstream provide yaw control in hover by thrust vectoring. These controls exchange functions in cruising flight. The Bell X-22A VTOL airplane configuration has a similar arrangement.

Investigations of powered models have been made by NASA at small and large scale to study the problems of operation of this concept through the transition speed range. Other studies have indicated reasonable performance for such designs; this discussion is restricted to the stability and control aspects. The studies have provided sufficient data to define the capabilities of the concept and, in general, show it to be quite satisfactory for V/STOL design. Rather than delineate the good features, attention will be directed primarily toward the problems determined in the studies as outlined in figure 3. It appeared likely that control problems in terms of trim requirements, power available, and cross-coupling effects might be anticipated. Possible duct stall and its relation to descent capabilities needed assessment. Effects of ground proximity are also treated.

The large-scale results to be shown in this paper are from tests of a model utilizing 4-foot diameter propellers. These duct units and the drive systems are from the Doak VZ-4DA VTOL airplane which completed its flight research program about 4 years ago. The smaller models tested at Langley Research Center were about 0.3 scale with respect to the large model.

NOTATION

a_y	lateral acceleration, ft/sec^2
C_D	drag coefficient
C_L	lift coefficient
C_l	rolling-moment coefficient
C_m	pitching-moment coefficient
C_n	yawing-moment coefficient
C_Y	side-force coefficient
D	duct exit diameter, ft
g	acceleration of gravity, ft/sec^2
HP	total input horsepower
h	ground height, distance from ground to fuselage under surface, ft
I	moment of inertia, slug-ft^2
i_D	duct incidence, measured with respect to fuselage reference line, deg
L	lift, lb
M_y	pitching moment, ft-lb
M_Z	yawing moment, ft-lb
R_D	rate of descent, ft/min
V	airspeed, knots
α	angle of attack of fuselage reference line, deg
β	angle of sideslip, deg
Δ	increment

Subscripts

F	front
R	rear
Y,Z	about the Y or Z axis
α,β	derivative of parameter with respect to α or β
$\ddot{\theta}$	pitching angular acceleration, M_y/I_y, rad/sec^2
∞	value out of ground effect
static	value at V = 0

DISCUSSION

Transition Characteristics

The transition characteristics of the large-scale model, tested in the Ames full-scale tunnel, and of the smaller model tested at Langley Research Center are plotted in figure 4. Pitching moments, duct angle, and power requirements are given as functions of flight speed for 1-g steady flight. Moments[1] are divided by the inertia representative of a 15,000-lb gross weight airplane to give pitching acceleration values. The small-scale test results show somewhat lower trim duct angles at low speeds; the differences are believed directly relatable to a duct stall phenomenon on the small-scale model to be discussed later. Peak pitching moments occur at 40 to 45 knots for both models, with the small-scale data indicating a peak about 20 percent higher than the large-scale results, and a reduction to zero at a lower flight speed (about 95 knots). Power required is a minimum at about 120 to 130 knots and is roughly half the power required for hover.

Longitudinal Trim and Control

The severity of these pitching-moment variations (fig. 4) in terms of the amount of control required to trim the aircraft are shown in figure 5. Control available and trim requirements are plotted as functions of steady-flight duct angle so that cruise velocities correspond to low duct angles at the left and hover corresponds to a 90° duct angle at the right on this chart. The trim required curve for $\Delta i_D = 0$ is for a center of gravity midway between the front and rear duct rotation axes. Stability about this center of gravity position was approximately neutral, and hence represents a rearmost advisable center of gravity for flight.

[1]Model moments were scaled to values for an airplane approximately the size of the Bell X-22A airplane. A scale factor of 0.67 was used for the large model, and 0.20 for the small model.

A boundary of total pitch control available is shown, the left branch displaying the pitch control provided by differential deflection of the duct exit vanes, 20° trailing edge up on the front and 20° down on the rear duct vanes. Vane effectiveness was linear to this deflection for duct angles to 50° or higher. At larger deflections there may be flow separation off the vane, especially for downward vane deflections at high duct angles where the vane protrudes into the free-stream flow. The right branch of the control-available curve bounds the combined effects of differential vanes with differential front-rear propeller thrust. Differential thrust is limited by duct stall for these model tests as thrust was changed by varying propeller rpm; thus, reducing thrust on the forward ducts increases the advance ratio until the inlet lip stalls. (Duct stall will be discussed in more detail later.)

These data show that control power is critical at about 40° duct angle (about 70 knots flight speed) where the margin between the trim requirement and the control available amounts to about 0.4 rad/sec^2 of pitch acceleration for a 15,000-lb airplane. This represents the control available to handle pitch and roll maneuvering.

The trim requirement can be reduced by deflecting the ducts so that the front duct incidence is less than the rear. The example shown, with the front duct incidence 10° less, about doubles the margin of control for maneuvering in the critical area. Similar gains in control margin can be provided by a moderate forward shift of the center of gravity. Thus, it appears that adequate control for maneuvering can readily be provided.

Descent Rate Limitations

The transition corridor will be limited in one respect for any ducted propeller. As descent rates increase, the advance ratios of the tilted propellers increase until the ducts stall, and the resulting blade stresses or vibration/buffet levels preclude higher rates of descent. In figure 6, curves of required duct angle as functions of flight speed are shown for constant descent rates. Several test boundaries are superposed. In all cases the stall conditions to be described apply to the forward pair of ducts only. The downwash from the front ducts reduces the effective angle of attack at the rear ducts, delaying stall to higher geometric duct angles.

The band labeled "incipient stall" was measured on the large-scale model and represents the earliest measurable indications of stall, generally not discernible by examination of force and moment characteristics. These stall beginnings would be encountered at a descent rate of about 600 ft/min at flight speeds of 55 knots and less. One isolated duct, properly instrumented to monitor blade stresses and vibration, was tested at higher advance ratios to define the boundary at which large stresses and vibrations occurred. This boundary corresponds to those conditions at which flow separation occurs in the duct inlet at the upstream lip (as illustrated in fig. 7), and probably represents the limit rates of descent in flight. High descent rates are possible at flight speeds above 55 knots. At lower speeds, although blade stresses and buffet levels are tolerable, because of the low dynamic pressure, thrust losses accompany the stall; the significance of these losses needs

further study. The incipient stall boundary was used to define the limit for control available from differential thrust (fig. 6); hence, the margins of control available as discussed were conservative. The difference between the incipient and deep lip stall boundaries emphasizes the need for adequate test instrumentation for exploring duct stall phenomena.

The lower boundary in figure 6 was determined in tests of the small-scale models. The outer surface of the duct stalled (see fig. 7) even at zero descent rate. Tests of a large isolated duct of the type used on the small model proved this to be a scale effect. Although the surface pressure distributions on the large duct indicated some degree of separation of the flow over the upper-outer surface, its effects were too slight to be discernible in force or moment data or in model vibration. With a slat installed at the upper leading edge and an enlarged lower lip radius, the small-scale model displayed stall characteristics similar to those measured at large scale.

In summary, then, these data emphasize the care which must be taken in interpreting ducted-propeller data, for various sources and degrees of duct stall phenomena might otherwise lead to erroneous conclusions in predicting flight characteristics.

Lateral-Directional Characteristics

Studies of the lateral-directional characteristics of the ducted-propeller models have revealed several problem areas. The first of these is illustrated in figure 8 where yawing moment as a function of sideslip is shown for three duct incidence settings with the vertical tail both on and off. The vertical-tail volume was sufficient to provide directional stability with the ducts set in the cruise configuration ($i_{D,F} = 5^\circ$, $i_{D,R} = 0^\circ$). However, C_{n_β} becomes increasingly unstable at low sideslip angles as duct incidence is increased. At 50° duct incidence, the vertical tail did not measurably change C_{n_β} at low β. Small-scale tests identified an area of flow separation at the tail-fuselage juncture which immersed an increasing tail area with increasing angle of attack. Fences installed near the base of the vertical tail on the large-scale model did not prevent the spread of flow separation. However, tail-fuselage fairings were developed on the small-scale model which alleviated the separation.

There has been general concern about the magnitude of the side force on vehicles with the broad lateral areas of ducted-propeller configurations. It is difficult to assess the magnitude of these side forces. On figure 9 the measured side-force gradients, C_{Y_β}, are ratioed to C_{L_α} in a first attempt to judge the magnitude. This ratio simply relates the side force to a quantity which is very well-defined and understood. The data show that with the ducts set for the cruise condition C_{Y_β} is 30 to 40 percent as large as C_{L_α}, and the ratio increases as duct incidence is increased at transition speeds.

Figure 10 was prepared to assess the results in more meaningful terms - lateral acceleration at various flight speeds. For a 50 ft/sec crosswind gust, and over the flight-speed range for which the ducts will be set in the cruise configuration, increments of about 0.6 to over 1.0 g will be felt. These

magnitudes would be evaluated best by comparison with those for a design with free propellers to determine whether the ducts themselves or the propeller disk area leads to the large side forces. Directly comparable data were not available. Data for a two-propeller STOL model are not representative since the propeller span to the wing-span ratio was relatively small. Some data for a four-propeller model with large wing-tilt angles, that is, in transition configurations, indicate responses of about 1/3 to 1/2 those for the ducted-propeller model. These results, although inconclusive, suggest a problem area peculiar to the ducted-fan design concept.

Free-flight tests of a small-scale model showed Dutch roll oscillations that were unstable at low speeds and still lightly damped at speeds for which 20° duct angle provides trim. Tests were terminated at that point for fear of damaging the model at higher flight speeds. The static data in figure 11 for the large-scale model with ducts set in the cruise configurations suggest that the airplane will have Dutch roll tendencies in cruising flight. The model is directionally stable (as was seen in fig. 8), but the gradient with sideslip is quite low so the model will be lightly damped. The yawing moments are coupled with large rolling moments which are conducive to Dutch roll and hence support the small-scale free-flight findings.

Effects of Ground Proximity

Tests of the effects of ground proximity have been made at both small and large scale. Figure 12 summarizes some of the hover results for $\alpha = 0^{\circ}$, $\beta = 0^{\circ}$, and zero roll. Lift and exit-vane control are given as functions of model height above ground. Height is measured to the fuselage undersurface, and is referenced to duct exit diameter. Small-scale data indicate lift increases at low heights and the lift at a height typical for wheel contact is about 20 percent above that with no ground effect. Results from large-scale tests did not include a similar minimum height, but do show that lift increases as the ground is approached.

On the small-scale model exit vanes were deflected differentially on the left and right ducts to control yaw. Losses in control effectiveness were measured at ground heights of less than 2 diameters. At touchdown, the loss is about 40 percent. Tests of the large-scale model at a ground height of about 0.7 diameter showed a loss of pitch control of over 30 percent which is in general agreement with the yaw-control results. Yaw-control tests on a four-propeller tilt-wing model, showing similar control-power losses, are analogous to the ducted-propeller tests since the ailerons used for yaw control operate in the propeller slipstream in a manner similar to the vanes in the duct slipstream.

Figure 13 summarizes the basic longitudinal characteristics of the large-scale model as affected by ground proximity for operation as a STOL or conventional airplane. Lift increases of 10 to 20 percent were measured at the lowest test height. These increases will be beneficial in arresting sink rate during landing flare. Drag reductions will provide additional acceleration on take-off ground roll. Pitching-moment changes mean that the trim requirement

changes with height. However, the magnitude of these moment changes at the low dynamic pressures during a landing approach or climbout after take-off is very small.

CONCLUDING REMARKS

This review of test results on V/STOL models utilizing tilting ducted propellers as combination lift/propulsion/control units may be summarized as follows:

Adequate control is available through the transition speed range. The control margins beyond the trim requirements can be increased through moderate center of gravity shifts and by appropriate configuration conversion techniques.

Duct stall phenomena should not impose undue limitations on the flight envelope.

Directional instability at low flight speeds, and lightly damped stability in cruise may require stability augmentation to reduce Dutch roll tendencies.

Apparently large side-force gradients in sideslip may noticeably reduce passenger comfort in gusty air; this problem needs further study.

Lift increases are measured in proximity to the ground. Large control losses are also encountered which are similar to losses measured for tilt-wing V/STOL designs.

LARGE-SCALE MODEL
THREE-QUARTER REAR VIEW

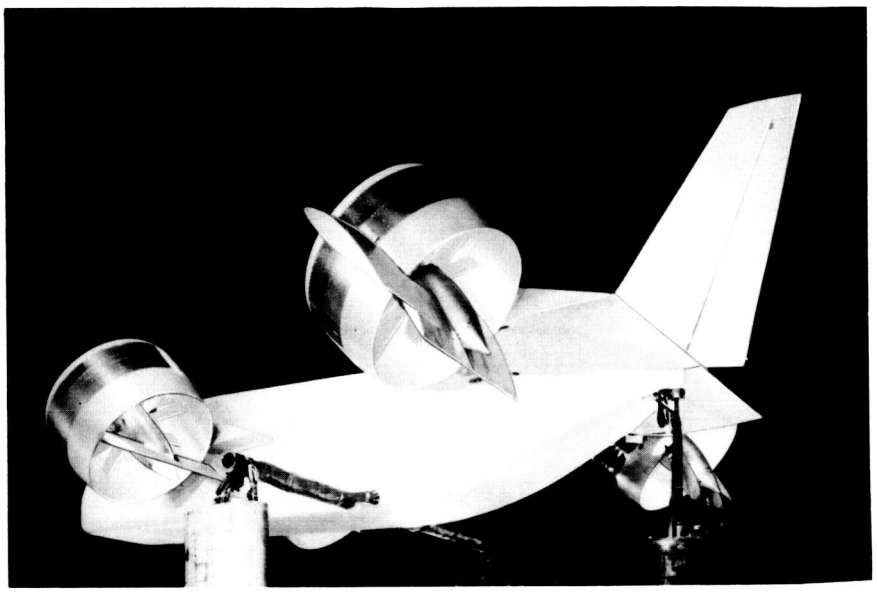

Figure 1

A-33529.1

LARGE-SCALE MODEL
OVERHEAD VIEW

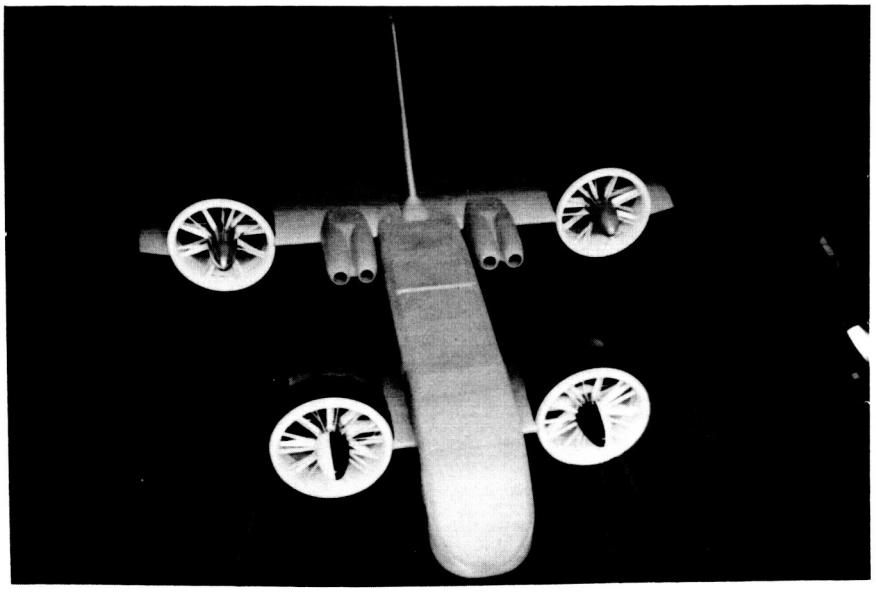

Figure 2

A-33532

STABILITY AND CONTROL INVESTIGATIONS OF DUCTED PROPELLER VTOL MODELS

- TRANSITION CHARACTERISTICS
- LONGITUDINAL STUDIES
  - TRIM AND CONTROL
  - DESCENT RATES
- LATERAL-DIRECTIONAL STUDIES
  - DIRECTIONAL STABILITY
  - SIDE FORCE
  - DUTCH ROLL
- GROUND PROXIMITY

Figure 3

TRANSITION CHARACTERISTICS

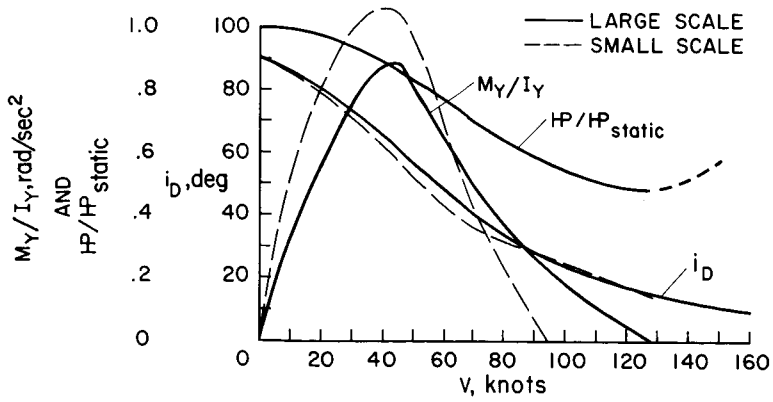

Figure 4

LONGITUDINAL TRIM AND CONTROL

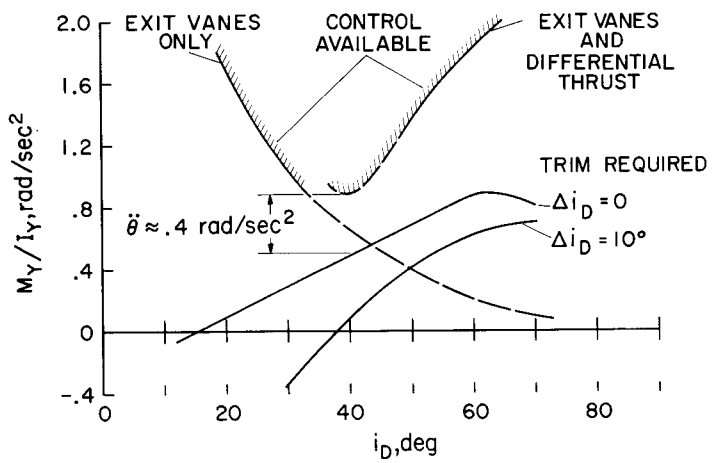

Figure 5

DESCENT-RATE LIMITATIONS

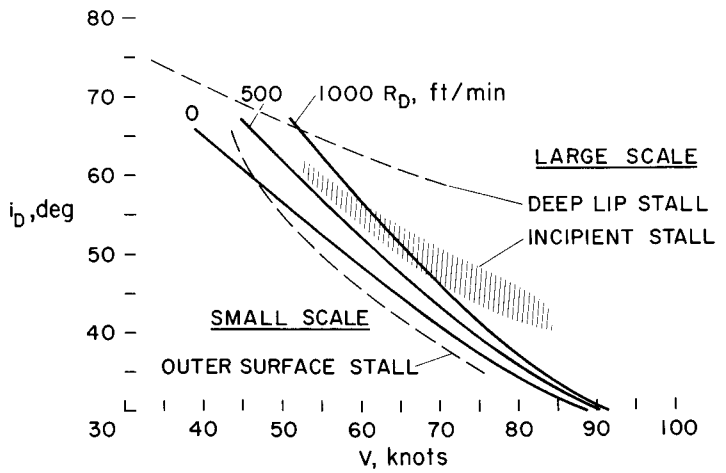

Figure 6

TYPES OF DUCT STALL

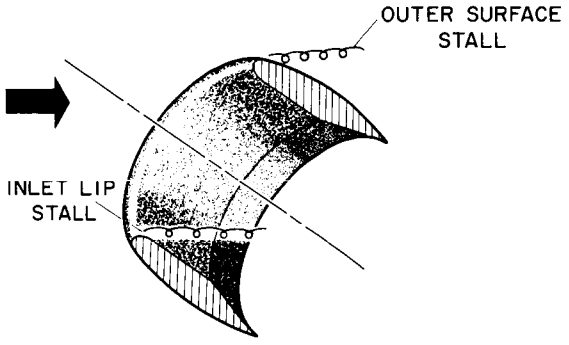

Figure 7

DIRECTIONAL STABILITY
$\alpha = 0°$

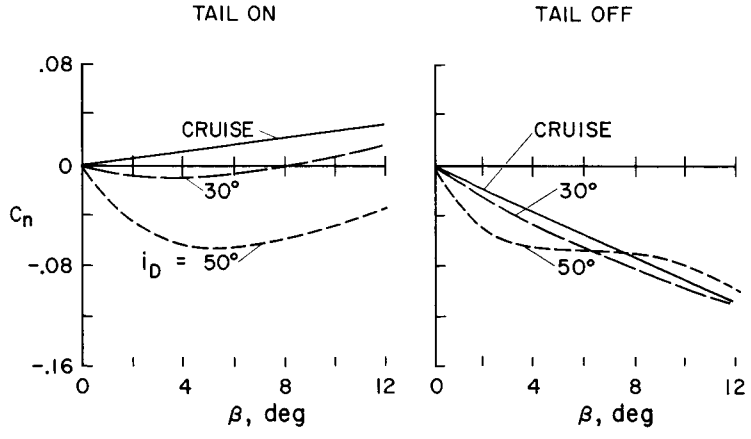

Figure 8

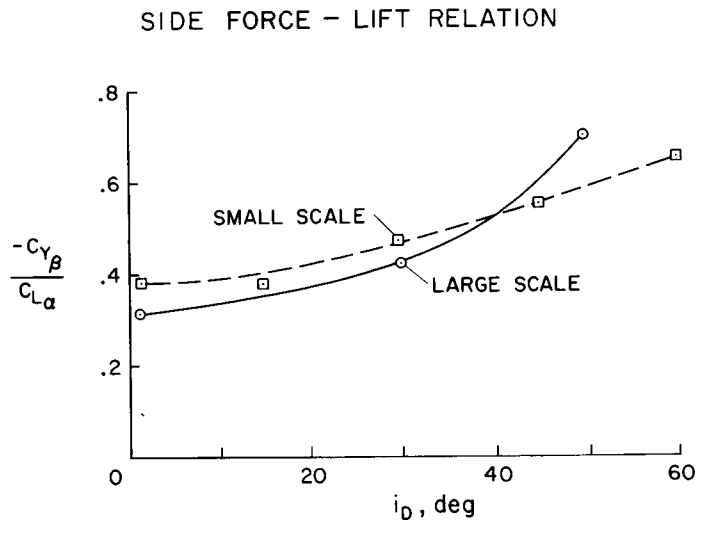

Figure 9

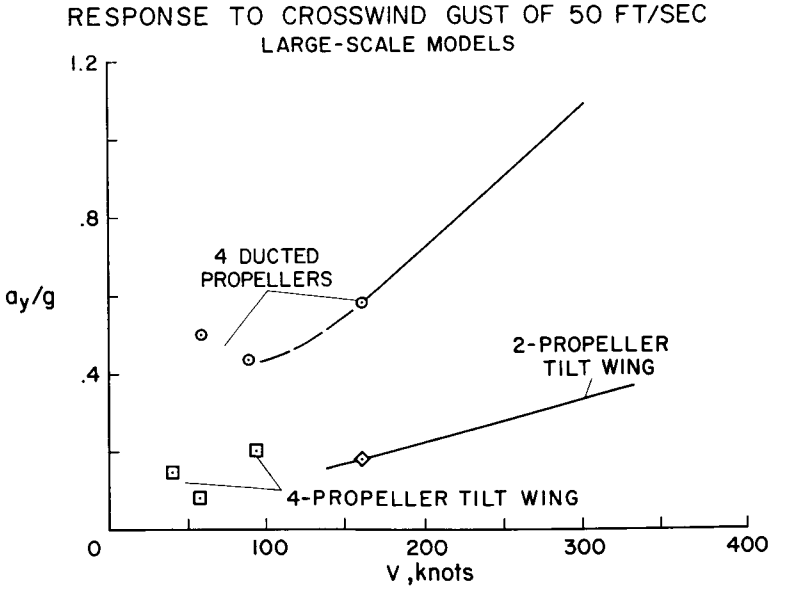

Figure 10

ROLL-YAW COUPLING
CRUISE CONFIGURATION LARGE-SCALE MODEL

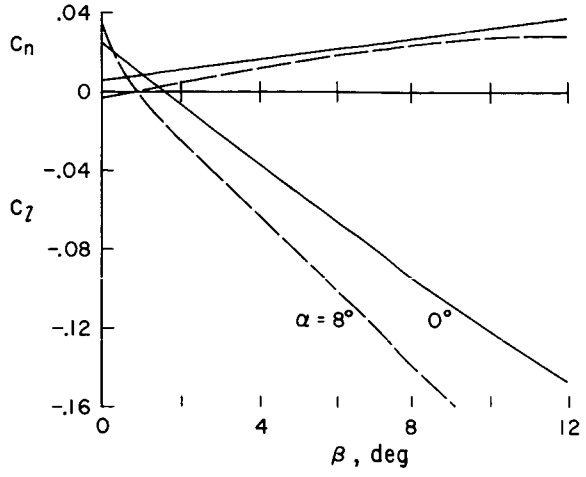

Figure 11

GROUND EFFECTS IN HOVER

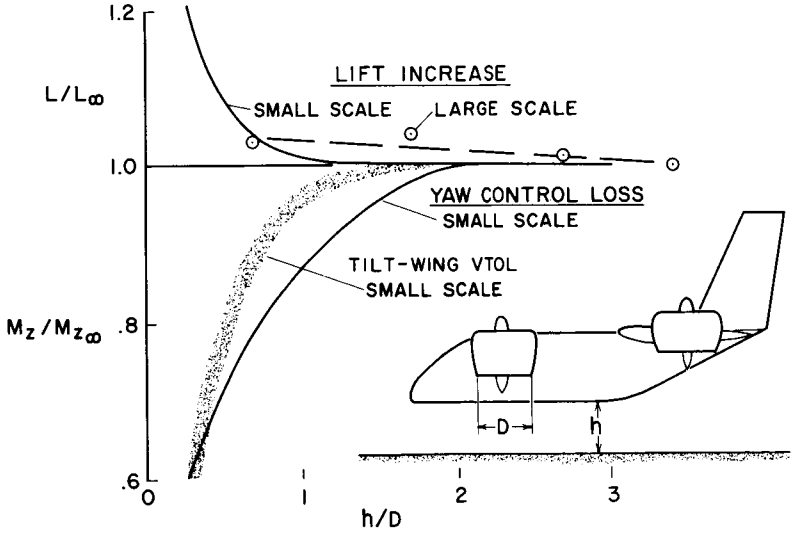

Figure 12

GROUND EFFECTS IN STOL OPERATION

LARGE-SCALE MODEL, $\alpha = 0°$

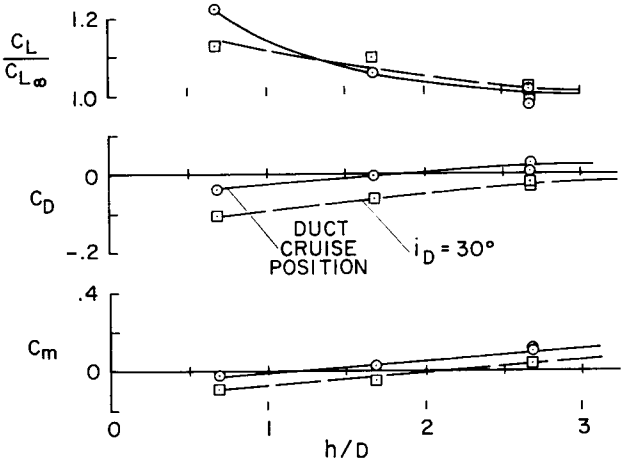

Figure 13

10. AN APPROACH TO EFFICIENT LOW-SPEED FLIGHT FOR FAN-POWERED V/STOL AIRCRAFT

By Marion O. McKinney, Lysle P. Parlett,
and William A. Newsom, Jr.

NASA Langley Research Center

SUMMARY

Exploratory tests have been performed at the Langley Research Center on a fan-powered V/STOL configuration which reduces the thrust required in transition flight to the desirably low values heretofore associated almost exclusively with tilt-wing and deflected-slipstream propeller-driven V/STOL configurations. The configuration employs cruise fans spaced out along the leading edge of a fixed wing having a large double-slotted trailing-edge flap. The fan exhaust is directed partly above and partly below the wing. That part of the fan exhaust which passes below the wing spreads out, blows virtually the entire flap system, and induces a circulation which efficiently produces large lift forces at low forward speeds.

Author

INTRODUCTION

The aerodynamicist has long known, and it has been pointed out many times, that the main feature required to get high efficiency in the transition speed range is to have the lift spread out more or less uniformly over as wide a span as possible. This requirement applies to the lift due to power as well as to the normal wing lift due to the free-stream flow. It has been possible to achieve desirable lift distributions with tilt-wing and deflected-slipstream propeller configurations in which the propellers blow fairly uniformly across the span. Until recently, however, all fan-powered configurations intended to accomplish this goal have had certain deficiencies, such as large internal losses, failure to achieve the full potential for inducing lift on the wing, or inherently low aspect ratio. This paper presents the results of some exploratory tests of a new fan-powered configuration which, by employing deflected-slipstream and jet-flap principles, produces large lift forces at high efficiency in the transition speed range.

SYMBOLS

A	aspect ratio
C_D	induced drag coefficient, $C_L^2/\pi A$

C_L lift coefficient, L/qS

$C_{L,\Gamma}$ lift coefficient due to jet-induced circulation

$C_{L,o}$ lift coefficient at $C_\mu = 0$ (no jet flow)

C_μ jet momentum coefficient, $m_j V_j/qS$

D drag, pounds

L lift, pounds

m_j jet mass flow rate, slugs/second

q_∞ free-stream dynamic pressure, $\left(\frac{\rho}{2} V^2\right)$, pounds/foot^2

R net resultant force, pounds

S wing area, feet^2

T net thrust, pounds

T_G gross thrust, pounds

V airspeed, feet/second

V_j jet exit velocity, feet/second

W weight of airplane, pounds

δ angle of jet deflection, degrees

δ_f angle of rear flap deflection, degrees

ρ air density, slugs/foot^3

DISCUSSION

The problem of thrust required in transition is illustrated in figure 1, which is a plot of thrust required against airspeed for level flight. The thrust required is divided by the weight of the airplane to make it nondimensional. The solid line to the right is the low-speed part of the thrust-required curve of a conventional airplane. In order to fly at speeds below the normal stalling speed, it is necessary to augment the aerodynamic lift of the airplane with power (or engine thrust). If this augmentation is done by simply adding vertical components of engine thrust, the thrust required is that

shown by the long-dash curve. In constructing this curve, it was assumed that the wing was operated at a lift coefficient of 2.0 throughout the transition speed range and that the extra thrust needed to support the airplane as the speed drops off was provided by tilting cruise fans mounted on the sides of the fuselage. The thrust required was then taken to be the total thrust required to provide the extra lift necessary and to propel the aircraft. Figure 1 also presents an induced-thrust curve. In constructing this curve it was assumed that the wing could produce as high a lift coefficient as is required for flight at the low speeds. If this lift were distributed in an elliptical span-load distribution across the entire span of the wing, the induced drag would be that calculated by the classical expression $C_L^2/\pi A$. The short-dash curve then shows the forward thrust required to propel such an airplane. Of course, the thrust required as calculated in this manner goes to infinity at zero airspeed. The important point, however, is that at intermediate speeds this induced-thrust curve is far below that calculated for the airplane with separate lifting engines. For example, the tick on the abscissa indicates approximately the speed at which approaches to vertical or short landings would be made. In this speed range, the thrust required would be markedly reduced if it were possible to operate on the induced-thrust curve instead of the one associated with the separate lifting engines. A new fan-powered configuration intended to have a thrust-required curve close to the induced-thrust curve of figure 1 is shown in figure 2.

The configuration has a wing of normal span, or aspect ratio, for a subsonic airplane; and it has high-bypass-ratio turbofan engines, of the type sometimes called cruise fans, spaced out across the span and blowing over the wing and flap to induce high lift on the wing. It was hoped that the part of the exhaust below the wing would spread laterally, blow through the slots of the flaps across the entire span, and induce a fairly high uniform lift across the wing by means of the jet-flap principle. In order to determine how well a configuration such as this will actually perform, a simple exploratory investigation is being conducted at the Langley Research Center with the small-scale semispan model shown in figure 3.

The model has a 3.5-foot-long rectangular wing with a 1-foot chord. The fans are 6 inches in diameter and have rectangular exits divided partly above and partly below the wing. The wing has a three-element slotted flap which will be described in detail. The tests completed to date are very limited in scope and there is no indication that any of the configurations tested are optimum. The model was tested first in still air to determine flap configurations that would give good slipstream turning effectiveness for hovering flight, and then, in forward flight using one of these flap configurations.

Before examining the results of these tests, it may be well to review one aspect of jet-flap aerodynamics to establish the definition of some terms. Figure 4 indicates that, for a jet flap, the lift is usually considered to be composed of three parts. The lift coefficient C_L is plotted against the jet momentum coefficient C_μ, which is the jet mass flow rate multiplied by the jet exit velocity divided by the free-stream dynamic pressure and wing area. This is the same momentum coefficient commonly used in boundary-layer control.

Also C_μ is a coefficient of gross thrust because the product $m_j V_j$ is the gross thrust of the fan. The lift is considered to be composed of $C_{L,o}$, which is the lift normally achieved in free-stream flow with no jet blowing; $C_\mu \sin \delta$, which is the lift due the vertical component of the deflected thrust; and $C_{L,\Gamma}$, which is the added circulation lift on the wing induced by the jet flow. This added circulation lift is usually considered to be a measure of the effectiveness of the jet flap and can be used to compare configurations having different amounts of physical flap, that is, different amounts of $C_{L,o}$.

Figure 5 shows a comparison of the added circulation lift due to the jet-flap action $C_{L,\Gamma}$ for the cruise-fan model shown in figure 3 with that for an idealized type of jet flap on a wing of the same aspect ratio. The upper curve is for a thin uniform jet sheet exhausting downward at a 45° angle all along the trailing edge of the wing. This jet-sheet configuration is chosen for comparison because it is generally accepted as being a very effective way of producing jet-induced circulation lift. The two lower curves show the results of tests with the present cruise-fan model. This model, as shown by the drawing in figure 5, has a double-slotted flap with a movable section ahead of the flap intended to improve the airflow into the first slot of the flap. The model was also provided with chordwise fences on the upper surface of the wing. These fences were in line with the edges of the fan exits and were as high as the fan exits. Without the fences, the flow from the upper fan exit will contract spanwise and thicken as it is deflected downward; that is, the upper part of the flow will not be deflected as much as that part immediately adjacent to the wing. The result of this distortion is a loss of turning effectiveness. The fences reduce the spanwise contraction and thereby reduce the thickening of the jet stream; thus, the turning effectiveness of the wing is increased. The fences are not employed on the bottom of the wing, where the fan flow naturally spreads spanwise into a continuous sheet which blows virtually through the entire slot and flap system.

The model was tested with and without fences. The data of figure 5 show that with the fences on, the added circulation lift induced by the fan was about 70 percent as great as that induced by the uniform jet sheet. It is also apparent that the contribution of the fences is very significant.

Similar data were obtained for other flap deflections, and these data have been plotted into a thrust-required curve as shown in figure 6. These test data are compared with the induced-thrust curve. This induced thrust is the same as shown in figure 1 and is simply the thrust required to overcome the drag calculated by the classical induced-drag equations. This induced-thrust curve was indicated in the early discussion to be a goal or a model of a good thrust-required curve. Figure 6 indicates that the thrust-required curve achieved with the model with the fans fairly widely spaced across the span is very nearly the same as the induced-thrust curve.

It can also be seen from figure 6 that the thrust losses involved when the flaps are deflected so that the fan exhaust is directed downward to produce lift for hovering flight are modest. At zero airspeed, a thrust-weight ratio of only 1.07 is required to support the aircraft for hovering flight, and

means that there was a thrust loss of only 7 percent in turning the slipstream essentially 90°.

The effects of some configuration variables on the performance in hovering flight are shown in figure 7, which presents the type of plot traditionally used to show the effectiveness of deflected-slipstream configurations in hovering flight. The ratio of total system lift to fan thrust is plotted against the ratio of net system drag to fan thrust. This drag is the total fore and aft force acting on the model and includes both fan thrust and wing drag. This plot can also be viewed as a polar plot to show the effectiveness of the wing flap system for turning the fan slipstream or vectoring its thrust. The radial lines show the slipstream deflection, or thrust vectoring angle; and the circular arcs show the ratio of resultant force to thrust, which is an indication of the efficiency of the system. The results in figure 7 are for 90° flap deflection. The data show the effect on hovering of two variables: the division of the fan exhaust above and below the wing, and the fences. The configuration in which all the fan exhaust goes beneath the wing is presented at the bottom of the key; and the test results for this configuration, indicated by the triangular symbol, show a high degree of slipstream turning, but a low degree of thrust recovery. The configuration in which the fan exhaust is split equally above and below the wing is shown at the top of the key. The data for this configuration, designated by a circular symbol, indicate substantially less slipstream-deflection angle and no better thrust recovery. The test results for the configuration in the center of the key, in which the exhaust is split with half as much going over the wing as goes beneath it, show substantially better results. With the fences off, the data show that the fan slipstream is turned about 82° with thrust recovery of 88 percent; and when the fences are installed, the turning angle increased to 88° and the thrust recovery, to 93 percent. This last condition is that shown at zero airspeed on the thrust-required curve of figure 6.

CONCLUDING REMARKS

Data from recent tests of a small semispan model of a turbofan-powered V/STOL configuration having a double-slotted trailing-edge flap indicate that the configuration has a desirably low thrust-required curve throughout the transition speed range. In this speed range, the thrust required is generally well below that calculated for a tilt-duct V/STOL configuration, and closely approximates the thrust required to overcome the induced drag as calculated by the classical induced-drag equation. Efficiency in hovering flight was good, a thrust-weight ratio of only 1.07 being required to support the aircraft at zero airspeed.

VARIATION OF THRUST REQUIRED WITH AIRSPEED

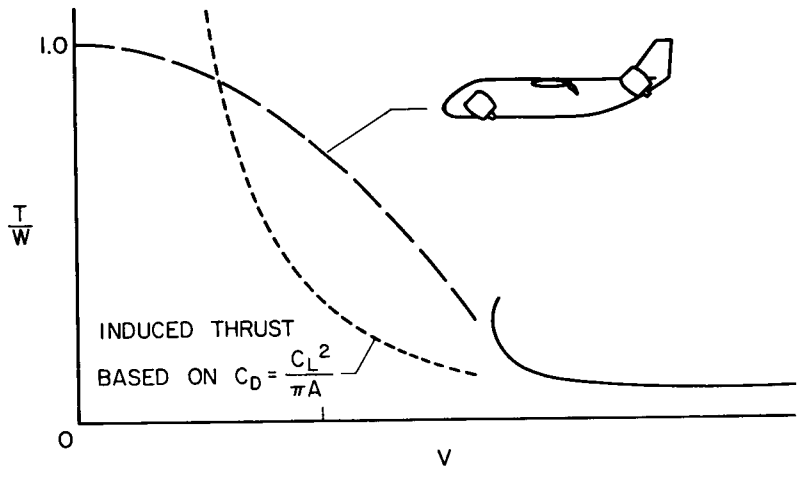

Figure 1

DEFLECTED-SLIPSTREAM CRUISE-FAN CONCEPT

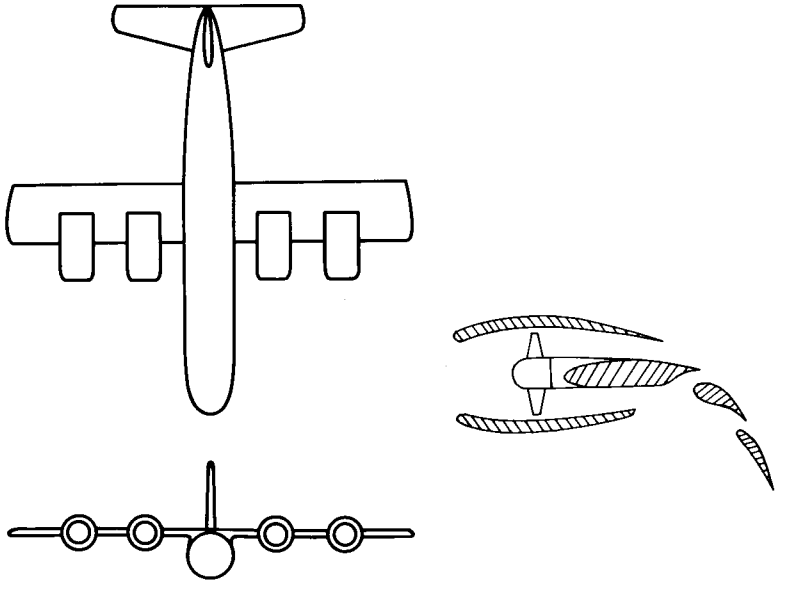

Figure 2

SEMISPAN TEST MODEL

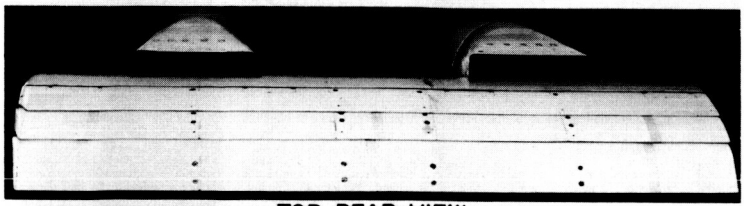

TOP REAR VIEW

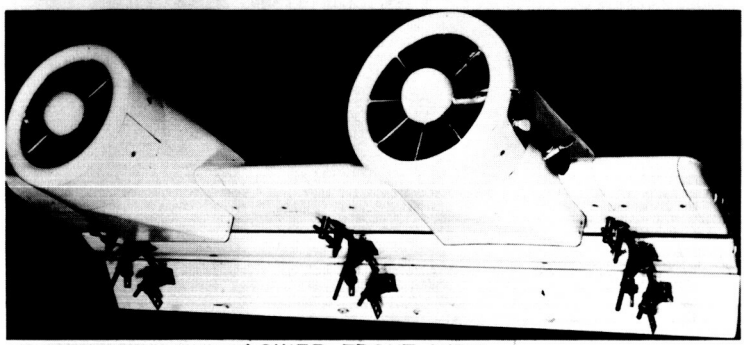

LOWER FRONT VIEW

Figure 3

LIFT BREAKDOWN FOR JET FLAP

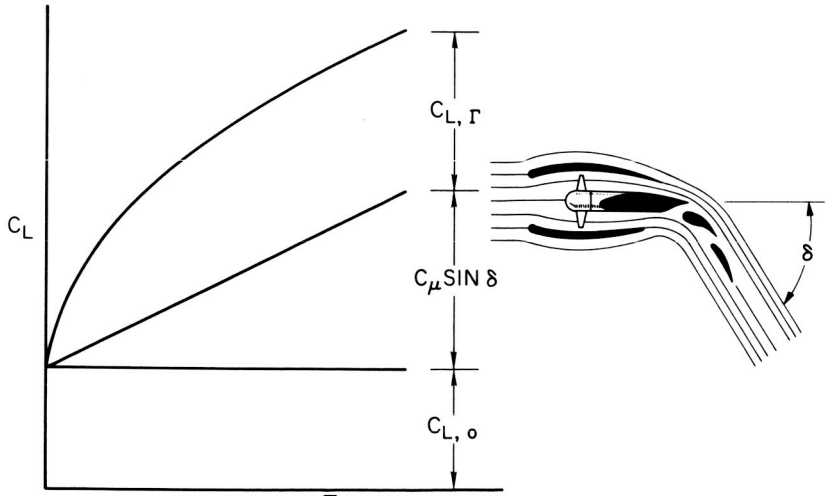

Figure 4

MEASURED JET-INDUCED LIFT

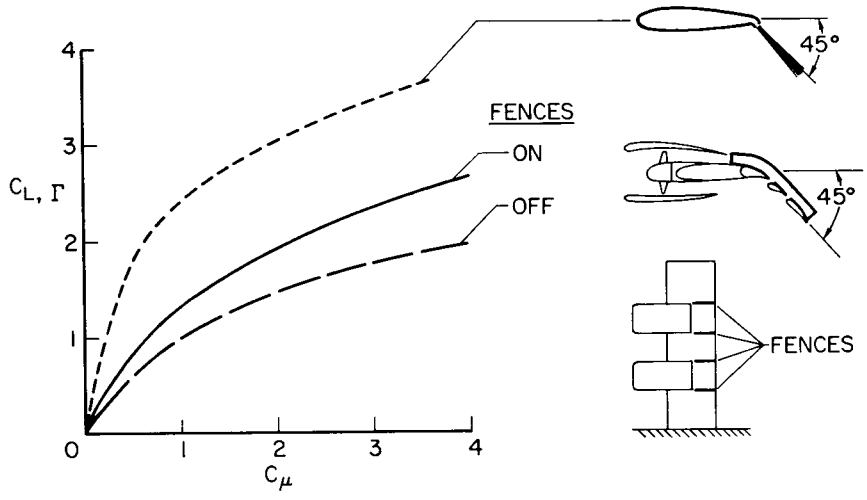

Figure 5

THRUST REQUIRED FOR TEST MODEL

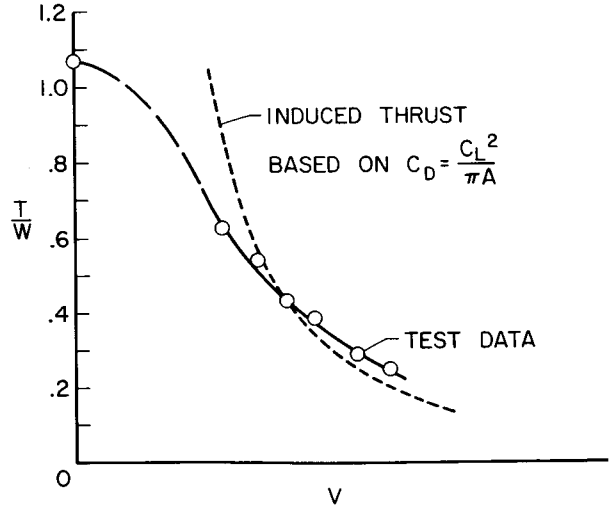

Figure 6

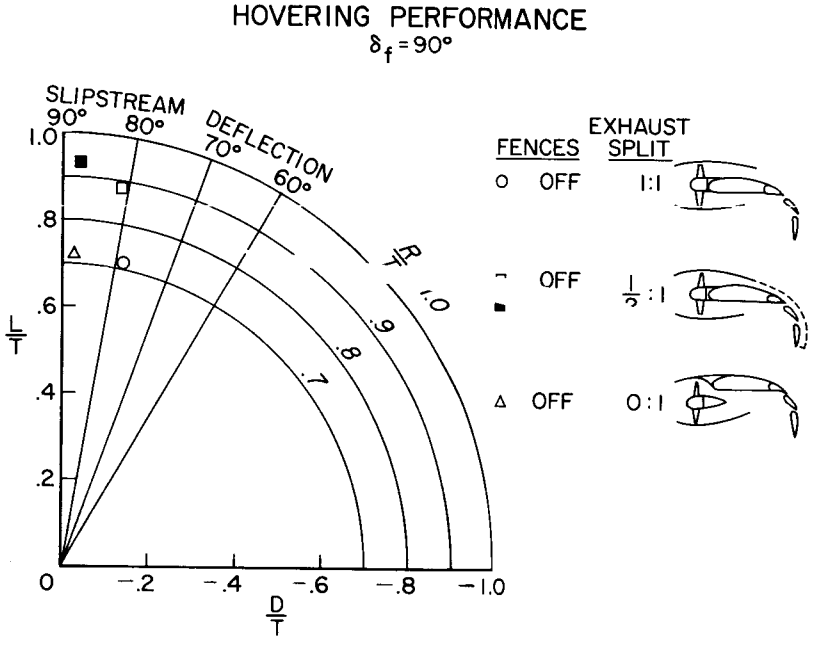
HOVERING PERFORMANCE
$\delta_f = 90°$
SLIPSTREAM DEFLECTION
90° 80° 70° 60°
1.0
.8
.6
.4
.2
0
$\frac{L}{T}$
$\frac{R}{T}$ 1.0
.9
.8
.7
−.2 −.4 −.6 −.8 −1.0
$\frac{D}{T}$
FENCES
EXHAUST SPLIT
○ OFF 1:1
OFF $\frac{1}{3}$:1
△ OFF 0:1

Figure 7

Page intentionally left blank

11. CRUISE PERFORMANCE AND STABILITY CONSIDERATIONS FOR JET V/STOL AIRCRAFT

By William J. Alford, Jr., and Roy V. Harris, Jr.

NASA Langley Research Center

SUMMARY

A study has been made of some of the conditions necessary to provide good cruise performance and stability characteristics for jet V/STOL aircraft with consideration of subsonic, supersonic, and multimission aspects. The study indicates that refinements in subsonic aerodynamic efficiency can be obtained by increases in wing span, reductions in wetted area, and improvements in airplane cleanliness. Refinements in supersonic efficiency can be obtained by increases in equivalent-body fineness ratio. Theoretical techniques and computer programs, which provide the modern aerodynamicist with rapid response time and flexibility in the overall design cycle, are available for complete configuration optimization.

Configurations utilizing composite-wing planforms with large fixed forewings are likely to have adverse wing-body pitching-moment characteristics and will require careful choice of vertical location of the horizontal tail to avoid pitch-up. Because of interactions of the lifting-jet system with the wing and horizontal tail, conflicts may exist between the cruise and V/STOL requirements for the composite-wing configurations.

For variable-sweep configurations, which offer high potential for multimission capability, an additional aerodynamic-center variation is associated with wing sweep. There are several schemes for minimizing this variation and also for controlling the aerodynamic-center shift associated with Mach number.

Author

INTRODUCTION

For V/STOL aircraft to provide desirable mission capability, the requirements of the take-off, transition, and landing modes must be satisfied without violating the principles for designing good cruise performance and stability characteristics into the aircraft.

It is the purpose of this paper to review some of the principles that should be considered to obtain good cruise performance and stability characteristics by presenting some recently declassified results on high-speed jet V/STOL aircraft, by describing some of the supersonic theoretical techniques and programs available for drag minimization, and by describing some areas of conflict between the requirements of the cruise and V/STOL

modes. Some of the more important subsonic, supersonic, and multimission performance and stability characteristics are considered.

SYMBOLS

b	wing span
C_D	drag coefficient
$C_{D,W}$	wave-drag coefficient based on frontal area
C_f	effective skin-friction coefficient
C_L	lift coefficient
C_m	pitching-moment coefficient
$\frac{\partial C_m}{\partial C_L}$	stability-level parameter
$\frac{\partial C_m}{\partial i_t}$	control-effectiveness parameter, deg
e	span efficiency factor
h	altitude
i_t	horizontal-tail incidence
L	lift
L/D	lift-drag ratio
M	Mach number
n	normal load factor, L/W
S	wing area
S_{wet}	wetted area
W	weight
α	angle of attack of reference line
θ	orientation angle of cutting plane
Λ	wing leading-edge sweep angle

Subscripts:

des	design
L	due to lift
max	maximum value
o	zero lift
opt	optimum
trim	conditions at $C_m = 0$

RELATIONSHIP OF PARAMETERS

Classic fundamentals are reviewed in this section to illustrate the parameters that will be considered and to show their relationship and magnitudes as well as to indicate the directions in which their variations should be guided to provide the highest performance and most desirable flying qualities.

The relationship between the performance and maneuverability parameters with the drag, stability, and control parameters is shown in figure 1. The data presented were obtained on a model of a jet V/STOL aircraft assumed to employ a vectored-thrust engine similar to that in the Hawker P 1127 VTOL airplane. (See refs. 1 and 2.)

With regard to stability, the parameters are the zero-lift pitching-moment coefficient $C_{m,o}$, the stability-level parameter $\frac{\partial C_m}{\partial C_L}$, and the control-effectiveness parameter $\frac{\partial C_m}{\partial i_t}$. A low value of $\frac{\partial C_m}{\partial C_L}$, consistent with acceptable handling qualities, is desirable in order to decrease trim drag and increase maneuvering capability. For a given level of $\frac{\partial C_m}{\partial C_L}$, a value of $C_{m,o}$ sufficient to provide trim at $(L/D)_{max}$ is desirable.

With regard to drag, the components or parameters are friction, wave, trim, and drag due to lift. The classical problem is to minimize each of these components without incurring weight penalties. To illustrate the effect of stability level on the trimmed drag polars, curves are shown in figure 1 for $\frac{\partial C_m}{\partial C_L}$ levels of 0, -0.10, and -0.20.

To illustrate the relationship of the performance and maneuverability with stability level, trimmed maximum lift-drag ratio and control-limited normal load

factor are shown in the right-hand side of figure 1. The highest values of $\left[(L/D)_{trim}\right]_{max}$ and n occur for the lower stability levels.

SUBSONIC CONSIDERATIONS

The subsonic aerodynamic efficiency, as measured by $(L/D)_{max}$, can be correlated linearly with the ratio of the span of an aircraft to the square root of its wetted area for given values of effective skin friction and span efficiency. Such a correlation for fighter, bomber, and transport aircraft is presented in figure 2. The correlating equation in this figure shows that the ratio of the span efficiency factor to the effective skin-friction coefficient is an additional governing parameter. The value of the inverse of this parameter, that is, C_f/e, is given on the mean-line fairing drawn through the data points. It should be noted that the effective skin-friction coefficient also includes components of form and pressure drag.

The data for the conventional aircraft are based on flight tests in the clean configuration. Addition of external stores or deterioration of surface cleanliness would seriously reduce these levels. For the V/STOL aircraft, the data were based largely on design studies since flight data on these types are, as yet, very limited.

For the data available on the V/STOL fighters (fig. 2(a)), the effective friction levels are essentially the same as those for the conventional aircraft; but because of lower values of $\frac{b}{\sqrt{S_{wet}}}$, the values of $(L/D)_{max}$ are lower. For the V/STOL transports (fig. 2(b)), both the effective friction levels and the span ratios are in an adverse direction; consequently, the performance parameters for the V/STOL transports are considerably lower than those for the conventional aircraft. This correlation clearly indicates the directions in which V/STOL configuration refinement should be made to improve the subsonic aerodynamic performance.

With regard to stability, one of the main tasks the aircraft designer is faced with, in trying to provide high performance levels and acceptable flying qualities, is the angle-of-attack divergence known as pitch-up, which results from nonlinear destabilizing pitching-moment characteristics. An example of the effect of wing planform geometry on pitching-moment linearity for wing-body combinations is shown in figure 3. Additional data on such wing-body combinations are presented in reference 3.

For the 20° sweptback wing with the relatively straight leading edge (see bottom curve in fig. 3), a reasonably linear pitching-moment variation with C_L is obtained. The addition of a highly swept low-aspect-ratio forewing to this 20° sweptback wing causes undesirably large destabilizing nonlinearities. Such a composite wing is representative of a variable-sweep wing with an outboard pivot, which, as will be shown subsequently, is desirable in controlling

the aerodynamic-center movement associated with wing sweep. As indicated by figure 3, the pitching-moment variation for the composite wing exhibits more destabilizing nonlinearity than that for the 45° sweptback wing shown for comparison.

The interaction between the flow field and the geometric layout of the composite wing is as follows: Since the forewing is highly swept and of low aspect ratio, its lift contribution is nonlinear and varies as α^2; and, because of its longitudinal location, this lift is destabilizing. The high-aspect-ratio outer panel with the lower sweep, on the other hand, provides a lift contribution that varies linearly with angle of attack; and, because of its longitudinal location, this lift is less destabilizing than that associated with the forewing. At the low lifts, therefore, the high-aspect-ratio portion of the wing is dominant but reaches its maximum level fairly early since it is flying in the upwash induced by the forewing. These induced angles cause early stall of the wing-tip sections, whereas the lift of the forewing continues to increase and thereby leads to the nonlinear destabilizing pitching-moment variations shown in figure 3.

In addition to the problem of cruise pitch linearity shown in figure 3, the addition of the forewing area could, depending on its relation to, and interaction with, the lifting jets, cause lift loss in the V/STOL modes. This subject is discussed in paper no. 12 by Alexander D. Hammond.

Two methods that may be used to provide acceptable pitching-moment variations for complete configurations employing composite wings are the utilization of wing flow-control devices and the proper choice of the vertical location of the horizontal tail. Results for a complete configuration for various vertical locations of the horizontal tail are presented in figure 4. As shown in this figure for the composite-wing—body configuration, the lowest tail location (designated H_1) provides the most desirable pitching-moment variation, with extremely nonlinear destabilizing contributions being associated with the higher tail locations (H_2 and H_3). For wing-body configurations whose pitching-moment curves are unstable and nonlinear, a high tail location further compounds these nonlinear characteristics. These data again indicate that in order for a high tail location to be effective, it should be combined only with wing-body configurations whose pitching-moment curves become stable at the higher lifts (ref. 4).

As indicated by the data of figure 4, the low tail provides the lowest initial level of stability since it is initially in a field of relatively high downwash. As the lift coefficient is increased, however, the tail moves out of the wing-body flow field and becomes more effective. For the highest tail locations, which are initially in a relatively undisturbed field, an increase in lift coefficient moves such tails into an even higher downwash field, with lowered dynamic pressures, and causes them to lose their contribution to stability.

In the V/STOL modes, the powered-lift system has a pronounced effect on the flow field in the region of the horizontal tail. This induced flow field

has, in general, less influence as the horizontal tail is moved higher above the wing chord plane. A conflict exists, therefore, between the V/STOL and cruise requirements with regard to horizontal-tail location, and more research is required to eliminate or satisfy the conflict. Some recent work on jet-induction effects is discussed in paper no. 13 by Richard D. Margason.

SUPERSONIC CONSIDERATIONS

To provide background and perspective for the various available supersonic theoretical techniques and programs, figure 5 presents a component breakdown for the drag polar of the V/STOL airplane of references 1 and 2 for a Mach number of 1.97. The data shown have been corrected, by a skin-friction extrapolation, to correspond to full-scale conditions at an altitude of 50,000 feet. For reference, the lift coefficient for maximum lift-drag ratio (that is, $C_{L,opt}$) is shown by the tick. In this plot, the various components are the equivalent flat-plate skin-friction coefficient, the zero-lift wave drag, the drag due to lift (which includes wave and vortex components), and the trim drag due to control-surface deflections.

For lift coefficients less than optimum, which would correspond to lower altitude flight, the wave drag tends to assume more importance in that it is almost twice the friction level. For lift coefficients above $C_{L,opt}$, where the aircraft would be in maneuvering flight, the drag due to lift becomes the dominant component. For cruise flight, at $C_{L,opt}$, all components, including the trim drag, become important. For the example shown, the trim drag associated with an assumed 10-percent stability level reduced the value of $(L/D)_{max}$ by approximately 10 percent. Higher levels of stability would cause even higher penalties. It is desirable, therefore, to utilize the lowest stability level possible, consistent with acceptable flying qualities, in order to minimize the trim drag and provide the highest value of $(L/D)_{max}$. Another method of controlling trim drag is by providing the proper level of zero-lift pitching-moment coefficient for a given stability level.

One of the items that makes some V/STOL aircraft designs more complex than conventional aircraft is the severe volumetric constraint imposed by the requirement for having dual-propulsive-system elements to provide lift as well as thrust. An example of the influence of this constraint on the equivalent-body fineness ratio and the associated wave-drag coefficient (based on frontal area) is presented in figure 6. The V/STOL configurations, from references 1, 2, 5, and 6, have lower equivalent-body fineness ratios and hence higher wave-drag coefficients than do the conventional take-off and landing configurations (CTOL). For these particular V/STOL configurations, which were designed around vectored-thrust engine concepts, the distributions of area were not too different from those for the CTOL configurations, which attempted to maintain the optimum area distributions of the length-volume Sears-Haack bodies as shown by the relation of the data points to the optimum curve. For configurations utilizing separate lift and cruise engine systems, the frontal area, for a given length, should be somewhat smaller than that for the vectored-thrust concepts;

this refinement would allow the fineness ratios to be higher and hence provide wave-drag coefficients somewhat closer to those for the CTOL configurations.

For higher supersonic Mach numbers ($M > 1.2$) and for configurations slender enough to satisfy the requirements of linearized supersonic theory, recent theoretical techniques and programs have been developed at the Langley Research Center in conjunction with the aircraft industry. These techniques and programs provide the modern aerodynamicist with a rapid response time and hence greater input and flexibility in the overall design cycle.

One of the most useful of the new techniques is a computer program (ref. 7) for the determination of aircraft wave drag at zero lift. Earlier efforts to utilize the linearized theory of Hayes (ref. 8) depended on laborious graphical schemes for determining the many equivalent bodies required. The current program accomplishes the geometric exercises within the computer in a matter of minutes. Print-out sheets are provided which give a component breakdown of each equivalent-body area distribution so that the effect of each component on the wave drag can be examined.

Shown in figure 7 is an example of how the airplane configuration is described to the computer. The computer input consists of a table of x,y,z coordinates which describe the airplane components. These data are independent of Mach number and need be determined only once. The computer is programed to take this input and make the necessary cuts at the required orientation angles, as shown by the angle θ, for each Mach number. The computer then derives the equivalent bodies, the corresponding mathematical source-sink distribution, and the resulting wave drag.

The correlation of experimental and computed wave-drag coefficients for complex complete configurations for the Mach number range from 1.4 to 3.2 is also shown in figure 7. The configurations represented by the data points vary from fighter vehicles with fineness ratios on the order of 7 to 9 (at the upper right) to bombers and transports with fineness ratios of about 13 (at the lower left). Very good agreement is indicated.

Another program is available, based on the work of reference 9, which uses the same geometric input data as those used in the wave-drag program to calculate the wetted areas and reference lengths of the various aircraft component parts from which the friction drag is obtained.

With regard to supersonic drag due to lift, the computer has been programed to calculate, for reference, the characteristics of the equivalent flat wing (ref. 10) and the optimum lower bound polar (ref. 11) in addition to those for the particular warped wing of interest. As shown in the sketch in figure 8, the wing surface is represented as a series of lifting elements which, when integrated, under the desired constraints, provide either the camber and twist surface necessary to support specified chord and span loadings or the aerodynamic characteristics of a specified warped surface. An example of the degree to which the theory is capable of predicting the aerodynamic characteristics is shown in figure 8. Excellent agreement is evident for both the flat wing ($C_{L,des} = 0$) and the twisted and cambered wing

with a design lift coefficient of 0.08, the drag of which is considerably lower in the useful lift-coefficient range.

In addition to providing improvements in the lift-drag ratios due to improved lifting efficiency, properly warped wings also provide a positive pitching-moment coefficient at zero lift $C_{m,o}$, which aids greatly in trimming the configuration. This is particularly true for wings with subsonic leading edges, where advantage can be taken of the induced upwash angles produced by the lifting apex portions of the wing. Some results of variation of zero-lift pitching-moment coefficient and $(L/D)_{max}$ with design lift coefficient are shown in figure 8 for a 70° swept arrow wing at $M = 2.05$. Sketches which indicate the degree of wing warp are shown at their respective design lift coefficients.

Note, in figure 8, that for the highest design lift coefficient (0.16), which provides the highest values of $C_{m,o}$, even though the linear theory is unable to represent the real flow over the highly distorted wing, both this wing and the wing designed for the more reasonable lift coefficient (0.08) give higher values of $(L/D)_{max}$ than the flat wing, which has a design lift coefficient of zero.

In complete configuration optimization, local interference effects must be carefully considered to provide the highest possible aerodynamic efficiency (ref. 12). An example of how these interference effects can be made favorable is illustrated in figure 9. Shown in figure 9 is an arrow wing with engine nacelles located beneath the wing, near the trailing edge, so that the compressions from the nacelle impinge on the receding slopes of the wing and the expansions from the wing impinge on the advancing slopes of the nacelle.

Illustrative aerodynamic characteristics of such a wing-nacelle combination, with an unreflexed wing trailing edge, are shown by the dashed-line curves in figure 9. The negative zero-lift pitching-moment coefficient is a result of the interference lift from the nacelle compressions acting on the rear portions of the wing surface, aft of the moment reference center. Note also that the maximum trimmed lift-drag ratio, for this configuration, occurs in the unstable region and requires considerable control deflections in the stable region with large reductions in $(L/D)_{max}$. This situation can be improved considerably by reflexing the wing trailing edge upward sufficiently (solid-line curves) to cancel the interference lift. This refinement thereby alleviates the adverse $C_{m,o}$ and reduces the pressure drag because the lower surface slopes, on which the nacelle interference pressures act, have been increased and the upper surface slopes have been decreased. The result of providing slightly lower drag and of canceling the adverse $C_{m,o}$ leads to values of $(L/D)_{max}$ that are substantially higher than those for the unreflexed configuration.

For configurations employing wing-mounted vertical tails, correct alinement with the local sidewash can provide tail-surface thrust components large enough to cancel their friction and wave drag. Such vertical tails may

therefore be utilized without drag penalty (ref. 12). A simple analysis has shown that the optimum alinement angle is one-half the average of the local sidewash angles (ref. 13).

To demonstrate how the aforementioned techniques and programs are utilized in complete airplane configuration optimization, figure 10 presents results for a 74° swept arrow-wing—body—vertical-tail combination with nacelles for a design Mach number of 2.6. This configuration is a high-performance supersonic-transport type and is not suggested as a possible V/STOL aircraft. Nevertheless, the design principles applied in this case might be used just as well for a V/STOL design, provided certain assumptions, to be discussed subsequently, are not violated. For reference, results for a flat-wing—body combination are also presented. The complete configuration incorporated a twisted and cambered wing to minimize the drag due to lift and to provide a positive value of $C_{m,o}$ so that the configuration was self-trimming at its design lift coefficient. The wing also utilized trailing-edge reflex, as discussed previously, to obtain drag benefits from the nacelles without incurring penalties in $C_{m,o}$ due to the nacelle interference lift. The vertical tails were alined to minimize their drag.

The theoretical results, obtained by utilizing the aforementioned techniques, are represented in figure 10 by the solid lines and show very good agreement with the experimental results for both the flat-wing—body combination and the complete configuration. More important is the fact that the complete configuration has lower drag values at reasonable lift coefficients than does the flat-wing—body combination. With regard to the maximum trimmed lift-drag ratios, those of the complete configuration are higher than those of the reference flat-wing configuration at reasonable stability levels. Also, the $\left[(L/D)_{trim}\right]_{max}$ variation for the complete configuration (square symbols) is far more tolerant of changes in stability level than that for the reference configuration (circular symbols).

In summarizing the theoretical techniques and programs, it is obvious that much-improved aerodynamic efficiency is achieved by their use and that they are capable of predicting the aerodynamic characteristics for configurations which satisfy the basic assumptions of linear theory. Because of the linear-theory assumptions, however, successful use of the programs requires some experience and judgment on the part of the user. The programs should not be expected to predict results for thick or low-fineness-ratio configurations having surface slopes that are high enough to cause flow separation or detached shocks. These types of configurations would not be suitable for efficient supersonic flight. The programs are extremely useful, however, in preliminary design analysis and can minimize the volume of wind-tunnel testing which will be required in the development of any new configuration.

MULTIMISSION CONSIDERATIONS

The requirements for high aerodynamic efficiency at subsonic and supersonic speeds are in some respects incompatible since optimum flight at subsonic speed is generally obtained for configurations with high span wings (see fig. 2) of relatively low sweeps (0° to 35°) and with equivalent-body fineness ratios of the order of 6 to 7. Optimum supersonic flight, on the other hand, is generally obtained for configurations with highly swept wings (preferably with subsonic leading and trailing edges) of lower aspect ratio and with equivalent-body fineness ratios between 11 and 13 (see fig. 10). Due to the present inability to change the flow laws substantially, the designer, in attempting to provide multimission capability (that is, provide efficient flight throughout the Mach and altitude spectrums with a single configuration), generally has to use some additional form of variable geometry (ref. 14). Of the many forms of variable geometry, variable wing sweep has received a great deal of attention and a considerable volume of information is now available. (For example, see refs. 1, 2, 3, 5, 6, and 14 to 22.)

With regard to performance, an indication of what should be possible in the way of multimission capability for V/STOL as well as for conventional aircraft is shown in figure 11, which presents illustrative $(L/D)_{max}$ variations with Mach number for optimum altitudes. In this figure, characteristics for fixed-wing configurations with subsonic and supersonic design Mach numbers are also shown. For these fixed-wing aircraft, all other combinations of Mach number and altitude are off-design conditions and the performance is seen to suffer. The performance possible with a multimission variable-sweep configuration is shown by the solid-line curve. In comparing these data with those for the fixed-wing aircraft, the performance would be expected to be slightly lower at the respective design points because of the fairing and surface cleanliness problems attendant with the moving parts; however, attractive performance levels which allow multimission capability throughout the Mach number range are indicated.

With regard to stability, as pointed out previously, it is desirable to have the lowest stability level possible, consistent with acceptable flying qualities, in order to minimize trim drag and to maximize the available control-limited maneuver load factor. For all configurations, both fixed and variable sweep, there is a rearward shift in the aerodynamic center that accompanies the transition from subsonic to supersonic speeds due to the change in the chordwise load distributions. For variable-sweep aircraft, an additional aerodynamic-center variation is present with wing sweep.

An example of the variation of the aerodynamic-center location with wing sweep is presented in figure 12. These data are for the V/STOL configuration of references 1 and 2. If an inboard pivot location is employed, as shown by the dashed-line wing, a large difference in stability level exists between the low-sweep and high-sweep positions (12 percent of the mean aerodynamic chord) and the center of gravity must be placed relatively far forward on the aircraft to provide stability throughout the sweep and Mach number ranges. For the inboard pivot shown, the overall aerodynamic-center variation between the

lowest sweep—lowest Mach number condition and the highest sweep—highest Mach number condition is approximately 25 percent of the mean aerodynamic chord.

If an outboard pivot is utilized, the stability level for the low-sweep condition can be made essentially the same as for the high-sweep condition and the overall aerodynamic-center variation with wing sweep and Mach number is reduced by approximately one-half. It should be noted that an important trade-off exists between pitching-moment-curve linearity (fig. 3) and the aerodynamic-center variation with wing sweep as affected by pivot locations (fig. 12) since the pivot locations govern the amount of fixed forewing area. In fact, it is this relationship between the size of the fixed forewing area and the size of the movable panel area, in combination with the longitudinal location of the movable panel, that determines the aerodynamic-center variation with wing sweep. A useful subsonic-lifting-surface-theory computer program is available at the Langley Research Center and allows a rapid systematic study of the effects of pivot location.

Earlier variable-sweep aircraft such as the Bell X-5 research airplane and the Grumman XF10F airplane successfully utilized wing translation as a method of adjusting the aerodynamic-center and center-of-gravity relationship. Although this approach was successful from aerodynamic and piloting considerations, it was reported to present weight and usable volume problems. This approach has not recently been utilized.

Another method of providing aerodynamic-center control with wing sweep, which essentially eliminates the adverse nonlinear destabilizing effects associated with the fixed forewing (fig. 3), is by use of double inboard pivots. (See ref. 21.) In this approach, two inboard pivots are used to vary the sweep of the inboard forewing as well as that of outboard wing so as to provide straight unbroken leading edges in both the low- and high-sweep positions. Using a free-floating wing apex (see ref. 17) is another method of controlling the aerodynamic-center variation associated with wing sweep.

With regard to control of the aerodynamic-center variation associated with Mach number (see fig. 12), several schemes are available, each having different degrees of mechanical complexity and reliability. One of the most obvious is to accept the aerodynamic-center shift and to change the center-of-gravity location by mass transfer. This approach is the one chosen by the designers of the Anglo-French Concorde supersonic transport, where fuel pumping is the mode of mass transfer. Some examples of other approaches use the following variable geometries: foldable, extendible, or variable-sweep canards; translating or variable-sweep horizontal tails; and extendible wing trailing edges.

For low-altitude transonic or supersonic flight, the dynamic pressure is high enough so that only a minimum amount of wing area is needed to sustain flight. In addition, the desire for providing the pilot with the least fatiguing ride and for increasing aircraft life leads to the requirements of low lift-curve slope and high wing loading, both of which are satisfied by minimum wing area. For configurations employing minimum-size wings, the tail span and tail volume become dominant factors in determining the longitudinal

characteristics. Some results obtained for models of V/STOL aircraft (ref. 5) indicate this fact. These results are presented in figure 13.

The sketch shown in the upper left-hand part of figure 13 is a variable-wing-sweep configuration with the wing sweep (outer panel) at 108° and the sketch shown in the upper right-hand part of the figure is a skewed-wing configuration with the wing in its 90° position. For these configurations, the small tail did not provide stability at the low lift coefficients although it was adequate for lower sweep angles (ref. 5). It is presumed that the vortices trailing from the wing tips, as shown in the sketches, produce high downwash angularities and render the small tail ineffective. Increasing the tail span to put its tip outboard of the vortices, in regions of upwash, produces a large stabilizing contribution at the expense of an increase in lift-curve slope. It should be noted, in this comparison, that since the tail volume was not held constant, the absolute contribution of tail span and tail volume cannot be separated conclusively.

SUMMARY OF RESULTS

A review of some of the conditions necessary to provide good cruise performance and stability characteristics for jet V/STOL aircraft - with particular consideration of the subsonic, supersonic, and multimission aspects - indicates the following points:

1. It is desirable to provide the lowest stability level possible, consistent with acceptable flying qualities, in order to minimize trim drag and to maximize control-limited maneuver load factor.

2. Refinements in subsonic aerodynamic efficiency for V/STOL aircraft can be obtained by increases in wing span, reduction in wetted area, and by careful attention to detail in the construction of the aircraft, especially in areas of high-lift systems, gaps, and surface finish.

3. Refinements in supersonic aerodynamic efficiency of V/STOL configurations can be obtained by increases in the equivalent-body fineness ratio. At present, the fineness ratios for V/STOL configurations are lower than those for conventional aircraft because of the volumetric constraints imposed by the use of dual propulsive systems.

4. Configurations that utilize composite-wing planforms with large fixed forewings are likely to have adverse wing-body pitching-moment characteristics, which will require careful choice of the vertical location of the horizontal tail to avoid pitch-up.

5. For the composite-wing configurations, conflicts between the requirements of the cruise and V/STOL modes may exist because of the interactions of the lifting-jet system with the wing and horizontal tail.

6. Theoretical techniques and programs are available which provide the modern aerodynamicist with rapid response time and flexibility in the overall design cycle. These techniques, with proper experience and judgment, provide excellent tools for use in preliminary design analysis and for minimizing the volume of wind-tunnel tests.

7. For variable-sweep configurations, which offer high potential for multimission capability, an additional aerodynamic-center variation is associated with wing sweep. There are several schemes for minimizing this variation and also for controlling the aerodynamic-center shift associated with Mach number.

REFERENCES

1. Luoma, Arvo A.; and Alford, William J., Jr.: Performance, Stability, and Control Characteristics at Transonic Speeds of Three V/STOL Airplanes With Wings of Variable Sweep. NASA TM X-321, 1960.

2. Foster, Gerald V.; and Morris, Odell A.: Aerodynamic Characteristics in Pitch at a Mach Number of 1.97 of Two Variable-Wing-Sweep V/STOL Configurations With Outboard Wing Panels Swept Back 75°. NASA TM X-322, 1960.

3. Spencer, Bernard, Jr.: Low-Speed Longitudinal Aerodynamic Characteristics Associated With Variations in the Geometry of the Fixed Portion of a Variable-Wing-Sweep Airplane Configuration Having an Outboard Pivot. NASA TM X-625, 1962.

4. Spreeman, Kenneth P.: Design Guide for Pitch-Up Evaluation and Investigation at High Subsonic Speeds of Possible Limitations Due to Wing-Aspect-Ratio Variations. NASA TM X-26, 1959.

5. Luoma, Arvo A.: Longitudinal Aerodynamic Characteristics at Transonic Speeds of Two V/STOL Airplane Configurations With Skewed and Variable-Sweep Wings. NASA TM X-527, 1961.

6. Morris, Odell A.; and Foster, Gerald V.: Static Longitudinal and Lateral Aerodynamic Characteristics at a Mach Number of 2.20 of a V/STOL Airplane Configuration With a Variable-Sweep Wing and With a Skewed Wing Design. NASA TM X-521, 1961.

7. Harris, Roy V., Jr.: An Analysis and Correlation of Aircraft Wave Drag. NASA TM X-947, 1964.

8. Hayes, Wallace D.: Linearized Supersonic Flow. Rept. No. AL-222, North Am. Aviation, Inc., June 18, 1947.

9. Peterson, John B., Jr.: A Comparison of Experimental and Theoretical Results for the Compressible Turbulent-Boundary-Layer Skin Friction With Zero Pressure Gradient. NASA TN D-1795, 1963.

10. Middleton, Wilbur D.; and Carlson, Harry W.: A Numerical Method for Calculating the Flat-Plate Pressure Distributions on Supersonic Wings of Arbitrary Planform. NASA TN D-2570, 1965.

11. Carlson, Harry W.; and Middleton, Wilbur D.: A Numerical Method for the Design of Camber Surfaces of Supersonic Wings With Arbitrary Planforms. NASA TN D-2341, 1964.

12. Robins, A. Warner; Morris, Odell A.; and Harris, Roy V., Jr.: Recent Research Results in the Aerodynamics of Supersonic Vehicles. Paper No. 65-717, Am. Inst. Aeron. Astronaut., Nov. 1965.

13. Landrum, Emma Jean: Effect of Nacelle Orientation on the Aerodynamic Characteristics of an Arrow Wing-Body Configuration at Mach Number 2.03. NASA TN D-3284, 1966.

14. Baals, Donald D.; and Polhamus, Edward C.: Variable Sweep Aircraft. Astronaut. Aerospace Eng., vol. 1, no. 5, June 1963, pp. 12-19.

15. Alford, William J., Jr.; and Henderson, William P.: An Exploratory Investigation of the Low-Speed Aerodynamic Characteristics of Variable-Wing-Sweep Airplane Configurations. NASA TM X-142, 1959.

16. Spencer, Bernard, Jr.: Stability and Control Characteristics at Low Subsonic Speeds of an Airplane Configuration Having Two Types of Variable-Sweep Wings. NASA TM X-303, 1960.

17. Polhamus, Edward C.; and Hammond, Alexander D.: Subsonic Aerodynamic Characteristics of an Airplane Configuration Utilizing a Variable-Sweep Wing Having a Free-Floating Apex. NASA TM X-1126, 1965.

18. Spearman, M. Leroy; and Foster, Gerald V.: Static Longitudinal and Lateral Aerodynamic Characteristics at a Mach Number of 2.01 of a Tailless Delta V/STOL Configuration Having Variable-Sweep Wing Panels. NASA TM X-634, 1961.

19. Luoma, Arvo A.: Longitudinal Aerodynamic Characteristics at Transonic Speeds of a V/STOL Airplane Configuration With a Fixed Delta Wing Having Auxiliary Variable-Sweep Outboard Panels. NASA TM X-661, 1961.

20. Foster, Gerald V.; and Morris, Odell A.: Stability and Control Characteristics at a Mach Number of 1.97 of an Airplane Configuration Having Two Types of Variable-Sweep Wings. NASA TM X-323, 1960.

21. Polhamus, Edward C.; Alford, William J., Jr.; and Foster, Gerald V.: Subsonic and Supersonic Aerodynamic Characteristics of an Airplane Configuration Utilizing Double-Pivot Variable-Sweep Wings. NASA TM X-743, 1962.

22. Luoma, Arvo A.: Stability and Control Characteristics at Transonic Speeds of a Variable-Wing-Sweep Airplane Configuration With Outboard Panels Swept 113.24° and 75°. NASA TM X-342, 1960.

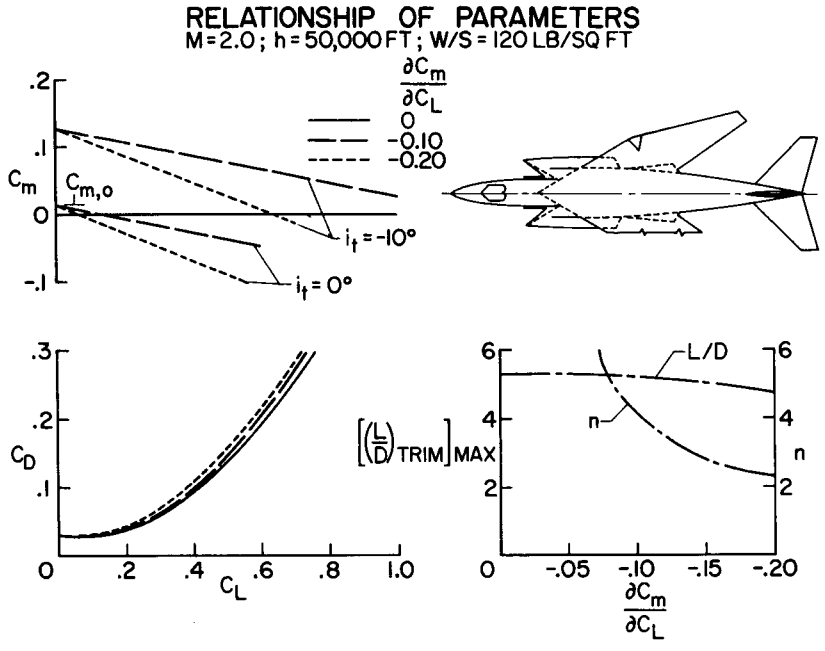
RELATIONSHIP OF PARAMETERS
M=2.0; h=50,000 FT; W/S=120 LB/SQ FT
∂Cm/∂CL
0
-0.10
-0.20
Cm
Cm,o
.2
.1
0
-.1
it = -10°
it = 0°
CD
.3
.2
.1
0
.2
.4
.6
.8
1.0
CL
[(L/D)TRIM]MAX
L/D
n
6
4
2
-.05
-.10
-.15
-.20
∂Cm/∂CL

Figure 1

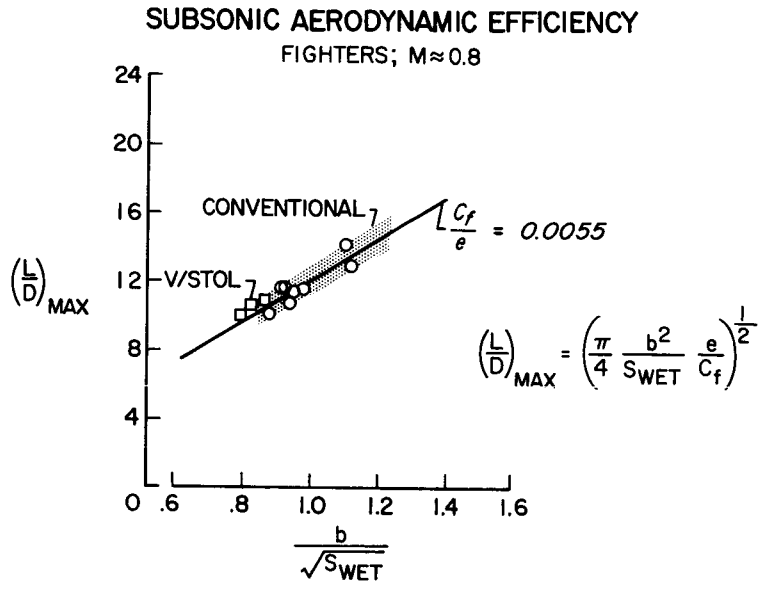

Figure 2(a)

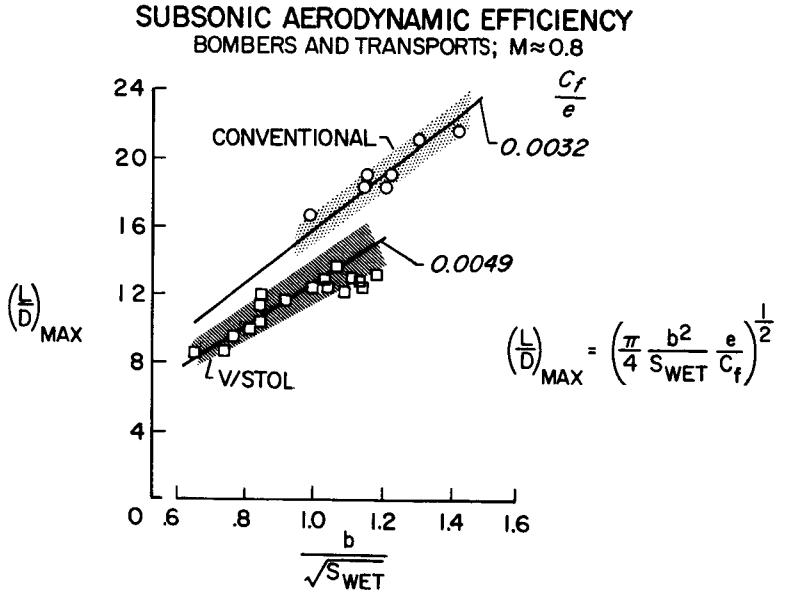

Figure 2(b)

PITCH-UP CONSIDERATIONS
WING-BODY

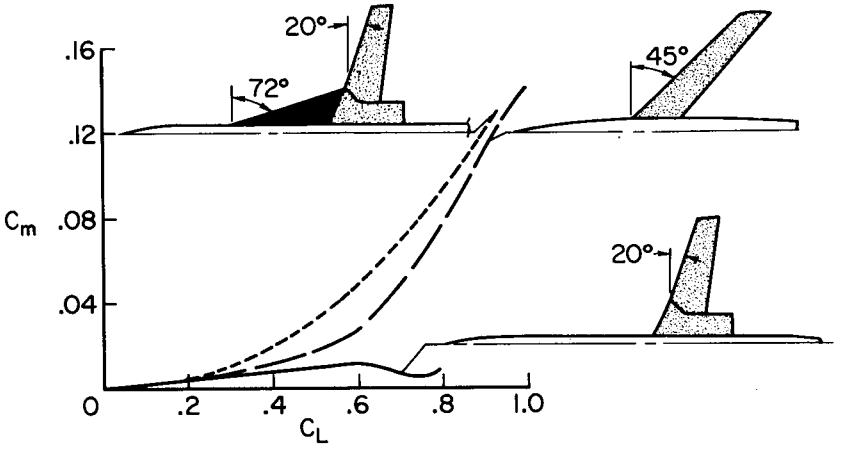

Figure 3

EFFECTS OF HORIZONTAL-TAIL HEIGHT

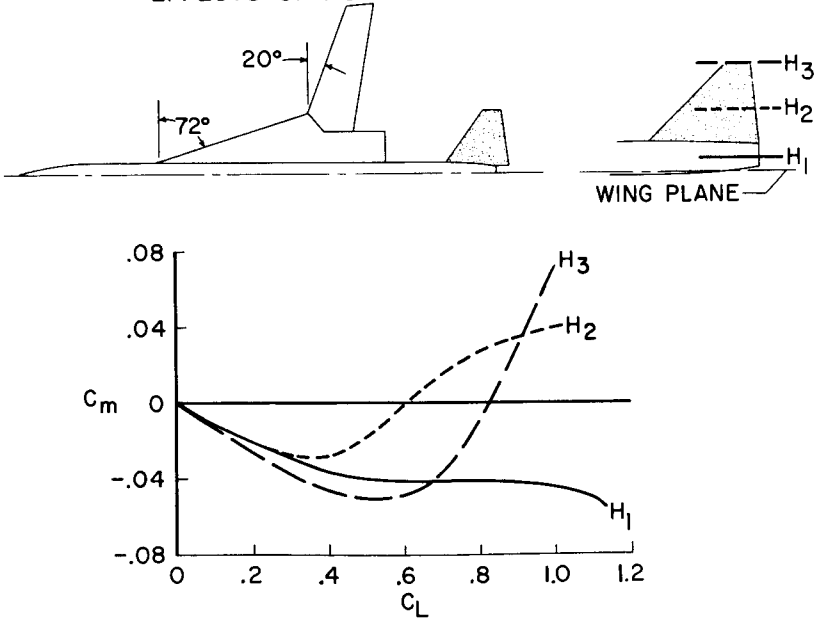

Figure 4

SUPERSONIC BREAKDOWN FOR V/STOL FIGHTER

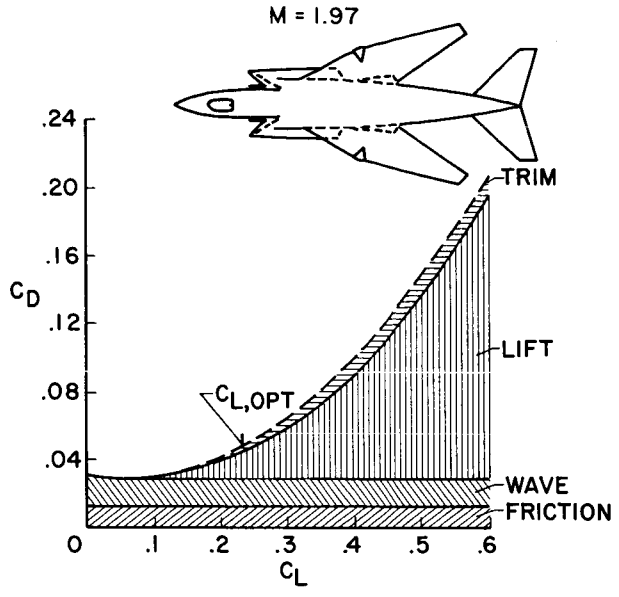

Figure 5

WAVE-DRAG COEFFICIENT
BASED ON FRONTAL AREA; M = 1.2

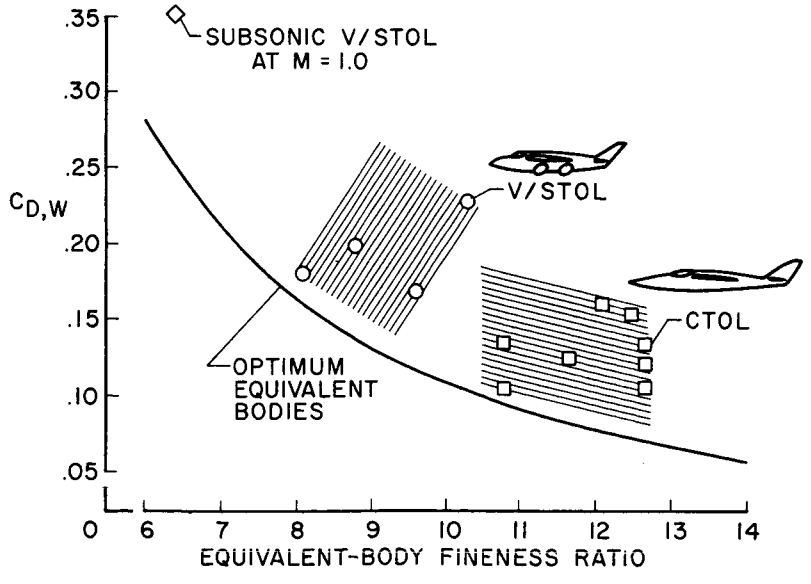

Figure 6

WAVE-DRAG PROGRAM AND CORRELATION

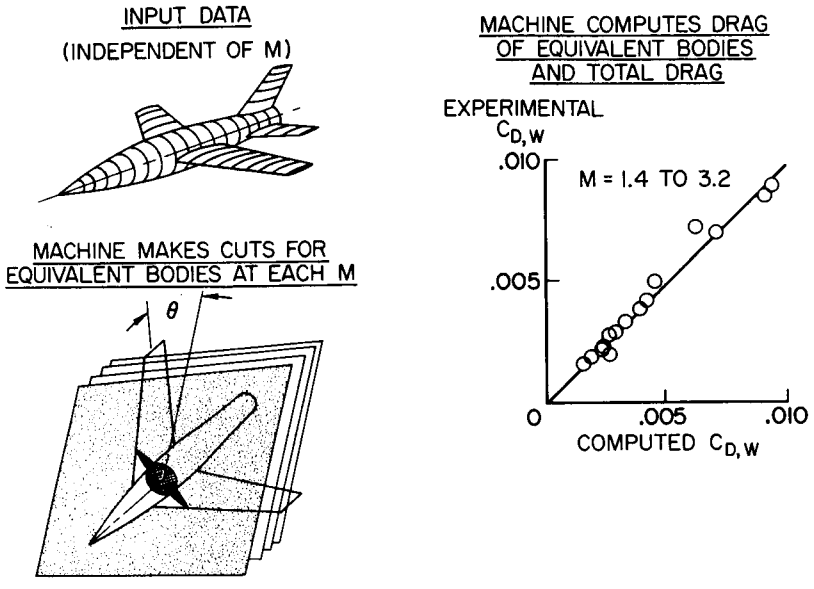

Figure 7

SUPERSONIC DRAG DUE TO LIFT AND EFFECTS OF WING WARP

M = 2.05 ; Λ = 70°

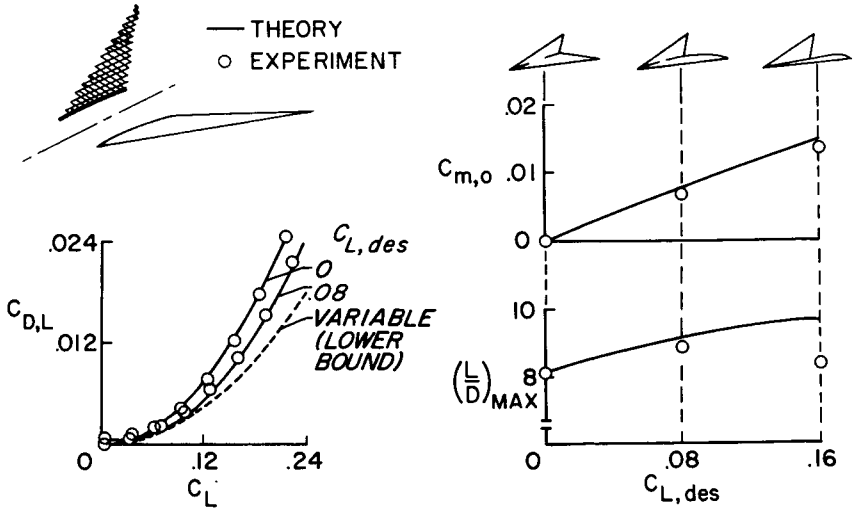

Figure 8

SUPERSONIC INTERFERENCE CONSIDERATIONS

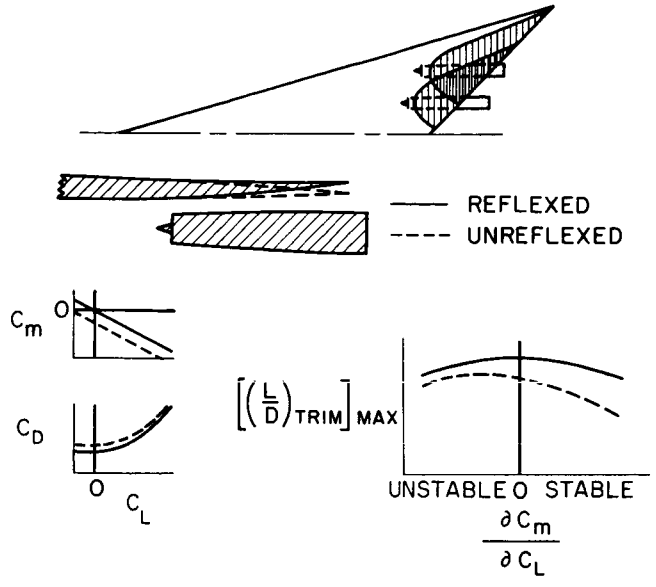

Figure 9

OPTIMIZATION OF COMPLETE CONFIGURATION
M = 2.6

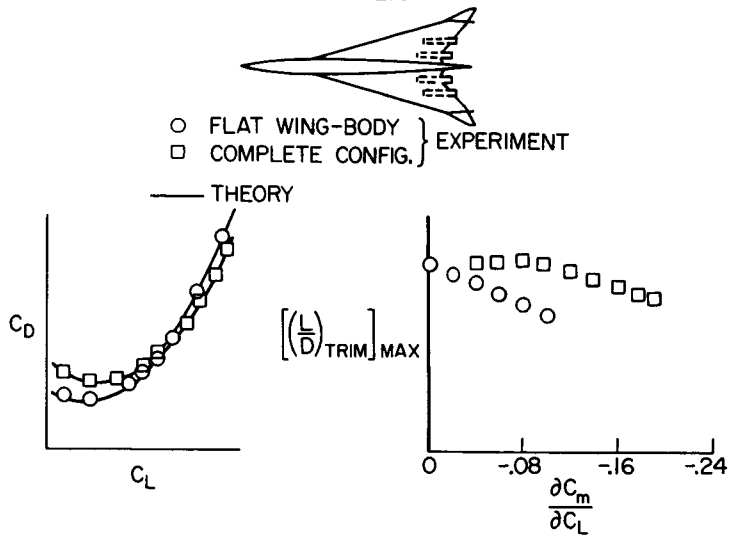

Figure 10

MULTIMISSION PERFORMANCE AT OPTIMUM ALTITUDE

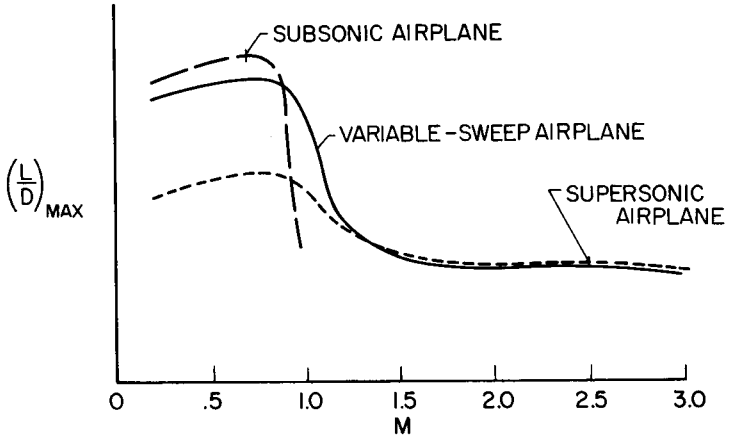

Figure 11

AERODYNAMIC-CENTER VARIATION WITH WING SWEEP AND MACH NUMBER

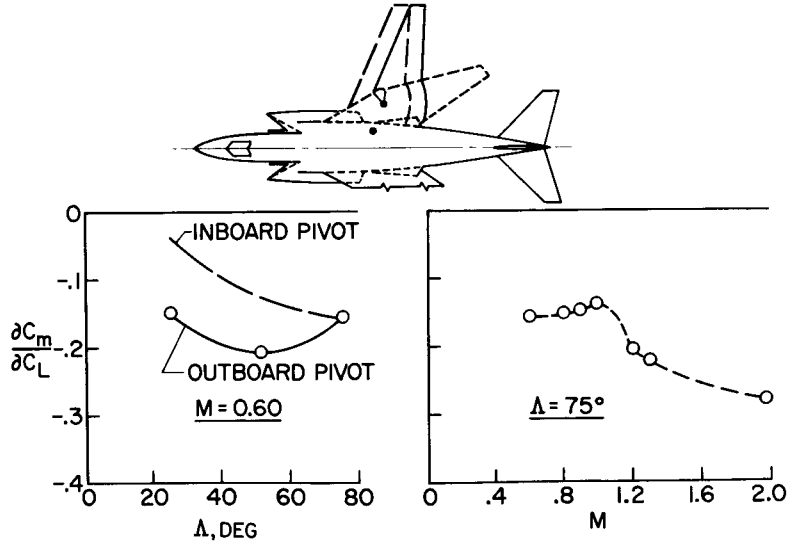

Figure 12

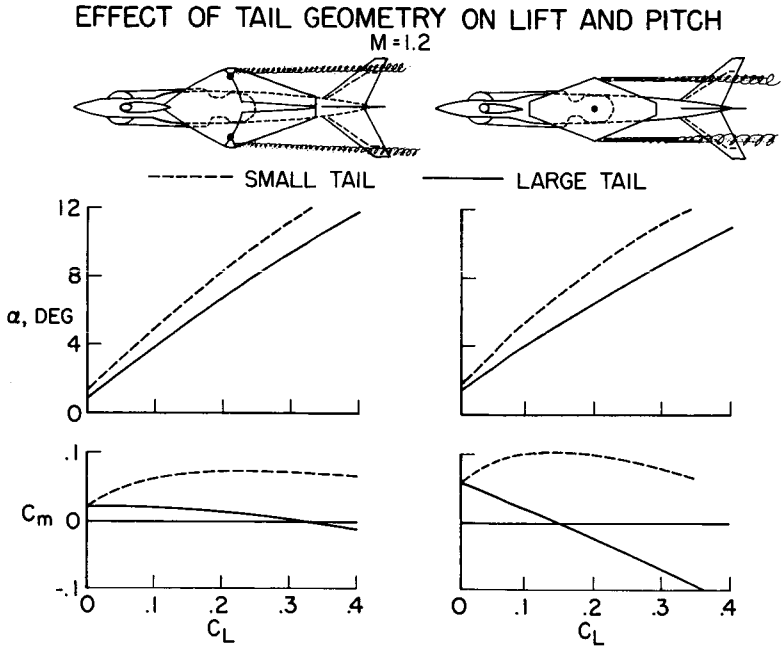
EFFECT OF TAIL GEOMETRY ON LIFT AND PITCH
M = 1.2
SMALL TAIL
LARGE TAIL
α, DEG
12
8
4
0
Cm
.1
0
-.1
0
.1
.2
.3
.4
CL

Figure 13

Page intentionally left blank

12. THRUST LOSSES IN HOVERING FOR JET VTOL AIRCRAFT

By Alexander D. Hammond

NASA Langley Research Center

SUMMARY

In order to determine the net hovering lift of a VTOL airplane, the magnitude of various installation losses that degrade the engine performance must be ascertained. Even though each of these losses may be only a few percent of the rated thrust, an accurate knowledge of each is required to make realistic estimates of the aircraft performance. An error of as little as 3 percent in the total lifting capacity in hovering would mean a reduction of 3 percent in gross weight, which in turn would reduce the fuel capacity and hence the design range by about 10 percent.

This paper is primarily concerned with two items; the jet-induced base loss encountered during hovering flight and the effect of ground proximity on this loss. The jet-induced base loss was found to be a function of the total planform area of the configuration and the rate of mixing of the exhaust gases and the surrounding air. Although from the standpoint of noise and ground erosion a rapid rate of mixing is desirable, the base loss becomes larger as the mixing rate increases.

The hovering ground effects for single-jet configurations can be satisfactorily predicted from available data. For multijet configurations the ground effects depend on the configurational arrangement and, although considerable data are available, tests on the particular multijet arrangement may be necessary.

Author

INTRODUCTION

The rated thrust of a jet engine, whether for a conventional aircraft or for a VTOL aircraft, is based on its performance with a bell-mouth inlet on a test stand using the particular design nozzle for the engine. The actual performance of the engine when installed in the airplane is degraded from the test-stand rating by various installation losses. Even though each of these losses may be only a few percent of the rated thrust, an accurate knowledge of each is required to make realistic estimates of the aircraft performance. An error of as little as 3 percent in the total lifting capacity in hovering would mean a reduction of 3 percent in gross weight, which in turn would reduce the fuel capacity and hence the design range by about 10 percent. There are several hovering thrust losses which must be considered, however, this discussion will be concerned primarily with two items; the aerodynamic lift loss in hovering resulting from the suction forces on the under surfaces of the airplane commonly referred to

as a base loss, and the aerodynamic ground effect on this base loss. In addition there are the basic nozzle losses common to all engine nozzle installations and the additional nozzle losses which might be peculiar to the VTOL airplane such as the losses resulting from thrust vectoring. The intake losses, presented in paper no. 15 by Tolhurst and Kelly, are dependent on the inlet configuration and, of course, the location of the inlet determines the severity of the thrust losses due to hot-gas ingestion. A complete discussion of hot-gas ingestion can be found in paper no. 14 by McLemore. One other item which must be accounted for, of course, is the thrust required for hovering control which is usually provided for by jet reaction controls or thrust vectoring, either of which downgrades the available thrust for hovering.

SYMBOLS

A_j	jet nozzle area, ft^2
D	nozzle diameter, ft
D_e	equivalent diameter; diameter of a single nozzle having the same area as the sum of several nozzles of a multijet configuration, ft
h	height of model above ground, ft
k	slope of line
ΔL	incremental lift, lb
ΔL_b	incremental lift due to base loss, lb
ΔL_g	incremental lift due to ground proximity, lb
p_t/p_o	total pressure ratio across nozzle exit
q_n	dynamic pressure at nozzle exit, lb/ft^2
q_x	dynamic pressure at distance x downstream of nozzle, lb/ft^2
S	total planform area, ft^2
T	jet thrust, lb
T_I	ideal jet thrust, lb
x	distance downstream from jet exit, ft

Subscripts:

i	intercept
MAX	maximum

DISCUSSION

The flow phenomenon which causes the hovering base loss is illustrated in figure 1 which shows a sketch of a nozzle with air exhausting vertically through a flat plate, representing a lift engine exhausting through the bottom of a fuselage. The lift losses ΔL_b, as measured on the plate, arise from the entrainment action of the jet which mixes with the surrounding air, sets up a crossflow over the bottom of the surface, and thereby induces suction pressures on the plate. The dynamic-pressure decay in the jet stream as well as the velocity of the crossflow would then be dependent on the mixing along the boundaries of the jet stream; this mixing in turn would be expected to depend on the turbulence of the flow. A summary of the results of two base loss investigations is shown in figure 2; these investigations were reported in reference 1 and were made to determine if there is in fact a relationship between the dynamic-pressure decay in a jet stream and the base loss. The lift losses measured on two circular plates with jets issuing from the center of the plates are also shown in figure 2. The sizes of the circular plates and of the nozzles are the same, but the characteristics of the flow issuing from the jets are different because of the plenum chamber design. In the first investigation, a large circular plenum (illustrated by the sketch at the top of fig. 2) with a long nozzle was chosen for static tests. In an attempt to build a plenum to go inside a small wind-tunnel model, a rather small rectangular plenum (illustrated by the sketch at the bottom of fig. 2) was utilized in the other investigation. The results from these investigations are shown on the left of figure 2. The decay of the jet is presented as the ratio of the maximum dynamic pressure measured in the jet stream at a distance x from the nozzle to the maximum dynamic pressure measured at the nozzle exit. The data for the circular plenum having smooth flow show only a small lift loss and little variation of this loss with pressure ratio. Also, the dynamic pressure does not decay rapidly. The original rectangular plenum shows a large lift loss which is affected by the jet pressure ratio, the larger losses occurring at the lower pressures. This configuration had a rapid loss in dynamic pressure. In order to determine if the jet flow characteristics were responsible for the large difference in lift loss between the two sets of data, the rectangular plenum was modified to improve the flow. The data for this improved configuration has considerably less lift loss; this loss is essentially constant with jet pressure ratio. Also a test was made for which the flow from the circular plenum was roughened, and the results from this test show a larger lift loss than the original smooth flow results. What seems to be even more significant, however, is that the data which indicate about the same base loss also show similar jet decay characteristics. This indicates that the rate of mixing of the jet efflux and the surrounding air is an important parameter and that a low rate of jet decay is desirable.

The arrangement of jets with respect to each other also influences the entrainment of the surrounding air. Additional data from reference 1 showing the effect of jet arrangement on the base loss and jet decay are presented in figure 3. The total exit area of the slots and of the four jets are equal to the area of the single jet and therefore have the same effective jet diameter. The total planform area of the configuration was varied by changing the size of the wings so that the ratio of the total planform area of the configuration to the jet area was a variable. There are two things shown by these data. First, the lift loss is a linear function of the square root of the planform to jet area ratio for all three jet arrangements. Second, lift loss is again seen to be a function of the decay characteristics, that is, the more rapid the decay, the larger the loss. A correlation of the base loss with jet decay characteristics by the method presented in reference 1 is shown in figure 4. The ratio of the lift loss over thrust to the square root of the planform to jet area ratio, that is, the slope of the curves at the top of figure 3, has been plotted against the square root of a jet decay parameter. This jet decay parameter is simply the ratio of the maximum rate of dynamic-pressure decay $\left[\frac{\partial(q_x/q_n)}{\partial(x/D_e)}\right]_{MAX}$ to the intercept $\left(x/D_e\right)$ at which this maximum slope occurs. It can be seen that all three configurations, the single-jet, the multijet, and the multislot configurations, as well as other single and multijet configurations, fall along a correlating line. The lift loss can be estimated for a configuration by the formula given at the bottom of figure 4 if the geometry of the configuration is known and the jet decay characteristics have been measured.

The data of figure 5 compare the data obtained for a single-jet and multijet arrangement using small cold jets (ref. 1) with the results obtained by using a J85 engine (ref. 2). The sizes of the square plates (fig. 5) were varied and the ratio of measured lift loss to thrust is again seen to be a linear function of the square root of the ratio of the planform area to jet area. Again it is seen that the multijet arrangement with the more rapid dynamic-pressure decay results in the largest base loss and that the curves for the large-scale J85 engine would also correlate in a similar manner to the small cold jets which were included in the data shown in figure 4.

Suppressor Nozzles

From the standpoint of base loss it has been shown that a rapid decay rate is not desirable. There are, however, the problems of ground erosion and noise on all jet VTOL airplanes. From the erosion and noise standpoint a rapid rate of dynamic pressure is very desirable, and an effort has been made to devise means of obtaining rapid reduction in the jet velocity. The Boeing Company has just completed a study for NASA to determine the effects of different nozzle configuration arrangements on jet decay. (See refs. 3 and 4.) A summary of some of the results of this investigation is presented in figures 6 and 7. A comparison of the dynamic-pressure ratio variation with distance downstream of the nozzle exit is presented in figure 6 for a circular, a single-slot, and a four-slot nozzle. The circular nozzle, of course, does not

decay very rapidly; however, the single-slot and multislot arrangements achieve the desired goal of rapid decay. The nozzle thrust losses for these suppressor nozzles are presented in figure 7. The ratio of the incremental lift or thrust loss to the ideal thrust is plotted against the dynamic-pressure reduction measured at a representative distance downstream ($x/D_e = 3.0$) for the nozzles shown in figure 6 along with other multislot nozzles investigated (refs. 3 and 4). It can be seen that the rapid decay comes at the expense of the basic nozzle efficiency, that is, the lower the dynamic pressure ratio, the larger the thrust loss. Also shown are the base losses measured on a simulated fuselage in the presence of the suppressor nozzles, the increment between the solid and dashed lines. This increment is also shown in reference 5 and is smaller than would be estimated from the correlation shown in figure 4. The apparent reason is that some of the base loss is already present in the basic nozzle loss as is discussed in reference 5.

From these results it can be seen that the requirement for rapid dynamic-pressure decay to prevent ground erosion and reduce the noise level has to be considered carefully in light of the larger nozzle and base losses that occur because of this rapid rate of dynamic-pressure decay.

Aerodynamic Ground Effect

The influence of the proximity of the ground on the base loss is illustrated in figure 8 where the flow characteristics are shown for a single-jet nozzle with air exhausting vertically through a flat plate at a height h above the ground. As the air from the jet impinges on the ground, it flows outward along the ground as shown. The entrainment of the surrounding air in this flow pattern creates the regions of negative pressures as indicated. The sketch on the right of the figure illustrates the flow pattern for multiple jets. The main difference between the two, of course, is the interaction of the flow between the jets which results in the so-called fountain effect that creates positive pressures in the region between the jets.

A number of model tests have been made of single-jet configurations to determine the effects of ground on the lift of jet VTOL configurations (refs. 6 to 8). A correlation of these results with the full-scale X-14A flight tests (ref. 9) is shown in figure 9. L. A. Wyatt (ref. 7) has correlated the data from a number of model tests and has derived an empirical method to determine the effects of ground on lift for single-jet configurations. It has been assumed that the two jet exits of the X-14A are so close together that they act like a single jet. The full-scale flight-test results are in good agreement with the scale model results (ref. 10) and with the calculated results using the method of Wyatt shown by the dashed curve.

The X-14A was a low-wing model with all the planform area essentially in the same plane as the jet exits. The effect of wing height on the lift loss in hovering near the ground can be estimated as shown in figure 10. The Wyatt method to estimate the curve for the wing-off or fuselage-alone configuration and the estimation of the curve for the low-wing configuration can be used to determine the increment due to the wing in the low position at a given height.

Shifting the increment due to the wing to account for the difference in wing height Δh between the low wing and high wing and combining this increment with the fuselage-alone data give an estimation for the high-wing case as shown by the dash-dot curve. The measured data, from reference 7, shown by the circle symbols, and the estimation for the high wing are in good agreement.

Although many multijet configurations have been investigated and the results reported in references 1, 8, and 11 to 15, the story for multijet configurations is not as clear as for single-jet configurations at this time. The effect of multijets on the hovering ground effects for one configuration is illustrated in figure 11 (ref. 1). The data for the four-jet configuration reverse in trend at about 3 diameters from the ground and begin to show a reduction in the ground effect lift loss. This trend is due to the so-called fountain effect between the jets and causes positive pressures in this region. (See fig. 8.) This effect of multijets would be expected to be very much a function of the configurational arrangement of the jets with respect to each other. Attempts to generalize on the results that are available and correlate them have not been successful. It is therefore necessary to rely on model tests for multijet configurations.

CONCLUDING REMARKS

The jet-induced base loss encountered in hovering is a function of the ratio of total configuration planform area to jet area and of the rate of decay of the jets. An accurate prediction of these base losses for a given configuration requires that the decay curves for full-scale engines, with the nozzles to be used in the aircraft installation, be known.

Although suppressor nozzles having rapid decay characteristics reduce ground erosion, both the basic nozzle losses and the base loss characteristics are detrimentally affected by the rapid rate of decay.

Hovering ground effects for single-jet cases can be satisfactorily predicted from available data. For multijet configurations the ground effects can be reduced as a result of the interaction of the jets with each other when very close to the ground. There are considerable test data for multijet model configurations near the ground; however, attempts to correlate these results have been unsuccessful and therefore it is necessary to rely on model tests for multijet configurations.

REFERENCES

1. Gentry, Garl L.; and Margason, Richard J.: Jet-Induced Lift Losses on VTOL Configurations Hovering In and Out of Ground Effect. NASA TN D-3166, 1966.

2. McLemore, H. Clyde: Jet-Induced Lift Loss of Jet VTOL Configurations in Hovering Condition. NASA TN D-3435, 1966.

3. Higgins, C. C.; and Wainwright, T. W.: Dynamic Pressure and Thrust Characteristics of Cold Jets Discharging From Several Exhaust Nozzles Designed for VTOL Downwash Suppression. NASA TN D-2263, 1964.

4. Higgins, C. C.; Kelly, D. P.; and Wainwright, T. W.: Exhaust Jet Wake and Thrust Characteristics of Several Nozzles Designed for VTOL Downwash Suppression - Tests In and Out of Ground Effect With 70° F and 1200° F Nozzle Discharge Temperatures. NASA CR-373, 1966.

5. Kuhn, Richard E.; and McKinney, Marion O., Jr.: NASA Research on the Aerodynamics of Jet VTOL Engine Installations. Aerodynamics of Power Plant Installation, Pt. II, AGARDograph 103, Oct. 1965, pp. 689-713.

6. Spreemann, Kenneth P.; and Sherman, Irving R.: Effects of Ground Proximity on the Thrust of a Simple Downward-Directed Jet Beneath a Flat Surface. NACA TN 4407, 1958.

7. Wyatt, L. A.: Static Tests of Ground Effect on Planforms Fitted With a Centrally-Located Round Lifting Jet. C.P. No. 749, Brit. A.R.C., 1964.

8. Vogler, Raymond D.: Interference Effects of Single and Multiple Round or Slotted Jets on a VTOL Model in Transition. NASA TN D-2380, 1964.

9. Rolls, L. Stewart: Jet VTOL Power Plant Experience During Flight Test of X-14A VTOL Research Vehicle. Aerodynamics of Power Plant Installation, Pt. II, AGARDograph 103, Oct. 1965, pp. 539-537.

10. Sherman, E. W., Jr.: Studies of VTOL Inlet Temperature Rise and Lift-Thrust. [Preprint] 860E, Soc. Automotive Engrs., Apr. 1964.

11. Langfelder, H.: Bodeneffekte bei Senkrechtstart-Flugzeugen. EWR-Nr. 37/62, Entwicklungsring Süd (München), Mar. 1963.

12. Seibold, Wilhelm: Untersuchungen Über die von Hubstrahlen an Senkrechtstartern Erzeugten Sekundärkräfte. Jahrb. 1962 WGLR.

13. Davenport, Edwin E.; and Spreemann, Kenneth P.: Thrust Characteristics of Multiple Lifting Jets in Ground Proximity. NASA TN D-513, 1960.

14. Vogler, Raymond D.: Effects of Various Arrangements of Slotted and Round Jet Exits on the Lift and Pitching-Moment Characteristics of a Rectangular-Base Model at Zero Forward Speed. NASA TN D-660, 1961.

15. Vogler, Raymond D.: Ground Effects on Single- and Multiple-Jet VTOL Models at Transition Speeds Over Stationary and Moving Ground Planes. NASA TN D-3213, 1966.

BASE LOSS

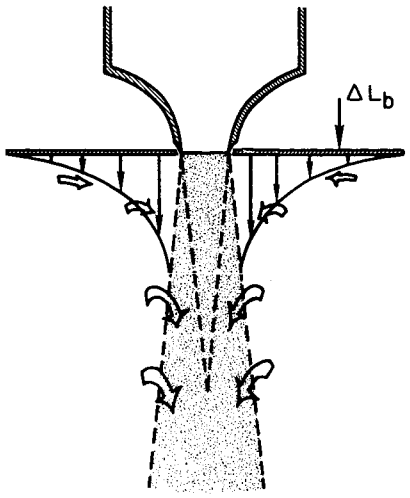

Figure 1

CORRELATION OF BASE LOSS WITH JET DECAY

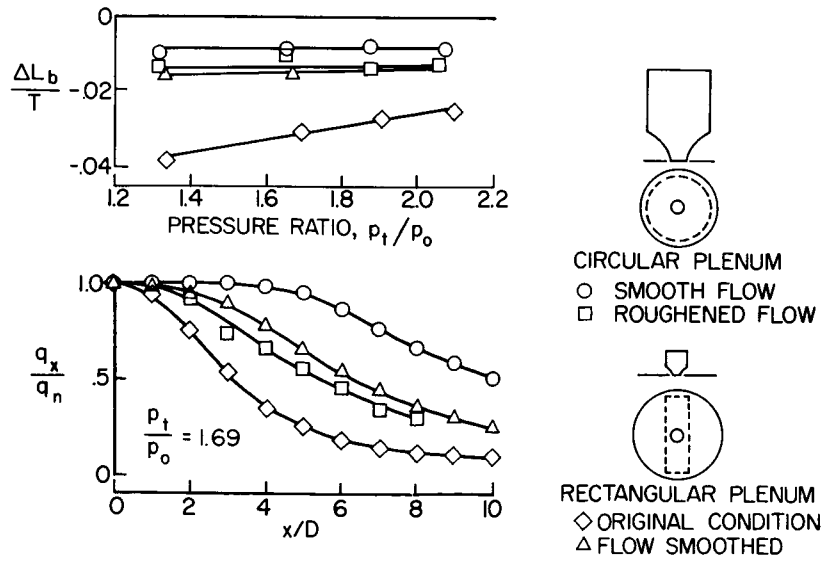

Figure 2

EFFECT OF JET ARRANGEMENT ON BASE LOSS AND JET DECAY

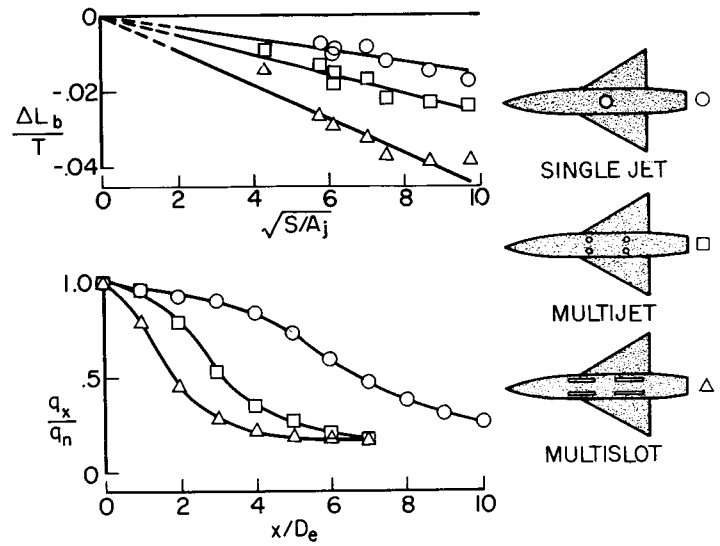

Figure 3

CORRELATION OF BASE LOSS WITH JET DECAY

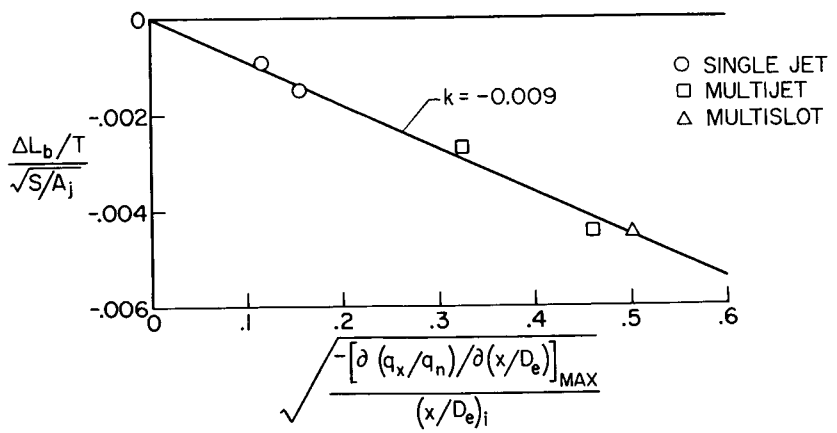

$$\frac{\Delta L_b}{T} = k\sqrt{S/A_j}\sqrt{\frac{-\left[\partial\,(q_x/q_n)/\partial(x/D_e)\right]_{MAX}}{(x/D_e)_i}}$$

Figure 4

COMPARISON OF SMALL SCALE WITH LARGE SCALE

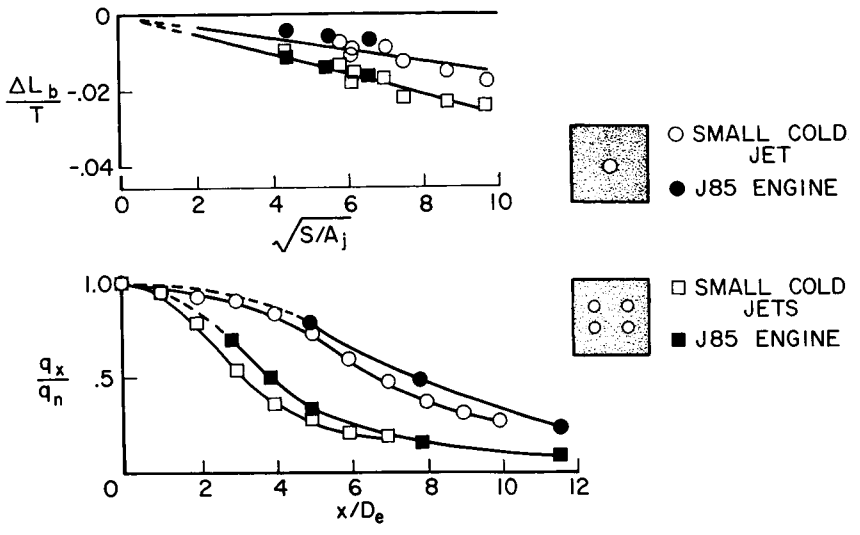

Figure 5

EFFECT OF NOZZLE CONFIGURATION ON JET DECAY

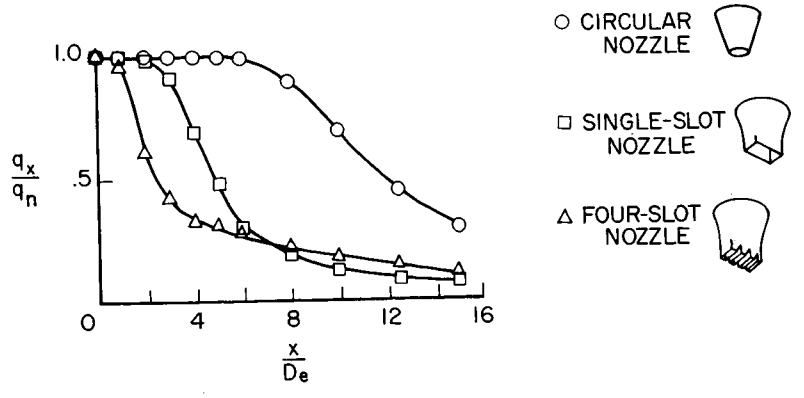

Figure 6

THRUST LOSSES WITH SUPPRESSOR NOZZLES

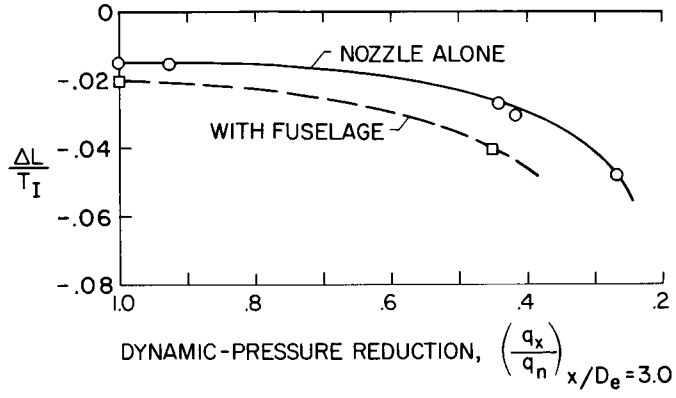

Figure 7

AERODYNAMIC GROUND EFFECTS
HOVERING FLIGHT

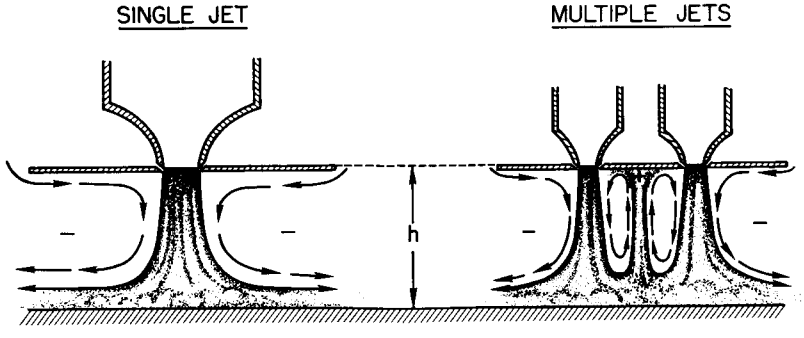

Figure 8

CORRELATION OF MODEL WITH FULL-SCALE X-14A

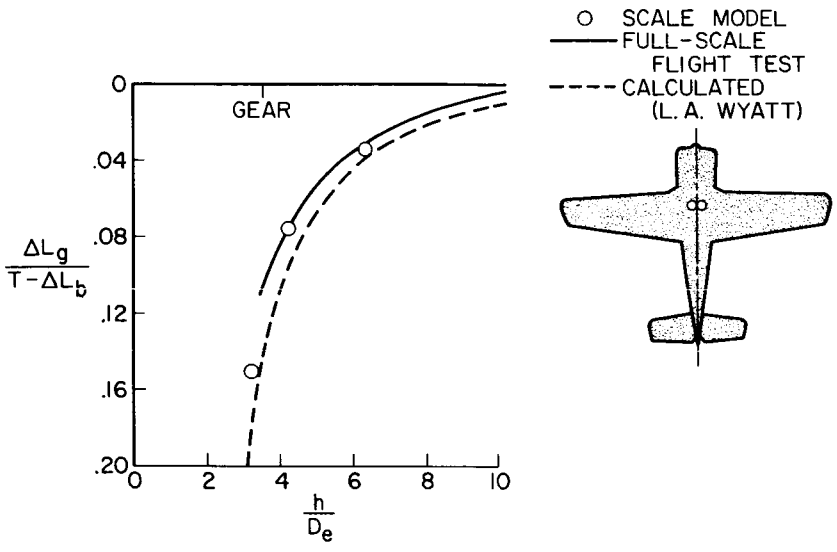

Figure 9

EFFECT OF WING HEIGHT

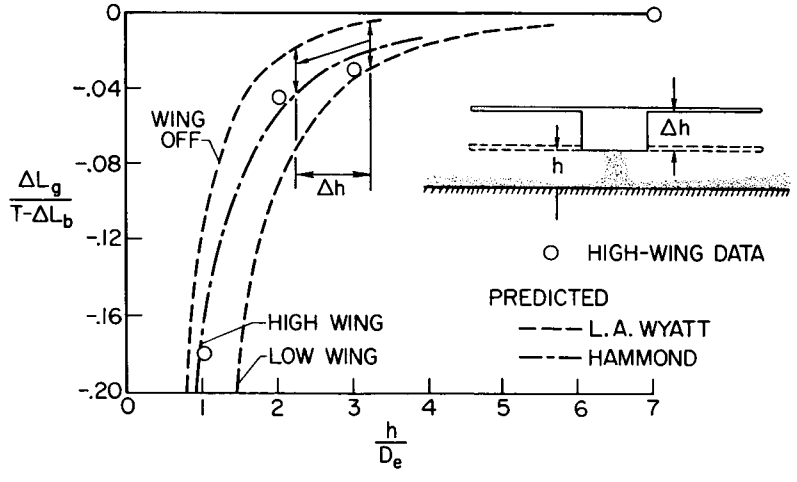

Figure 10

EFFECT OF MULTIPLE JETS

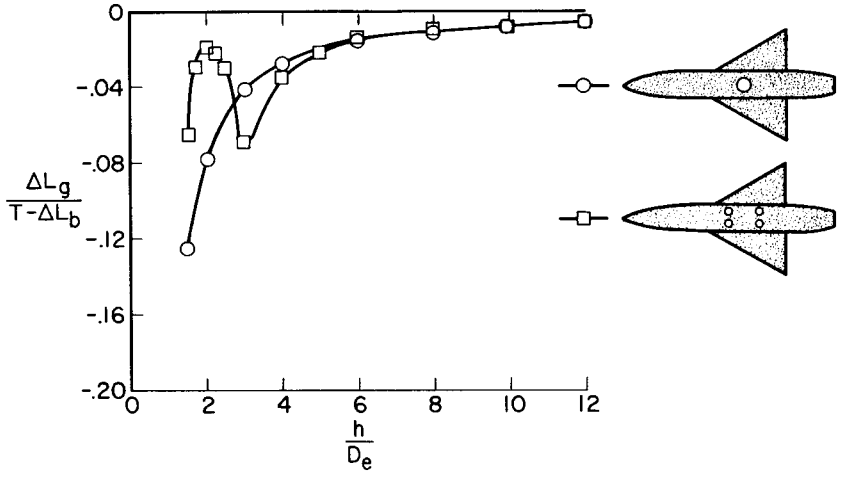

Figure 11

13. JET-INDUCED EFFECTS IN TRANSITION FLIGHT

By Richard J. Margason

NASA Langley Research Center

SUMMARY

Some of the characteristics of jet-powered VTOL fighter airplanes in transition from jet-supported hover to wing-supported forward flight are presented. Wind-tunnel investigations at the Langley Research Center have shown that interference between the jet wakes and the free stream causes significant increments of nose-up pitching moment and lift loss. Some methods of reducing these interference increments by configuration variations, such as changes in the wing planform and jet arrangement, are presented. The effects of the jet on the tail contribution to stability are also shown to be largely configuration dependent. The evidence indicates that configurations can be devised which have very little effect of power on longitudinal stability. Jet-induced rolling moments in sideslip may be a serious problem, and at present there appears to be little hope of completely eliminating this problem. Therefore, it is necessary to design the controls to handle these jet-induced rolling moments.

Author

INTRODUCTION

There is currently much interest in vertical take-off and landing (VTOL) airplanes powered by jet engines. One type of airplane which is now under study is a fighter configuration employing lift engines and lift-cruise engines. This airplane is capable of performing missions requiring cruise at high subsonic or supersonic speeds. The purpose of this paper is to present some of the characteristics of jet-powered VTOL fighter configurations in the transition from jet-supported hover to wing-supported forward flight. In particular, the interference effects induced on the airplane by the interaction between the free stream and the jet wakes are discussed in three parts: interference on the basic wing-body, interference on the tail contribution to stability, and interference on the lateral stability characteristics, with particular reference to roll control.

SYMBOLS

A_j jet nozzle area, feet^2

b wing span, feet

C_m pitching-moment coefficient, $\frac{M_Y}{qS\bar{c}}$

$\bar{c}$ mean aerodynamic chord, feet

D_e equivalent diameter; diameter of a single nozzle having the same area as the sum of several nozzles of a multijet configuration, feet

I_X lateral moment of inertia, $feet^4$

L lift, including jet force, pounds

ΔL increment in lift due to interference, pounds

M_X rolling moment, foot-pounds

M_Y pitching moment, foot-pounds

ΔM increment in pitching moment due to interference, foot-pounds

q free-stream dynamic pressure, pounds per $foot^2$

S wing area, $feet^2$

T thrust, pounds

V_j jet velocity, feet per second

V_∞ free-stream velocity, feet per second

W airplane gross weight, pounds

α angle of attack, degrees

β angle of sideslip, degrees

δ_f flap deflection angle, degrees

ρ_j air density in jet, slugs per $foot^3$

ρ_∞ free-stream air density, slugs per $foot^3$

DISCUSSION

In paper no. 12, Alexander D. Hammond discussed the hovering interference effects in detail. These effects were attributed primarily to the suction

pressures induced on the lower surfaces of the airplane by viscous mixing. In transition from hover to forward flight, a second mechanism comes into operation, which is illustrated in figure 1 by a jet VTOL fighter configuration. It is powered by three lift engines located in the forward portion of the fuselage and by two cruise engines located one on each side of the fuselage. The cruise engines can be deflected near the rear portion of the fuselage to provide lift. The wakes from the lift engines merge and are quickly transformed into a rolled-up vortex pair (ref. 1). The same phenomenon occurs for the individual wakes from the lift-cruise engines. The rolling up of these wakes into vortices is the primary cause of the interference effects in transition flight. The vortices change the flow field in the region of the model and induce additional suction pressures on the lower surface of the fuselage and wing of the airplane. These additional pressures cause a loss in lift and a nose-up pitching moment, as illustrated in figure 2.

The data of figure 2 illustrate typical trends for a tail-off configuration. Plotted are the lift divided by the thrust as a function of the angle of attack on the left and the pitching moment as a function of the angle of attack on the right. In hover, the jets produce a lift which is equal to the net thrust. At forward velocity the wing develops additional lift. In the absence of interference effects, lift from these two sources could be added together to produce the solid curve. The jet-induced effects, however, cause a loss in lift, and the actual lift measured in a wind tunnel is shown by the symbols. The difference between the calculated and measured curves is the interference lift loss, which is generally independent of angle of attack.

The situation with regard to pitching moments is shown at the right in figure 2. In hover, the jets are placed so that they produce zero pitching moment from direct thrust forces. For a forward velocity, the power-off pitching moment due to aerodynamic loads might follow a variation such as that shown. The measured power-on moment, however, is usually more positive than the power-off moment. The difference is the interference moment. This interference pitching moment arises from the same suction pressures which cause the lift loss, but these suction pressures are induced primarily beside and behind the jets, and, therefore, produce a nose-up increment. Like the lift increment, the pitching-moment increment is generally independent of angle of attack for the tail-off configuration.

Interference Effects on Wing-Body

Although the wing-body interference increments are usually independent of angle of attack, they are a function of several other parameters. The most obvious of these is the planform area of the configuration. The larger the area surrounding the jets, the larger the increments would be. The interference increments are also a function of the distribution of area and of the forward velocity, as shown in figure 3. These data, obtained from reference 2, are for a model with a ratio of total projected wing-body planform area to jet nozzle area of 38. The interference pitching-moment increment nondimensionalized by dividing by thrust times the equivalent diameter of the jet exit and the lift-loss increment divided by the thrust are presented as functions of an

effective velocity parameter. This parameter is the square root of the ratio of the dynamic pressure of the free stream to the dynamic pressure of the jet and is used, as suggested in reference 1, because it accounts for the density of the jet and, therefore, accounts for temperature effects in applying the data to hot-jet configurations. Zero refers to zero forward velocity or hovering. The transition flight speeds are represented by values of the effective velocity ratio up to about 0.25. Data are shown for a four-jet model with two wing configurations. The lift loss is essentially independent of the wing sweep; however, the nose-up pitching moment is higher for the sweptback wing because some of the areas on which the suction pressures act are farther behind the moment reference point for this wing. In general, it is desirable to minimize the area behind the jets.

The arrangement of the jets can have a large effect on the magnitude of the induced interference, as shown in figure 4. Data for a different four-jet configuration are compared with data for a configuration in which the same total jet area is distributed along a central slot (ref. 3). This arrangement might represent a row of lift engines. It can be seen that changing from the rectangular array to the linear slot gives a drastic reduction in both the lift loss and the nose-up pitching moment.

An additional point can be made by comparing the data from the four-jet configuration in figure 4 with the results for the low-wing-sweep four-jet configuration in figure 3. The arrangement of the jets is similar, but the model of figure 4 has a larger ratio of total planform area to jet area. It should be noted that most of this area increase is due to a larger fuselage, which places more area closer to the jets. As a result, this model has significantly larger interference increments than the low-wing-sweep model of figure 3. This comparison again points out the importance of the ratio of planform area to jet area and the distribution of the planform area. Up to this point, all the data presented deal with the effects of exit flow.

In figure 5, data are presented for a configuration for which both the inlet and the exit flow could be simulated. The model represents a five-jet configuration with three lift engines simulated in the forward portion of the fuselage and two lift-cruise engines with deflected thrust simulated in the rear portion of the fuselage. The inlets of the lift engines are on the upper surface of the fuselage, and those of the lift-cruise engines are on the side of the forward portion of the fuselage. With the inlets closed, that is, with exit flow only, this model shows increments of lift loss and nose-up pitching moment similar to those discussed previously. Opening the inlets adds an increment to the nose-up pitching moment but does not affect the lift loss. These data indicate that the nose-up moment induced by the inlet is a factor to be considered, but for this model it is much smaller than that induced by the exit flow.

Additional data on the interference effects are presented in references 1 to 6. In particular, some of the effects of ground proximity are discussed in reference 6, and the effect of flap deflection for one configuration is presented in reference 1. Additional unpublished data obtained at the NASA Langley

Research Center indicate that the effect of flap deflection may be critically dependent upon the location of the jets with respect to the flap.

Interference Effects on Tail Contribution to Stability

All the previous data have been for the basic wing-body configuration with the tail off. In addition to the suction pressures the jets induce on the fuselage and wing lower surface, the jets also induce a large downwash at the horizontal tail. The downwash at the tail causes an additional nose-up pitching moment, as shown in figure 6. The additional increment of pitching moment corresponds to a downwash angle of about 5°.

Unlike the jet induced moment on the wing-body, which is generally independent of angle of attack, the downwash at the horizontal tail is a function of angle of attack and can, therefore, change both the trim and the stability of the tail-on configuration. The effect of power on the tail contribution to stability is highly dependent on the flow field in which the tail operates and, in particular, on the flow field generated by the parts of the airplane ahead of the wing proper.

Figure 7 illustrates an airplane in cruising flight. On most modern high-speed jet airplanes there are inlets or other elements such as fixed forewings for variable-sweep wings which produce lift and shed vortices inboard. As Alford and Harris indicated in paper no. 11, it is desirable that the tail be located below this trailing vortex system. This arrangement would insure that the tail would move away from the vortices as the angle of attack is increased. For the jet VTOL airplane, however, the situation is different, as shown in figure 8. The inboard vortices can be pulled below the horizontal tail by the action of the lifting jets. Then as the angle of attack is increased, the tail is forced to traverse through these vortices. The severity of the problem thus created depends on many configuration variables, all of which have not yet been isolated.

A particularly severe example is presented in figure 9 for a four-jet configuration with a fixed forewing and large inlets placed well forward (ref. 5). With the power off, there is a linear and stable variation of pitching moment with angle of attack and a stable break at the stall. With the power on, there is a nose-up increment, but it is no longer invariant with angle of attack. It increases very rapidly as the angle of attack is increased and results in an extremely unstable configuration.

Data for two other configurations are shown in figure 10. For the configuration with short inlets and no variable-sweep wing glove, the power effect on stability is essentially zero, as indicated by the fact that the two curves are nearly parallel. For the other configuration, which has long inlets and a fixed forewing, a reduction in stability due to power is encountered. However, it is not as severe as that shown for the configuration in figure 9. The primary difference between the configurations appears to be in the size and length of the lifting elements forward of the wing. The differences in tail length and tail configuration may also contribute to the differences in stability.

The destabilizing influence of elements which carry lift and are located ahead of the main wing was described by Alford and Harris in paper no. 11 of this conference. This effect can be seen by comparing the two power-off curves in figure 10. The primary point here is that the effects of power on longitudinal stability can be kept small. Additional work will be required to learn all the ground rules involved.

Interference Effects on Lateral Control

Another aspect of the interference effects is the jet-induced effects on the lateral control characteristics. The same jet-induced suction pressures which cause a nose-up pitching moment can also cause a rolling moment in a sideslipping condition. In figure 11, the effect of sideslip on rolling moment is presented. The sideslip angle resulting from an assumed 30-knot crosswind increases as the velocity decreases and would reach 90° at zero velocity. In the plot at the bottom of the figure, the rolling-moment parameter is plotted as a function of velocity for a 30 000-pound airplane. The curve with the circles indicates the rolling moment that would be encountered. This rolling moment must be cancelled by the control available, shown by the long-dash—short-dash curve. The control available at forward speeds is a combination of that due to the roll from the tip jets plus the rolling moment obtained from the aerodynamic control surface on the airplane. The lower speed range where the moments are quite large is most critical, as indicated by comparing the control-required curve with the hover control that would be provided for an airplane of this size. This available hover control, shown by the diamond, corresponds to a rolling acceleration of 1.2 radians per second^2 and is supplied by roll jets near the wing tips. Unfortunately, the amount of roll control available from the tip jets decreases with increasing speed because of the interference effects between the jets and the wing area surrounding them (ref. 4). For the configuration shown, the total control available is slightly greater than that required, but there is little margin for complacency. Obviously, operation in crosswinds is undesirable but not always possible to avoid. When an airplane is close to the ground, a pilot tends to sense velocity and direction with respect to the ground and can thus lose track of the direction of the approaching wind. The point is that these rolling moments can be quite significant and must be accounted for in the design of the airplane. In paper no. 16, Anderson discusses the handling qualities aspect of this problem with specific reference to criteria for roll control.

CONCLUDING REMARKS

The results indicate that significant increments of nose-up pitching moment and loss in lift can be induced on jet VTOL configurations in transition. Some methods of minimizing these interference increments by configuration variations, such as changes in the wing planform and jet arrangement, have been presented. The effects of the jet on the tail contribution to stability are also shown to be largely configuration dependent. Even though all the parameters involved are not fully understood at this time, the evidence indicates that configurations

can be devised which have very little effect of power on longitudinal stability. It appears that the jet-induced rolling moments in sideslip may be a serious problem, but very little information is available. At present there appears to be little hope of completely eliminating the problem; therefore, it is necessary to design the controls to handle these jet-induced rolling moments.

REFERENCES

1. Williams, John; and Wood, Maurice N.: Aerodynamic Interference Effects With Jet Lift Schemes on V/STOL Aircraft at Forward Speeds. Aerodynamics of Power Plant Installation, Pt. II, AGARDograph 103, Oct. 1965, pp. 625-651.

2. Otis, James H., Jr.: Induced Interference Effects on a Four-Jet VTOL Configuration With Various Wing Planforms in the Transition Speed Range. NASA TN D-1400, 1962.

3. Vogler, Raymond D.: Interference Effects of Single and Multiple Round or Slotted Jets on a VTOL Model in Transition. NASA TN D-2380, 1964.

4. Kuhn, Richard E.; and McKinney, Marion O., Jr.: NASA Research on the Aerodynamics of Jet VTOL Engine Installations. Aerodynamics of Power Plant Installation, Pt. II, AGARDograph 103, Oct. 1965, pp. 689-713.

5. Vogler, Raymond D.; and Kuhn, Richard E.: Longitudinal and Lateral Stability Characteristics of Two Four-Jet VTOL Models in the Transition Speed Range. NASA TM X-1092, 1965.

6. Vogler, Raymond D.: Ground Effects on Single- and Multiple-Jet VTOL Models at Transition Speeds Over Stationary and Moving Ground Planes. NASA TN D-3213, 1966.

JET WAKES IN TRANSITION FLIGHT

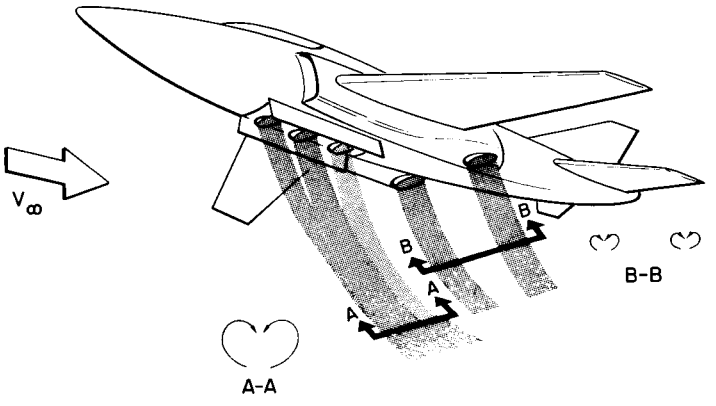

Figure 1

JET INTERFERENCE IN TRANSITION FLIGHT
TAIL OFF

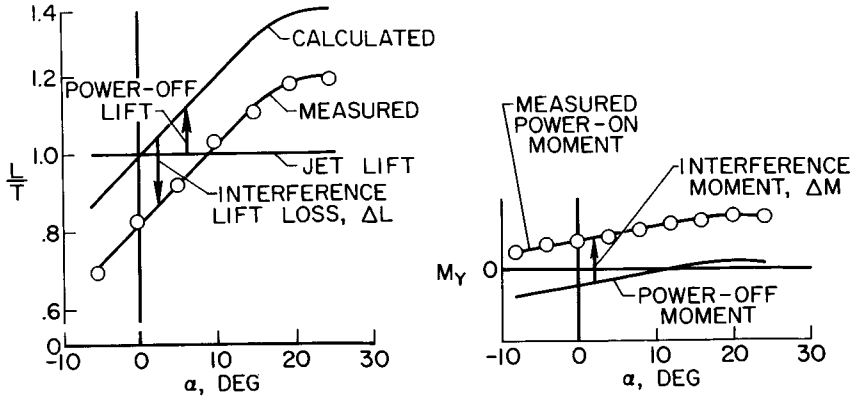

Figure 2

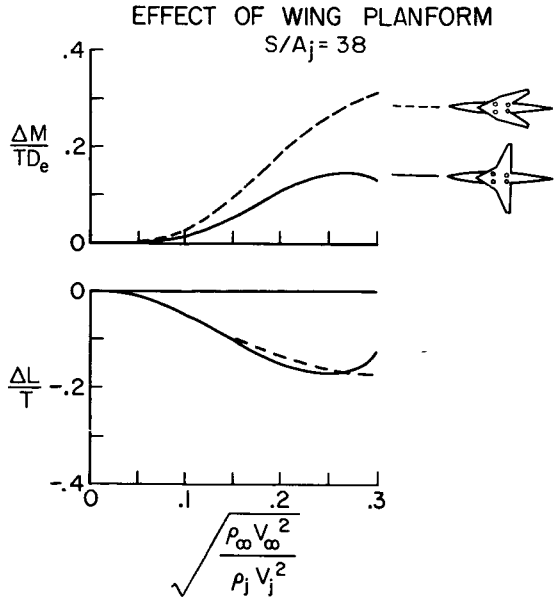

Figure 3

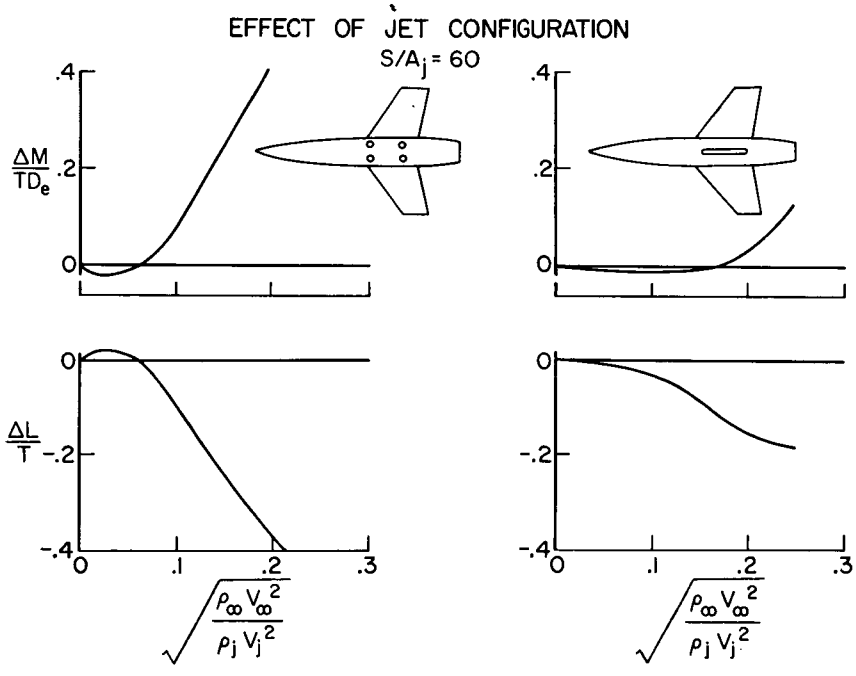

Figure 4

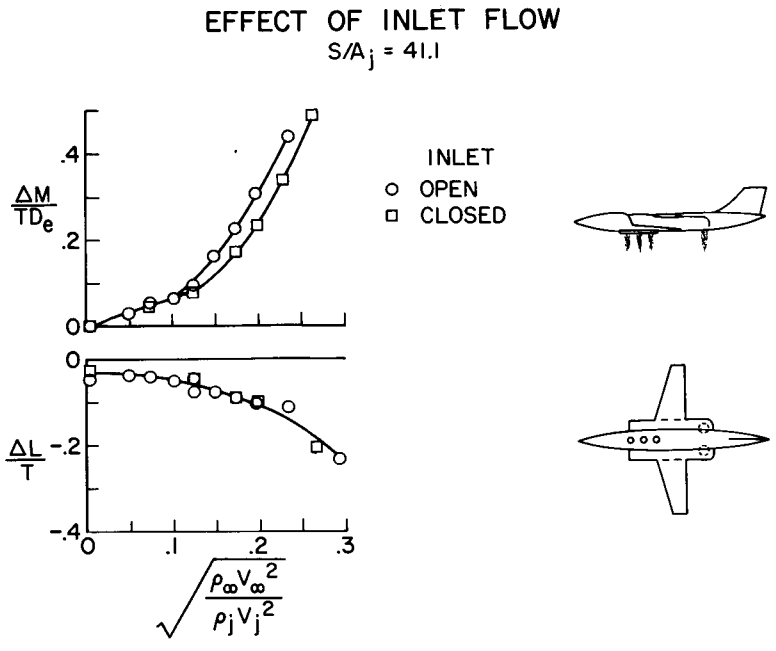

Figure 5

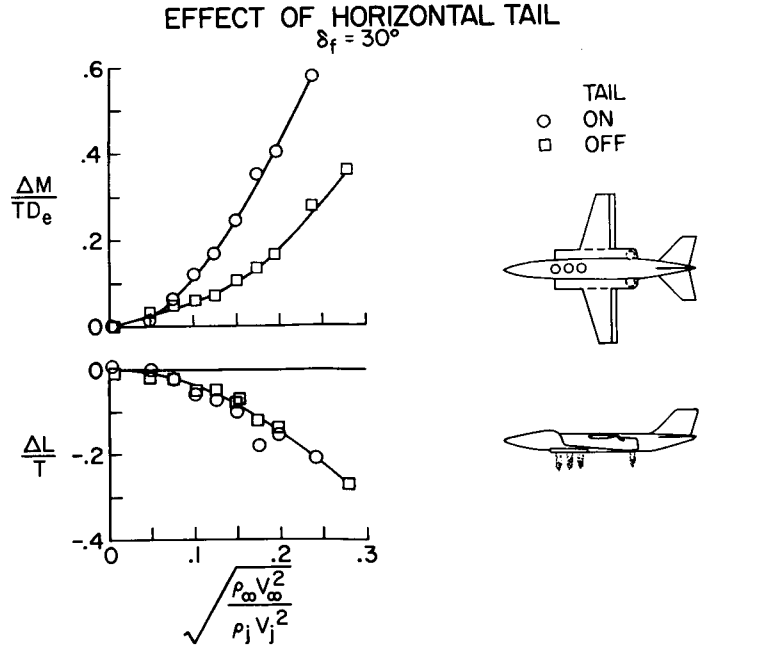

Figure 6

VORTEX PATHS IN CRUISE

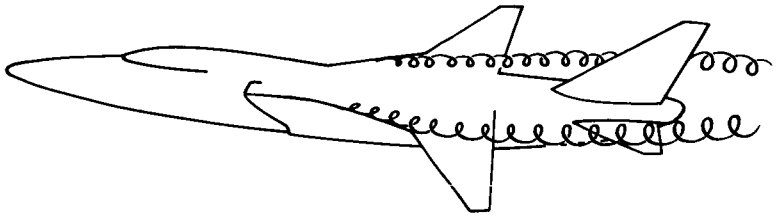

Figure 7

VORTEX PATHS IN TRANSITION FLIGHT

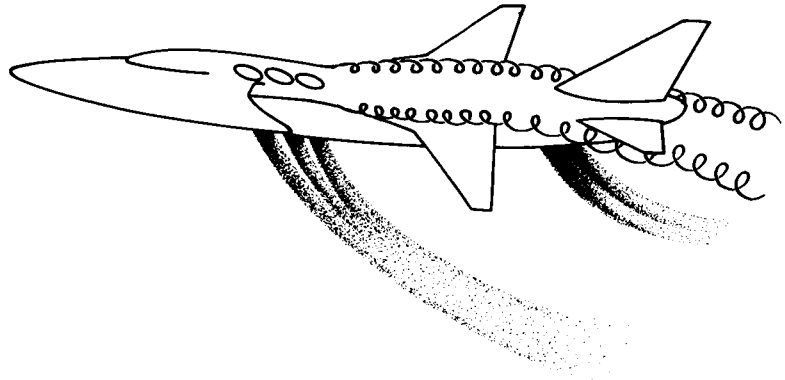

Figure 8

EFFECT OF POWER ON LONGITUDINAL STABILITY
FOUR-JET MODEL

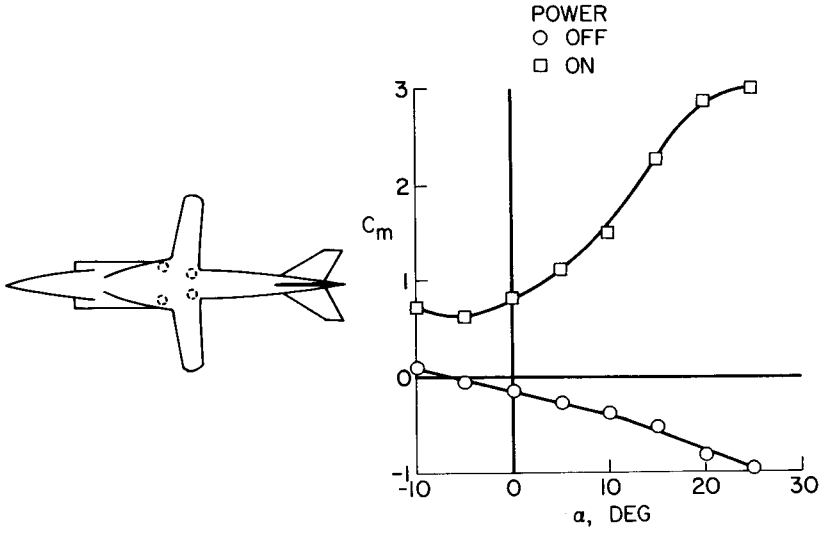

Figure 9

EFFECT OF POWER ON LONGITUDINAL STABILITY
FIVE-JET MODEL

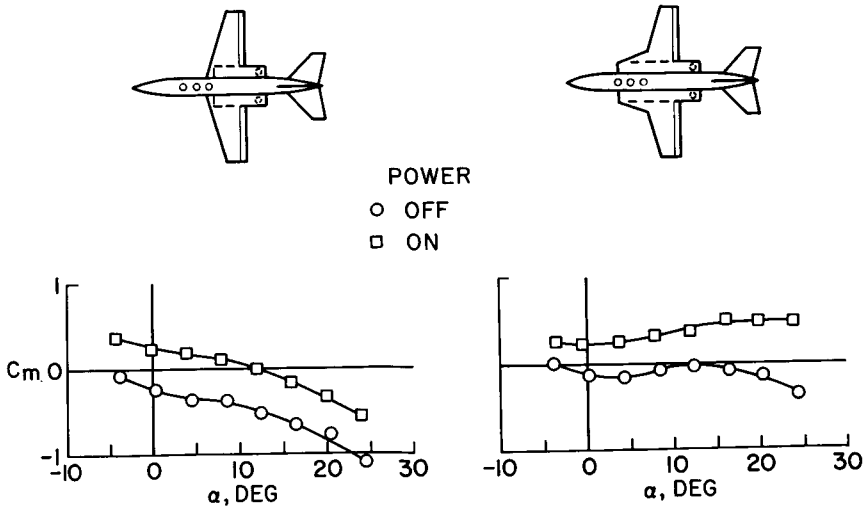

Figure 10

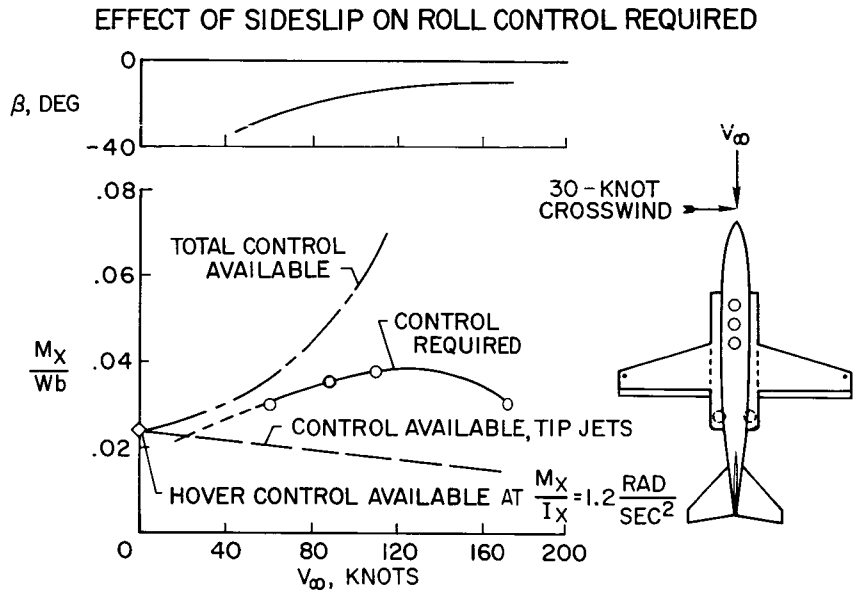
EFFECT OF SIDESLIP ON ROLL CONTROL REQUIRED
β, DEG
0
-40
.08
.06
.04
.02
Mx/Wb
TOTAL CONTROL AVAILABLE
CONTROL REQUIRED
CONTROL AVAILABLE, TIP JETS
HOVER CONTROL AVAILABLE AT Mx/Ix = 1.2 RAD/SEC2
0
40
80
120
160
200
V∞, KNOTS
V∞
30-KNOT CROSSWIND

Figure 11

Page intentionally left blank

14. CONSIDERATIONS OF HOT-GAS INGESTION FOR JET V/STOL AIRCRAFT

By H. Clyde McLemore

NASA Langley Research Center

SUMMARY

Hot-gas ingestion tests have been conducted out of doors at the Langley Research Center on a relatively large-scale fighter-type VTOL model. The model had a J85 turbojet engine mounted in the fuselage, which could be fitted with various inlet and exhaust arrangements. Results of tests of the Langley model and other research vehicles and models have shown that aircraft configuration - particularly the exhaust and inlet arrangement - and surface winds can greatly alter the hot-gas ingestion problem. Deflecting the engine exhaust gases rearward and making rolling take-offs to stay ahead of the hot-gas field appears to be one solution to the hot-gas ingestion problem. Another solution is to design the aircraft so that components such as wings shield the engine inlets from the direct path of the hot exhaust gases and so that the fountain effect caused by multiple-exhaust-nozzle configurations is minimized.

Author

INTRODUCTION

Hot-gas ingestion is the taking into the engine inlet of hot exhaust gases or of air heated by the hot exhaust. Hot-gas ingestion is a serious problem for jet VTOL aircraft because elevated inlet air temperatures cause an engine thrust loss and, since jet VTOL aircraft need all available thrust, any circumstance that reduces thrust becomes a problem. Although hot-gas ingestion is recognized as a serious problem (ref. 1), very little systematic work has been done in this field. However, some work on specific configurations has been done by several investigators (refs. 2 to 5) and, during the past year, the Langley Research Center has initiated a program to study, on a systematic basis, the hot-gas ingestion problem of jet VTOL fighter configurations. This report is in the nature of a progress report on this Langley work with results of other investigators used where appropriate.

SYMBOLS

D	diameter of nozzle
D_e	effective nozzle diameter
EGT	exhaust-gas temperature, ^{o}F

h nozzle height above ground

t time, sec

ΔT inlet temperature rise, ^{o}F

HOT-GAS INGESTION PROBLEM

The general problem of hot-gas ingestion is illustrated in figure 1. In general, the hot exhaust flow strikes the ground and circulates back into the engine inlet. The problem is the elevated inlet air temperatures and not the contamination of the air.

Hot-gas ingestion is a serious problem for jet VTOL aircraft because a thrust loss occurs as a result of elevated inlet air temperatures. For instance, an inlet temperature rise of 40^{o} F would cause about a 15-percent thrust loss. Another reason for concern is that the engine compressor may stall as a result of a very rapid rise in inlet temperature or an uneven temperature distribution about the face of the engine inlet. Of course, compressor stall would result in a large abrupt thrust loss.

The causes of hot-gas ingestion are shown in figure 1 to be (a) buoyancy of the hot gases which makes them rise to the vicinity of the engine inlets with a resulting elevation in inlet temperatures, (b) surface winds which blow the hot exhaust gases back toward the aircraft, and (c) airplane configuration - particularly the engine exhaust and inlet arrangement.

TEST CONFIGURATIONS

The models and test vehicle from which the data for this report were obtained are shown in figure 2. The sketch at the top left shows the Langley model which represents approximately a 1/3-scale model of a high-wing VTOL fighter airplane. The model is powered by a single J85 engine mounted in the fuselage, which can be fitted with various exhaust and inlet arrangements. For example, the exhaust gas can be split to exhaust through four small nozzles in a rectangular arrangement as indicated by the solid-line circles or can be exhausted through a single large nozzle as indicated by the dash-line circle. In addition, the model can take inlet air through forward-facing side inlets or through upper-surface inlets directly above the exits.

The sketch at the top right represents a small-scale high-wing model tested by Bell Aerosystems Company under contract to the Navy. This model is also a general research model and can be arranged to represent many different configurations, some of which duplicate the Langley model.

The center sketch represents a NORAIR model which is being tested at the Ames Research Center. This model has five J85 engines mounted vertically in the fuselage and two propulsion engines at the rear of the fuselage with their

exhaust diverted downward for VTOL lift. These propulsion engines can be fitted with inlets at different positions beside or above the fuselage.

The sketch at the bottom left shows the Lockheed CL-757 flying test vehicle. It has an open framework structure and three J85 engines mounted vertically at each wing tip.

The sketch at the bottom right shows a small-scale North American high-wing model. This model has four circular nozzles in a rectangular pattern and two rectangular nozzles inside of the larger four-nozzle pattern and has forward-facing side inlets. During tests of all these configurations the exhaust temperature was approximately 1200° F and the nozzle pressure ratio was approximately 2. These conditions are generally representative of the conditions for pure turbojet lift engines.

RESULTS AND DISCUSSION

Single-Nozzle Configurations

Still air.- The source of hot-gas ingestion for a single-nozzle configuration without surface winds is shown schematically in figure 3. The exhaust stream strikes the ground and spreads radially. Because of its momentum the main exhaust stream is carried far away and probably is not ingested. As the main exhaust stream flows outward, it entrains surrounding air, however, and slows down. During the entrainment process some of the hot gases are left behind and, as these hot gases rise because of buoyancy, they are close enough to the inlet to be sucked in, resulting in elevated temperatures in the engine inlet.

The temperature rise associated with single-nozzle configurations in still air is shown in figure 4. The results from two investigations using similar models are presented, and the shaded areas indicate the spread of temperatures obtained for several tests. These results show that the inlet temperature rise was of the order of 10° to 20°. This is a fairly modest temperature rise, but even this low temperature would result in a 4- to 7-percent thrust loss.

Surface winds.- The effect of surface winds on the hot-gas cloud of a single-nozzle configuration is shown schematically in figure 5. With a 2- to 3-knot wind the exhaust cloud spreads out only a distance of 20 to 30 nozzle diameters as compared with 50 to 60 nozzle diameters without wind (fig. 3). As the exhaust gases rise, the wind blows them back toward the engine inlet where they can be readily ingested. It would be expected that, where the engine is ingesting the main parts of its exhaust, the inlet air would be hotter than that for the condition of still air. Some theoretical and experimental results showing the extent of the hot-gas cloud with and without winds are presented in reference 6.

The temperature rise associated with surface winds is shown in figure 6. The models used had a top inlet, a single nozzle, and a nozzle height of

approximately 2 nozzle diameters. The lower shaded area shows the results of tests at full power with the Langley model. These data indicate an inlet temperature rise of 25° to 35° at a wind speed of about 8 knots as compared with 10° to 20° without wind. This 25° to 35° temperature rise would result in about a 12-percent loss of engine thrust. The upper shaded area shows the inlet temperature rise at idle power as measured with the Bell model for essentially the same configuration as the Langley model. The inlet temperature rise is seen to be as high as 70°. The reason the higher temperature rise occurs with idle power is probably that the exhaust-gas temperature is almost as high as that with full power and, since the exhaust velocity is much lower, the hot gas does not spread as far and thus flows back into the engine inlet while it is still hot. This high temperature with idle power, of course, would indicate that jet VTOL aircraft should not operate at idle power on the ground for prolonged periods of time without deflecting the exhaust gases away from the aircraft.

An operating technique that is generally in use to avoid this high-temperature condition is to start the engines and check them out with exhaust nozzles deflected rearward to direct the exhaust away from the aircraft. When the pilot is ready to take off, he would advance the throttle as far as possible without the aircraft starting to move forward. Then he would deflect the nozzles downward for vertical take-off and advance the throttle to full power. Discussions with NASA pilots who have flown jet VTOL aircraft have indicated that it would require approximately 5 seconds from the time the nozzles were deflected downward to the time the engines were brought up to full power for the pilot to make final checks of engine operation and to establish trim before leaving the ground. This take-off procedure would minimize the time that the aircraft would be operating in the hot-gas environment. This nozzle-deflection procedure was used for all Langley tests.

Time histories.- The take-off time element brings up the question of how quickly the temperature rise occurs. Time histories of the temperature rise of the Langley model with a top inlet and a single nozzle at a height of 2 nozzle diameters for the conditions of still air and of 5- to 8-knot winds are therefore presented in figure 7. The data for still air show that the temperature rise was fairly slow and the pilot would probably be able to make the take-off before encountering the worst of the hot-gas ingestion. With surface winds, however, the temperature rise occurred very quickly. The nozzles were deflected downward at zero time. In 5 seconds the inlet-air temperature rise was 30°, and in 7 seconds the engine compressor stalled with an abrupt loss in thrust. Sequence photographs of the development of the hot-gas cloud are given in figure 8. These photographs were made for the Langley model with a top inlet and a single nozzle at a height of 2 nozzle diameters. There was a 5- to 8-knot wind from right to left. The time interval between photographs was 0.2 second. The radius of the concrete pad was 25 feet. A pulse of smoke was injected into the upwind side of the nozzle at zero time, and it can be seen that the exhaust gases spread only a short distance before they rose and were blown back into the inlet. The engine apparently began to ingest the hot gases in about 1 second; this rapid ingestion agrees with the rapid onset of the temperature rise shown in figure 7.

This rapid temperature rise, which tends to cause compressor stall, may be a more serious problem than the maximum level of the temperature. It is apparent from figures 3 to 8 that wind is an important factor in the problem of hot-gas ingestion for the single-nozzle configuration.

Multiple-Nozzle Configurations

Still air.- The fundamental characteristics in still air of the exhaust-gas flow for the configuration with two lift engines some distance apart are shown in figure 9. The ordinate is the nozzle height in effective diameters. The effective diameter is the diameter of a circle whose area is equal to the sum of the areas of all the nozzles. A part of the exhaust gas spreads out radially, in a manner similar to that of a single jet, and is not ingested. Another part of the exhaust gas flows toward the center and, since it cannot escape in this direction, it goes upward in a fountain between the engines. The gases in this fountain are very accessible to the engine inlets and are still very hot because they have not traveled far and very little mixing has taken place. This, of course, is what happens when there is no airframe between the engines. An airframe would modify the flow somewhat, but the hot gases would still tend to flow upward between the engines and spread out along, or around, the underside of the airframe.

The inlet temperature rise in still air as a function of the height of the jet nozzles above the ground in effective nozzle diameters is presented in figure 10 for three multiple-nozzle models. The data shown are for the Langley, Bell, and North American models for ratios of nozzle height to effective nozzle diameter. All three models had four exhaust nozzles arranged in a rectangular pattern and were tested with side inlets. The Langley model was also tested with a single top inlet instead of the side inlets.

The data show that both side and top inlets experienced very high temperatures when the model was near the ground, with the top inlet experiencing the much higher temperature. These very high temperatures which occurred within 2 seconds after downward deflection of the exhaust nozzles would make VTOL operation impossible. The thrust loss would be too great and the engine compressor would probably stall. As nozzle height was increased, the temperature rise decreased very rapidly; at a height of 5 nozzle diameters the temperature rise was of the order of 20°, a temperature rise no greater than that experienced by the single-nozzle configuration.

Surface winds.- The inlet temperature rise as a function of wind speed in knots for the four-nozzle configuration is shown in figure 11. Since all the Langley tests have been conducted out of doors, the wind speeds are for the existing ground winds at the time of the tests. The data are for head-on winds and exhaust nozzle heights of 2.5 and 5 effective nozzle diameters for the four-nozzle configuration with either top or side inlets. The shaded areas represent the scatter of several test points for each configuration. These temperatures occurred within 2 seconds after downward nozzle deflection. Wind velocity seems to have some effect on hot-gas ingestion, but the inlet configuration is seen to be a much more important parameter. The data do indicate,

however, that wind speeds above 15 knots tend to decrease the hot-gas ingestion. Since results for still and near-still air at normal landing-gear heights of 2 to 3 nozzle diameters showed an inlet temperature rise too great for VTOL operation, it appears that the rolling take-off technique would be required here. Of course, vertical take-off over a raised grating of some sort would be effective in reducing hot-gas ingestion, but this does not seem to be a very practical solution for operational aircraft.

The important point to be gained from these data is not that the hot-gas ingestion problem is very bad for multiengine configurations, but that it is very configuration dependent. For example, if all the exhaust nozzles were grouped very close together, they would be expected to act effectively as a single nozzle and to give the lower inlet air temperatures associated with a single-nozzle configuration mainly because the close spacing would eliminate the fountain of hot gases between the jets. There may be other ways to eliminate this fountain of hot gases which apparently causes the high inlet temperatures. For example, some tests with the Bell model with four exhaust nozzles in line and with upper-surface inlets showed an inlet temperature rise of only about 10° F. Another important configuration parameter might be wing position. Some tests of the NORAIR model at the Ames Research Center have shown that much lower inlet air temperatures were obtained when the wing was in a low position than when it was in a high position. All these various results simply indicate that the hot-gas ingestion problem is very configuration dependent and, at this time, not enough is known to generalize on the problem or make a reliable prediction of inlet air temperature for arbitrary configurations.

The effect of winds on a very different type of multiengine configuration - one with very widely spaced engines - is shown in figure 12. The configuration is the Lockheed CL-757 flying test vehicle, a front view of which is sketched on the right-hand side of the figure. A plan view of the configuration is shown in figure 2. The CL-757 has three engines mounted on each wing tip with very little airframe between them. For the wind condition illustrated in figure 12 it would be expected that the winds would blow the fountain of hot gases between the engines toward the downwind engines. The temperature rise in degrees Fahrenheit was obtained for various stations around the face of the center downwind-engine inlet and is shown on the left-hand side of the figure. These temperatures are incremental values above an ambient temperature of 53° F. Some of the temperatures are relatively high and there is a large temperature distortion across the engine inlet. This distortion and the high inlet temperatures together caused the engine compressor to stall with an abrupt loss in thrust.

There are other instances in which a rapid temperature rise and severe temperature distortions such as these have caused compressor stall. For some test conditions the large multiple-engine NORAIR model at the Ames Research Center (fig. 2) has experienced distorted and very high inlet temperatures which have resulted in compressor stall for one or more engines.

It has been emphasized that in many investigations engine-compressor stall has been encountered as a result of inlet temperature distortion or rapid inlet temperature rise. The compressor-stall problem was probably worse for these

research models and test vehicles than it will be for operational aircraft because early versions of engines which were particularly sensitive to temperature effects were used. Later versions of these engines are known to be less sensitive to the rate of temperature rise or to temperature distortion. These factors, however, should continue to be given consideration in V/STOL engine technology.

CONCLUDING REMARKS

One of the principal causes of the hot-gas ingestion problem is the aircraft configuration, that is, the arrangement of engine nozzles and inlets. For multiple-nozzle configurations, the exhaust gas tends to flow upward between the nozzles where it may reach the vicinity of the inlets very quickly while it is still very hot. The solution to this situation appears to be to group the engine exhaust nozzles in such a manner that the hot-gas fountain effects are minimized and to design the aircraft so that components such as the wing shield the inlets from the direct path of the hot gases. The other major cause of the hot-gas ingestion problem is surface winds. The winds blow the far-field gases back toward the aircraft and into the inlets before these gases have had time to mix with the surrounding air and cool off. The wind problem is difficult to assess since different configurations are affected differently by winds. One solution to the wind problem, and perhaps the configuration problem as well, appears to be to deflect the engine exhaust so that it is directed away from the aircraft and to make rolling take-offs as a means of staying ahead of the hot-gas field.

One observation that should be made is that the state of the art of the hot-gas ingestion problem is still in an exploratory stage. It is certainly not such that the inlet temperature rise can be predicted for any particular configuration or operating condition. At the present time, therefore, in the development of a VTOL airplane, hot-gas ingestion tests should be made for the particular configurations and operating conditions that are expected to be encountered.

REFERENCES

1. McKinney, M. O., Jr.; Kuhn, R. E.; and Reeder, J. P.: Aerodynamics and Flying Qualities of Jet V/STOL Airplanes. [Preprint] 864A, Soc. Automotive Engrs., Apr. 1964.

2. Speth, Robert F.; and Ryan, Patrick E.: A Generalized Experimental Study of Inlet Temperature Rise of Jet VTOL Aircraft in Ground Effect. Rept. 2099-928003 (Contract No. N600(19)63320), Bell Aerosystems Co., Apr. 5, 1966.

3. Mohne, E. A.: V/STOL Exhaust Gas Ingestion Test Hovering Test Facility. NA 64-1142, North Am. Aviation, Inc., Mar. 1964.

4. Smith, Fred: CL 757 Flight Test Results. Rept. No. LR 18781 (Contract AF 33(657)-10534), Lockheed - California Co., Apr. 28, 1965.

5. Rolls, L. Stewart: Operational Experiences With the X-14A Deflected-Jet VTOL Aircraft. Conference on Aircraft Operating Problems, NASA SP-83, 1965, pp. 299-307.

6. Cox, M.; and Abbott, W. A.: Studies of the Flow Fields Created by Single Vertical Jets Directed Downwards Upon a Horizontal Surface. N.G.T.E. Mem. No. M.390, Min. Aviation (Brit.), Oct. 1964.

HOT-GAS INGESTION

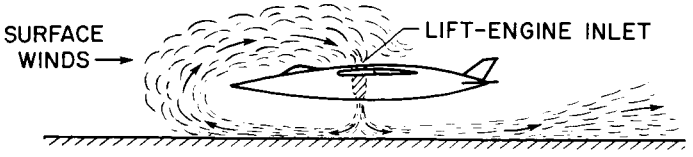

REASONS FOR CONCERN

- THRUST LOSS
  - TEMPERATURE RISE OF 40°F CAUSES 15% LOSS OF THRUST
- COMPRESSOR STALL
  - RAPID TEMPERATURE RISE
  - TEMPERATURE DISTRIBUTION

CAUSES

- BUOYANCY OF HOT EXHAUST
- SURFACE WINDS
- CONFIGURATION
  - EXHAUST AND INLET ARRANGEMENT

Figure 1

VTOL MODELS AND TEST VEHICLE

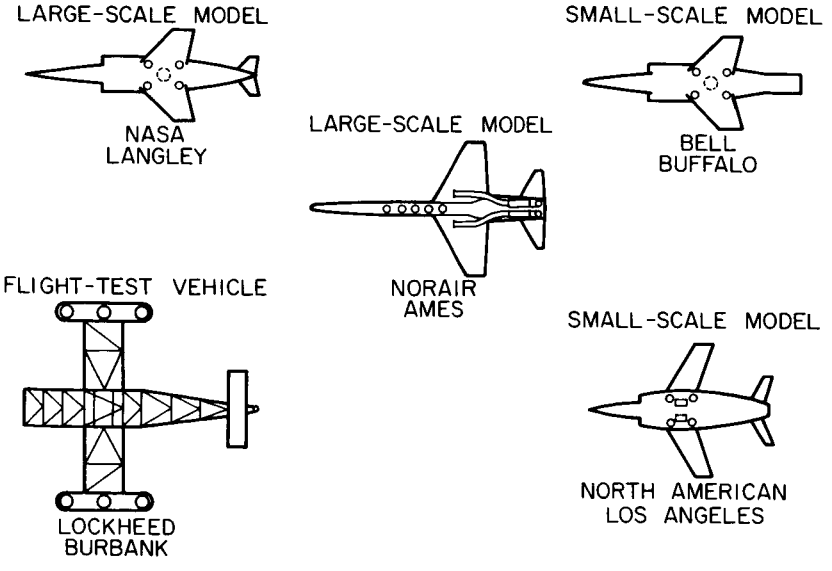

Figure 2

EXTENT OF HOT-GAS CLOUD IN STILL AIR

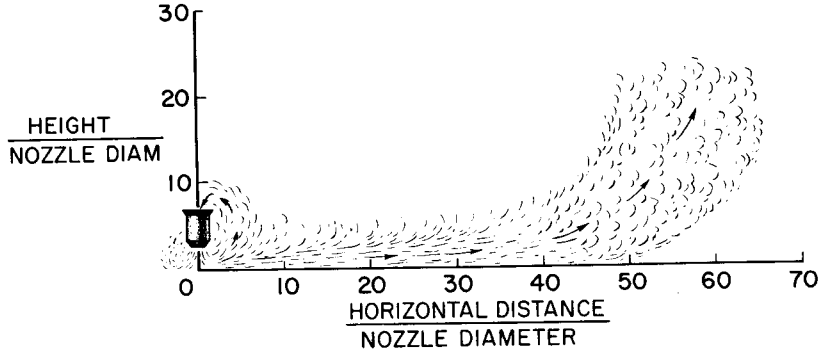

Figure 3

INLET TEMPERATURE RISE IN STILL AIR
TOP INLET; SINGLE NOZZLE; EGT ≈ 1200°F

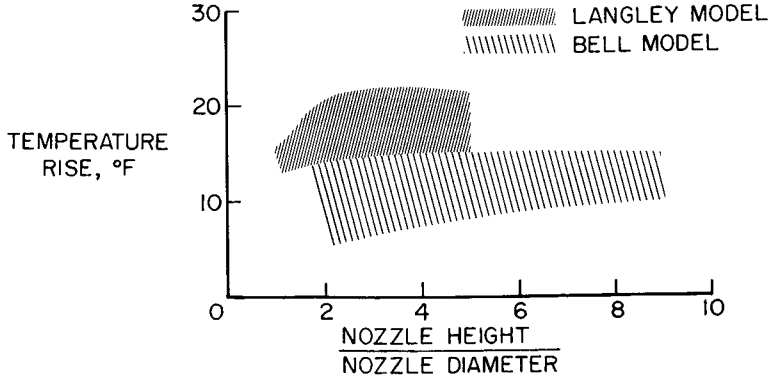

Figure 4

EXTENT OF HOT-GAS CLOUD WITH WIND

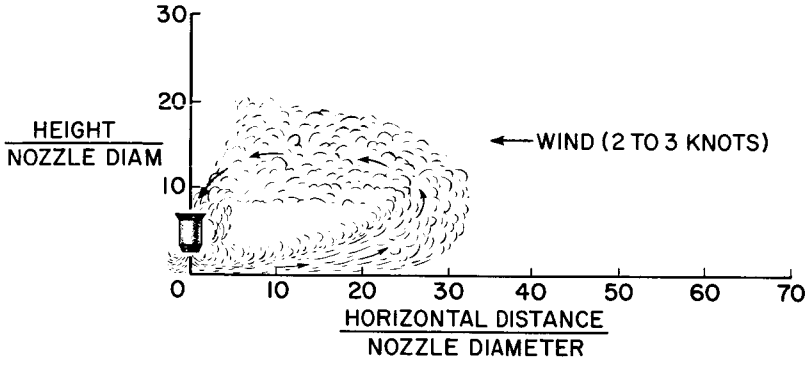

Figure 5

INLET TEMPERATURE RISE WITH WIND
TOP INLET; SINGLE NOZZLE; h/D ≈ 2

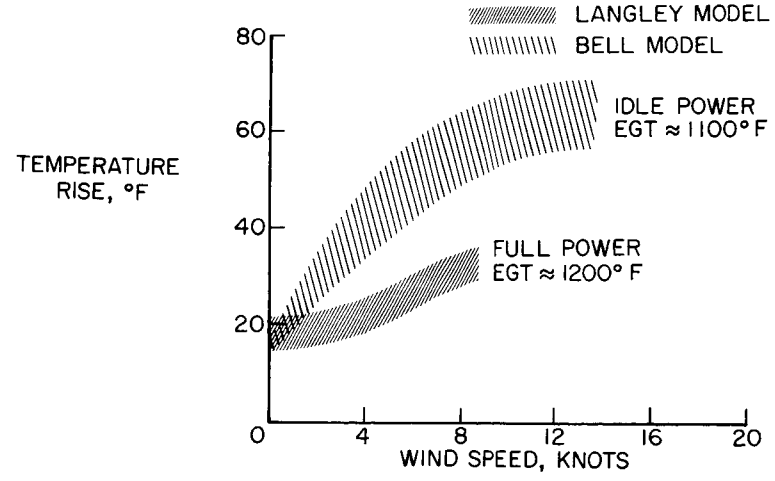

Figure 6

TIME HISTORY OF TEMPERATURE RISE
LANGLEY MODEL; TOP INLET; SINGLE NOZZLE; EGT ≈ 1200° F

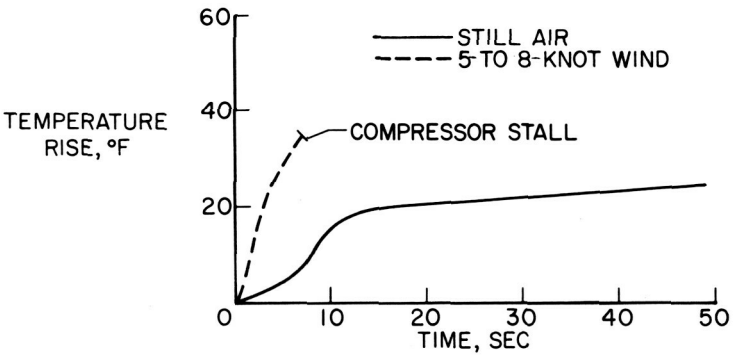

Figure 7

SEQUENCE PHOTOGRAPHS OF HOT-GAS CLOUD
FULL POWER; TOP INLET; SINGLE NOZZLE
← 5- TO 8-KNOT WIND

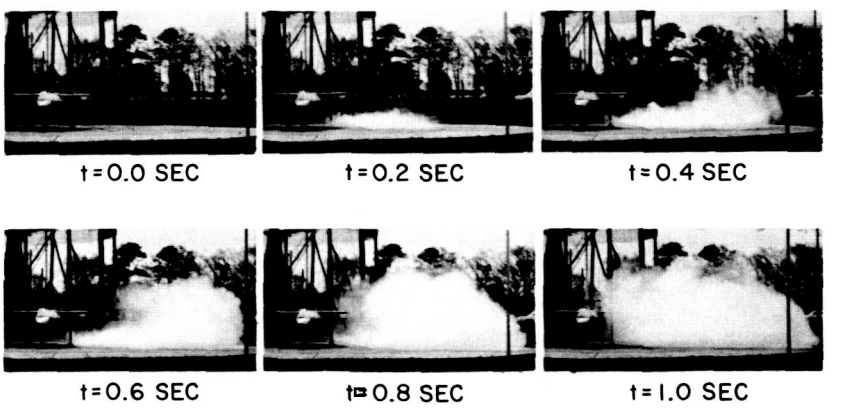

Figure 8 L-2652-8

EXTENT OF HOT-GAS CLOUD IN STILL AIR

MULTIPLE NOZZLES

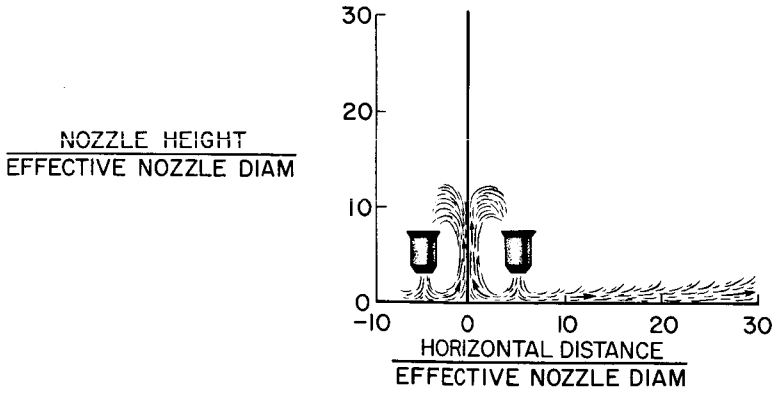

Figure 9

INLET TEMPERATURE RISE IN STILL AIR

MULTIPLE NOZZLES ; EGT ≈ 1200° F

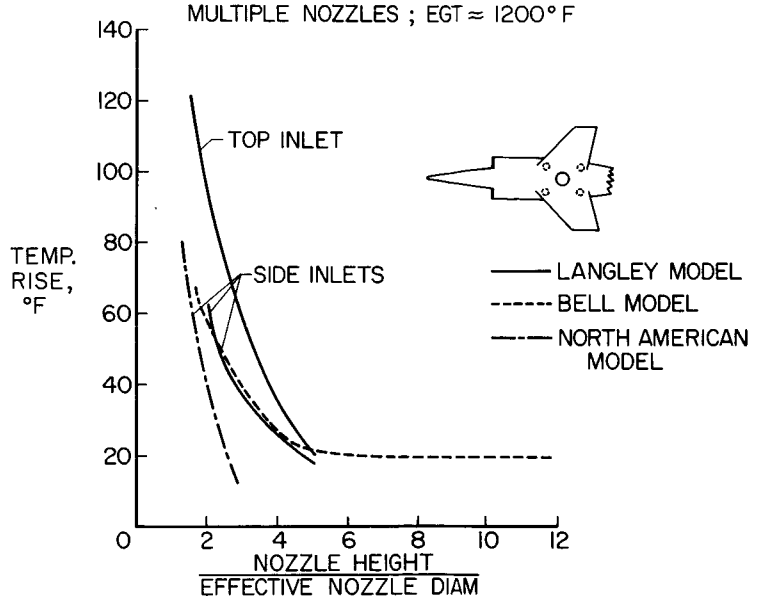

Figure 10

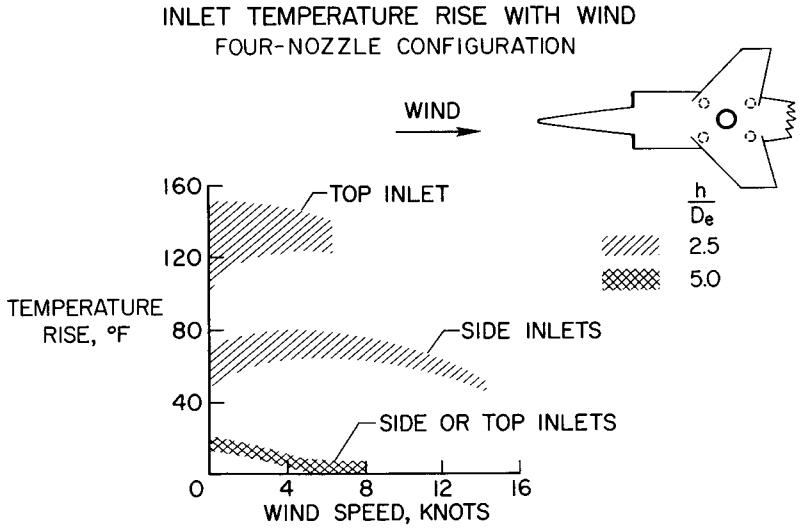

Figure 11

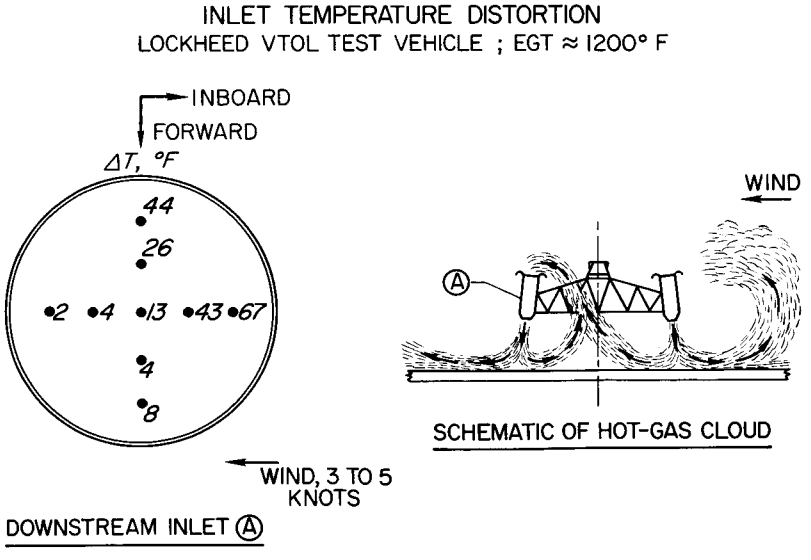

Figure 12

15. CHARACTERISTICS OF TWO LARGE-SCALE JET-LIFT PROPULSION SYSTEMS

By William H. Tolhurst, Jr., and Mark W. Kelly
Ames Research Center

SUMMARY

The characteristics of jet-lift VTOL aircraft have been investigated at the Ames Research Center in experimental studies of two full-scale configurations having YJ-85 GE-5 turbojet engines as simulated lift engines. One model simulated a supersonic fighter-type airplane and was used to determine the effects of wing and cruise engine inlet position on exhaust gas ingestion during static operation near the ground. The other model represented a wing-mounted lift-engine pod suitable for use on a transport type airplane. This model was used to determine engine inlet pressure recovery and flow distortion, induced aerodynamic effects, and some aspects of lift engine operation during forward flight.

Presented in this paper are time histories, obtained during the static tests, of engine inlet pressure, and exhaust gas pressure and temperature, the change of jet-induced lift loss with variation of height above the ground, some sound pressure level measurements and a brief table evaluating the various configurations for susceptibility to exhaust gas ingestion. Data presented for the lift-engine pod test in the wind tunnel are the inlet flow distortion and pressure recovery for ratios of free-stream velocity to inlet velocity up to 2.8, angles of attack up to 16°, and angles of yaw to 8° for several types of engine inlets. Also presented are the effects of engine operation on the aerodynamic lift forces during forward flight and engine windmilling performance at various angles of attack at 150 knots airspeed.

The results indicated that the engine inlets may ingest exhaust gases with temperatures of the order of 200° F, and that ingestion of this intensity could cause the engines to stall. By properly locating the inlets with respect to the exhaust nozzles and by taking advantage of the shielding effect of the wing, ingestion was avoided. There did not appear to be any extreme problems in operating the lift engines at free-stream speeds up to 150 knots. These engines operated very well with a simple bell-mouth inlet. Engines located ahead of the wing reduced the overall lift of the aircraft while engines located behind the wing increased the lift.

INTRODUCTION

The use of turbojet engines as the lifting elements in VTOL aircraft involves several research areas. Some of these are ground interference effects on the forces and moments, recirculation of the engine exhaust flow

back into the engine inlets, the effects of cross flow on the engine inlet airflow distortion and pressure recovery, and the induced aerodynamic effects in forward flight.

To study these problem areas, investigations have been conducted at the Ames Research Center with two large-scale models using YJ85 GE-5 turbojet engines as lift engines. This paper presents some of the results of these investigations, in particular, exhaust gas ingestion, inlet flow distortion and pressure recovery, the implications of these effects on engine operation, and the aerodynamic forces induced by the flow through the propulsion system.

SYMBOLS

α	angle of attack of wing chord plane, deg
D_i	jet engine inlet diameter, ft
D	jet engine tail-pipe diameter, ft
δ	density ratio
F	engine gross thrust, lb
F_{max}	maximum engine gross thrust, lb
L	lifting force on model, lb
h	height of model above ground, ft
$P_{T_{max}}$	maximum local total pressure in engine inlet, psf
$P_{T_{min}}$	minimum local total pressure in engine inlet, psf
$P_{T_{av}}$	integrated average total pressure in engine inlet, psf
P_T	total pressure in free stream, psf
V_i	velocity in engine inlet, fps
V_∞	velocity in free stream, fps
ψ	angle of yaw, deg

MODELS AND APPARATUS

The model used in the exhaust gas ingestion investigation is shown in figure 1 installed on the outdoor static test facility at Ames Research Center. The strut mounting system was capable of changing the model elevation from

2.7 to 10 tail-pipe diameters measured from the bottom of the fuselage at the location of the lift engines. The angle of attack of the model could be varied as much as $\pm 10^{\circ}$ depending on the height above ground.

The model contained five YJ85 GE-5 turbojet engines mounted in the fuselage in tandem with an inclination of 10° forward of the vertical (fig. 2). This inclination allowed the use of a relatively large radius bell-mouth entry on the forward side of the inlet.

Deflector doors were mounted on the lower surface of the fuselage at the exhaust nozzle of each engine. Two cruise engines were mounted horizontally in the tail of the model. The tail-pipe consisted of a 90° elbow which directed the exhaust gas downward to simulate the exhaust of a vectored-thrust engine. Inlets for these two engines could be located in three different places. In the top-mounted position the two inlets were installed side-by-side just behind the aft lift engine inlet, as shown in figure 2. In the rear position the inlets were located on either side of the fuselage in about the same vertical plane as for the top inlet but slightly below the fuselage center-line plane. In the forward or front positions the inlets were also slightly below the fuselage center-line plane but were extended well forward of the wing leading edge.

In addition to the two positions indicated in figure 2, the wing could be located mid-way between the two positions shown. The wing could also be located 56 inches forward of the position indicated and at the same three vertical heights. The horizontal tail remained fixed in the position indicated.

The normal and axial forces were measured by means of three load cells supporting the model. Inlet temperatures were obtained from rakes of rapid-response thermocouples located near the compressor plane of each engine. Engine tail-pipe pressure and temperature were also measured with all data being recorded on oscillographs to obtain time histories of each variable. Sound pressure level measurements were obtained by means of a hand-held sound level meter set at the flat response or "C" setting.

The model used for the forward flight portion of the investigation is shown in figure 3 installed in the Ames 40- by 80-foot wind tunnel. The model was representative of a wing-mounted lift-engine pod similar to that proposed for some transport and cargo aircraft. The pod contained five YJ85 GE-5 turbo-jet engines mounted in tandem as in the previous model. Unlike the static test model the wing was fixed in the position sketched in figure 4.

On this model the engine inlet pressures were measured by means of total pressure probes arranged to give the integrated average pressure over the inlet area as well as the local pressure. Inlet temperatures were measured by one thermocouple in each inlet. Tail-pipe pressures and temperatures were measured on each engine. The model was mounted on the three-strut support system and the model total forces were measured on the wind-tunnel balance systems. The data were obtained for this model after steady-state flow conditions were established.

TESTS AND PROCEDURES

Static Tests

The exhaust gas ingestion tests were conducted at five different heights above the ground plane from 2.7 to 10 tail-pipe diameters. At each height the engines were brought up to 70 percent rpm with the deflector doors deflected to 50° aft from the vertical. When steady flow conditions were obtained, all engines were simultaneously accelerated to full power as rapidly as possible, and, at the same time, all deflector doors were simultaneously deflected to a position that produced thrust normal to the model center line.

The engines were held at full power for a time interval which varied from 30 seconds at the maximum model height above ground to 5 seconds at the minimum height. The time histories of all variables were obtained from the time at which all engines were stabilized at 70 percent rpm until several seconds after reduction in speed from full power.

Data were obtained at ±3° as well as 0° angle of attack.

Atmospheric pressure and temperature as well as wind velocity and direction were recorded for each run. While most of the data were obtained with the wind velocity at 5 knots or less, some data were obtained at 15 knots to determine the effect of wind velocity on ingestion.

Wind-Tunnel Tests

The wind-tunnel tests were conducted at free-stream velocities ranging from 0 to 150 knots (which corresponds to a dynamic pressure from 0 to 76 psf). Engine thrust was varied from 0 (power off) to maximum available. The angle-of-attack range investigated was from 0° to +16°, and the yaw angle range extended from 0° to +8°.

RESULTS AND DISCUSSION

Static Test Characteristics

Exhaust gas ingestion.- During the early part of this test it was determined that there were two distinct types of exhaust gas ingestion that required consideration. The first type was characterized by exhaust flow that extended along the ground for some distance away from the airplane. After a large decrease in velocity these exhaust gases floated upward as a cloud of hot gas which eventually circulated back to the inlet. The mixing between the exhaust gas and the atmosphere was such that the temperature of the gas ingested in the engine inlets was only a few degrees higher than ambient air temperature.

The second type of exhaust gas ingestion was characterized by the high velocity exhaust jet meeting another exhaust jet flowing in the opposite direction. This resulted in an upward flow of gases having high temperature with little opportunity for mixing with the ambient air. These hot exhaust gases entered the engine inlet in a fairly localized region of the inlet. This localized flow of hot gases occasionally distorted the temperature distribution at the face of the engine compressor sufficiently to stall the engine.

The first type of ingestion is more dependent on atmospheric conditions than on airplane configuration. Since the resulting rise in inlet temperature is relatively modest, the only result will be loss of vertical thrust. However, the second type of ingestion can cause loss of one or more engines by causing a compressor to stall. This second type of ingestion was investigated during this test.

Figure 5 shows the results for a configuration having high ingestion of exhaust gas. The pattern of the exhaust gas flow is indicated by the arrows in the sketch. The lift engine exhaust gas flows down to the ground and there turns parallel to the ground. The portion of the gases which are flowing aft along the ground meet with the cruise engine gas which is flowing forward. These two flows combine and flow upward in a high temperature turbulent flow. As indicated, some of this exhaust gas entered the inlets for the cruise engines. The remainder flowed up to the wing which deflected a portion of the exhaust gases to the vicinity of the lift engine inlets. These exhaust gases were drawn into the engine inlets. As shown in the representative time histories in figure 5, the local inlet temperature was nearly 200° F.

The initial value shown on these time histories is for all six engines operating at low thrust and with the exhaust deflected aft. Under these conditions no ingestion was encountered. This may be verified by the low initial inlet temperature of 38° F (which was the same as the ambient temperature). About two seconds after the start of the record the engine was accelerated to full thrust and the exhaust gases were simultaneously directed straight down. Immediately after reaching full thrust, exhaust gas was ingested in the inlet. This is shown by the large increase and violent fluctuations in inlet temperature. About three seconds after the engines reached full thrust an extremely hot gust was ingested which caused the engine to stall. This is indicated by the sudden decrease in exhaust gas pressure and increase in exhaust gas temperature. These results are shown for engine number 3. Engine number 4 stalled about three seconds later with like indications of exhaust gas ingestion and compressor stall.

Figure 6 shows a configuration that ingested very little exhaust gas. The engines were accelerated following the same procedure as before. However, in this case the inlet temperature remained at about 56° F (which was the ambient value for this test), indicating that there was very little if any ingestion. These same results were also indicated for all the other inlets in this case. It should be noted that these particular data were obtained under very moderate wind conditions, about 4 knots from the tail. The effects of strong winds or wind from other directions could modify these results.

Other configurations tested and some brief comments concerning the effect of configuration on the ingestion are summarized in table I.

The nomenclature concerning the positions of the wing and the cruise inlets is defined in the section "Models and Apparatus." In addition, two combinations of lift engines were tested, the arrangement shown in figure 5 using the front four engines and another arrangement using the front three engines and the rearmost (or engine number 5). In this case engine number 4 inlet and tail pipe were covered to prevent any flow through the engine.

The second arrangement produced a separation of about two tail-pipe diameters between engines 3 and 5 which resulted in the exhaust gases from these two engines meeting and being directed upward in a high velocity stream as was described before for the configuration having high ingestion. When the engines were spaced close together, as were the front three engines, the jets tended to be entrained by each other and formed a single jet of oblong cross section.

From the foregoing results it is possible to define some general design provisions which have been found to alleviate exhaust gas ingestion. It is generally beneficial to locate the cruise engine inlets high on the fuselage and away from the exhaust nozzles and to place the wing to act as a shield between the exhaust nozzles and the inlets. A low wing provides more protection against ingestion than does a high wing because the hot exhaust gases deflected by the low wing are directed back into the vicinity of the exhaust nozzles and are captured by jet entrainment. With a high wing the exhaust gases may flow around the wing and be drawn into the inlet. It is also beneficial to group the lifting engines as close together as possible. When the engines are spaced apart from each other, the exhaust gases meet between the engines and are directed upward in a high velocity, high-temperature stream which may be ingested by the inlets.

Jet induced lift loss.- While a configuration having a low wing may protect the engine inlets from exhaust gas ingestion, the jet induced lift loss that might be incurred from a wing in this position must be considered. Figure 7 shows the ratio of total lift to the sum of the thrust of the individual engines as a function of height above the ground plane for three configurations. Here it is seen that with engines 1, 2, 3, and 5 along with the cruise engines operating with the wings off or with the wings on, there is a slight decreased in lift loss as the ground height is decreased. With the other configuration (engines 1, 2, 3, 4 and the two cruise engines) there is very little change in net lift with variation in height. From this it may be concluded that, for this type of configuration, the so-called "suck-down" effect would be of secondary concern when compared to the problem of exhaust gas ingestion in design considerations.

Noise measurements.- Since the noise of jet VTOL airplanes is a matter of concern in some applications, some noise level measurements were made during these tests. Early in the program it appeared to test observers that the noise was not nearly so severe as would be anticipated for operation of six of these engines. Measurements were made with various numbers of engines operating and some of the results are shown in figure 8. This figure presents a plot of sound pressure level in decibels as a function of the number of engines

operating. As shown by the measurements indicated here, the sound pressure level first increased but then decreased as additional engines were brought into operation. The cross-hatched area represents the bounds of the variation in sound pressure level measured by two independent systems during these tests. Also shown in this figure is the theoretical increase in noise that would be expected from a simple addition of the sound level generated by the individual engines. The reason for the reduction in sound pressure level obtained experimentally is not understood at the present time. However, it should be noted that the exhaust jets of the five lift engines mix very rapidly to form a long rectangular jet. Such jets, which have a larger perimeter compared to their area than do circular jets, are known to provide sound suppression. Therefore, it might be expected that the sound pressure level should not increase as rapidly as indicated by the theoretical curve which assumes no combining of the jets. No general conclusions can be drawn from this limited amount of data; however, it does appear that significant sound attenuation or cancellation effects may exist.

Forward Flight Characteristics

Inlet performance.- The inlet performance obtained with the simple bell-mouth inlets is shown in figure 9 over a range of free-stream velocities from 0 to 150 knots. These results were obtained with all five engines operating simultaneously. These data show that these simple inlets gave relatively low inlet flow distortion levels and high inlet pressure recoveries over a wide range of velocity ratios. (A velocity ratio of 2.8 corresponds to a flight speed of 150 knots with the engines set at idle power.) It should be noted that, since the engines were inclined 10° forward of the vertical, it was possible to provide a relatively large radius on the upstream side of the bell mouth.

Figures 10(a), (b), and (c) present inlet flow distortion and pressure recovery as a function of angle of attack for various velocity ratios. These data show that, except for the inlet for the number 2 engine, the flow distortion and pressure recovery were not seriously affected by angle of attack. The high flow distortion level shown for the inlet of engine number 2 was caused by a high angularity of the external flow at junction of the wing leading edge with the lift engine pod. However, the distortion level shown for the number 2 engine inlet is still below the value of 10 percent specified as an operational maximum for this engine.

The effect of sideslip on pressure recovery and flow distortion for the bell-mouth inlets is shown in figure 11. Comparison of these results with those of figure 10(a) shows that sideslip increased the flow distortion index of the number 2 engine inlet from a value of about 0.075 to 0.12 at angle of attack.

The flow distortion and pressure recovery of scoop-type inlets is shown on figures 12(a), (b), and (c). By comparing the results shown on figure 12 with those on figure 10 it may be seen that the scoop inlets were more sensitive to angle of attack and velocity ratio than were the bell-mouth inlets. The high distortion level shown on figure 12(b) for the number 2 engine inlet

was caused by flow separation from the upper surface of the scoop on the number 1 engine inlet. This separated flow entered the number 2 engine inlet and caused the high distortion shown at 16° angle of attack. This problem could be alleviated by using a smaller scoop angle setting for the number 1 engine inlet. However, there was then insufficient inlet area for the number 1 engine under conditions of high power and low flight speeds. This problem could be solved, of course, by the addition of pressure-operated louvers in the scoops or by other means of increasing the inlet area.

The effect of adding sides to the scoop inlets is shown on figure 13. These results show that the addition of sides (or end plates) increased the inlet flow distortion and reduced the pressure recovery.

Figures 14(a), (b), and (c) present the flow distortion and pressure recovery characteristics of the bell-mouth inlets equipped with side-folding doors. These doors were equipped with longitudinal hinges and opened laterally away from the inlets. In the fully opened position the surface of the door served to increase the size of the bell mouth as shown on the sketch on figure 14(a). As may be seen by comparison of the results presented on figure 14 with those presented on figure 10 the side-folding doors significantly reduced the flow distortion of the number 2 engine inlet. The use of the side-folding doors reduced the external flow distortion caused by the intersection of the wing leading edge with the lift engine pod, but increased the flow distortion in the number 1 engine inlet. This was caused by a similar type of external flow distortion caused by the intersection of the leading edge of the side-folding door with the lift-engine pod, and probably could be eliminated by extending the leading edge of the door further ahead of the inlet.

The effects of sideslip angle on the flow distortion and pressure recovery of the inlets with the side-folding doors are shown on figures 15(a), (b), and (c). Comparison of these data with those of figure 11 shows that the side-folding doors significantly reduced the flow distortion of the number 2 engine inlet at high angles of sideslip and angles of attack.

Induced lift.- The effect of engine operation on the lift characteristics of the complete model is shown on figure 16. This figure shows the ratio of induced lift to the lift component of the engine's static thrust as a function of the ratio of free-stream momentum to jet momentum per unit area. The results obtained with only the number 1 engine operating show that there was a significant loss of lift due to engine operation throughout the flight speed range. This engine was located ahead of the wing and caused a downwash on the wing. Conversely, operation of the number 5 engine, which was located slightly aft of the wing, induced a favorable lift effect throughout the flight speed range. The number 3 engine, which was located approximately at the mid-chord of the wing, had relatively small induced lift effectiveness. When all five engines were operated simultaneously, these various induced effects cancelled each other so that the induced lift with all five engines operating was essentially zero. These data indicate that it should be possible, by judicious arrangement of the lift engines, to create favorable interference effects between the engine flow and the flow over the wing so that beneficial lift effects are obtained. This would, of course, improve the STOL takeoff performance of jet-lift aircraft.

Engine operation.- Some general observations concerning the operation of the engines during these tests in the wind tunnel are provided here, since there is relatively little information available on the operational aspects of turbojet-lift-engine configurations. First, there were no serious problems connected with exhaust gas ingestion; that is, no extremely high temperature air was ingested into the inlets, and no engines stalled as a result of hot gas ingestion. This was so even though at times the engines were started at zero free-stream velocity in the wind tunnel, and the wind-tunnel walls constrained the exhaust flow and directed it back to the vicinity of the inlets. However, the configuration was 20 feet from the wind-tunnel floor, and the exhaust gases were well mixed with cool air by the time they recirculated to the engine inlets. Therefore, the inlet temperature rise was modest (of the order of 20° to 30° F). At free-stream velocities of 20 to 30 knots all traces of exhaust gas ingestion in the inlets had disappeared.

Another possible problem of an operational nature is that of starting the engines at high flight speeds with the engines operating in an extreme crossflow environment. Some aspects of this problem are shown on figure 17, which presents engine windmilling speed as a function of angle of attack at a free-stream velocity of 150 knots. These data indicate that back pressure existed across some of the engines (e.g., engine number 3 which had a negative windmill speed at positive angles of attack). However, as has been shown previously by Rolls Royce, the use of a simple spoiler ahead of the engine exhaust nozzle provides a favorable pressure drop across the engine. The beneficial effects of such a spoiler are shown in figure 17 for the number 1 engine, which was so equipped. As a point of reference, the minimum engine speed for a successful start of these engines was 10 percent of rated speed. Calculations indicate that this engine speed would be achieved for the number 1 engine by windmilling if the flight speed were increased to approximately 250 knots. Therefore, windmill starts of lift engines appear feasible with the use of relatively simple devices to generate a favorable pressure gradient across the engine. An additional point of interest is that, when the number 1 engine was started, its exhaust flow created an effective aerodynamic baffle ahead of the number 2 engine, thereby improving its windmilling speed. The number 2 engine, when started, created an aerodynamic baffle ahead of the number 3 engine, and so on down the line. Therefore, it appears that the addition of a single spoiler ahead of the forward engine would be sufficient to create a favorable pressure environment for starting all of the engines, provided they could be started one at a time. It should be noted that no problems were encountered in starting any of these engines at air speeds up to 150 knots and angles of attack up to 12° with the standard electric starters provided on these engines.

CONCLUSIONS

The following conclusions may be drawn from the investigations of jet-lift VTOL aircraft configurations described in this paper.

1. The engine inlets may ingest exhaust gases having temperatures of the order of 200° F unless suitable design measures are taken to avoid this.

Fortunately, it appears that, if the inlets are located properly with respect to the exhaust flow, and maximum advantage is taken of the shielding effect of the wing and fuselage, these extremely high inlet temperatures can be avoided. However, the present state-of-the-art for predicting the occurrence of exhaust gas ingestion is such that experimental study of new designs is required to ensure that they are free of ingestion.

2. There do not appear to be any extreme problems connected with the operation of turbojet lift engines in the high crossflow environment encountered during the transition from jet-supported flight to wing supported flight. In fact, these engines operated very well behind simple bell-mouth inlets. (One qualification should be made here. These engines were inclined 10° forward of the vertical, and this allowed the use of a relatively generous radius of curvature on the upstream side of the inlet.)

3. Operation of the lift engines may produce significant interference effects on the overall lift characteristics of the aircraft. These interference effects may be either favorable or unfavorable. It appears that engines located ahead of the wing will generate unfavorable lift interference, and that engines located near the wing trailing edge will generate favorable lift interference. Thus, it appears that the short take-off performance of jet-lift VTOL aircraft could be improved by the judicious arrangement of the engines with respect to the wing.

TABLE OF CONFIGURATIONS

Configuration		Lift engine no.	Remarks (Test points at h/D = 8.7, 6.5, 4.5, 3.0, 2.4)
Cruise inlet location	Wing position		
Top	Mid/aft	1,2,3, 4, and cruise	Ingestion and stall on engine nos. 3, 4 at h/D = 3.0. Ingestion but no stall at all other h/D points.
Top	Low/aft	↓	Very small amount of ingestion and no stall at all h/D points.
Rear	Low/aft		Ingestion at h/D = 2.4, 3.0 but no stall. Small amounts of ingestion at other h/D points.
Rear	High/aft		Ingestion and stalls at all h/D points. Configuration considered inoperable.
Front	High/aft		Ingestion at all h/D points. Stall at h/D = 3.0 only.
Front	Low/aft		Ingestion and stall at h/D = 2.4, 3.0, small amount of ingestion and no stalls at all other h/D points.
Top	High/fwd	1,2,3, 5, and cruise	Ingestion but no stall at h/D = 8.7, 6.5, ingestion and stall at all other h/D points.
Top	Mid/fwd	↓	Ingestion and stall at h/D = 3.0. Ingestion but no stall at all other h/D points.
Top	Low/fwd		Small amount of ingestion at all h/D points and no stall.
Rear	Low/fwd		Ingestion but no stall at all h/D points.
Front	Low/fwd		Ingestion in cruise engines at all h/D points. No ingestion in lift engines at h/D = 8.7, 6.5. Ingestion and stall at h/D = 3.0.
Front	High/fwd		Ingestion at all h/D points. Stall at h/D = 3.0 only.
Top	Low/fwd	3,4,5	Small amount of ingestion at h/D = 2.4. Very small amount at all other h/D points. No stall.
Top	High/fwd	↓	Very small amount of ingestion at h/D = 2.4. No ingestion at all other h/D points.

VTOL GROUND EFFECTS AND INGESTION TEST MODEL

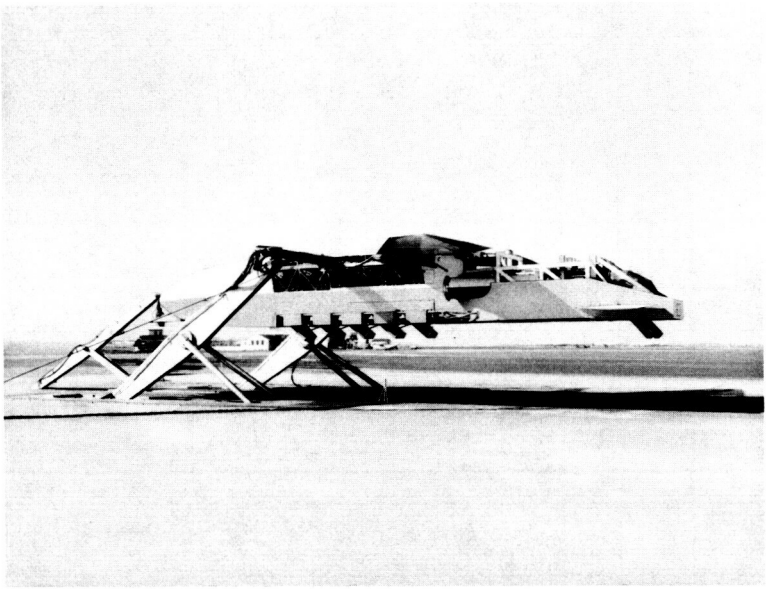

A-36209.1

Figure 1

VTOL GROUND EFFECTS AND INGESTION TEST MODEL

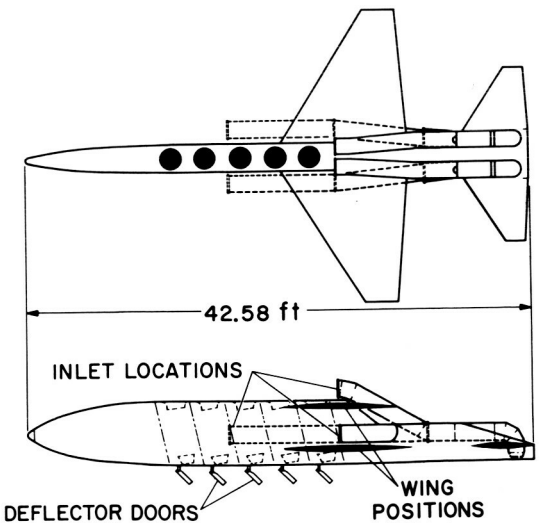

Figure 2

LIFT-ENGINE POD MODEL

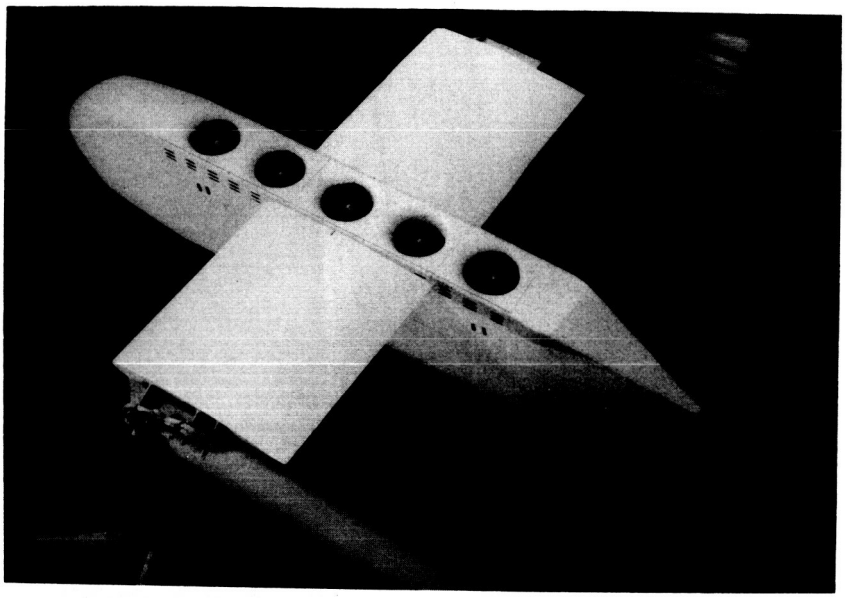

A-33628.1

Figure 3

LIFT-ENGINE POD MODEL

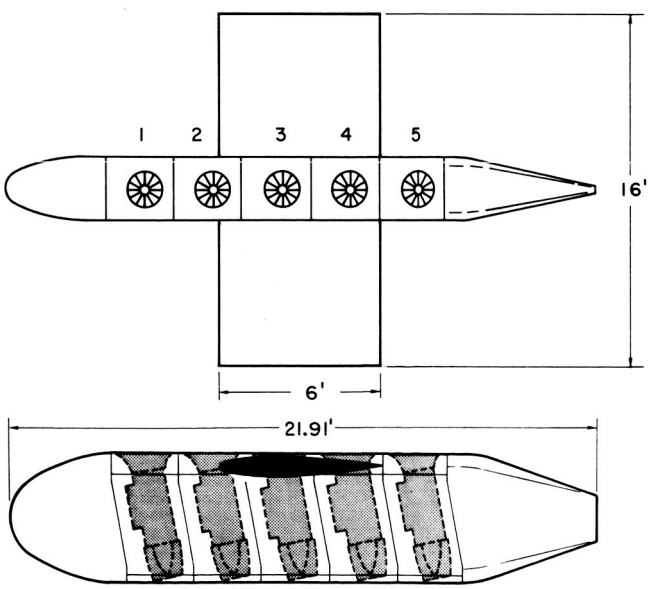

Figure 4

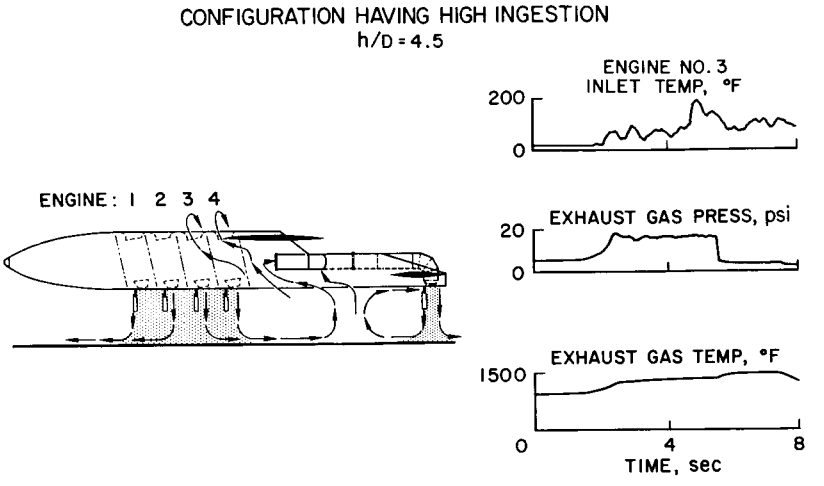

Figure 5

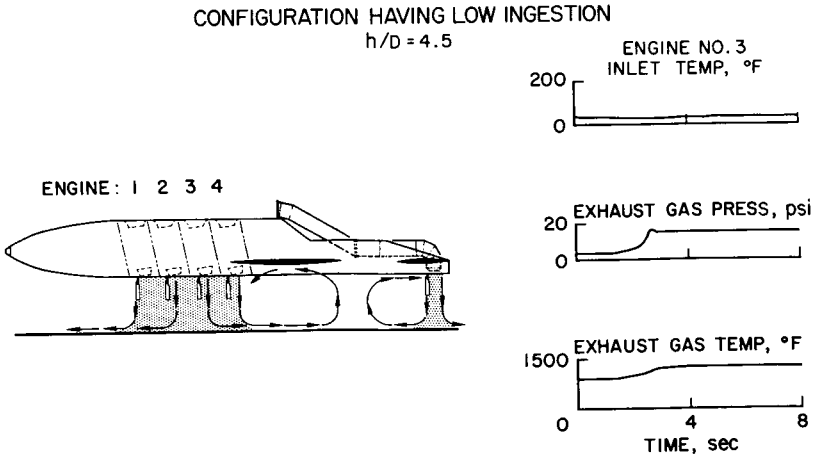

Figure 6

JET INDUCED LIFT LOSS

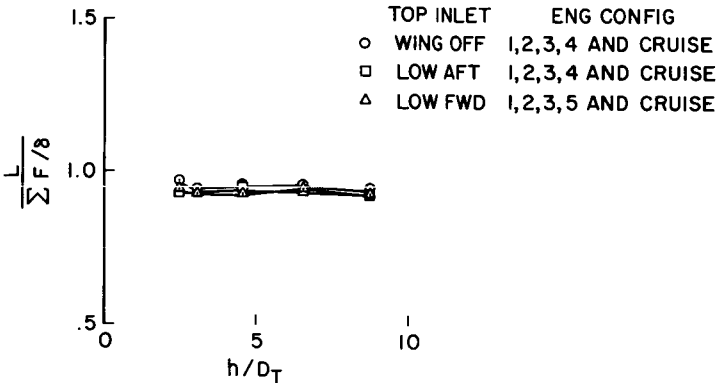

Figure 7

SOUND PRESSURE LEVEL WITH VARIOUS NUMBERS OF ENGINES OPERATING

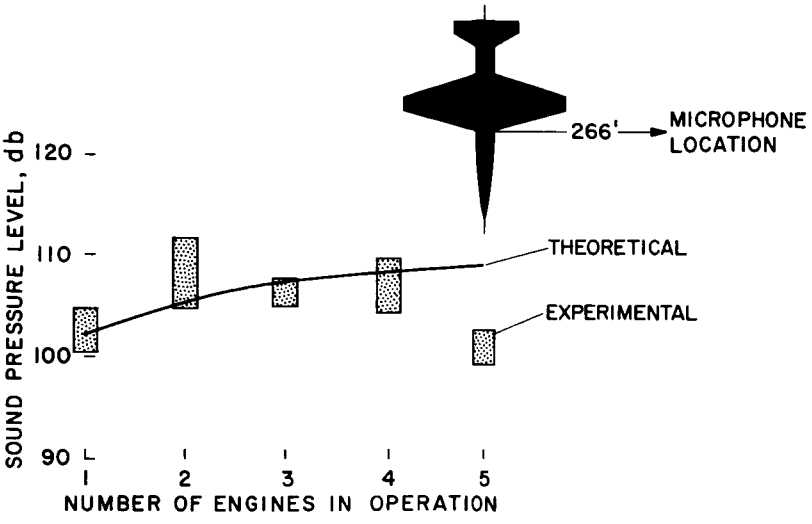

Figure 8

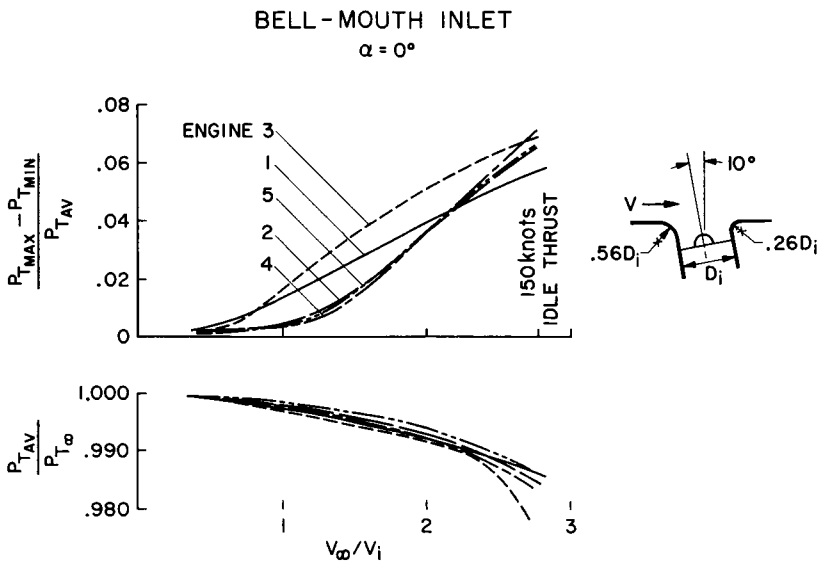

Figure 9

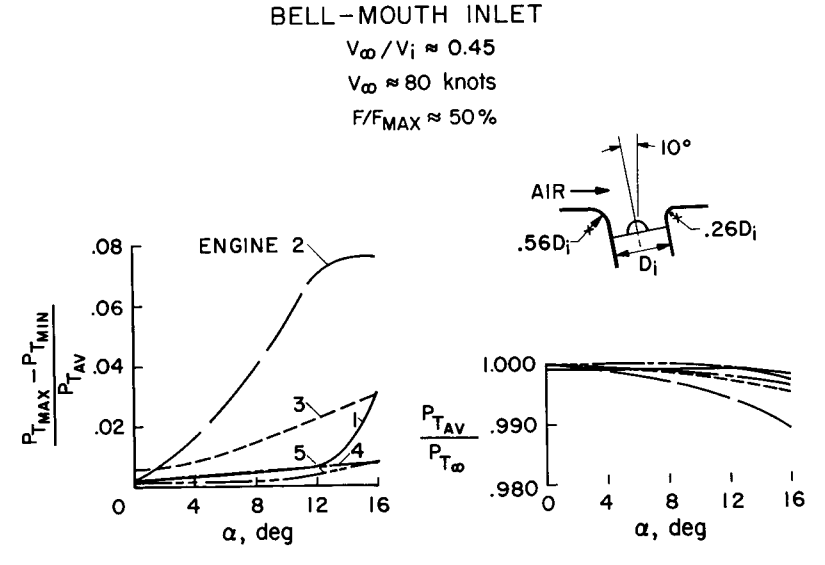

Figure 10(a)

BELL-MOUTH INLET

$V_\infty/V_i \approx 1.30$

$V_\infty \approx 80$ knots

$F/F_{MAX} \approx 23\%$

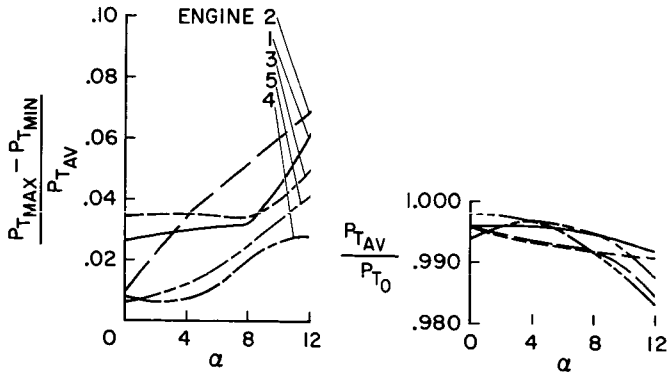

Figure 10(b)

BELL-MOUTH INLET

$V_\infty/V_i \approx 2.8$

$V_\infty \approx 150$ knots

F/F_{MAX} = IDLE

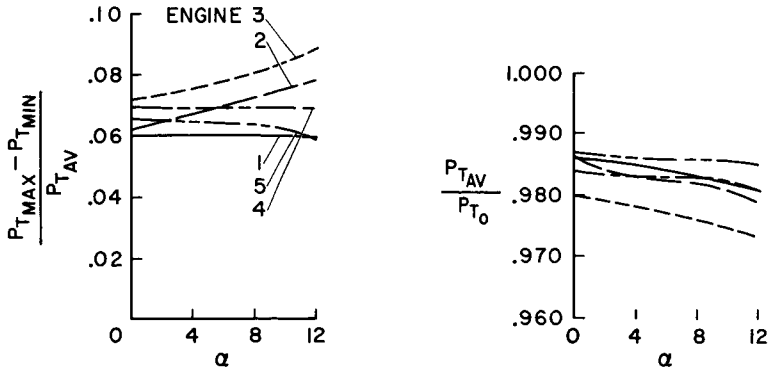

Figure 10(c)

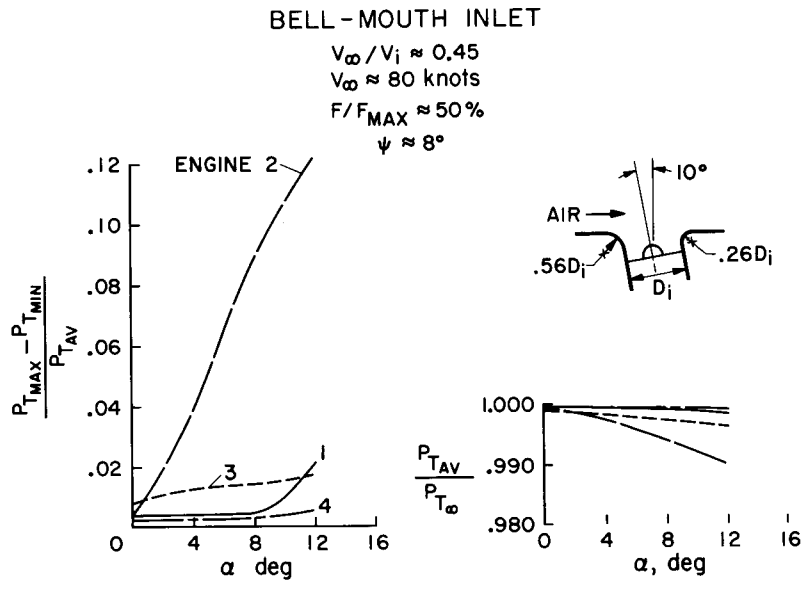

Figure 11

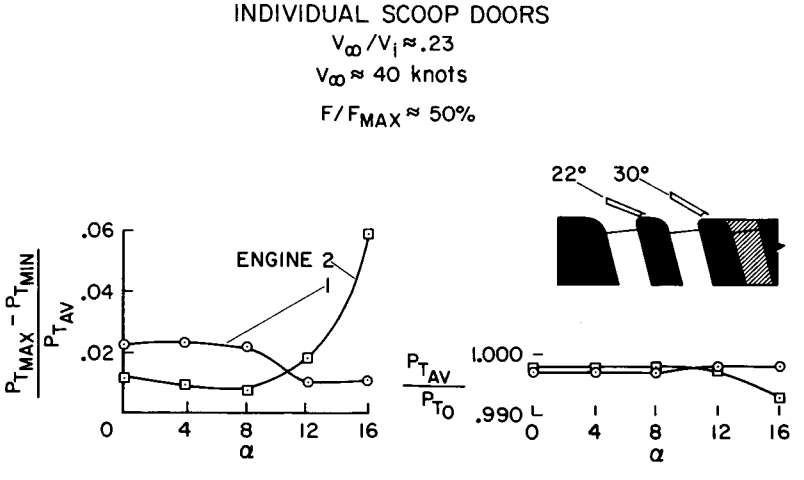

Figure 12(a)

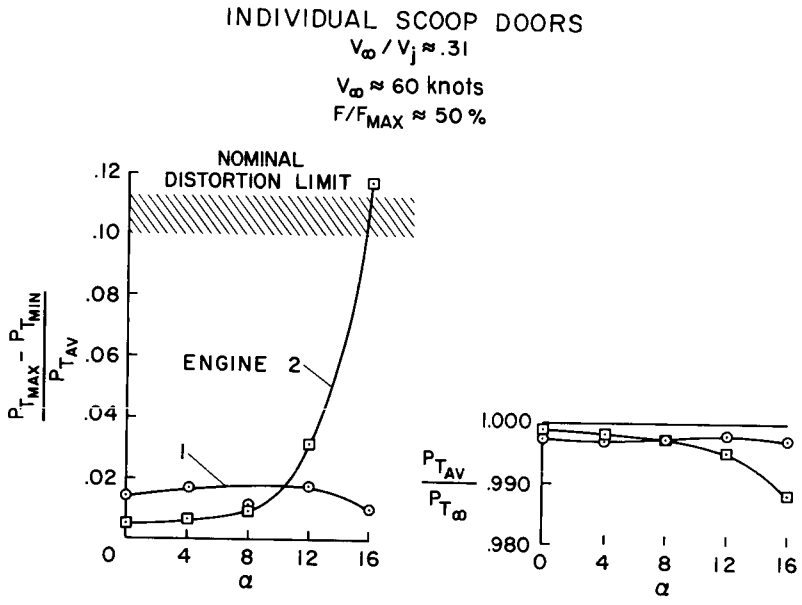

Figure 12(b)

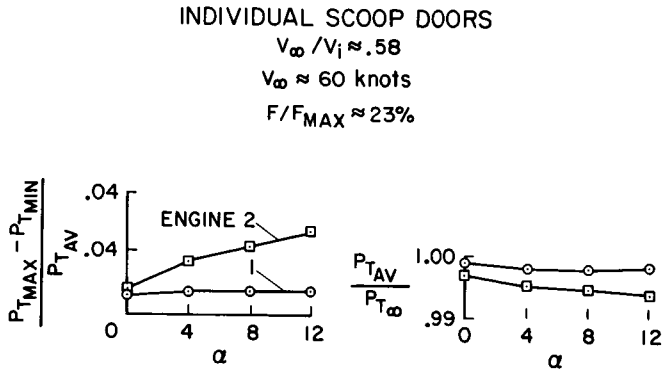

Figure 12(c)

INDIVIDUAL SCOOP DOORS WITH SIDES

$V_\infty / V_j \approx .47$

$V_\infty \approx 64$ knots

$F/F_{MAX} \approx 50\%$

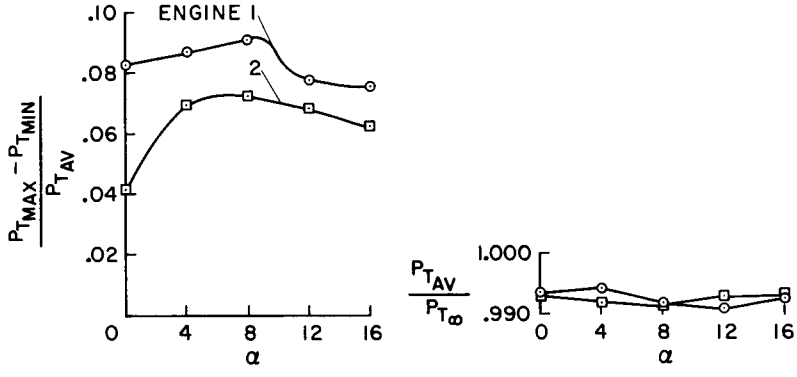

Figure 13

SIDE-FOLDING DOORS

$V_\infty / V_j \approx 0.45$

$V_\infty \approx 80$ knots

$F/F_{MAX} \approx 50\%$

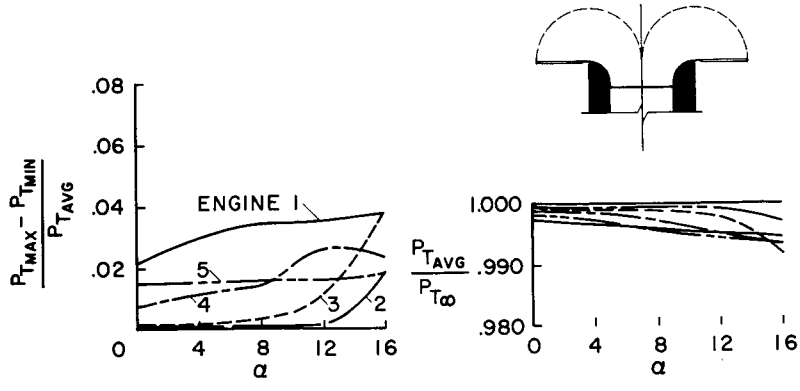

Figure 14(a)

SIDE FOLDING DOORS
$V_\infty / V_i \approx 1.27$
$V_\infty \approx 150$ knots
$F/F_{MAX} \approx 23\%$

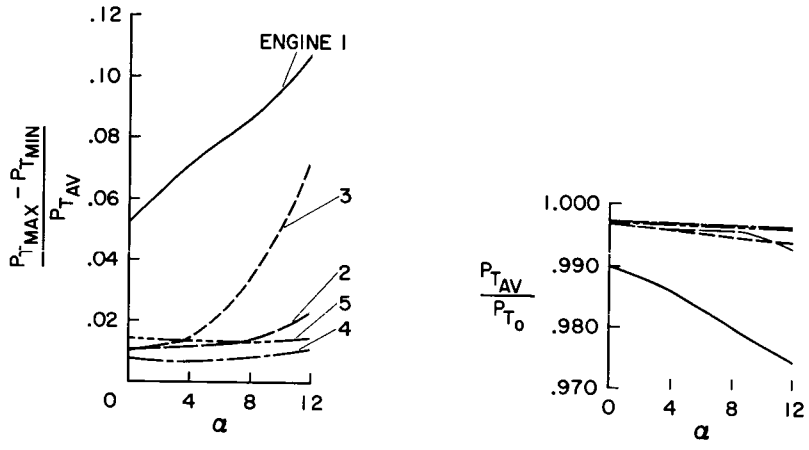

Figure 14(b)

SIDE FOLDING DOORS
$V_\infty / V_i \approx 2.76$
$V_\infty \approx 150$ knots
F/F_{MAX} = IDLE

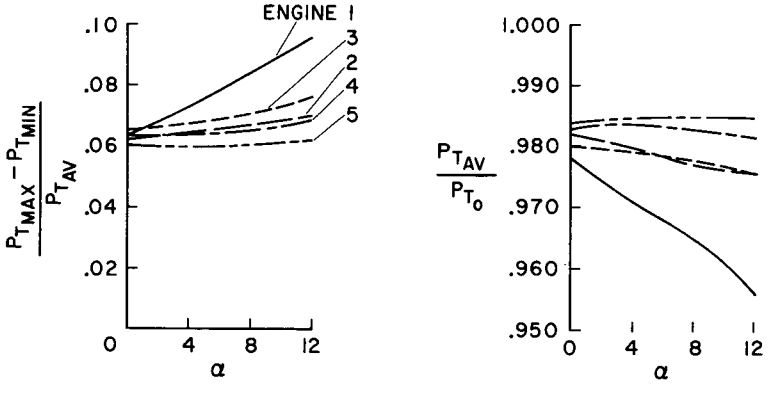

Figure 14(c)

SIDE FOLDING DOORS
$V_\infty / V_i \approx .67$
$V_\infty \approx 125$ knots
$F / F_{MAX} \approx 50\%$
$\psi = 6°$

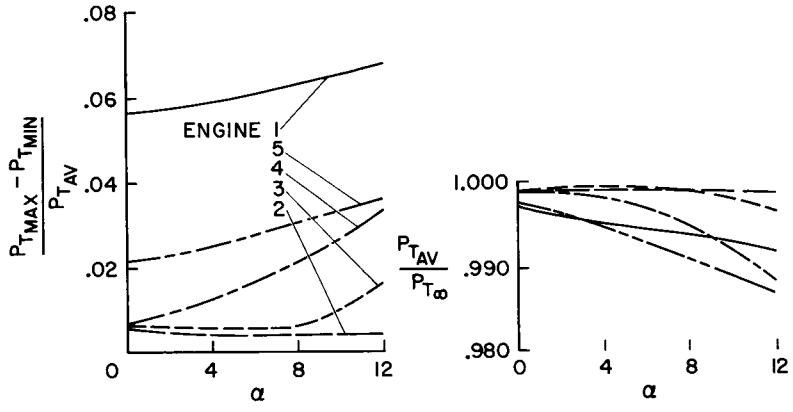

Figure 15(a)

SIDE FOLDING DOORS
$V_\infty / V_i \approx 1.28$
$V_\infty \approx 150$ knots
$F / F_{MAX} \approx 23\%$
$\psi = 6°$

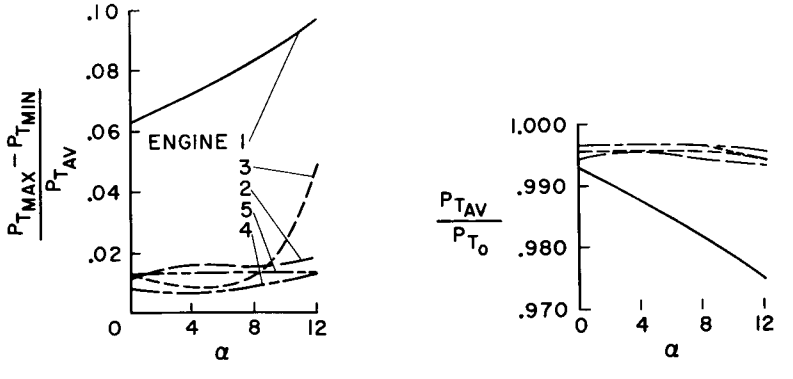

Figure 15(b)

SIDE FOLDING DOORS
$V_\infty / V_j \approx 2.69$
$V_\infty \approx 150$ knots
$F/F_{MAX} \approx$ IDLE
$\psi = 6°$

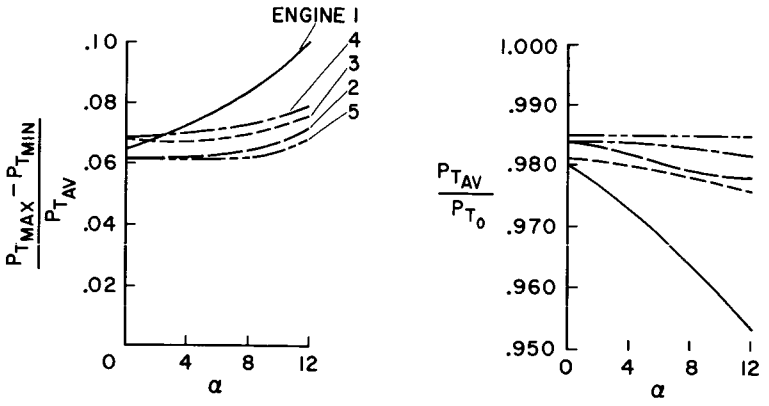

Figure 15(c)

ENGINE INDUCED EFFECTS

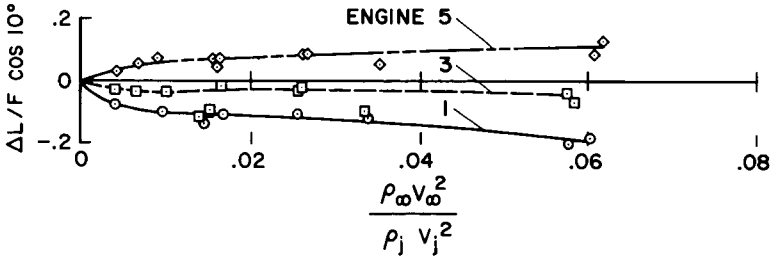

Figure 16

WINDMILL RPM AT 150 KNOTS

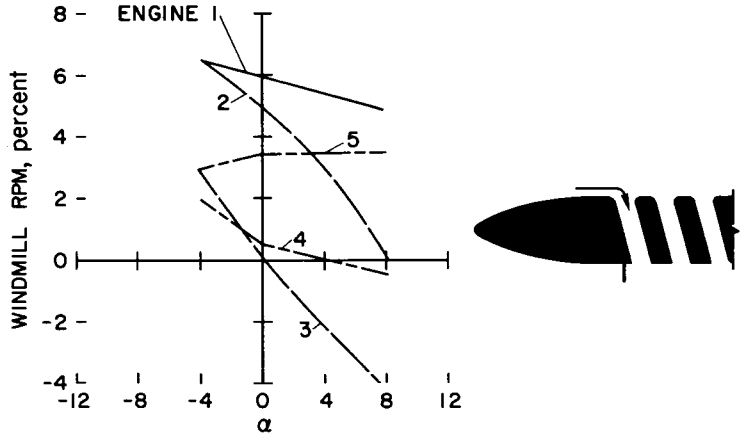

Figure 17

16. CONSIDERATIONS FOR REVISION OF V/STOL HANDLING QUALITIES CRITERIA

By Seth B. Anderson
Ames Research Center

SUMMARY

24622

A review of selected V/STOL handling qualities has been made to provide information to be used to update and revise V/STOL handling qualities requirements. Comparisons are made of recent flight and simulator results with existing V/STOL requirements. The results show that improved guidelines are becoming available to aid the designer of V/STOL aircraft.

INTRODUCTION

Author

Handling qualities requirements must be carefully formulated so they do not unduly restrict the many compromises that must be made in the design of new aircraft. V/STOL aircraft are particularly sensitive to detailed requirements because there is a direct trade off between performance and the amount of control needed for hover. We must learn more about the values of hover control power needed for different size aircraft before we can establish requirements for hover control as well as for many other factors.

It is intended here to review information that can be used (fig. 1) for updating V/STOL handling qualities and to point out that limitations in current knowledge preclude treating these as requirements. Numerous analytical, flight, and simulator studies have been directed at improving our understanding of V/STOL handling qualities since the first NASA report on this subject was published in 1960.[1] It is indeed a challenging task to convert information from many of these studies to general handling qualities criteria because, for the most part, the results pertain to specific configurations. The lateral-directional control results have been particularly difficult to generalize because the total control requirements depend on many interrelated factors.

The discussion will include also a comparison of recent flight and simulator results with proposed V/STOL requirements. Although many advanced VTOL aircraft, such as the P.1127, Balzac, VJ-101, XV-5A, and XC-142, have been in flight status for a number of years, relatively little quantitative flight data has been obtained on the stability and control and handling qualities of these aircraft. Even when sufficient operational experience is obtained with a V/STOL aircraft to define control requirements for maneuvering, one must be careful when generalizing on the results for a specific aircraft. It obviously would not be appropriate, for example, to base directional control power requirements for a jet lift transport on the results of a small helicopter.

It should be recognized that handling qualities are by their very nature difficult to define, difficult to measure, and always somewhat subjective. It is hoped that this paper will provide a better understanding of why it is more meaningful to develop V/STOL criteria instead of requirements.

CLARIFICATION OF DEFINITIONS

Before specific V/STOL handling qualities are discussed, it is helpful to distinguish between the terms "criteria" and "requirements" commonly used in discussions of handling qualities. One criticism of the recommendations for V/STOL handling qualities (e.g., ref. 2) is that they contain a mixture of criteria and requirements (fig. 2) so that the user tends to interpret the meaning to suit his purpose.

Criteria

Criteria can be defined as standards for judging. They should therefore provide qualitative background information. It is necessary to understand the purpose as well as the various factors related to the criteria. For example, roll-control criteria should not only point out the magnitude of a desired bank-angle change, but should also make it clear that control power must be sufficient to maneuver in particular tasks and to provide control for trim and disturbances as well. In discussing criteria it has been suggested that background and reference material be supplied so that the designer could use his own judgment in applying the criteria to his design. Criteria could then serve as a guide in establishing specifications or requirements for a given aircraft.

Requirements are quantitative measures of particular flight characteristics of a particular vehicle. Thus they should be easily measurable in flight and be related as directly as possible to the pilot's impression of the aircraft's behavior. They are the specifications against which to assess production aircraft. Requirements for one class of aircraft should not be used as a yardstick for another class of aircraft.

Although both criteria and requirements are needed for V/STOL aircraft, it is necessary to first provide meaningful criteria. Accordingly, the discussion in this paper is so oriented.

RESULTS AND DISCUSSION

It is not intended to cover all the V/STOL criteria needing revision, but only selected ones that have proved to be controversial.

Longitudinal Characteristics

The areas to be covered on longitudinal characteristics are shown in figure 3.

Static stability with respect to speed.- No one will question that both stick-fixed and stick-free stability with respect to speed are desirable (fig. 4), yet even conventional aircraft have been designed with only stick-free stability in the landing approach. Such aircraft have been found to be unacceptable under instrument conditions, particularly in rough air. Speed stability is particularly important for V/STOL aircraft because these aircraft are operated at speeds where drag increases with decreasing speed which makes flight-path control difficult.

On the other hand, numerous investigations[3] have pointed out the adverse effects of too much speed stability (M_u). Too much speed stability causes excessive response to horizontal gusts, increases the requirement for angular velocity damping (M_q), and for tilt wing or tilt duct aircraft, limits the usable speed range at a given wing/duct angle.

Angle-of-attack stability.- In addition to speed stability, angle-of-attack stability must be considered. In operating STOL aircraft (BLC C-130,[4] Breguet 941,[5] and UF-XS[6]), the pilot uses angle of attack as a reference during approach and wants the aircraft to return to the reference angle of attack as well as to the reference airspeed when the aircraft is disturbed. Angle-of-attack instability limits the operational angle-of-attack range of the P.1127 aircraft to a very low value of 8° which in turn results in a maximum allowable glide slope angle of only 10° in landing approach. The XV-4 (Hummingbird) also had angle-of-attack instability as well as marginal longitudinal control power, and this aircraft crashed. The XV-5A and Balzac aircraft have angle-of-attack instability which limits operation in transition.

Dynamic stability.- There has been a lack of adequate criteria for the short-period and the long-period (phugoid) modes for V/STOL aircraft and for the conventional aircraft as well, particularly in the period range around 8 to 12 seconds. Requirements[7] for V/STOL aircraft in terms of a period-damping relationship are not directly related to the criteria familiar to a pilot. In any landing approach of a VTOL or conventional aircraft, the pilot is concerned primarily with controlling flight-path angle; however, the factors which affect control depend on the aircraft type. Recent studies[8] for conventional aircraft with high aspect ratios indicate that lift-curve slope, C_{L_α}, and normal acceleration variation with angle of attack, N_α, terms as well as frequency-damping parameters affect flight-path control. It is interesting that for aircraft with lower aspect ratio, such as the F-8C Crusader,[9] flight-path control in carrier approaches was markedly improved with a direct-lift type of control which in a sense is a means of increasing C_{L_α}. Since landing approaches for V/STOL aircraft are made with a very low effective C_{L_α}, engine power is used as a direct lift control. It is apparent that factors in addition to period damping must be considered in arriving at dynamic-stability boundaries for V/STOL aircraft. Some of the current VTOL aircraft, such as the P.1127 and VJ-101C, which appear to need improved damping in STOL approaches,

particularly for instrument operation, may actually need more lift control. The interplay of these factors is inadequately defined for V/STOL aircraft and should be studied with greater emphasis as soon as more sophisticated variable stability VTOL aircraft become available.

Response and damping.- Longitudinal response and damping in hover will be discussed together with lateral control criteria; however, it should be noted here that flight experience bears out the fact that longitudinal control requirements in hover are generally less severe than roll control requirements. For some VTOL types, such as the X-14A and the P.1127, flight experience has shown little need for damping augmentation; in fact, zero angular rate damping can be tolerated in VFR operation. However, analytical studies[10] and flight tests[11] have indicated that for some configurations, such as the tilt duct types, where the speed stability parameter M_u is large, both damping and increased control power will be required, particularly for IFR and rough-air operation.

Lateral-Directional Characteristics

The lateral-directional characteristics to be discussed are outlined in figure 5.

Functions of roll control.- The roll control must be powerful enough to serve a number of functions; in figure 6 these are grouped into three broad categories. Lateral control is needed for trimming, for controlling upset, and for maneuvering. Unfortunately, it has not been easy to separate these individual needs, and to the pilot the amount of lateral control needed appears as a total requirement. Upon examination, however, the pilot rating of a given configuration reflects consideration for all the aforementioned aspects. Values of trim control power needed can be calculated from the geometry of the vehicle and the static stability values. Power needed for upset and maneuver is not only affected by the configuration, but by the aircraft size; and the specific maneuvers required and the gust environment must be known. Upsets, in addition, are a function of self-induced flows. Some of these factors which affect roll control power requirements will be considered next in more detail.

Aircraft size effects.- Size effects both from upset and maneuver standpoints are shown in figure 7. A number of studies[12,13] have examined the effect of gust upsets and concluded that the magnitude of an upset, in rad/sec^2, is inversely proportional to the square root of the weight. Although the upsetting moments actually increase with increase in aircraft size because of the area exposed, the moments of inertia increase at a greater rate, resulting in a decrease in the upsetting accelerations. The control power required for maneuvering is shown also in figure 7. One can assume that the maneuver requirement will be essentially similar for similar types of aircraft for the same mission or task even though the weight may vary considerably. However, it is also logical to assume the basic level of maneuvering control power required will be generally lower for larger size aircraft such as transports, since the task itself will not require large and rapid

maneuvers. This suggests that the total control power required for maneuvering should be specified for V/STOL aircraft by classes as is done for conventional aircraft.

As far as the effect on engine power plant is concerned, total control power required for maneuvering can be divided further into (1) steady state or long-term aspects to offset aerodynamic effects (speed stability, M_u, or rolling moment due to side velocity, L_v) when operating in steady winds and (2) the short-term control inputs required to reposition the aircraft. The steady trim requirements are a function of configuration and the short-term input is largely a function of the control system used (to be discussed later).

One final point to be made from these curves is that at the lower gross weights, gust and self-induced disturbances dominate the demands for control power, while at the higher gross weights the maneuver task dictates the amount needed.

At this point we ask how well does this description of size effects fit available data. Control power values that have been used in operating various VTOL aircraft are compared in figure 8 with the sizing formula $(W + 1000)^{1/3}$. The example aircraft do not appear to follow any scaling rule. For example, the X-14A has 1/4 the weight of the P.1127 but requires less control power. Note also that the control power values for the various aircraft are larger than the AGARD formula, which is basically a maneuvering requirement. If it is assumed for simplicity that the same maneuvering task is used for each aircraft, the P.1127 requires high control power for trim to offset a very large dihedral effect (L_v) as does the XV-5A, the Balzac, and the Mirage III-V. The SC-1 also has recently been shown to have a large L_v requirement at higher angles of attack. The low control-power value appears adequate for the VJ-101C when an attitude stability system is used; however, the control power is nominally rated at 1.2 rad/sec^2, but actually 7 rad/sec^2 is available if one is willing to reduce power completely on one engine. The lateral trim control required for this aircraft is very small, and gust upsets are minimized by the attitude stability system. For the X-19A, roll control power was adequate although there were a number of mechanical control systems problems with this aircraft. The XC-142 has 1.2 rad/sec^2 available in roll, which is judged ample for hovering, but may not be entirely satisfactory at slow speeds.[14] During STOL operation at speeds below about 25 knots, ground effect and recirculation disturbances can exceed the control available, as evidenced by the landing accident in 1965.

There are two further considerations that affect control power requirements. These are (1) the type of control system, and (2) the sensitivity or stick gearing.

Effect of type of control system.- The type of control system (i.e., controlling acceleration, rate, or attitude) has important effects on the overall control power the pilot needs, as shown in paper no. 17 by Greif. Studies were made on the Ames six-degrees-of-freedom motion simulator of control power required for maneuvering with no gust or trim inputs. These results indicate the improvement in lowering the allowable power for basic maneuvering. To

hover in a steady 30-knot crosswind, a given aircraft configuration will require the same control power regardless of the type of control system used. For repositioning the aircraft after gust or self-induced upsets, however, the rate-damped system (typified by the P.1127 and the X-14A) has limitations on how low the control power can be and still permit command of the situation. The effects of this lower limit of control power have been demonstrated dramatically in three landing accidents to the X-14A when maximum roll control power was of the order of 0.5 to 0.7 rad/sec^2. With the rate-damped system the pilot must supply both stability and damping which can be done only if the response is adequate to quickly correct for errors. Studies[15] have shown that at low values of control power the pilot cannot anticipate (supply precise lead inputs) the response to his input well enough to prevent divergence in a confined area task. With an attitude stabilized system, such as used in the VJ-101C, the pilot is not required to correct for induced disturbances or for gust upsets. Since this is accomplished for him, he has only to impose his maneuvering commands.

Effect of sensitivity.- Sensitivity or gearing (control power per unit deflection of the control) has important effects on the amount of control moment available. It was recognized early in studies of lateral control requirements for the P.1127, for example, that stick gearing changes which increased sensitivity were just as important in achieving pilot acceptance of lateral behavior in hover as increases in total control power. Recent studies at Ames have reemphasized the importance of sensitivity considerations for STOL aircraft with wheel-type controls. Figure 9 shows the effect of wheel gearing on control power requirements taken from both simulator and flight tests of a large STOL aircraft for a maneuvering task in the landing approach. The changes in sensitivity were made by keeping the total wheel travel constant (at $\pm 90^{\circ}$) but varying the gain so that full control power was available at the first part of the wheel deflection. The force gradient was approximately 0.25 lb/deg for these tests. It can be observed that this nonlinear type of gearing has a distinct effect on control-power requirements. The effect of wheel gearing in terms of bank-angle response is presented in figure 10. For comparison purposes conventional control aircraft and the modified 707 BLC aircraft (discussed in paper no. 20 by Quigley) with increased wheel sensitivity of the nonlinear type is shown also. The results suggest that the roll response specification of 8° after the first second for the C5A aircraft could be reduced without affecting pilot rating by employing increased wheel sensitivity of the nonlinear type.

Tests of changing the sensitivity of stick controls in variable stability VTOL aircraft (X-14A[16] and VHC-1 helicopter) showed a favorable reduction in pilot work load during precision hovering, but did not show a pronounced effect of sensitivity for the maneuvering task. It should be noted, however, that in these tests sensitivity was changed by reducing stick throw for a constant control power. The pilot sharply down-rated the lower stick throws (higher sensitivity) whenever the maneuvers required going against the physical limits of stick travel. Further considerations of sensitivity are covered in papers nos. 17 and 18 by Greif and Garren.

It should be kept in mind that sensitivity effects must be acceptable also for high-speed operation. Nonlinear gearing has advantages in this respect since the hover control would be phased out as speed increases.

In summary, this part of the discussion has shown that a simple weighting formula for control power is not easy to supply because of the separate inputs required for trim, upset, and maneuvering. To arrive at meaningful criteria, it must be recognized that these inputs depend on configuration and class of aircraft. In addition, the type of control system must be considered, and control system gearing or sensitivity is an important item. It should be remembered that the points discussed for the lateral control will apply in general to the longitudinal control, also.

Translational control.- It has been suggested in a number of studies[1,12] that control power levels may be reduced when the engine thrust is vectored to produce translation instead of tilting the aircraft. This method of control is shown schematically in figure 11. The use of a movable vane in the engine exhaust has been flight tested on the X-14A and the control system has been investigated in studies using the Ames six-degrees-of-freedom motion simulator. A translational control has obvious advantages for large aircraft where large roll inertia severely limits the angular response.

Results of the simulator study are presented in figure 12 in terms of pilot rating (table I) of roll control power required for various methods of translational vane control. The task for each type of control was to reposition the aircraft laterally as rapidly as desired in a gust-free environment and with no aerodynamic inputs. Stick sensitivity and roll damping were set at optimized values. It can be observed that for the lower range of control powers programming the vane as a function of bank angle reduced the angular acceleration requirements for a given pilot rating, but did not achieve a satisfactory pilot rating. This "quickening" in side acceleration is similar to the cyclic effect in a helicopter rotor. When the vane was actuated by a thumb controller on top of the stick, angular acceleration requirements were markedly reduced, as would be expected since for these tests there was little tendency for the pilot to produce bank upsets.

Flight tests with the vane on the X-14A VTOL aircraft bear out trends shown by the simulator tests. More operational flight experience must be obtained, however, to establish a trade-off between vane control and bank-angle control to account for upsets and trim requirements. Further work needs to be directed at IFR tasks where lateral positioning is more demanding.

Lateral-directional cross coupling.- In current handling-qualities requirements[2] the cross-coupling problem is treated in terms of adverse yaw generated in a rudder-fixed roll. The allowable sideslip angle is large, 15° to 20°, and is independent of the aircraft type. Studies[17] with large STOL aircraft have indicated that a size effect should be included in the criteria which considers sideslip divergence rate and the frequency (period) of the aircraft. Indications are that larger aircraft with resultant long directional periods will not tolerate as much sideslip divergence since the pilot cannot precisely position the rudder for corrective inputs. Further

discussions on cross-coupling effects for STOL aircraft are covered in paper no. 20 by Quigley.

Directional response and damping.- Early experience with helicopters established the requirements for large values of directional control power. These values were necessary primarily because of the large directional trim change with power peculiar to single-rotor aircraft. Recent experience with most VTOL aircraft has indicated that very low yaw response is acceptable, emphasizing again the importance of examining in detail the individual components making up the requirement for total control power. Even though the yaw axis requires only a fraction of the control power required for roll and pitch, flight experience has shown that some additional factors are significant. (1) Adequate control for upsets, such as the XC-142 has encountered in ground effect in STOL landings, must be considered for some designs. (2) A change in rudder effectiveness with height above the ground can be undesirable, as evidenced by the landing incident with the XC-142. (3) Nonlinear directional characteristics are undesirable. Primarily because of engine inlet moments, some jet VTOL configurations, such as the P.1127 and XV-5A, require nonlinear rudder inputs when turning out of wind. Pilots seem willing to accept poor response, but object very strongly to the nonlinear behavior. The present requirements[2] state only that it should be possible to turn 360° and nonlinear aspects are not adequately covered.

Hovering and Vertical Flight Characteristics

Hovering and vertical flight areas to be discussed are shown in figure 13.

Height control and hovering precision.- The present requirements[2] in height control and hovering precision are very strict because they are based on helicopter experience. Control of ±1 ft/sec, which may be required for rescue missions, can certainly be relaxed for vehicles not requiring continuous hover. Height control has not proved to be a large problem on VTOL aircraft and vertical height damping has not been required even for aircraft with suck down and unsteady ground effects. The criteria should consider, however, the effects of nonlinear trim changes near the ground; for the P.1127 aircraft a nose-down tendency in ground effect changes in magnitude with aircraft attitude (becoming larger as the aircraft noses down). In this sense precision of height control should consider aircraft attitude. Cross coupling between height control and pitch could prove to be a problem for some designs, for example, those which obtain height control by a combination of lift engines and deflected cruise engines. The thrust response of the lift engines would undoubtedly be better than the cruise engines and lift pitch coupling could result. In addition, when the forward lift engines are used for roll control, the total thrust change results in a pitch change. This problem could be more severe in ground effect.

Vertical thrust margins.- Several studies[18] show the interrelationship between thrust-weight ratio, T/W, and vertical height damping, and provide a basis for reasonably sound requirements for both takeoff and landing. The thrust margins needed for simultaneous control about several axes has not,

however, been covered adequately. The requirement[2] that T/W should not be less than 1 when full control is applied about one axis with 50-percent control applied about the remaining axes is very conservative in light of actual VTOL experience. For example, operating the P.1127 with a demand bleed system and the VJ-101C aircraft with a thrust modulation control system has been found to be acceptable in spite of the fact that T/W values less than 1 occur during pronounced control activity. Operations with these aircraft in take-off have shown that this condition is acceptable because control inputs are needed for only a short time. The question of how much altitude loss can be permitted is difficult to answer without more operational experience. Studies[12] have shown that simultaneous control inputs in roll and pitch usually occur as discrete large control deflections for a short time. The requirement should recognize that altitude may be lost for some specific time period. In addition, since the large control inputs are held for only a short time, engine over-temperature may be acceptable for that time.

Plans for Revising V/STOL Critieria

From the foregoing discussion in which just a few areas were covered, it is apparent that additional work remains to be done to update and revise the V/STOL handling qualities. The plans for this are shown on figure 14. An AGARD committee chaired by the NASA has been formed to update and revise AGARD report no. 408 and change its emphasis from requirements to criteria. This group has the possible advantage of obtaining recent flight experience inputs from the various NATO nation flight programs.

The NASA together with the DOD and FAA have formed another committee to help guide research of handling qualities for conventional and V/STOL aircraft. The Navy BuWeps will operate the variable stability and control X-22A VTOL aircraft under a tri-service arrangement to provide answers to handling qualities questions. The USAF has a program underway directed at writing V/STOL handling qualities requirements over a 3-year period. The Army, too, has plans for writing V/STOL handling qualities specifications peculiar to their needs. Because of these varied approaches it is important that a coordinated effort be made so that nonconflicting requirements evolve and duplication is avoided.

CONCLUDING REMARKS

A review of a number of selected V/STOL handling qualities shows that improved guidelines are available to aid the designer of V/STOL aircraft. Studies have shown that control power for small size (weight) aircraft is needed primarily for gust or upset corrections, while for large-size aircraft the maneuvering task may dominate the control power required. Present V/STOL requirements do not adequately account for sizing of aircraft. The requirements should take into account the class of aircraft as well as allow for the benefits in reduced control power accruing from the use of attitude stability systems, nonlinear gearing, and translational control. It is encouraging to

note that steps are being taken to update and revise existing V/STOL handling qualities requirements.

REFERENCES

1. Anderson, Seth B.: An Examination of Handling Qualities Criteria for V/STOL Aircraft. NASA TN D-331, 1960.

2. Botrel, A.: Recommendations for V/STOL Handling Qualities. AGARD Rep. 408, Oct. 1962.

3. Tapscott, Robert J.: Criteria for Primary Handling Qualities Characteristics of VTOL Aircraft in Hovering and Low-Speed Flight. Presented at NASA Conference on V/STOL Aircraft, Langley Research Center, Nov. 17-18, 1960, pp. 195-205.

4. Quigley, Hervey C., and Innis, Robert C.: Handling Qualities and Operational Problems of a Large Four-Propeller STOL Transport Airplane. NASA TN D-1647, 1963.

5. Quigley, Hervey C., Innis, Robert C., and Holzhauser, Curt A.: A Flight Investigation of the Performance, Handling Qualities, and Operational Characteristics of a Deflected Slipstream STOL Transport Airplane Having Four Interconnected Propellers. NASA TN D-2231, 1964.

6. Holzhauser, Curt A., Innis, Robert C., and Vomaske, Richard F.: A Flight and Simulator Study of the Handling Qualities of a Deflected Slipstream STOL Seaplane Having Four Propellers and Boundary-Layer Control. NASA TN D-2966, 1965.

7. Curry, Paul R., and Matthews, James T., Jr.: Suggested Requirements for V/STOL Flying Qualities. USAAML 65-45, RTM 37, U. S. Army Aviation Materiel Laboratories, Fort Eustis, Va., June 1965.

8. Shomber, H. A., and Gertsen, W. M.: Longitudinal Handling Qualities Criteria: An Evaluation. AIAA Paper 65-780, 1965.

9. Nemoff, Alfred J.: Direct Lift Control for the Handling Approach. Presented at the Soc. of Exptl. Test Pilots Ninth Annual Symp., Sept. 24-25, 1965, Sec. 1965 Issue, vol. 7, no. 4, pp. 47-58.

10. Stapleford, R. L., Wolkovitch, J., Magdaleno, R. E., Shortwell, C. P., and Johnson, W. A.: An Analytical Study of V/STOL Handling Qualities in Hover and Transition. AFFDL-TR-65-73, Systems Technology, Inc., Oct. 1965.

11. Kelley, Henry L., and Champine, Robert A.: Flight Operating Problems and Aerodynamic and Performance Characteristics of a Fixed-Wing, Tilt-Duct, VTOL Research Aircraft. NASA TN D-1802, 1963.

12. Lollar, Thomas E., Bus, Frank J., and Dolliver, David M.: Control Requirements and Control Methods for Large V/STOL Aircraft. SAE Rep. 650808, Oct. 1965.

13. Johnston, J. Ford, and Friend, Carl F.: Effect of Size on VTOL Hover and Low Speed Handling Qualities. Proc. First National V/STOL Aircraft Symp., Nov. 3-4, 1965, Wright-Patterson AFB, Ohio, pp. I-134-150.

14. Ransone, Robin K., and Jones, Gay E.: XC-142A V/STOL Transport Tri-Service Limited Category I Evaluation. FTC-TR-65-27, Jan. 1966.

15. Lollar, Thomas E.: A Rationale for the Determination of Certain VTOL Handling Qualities Criteria. AGARD Rep. 471, 1963.

16. Rolls, L. Stewart, Drinkwater, Fred J., III, and Innis, Robert C.: Effects of Lateral Control Characteristics on Hovering a Jet Lift VTOL Aircraft. NASA TN D-2701, 1965.

17. Anderson, S. B., Quigley, H. C., and Innis, R. C.: Stability and Control Considerations for STOL Aircraft. Presented at CASI/AIAA Low-Speed Flight Meeting, Oct. 18-19, 1965, Montreal, Canada, AIAA Paper 65-715.

18. Gerdes, Ronald M.: A Piloted Motion Simulator Investigation of VTOL Height-Control Requirements. NASA TN D-2451, 1964.

TABLE I.- PILOT OPINION RATING SYSTEM

	Adjective rating	Numerical rating	Description	Primary mission accomplished	Can be landed
Normal operation	Satisfactory	1	Excellent, includes optimum	Yes	Yes
		2	Good, pleasant to fly	Yes	Yes
		3	Satisfactory, but with some mildly unpleasant characteristics	Yes	Yes
Emergency operation	Unsatisfactory	4	Acceptable, but with unpleasant characteristics	Yes	Yes
		5	Unacceptable for normal operation	Doubtful	Yes
		6	Acceptable for emergency condition only[1]	Doubtful	Yes
No operation	Unacceptable	7	Unacceptable even for emergency condition[1]	No	Doubtful
		8	Unacceptable - dangerous	No	No
		9	Unacceptable - uncontrollable	No	No

[1]Failure of a stability augmenter

PURPOSE OF PRESENTATION

- TO REVIEW INFORMATION FOR UPDATING V/STOL HANDLING CRITERIA
- TO DISCUSS AND COMPARE EXISTING REQUIREMENTS WITH RECENT FLIGHT AND SIMULATOR RESULTS
- TO POINT OUT PLANS FOR REVISING CRITERIA

Figure 1

CLARIFICATION OF DEFINITIONS

- CRITERIA (A STANDARD FOR JUDGING)
  - STANDARDS USED TO PROVIDE GUIDANCE TO THE DESIGNER
- REQUIREMENTS OR SPECIFICATIONS
  - DESIGNATION OF PARTICULARS USED AS A STANDARD FOR EVALUATION

Figure 2

LONGITUDINAL CHARACTERISTICS NEEDING REVISION

- STATIC STABILITY WITH RESPECT TO SPEED
  - STICK-FIXED & STICK-FREE STABILITY
  - EXCESSIVE SPEED STABILITY
- ANGLE-OF-ATTACK STABILITY
  - PITCH UP
- DYNAMIC STABILITY
- RESPONSE AND DAMPING IN HOVER
  - AUGMENTATION

Figure 3

LONGITUDINAL STABILITY CHARACTERISTICS
LOW SPEED

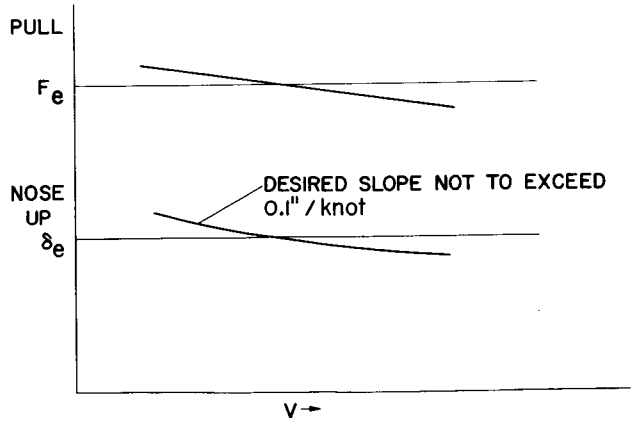

Figure 4

LATERAL-DIRECTIONAL CHARACTERISTICS TO BE DISCUSSED

- RESPONSE AND DAMPING IN HOVER
  - FUNCTIONS OF ROLL CONTROL
  - EFFECTS OF SIZE
  - COMPARISONS WITH CURRENT CRITERIA
  - EFFECTS OF TYPE OF CONTROL SYSTEM
  - EFFECTS OF SENSITIVITY (STICK GEARING)
  - TRANSLATIONAL CONTROL

Figure 5

ROLL CONTROL FUNCTIONS

- TRIM
  - TRIM AIRCRAFT FOR AERODYNAMIC, INERTIAL, AND POWER-PLANT ASYMMETRIES
  - MAINTAIN ATTITUDE IN SIDEWARD FLIGHT OR POSITION IN STEADY CROSSWINDS
- UPSET
  - MAINTAIN ATTITUDE OR POSITION IN GUSTY AIR AND IN GROUND-EFFECT DISTURBANCES
- MANEUVER
  - PERFORM MANEUVERS REQUIRED FOR MISSION

Figure 6

CONTROL POWER TRENDS WITH WEIGHT

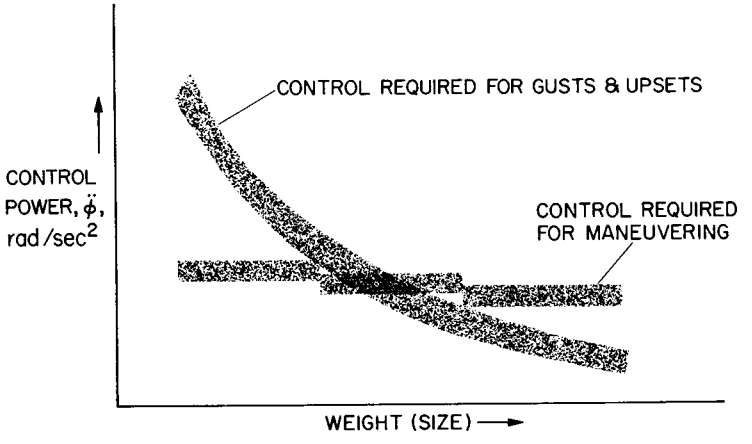

Figure 7

COMPARISON OF VTOL AIRCRAFT ROLL CONTROL POWER WITH AGARD REQUIREMENT

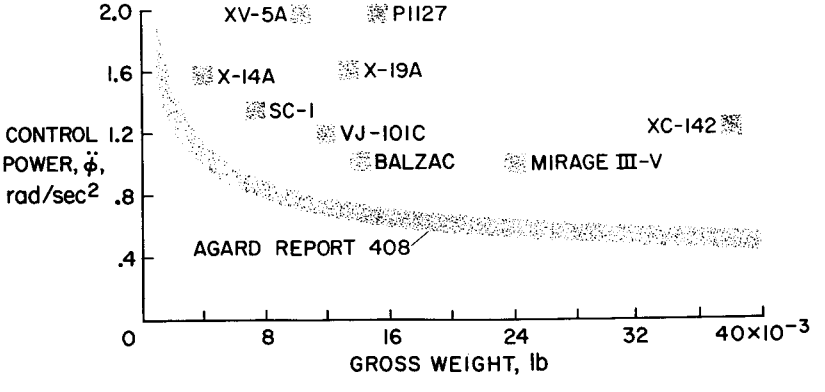

Figure 8

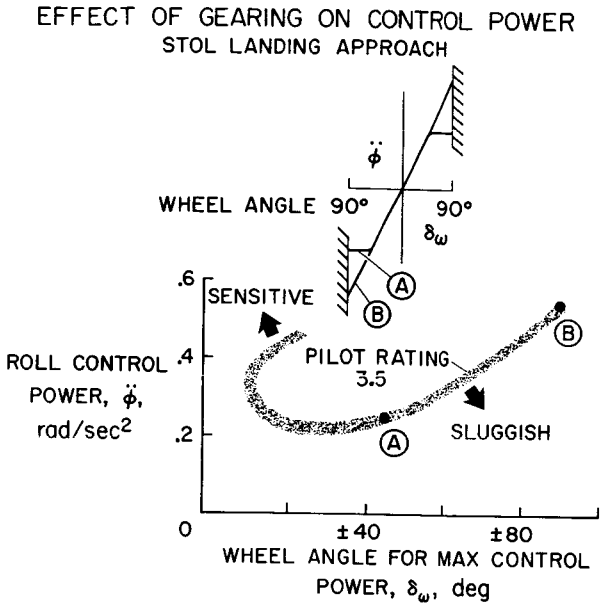

Figure 9

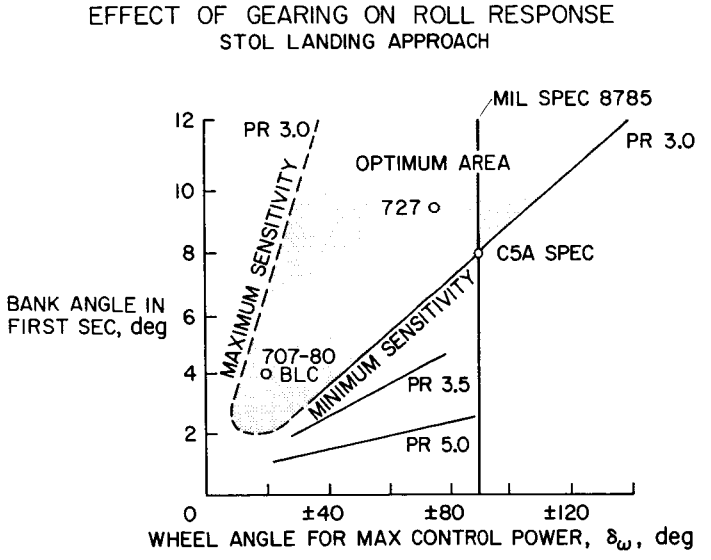

Figure 10

TRANSLATIONAL CONTROL METHODS
X-14A

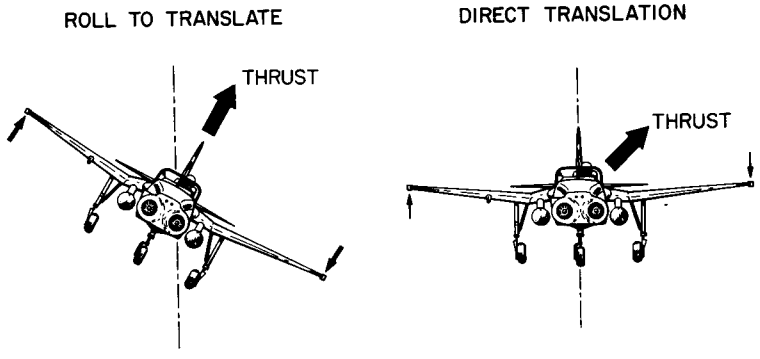

Figure 11

EFFECT OF LATERAL ACCELERATION VANE ON CONTROL POWER FOR HOVERING

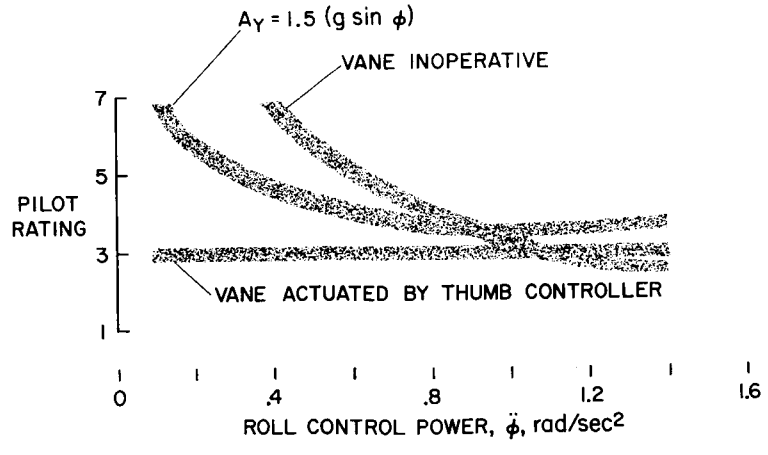

Figure 12

HOVERING AND VERTICAL FLIGHT CHARACTERISTICS NEEDING REVISION

- HEIGHT CONTROL AND HOVERING PRECISION
  - EFFECT OF AIRCRAFT ATTITUDE
  - CROSS-COUPLING EFFECTS
- VERTICAL THRUST MARGINS
  - SIMULTANEOUS USE OF CONTROLS

Figure 13

PLANS FOR REVISING CRITERIA

- FORMATION OF AGARD V/STOL HANDLING QUALITIES COMMITTEE
  - RESULTS FROM NATO NATION AIRCRAFT
  - CHANGE TO CRITERIA FORMAT
- INTERAGENCY COMMITTEE
  - DOD/NASA/FAA

Figure 14

Page intentionally left blank

17. SIMULATOR INVESTIGATIONS OF VARIOUS CONTROL SYSTEMS FOR VTOL AIRCRAFT

By Richard K. Greif, Emmett B. Fry, Terrence D. Gossett*,
and Ronald M. Gerdes
Ames Research Center

INTRODUCTION

A comprehensive program is under way at the Ames Research Center to investigate control system requirements for VTOL aircraft. In its preliminary phase extensive use is being made of advanced simulation techniques, with a six-degree-of-freedom motion simulator serving as the primary research tool. Initial concentration is placed on the hovering task together with the small maneuvers associated with hover. A portion of the program, comparing simplified control concepts, has been completed.

A great deal of experimental information already exists on this subject (refs. 1 to 5). Unfortunately, most of it was obtained from unrelated systems so that valid comparisons are practically impossible. Analytical studies are also in relative abundance (refs. 6 to 12), but most are still awaiting experimental verification. Consequently, the choice of a control system is still subject to conjecture, and the potential versatility and utility of the VTOL concept is susceptible to compromise.

The critical characteristics which must be considered for any control system are handling qualities and control power requirements (ref. 13). Control systems used in the past gave indications that good handling qualities are synonymous with a requirement for large control powers. For some VTOL aircraft, this presents no serious problem. For others, however, control power is critically equated to payload; in fact, some otherwise promising VTOL concepts appear destined to failure unless systems can be devised which operate at low control power levels. With this consideration in mind, the Ames program is designed to systematically study a wide variety of control systems, with emphasis placed on the improvement of handling qualities and the reduction of control power requirements.

This paper is in two parts. Since the simulator used in the program is relatively new and unique, an explanation of its characteristics and discussion of its suitability to the VTOL problem is covered in the first part of the paper. The second part of the paper discusses the results of a study designed to optimize and compare three control system concepts applying to VTOL aircraft which require attitude changes in order to maneuver. They were: an acceleration system, a rate system, and an attitude system.

*With Army Aeronautical Activity.

NOTATION

I_x roll moment of inertia, lb-ft-sec^2 (or slug-ft^2)

L rolling moment, lb-ft

L_p roll rate feedback gain, lb-ft-sec/rad

$\frac{L_p}{I_x}$ = rate damping, 1/sec

L_δ roll control gain, lb-ft/in.

$\frac{L_\delta}{I_x}$ = control sensitivity, rad/sec^2/in.

L_φ roll attitude feedback gain, lb-ft/rad

$\frac{L_\varphi}{I_x}$ = attitude feedback, 1/sec^2

p body-axis roll rate, rad/sec

PR pilot rating

ss steady-state

δ control displacement, in.

ζ damping ratio, damping/critical damping

φ Euler angle roll attitude, rad

φ_{ss}/δ bank angle sensitivity, rad/in.

ω_n undamped natural frequency, rad/sec

EQUIPMENT

Description of the Simulator

The six-degree-of-freedom motion simulator used for this study was designed primarily to investigate the VTOL flight regime (see fig. 1). In its present configuration, the simulator is suitable for visual hovering tasks. Large doors in front of the simulator are opened for all data runs to provide the pilot with an actual outdoor scene, thus avoiding the necessity for artificial displays. This adds a great deal to the realism of the simulation, and also helps to overcome the pilot's feeling of confinement.

All simulator rotational limits are ±45° and the translational limits are ±9 feet. This amount of linear travel is somewhat restrictive, but experience has shown that general hovering tasks, including limited maneuvering such as "quick stops," can be accomplished without resorting to motion "washout" techniques. All motions, therefore, occur just as they would in actual flight.

Power is provided by electric motors which are employed in Ward-Leonard type servo systems. Silent chains transmit power to the angular modes, while cables transfer power to the linear modes. Combined with good frequency response, the resultant motion is described by pilots as being very effective in reproducing the important sensations of actual flight.

Simulator Validation

Before using the simulator for general VTOL research, a study was made to determine how well its results might compare with those obtained in actual flight. A few results from this study are presented in figure 2.

The airplane used for comparison was the Bell X-14 jet-lift VTOL. It was equipped with a rate-damped control system in which both control power and damping could be varied (ref. 14). With the simulator mechanized in a near identical way, concurrent tests were run to evaluate various combinations of control power and damping on the basis of a near similar task.

The bands indicate the combinations resulting in both a 3-1/2 and a 6-1/2 pilot rating. Good agreement between simulator and flight is apparent in both cases. This result does not mean that flight research is no longer necessary. It does indicate, however, that the simulator is capable of providing valid preliminary results, so that subsequent flight tests can be abbreviated.

TESTS

The control systems tests discussed in the remainder of this paper are concerned with VTOL aircraft which require attitude changes in order to translate. As illustrated in figure 3, such aircraft are characterized by thrust vectors fixed in relation to the aircraft, thus requiring rotation of the entire vehicle in order to generate a horizontal force.

Description of Systems Studied

Three concepts for controlling attitude have been tested and compared. For purposes of discussion, they will be referred to as: the acceleration system, the rate system, and the attitude system. The descriptive elements of each system are presented in figure 4.

The acceleration system has no stabilizing feedbacks. As its time history shows, stick deflections produce steady-state acceleration, and the pilot

must provide his own stability and angular-rate damping while controlling attitude. The control-system variables pertinent to this system are control power and control sensitivity.

The rate system is obtained simply by providing the acceleration system with angular-rate feedback. For this case, stick deflections produce steady-state rate. Controlling attitude requires the pilot to provide his own attitude stability, but he does not have to worry about excessive rate buildup. The variables associated with the rate system are control power, control sensitivity, and damping. Damping is simply the gain in the rate feedback loop.

The attitude system goes one step beyond the rate system by incorporating attitude feedback in addition to rate feedback. Pilots using this system command steady-state attitude proportional to stick deflection, and all stabilizing requirements are automatically provided. The variables which describe the attitude system are control power, control sensitivity, damping, and frequency. Frequency refers here to the undamped natural frequency of the system. It is a commonly used measure of the stability of a second-order system; more precisely, frequency is equal to the square root of the gain in the attitude feedback loop. The actual oscillatory characteristics of an attitude system are not defined by frequency alone, but by frequency and damping together. To illustrate this, the time history shown in the bottom of figure 4 is typical of an attitude system which is somewhat underdamped; that is, if damping were increased, the oscillations could be made to disappear.

Each of the three systems had proportional control; that is, the output of the pilot's controller varied linearly with his input. In addition, all feedback terms considered were linear.

The conditions for the tests are shown in table I. The control geometry shown was unchanged throughout the tests. Simplicity was stressed to insure a basic understanding of each control system before subjecting it to complex conditions (as will be done later).

For all of the test conditions, the simulator was operated in the six-degree mode. However, systematic data were generated for the roll axis only. This was done for the following reasons: first, the roll axis has been consistently indicated as a more critical axis than pitch or yaw; in addition, roll-axis data should qualitatively apply to subsequent tests of the pitch axis. From the latter standpoint, the pitch-axis parameters were varied identically with the roll-axis parameters throughout the tests, and abbreviated testing of the pitch axis is planned at a later date. Since the yaw axis was not considered of primary concern, it was maintained as a satisfactory rate system for the duration of testing.

Three pilots, each with a diverse test background including considerable VTOL experience, participated in the test. Two of the pilots were used in all phases of the study, and the third was used for selected verification of the results. The pilots performed the same tasks and used the same method of evaluation. This method was based upon the well-known Cooper Pilot Rating System (ref. 15).

The simulator tasks which formed the basis for evaluation are shown in table II. Since the main intent was to establish a common basis for system comparison, no attempt was made to define tasks which would be universally representative of actual flight situations. (In actuality it is now generally agreed that the VTOL task is not universal in the first place; that is, it will vary greatly from vehicle to vehicle, depending on the mission.) The simulator task was simply designed as a general hover task and a general maneuver task. The hover task was divided into two parts: precision hovering at a point in space, and precision altitude changes to simulate the takeoff and landing modes. The maneuver task included both translation start-stops and roll reversals. Bank angle maximums of 12° were used frequently in the maneuver task.

Because of their nature, the simulator tasks are believed to be more demanding than their counterparts in flight, at least for the majority of VTOL aircraft. For example, the precision hover task involved the pilot's ability to hover a given system within limits on the order of ±2 feet. It is obvious that many VTOL aircraft, though fully suitable for their own design mission, would have difficulty hovering within limits several times this amount. For the maneuvering case, the start-stops were performed by moving rapidly from one hover point to another, separated by distances of about 15 feet. While this might represent a realistic situation in actual flight, the existence of physical travel limits in the simulator tend to make pilots critical of errors which might be unnoticed in flight.

The foregoing was pointed out in order to reemphasize the fact that the simulator results are valid primarily for comparison purposes, and should not be taken in an absolute quantitative sense. Accurate definitions of system requirements will still depend on subsequent flight tests, where tasks can be expanded in a more realistic manner.

RESULTS AND DISCUSSION

The tests began with the optimization of variables for each of the systems previously described. When this was completed, each system was optimized, and a comparison of systems was undertaken. During the optimization studies, control power was held constant at a relatively high value (2 rad/sec^2) in order to minimize any influence it may have had on the results.

In the determination of optimums, none of the variables had a strong effect on pilot rating in the area near the optimum. Optimum values for the variables are therefore presented in ranges (or bands) rather than points (or lines). The widths of these ranges (or bands) were arbitrarily established to include a pilot-rating deviation of about 1/4 to either side of the mean.

Optimization of Parameters

Acceleration system.- Figure 5 simply shows the variation of pilot rating over a wide range of control sensitivity. The curve indicates that sensitivity

does not have a strong effect on pilot rating; in fact, minimum pilot rating is essentially constant between 0.4 and 0.8 rad/sec^2/in. This is shown as the range of optimum sensitivity for the acceleration system.

Since there are no other variables to optimize here, we can proceed to a discussion of the rate system. Before continuing, however, it should be noted that this type of test was used to determine optimum control sensitivity for the rate system, and later on for the attitude system. For the rate system, the test was merely repeated at various levels of constant damping. Results here served as a starting point, since the acceleration system can be considered as a rate system with zero damping.

Rate system.- Figure 6 shows the effect of damping on the optimum sensitivity range for the rate system. This is indicated by a band which was drawn through the optimum sensitivity ranges found at various levels of constant damping. The intercepts on the zero damping axis correspond to the acceleration system just discussed. Increasing the damping does not change the optimum sensitivity range until damping values of about -5 per second are reached. Beyond that point, increases in sensitivity are required to compensate for the sluggishness of the system. Otherwise, stick motions to produce desired roll rates become uncomfortably large. This result can be understood through study of the relationship $p_{ss}/\delta = (L_\delta/I_x)/(L_p/I_x)$.

An optimum damping range from -2 to -5 per second was found by examining the variation of pilot ratings along the optimum sensitivity band. This results in an optimum area in which optimum sensitivity lies between 0.4 and 0.8 rad/sec^2/in., the same as for the acceleration system. The optimum sensitivity and damping ranges for the rate system provide a starting point for discussion of the attitude system. In other words, the next figure will show what happens to these ranges as attitude feedback is applied.

Attitude system.- Figure 7 shows the variation in optimum control sensitivity with frequency. The intercepts at zero frequency correspond to the optimum sensitivity range for the rate system discussed in the preceding figure. As frequency is increased, the optimum sensitivity values at first remain constant, and finally start to increase at frequencies above 2 rad/sec. The increase in sensitivity is required to overcome the increasing stability of the system (a situation somewhat analogous to the sluggishness of the rate system at high values of damping).

In the upper right-hand corner of figure 7 is an equation showing the relationship of bank-angle sensitivity to control sensitivity and frequency. In this expression bank-angle sensitivity is used to express the steady-state bank-angle relationship to stick deflection. In the frequency range where optimum control sensitivity is relatively constant, optimum bank-angle sensitivity must approach infinity as frequency goes to zero. This corresponds, of course, to the fact that bank-angle sensitivity for a rate system is infinite. At high values of frequency, where optimum control sensitivity is increasing, bank-angle sensitivity appears to approach a constant range from about 0.04 to 0.06 rad/in. For the control stick geometry used in these tests, this range could be re-expressed as from about $1/2^\circ$ to 1° of bank per degree of stick

deflection. The important thing to note here is that for frequencies less than 3 rad/sec, the pilots apparently evaluate stick sensitivity on the basis of initial acceleration response rather than stick deflection to achieve a given bank angle or attitude.

The determination of optimum control sensitivities for the attitude system was done at optimum levels of damping. In actuality, there were some interacting effects between these variables, thus requiring reiterative tests to optimize both. In other words, the sensitivity results imply optimum damping, and the damping results in the next figure imply optimum sensitivity.

Figure 8 shows the variation of optimum damping for the attitude system. Once again the intercepts at zero frequency represent the values required for a rate system. It is important to note that the damping parameter used on the ordinate is the damping-to-inertia ratio, and not the familiar damping ratio ζ normally used to describe second-order systems of this type. Using the relationship $L_p/I_x = 2\zeta\omega_n$, values of ζ appear as lines of constant slope in figure 8. The curve shows that optimum damping-to-inertia ratio is relatively constant with frequency up to frequencies of about 3.0 rad/sec. This indicates that pilots are more concerned with a basic level of damping rather than the overshoot or undershoot characteristics which occur as a function of damping ratio ζ. For frequencies above 3.0 rad/sec, however, optimum damping appears to be asymptotic to a constant ζ of around 0.5.

The determination of optimum frequency was performed at three levels of control power. Holding control power constant, frequency was varied over a range from 0 to 4 rad/sec. At each frequency, control sensitivity and damping were set at optimum values, and pilot ratings were obtained. The results of pilot rating versus frequency are shown in figure 9. For control powers greater than 0.5, optimum frequency lies in a band between 1.4 and 2.6 rad/sec. At frequencies below 1.4 rad/sec, the system is insufficiently stable, and too much pilot attention is necessary to control attitude. Above 2.6 rad/sec the system is overly stable to the extent that maneuvering is made difficult by the necessity for large control motions. When control sensitivity is increased to alleviate the maneuvering problem, the system becomes oversensitive in hover. The overall effect is described by the pilots as one of excessive "stiffness."

Table III summarizes the results of the optimization studies. Each of the three systems was then optimized (at the mean values of the optimum parameters shown in this table) and tested at various levels of control power.

System Comparisons

Figure 10 presents the variation of pilot rating with control power for an acceleration system, a rate system, and an attitude system. Each system was optimized according to the results in the summary chart.

The acceleration system is shown to be unsatisfactory for the simulator task regardless of control power. On the other hand, the rate system and the

attitude system are both satisfactory if provided with enough control power. The important difference indicated here is that the attitude system becomes satisfactory at 30- to 40-percent less control power than the rate system.

At large levels of control power, the rate system approaches a constant rating just a little better than 3. The attitude system is rated as a 2. This represents a significant improvement in handling qualities when one considers that pilot ratings better than 2 are practically never given. The superiority of the attitude system reflects itself mainly in the hovering and precision maneuvering modes. It allows these tasks to be performed with little effort, whereas the rate system requires constant pilot attention. For random maneuvering, the two systems feel very much alike, with the rate system being somewhat more responsive.

Figure 10 contains some interesting implications regarding failures. For example, if a satisfactory (pilot rating of 3-1/2) attitude system should experience a failure in its attitude feedback loop, it would revert to a rate system with a pilot rating of about 5. This is because its sensitivity and damping are essentially the same as those for the rate system shown in the same figure. Likewise, if a satisfactory attitude system lost both its feedback loops, it would revert to an acceptable (for emergency operation) acceleration system. The only case not shown here is the one for a failure of the damping loop in the attitude system. Preliminary tests showed that this condition may result in a system so oscillatory as to be unacceptable even for emergency operation. Additional tests are planned to investigate all possible failure conditions.

While these results indicate a definite superiority of the attitude system, the question arises as to whether this system can be made to operate at lower control-power levels without compromising its handling qualities. The answer to this question requires an understanding of all the factors which affect the control power requirements for the attitude system. These factors are summarized in figure 11.

Figure 11 shows the variation of control power required to maintain a constant pilot rating as frequency is increased from 0 to about 3 rad/sec. The rating of 2-1/2 was chosen to be representative of superior, rather than just satisfactory, handling qualities. In other words, any system which achieved this rating had to be more than just satisfactory in coping with the simulator tasks.

The 2-1/2 boundary seems to be influenced by four factors. On the left the curve appears asymptotic to an attitude stability level corresponding to a frequency of about 0.2 rad/sec. (This result re-illustrates the deficiency of the rate system.) Since these tests were run in calm air, it should be noted that the stability level of 0.2 is a minimum; that is, if upset conditions, such as gusts or ground effect, were imposed, the stability level would surely move to the right. The nature of these effects will require further investigation.

The factor most influential on the lower limit of control power appears to be associated with maneuvering response. For the linear systems of this

type there is a level of control power below which response is simply insufficient.

A factor closely associated with insufficient response becomes important at intermediate frequencies. This factor is insufficient bank angle. As shown in the figure, a bank-angle capability of at least 0.2 radian is required to achieve a 2-1/2 pilot rating. (Note here that bank-angle boundaries are represented by curves proportional to frequency squared.) The importance of bank angle is associated primarily with maneuverability; that is, adequate maneuverability to perform a given task requires a certain bank angle in order to generate the necessary horizontal forces.

At frequencies greater than about 3.5 rad/sec, the attitude system finally becomes uncomfortable to the pilot. Since he basically objects to the stiffness of the system in this region, no amount of control power will solve the situation.

In summary, this figure clearly shows some areas for future research. One of the most promising would be to further develop the attitude system in the range of frequencies from 1.4 to 2.6 rad/sec. These are the systems producing the best handling qualities for the least amount of control power. While handling qualities are already near optimum, possibilities exist for their achievement at lower levels of control power. The problem is to somehow overcome the insufficient response and insufficient bank-angle restrictions. This might be accomplished in several ways. For example, previous research has shown that the use of nonproportional control in the pilot's stick can be beneficial in the improvement of response at low control powers. (An extreme case of nonproportional control, known as the on-off system, is discussed in the paper by Garren and Kelly.) On the other hand, bank-angle insufficiencies can be eliminated by the incorporation of nonlinear feedback techniques. It remains to be determined whether nonproportional and/or nonlinear systems have any adverse characteristics of their own. Response problems in maneuvering might also be overcome by combining the attitude system with some form of thrust vectoring capability. As discussed in the paper by Anderson, the use of direct thrust vector control eliminates the need for large attitude changes and might result in significant control power reductions. Here again, the possible adverse characteristics of such systems must be determined.

CONCLUDING COMMENTS

The nature of this study was so basic that no attempt will be made to form specific conclusions. However, an important trend has already become clear, that is, that handling qualities improve and control powers decrease as the pilot is relieved of stabilization workloads which can be more efficiently handled by automatic stabilization techniques.

With this consideration in mind, and with the information herein serving as fundamental background material, additional research is already under way to further define the requirements for a safe and efficient VTOL control system. As promising systems are developed, they will be evaluated under increasingly complex conditions, until final evaluation can be performed in actual flight.

REFERENCES

1. Salmirs, Seymour; and Tapscott, Robert J.: The Effects of Various Combinations of Damping and Control Power on Helicopter Handling Qualities During Both Instrument and Visual Flight. NASA TN D-58, 1959.

2. Rolls, Stewart L.; and Drinkwater, Fred J.: A Flight Determination of the Attitude Control Power and Damping Requirements for a Visual Hovering Task in the Variable Stability and Control X-14 Research Vehicle. NASA TN D-1328, 1962.

3. Rolls, Stewart L.; Drinkwater, Fred J.; and Innis, Robert C.: Hovering Lateral Control Requirements Based on a Jet Lift VTOL Aircraft. NASA TN D-2701, 1965.

4. Garren, John F.; Kelly, James R.; and Reeder, John P.: A Visual Flight Investigation of Hovering and Low-Speed VTOL Control Requirements. NASA TN D-2788, 1965.

5. Faye, Alan E., Jr.: Attitude Control Requirements for Hovering Determined Through the Use of a Piloted Flight Simulator. NASA TN D-792, 1961.

6. Savant, C. J.: Basic Feedback Control System Design. McGraw-Hill Book Co., Inc., N. Y., 1958.

7. Graham, D.; and McRuer, D. T.: Analysis of Nonlinear Control Systems. John Wiley and Sons, 1961.

8. Norair, Div. of Northrop Aircraft: Methods of Analysis and Synthesis of Piloted Aircraft Flight Control Systems. BuAer Rep. AE-61-4-I, Mar. 1952.

9. Truxal, J. G.: Automatic Feedback Control System Synthesis. McGraw-Hill Book Co., Inc., N. Y., 1955.

10. Gardner, M. F.; and Barnes, J. L.: Transients in Linear Systems. John Wiley and Sons, N. Y., 1942.

11. D'Azzo, J. J.; and Houpis, C. H.: Feedback Control System Analysis and Synthesis. McGraw-Hill Book Co., Inc., N. Y., 1960.

12. Ku, Y. H.: Analysis and Control of Linear Systems. International Textbook Co., Scranton, Pa., 1962.

13. Pauli, Frank A.; Hegarty, Daniel M.; and Walsh, Thomas M.: A System for Varying the Stability and Control of a Deflected Jet Fixed Wing VTOL Aircraft. NASA TN D-2700, 1965.

14. Cooper, George E.: Understanding and Interpreting Pilot Opinion. Aero. Eng. Rev., vol. 16, no. 3, Mar. 1957, pp. 47-51, 56.

15. Anderson, Seth B.: An Examination of Handling Qualities Criteria for V/STOL Aircraft. NASA TN D-331, 1960.

TABLE I

TEST CONDITIONS

- CALM AIR (NO GUSTS, CROSSWINDS, OR GROUND EFFECT)
- IDEAL SYSTEMS (NO ACTUATOR DYNAMICS, ETC.)
- NO GYROSCOPICS OR CROSS COUPLING
- CONSTANT CONTROL GEOMETRY

	MAXIMUM CONTROL DEFLECTION, in.	FORCE GRADIENT, lb/in.	BREAKOUT FRICTION, lb	
ROLL	±5	1.8	1	CENTER STICK
PITCH	±5	1.8	1	
YAW	±2.5	0	6	RUDDER PEDALS
THROTTLE	FIGHTER TYPE QUADRANT			

TABLE II

TASKS

INVESTIGATING ROLL CHARACTERISTICS ONLY

- HOVER TASKS
  - PRECISION HOVERING, WITHIN ± 2ft
  - TAKE-OFF AND LANDING
- MANEUVER TASKS
  - TRANSLATION START-STOPS, MAX OF 18ft
  - ROLL REVERSALS

TABLE III

OPTIMUM PARAMETER SUMMARY

● ACCELERATION SYSTEM				
OPTIMUM CONTROL SENSITIVITY	.4	TO	.8	rad/sec²/in
● RATE SYSTEM				
OPTIMUM CONTROL SENSITIVITY	.4	TO	.8	rad/sec²/in
OPTIMUM DAMPING	-2	TO	-5	1/sec
● ATTITUDE SYSTEM				
OPTIMUM CONTROL SENSITIVITY	.4	TO	.8	rad/sec²/in
OPTIMUM DAMPING	-2	TO	-4	1/sec
OPTIMUM FREQUENCY	1.4	TO	2.6	rad/sec

AMES SIX-DEGREE-OF-FREEDOM SIMULATOR

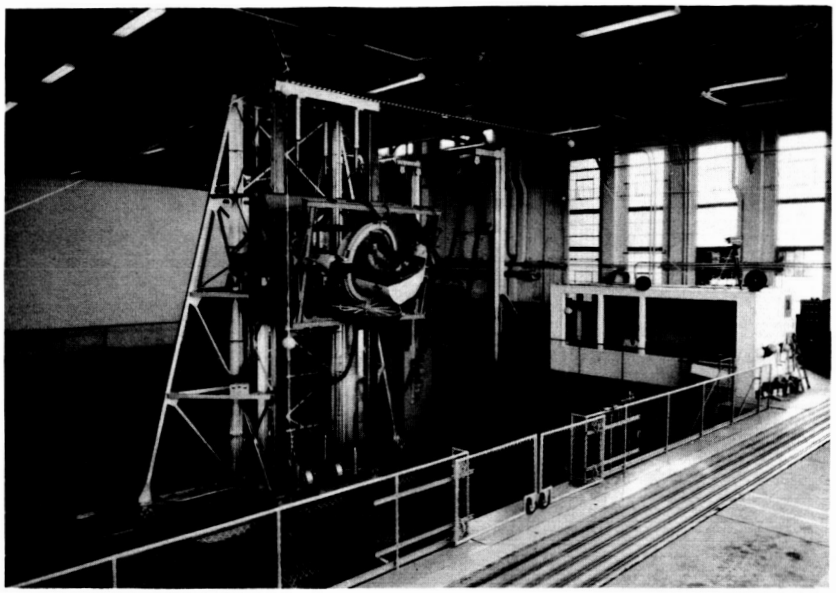

Figure 1

A-36014

COMPARISON OF SIX-DEGREE-OF-FREEDOM SIMULATION AND FLIGHT, X-14

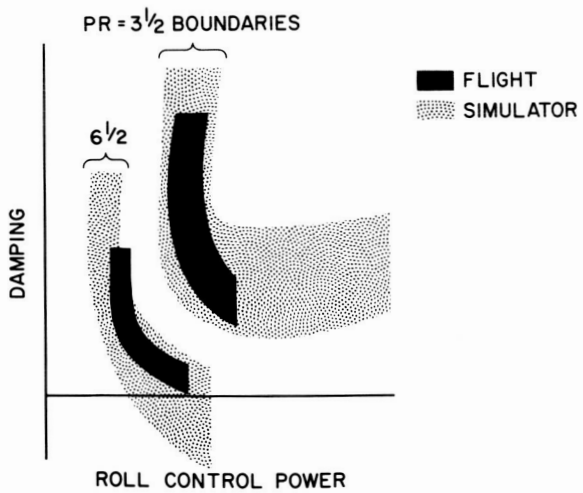

Figure 2

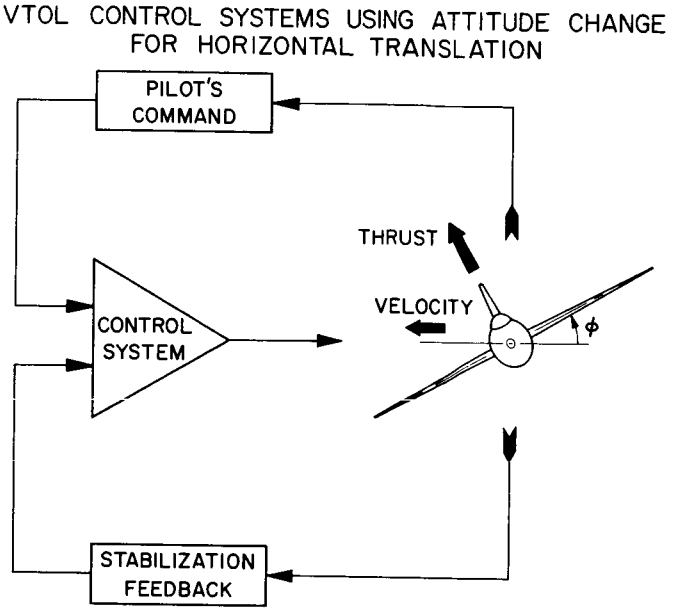

Figure 3

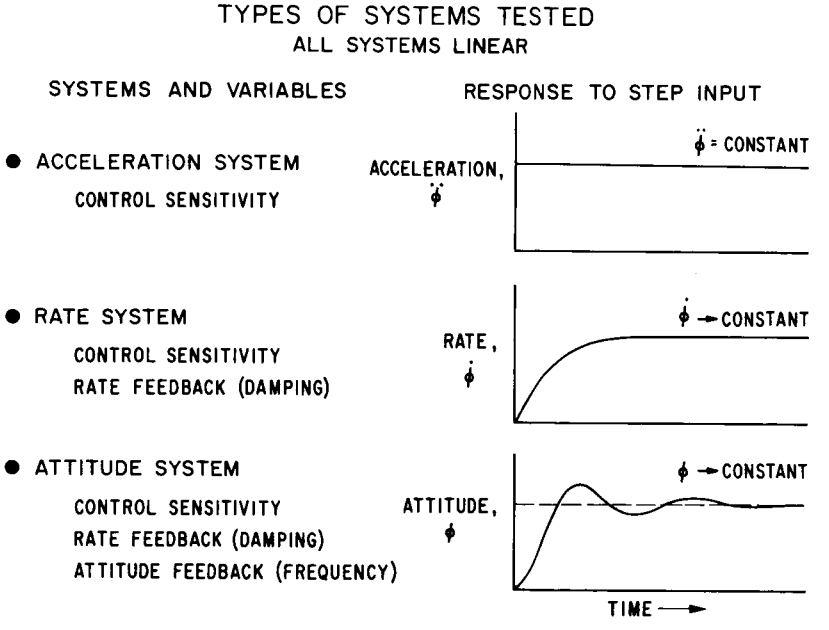

Figure 4

ACCELERATION SYSTEM
EFFECT OF CONTROL SENSITIVITY ON PILOT RATING

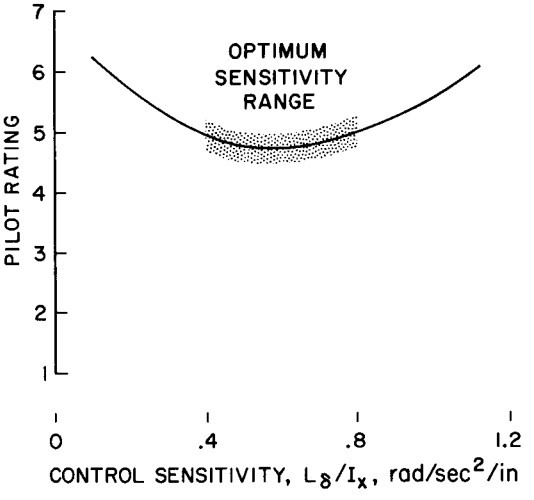

Figure 5

RATE SYSTEMS
VARIATION OF OPTIMUM CONTROL SENSITIVITY WITH DAMPING
(INCLUDING RANGE OF OPTIMUM DAMPING)

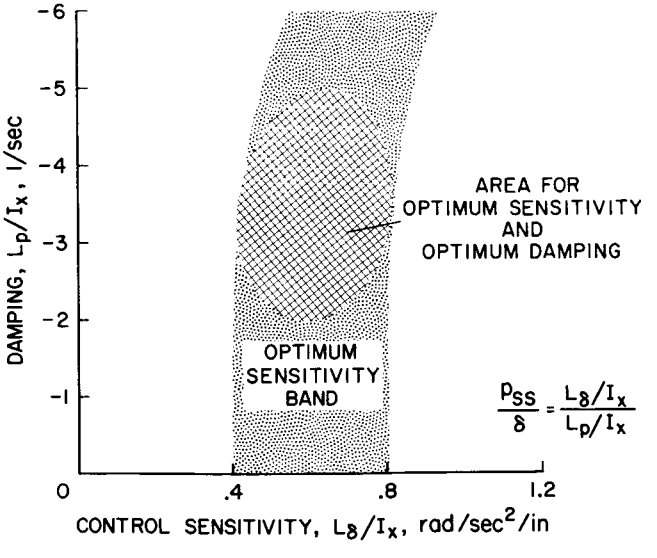

Figure 6

ATTITUDE SYSTEMS

VARIATION OF OPTIMUM CONTROL SENSITIVITY WITH FREQUENCY

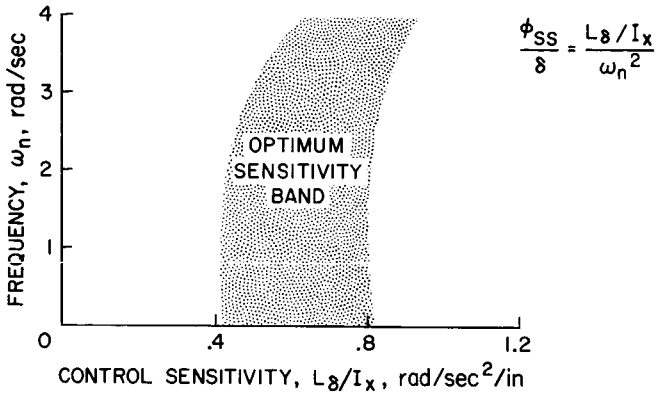

Figure 7

ATTITUDE SYSTEMS

VARIATION OF OPTIMUM DAMPING WITH FREQUENCY

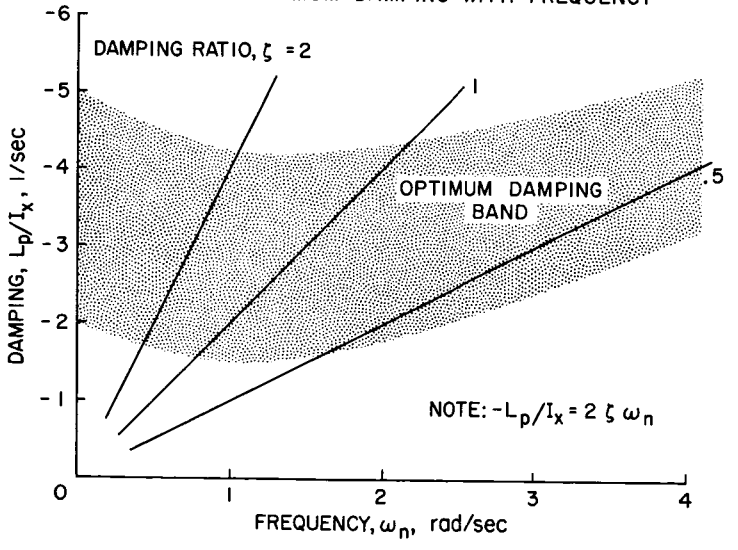

Figure 8

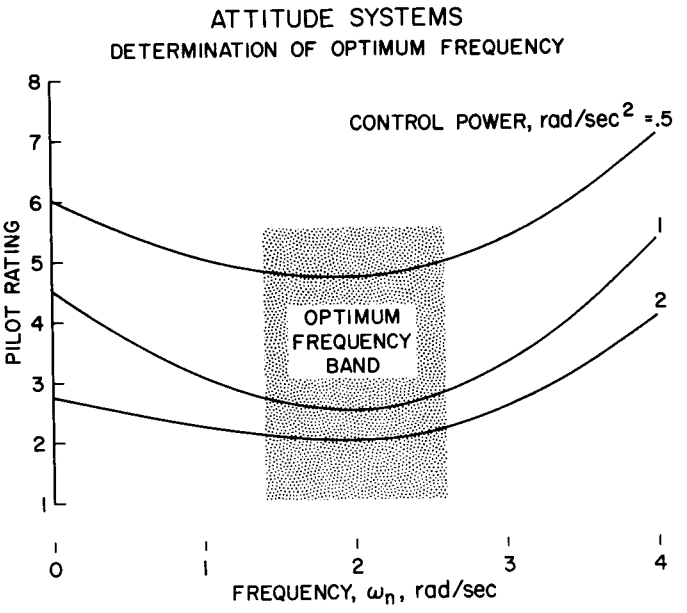

Figure 9

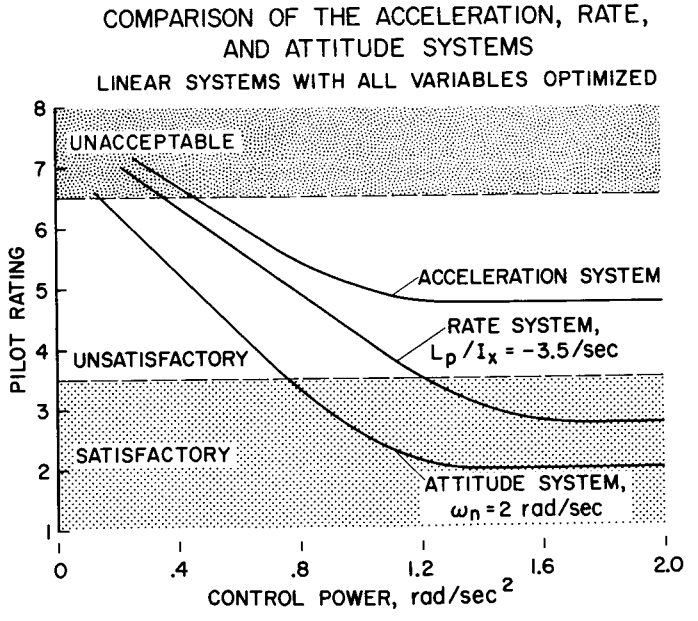

Figure 10

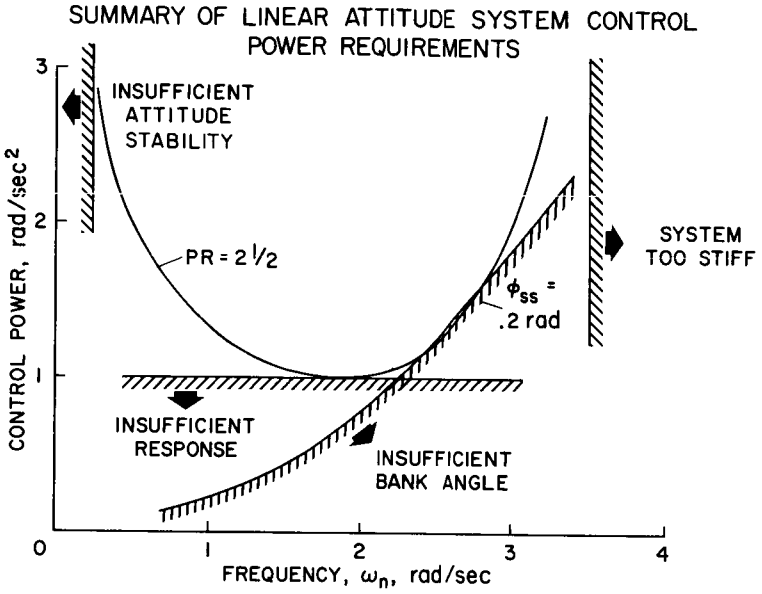
SUMMARY OF LINEAR ATTITUDE SYSTEM CONTROL POWER REQUIREMENTS
INSUFFICIENT ATTITUDE STABILITY
PR = 2 1/2
SYSTEM TOO STIFF
ϕ_{ss} = .2 rad
INSUFFICIENT RESPONSE
INSUFFICIENT BANK ANGLE
CONTROL POWER, rad/sec^2
FREQUENCY, ω_n, rad/sec
0
1
2
3
4

Figure 11

Page intentionally left blank

18. FLIGHT STUDY OF ON-OFF CONTROL FOR V/STOL AIRCRAFT

By John F. Garren, Jr., and James R. Kelly

NASA Langley Research Center

SUMMARY

Because of the severe performance penalties associated with providing high levels of control power in V/STOL aircraft, methods which offer a potential for reducing control power requirements warrant consideration. One such method is the on-off type of control. The lateral results of a visual flight investigation utilizing an on-off pitch and roll control in the variable-stability helicopter at Langley are presented. The size of the control dead band was found to be a critical parameter in providing acceptable handling characteristics. The significant reduction in control power requirements realized by using the on-off control is illustrated by a comparison with the results of a similar investigation using a proportional control system. The effects of angular-velocity damping, trim requirements, and disturbances are discussed.

INTRODUCTION

The potential application of on-off control techniques for V/STOL aircraft was recently brought to the attention of the NASA for serious consideration as a result of research related to landing a manned vehicle on the moon. Studies of the lunar-landing problem using on-off control techniques had indicated the control moment requirement to be substantially less than the current V/STOL criteria, which are based on experience with proportional controls. Although there are significant differences in mission requirements for lunar-landing vehicles and for the operation of V/STOL aircraft, if the control moment reduction were achieved largely as a result of the type of control being used, then the potential application of on-off control techniques to V/STOL aircraft obviously would be of great interest.

Early in 1965 the NASA employed the variable-stability helicopter described in reference 1 to perform in-flight studies with an on-off control. Figure 1, which is a plot of control moment against stick position, compares the type of on-off control used in this study with the more conventional proportional control. In the case of the on-off control a small dead band is provided within which motion of the control produces no moment. When the control has moved past the dead-band threshold, the maximum amount of moment available is generated. Moving the control beyond this point generates no further moment. Rather than putting mechanical stops at the edge of the dead band, overtravel of the stick was permitted.

The purpose of the on-off control study was threefold: first, to establish the major parameters which influence application of the on-off control; next, to assess the handling characteristics provided by the on-off control technique for VTOL operation; finally, to determine the associated control moment requirement. The on-off control was used for both the pitch and roll axes; a proportional system was used for controlling heading and altitude. For the purpose of this paper, the results obtained with the on-off control can be sufficiently illustrated by considering either axis. Because the roll axis has been generally more critical for VTOL aircraft, only the roll results are presented in this paper (a complete discussion of the results for both axes is presented in reference 2). In addition, these results are compared with the results from a proportional control study and with the on-off results obtained with the lunar-landing research vehicle at the NASA Flight Research Center. The effects of trim changes and disturbances are also discussed in this paper.

DEFINITIONS

Terms in this paper which need a specific definition are as follows: Control power is the ratio of maximum control moment available to aircraft inertia, and hence, the maximum angular acceleration capability. Sensitivity is the angular acceleration per unit of control travel. Angular-velocity damping is the angular acceleration which is proportional to and opposes angular velocity; the damping is therefore the reciprocal of the angular response time constant.

PILOT TASKS

The fundamental requirements for VTOL operation dictated the selection of the piloting tasks which were performed during the evaluation of each test condition. For discussion purposes the tasks were divided into categories of maneuvering and precision. The maneuvering tasks included both lateral and longitudinal quick starts and stops. For the lateral task this maneuver was accomplished by accelerating the aircraft rapidly to about 25 knots in sideward flight and then decelerating it to a hover over a preselected spot; acceleration to about 45 knots was used for the longitudinal task. Turn reversals involving rapid S-turns to realine with the runway after an intentional misalinement were performed during the 45-knot landing approaches. The precision tasks included hovering and vertical landings. Precision hovering amounted to steadying the aircraft, moving it a few feet and steadying it again, and remaining positioned at a spot over the ground. If precision hovering could be accomplished satisfactorily, the pilot would attempt a vertical landing. In addition to the research with the variable-stability helicopter, the Ames six-degree-of-freedom simulator was used effectively to study the precision tasks. The pilots used the familiar Cooper pilot-opinion rating system (ref. 3) which consists of numerical ratings ranging from 1 to 10. A rating of $3\frac{1}{2}$ separates

satisfactory from unsatisfactory conditions; a rating of $6\frac{1}{2}$ separates unsatisfactory from unacceptable conditions.

RESULTS AND DISCUSSION

Control Stick Characteristics

During the initial flight, both a center-mounted and side-mounted (or side-arm) control stick were evaluated. The pilots indicated a preference for the side-mounted stick, primarily because an armrest was available with this control. Since the pilots noted, however, that the choice of either control would not alter the results, the tests were conducted solely with the side control. The force gradient on the control stick was fairly light (approximately 1.3 pounds per inch) and the breakout forces and other friction were negligible.

The size of the control dead band (see fig. 1) is one parameter which must be considered in the utilization of an on-off control. Four different dead-band values ranging from ±1/8 inch to ±1 inch were tested and it was found that the size of this dead band was a very critical parameter. The optimum value of the dead band appeared to be about ±1/4 inch and it was held at this value throughout the testing. For dead-band values as large as ±1 inch the pilot could not command the response precisely when desired; for the smaller value of ±1/8 inch, motion of the pilot's hand caused the control to be triggered inadvertently, which, of course, was highly undesirable.

On-Off Results for No Disturbances

Figure 2 illustrates the range of parameters covered during these tests as compared with the range covered during typical proportional control studies. On the vertical scale is plotted angular-velocity damping and on the horizontal axis is plotted control power. The small region near the origin is the range of parameters covered during the on-off tests; as will be shown, it was possible to define a satisfactory region within this area. The larger region at much higher control powers represents the range which must be considered to establish a satisfactory region for maneuvering with a proportional control system.

The small on-off test region shown in figure 2 has been expanded in figure 3, in which the pilot ratings obtained during the maneuver tasks for various combinations of damping and control power are presented. Several maneuver tasks were performed; however, the ratings shown in this figure were obtained for the task which yielded the poorest pilot rating. Although these results are specifically for the lateral axis, the longitudinal results were quite similar and the discussion of the lateral results applies equally well to the longitudinal axis.

Figure 3 shows that only one test condition was considered satisfactory; all the other conditions were unsatisfactory for maneuvering for one reason or another. For the two lowest control power conditions at zero damping, the

weak angular acceleration capability required the pilot to supply a potentially dangerous amount of lead time, or anticipation, for executing maneuvers. For the condition of high control power and zero damping, the control power was sufficiently powerful to produce the desired angular rates but was not sufficiently powerful to arrest these rates. Consequently, uncomfortable attitude changes tended to occur before the angular rate could be stopped. Consideration of these comments suggested the provision of angular-velocity damping which should be beneficial in restricting the build-up of excessively high angular rates, and at the same time, should aid the pilot in stopping the angular rate once the desired attitude was approached. As a result of increasing the damping to 0.5/sec, it is seen that the control power of 0.2 rad/sec^2 was satisfactory for all the maneuver tasks performed. Further increase in the damping to 1.0/sec resulted again in unsatisfactory control because the damping restricted the maximum angular rate that the pilot could develop for maneuvering.

In order to facilitate comparison with other studies, the location of a $3\frac{1}{2}$ boundary has been estimated in figure 3. Although this $3\frac{1}{2}$ boundary is by no means precise, pilot commentary indicated that increasing the control power much beyond 0.2 rad/sec^2 would result in an extremely sensitive control for precision work, whereas reducing it much below this value would result in a limited angular rate capability.

Comparison With Proportional Control Results

Figure 4 offers a comparison between the on-off results and a proportional control study which was conducted with the same equipment. Other similarities between these two investigations include the use of identical tasks and some of the same test pilots. The $3\frac{1}{2}$ boundary for the on-off control has been replotted from figure 3. The data for the $3\frac{1}{2}$ boundary and for the $6\frac{1}{2}$ boundary for the proportional control was plotted from data presented in reference 4. It is seen that the minimum satisfactory control power for the proportional control was about 0.75 rad/sec^2 as compared with less than 0.2 rad/sec^2 for the on-off control. With the proportional control, control powers as low as 0.2 rad/sec^2 were rated completely unsatisfactory.

Another interesting point which can be made from figure 4 is related to the relatively small size of the satisfactory region for the on-off control. The fact that this region is indeed quite small has also been confirmed by tests on the Ames six-degree-of-freedom simulator. The small, closed nature of this region is likely to place a more exacting burden on the designer. For example, the reduction in aircraft inertia, which accompanies expenditure of fuel and stores, results in an increase in control power. Although this is a shift in the favorable direction for proportional systems, an increase in control power for the on-off control might shift the response into an unsatisfactory region. However, for the single test condition which was flown within the satisfactory on-off region, the pilots commented that the precision was as good as that

previously experienced with proportional controls and that the maneuverability was adequate. In fact, analysis of the angular-velocity time histories indicated that about the same angular rates were used for the test condition within the satisfactory on-off region as for test conditions on the satisfactory boundary for the proportional control. It should be noted that all the pilots adapted to the on-off control very readily, the learning time per pilot being on the order of only 10 minutes.

It is logical at this point to consider reasons why the on-off control provides such benefits. It is believed that the benefits are related primarily to the fact that the on-off control, in effect, provides a high sensitivity without causing the touchiness usually associated with high sensitivities. In other words, the small dead band puts the full control capability at the pilot's finger tips and further serves to prevent inadvertent stick motions from affecting the aircraft.

Comparison With On-Off Results From Lunar-Landing Studies

Additional studies with on-off control techniques have similarly indicated satisfactory maneuverability for low control powers. A comparison of the present results with results from the lunar-landing research vehicle (LLRV) (see ref. 5) at the NASA Flight Research Center is shown on figure 5 which is a plot of pilot rating against control power. The proportional results discussed previously have been replotted solely to emphasize the low magnitude of the control power for the two on-off studies.

For the lunar mission it is advantageous to use an on-off type of damping rather than the linear, or aerodynamic, damping simulated in the present study; thus, the comparison is made only on the basis of the control power that was provided. This figure shows that rather good agreement was obtained between the two on-off studies in the region where comparable values of control powers were tested. As a matter of interest, it is noted that in the LLRV the pilot rating continued to improve with increased control power. Although the present study did not evaluate control powers higher than 0.2 rad/sec^2, as mentioned previously, the pilots felt that going much above this value would aggravate precise control and cause control deterioration. Differences in pilot location relative to the axis of rotation, differences in controller characteristics, and also possible differences in mission philosophy between lunar operation and conventional VTOL operation might account for this apparent variation. At any rate, in both applications, the use of nonlinear control techniques has permitted a significant reduction in the amount of control power that would otherwise be required for maneuvering.

Effects of Disturbances

Thus far only the control power required to maneuver the aircraft has been considered. In practice, this requirement represents but one of several demands on control power. As a function of aircraft configuration and size, varying amounts of control power must be provided to compensate for trim

changes and to permit corrections to random disturbances. Trim changes, such as would occur as a result of changes in the aircraft center-of-gravity position, were tested. These results indicated that the pilot could handle a trim change of only about 15 percent of the available control power without having any adverse effect on the controllability. Beyond 15 percent the degradation in control does become apparent.

The other aspect of these disturbance tests was to determine the effects of random disturbances on the handling characteristics when the on-off control is used. Figure 6 is a sample time history of the random disturbance amplitude used to excite the aircraft. The figure indicates that the primary peaks occurred only a few times per minute and were of relatively short duration. In common with the familiar rule of thumb for natural turbulence, these peaks correspond in amplitude to about $2\frac{1}{2}$ to 3 times the root-mean-square value of the disturbance.

In figure 7 pilot ratings are plotted as a function of the angular acceleration produced by the peak disturbances. Only the precision tasks were performed during the random disturbance tests on the assumption that random disturbances would be most detrimental to precision flight and also on the assumption that under conditions of heavy disturbances the pilot would be most concerned with keeping the aircraft level and would do as little maneuvering as possible. The combination of control power and damping which was selected for this test was 0.2 rad/sec^2 and 0.5/sec, respectively, and has already been established as providing satisfactory characteristics for the zero disturbance flights. It is seen from this figure that the degradation of the rating is fairly mild up to a peak disturbance level of 0.12 rad/sec^2 where the handling characteristics begin to become unsatisfactory. It is realized, of course, that a disturbance of 0.12 rad/sec^2 is equivalent to 60 percent of the control power provided. It is thought to be significant that the pilots were able to cope satisfactorily with disturbances of this size.

CONCLUDING REMARKS

The results of these studies have indicated that substantial reductions in the control power required for maneuvering can be achieved by use of nonlinear control techniques. In addition to providing a control system which seemed natural and comfortable to the pilot, the on-off control was found capable of handling small trim changes and moderate disturbances. It is concluded, therefore, that practical application of the on-off control would most likely occur in aircraft where the primary requirement for control power is maneuvering (for example, in cases where susceptibility to random angular disturbances is small and where trim changes are either kept small or handled by an alternate control source).

REFERENCES

1. Garren, John F., Jr.; and Kelly, James R.: Description of an Analog Computer Approach to V/STOL Simulation Employing a Variable-Stability Helicopter. NASA TN D-1970, 1964.

2. Garren, John F., Jr.; DiCarlo, Daniel J.; and Driscoll, Norman R.: Flight Investigation of an On-Off Control for V/STOL Aircraft Under Visual Conditions. NASA TN D-3436, 1966.

3. Cooper, George E.: Understanding and Interpreting Pilot Opinion. Aeron. Eng. Rev., vol. 16, no. 3, Mar. 1957, pp. 47-51, 56.

4. Garren, John F., Jr.; Kelly, James R.; and Reeder, John P.: A Visual Flight Investigation of Hovering and Low-Speed VTOL Control Requirements. NASA TN D-2788, 1965.

5. Bellman, Donald R.; and Matranga, Gene J.: Design and Operational Characteristics of a Lunar-Landing Research Vehicle. NASA TN D-3023, 1965.

COMPARISON OF ON-OFF AND PROPORTIONAL CONTROLS

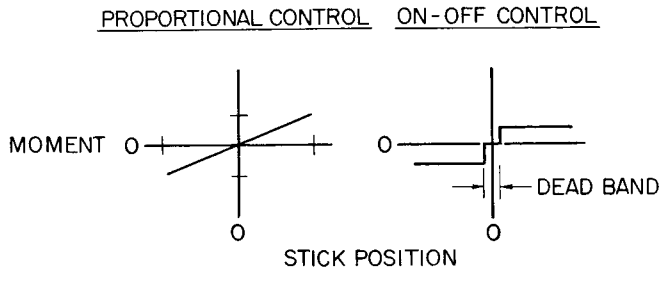

Figure 1

RANGE OF RESPONSE PARAMETERS TESTED

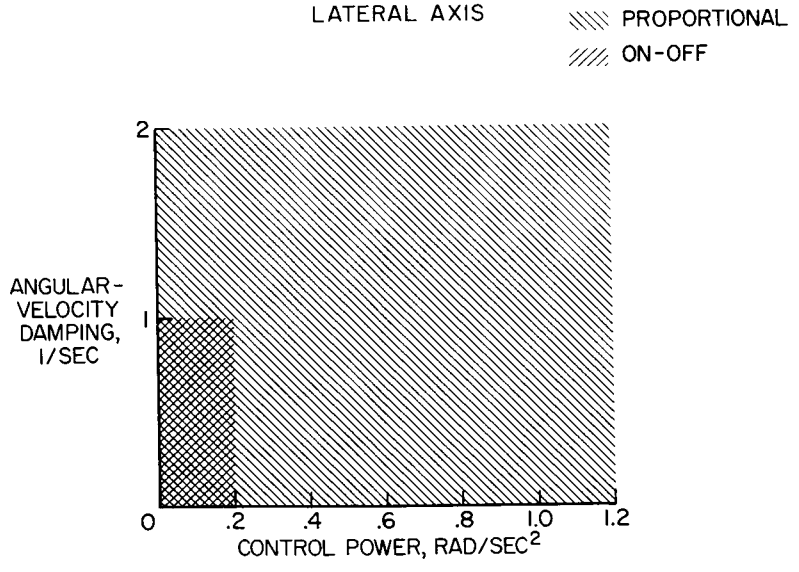

Figure 2

ON-OFF CONTROL RESULTS FOR MANEUVERING TASKS
LATERAL AXIS

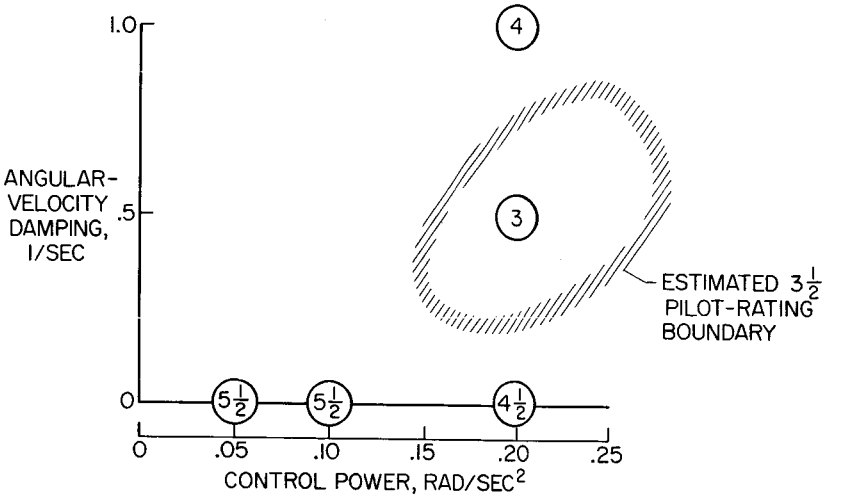

Figure 3

COMPARISON OF ON-OFF AND PROPORTIONAL CONTROL RESULTS FOR MANEUVERING TASKS
LATERAL AXIS

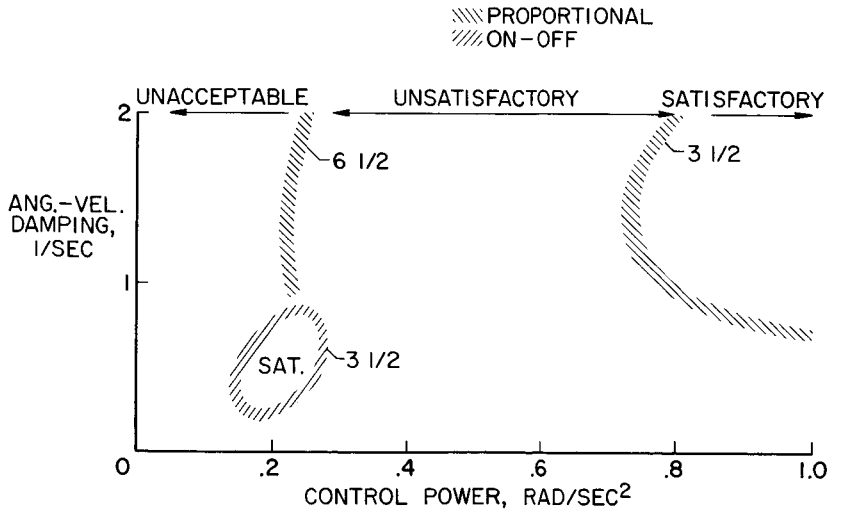

Figure 4

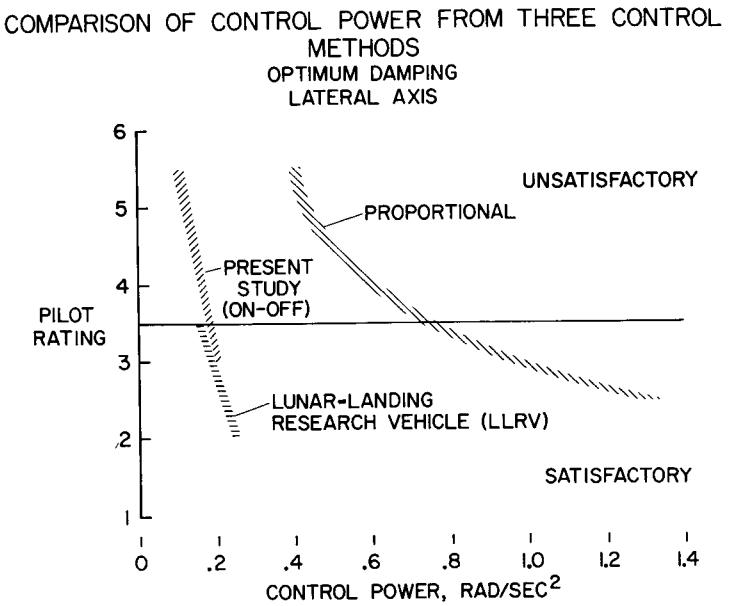

Figure 5

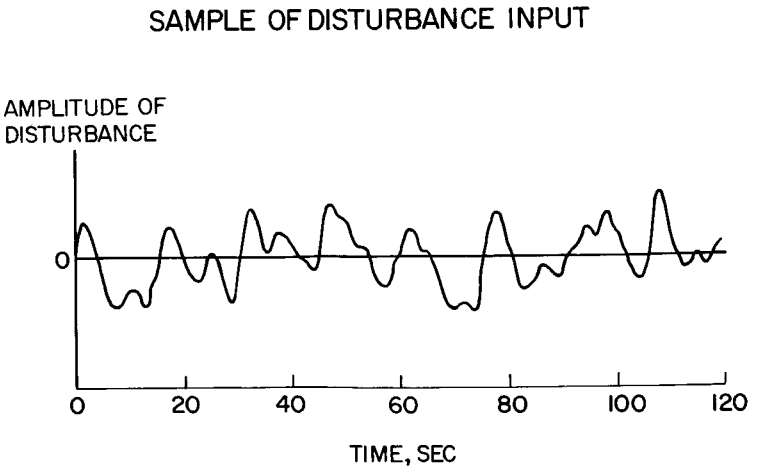

Figure 6

DISTURBANCE EFFECTS ON ON-OFF CONTROL DURING PRECISION TASKS

CONTROL POWER, 0.2 RAD/SEC^2; ANGULAR-VELOCITY DAMPING, 0.5/SEC

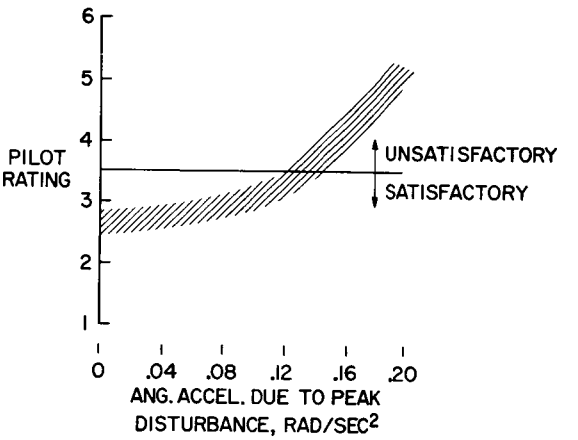

Figure 7

Page intentionally left blank

19. RESULTS OF A BRIEF FLIGHT INVESTIGATION OF A COIN-TYPE STOL AIRCRAFT

By Terrell W. Feistel, Curt A. Holzhauser,
and Robert C. Innis
Ames Research Center

SUMMARY

This paper shows that a current generation COIN aircraft is capable of good low-speed performance and handling qualities when flown in the STOL regime, provided the possibility of engine failure is ignored or a suitable safeguard, such as cross shafting, is incorporated. This performance is achieved in spite of the flaps having only medium effectiveness because the aircraft has a low aspect ratio, a high power loading, and a landing gear designed for no-flare landings. However, when it is flown above the minimum single engine control speed, in compliance with the safety restrictions for twin-engine airplanes, major aspects of the performance are no better than that obtainable with many small twin engine aircraft in current production, and most of the original objectives of the COIN concept are compromised.

INTRODUCTION

A continuing need exists for the development of a small, uncomplicated aircraft with good high-lift capability to allow operation from short, unimproved fields. Proposed uses are for transportation, in the so-called underdeveloped countries, and also as a counter-insurgency (or COIN) aircraft. Many previous papers and reports have pointed out the large maximum lift capabilities of propeller driven STOL airplanes. However, operational utilization of these lift capabilities has been limited by inadequate descent performance, poor handling qualities, and concern over the loss of an engine. To examine these problem areas further and to obtain additional operational experience with STOL aircraft (as well as for evaluation as a possible NASA STOL research aircraft), 10 hours of flight testing were performed in the first flying prototype COIN, the Convair Model 48 "Charger."

SYMBOLS

C_D power-on drag coefficient

C_L lift coefficient

$\overline{C}_F$ mean equivalent skin friction coefficient in cruise

$\equiv C_{D_{cruise}} - \frac{C^2_{L_{cruise}}}{\pi AR}$ (where AR is actual geometric aspect ratio, $\frac{b^2}{S}$)

$\frac{R}{S}$ rate of sink, fps or fpm

$\overline{Re}$ mean Reynolds number in cruise $\equiv \overline{l} \times \frac{V}{\gamma}$ (where $\overline{l}$ is the mean wetted surface length and γ is the kinematic viscosity of air)

SHP shaft horsepower

S_L total landing distance over 50 ft

T'_c thrust coefficient

V_k indicated airspeed, knots

V_{MC} minimum single-engine control speed, knots

$\frac{W}{S}$ wing loading, lb/sq ft

α indicated angle of attack, deg

δ_F flap deflection, deg

γ flight-path angle, deg

DESCRIPTION OF TEST AIRPLANE

Figure 1 shows the airplane in an STOL landing approach. The airplane had two 650 SHP PT6A engines driving opposite rotation propellers, with tips rotating upward in the center, and retractable Krueger flaps to protect the inboard leading edges of the wing; the wing was completely immersed in the propeller slipstream and incorporated a single-slotted, double-hinged, 44-percent chord flap which was deflected at $60^\circ + 30^\circ$ for the landing approach and at 20° for take-off. (The flap geometry is shown on the inset.) Lateral control was with spoilers only and longitudinal control incorporated a free-floating horizontal tail.

All of the take-offs and landings, and most of the total NASA flight time, were in the STOL regime (that is, at speeds below power-off stall speed and below the minimum single engine control speed) since the ability to operate in this region represented the only truly unique capability of the aircraft and was the principal subject of our interest.

Instrumentation

The flight test data were obtained from information recorded with an on-board tape deck and photo panel, the taped data being recorded on oscillograph paper subsequent to the flights. Correlation was made through voice contact with the pilot and with a time-coding system.

HANDLING QUALITIES DISCUSSION

The first area to be discussed will be STOL handling qualities; later, the STOL landing and descent capabilities will be covered in detail.

The handling-quality areas that were anticipated to be of most concern during the preliminary design phase for the COIN aircraft are listed in figure 2. The most significant of these, the engine-out roll control problem, will be discussed in detail later (along with the performance aspects).

Tail Location

A high or low horizontal tail location was the object of much discussion for the various COIN configurations proposed. Initially, concern was expressed that a high horizontal tail configuration would have unacceptable pitch-up characteristics as well as undesirable pitching-moment response due to thrust change. Very little longitudinal trim increment with power change was evident from the flight test data for the test airplane in the landing approach, and the pilot's opinion was that the airplane's pitch response to throttle changes was good. (A similar result was obtained in the simulator studies of reference 1.)

Pitch-up

The pitch-up problem also proved to be of little consequence. The only pitch-up tendency encountered was during a stall in the wave-off condition in which a small increment in forward stick was required at the minimum speed. (As flown during these NASA flights the propellers were rotating up in the center, a possibly relevant factor which helped to counteract the "roll-up" of the wing-tip vortices.)

Turn Coordination

The problem of high adverse sideslip being produced during a turn at high C_L, as is so often evidenced by the larger STOL aircraft, has not proven so serious with the smaller craft, such as the Charger and the Ryan VZ-3. The reason is evident from the data presented in reference 2. With directional periods of less than approximately 8 seconds, the pilot is able to adequately

coordinate the turn with rudder and has not as much tendency to over-control or to produce out-of-phase inputs as with the larger aircraft.

Control System Characteristics

The problems encountered with the non-boosted control system of this airplane were not precisely as might have been anticipated. The free flying horizontal stabilizer-elevator system, controlled by a small trailing edge tab connected directly to the stick, proved highly successful in producing adequate and responsive control moments with low stick forces; it even produced a desirable quickening effect to rapid longitudinal inputs, due to the dynamic overshoot tendency of the free floating stabilizer. The all-mechanical lateral control system, however, was deficient because of the high mass and resultant moments of inertia of the circular-arc spoilers used which, combined with the sensitive longitudinal system, produced a force disharmony and resulted in inadvertent pitch inputs from lateral control motions.

Handling Qualities Summary

The lack of any seriously objectionable aerodynamic stability and control characteristics, for current STOL capability of the aircraft at least, indicates that STOL handling qualities can be considered of secondary importance to other COIN problems, with engine-out characteristics being in the forefront. (This is not to state that the handling qualities were good, but that they were acceptable for a test-bed airplane.) Improving the STOL capability, however, to allow operation in the 40-50 knot region, would necessitate, as a minimum, an upgrading of the lateral and directional control power capabilities. The table below shows some of the significant control power and response characteristics (in the landing approach condition) of the aircraft, as flown:

CONTROL RESPONSE CHARACTERISTICS

(NOMINAL STOL DESCENT CONDITION, V_k = 55-60, R/S = 600-800 fpm)

Quality	Longitudinal	Lateral	Directional
Control power (max acceleration)	$\approx$ 1.2 rad/sec^2	0.7 rad/sec^2	0.3 rad/sec^2
Response after 1 sec (measured)	$\approx 14^o$	10^o	7^o
Pilot rating (control)	3	3-1/2	3

STOL LANDING PERFORMANCE

Figure 3 shows actual STOL landing distances for the Charger, as flown by the NASA test pilot, as a function of approach descent angle; representative Breguet 941 (ref. 3) distances are superimposed for comparison, the open points represent the air distance over 50 feet and the closed points represent the total distance to a stop. (The wing loadings for the Charger were from 35 to 40 lb/sq ft and all approaches were made at 55 to 60 knots.) The variation with descent angle of air distance over 50 feet is noteworthy; it points out the great importance of attaining good descent performance along with low speed, for short field landings.

The sink speed placard of 16 fps for the prototype Charger landing gear is significant; the no-flare landings it enabled were a distinct advantage and made possible a great reduction in landing distance and improvement in touchdown point consistency over the conventional full flare.

It should be noted, with regard to the Charger landings, that the NASA pilot was primarily investigating different combinations of approach speed and sink rate and did not optimize the ground roll (as evidenced by the increased ground distance at the higher angles, caused by bouncing). During the Convair flight testing, actual landing distances as low as 600 feet over a 50-foot obstacle were achieved. Superimposed on the data are calculated distances for landing over a 50-foot obstacle, touching down with no flare, and stopping with an average deceleration of 1/2 g; these calculated landing distances will be used in subsequent plots as a guide to show the probable trend of landing distance variation as approach angle and speed are varied.

Primary emphasis in the remainder of the paper will be on the STOL landing regime because this has proven to be the biggest problem area, and the take-off distance, of this as with most projected STOL aircraft, is consistently less than that for landing. In the Charger flight tests, both by NASA and by Convair, the take-off distances over 50 feet, minimum as well as average, were approximately 100 feet less than those for landing.

STOL DESCENT CAPABILITY

The descent characteristics in the landing approach condition, as derived from the NASA flight test data, are presented in figure 4. Sink rate is plotted as a function of speed, for constant throttle settings, with angle-of-attack values superimposed. The maximum descent capability was limited by buffeting and lateral unsteadiness which necessitated an adequate margin from the stall for the STOL landing approach. (The indicated angle of attack for the stall varied from approximately 20° to 35° as power was increased from idle to NRP.) The nominal approach condition for a STOL landing was made at 55 to 60 knots with 600 to 800 fpm rate of sink (corresponding to more than half the NRP). It is significant that this was approximately 10 knots below the power-off stall speed of 67 knots.

The descent condition for the Breguet 941, as flown in the NASA tests of 1963 (ref. 3), is also indicated and is approximately the same as that shown for the subject airplane. The similarity of the descent conditions for these two fairly dissimilar craft is striking. The fact that the Breguet can descend at the same angle as the Charger, despite its higher aspect ratio (6-1/2 vs. 4-1/2), is attributable to its superior flap effectiveness.

ENGINE OUT CHARACTERISTICS

Figure 5 is another descent characteristics plot with data from the previous one shown for comparison. The information on the right-hand side of the plot includes single-engine flight test data and shows the effect of flying the test aircraft strictly as a twin-engine airplane (i.e., approaching above the minimum single-engine control speed, V_{MC}). A probable V_{MC} approach condition is shown with a speed of approximately 80 knots and 900 fpm rate of sink. The take-off flap setting is seen to represent a feasible condition for an engine-out landing, and indicates the degradation of lift capability that would be necessary under these ground rules. (The minimum sink rate for single-engine flight with landing flaps is 1900 fpm, beyond the 20-fps COIN landing gear design limit.)

The engine-out speed limitation indicated on the plot was on lateral control (rather than directional, as is usually the case with conventional aircraft). This comes about because of the basic deflected slipstream principle being utilized which dictates an asymmetrical loss of lift proportional to the loss of thrust of the corresponding propeller. The result is that the only way to counter the rolling moment produced is by spoiling the lift and/or reducing the thrust on the appropriate side.

COMPARISON OF DESCENT AND LANDING PERFORMANCES

Figure 6 is a comparison plot to show the descent characteristics and potential landing distances for the two modes previously discussed and to compare these with those for some existing medium-field-length utility transports with similar wing loadings. The calculated, no-flare landing distance lines are superimposed on the conventional descent plot. The nominal STOL approach condition for the test aircraft falls below the 800-foot landing distance line while the calculated distance for the V_{MC} approach condition is about 1100 feet. A representative shaded area is shown to indicate the maximum performance approach condition of the Caribou-Mohawk-Buffalo types. (Maximum performance landings of the Caribou result in a distance over 50 ft of approximately 1000 ft, including the flare.)

Engine-Out Provisions

As is evident from the comparison with the Caribou, the existing COIN configuration, when flown strictly as a twin-engined airplane, has no

performance advantage over many twins in current production and cannot properly be termed an STOL. The Convair Charger, to overcome this difficulty, was equipped with a "torque equalizer" device which was to automatically throttle back one engine in the event of the failure of the other, and to provide "single-engine survivability" by allowing the pilot to eject with the airplane still upright. A superior solution, of course, to the engine-out problem (but one which was ruled out in the original competition) is to provide highly reliable cross shafting to allow the power from one engine to be transmitted to both propellers. A practical cross-shafting system, of course, requires propellers, gear boxes, and shafting with an inherently higher order of reliability than the engines. Other, and perhaps more important, advantages of cross shafting lie in its adaptability to improved means of lateral-directional control through asymmetrical propeller pitch phasing, and in much improved thrust response without asymmetry for maximum performance in take-offs, reverse-thrust landings, and full power wave-offs. The Breguet 941 serves as an excellent example of all these applications.

It is noteworthy that the test airplane, if equipped with cross shafting, would be capable of descending at the nominal STOL approach condition with one engine at military power and, it would have a wave-off capability with flaps retracted to the take-off setting (assuming a fast retract mechanism were incorporated).

STOL APPROACH POLAR

Figure 7 shows the actual power-on, lift-drag polars of the airplane as derived from flight test data. Lines of constant thrust coefficient are plotted with angle-of-attack values superimposed. The nominal STOL approach condition is indicated, and the Breguet 941 condition is shown for comparison. The figure points up the large disparity between the realizable $C_{L_{max}}$ capability of the airplane and the actual C_L used in a landing approach, which is representative of most STOL designs. This disparity is due partly to the steep descent capability required for short landing distances over an obstacle and partly to a stall margin of approximately 10 knots and 10° α, which is usually demanded by the pilot.

COMPARATIVE POLAR DIAGRAM

Figure 8 is a C_L - C_D plot showing lines of constant, calculated, no-flare landing distances over 50 ft for a wing loading of 40 lb/sq ft; also shown for reference is the 20 fps sink-rate line which is the landing gear design limit specified for the COIN. The form of the curves illustrates the need for good descent capability (that is, high drag to accompany high lift) for the achievement of a short landing over an obstacle; the nominal STOL approach condition of the test aircraft is again indicated for reference. Another approach condition is sketched to show what might be achievable with any of several possible means of improving flap effectiveness of the "conventional" COIN configuration. By improving the turning efficiency to allow

an increase in the usable C_L to the order of 7 and the attainment of a 10^o-15^o descent angle, the no-flare landing distance could be reduced to less than 400 feet. One possible means of achieving such an improvement in descent performance might be through the use of a rotating-cylinder flap arrangement; others might include the use of boundary layer control, either suction or blowing, or of jet flaps. Even a well designed double or triple slotted flap arrangement such as used in the Breguet would represent a great improvement in turning effectiveness (and, consequently, landing performance) over the current COIN capability as is evidenced by the typical STOL descent condition shown for the Ryan VZ-3 (this aircraft had an aspect ratio of 4-1/2 also).

Another area which would seem to be a fruitful possibility for future research would be to consider various means of eliminating the dependency of lift on thrust (i.e., forsaking the deflected slipstream principle). Such an approach (assuming good low-speed capability were maintained) might improve descent capability as well as eliminate problems of asymmetry due to the loss of an engine. A configuration change would be almost unavoidable and would most likely result in a single propeller axis design with augmented lifting surfaces. A pusher canard or tandem-wing configuration might be likely candidates.

CRUISE PERFORMANCE OF STOL AIRCRAFT

The high speed performance of the present generation of COIN aircraft has fallen somewhat below the early expectations. It has been found that high power and small size alone are not sufficient to assure respectable high speed capability. Figure 9 (derived from ref. 4) shows a comparison of the equivalent mean skin-friction drags of various airplanes. The approximate net parasite drag at cruise, $\overline{C}_F$, based on wetted area (which corresponds to an equivalent skin friction drag), is plotted against the approximate average Reynolds number, $\overline{R}e$, for the airplane in the condition tested; lines of flat plate laminar and turbulent skin friction coefficients are shown for comparison. It can be seen that high performance sailplanes reach a mean skin-friction drag coefficient approaching that of a turbulent flat plate, but that most powered airplanes have drag levels somewhat higher; the Breguet 941 falls in this category with $C_F \approx 0.005$. According to the NASA flight test data in the "clean" configuration at normal rated power, and using the manufacturer's estimate for propeller efficiency, the Convair Charger had $C_F \approx 0.008$, a relatively high value. That good STOL performance and reasonable drag values in cruise need not be mutually exclusive is evident from the data shown for the Breguet 941; even though this airplane is by no means optimized for cruise, it has a reasonably low cruise drag along with its good low speed performance. If STOL performance is the primary goal, however, the proper path toward reasonable cruise performance is probably to incorporate detailed modifications into the design after the general configuration has been tailored to achieve good low-speed performance and handling qualities and not vice versa. Such items as leakage through retracted flaps and landing gear doors, separation off of afterbodies and canopies, and poor nacelle drag and propeller performance can often be corrected by detailed attention to individualized fixes

with consequent large reductions in drag and with little or no decrement (and possibly an increment) in low-speed performance.

CONCLUDING REMARKS

This paper shows that a current generation COIN aircraft is capable of good low-speed performance and handling qualities when flown in the STOL regime, provided the possibility of engine failure is ignored or a suitable safeguard, such as cross shafting, is incorporated. This performance is achieved in spite of the flaps having only medium effectiveness because the aircraft has a low aspect ratio, a high power loading, and a landing gear designed for no-flare landings. However, when it is flown above the minimum single engine control speed, in compliance with the safety restrictions for twin-engine airplanes, major aspects of the performance are no better than that obtainable with many small twins in current production, and most of the original objectives of the COIN concept are compromised.

Also, it was hoped to point out that, through proper utilization of current advances in the state of the art, substantial improvements are possible to enable the design of much needed aircraft, either COIN or short-haul transport, with truly unique short-field capabilities.

REFERENCES

1. Vomaske, R. F.; and Drinkwater, F. J., III: A Simulator Study to Determine Pilot Opinion of the Trim Changes With Power for Deflected Slipstream STOL Airplanes. NASA TN D-3246, 1966.

2. Anderson, S. B.; Quigley, H. C.; and Innis, R. C.: Stability and Control Considerations for STOL Aircraft. AIAA 65-715, presented at CASI/AIAA Low-Speed Flight Meeting, Montreal, Canada, Oct. 18-19, 1965.

3. Quigley, H. C.; Innis, R. C.; and Holzhauser, C. A.: A Flight Investigation of the Performance, Handling Qualities, and Operational Characteristics of a Deflected Slipstream STOL Transport Airplane Having Four Interconnected Propellers. NASA TN D-2231, 1964.

4. Raspet, August: Application of Sailplane Performance Analysis to Airplanes. Aero. Engr. Review, vol. 13, no. 8, Aug. 1954.

STOL LANDING APPROACH
$\delta_F = 60/30$

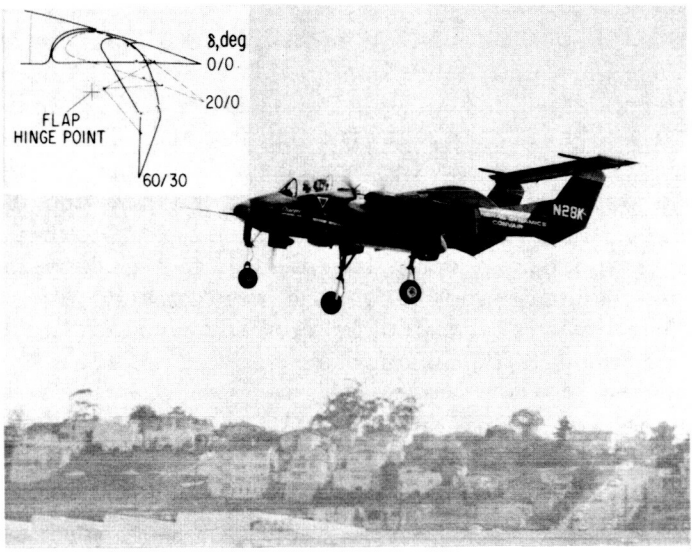

Figure 1

AAA036-1

COIN HANDLING QUALITIES TO BE DISCUSSED

- ENGINE-OUT ASYMMETRY
- HORIZONTAL-TAIL LOCATION
  - PITCH RESPONSE WITH POWER
  - PITCH-UP
- HIGH ADVERSE SIDESLIP
- NONBOOSTED CONTROL SYSTEM

Figure 2

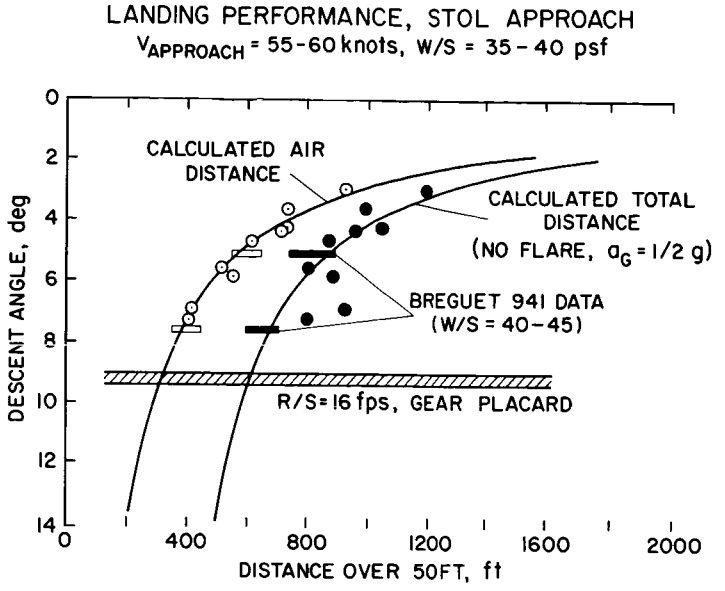

Figure 3

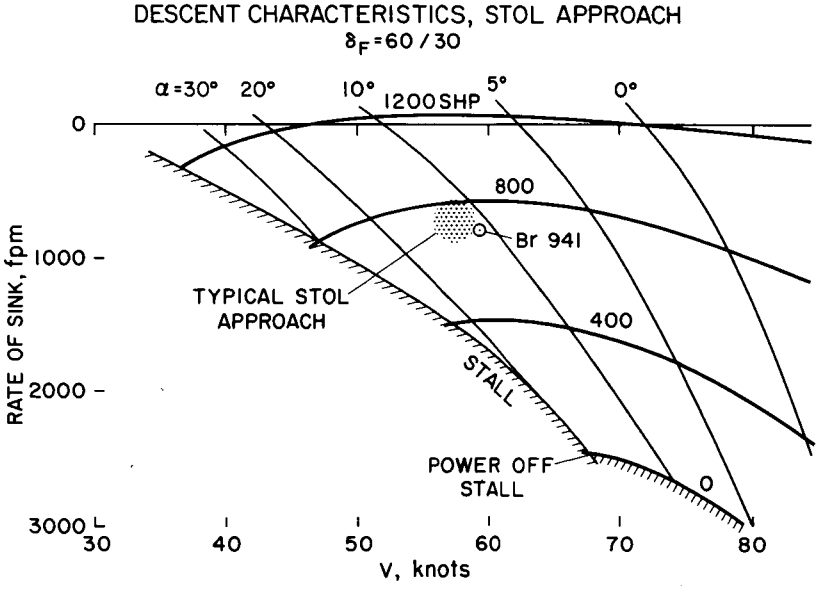

Figure 4

EFFECT OF ENGINE-OUT ON LANDING APPROACH

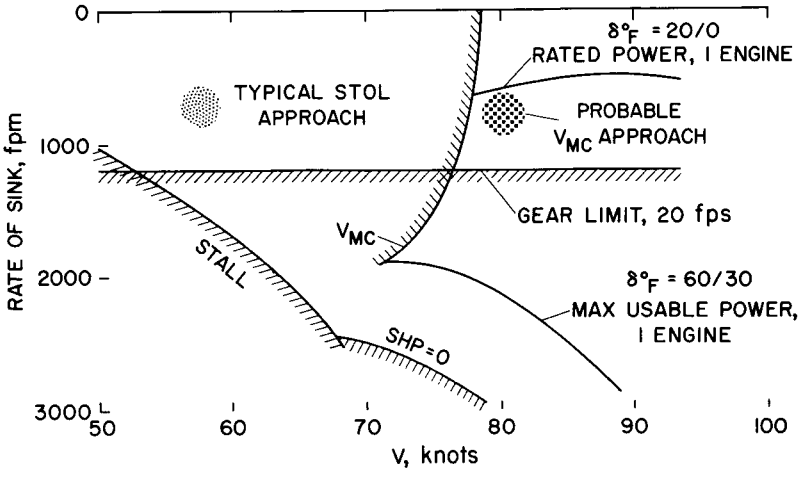

Figure 5

COMPARISON OF LANDING PERFORMANCE

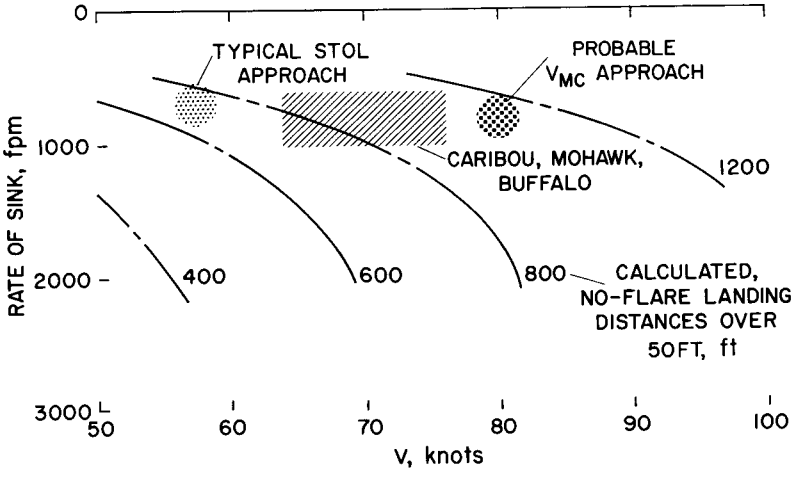

Figure 6

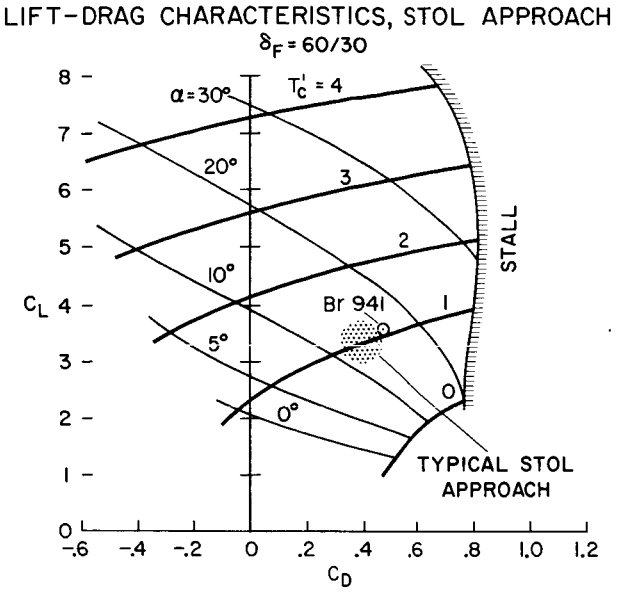

Figure 7

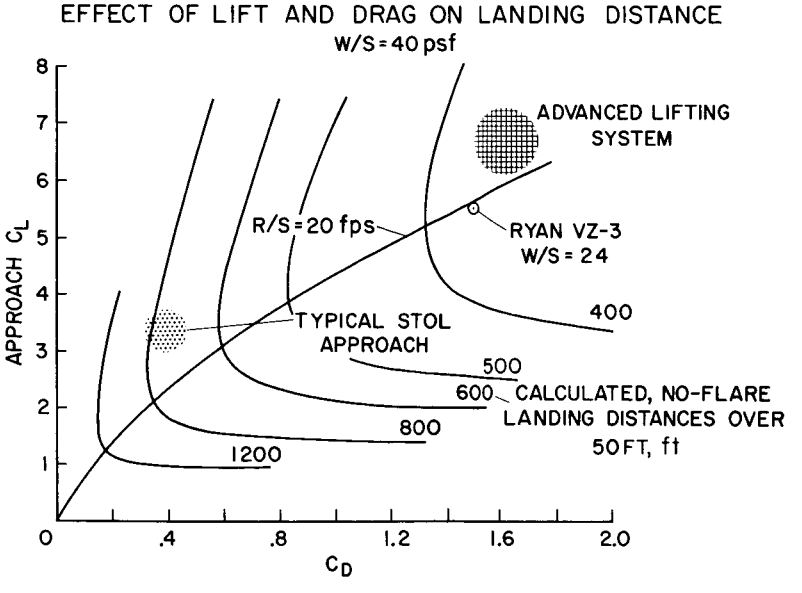

Figure 8

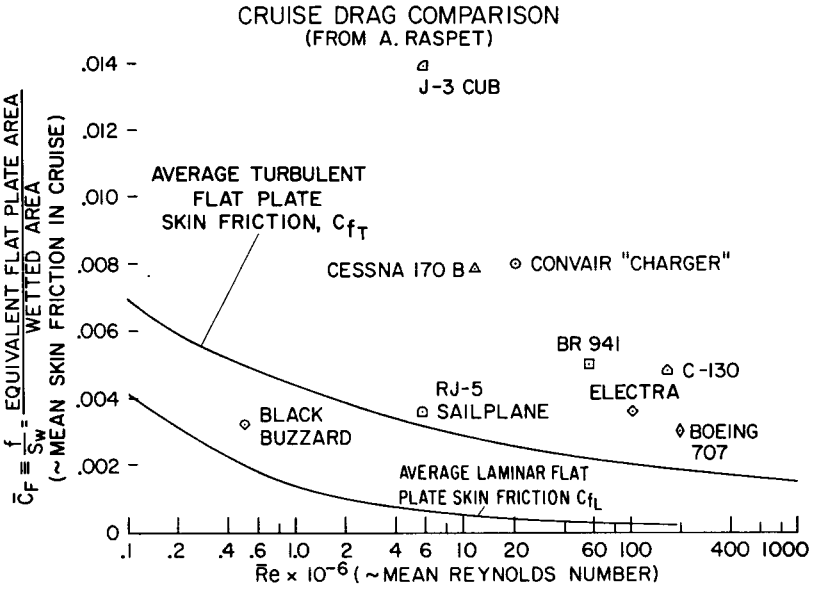
CRUISE DRAG COMPARISON
(FROM A. RASPET)
J-3 CUB
AVERAGE TURBULENT
FLAT PLATE
SKIN FRICTION, C_{f_T}
CESSNA 170 B
CONVAIR "CHARGER"
BR 941
C-130
ELECTRA
RJ-5
SAILPLANE
BLACK
BUZZARD
BOEING
707
AVERAGE LAMINAR FLAT
PLATE SKIN FRICTION C_{f_L}
$\bar{C}_F \equiv \frac{f}{S_w} = \frac{\text{EQUIVALENT FLAT PLATE AREA}}{\text{WETTED AREA}}$
(~MEAN SKIN FRICTION IN CRUISE)
.014
.012
.010
.008
.006
.004
.002
0
.1 .2 .4 .6 1.0 2 4 6 10 20 60 100 400 1000
$\bar{R}e \times 10^{-6}$ (~MEAN REYNOLDS NUMBER)

Figure 9

20. LATERAL-DIRECTIONAL AUGMENTATION CRITERIA FOR JET SWEPT-WING TRANSPORT AIRPLANES OPERATING AT STOL AIRSPEEDS

By Hervey C. Quigley, Richard F. Vomaske,
and Robert C. Innis
Ames Research Center

SUMMARY

A flight and simulator study of the lateral-directional characteristics of a typical swept-wing jet transport operating at landing approach speeds between 80 and 90 knots has shown the need for augmentation to achieve satisfactory handling qualities. Primary considerations must be given to the yaw axis, to increasing the Dutch-roll damping, and to improving turn coordination. Lateral axis augmentation to reduce the dihedral effect, to increase the roll damping, and to stabilize the spiral mode must also be considered. The control authority required in the augmentation system will depend on the maneuvering required in the landing approach. Flight tests have demonstrated that with proper augmentation, satisfactory handling qualities are possible at a landing approach speed as low as 80 knots.

INTRODUCTION

Flight tests have demonstrated that the application of high lift devices to the swept wings of jet transport airplanes can substantially reduce the landing approach speed and the landing distance of jet transports (refs. 1 and 2). With good handling qualities, the lower speeds mean shorter runway requirements and greater safety. Unfortunately, the handling qualities of airplanes tend to deteriorate as landing speeds are reduced or the size of the airplane is increased (ref. 3). This has been illustrated by the problems that have faced the C-5A program from the beginning. Compared to present day jet transport, the C-5A is not only larger, but must land slower and fly at a higher lift coefficient because of a higher wing loading. The studies of the C-5A airplane and other proposed swept-wing transports have shown that to achieve good handling qualities, stability characteristics will have to be improved artificially with an augmentation system.

This paper will present some of the results of a ground-based simulator and flight study of the handling qualities of a typical swept-wing jet in the landing approach at high lift coefficients and low airspeed. The topics to be discussed are:

1. Effect of reduced landing approach speed on handling qualities;

2. Pilot opinion of changes in lateral-directional characteristics;

3. Augmentation criteria for satisfactory handling qualities.

SYMBOLS

BLC	boundary layer control
g	acceleration of gravity, ft/sec^2
IFR	instrument flight rules
I_{xx}	roll moment of inertia
I_{yy}	yaw moment of inertia
L	$\frac{\text{rolling moment}}{I_{xx}}$, rad/sec^2
L_β	$\frac{\partial L}{\partial \beta}$, 1/sec^2
N	$\frac{\text{yawing moment}}{I_{zz}}$, rad/sec^2
N_p	$\frac{\partial N}{\partial p}$, 1/sec
p	roll rate, rad/sec
T_2	time to double amplitude
$T_{1/2}$	time to half amplitude
V	knots or ft/sec
VFR	visual flight rule
$\frac{\Delta\beta}{\Delta\varphi}$	peak sideslip angle to peak bank angle ratio in turn entries
β	sideslip angle, rad or deg
φ	bank angle, rad or deg
ζ	damping ratio
ω_d	Dutch-roll frequency

TESTS

The Boeing 367-80 prototype jet transport shown in figure 1 was used as the test airplane, and its characteristics were programmed on the simulator as the basic configuration. The airplane is a highly modified version of a present day swept-wing jet. It has a powered-lift boundary-layer-control system with highly deflected trailing-edge flaps, a fixed slat on the wing leading edge, and an inverted slat on the leading edge of the enlarged horizontal-tail surface. These high-lift devices enable the airplane to make approaches at speeds as low as 80 knots. (See refs. 1 and 2 for more detailed description of airplane and equipment.) The airplane as flown in these tests had a fully powered irreversible control system with force bungees for all three axes. The augmentation system drove the rudder and aileron without feedback to the pilot in response to multiple inputs which had variable gains.

The study consisted of pilot evaluations of parameters over a wide range on the Ames three-degree-of-motion transport simulator followed by a flight evaluation of a few selected conditions. The pilot's evaluation task both on the simulator and in flight consisted of a series of maneuvers at altitude to evaluate control and response characteristics followed by VFR and IFR landing approaches with 200-foot lateral offsets.

RESULTS AND DISCUSSION

Effect of Approach Speed on Handling Qualities

As a background to the low-speed study, the effect on handling qualities of reducing the approach speed of the test airplane was determined from data from previous flight tests. The pilot opinion of the general lateral-directional and longitudinal handling qualities is shown in figure 2. The data show the variation of the pilot rating, as defined by the Cooper Rating system (ref. 4), with landing approach speed between 80 and 140 knots. The flap deflection and BLC conditions were not constant over the speed range, but were set to give a reasonable angle of attack at the approach speed being flown. For approach speeds of present day jets, that is, above 130 knots, the longitudinal characteristics are good and still acceptable (pilot rating of 4) at the low approach speed of 80 knots. The lateral-directional characteristics, on the other hand, are only acceptable at the higher speed and become unsafe for IFR operation (i.e., pilot rating greater than 6-1/2) at the low approach speed. This study concentrated, therefore, on what was required to improve the lateral-directional characteristics. Further research is required for determining a method of improving the longitudinal characteristics at low airspeed.

To determine the reasons for the poor handling qualities at low speed, the control characteristics were examined first. The variation of available control power with approach speed is shown in figure 3 for all three axes of the airplane. Longitudinal and directional control power decreases

proportionately to dynamic pressure as airspeed is reduced. The lateral control, which is a combination aileron and spoiler system, decreases at the higher approach speeds as speed is reduced, but when flap deflection is increased and BLC applied at the lower airspeeds, the spoilers become more effective and the control power increases. The pilots considered the control power about all three axes adequate for normal maneuvering and for the evaluation task. The directional control power at the low airspeeds was too low for engine-out operation. Operation below minimum control speed was necessary, but this problem was disregarded by the pilot when rating any of the characteristics in this study.

The lateral and directional damping characteristics were examined next. The variation of roll time constant and Dutch-roll damping ratio with approach speed is shown on figure 4. The roll damping is low (time constant greater than 1.0) at airspeeds less than 100 knots. The Dutch-roll damping, which is low (damping ratio less than 0.1) even at the higher speeds, becomes negative below 110 knots. The divergent Dutch-roll oscillation at low airspeeds results from the high dihedral effect of swept wings operating at high lift coefficients and from their low yaw-rate damping. It is obvious that damping is one of the chief reasons for poor handling qualities at low airspeed.

Figure 5 shows the variations with airspeed of the directional stability (in terms of the Dutch-roll frequency) and of the ratio of sideslip to bank angle (in rudder-fixed turn entries). These characteristics are related to what pilots call turn coordination. Poor turn coordination will always accompany low stability because high sideslip angle must be generated in rudder-fixed turn entries. Sideslip to bank angle ratio $\Delta\beta/\Delta\varphi$ is a measure of turn coordination. The test airplane at 80 knots, for example, had a $\Delta\beta/\Delta\varphi$ of about 0.8, that is, for a rudder-fixed bank turn of 10° a peak sideslip of 8° would develop. References 3 and 5 have shown that when $\Delta\beta/\Delta\varphi$ is above 0.3, turn coordination will become a problem.

The analysis of the effect of approach speed on handling qualities has shown two of the characteristics that are responsible for the deterioration of handling qualities with decreasing airspeed. They are low damping and poor turn coordination. The study was, therefore, directed at obtaining good handling qualities by augmenting these characteristics at airspeeds between 80 and 90 knots.

Yaw Axis Augmentation Considerations

Damping.- Figure 6 shows the influence on pilot rating of the Dutch-roll damping parameter $\zeta\omega_d$, that is, Dutch-roll damping ratio times Dutch-roll frequency. The parameter $\zeta\omega_d$ is inversely proportional to time to halve or to double the amplitude of the Dutch-roll oscillation. These data are for the airplane with satisfactory turn coordination and for a range of directional stabilities with ω_d between 0.52 and 1.05. The range shown by the shaded area is the scatter in the pilot opinion data due to the different frequencies. The low stability points were usually rated near the top of the shaded area and the higher stability, near the bottom of the shaded area. Sideslip rate

damping, commonly known as $\dot{\beta}$ damping, was used to increase the damping. The advantages of $\dot{\beta}$ damping are discussed in reference 3. These data show a large improvement (lower number) in pilot rating as damping is increased. The minimum damping parameter for a satisfactory rating was $\zeta\omega_n$ of about 0.1; a value of the parameter between 0.3 and 0.4 had more favorable pilot rating. Based on these results, a damping value of $\zeta\omega_d = 0.09$ was used during the other parameter variation studies. This level of damping was satisfactory, but not large enough to overshadow the effects of other parameter changes.

Turn coordination.- As was pointed out earlier, the turn coordination characteristics of the airplane were unacceptable. Figure 7 shows the effect of two of the parameters that have a strong influence on the turn entry characteristics. The variation of sideslip to bank-angle ratio, $\Delta\beta/\Delta\varphi$, with yawing moment due to roll rate, N_p, is shown for three values of directional stability (in terms of ω_d). For the test airplane the adverse yaw due to aileron and spoiler deflection was near zero, so N_{δ_a} was not considered a variable in these tests. (See ref. 5 for discussion of the $N_{\delta a}$ effect.) The basic airplane at an approach speed of between 80 to 90 knots has an ω_d between 0.78 and 0.52 with an N_p of between a negative 0.2 and negative 0.1, resulting in an $\Delta\beta/\Delta\varphi$ of about 0.8. A value of between 0.2 and 0.3 is desirable. The data indicate two methods of improving turn coordination: (1) increasing the directional stability ω_d, or (2) increasing N_p, the yawing moments due to roll rate - preferably both. Theory (ref. 3) shows that to achieve minimum sideslip in turn entries, N_p must equal the acceleration of gravity divided by the velocity, g/V. At N_p equal to g/V, the value of $\Delta\beta/\Delta\varphi$ is a minimum and is the ratio of steady sideslip to steady-state bank angle in a rudder-fixed steady turn. The value of steady-state $\Delta\beta/\Delta\varphi$ in a turn is a function of the directional stability and yaw-rate damping. At an N_p greater than g/V there is a small negative $\Delta\beta/\Delta\varphi$, which causes some problems and will be discussed later.

The variation of the pilot rating of the lateral-directional characteristics with N_p for three Dutch-roll frequencies is presented in figure 8. The curves in figures 7 and 8 have similar shapes except that figure 8 is extended to high positive values of N_p where pilot rating shows a rapid deterioration because of the pilot's tendency to induce a lateral-directional oscillation when $\Delta\beta/\Delta\varphi$ is negative and the Dutch-roll damping is low. Reasons for the pilot-induced oscillation are discussed in reference 6. This occurs, fortunately, at values of N_p above what is optimum for turn coordination. Although turn coordination can be improved by changing either N_p or ω_d, flight experience has shown that N_p is the most effective and easiest to mechanize.

The ratio of sideslip to bank angle appears to be a good parameter to consider for a handling quality criterion. It is difficult to calculate without the aid of a computer, but easy to measure in flight (see ref. 3). Figure 9 shows the variation of pilot rating with the sideslip to bank-angle ratio. The shaded area reflects the variation due to different values of directional stability and normal scatter of the pilot rating. Near $\Delta\beta/\Delta\varphi = 0$, a discontinuity exists because $\Delta\beta$ is determined by the sideslip in a steady-state turn. These data show that a $\Delta\beta/\Delta\varphi$ of less than 0.3 is required for a satisfactory pilot rating. The requirement for $\Delta\beta/\Delta\varphi$ to be less than 0.3 for a satisfactory rating agrees with the results of a similar investigation with the same

airplane at 135 knots approach speed (ref. 5). The shaded area to the left of zero is rated as poor because of the tendency for pilot-induced oscillation discussed earlier.

Lateral Axis Augmentation Considerations

Dihedral effect.- All of the preceding data discussed have been for an airplane with the inherently high dihedral effects ($L_\beta = -1.03$) of swept wings at high lift coefficients. To determine the effect of dihedral on the results obtained, the study included the effect of dihedral. Figure 10 shows the variation of pilot rating with dihedral effects, $-L_\beta$, for two values of N_p and for three values of direction stability, ω_d. When N_p is zero and the stability is low (ω_d less than 1) the pilot rating improves when $-L_\beta$ is reduced to near zero, but for $N_p = 0.24$, which is near optimum for turn coordination, little effect of dihedral is evident. These results indicate that the pilot is not as critical of the sideslip, which will develop when $N_p = 0$ if the airplane is not also disturbed in roll because of high $-L_\beta$. When $N_p = 0.24$, little sideslip will accompany maneuvering and, therefore, the dihedral effect will be of little consequence to the pilot. In mild turbulence at STOL airspeeds, reduced dihedral effect is preferable because of the high sideslip angles due to gusts encountered at low speed. For a satisfactory rating, augmentation to reduce the dihedral effects will not be necessary if the airplane has good turn coordination and damping.

Roll damping.- Another way in which lateral augmentation can improve the handling qualities is by increasing roll damping. Roll damping was low at an approach speed of about 90 knots, but if the other characteristics were good, the low roll damping was not too objectionable. An increase in roll damping from a time constant of 1.0 to 0.6 improved the pilot rating only about half a rating point for an airplane with good turn characteristics and damping. Reference 7 shows roll time constants above 1.3 are unsatisfactory and will require augmentation.

Spiral stability.- The study pointed out that pilots are particularly sensitive to lateral spiral stability characteristics. Figure 11 shows the pilot rating variation with spiral stability in terms of the reciprocal of the time to half amplitude for a stable condition and in terms of the reciprocal of the time to double amplitude for an unstable or divergent condition. Spiral divergence that exceeds doubling the bank-angle amplitude in a control fixed turn in less than 15 seconds ($1/T_2 = 0.067$) will result in an unsatisfactory pilot rating. A slightly stable condition ($T/(1/2) \doteq 20$ sec) was considered optimum (minimum pilot rating), but a condition with high spiral stability was objectionable because of the necessity of holding lateral control in a steady turn. The inherent spiral stability of the test airplane was within these limits. Spiral augmentation was required, however, when the dihedral effect was reduced to near zero.

Improvements With Augmentation

Figure 12 shows the improvements in handling qualities that were realized with augmentation of the test airplane in this investigation. The data show the pilot opinion of the lateral-directional handling qualities of the unaugmented and the augmented airplane. The basic or unaugmented values are the same as were presented at the beginning of the paper. The airplane with only a yaw axis augmentation system, that is, $\dot{\beta}$ damping and turn coordination, was rated satisfactory with a pilot rating of 3 to 3-1/2. With lateral axis augmentation to reduce dihedral and stabilize the spiral mode, a pilot rating of 2-1/2 was possible.

Control Authority Required for Augmentation

Any of the characteristics discussed can be achieved artificially with an augmentation system. The system itself will not be discussed, but a brief discussion on the control authority required seems pertinent. Since lateral control requirements are high for STOL flight, there should be no problem in providing the required rolling moments for lateral augmentation, such as roll damping or spiral stability. A lateral augmentation system with an authority of less than 25 percent of maximum lateral control could provide any of the lateral characteristics discussed.

The rudder authority required for directional augmentation, on the other hand, was high. Figure 13 shows the rudder required for yaw due to rolling or N_p augmentation for turn coordination. The yaw angular acceleration variation with roll rate for four values of N_p is shown as the solid diagonal lines. The values shown are for an optimum N_p of 0.24, a lower value of $N_p = 0.1$, which will be sufficient for a satisfactory pilot rating, and zero and basic N_p. The dashed lines are the yaw acceleration available with rudder deflections with roll rate for 10°, 20°, and 30° rudder authority in the augmenter. The line of zero rudder authority is therefore identical to the line for basic $N_p (N_p = -0.2)$. An augmenter designed for optimum turn coordination would have to provide an N_p of 0.24 and a rudder authority from 25° to 30° (maximum rudder for the test airplane was 25°) for the peak roll rate of 7° to 10° per second that was normally used in the evaluation maneuvers. Going to a satisfactory level of N_p equal to 0.1 and a rudder authority of only 10°, which was the limit of rudder authority in the test airplane, proved to be sufficient for a satisfactory rating when the dihedral effect was reduced and spiral mode stabilized. In this case the N_p would be equal to 0.1 up to a roll rate of 4° per second where the rudder would be the limiting factor. At higher values of roll rate, the effective N_p would reduce to a value where the lines of constant N_p cross the lines of constant rudder deflection. For example, at a roll rate of about 7° per second the effective N_p has dropped to zero for 10° of rudder authority. The resultant nonlinearity was considered acceptable by the pilot for the evaluation maneuvers. The maximum rudder authority required for augmentation will depend, therefore, on the maneuvering required in the landing approach. The rudder deflection required to augment the damping is low compared to that for turn coordination augmentation.

CONCLUDING REMARKS

In summary, reducing the landing approach speed of a typical jet transport airplane causes the handling qualities to deteriorate unless proper augmentation is provided. Both yaw axis and lateral axis augmentation must be considered if handling qualities are to be satisfactory. Primary consideration must be given to the yaw axis first, to damp the Dutch-roll to a satisfactory level, and second, to improve turn coordination by eliminating the large sideslip excursions that develop with low stability and adverse yaw due to roll rate inherent at low airspeeds.

Secondary consideration must be given the lateral axis augmentation to increase roll-rate damping, to reduce dihedral effect, and to stabilize the roll spiral mode.

Augmentation will of necessity complicate a jet transport airplane and make it more costly, but good handling qualities will increase the utility by decreasing the limitation on the operation of the airplane at its minimum approach speed. Good handling qualities will increase the safety in the landing approach by giving the pilot an airplane that is not only easier to fly, but one he likes to fly in the STOL mode.

REFERENCES

1. Schade, Robert O.; and Crane, Harold L.: Low-Speed Flight Characteristics of a Powered-Lift Jet Transport During Landing Approach. Presented at NASA Conference on Aircraft Operating Problems, Langley Research Center, May 10-12, 1965. NASA SP-83, 1965.

2. Gratzer, L. B.; and O'Donnell, T. J.: The Development of a BLC High-Lift System for High Speed Airplanes. Presented at the Transport Aircraft Design and Operations Meeting of the AIAA, Aug. 10-12, 1964 (AIAA Paper no. 64-589).

3. Anderson, S. B.; Quigley, H. C.; and Innis, R. C.: Stability and Control Considerations for STOL Aircraft. Presented at CASI/AIAA Low-Speed Flight Meeting, Montreal, Canada, Oct. 18-19, 1965 (AIAA Paper no. 65-715).

4. Cooper, George E.: Understanding and Interpreting Pilot Opinion. Aero. Eng. Rev., vol. 16, no. 3, March 1957, pp. 47-51, 56.

5. McNeill, Walter E.; and Innis, Robert C.: The Effect of Yaw Coupling in Turning Maneuvers of Large Transport Aircraft. Presented at NASA Conference on Aircraft Operating Problems, Langley Research Center, May 10-12, 1965. NASA SP-83, 1965.

6. Stapleford, Robert W.; Johnson, Donald E.; Teper, Gary L.; and Weir, David H.: Development of Satisfactory Lateral-Directional Handling Qualities in the Landing Approach. NASA CR-239, 1965.

TEST AIRPLANE

Figure 1 A-33973-1

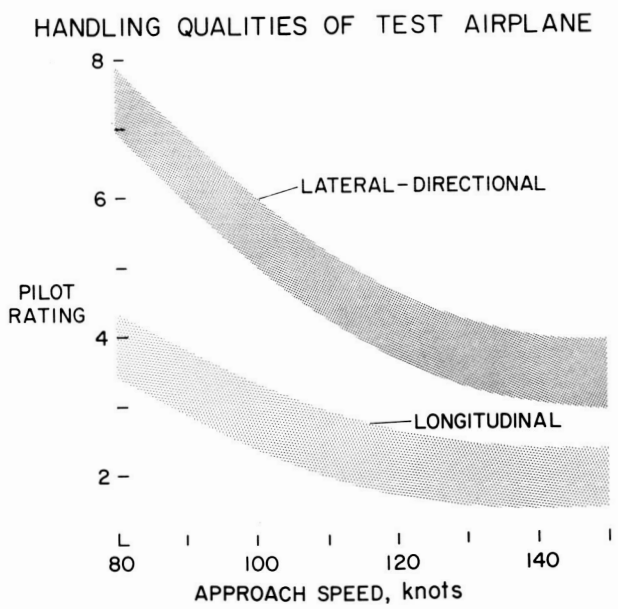

Figure 2

CONTROL POWER

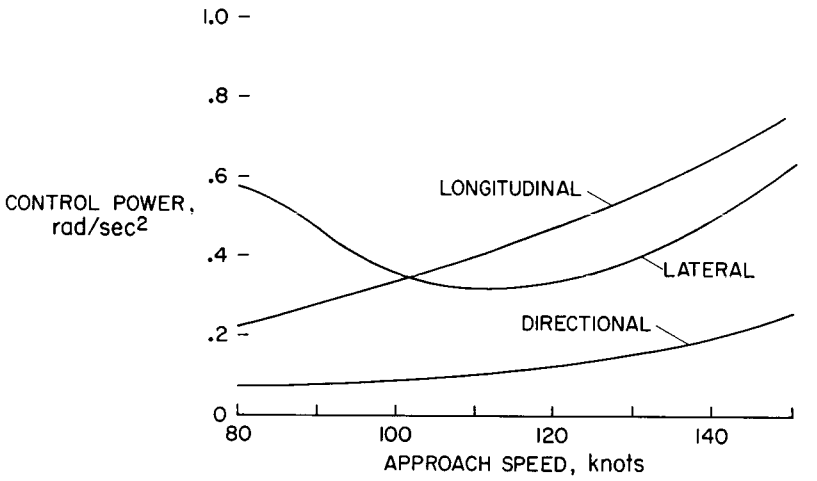

Figure 3

LATERAL-DIRECTIONAL DAMPING

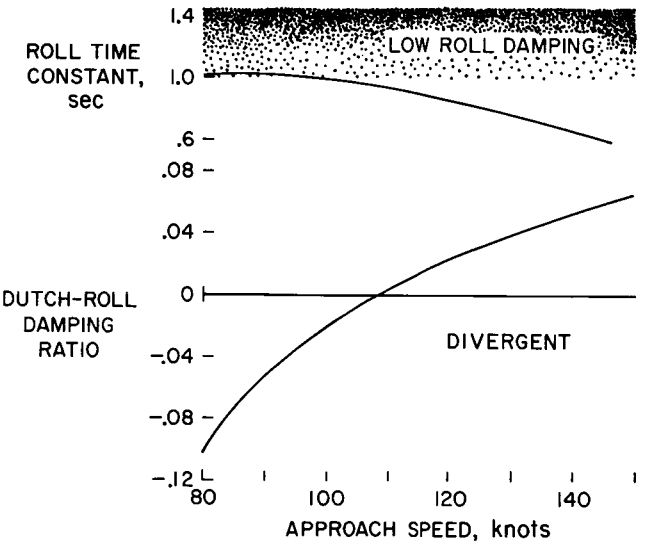

Figure 4

DIRECTIONAL STABILITY AND TURN ENTRY CHARACTERISTICS

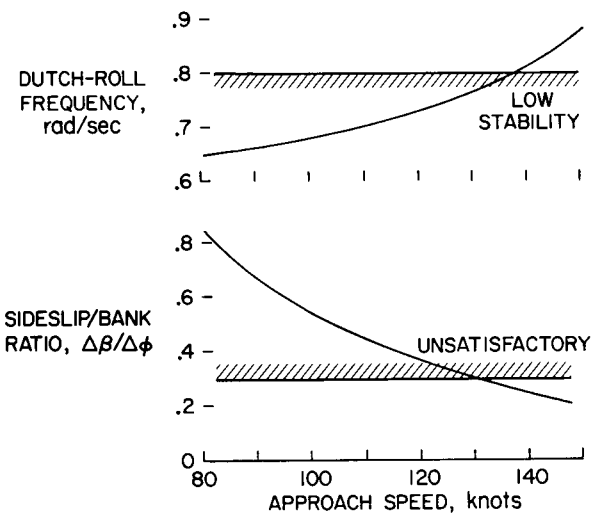

Figure 5

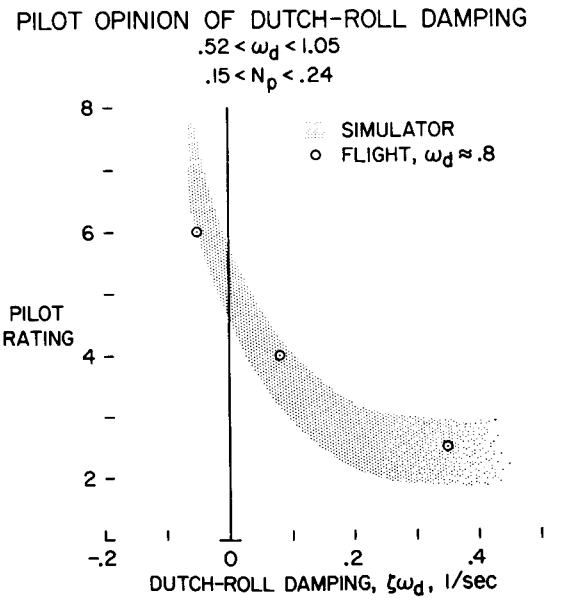

Figure 6

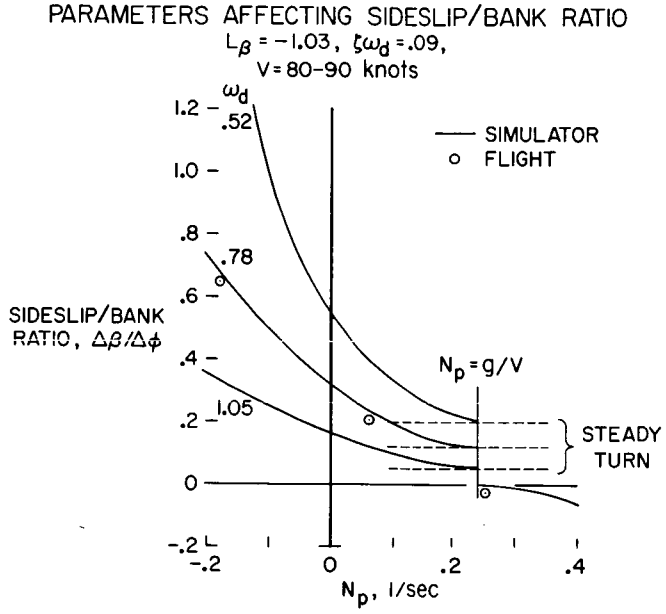

Figure 7

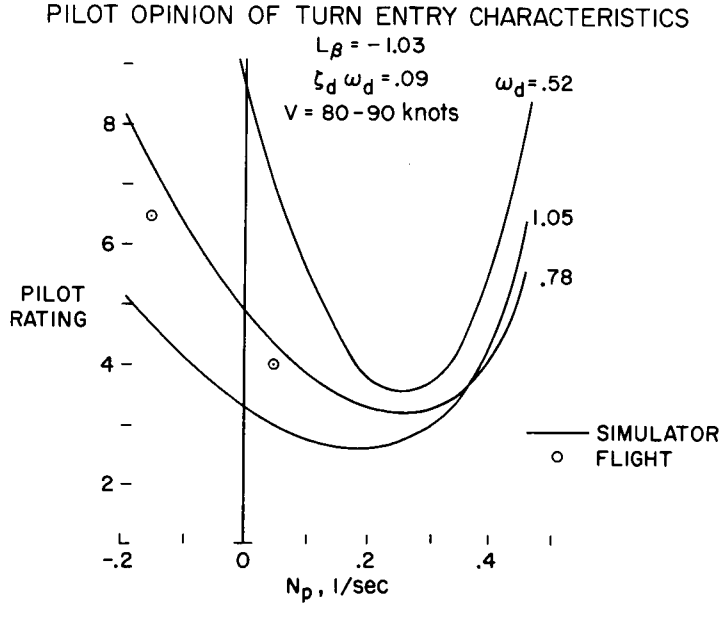

Figure 8

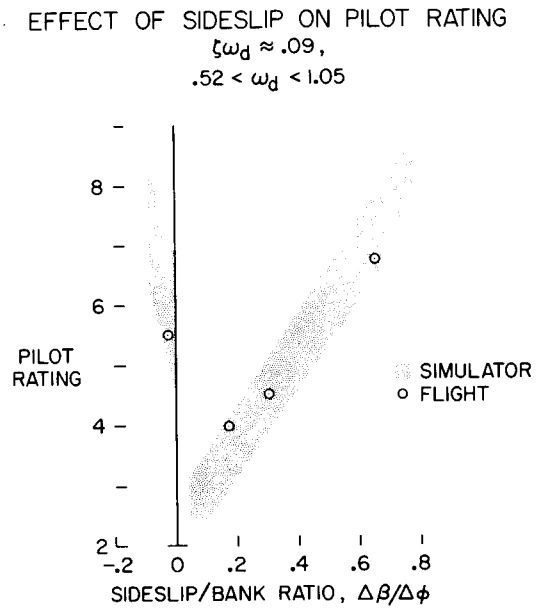

Figure 9

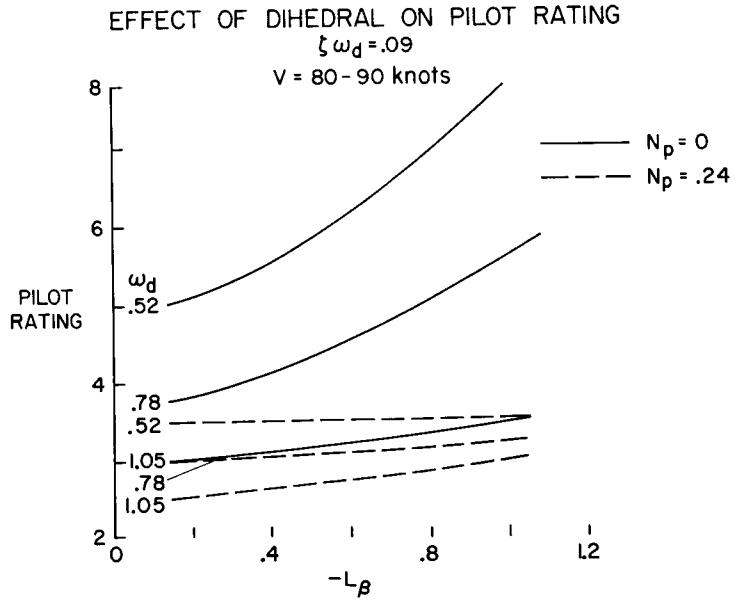

Figure 10

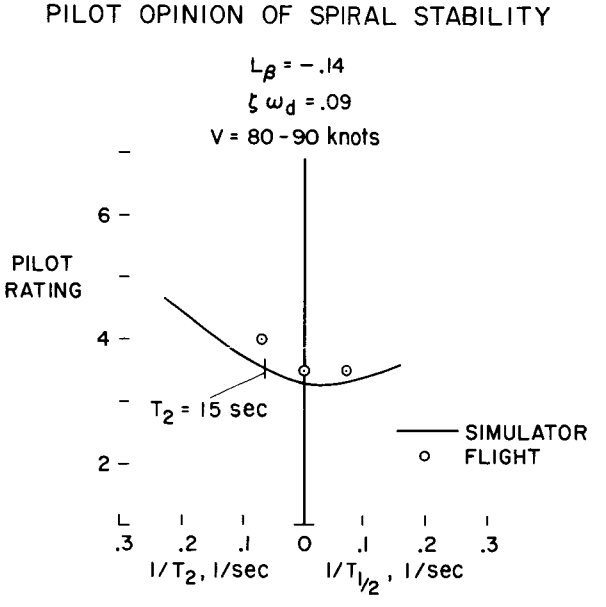

Figure 11

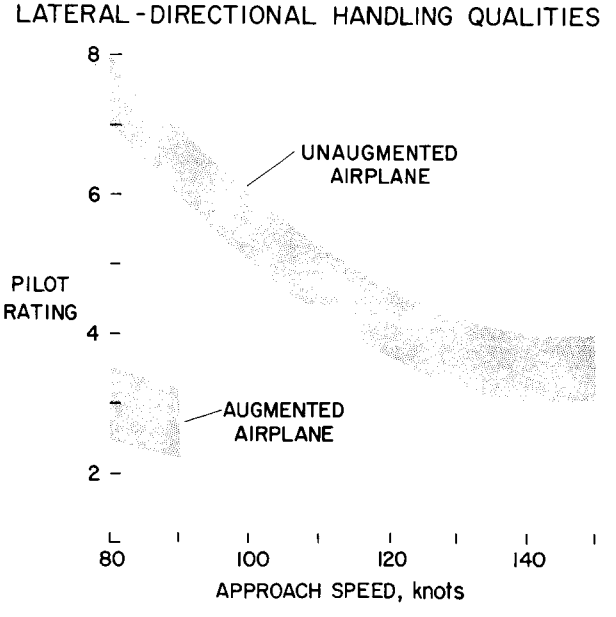

Figure 12

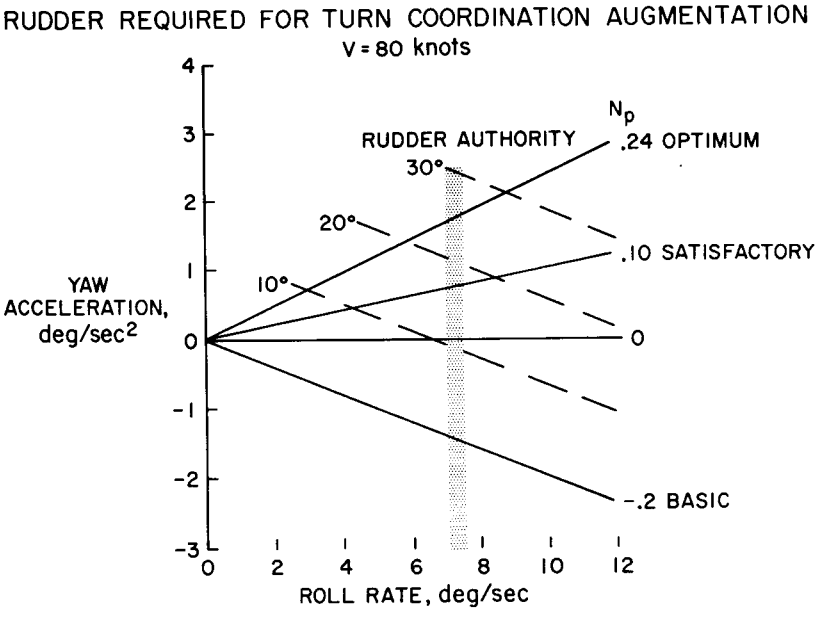
RUDDER REQUIRED FOR TURN COORDINATION AUGMENTATION
V = 80 knots
YAW ACCELERATION, deg/sec²
ROLL RATE, deg/sec
RUDDER AUTHORITY
Np
.24 OPTIMUM
.10 SATISFACTORY
0
-.2 BASIC
30°
20°
10°
4
3
2
1
0
-1
-2
-3
0
2
4
6
8
10
12

Figure 13

SESSION III - V/STOL CONFERENCE

Remarks by Session Chairman - Wallace H. Deckert

Last year NASA awarded contracts to the Boeing Company, Ling-Temco-Vought, and Lockheed Aircraft Corporation to study the feasibility of V/STOL concepts for short-haul transport aircraft. The agenda for this session consists of presentations, by the contractors, which summarize study results.

The studies are scheduled to be completed in the next few weeks. Since a large body of information must be summarized in a short period of time, and since the studies have not been completed, the contractors' presentations can best be described as previews of the final reports. The final reports will be made available to the aeronautical community.

The purpose of the study is to determine which of the V/STOL concepts are the most promising for development into successful commercial short-haul transports and to indicate the research that is required to develop the most promising V/STOL concepts into useful aircraft. It should be noted that the most promising concepts - not concept - are to be determined. It is not expected that, at the conclusion of this study, this complex subject will have converged to the one most promising concept. Because of the complexity of the subject, the opinions of three contractors were solicited. The results of this study are of interest to NASA primarily as guidelines for orienting future research.

The scope of the study is limited primarily to aircraft design as opposed to a study of the total transportation system. For example, economic aspects are limited in this study solely to the determination of aircraft direct operating costs. The technical and economic aspects of V/STOL transportation systems are being evaluated by others, particularly the Federal Aviation Agency.

Both NASA and the contractors participated in the selection of the concepts to be studied. The contractors were required to study certain concepts. However, each contractor was asked to recommend any additional concepts that were considered to be appropriate. The concepts to be studied by each contractor were then determined by negotiation. It should be noted that the contractors were required to study certain basic concepts - not specific configurations. For example, study of the tilt-wing concept was required, but the entire design approach was to be determined by the contractor.

Design criteria for this study are shown in figure 1. The aircraft were required to meet the 500 statute mile range requirement while operating at minimum, or near minimum, direct operating cost. Thus cruise speed and cruise altitude were not specified. Reserve fuel was specified as the fuel required for a 30 minute hold at 5000 feet standard day altitude with holding airspeed for (or near) maximum endurance plus the fuel required to complete a go-around due to an aborted landing.

The basic payload requirement for all designs was 60 passengers. Some configurations are also being sized for 90 and 120 passenger payloads.

Payload was based on 200 pounds per passenger (including baggage) plus a revenue cargo payload of 10 percent of the passenger payload.

For the takeoff and landing criteria that were specified, field lengths for the STOL aircraft correspond to approach speeds of about 55 knots and 85 knots for field lengths of 1000 and 2000 feet, respectively.

Propulsion systems were to be selected on the basis that the system could be (not will be) commercially available by 1970. Revised versions of presently designed engines were permitted.

The thrust/weight ratio requirements presented in figure 1 were for a trimmed aircraft on a sea level 86° F day. An engine emergency contingency rating, based on increasing normal takeoff gas generator power by 10 percent, was permitted.

The basic control requirements for 60 passenger aircraft are shown in figure 1. For 90 and 120 passenger aircraft, the control requirements were reduced to 90 and 80 percent of the values shown. Since control requirements are not well-defined, particularly for VTOL aircraft, the study includes design of some 60 passenger VTOL aircraft to one-half of the basic control values shown in figure 1.

The contractors will use three abbreviations to classify the various short-haul aircraft, namely, VTOL, V/STOL, and STOL. V/STOL is often used in a broad sense, but when used to describe a particular design, V/STOL has a specific meaning. VTOL, V/STOL, and STOL aircraft were all sized for a 500 mile range, but V/STOL aircraft must operate as a STOL to meet the 500 mile range requirement. When operated as a VTOL, the V/STOL aircraft have a range of 50 miles at maximum payload.

DESIGN CRITERIA FOR V/STOL STUDY

- RANGE · · · · · · · · 500 STATUTE MILES
- PAYLOAD · · · · · · · · 60, 90, AND 120 PASSENGERS
- FIELD LENGTH · · · · · · · · · VTOL — AS REQUIRED
  STOL — 1000 AND 2000 ft
- PROPULSION SYSTEM · · · · · · · · AVAILABLE BY 1970
- T/W REQUIREMENTS FOR VTOL AIRCRAFT
  T/W = 1.15 (ALL ENGINES)
  T/W = 1.05 (CRITICAL ENGINE INOPERATIVE)
- CONTROL REQUIREMENTS FOR 60 PASSENGER AIRCRAFT

	VTOL	STOL
PITCH	.60 rad/sec^2	.40 rad/sec^2
ROLL	1.20	.45
YAW	.50	.20

Figure 1

Page intentionally left blank

21a. REVIEW AND EVALUATION OF BOEING DESIGNS FOR THE NASA SHORT-HAUL COMMERCIAL TRANSPORT STUDY

By Bernard L. Fry
The Boeing Company

CONFIGURATION ANALYSIS

24627

The scope of this paper does not permit detailed discussion of all the design tradeoffs. Therefore, the concepts and some typical design tradeoffs are discussed briefly. The dimensions, areas, engine sizes, and similar general characteristics of the aircraft are given in table I, and weight summaries are compared in table II. The mission profile is shown in figure 1.

Author

Tilt Wing VTOL

The tilt wing aircraft shown in figure 2 has four engines and four propellers interconnected in the usual manner. Pitch control in hover is provided by monocyclic (single-axis cyclic control) propellers, yaw control by a spoiler-deflector system, and roll control by differential collective propeller blade angle. Therefore, the complete vertical takeoff system is contained within the wing; there is no tail rotor, no tail shafting, and no aft gear box.

Control.- Since the losses in vertical lift capability due to control application are small, the critical hover criteron is that which stipulates a T/W of 1.05 trimmed with one engine failed. These losses are shown in figure 3; the required amounts of control at a T/W = 1 (50 percent roll, 20 percent yaw, and 20 percent pitch) produce a total lift loss of 2.7 percent.

The desired angular accelerations in roll and yaw, roll by differential collective pitch and yaw by a spoiler-deflector system, are provided without penalties. The spoiler-deflector system has advantages over a differential flap system in that there is no loss of control power in ground effect, and, since no upward flap travel is needed, the flap design can be optimized for transition performance.

In pitch, the required rather than the desired angular acceleration is provided because it is near the limit of control which can be obtained with monocyclic pitch control on a large four-propeller aircraft. The limit is set by the maximum thrust offset, of the order 0.25 propeller radius. (Much larger amounts of control are available for two-propeller of lower gross-weight machines because they have a more favorable relationship between propeller diameter and pitch inertia.) However, current investigation of additional longitudinal control capability, obtained by linking wing tilt and flap deflection to the stick, shows that the desired value of initial pitch acceleration can be obtained, as well as any desired level of longitudinal acceleration control.

Propulsion.- The propeller size chosen for this aircraft results from the upper and lower limits of propeller diameter being close together. The lower limit of 21 feet is given by a combination of the low tip speed (850 fps) desired from the noise standpoint, the maximum blade lift coefficient required for adequate monocyclic control margins, and the maximum blade solidity desirable for propeller efficiency in hover and reasonable monocyclic control load. The 21-foot diameter is close to the upper limit for which propeller clearance can be provided in a wing-down emergency landing without compromising landing-gear design. Provision of such clearance is obviously desirable, though by no means mandatory. For one thing, it simplifies ground handling during maintenance and overhaul. Even more important, the high wing loading which stems from the use of minimum-diameter propellers gives minimum gust sensitivity and maximum cruise performance.

Wing design.- The wing is sized to provide the same relationship between propeller disk and wing areas which were found necessary for good transition aerodynamic characteristics in Vertol Division's wind tunnel tests of other tilt wing configurations. This relationship is based on area with flaps extended. The area has been provided in chord and the wing does not extend spanwise beyond the outboard nacelle. This was done to increase span loading and thus improve the aircraft's gust sensitivity. Gust sensitivity is important for short stage lengths, when the aircraft will cruise at low altitude and high equivalent airspeed.

Tilting the thrust axis upward relative to the wing chord at intermediate wing angles can alleviate transition flow-separation problems and thus free the wing area from its dependency on propeller size. This promising feature is currently under investigation, but it was not sufficiently defined at the beginning of the study to be included in this design.

Performance.- The results of design cruise speed and altitude studies are presented in figures 4 and 5. Low cruise altitudes give low block times because they reduce climb and descent time, but they increase the fuel requirements and, therefore, the size and cost of the aircraft. The effect of altitude on these parameters and the resulting direct operating costs are given in figure 4, which shows a smaller aircraft with a high cruise altitude and higher block time is preferable. There is a similar tradeoff with design cruise speed. Here, the low propeller efficiencies at high speeds contribute to progressively greater fuel requirements and higher design gross weights. Figure 5 shows that the decrease in block time with increasing cruise speed outweighs the effect of increased aircraft size on direct operating costs, and that the higher design cruise speed is desirable.

Technical risk.- The tilt wing concept has little technical risk, compared with other VTOL concepts. The first tilt wing, the VZ-2, was a somewhat crude research aircraft intended to demonstrate the feasibility of the concept. However, it was eventually used to provide tilt wing experience for a large number of pilots, and it proved easy to fly. The more sophisticated CL-84 and XC-142 aircraft are also successful and their problems are mainly those to which general engineering solutions apply, rather than problems particular to the concept.

R and D required.- The major research and development requirements for the tilt wing configuration presented here are confinded to the monocyclic pitch control system. Full-scale propeller, hub, and control system hardware needs to be developed and tested through the complete transition speed range to provide stress, aerodynamic, and dynamic-load data.

Jet Lift VTOL

The general layout of the aircraft (shown in fig. 6) was chosen so that all hover control is provided by modulation or deflection of engine thrust. No additional control devices are required. The 10 lift engines are mounted in pods at the tips of the swept-forward wing. Therefore, their center of lift is forward of the center of gravity and the four cruise turbofans mounted on the rear fuselage can be used for lift in hover. This layout permits roll control to be obtained via differential lift turbofan thrust, yaw control through differential longitudinal tilting of the lift turbofan nozzles, and pitch control by differential thrust of the forward eight lift engines and the cruise engines. Direct translation control is also possible with the lift turbofan nozzles.

Propulsion.- The tip position for the lift engine pods was chosen in preference to a more inboard location for several reasons. The tip position permits using smaller lift engines, since the increased control arm outweighs the increased roll inertia (see fig. 7). An inboard location would increase interference drag and not give the favorable end-plate effect of the tip pod. The inboard location would also require the pod to be beneath the wing and, since it would also lack some of the favorable effect of wing dihedral on jet-efflux ground clearance, a high wing would have been required to make this clearance adequate. The tip location gives good clearance on a low wing aircraft. Reference 1 indicates that the tip location also avoids unfavorable interactions of propulsion and airframe aerodynamics. The tip pod location increases wing weight approximately 25 percent, but this is offset by the absence of separate hover control devices and the penalties which would be incurred by a high wing and fuselage-mounted landing gear. The low wing is also preferred for ditching and for maintenance accessibility.

The choice of number of lift engines is somewhat subjective. While a large number of engines minimizes engine size, and the effect of an engine out, fewer engines are obviously desirable for reduced maintenance cost. The thrust-to-weight ratio (total lift-engine thrust to gross weight) varies with number of lift engines as follows:

1. Eight engines: 1.24
2. Ten engines: 1.19
3. Twelve engines: 1.17

Ten engines were chosen as a compromise between these factors. While eight does not increase installed thrust to a prohibitive degree, it does result in a very large, high-drag, pod design.

A summary of the thrust modulation required for control is given in table III. The lift-engine bypass ratio of 2.5 was chosen as a compromise

between noise propagation and engine size and weight. The large amount of lift-engine running time dictated by the taxi, takeoff, approach, and landing ground rules favored turbofan engines for low specific fuel consumption.

Wing design.- The wing loading of 115 pounds per square foot was chosen as the maximum permissible if emergency conventional landings were to be feasible. This loading has proved to be compatible with satisfactory transition performance.

Performance.- The jet-lift VTOL is designed to cruise at 30,000 feet for the 500 statute-mile stage length. The cruise Mach number of 0.8 is comparable to that of contemporary short-range jet transports. Higher cruise speeds would demand more highly swept or thinner wings and tail surfaces, with attendant weight penalties. Higher cruise speeds might still improve direct operating costs slightly at the long stage lengths, but they would worsen the operating costs at the short stage lengths, where the cruise speed would be EAS-limited.

Technical risk.- The technical feasibility of the jet-lift concept has been well established by the many aircraft of this type, ranging from the original Rolls Royce Flying Bedstead to the highly successful Hawker P1127, for which production quantities are under procurement.

R and D required.- The airframe is, for the most part, quite straightforward; the required research effort is in the propulsion area. Lift turbofan engines are being developed, but care must be taken to ensure that their thrust response characteristics are adequate for flight control via modulation, and that satisfactory noise suppression is achieved. Research is also required in the aerodynamic interactions between the propulsion system and airframe (e.g., suck down, stability in ground effect, the transition lift, drag and trim), and in design of lift engine intakes when engine spin axis is normal to the free-stream flow.

Stowed Rotor VTOL

Several concepts of stopped or stowed rotor aircraft were considered before selection of the tandem configuration shown in figure 8. Configurations with a folded trailed single rotor, but no rotor fairing (i.e., not stowed), were not examined in detail because of the drag penalty of the exposed trailed rotor. The drag penalty is discussed in reference 2 and illustrated in figure 9. The trailed rotor concept may also have dynamics and handling problems associated with unsupported blades of relatively low stiffness.

Rotor.- Single-rotor shaft-driven and warm cycle gas-driven types were analyzed. It was found that the rotor stowage problem was more severe than that of the tandem configuration since the rotor locations of the latter permitted stowage without retraction of the rotor hub or transmission. The central location of the single rotor dictates the use of hub retraction for stowage, if adequate airframe clearance is maintained when the rotor is deployed. The alternative is a large central hub body into which the blades retract. Both of these solutions impose severe penalties of weight and complexity on single rotor configurations. The bulky, high-torque-loading transmission associated with a

single large-diameter shaft-driven rotor also presents weight and installation problems which are compounded by hub retraction. In addition, a single-rotor aircraft (assuming the blades are rigid) may experience cyclic pitching and rolling moments as the rotor is stopped for conversion; this is not the case with the synchronized rotors of a tandem configuration.

Propulsion.- The tandem configuration presented in figure 8 is powered by four convertible turbofan engines. The thrust of the fans can be modulated at constant power-turbine speed by variable inlet vanes while shaft power is also provided to drive the rotors. During hover and low-speed flight the fans are decoupled. For transition, the fans are engaged to provide propulsive thrust and at the same time shaft power is provided for rotor lift. Conversion to the cruise configuration is accomplished by unloading, decoupling, braking, and stopping the rotors, which are then folded in the trailing position and enclosed by retraction of the doors and fairings on the fuselage and aft pylon. When the fairings are open, they clear the rotor for hover and transition. The droop stops of the rotor blades are centrifugally operated to lock out the flapping hinges when the rotor is stopped for conversion.

Performance.- The wing and its high-lift devices have been designed to permit conversion at 130 knots EAS using a 1.2 V_{stall} criteria. The wing is swept to improve ride qualities, reduce fatigue loadings, and attain correct c.g. location.

Hover control.- Hover control is accomplished in the usual tandem helicopter manner, i.e., differential collective in pitch, collective cyclic for roll, and differential cyclic in yaw. The desired initial angular acceleration values can be provided with negligible power penalties.

Technical risk.- The stowed rotor aircraft is a comparatively recent development and is the only aircraft considered in this study for which there has been no flight research. Some exploratory wind-tunnel tests have been made, but the concept must be considered to have a higher degree of technical risk than the other configurations.

R and D required.- Development of the convertible fan engines is required, although this is largely a matter of integrating proven components. The major problem is, of course, the conversion process. Research must be conducted into the mechanical, dynamic, aerodynamic, and stress problems associated with stowing, stopping and folding the rotor blades, and the reverse process of deploying and spinning up the rotors. Stability during the conversion requires investigation, and the phasing and mixing of the helicopter and conventional flight control systems must be determined. While the size and configuration of the other concepts can be determined with a reasonable degree of confidence, the stowed rotor could change radically as a result of research. For instance, if it were determined that a transition speed higher than that assumed in this study were feasible, the wing size and the flap complexity could be reduced, with a favorable effect on aircraft size and cost.

Lift-Fan VTOL

The lift-fan VTOL aircraft, illustrated in figure 10, uses turbine-driven lift fans of the type developed by General Electric for the XV-5A aircraft. Each of the four fans (bypass ratio 8) is driven by a lightweight gas generator (pressureratio 12) of the lift turbojet type. In hover, the lift of the fans is supplemented by the thrust of the cruise turbofans (bypass ratio 3) which is deflected downward.

Integration of fan location and wing design.- Since the number of fans is small, a satisfactory fan location to permit hover control via thrust modulation or deflection is not possible without extensive cross-ducting to cope with an engine-out situation. The fans have therefore been installed in the wing root with cross ducting in the roll sense only.

The root chord is dictated by the wing thickness required to contain the fans. Therefore, if excessive taper ratio is to be avoided, the lower limit of wing area is dictated by root chord and aspect ratio. The combination of aspect ratio and wing area is dictated by cruise considerations.

Hover control.- Hover control is achieved via nozzles at the aircraft extremities. The nozzles are fed by turbocompressors which are driven by air bled from the ducts that couple the gas generators to the fans. The ducting system from the turbocompressors to the nozzles is arranged to feed each nozzle by two compressors in order to maintain control in the event of an engine failure. Fuel is burned at the nozzles to provide additional thrust when high control powers are demanded. The burner at each nozzle consists of several segments, one of which is continuously lit in hover and transition to serve as a pilot light. High control power demand feeds fuel to the remaining burner segments. The control system is also designed to contribute to the net lift in the engine-out case. The control system is designed to provide the required, rather than the desired, angular accelerations since designing for the higher values would result in a weight penalty of approximately 2 percent of gross weight.

R and D required.- Like the jet lift, the most pressing need for research is in noise suppression of the deflected cruise thrust and lift fans and, in this case, of the bleed and burn control system also. The control turbocompressors and nozzles, lift fans and associated gas generators, and the cruise engine deflector nozzles must also be developed, although most of these items are extensions of existing technology.

Fan-In-Wing STOL

In this STOL configuration, shown in figure 11 and described fully in reference 3, wing lift is supplemented by fans located in the wing and by deflection of cruise engine thrust.

Propulsion.- A combined T/W from both cruise and lift systems of 0.70 is necessary to meet the balanced field length of 2000 feet over a 35-foot obstacle.

The cruise engine size was selected to provide good climb performance as well as the required cruise thrust. These (bypass ratio 3) engines give a net T/W of 0.29 when the thrust is deflected. A lift fan T/W of 0.41 supplies the remaining lift necessary to meet the 0.70 total T/W.

No reaction-control system is required for the STOL airplane. Aileron and rudder power is augmented by applying boundary layer control to these surfaces. Air for this purpose is bled from the lift-fan gas generators.

Lift-fan gas generators are sized to drive the lift fans and to supply the bleed air needed for control surface blowing. They are much smaller than for the VTOL configurations, where they also powered the reaction-control system. This reduction in size and the absence of the control system turbocompressors allows a much smaller engine compartment above the body. No increase in frontal area is necessary to house the gas generators.

Wing design.- The wing design incorporates double slotted flaps at the trailing edge and Krueger flaps and slots at the leading edge.

R and D required.- The items requiring research for this aircraft include handling qualities at STOL speeds, the boundary layer control system on the control surfaces, and the lift fans and associated gas generators.

Turbofan STOL

This aircraft (described more fully in ref. 3) was designed to permit evaluation of a STOL aircraft that does not employ auxiliary vertical-lift devices other than externally blown flaps. The turbofan STOL is shown in figure 12.

High lift and control devices.- The flap system on this aircraft is similar to that which Boeing proposed for the C-5A Heavy Logistic Transport. At the leading edge, a simple Krueger flap is located inboard of the inboard engine. Outboard of the inboard engine to the wing tip, a flexible (drooping) leading edge is employed combined with hinged slats which form part of the lower leading-edge surface in the stowed position.

The trailing-edge flap system consists of two double segmented and double slotted flaps per wing. The aft segment of each flap is movable relative to the main segment. A linkage system regulates motion of the aft segment as a function of the main flap travel and also allows a limited independent aft segment travel. The independent aft segment of the outboard flap also functions as a flaperon to provide supplemental lateral control and trim.

Spoilers are located in the upper surface of the wing aft of the rear spar to augment lateral control and provide aerodynamic braking for both flight and ground operation.

Stability and control studies indicate that blowing of the elevator and ailerons is not necessary, but marginal conditions exist for the rudder.

Wing design.- The wing was sized for a wing loading of 85 psf at takeoff. Wing sweep was limited to 25° to increase the lift at low speeds. A high wing was selected since close proximity of the ground would adversely affect the flap performance.

Propulsion.- Four powerplants were used to cover a large percentage of the flap span with exhaust air and to reduce the yawing moment due to engine failure. The short duct fan engine installation incorporates thrust reversers for both the primary and secondary air. Both deflectors are of the same basic design which incorporates a translating sleeve with integral blocker doors which direct the flow forward through concentric rings of turning vanes. The effective thrust-to-weight ratio of the turbofans on an 86° F day at sea level was limited to 0.41 since it is believed that a higher ratio would result in undesirable pitching moments caused by the flap. The net T/W of 0.41 on a 85° F day corresponds to a gross value at S.L./Std. temperature of 0.47. Center line of thrust is at a small angle with the wing chord. The angle is chosen to give optimum flow conditions over the flap. C-5A experience showed that an angle of 4-1/2° was optimum for both low speed and high speed flight.

R and D required.- The major research requirements for this type of aircraft are confined to ensuring satisfactory stability and control characteristics in the STOL flight regime. The externally blown flap has been investigated in wind-tunnel tests and will be further developed in the C-5A program.

COST COMPARISONS

Acquisition Cost

These costs are summarized in figures 13 and 14. As might be expected, the turbofan STOL is the least expensive aircraft by virtue of its lack of propulsion system complexity, while the fan in wing STOL which has a lifting propulsion system but no VTOL controls, falls between the turbofan STOL and the least costly VTOL, the tilt wing. The latter aircraft's low cost relative to the other VTOL concepts is due not only to its lower gross weight, but also to the low cost per pound of transmissions and rotors compared with engine costs. The latter fact is also responsible for the stowed rotor cost not greatly exceeding the jet lift and lift fan concept costs despite its much higher weight. Although the jet lift propulsion system consists solely of engines, its propulsion cost does not greatly exceed that of the lift fan aircraft because it has only two basic propulsion and VTOL control devices as against five for the lift fan type.

Direct Operating Cost

The direct operating costs of the six aircraft types are given in figure 15 as a function of stage length. The values shown for the two STOL aircraft include the taxi time and approach and landing pattern given in the ground

rules. These rules were not felt to be representative of the operating procedure for VTOL aircraft and therefore, while the rules were adhered to in sizing these aircraft, the direct operating costs are based on zero taxi time and an allowance of 2 minutes for approach and landing and 1 minute for takeoff.

The STOL aircraft have, as would be expected, the lowest direct operating cost at the 500-mile stage length due to their small size and relatively low complexity. This advantage is lost at the lower stage lengths where the higher nonproductive air time begins to have a significant effect. The direct operating cost of the fan-in-wing STOL rises to the same general level as the jet type VTOL aircraft. The jet lift and the lift fan VTOL types suffer in general level because of their high acquisition cost and this is compounded at the low stage lengths by the high propulsion system maintenance cost and hover fuel flow. While the DOC of the stowed rotor does not escalate with reduced stage lengths as much as some of the other types the general level is high because of its poor specific range, high first cost and high airframe maintenance cost. The tilt wing achieves the best overall DOC. It falls between the STOL and jet type VTOL aircraft at the higher stage lengths and has the lowest cost of all the aircraft at short distances. This can be attributed to its relatively modest size and first cost, good specific range, and reasonable fuel flow in hover and transition.

PUBLIC ACCEPTANCE

Noise

This is certainly the overriding factor in the practical application of V/STOL aircraft to short haul intercity transport. The intensity and duration of takeoff and landing noise are most important; sound levels generated in low-altitude flight are secondary. Figure 16 presents comparisons of takeoff noise at a distance of 500 feet from the aircraft, and of ground level noise due to the aircraft flying at 300 knots at 2000 feet. The perceived noise levels given in this figure are conservative since they include the noise total generated in all frequency bands. All of the noise is not necessarily heard simultaneously at any one point.

The noise levels follow the expected pattern with the jet being the highest and the tilt wing fairly low. The rather high noise level of the stowed rotor helicopter is due to the large size of this aircraft and the high blade loading associated with three-bladed rotors operating at 10.7 psf disk loading. These rotor parameters are compromises occasioned by the folding requirement. The jet lift noise level is not as high as one might anticipate from 80,000 lb of jet thrust. However, the lift engines have a bypass ratio of 2.5 and are run in hover at only 70 percent power, due to the high installed thrust to weight ratio required for engine-out control considerations.

Ride Qualities

Since these short haul transports will spend much of their flight time at low altitudes, the gust sensitivity, as it effects passenger comfort, is of greater importance than with long range high flying aircraft. Poor ride qualities could severely affect the economy of the aircraft by forcing flights in turbulent conditions to be made well below the normal cruise speed. The gust sensitivity of the various types is compared in figure 17. The values for the Electra are given for comparative purposes. The tilt wing, which has no higher gust sensitivity than the Electra, is the most sensitive; the jet lift, which was high wing loading and low aspect ratio, is at the opposite end of the scale.

Passenger Appeal

What might be called general passenger appeal has played a part in the development of the commercial airline market. The introduction of jet aircraft met with general enthusiasm from the public, initially because of decreased journey time but, after experiencing jet travel, quietness and smoothness became additional factors in "jet appeal."

In the case of V/STOL aircraft, the convenience of city center to city center travel is the major time saving. By comparison, the differences in block time between the various aircraft over short stage lengths is minor. Therefore passenger appeal will be a matter of comfort dependent on noise, vibration, smoothness of transition, etc. While this section of the paper is intended to compare the concepts, this point is too subjective for meaningful comparison.

MOST PROMISING CONCEPTS

One of the study objectives was to select the three most promising concepts, of which one should be a STOL type, for further investigation of sensitivity of size and cost to required payload, control power, operation over a hypothetical route structure, production quantities, and utilization. This second phase of the study is currently under way. The most promising concepts have been chosen as follows.

Turbofan STOL

This is an obvious choice in view of its small size, relative simplicity, low technical risk, low acquisition cost and low direct operating cost at all but the very short stage lengths.

Tilt Wing VTOL

Of the four VTOL concepts the tilt wing is the smallest and the least costly to acquire and operate. It is also the aircraft with the least noise

problem, particularly if some compromise of size and performance is made by using low tip speeds, as is the case with the tilt wing presented in this paper. The tilt wing has the advantage of a simple conversion process which does not require starting or stopping of engines. It is a proven, well-understood concept with much research and development work behind it.

Lift-Fan VTOL and Jet-Lift VTOL

The choice of a third concept was more difficult. The fan-in-wing STOL was eliminated because its capability is matched by the less complex turbofan STOL for the 2000-foot field length considered in this study. It would, however, be a good configuration for STOL distances below 2000 feet. The stowed rotor does not have competitive direct operating costs and therefore this left the lift-fan and jet-lift VTOL aircraft. There is little difference in weight, acquisition cost, or direct operating cost between these aircraft. Both types have a noise problem and both have low gust sensitivity. It was therefore decided that both types would be included in the second phase of the study.

CONCLUSIONS AND RECOMMENDATIONS

In interpreting the results of a study such as this, it is necessary to consider both the confidence level of the technical inputs and the effect of the ground rules on the results. With the exception of the stowed rotor concept, all of the aircraft have a well defined technical background and the resulting preliminary designs have a fair degree of confidence. The stowed rotor design, which did not show up very well in comparison with the other types, has a relatively low confidence level since there is little background data or research available. The assumed conversion speed may have a considerable effect on aircraft size, and the weight penalties associated with rotor folding and retraction are somewhat nebulous at present. There is an infinite variety of possible approaches to converting a helicopter into a conventional airplane in flight. A significant breakthrough in this area might change the competitive position of this type of aircraft.

The ground rules of this study were not conducive to low direct operating costs, expecially at low stage length. The aircraft were required to be self supporting, have the conveniences associated with current commercial aircraft, carry fuel for conventional approach and landing patterns, and be designed for the not-so-short stage length of 500 statute miles. Despite these requirements, the operating costs are no higher than those of current transport helicopters at 25 miles stage length, and little greater than conventional short haul transports at the higher stage lengths. However, these costs must be reduced if air transport is to compete with surface travel in the short haul intercity market.

Therefore the design requirements must be scrutinized closely. It has become customary for short haul aircraft to be self-supporting. However, these aircraft only require 2 to 3 pounds of thrust for every 10 pounds of weight added. The VTOL requires about 12 pounds. Such items as stairs, auxiliary

power units, and ground air conditioning could be built into landing pads without affecting turnaround time, and VTOL aircraft need not carry galleys, multiple toilets, or deluxe furnishings. Fuel requirements can be tailored for the short approach and landing patterns of which the VTOL is capable, and a go-around fuel reserve is probably not required. VTOL aircraft can make final approach adjustments at very low speeds. Applying this philosophy, the design gross weight of the tilt-wing aircraft in this study could be reduced from 71,704 pounds to 56,500 pounds for the same payload and range, with corresponding reductions in direct operating cost of approximately 20 percent.

It should be remembered that, although this study has shown that from most standpoints the V/STOL is a practical vehicle for commercial short haul transportation, noise reduction is the key to acceptance of these aircraft. Noise reduction is the most important item of required research.

REFERENCES

1. Emslie, K.: Wind Tunnel Tests on Models of V.T.O. Aircraft, AIAA Paper 65-720, 1965.

2. Stephniewski, W.; and Young, M.: Helicopter and Propeller-Type VTOL Aircraft in the Light of Technologies. SAE Paper 65-0193, 1965.

3. Zabinski, J.: Review of Boeing STOL Designs for NASA Short Haul Transport Study. Proceedings of NASA V/STOL Conference, April 1966.

TABLE I.- COMPARISON OF GENERAL CHARACTERISTICS

Item	Tilt Wing VTOL	Jet Lift VTOL	Stowed Rotor VTOL	Lift Fan VTOL	Fan-in-Wing STOL	Turbofan STOL
WEIGHTS						
Design gross weight, lb	71704	80758	94455	79191	65329	62824
Operating weight empty, lb	51704	55568	68447	55309	44410	42310
Weight empty, lb	50254	54098	66997	53859	42960	40924
PHYSICAL DATA						
Fuselage length, ft	79.5	80	79	82.5	78.5	80
Wing loading, psf	91	115	108	75	80	85
Wing area, sq ft	787	712	875	1055	823	749
Wing span, ft	79.5	55	70	58.6	65.4	68
Aspect ratio	8.02	4.25	5.6	3.27	5.2	6.17
1/4-chord sweep, deg	0	-25	29	35	25	25
r/c root ℄, percent	18	17	18	14.5	13.6	13.6
r/c tip, percent	9	11 from 0.3 b/2 to tip	9	9	8.2	9
DESIGN CRUISE CONDITIONS						
Cruise speed, knots	380	466	340	466	472	472
Cruise altitude, ft	30000	30000	25000	30000	30000	30000
STRUCTURAL LIMITS						
V_{MO}, knots EAS	390	400	350	400	400	400
M_{MO}	0.72	0.83	0.65	0.83	0.83	0.83
V_D, knots EAS	425	450	390	450	450	450
N Limit	2.9	2.5	2.5	2.5	2.5	2.5
ROTORS OR PROPELLERS						
Diameter, ft	21.1	--	75	--	--	--
Number of blades	4	--	3	--	--	--
Solidity	0.25	--	0.07	--	--	--
Maximum tip speed, fps	850	--	740	--	--	--
CRUISE POWERPLANTS						
Number	4	4	4	4	2	4
Maximum thrust, lb	--	6950	--	6960	11426	7482
Maximum power, shp	6741	--	7300	--	--	--
Bypass ratio	--	3	6	3	3	3
Pressure ratio	20	16	20	16	20	16
T_4	2600	2600	2600	2600	2600	2600
LIFT POWERPLANTS						
Number	--	10	--	4 gas gen. 4 fans	4 gas gen. 2 fans	--
Maximum thrust, lb	--	9970	--	15983	13775	--
Bypass ratio	--	2.5	--	8 (fans)	8 (fans)	--
Pressure ratio	--	7	--	12 (gen.)	12 (gen.)	--
T_4	--	2360	--	2600	2600	--

TABLE II.- WEIGHT SUMMARY

Item	Tilt Wing VTOL	Jet Lift VTOL	Stowed Rotor VTOL	Lift Fan VTOL	Fan-in-Wing STOL	Turbofan STOL
Rotors	4605	--	9456	--	--	--
Wing	5250	7000	5050	5774	5830	5895
Tail	1937	2023	2300	2557	2120	1765
Body	9620	10450	13002	11890	10510	9990
Alighting gear	2775	3250	3750	3180	2630	2554
Flight controls	4172	1849	3375	2000	2000	2150
Reaction controls	--	--	--	2030	--	--
Power plant instl	(11000)	(18301)	(19054)	(15386)	(8880)	(7673)
Engine and nacelle instl	5340	17801	9454	11456	7240	7273
Drive system	5310	--	9100	--	--	--
Fan instl	--	--	--	3480	1240	--
Fuel system	350	500	500	450	400	400
Auxiliary powerplant	530	530	530	530	530	530
Instrumentation and navig'n	675	770	690	700	710	675
Electrical and hydraulic	2450	2505	2450	2450	2450	2450
Electronics	750	750	750	750	750	750
Furnishings and equip't	5120	5220	5120	5182	5160	5122
Air conditioning and deicing	1370	1450	1470	1430	1390	1370
WEIGHT EMPTY	(50254)	(54098)	(66997)	(53859)	(42960)	(40924)
Crew and crew baggage	520	520	520	520	520	520
Unusable fuel	175	175	175	175	175	175
Engine oil	100	120	100	100	100	100
Passenger service equip't	655	655	655	655	655	655
OPERATING WEIGHT EMPTY	(51704)	(55568)	(68447)	(55309)	(44410)	(42310)
Passengers (60) and luggage	13200	13200	13200	13200	13200	13200
Fuel	6800	11990	12808	10682	7719	7250
TAKEOFF GROSS WEIGHT	(71704)	(80758)	(94455)	(79191)	(65329)	(62824)

TABLE III.- HOVER CONTROL FOR JET-LIFT VTOL

Item	Roll	Pitch	Yaw
Means of control	Differential thrust	Differential thrust	Differential nozzle, longitudinal deflection
Engines used	All lift engines	All cruise engines fwd & lift engines	All lift engines
Control authority per engine . . .	±1500 lb	Cruise engines: ±1785 lb Lift engines: ±800 lb	±8.3°
Maximum angular accelerations (radians / second^2)			
Sea-level standard all engines operating	0.974	0.3	0.25
Sea level, 86° F, T/W = 1 one engine failed, one axis only	0.65	0.3	0.25
Sea level, 86° F, T/W = 1 one engine failed, simultaneous control	0.3 (50% × 0.6)	0.06 (20% × 0.3)	0.25

MISSION GROUND RULES

DISTANCE CREDIT FOR CLIMB
CRUISE AND DESCENT ONLY
CLIMB + DESCENT
< CRUISE DISTANCE

1000 FT. V_{CON} @ A, B AND C

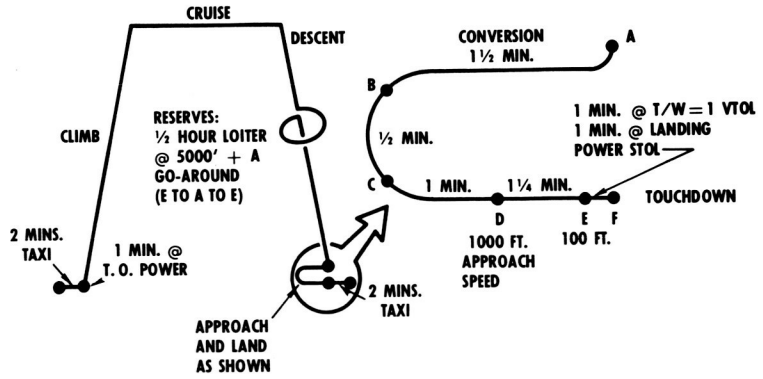

MISSION PROFILE APPROACH PATTERN

Figure 1

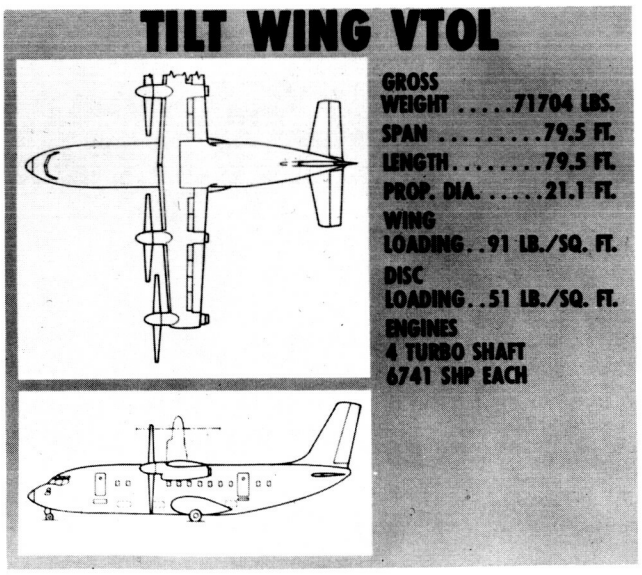

Figure 2

TILT WING, THRUST MARGINS REQUIRED FOR CONTROL

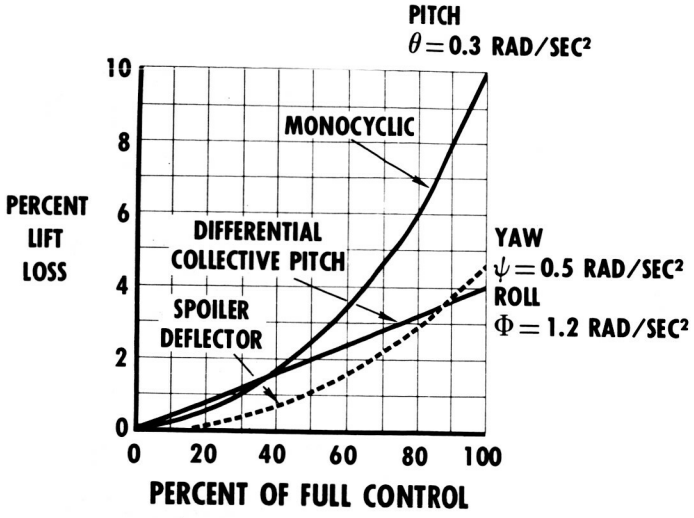

Figure 3

TILT WING, TYPICAL CRUISE ALTITUDE—DOC TRADE OFF

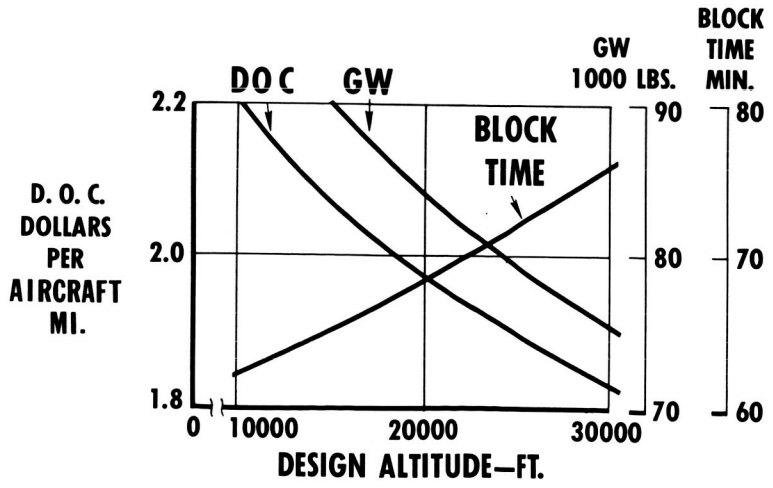

Figure 4

TILT WING, TYPICAL V_{CRUISE} — DOC TRADE OFF

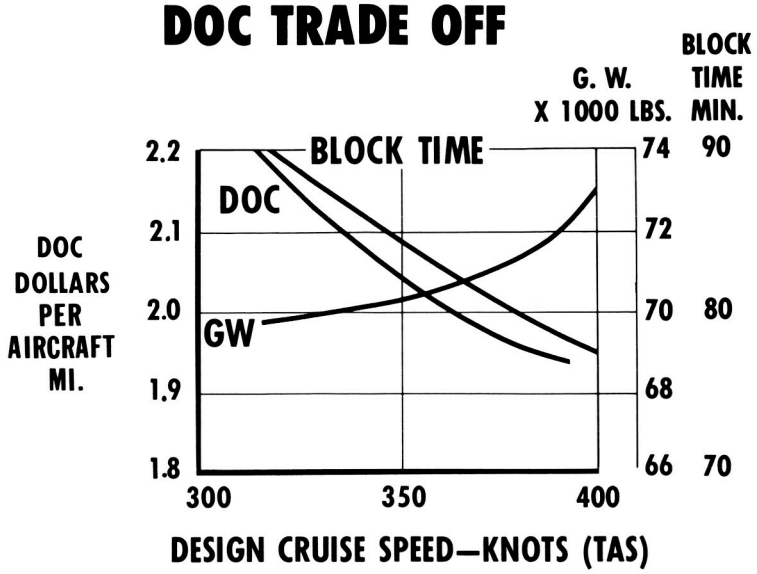

Figure 5

JET LIFT VTOL

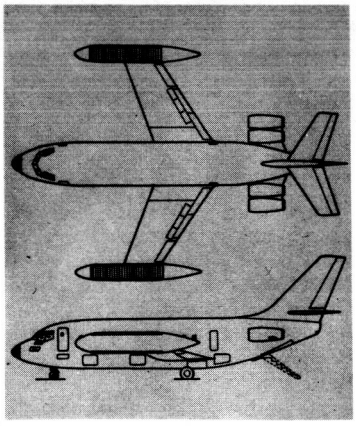

GROSS WEIGHT . . . . 80758 LBS.

SPAN (OVERALL) . . . . . 59.0 FT.

LENGTH . . . . . 80.0 FT.

WING LOADING . . . . . 115 LBS. PER SQ. FT.

ENGINES:
CRUISE—4 BYPASS RATIO 3 TURBOFANS 6950 LBS. THRUST

LIFT—10 BYPASS RATIO 2.5 TURBOFANS 9900 LBS. THRUST

Figure 6

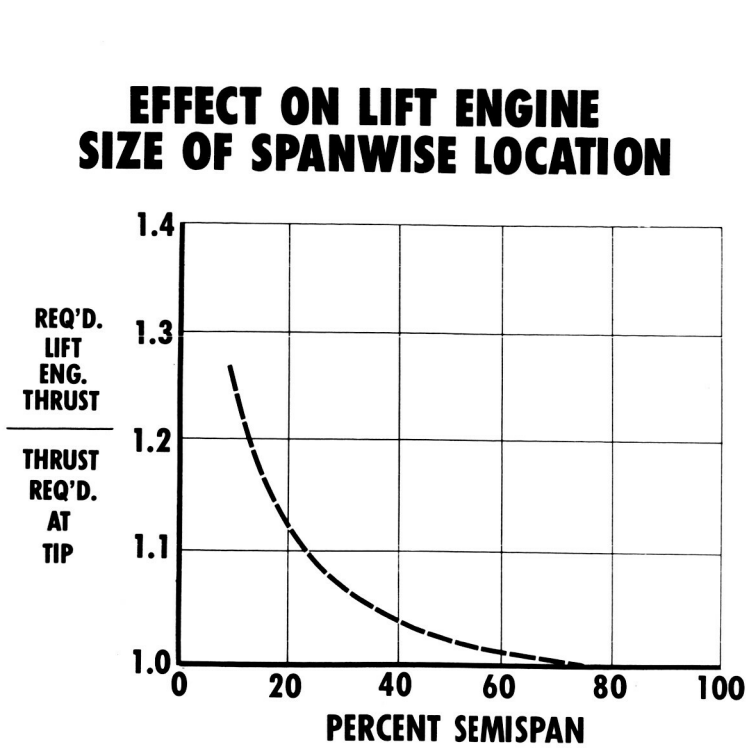

Figure 7

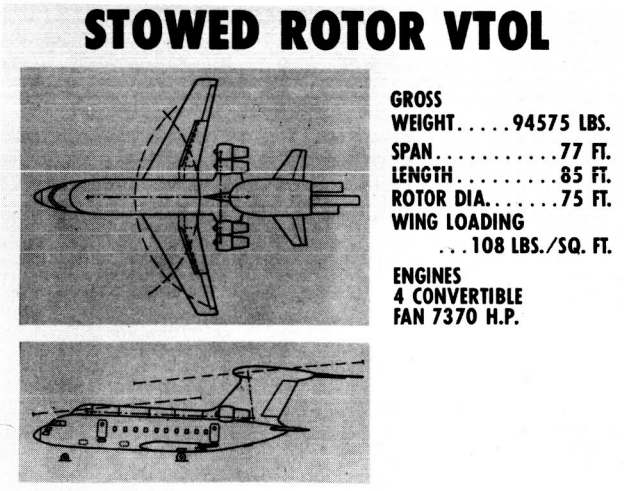

Figure 8

DRAG COMPARISON OF CONVERTIBLE HELICOPTERS

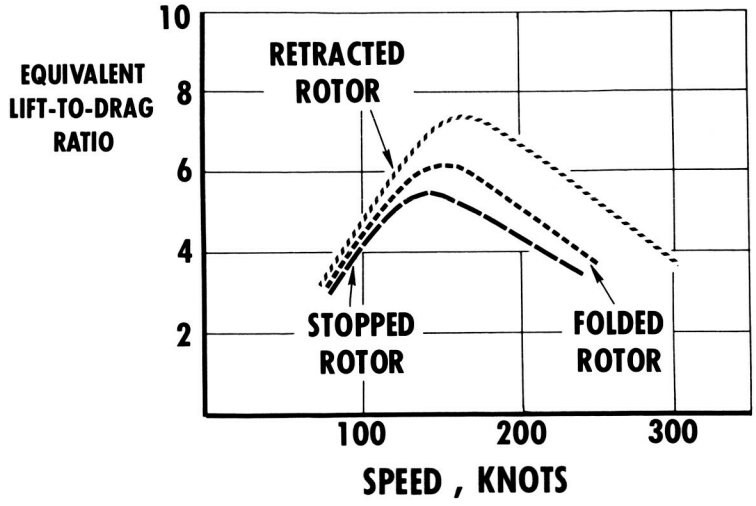

Figure 9

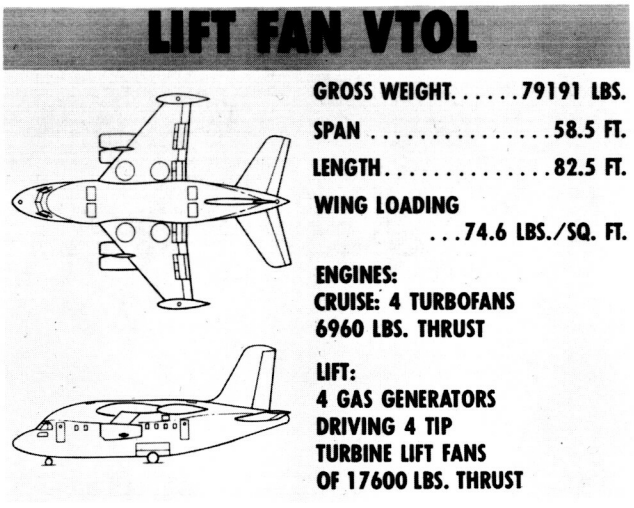

Figure 10

Figure 11

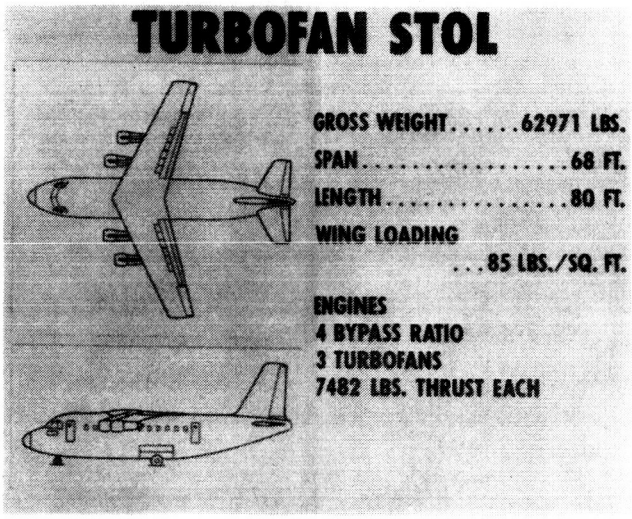

Figure 12

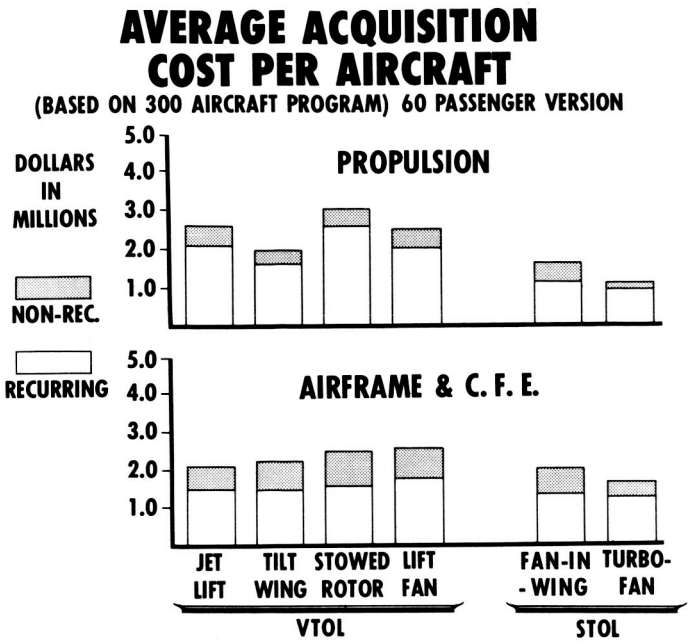

Figure 13

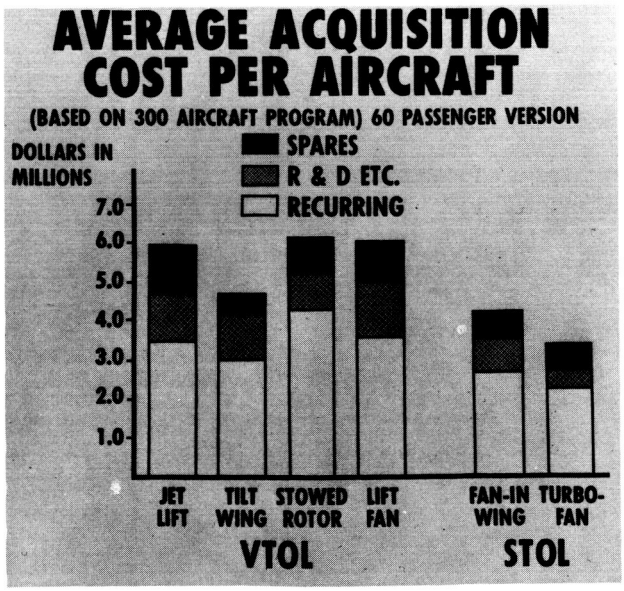

Figure 14

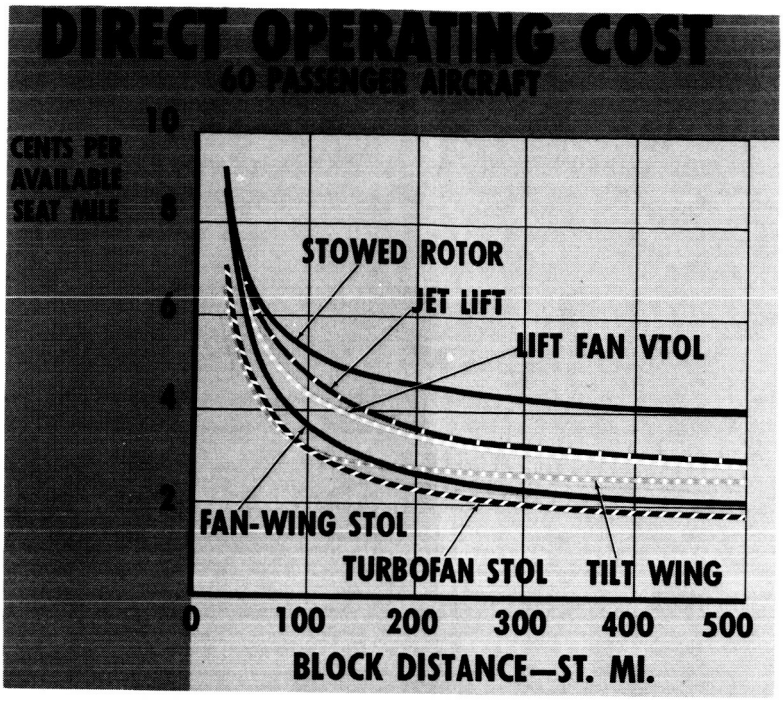

Figure 15

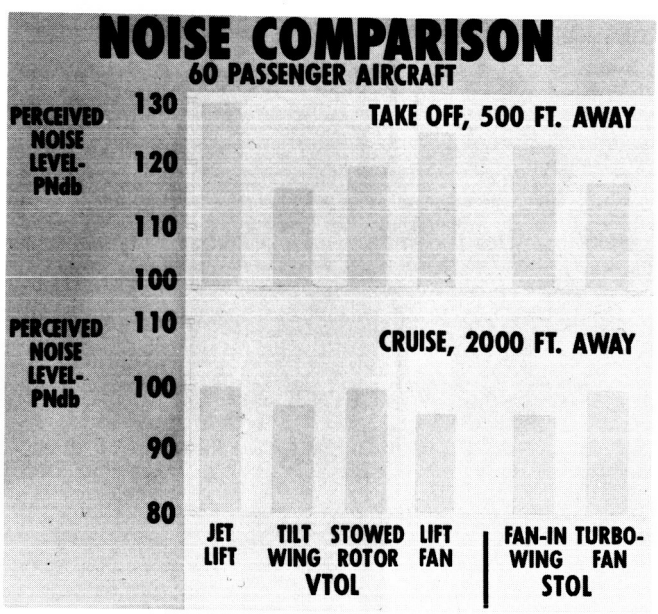

Figure 16

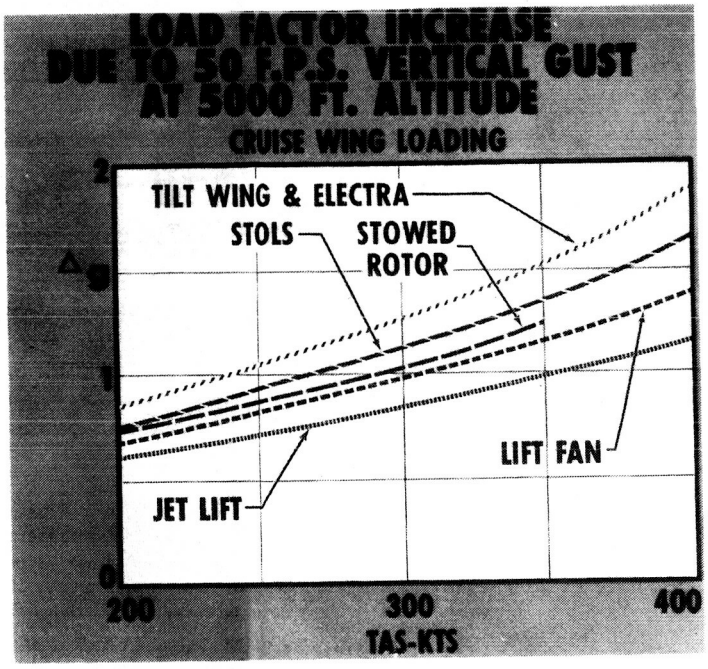
LOAD FACTOR INCREASE
DUE TO 50 F.P.S. VERTICAL GUST
AT 5000 FT. ALTITUDE
CRUISE WING LOADING
2
1
0
ΔnZ
TILT WING & ELECTRA
STOLS
STOWED
ROTOR
LIFT FAN
JET LIFT
200
300
400
TAS-KTS

Figure 17

21b. A REVIEW OF STOL DESIGNS FOR THE NASA SHORT-HAUL TRANSPORT STUDY

By Joseph M. Zabinsky
The Boeing Company

INTRODUCTION

Many concepts of V/STOL aircraft have been investigated during the last decade. This work has resulted in flying prototypes, ranging from somewhat primitive research aircraft to more sophisticated second-generation models suitable for operational evaluation. Several concepts have emerged as practical configurations. More recently, concepts of the helicopter type which can be converted in flight to a conventional aircraft configuration have evolved. The state of the art in V/STOL technology has now reached the point where the application of these V/STOL aircraft to civil transportation can be evaluated with a reasonable degree of confidence.

This paper presents some of the results obtained in the first phase of a study of VTOL and STOL short-haul transports conducted by The Boeing Company for NASA's Ames Research Center. Four VTOL aircraft were studied: the tilt wing, jet lift, lift fan, and stowed-rotor concepts. Two STOL types, the fan-in-wing and the externally blown flap turbofan, were studied.

STUDY GROUND RULES

The aircraft were designed for minimum direct operating cost at their maximum stage length of 500 statute miles with a payload of 60 passengers (200 lb each with baggage) and 1200 pounds of revenue cargo. A crew of three was specified and the aircraft were required to have two toilets and provision for serving beverages. Two integral airstairs were assumed in each aircraft and an Auxiliary Power Unit was stipulated.

The design takeoff condition was sea level, 86° F, and the most severe hover criteria were as follows:

1. Most critical engine out, T/W = 1.0 trimmed, and 50-percent roll control, 20-percent pitch control, and 20-percent yaw control.

2. Most critical engine out, T/W = 1.05 trimmed, but no control input.

The following initial angular accelerations (radians per second squared) were specified:

	Required	Desired
Roll	0.6	1.2
Pitch	0.3	0.6
Yaw	0.25	0.5

It was assumed that under emergency conditions (i.e., engine out) a contingency rating of 10-percent power or 7-percent thrust above the normal maximum was available.

The STOL aircraft were required to have a balanced field length of 2000 feet. The takeoff was over a 35-foot obstacle and the landing over a 50-foot obstacle. For takeoff, the field length was taken to be the distance to clear 35 feet with one engine failed, and for landing, the distance to land over the 50-foot obstacle multiplied by 1.67.

ANALYSIS OF DESIGN PARAMETERS

Figure 1 puts the 2000-foot field length in perspective. This figure shows the combination of aerodynamic and propulsive forces required for various field lengths. For very short field lengths the aerodynamic force contribution is negligible, and the propulsion system is dominant. This is the region of the V/STOL airplanes.

As field length increases, the line on the figure separating the aerodynamic and propulsion contribution becomes a widening band. This indicates the variation in the aerodynamic portion of the lift that is possible at any given distance, through changes in wing loading, aspect ratio, flap complexity, and various forms of high lift.

For the 2000-foot field length, either high lift or lift propulsion STOL airplanes are feasible. It is between these types that a choice is to be made. For this study the lift propulsion type was specified as having a lift fan in wing, and the high-lift type selected had an externally blown flap boundary-layer-control system.

At the short end of the field-length spectrum is the V/STOL airplane. A fan-in-wing airplane, designed to perform the basic mission from a vertical takeoff, is shown in figure 2. The wing design is dominated by the fan installation; thus, the desired wing loading and aspect ratio cannot always be attained.

The thrust required in terms of installed thrust-to-weight ratio for various field-length designs is shown in figure 3. The reduction in T/W with increasing field length is the main cause of the gross weight reduction shown on figure 4. The heavy solid line is the locus of design point airplanes, each capable of flying the basic mission from the indicated field length. The dotted line represents the overload and off-load performance of one of these airplanes and is typical of any of them. As the airplane is operated along this line, other changes occur which are important, especially to a commercial airplane. In particular, the load factor varies approximately with gross weight. For commercial use it is important to determine if there are circumstances when a reduction in design-load factor may be permitted for overload. The usefulness of the overload capability for commercial airplanes may depend on the answers to such questions.

As the design field length increases, there is a corresponding decrease in the vertical capability, until the point is reached at which the VTOL weight is the empty weight. This point forms a cutoff for the V/STOL type.

It is apparent from the V/STOL cutoff that the 2000-foot field length airplane will not have any vertical capability, and therefore the control system will be designed for the 2000-foot case. Figure 5 is a curve of minimum flying speed associated with various field lengths. These are minimum control speeds which result in approach speeds for the indicated distances. Superimposed on this curve are areas showing the type of control required for various speed ranges and consequently for the different field lengths. For the design distance of 2000 feet, a conventional aerodynamic control system will be adequate. In parametrically examining STOL airplanes with other design distances, the aerodynamic control was used. For this reason the designs for distances less than 2000 feet will be somewhat optimistic.

Fan-in-Wing STOL

The first of these 2000-foot airplanes, a fan-in-wing STOL, is shown in figure 6. It is apparent that the fan size no longer dominates the wing and that the reduction in required lift thrust permitted the use of one fan in each wing.

The variation of thrust required with field length is shown in figure 7. This figure shows the available thrust on an 86° F day at sea level. As the field length increases, the lift propulsion required decreases, but the ratio of weight of lift propulsion to lift thrust increases because the installation weight of the fans does not decrease as fast as the thrust.

The choice of flap design for the fan-in-wing STOL stems from two requirements. At the flying speed associated with a particular field length, the obvious use of a flap is to increase C_L and thereby reduce the size of the lift propulsion system. This is worthwhile only if the weight of the flap necessary to produce the lift increment is less than the weight of propulsion system it replaces. At the low speeds associated with short field lengths it is lighter to use thrust and ignore lift. As the design field length and flying speed increase, the increment in lift for a given weight of flap increases with the square of the velocity. For that reason the flap system associated with these airplanes becomes more complex, leading to higher usable lift coefficients as the field length increases. At the 2000-foot design point the wing was equipped with a double-slotted flap which provided a maximum power-off C_L of about 2.5.

The second requirement is best illustrated at a short-field-design point where thrust can be obtained at less weight than lift. This design would use a flap to reduce the speed at which the airplane can operate with the lift propulsion shut off. This speed is directly related to the traffic speed and to the structural design speed of such things as wheels, and lift engine doors, which are only used during takeoff and landing, but must be extended into the airstream before the low speed associated with the short field length

can be achieved. The weight savings that can be realized in this way will far exceed the weight of the appropriate flap.

The variation of gross weight with field length is shown in figure 8. The change in slope for the design-point airplanes as the lift propulsion decreases is due to the installation effect mentioned above. A knee to the curve occurs in the region of 2000 feet indicating that the design point is still in a good region for this concept.

A feature of the lift-propulsion STOL design is its ability to always match the cruise propulsion to the conventional flight requirements. For this reason the airplane always operates economically in cruise.

The overload characteristic of the 2000-foot airplane is similar to that of the V/STOL airplanes. The off load performance is limited by the minimum control speed. As the airplane weight is reduced the change in approach speed and, therefore, field length is small.

HIGH-LIFT STOL

The second type of STOL designed for 2000 feet used an externally blown flap to provide high lift through boundary-layer control. Such a system is shown schematically in figure 9. The engine exhaust spreads under the wing, passes through the slots, and energizes the boundary layer. A variable trailing-edge flap segment is used for flight path control. This drag flap is deflected to rotate the force vector.

A sample of wind-tunnel data for an externally blown flap is shown in figure 10. Lift (C_L) and drag (C_D) coefficients are shown for the extreme positions of the drag flap and three values of thrust coefficient (C_j). The solid lines represent the data with the drag flap undeflected with respect to its main flap. At $C_j = 0.6$ the dotted line is data with the drag flap in the deflected position. At the approach C_L the horizontal forces can vary from thrust, which is sufficient for go around, to drag, for deceleration and approach, all at constant power setting.

The 2000-foot STOL airplane, using the externally blown flap, is shown in figure 11. The airplane is very conventional in appearance. Four cruise engines are used to give good spanwise flap coverage. When thrust in excess of that required for cruise is needed for STOL performance, it is provided by increasing the size of the cruise engines. Small amounts of extra thrust are relatively cheap, since a new installation is not required and the installation weight-to-thrust ratio will remain fairly constant. Putting extra thrust into the cruise system for takeoff and landing causes a mismatch for level flight which grows increasingly severe as the field length decreases. This mismatch is minimized by the choice of bypass ratio. The characteristic variation of thrust with speed and bypass ratio allows a good cruise match to be maintained by increasing the bypass ratio as the thrust required increases.

The thrust required for this STOL is shown in figure 12 in relation to the fan-in-wing STOL and V/STOL requirements. For the high-lift system the cruise thrust needs to be augmented by about 50 percent for the 2000-foot field length. The total thrust-to-weight ratio approaches 1.0 at a field length of about 1200 feet. The effect of this thrust requirement on the gross weight of these airplanes as they vary with field length is shown in figure 13. A knee in the high-lift line occurs at about 2000 feet with the weight increasing rapidly at lower field lengths. This change in slope is the effect of the extra thrust which is being put into the cruise system to provide the high lift. In addition, an increasingly poor cruise match with attendant fuel penalties results.

The overload performance is similar to that of the other designs and, as with the fan-in-wing STOL, the off-load performance is limited by the minimum control speed.

CONCLUSIONS

A comparison of the 2000-foot field length designs is shown in figure 14. They differ mainly in the number of propulsion units and in the total installed thrust. The weights differ by only about 2000 pounds, or less than 3 percent.

The fan in wing has two cruise engines, two lift fans, and four gas generators to drive the fans for a total installed thrust-to-weight ratio of 0.77. The externally blown flap design has four cruise engines with a total thrust-to-weight ratio of 0.47. These thrust-to-weight ratios are for sea-level standard conditions.

The externally blown flap is preferred for the 2000-foot field length design. The number of units and total energy of the propulsion system are the predominant differences between the two STOL designs at a design field length of 2000 feet. For shorter field lengths, the fan-in-wing design would be superior because the rapid increase in thrust required causes the high-lift design to become significantly heavier than the lift propulsion design.

At longer field lengths the high-lift design will be superior because there will be no appreciable reduction in weight for the fan-in-wing design due to the cost of installing even small amounts of lift thrust.

BIBLIOGRAPHY

1. The Boeing Company: CX-6 V/STOL Assault Transport - Final Report. D6-16159, Aug. 1965.

2. Kuhn, R. E.; and Hammond, A. D.: Control Requirements Affecting STOL's. Astronaut. and Aeronaut., May 1965.

3. Kuhn, R. E.; Kelly, M. W.; and Holzhauser, C. A.: Bringing V/STOL's Down Town. Aeronaut. and Astronaut., Sept. 1965.

4. Wimpress, John K.: Shortening the Take Off and Landing Distances of High Speed Aircraft. D6-16168, The Boeing Co., Renton, Washington, June 1965. (Also Aeronaut. and Astronaut., Feb. 1966).

5. Zabinsky, Joseph M.: The Effect of Propulsion System Parameters on Vertical Take Off and Landing Performance of a Transport Aircraft. SAE-ASME no. 860, Air Transport and Space Meeting, New York, N. Y., April 1964.

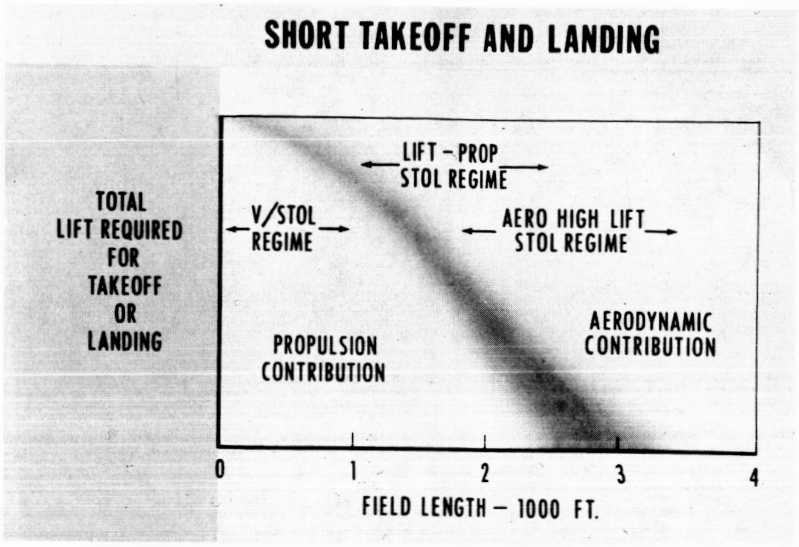

Figure 1

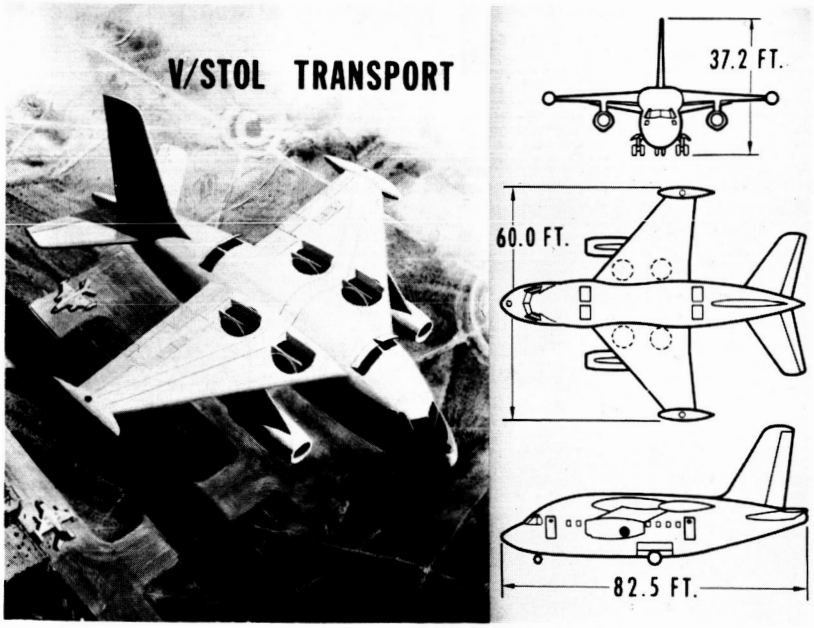

Figure 2

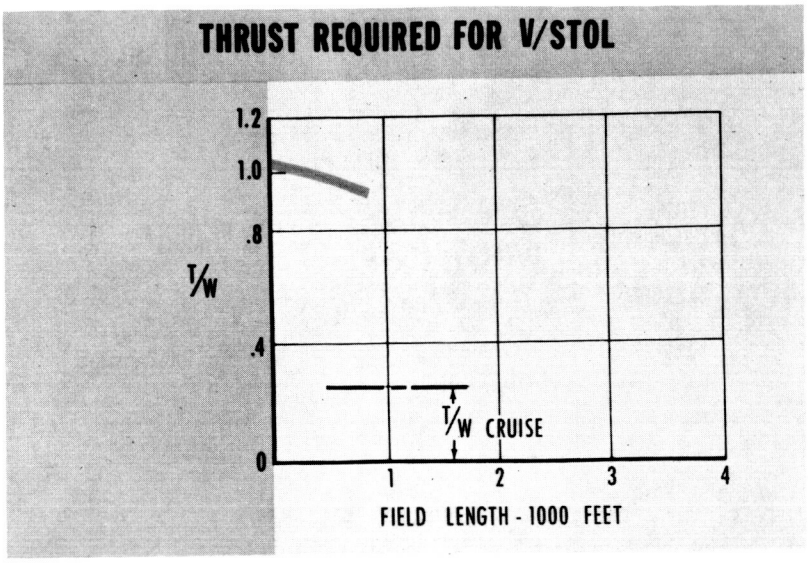

Figure 3

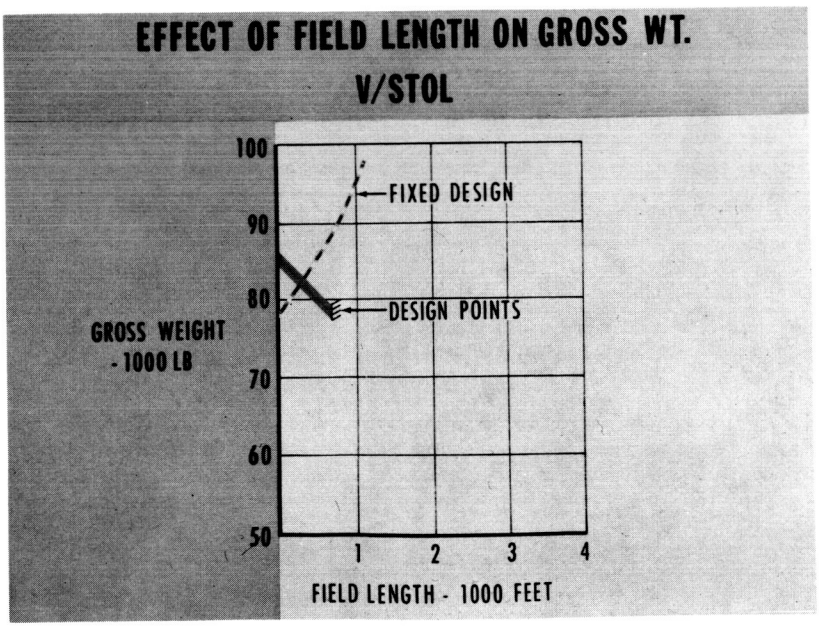

Figure 4

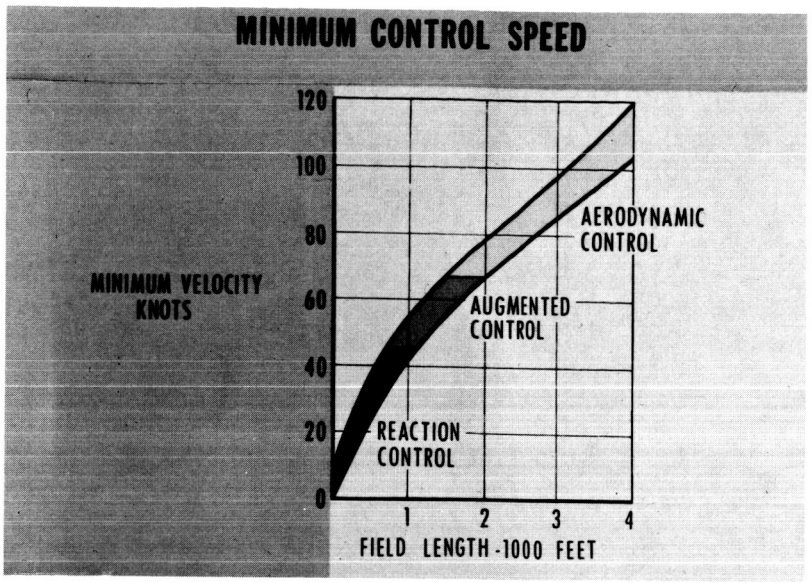

Figure 5

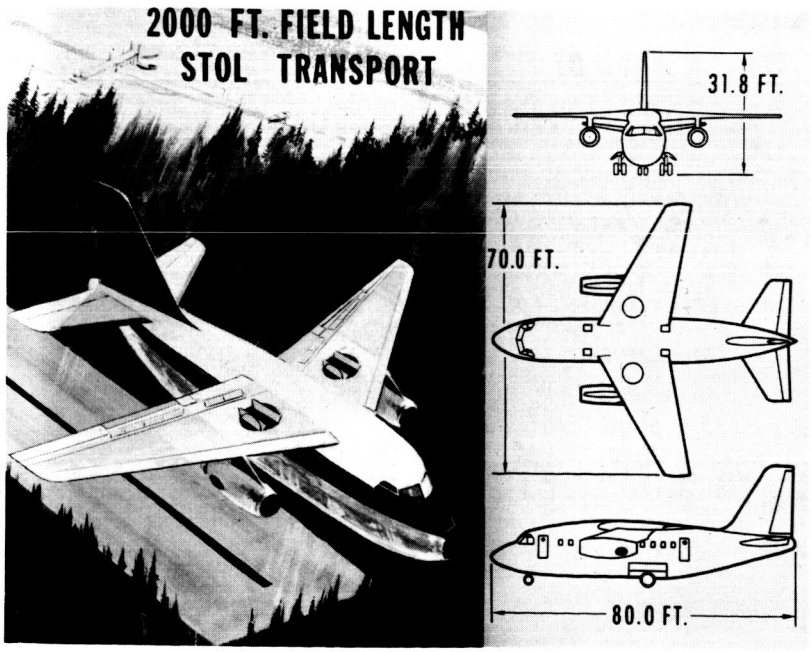

Figure 6

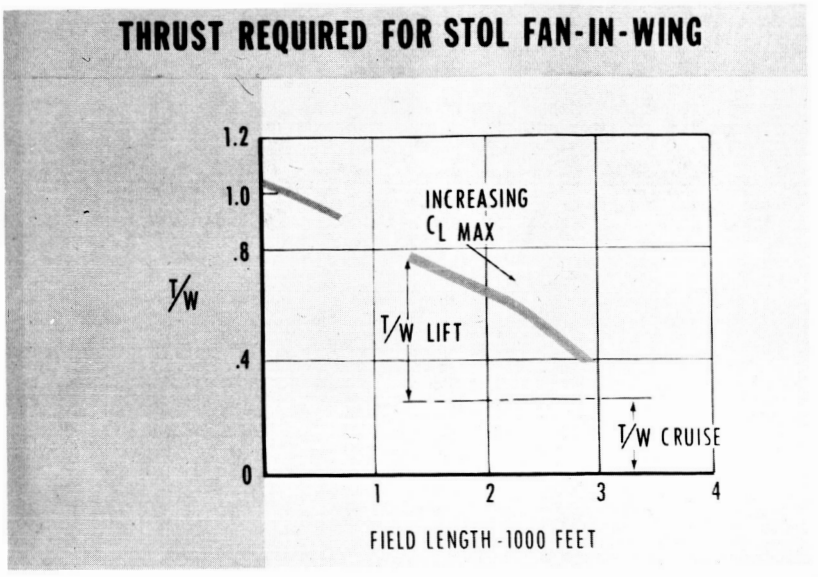

Figure 7

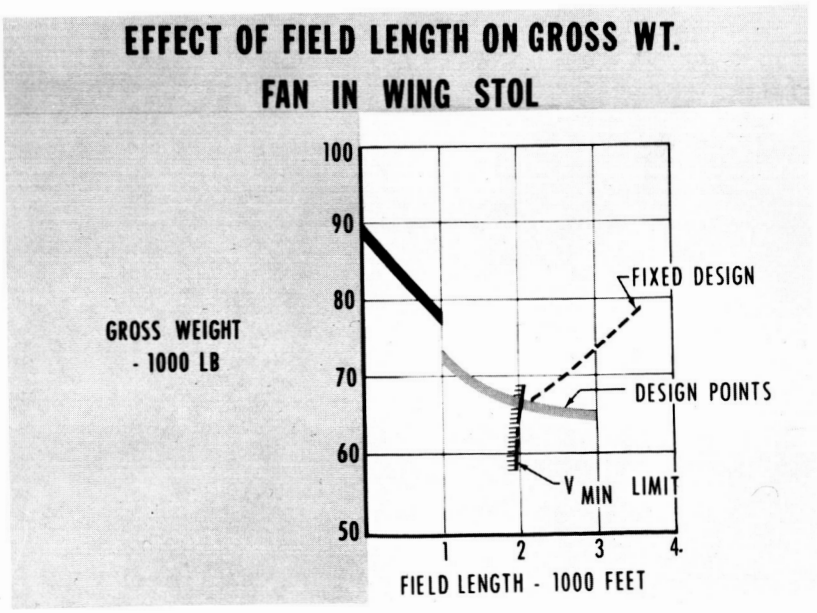

Figure 8

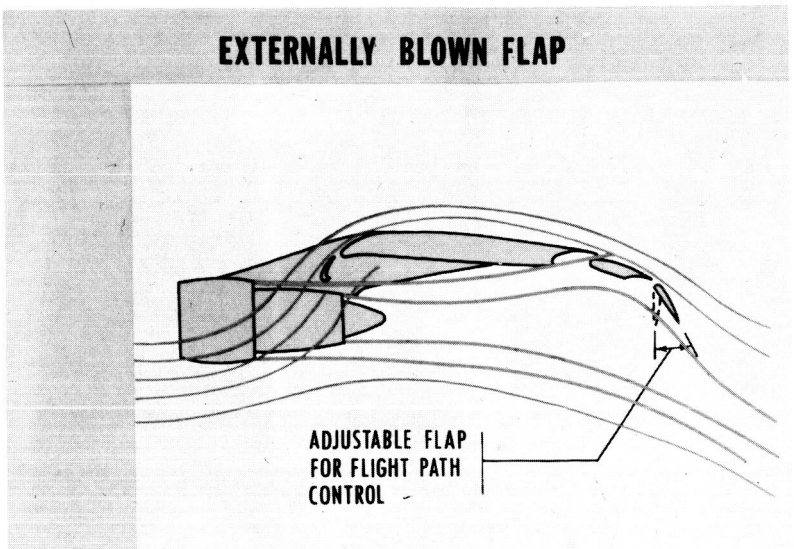

Figure 9

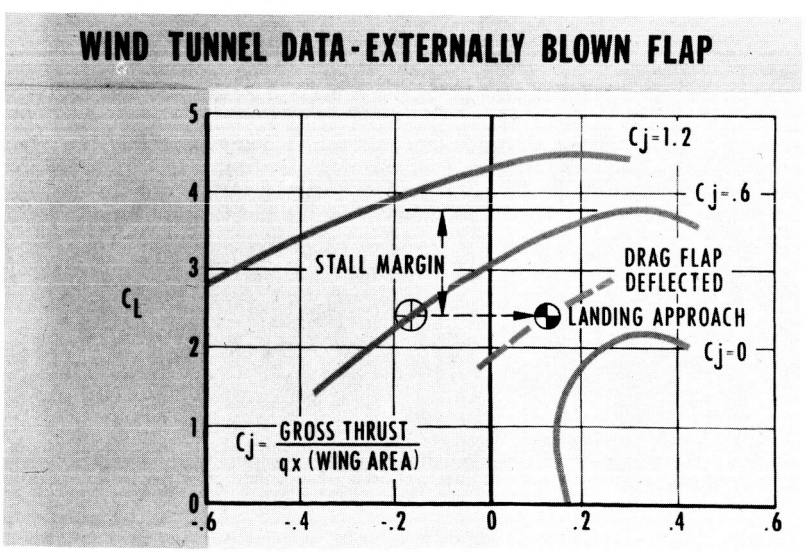

Figure 10

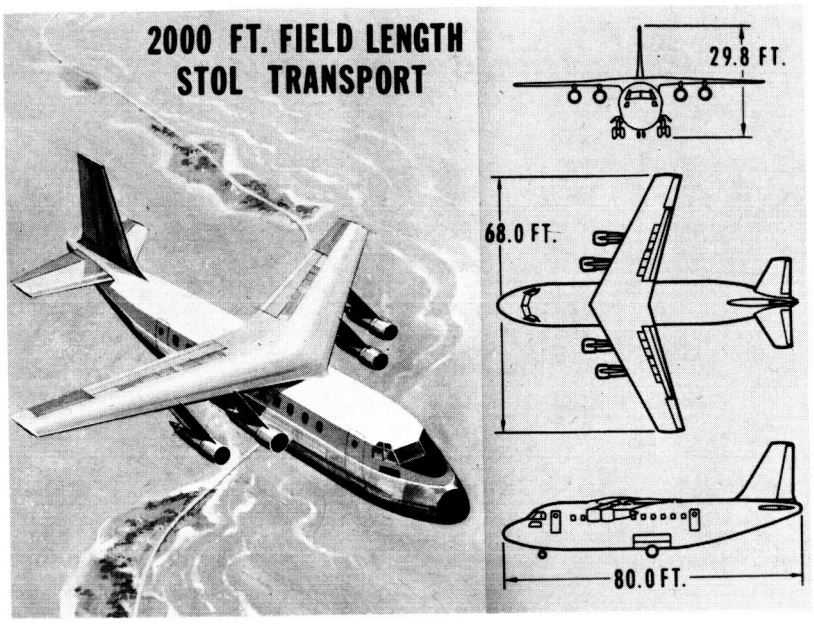

Figure 11

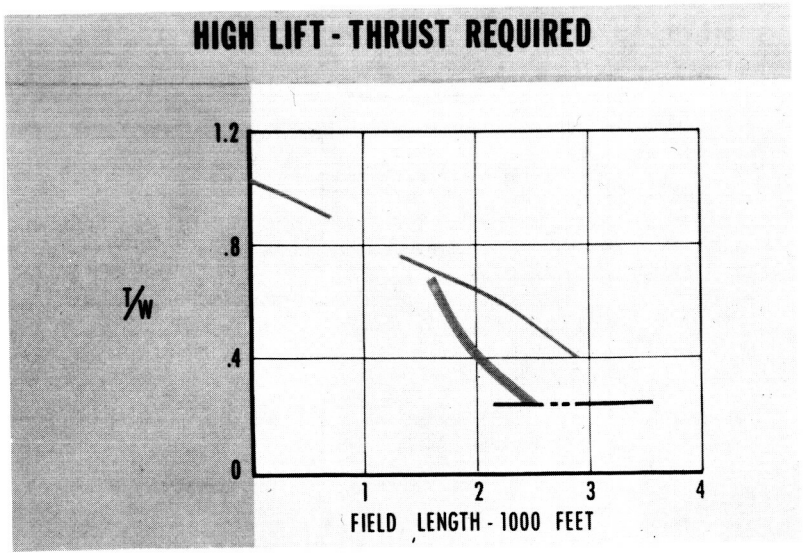

Figure 12

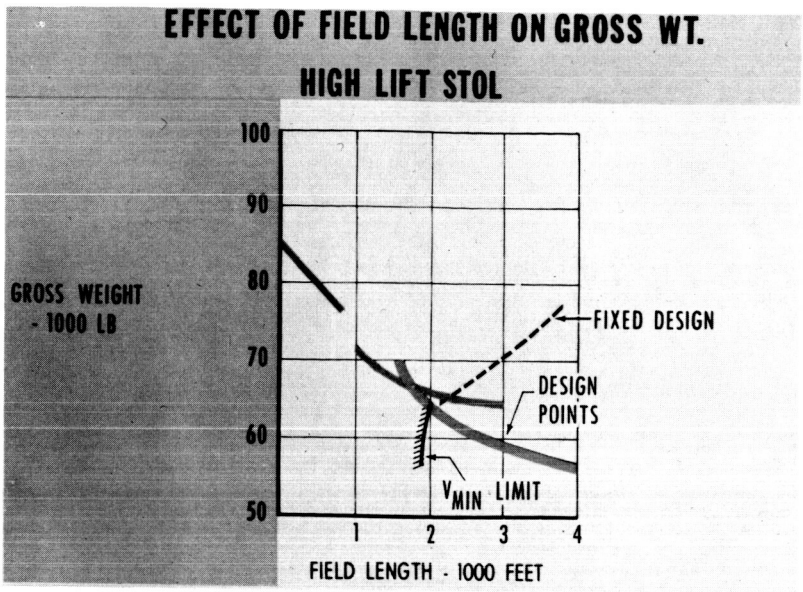

Figure 13

STOL COMPARISION

	HIGH LIFT (EXTERNALLY BLOWN)	LIFT THRUST (FAN-IN-WING)
GROSS WEIGHT - LB.	63,700	65,800
PROPULSION		
CRUISE		
TURBO FAN	4 ENGINES	2 ENGINES
T/W CRUISE	0.47	0.35
LIFT FAN		2 LIFT FANS 4 GAS GENERATORS
T/W LIFT		0.42
T/W TOTAL	0.47	0.77

Figure 14

Page intentionally left blank

22. SUMMARY OF LING-TEMCO-VOUGHT FEASIBILITY STUDIES

By Keith R. Marsh, Jesse J. Santamaria,
and Robert B. English

SUMMARY

The technical feasibility of many V/STOL concepts has been proven by wind-tunnel tests and flying prototypes. It now is considered appropriate to study the applicability of V/STOL to short-haul transport requirements.

A feasibility study has been performed for 10 point design of 60 passenger transports. Four of these were extended to 90 passenger and 120 passenger transports. For these 18 point designs, operational and economic analyses were made to identify specific research which will reduce the technical risk associated with their development.

INTRODUCTION

Purpose

The bulk of the population gain expected by 1980 will be in urban areas. At least three supermetropolitan regions - the northeast corridor, the Great Lakes area, and along the California Pacific coast - will exist by 1980. They will each extend approximately 400 miles and they alone will contain approximately 50 percent of the country's population.

The airports to serve these supermetropolitan areas are being forced to increase in size and thus move farther from the population centers to find adequate space and avoid problems associated with community acceptance. As a result of this and the increasing congestion on urban highways, the short-haul traveler is faced with a dilemma - the lack of a rapid short-haul transport system.

V/STOL short-haul transport aircraft systems operating to and from very small airports are considered to be one method for solving the dilemma of the short-haul traveler. As a result, LTV, under contract to the NASA, Ames Research Center, has studied the feasibility of various V/STOL concepts as short-haul transport aircraft. The purpose was to determine which of the V/STOL concepts studied were most promising for development into successful commerical short-haul transports and to indicate the specific research work that is required to develop the most promising V/STOL concepts into useful aircraft.

Concepts Studied

During this study, LTV has evaluated 10 designs incorporating three different propulsion system concepts - turboprops, fan in wing, and propulsive wing (fig. 1). The turboprop powered designs use a washed wing philosophy with wing tilt applied as required to meet the specific slow speed design criteria. The fan-in-wing designs use the pure fan-in-wing philosophy with all of the hot gas from the gas generator deflected to drive the wing fans for take-off and landing, and ducted straight aft in a conventional turbojet manner for cruise. The propulsive wing designs, which are considered for STOL operations only, use a jet flap concept in conjunction with the propulsive wing to develop high induced lift coefficients for slow speed flight. The propulsion system of the propulsive wing design is a high-bypass ratio turbofan system for cruising flight.

For the turboprop powered and fan-in-wing propulsion system concept, VTOL, V/STOL, and STOL point designs were considered, and for all three propulsion system concepts the STOL point designs considered were for operation from 1000- and 2000-foot fields (see fig. 2). All point designs were optimized to give a minimum direct operation cost on a 500-mile stage length.

Study Approach

The approach used by LTV (fig. 3) began with a series of parametric studies which selected the characteristics of designs that would perform the design mission. The constraints imposed by FAR airworthiness requirements and the ground rules established for this study by reference 1 were used. The designs represented by these combinations of characteristics were then analyzed to determine their direct operating costs (DOC) on the design stage length. That combination of characteristics which resulted in a near minimum DOC on the design stage length and had the desired landing and take-off performance was then selected as the optimum for each point design. These optimum point designs were evaluated for their economic and operational characteristics. From this analysis, the fan-in-wing V/STOL, tilt-wing VTOL, turboprop powered 2000-foot STOL, and propulsive wing 2000-foot STOL were selected as the point designs which warranted additional study. Additional analyses of these point designs included the evaluation of 90 and 120 passenger versions, studies of the sensitivity of selected designs to the variation of selected variables, and extended economic analyses. The characteristics of the most promising concept were then identified and the areas requiring research were defined. Finally, the inadequacies of existing airworthiness requirements to cope with the novel flight capabilities of V/STOL aircraft were noted.

Propulsion System State of the Art

The aircraft designs to be evaluated during this study were to utilize propulsion system technology representative of the 1970 time period (see fig. 4). The GE1 gas generator technology was selected as representative of a good compromise to provide the cruise power for all designs being evaluated.

Some of the more important characteristics of this power plant are a 2200° F turbine inlet temperature, and when configured as a turbojet engine, a thrust-to-weight ratio of 8:1. When configured as a turboshaft engine, this engine has a 7:1 horsepower-to-weight ratio.

DESIGN INTEGRATION STUDIES

To simplify the description of each propulsion system concept, a representative general arrangement of each will be presented, beginning with a discussion of the turboprop powered airplane.

Turboprop Powered Concepts

As shown in figure 5, the VTOL turboprop is a high wing airplane, powered by four turboshaft engines, driving four propellers. The wing is provided with leading-edge slats and full-span double slotted trailing-edge flaps to compensate for the high wing loading which is desirable for minimum DOC. Ailerons form the trailing edge of the flaps from the inboard engine nacelle to the wing tip. The horizontal tail is mounted high on the vertical fin which is a conventional fin and rudder arrangement.

The fuselage has a modified oval cross section and its length is established by the combined requirements of cockpit space, passenger cabin and its facilities, and an aft fuselage shaped for low drag. Two doors are provided for access to the fuselage. In addition to the access doors, passenger and crew escape hatches are located on each side of the fuselage in the passenger cabin. Each passenger is provided with 2 cubic feet carry-on baggage volume.

Cargo and baggage compartment access doors are located at a convenient height on the lower side of the fuselage. Space is provided for 1200 pounds of revenue cargo at a density of 10 pounds per cubic foot, and stowed baggage space is provided assuming each passenger carries the baggage limits allowable without excess baggage charges.

The unique characteristics of the V/STOL turboprop powered airplanes are the tilting wing (in all but the 2000-foot STOL), a transmission system interconnecting all engines, and the use of jet engines for longitudinal control (in all but the 2000-foot STOL).

The turboprop design philosophy used by LTV is based on the XC-142A with one major exception which is the use of jet engines for pitch control in place of the tail rotor. The pitch engines are sized so that each engine provides all the thrust necessary for all the trim and half the pitch control required, thereby providing more than the minimum requirement when one pitch engine is out.

Two main reasons for this installation are that the safety margin is increased by the redundant pitch system and, at the relatively high cruise speed, the drag is considerably reduced by the elimination of the tail rotor.

As in the XC-142A, the engines are mounted directly aft of the propellers (see fig. 6) keeping the cross shafting unloaded except when unsymmetrical thrust is desired, such as for control. The wing has no geometric dihedral and the leading-edge beam from which the cross shafting is supported, is straight, thus eliminating the need for a gearbox between the left- and right-hand sets of engines.

The control producing devices are as follows:

- Pitch engines during hover and transition, and a unit horizontal tail during cruise flight provide longitudinal control.

- For cruising flight the airplane utilizes the conventional ailerons and rudder for lateral and directional control. During hover and transition, the lateral-directional control is obtained by combining the varying thrust of the propellers, ailerons, and rudder. These are connected by a roll-yaw integrator which is a mechanical linkage that accepts pilot stabilization, trim, and wing position inputs. Output is diverted to the propellers, rudder, and ailerons in the direction and magnitude required for pure rolling or yawing.

Fan-In-Wing Concepts

As shown in figure 7, the V/STOL fan in wing is a high wing airplane. It is powered by six wing-mounted turbojet engines driving four tip turbine fans installed in the wing and one tip turbine fan installed in the fuselage nose. The wing has trailing-edge flaps on the inboard section and combination trailing-edge flaps and ailerons on the outboard section. The horizontal tail is mounted on the top of the vertical fin which is a conventional fin and rudder arrangement.

The fuselage, other than the differences necessitated by the installations of the nose fan, is similar to the fuselage of the turboprop powered airplanes, as are the crew and passenger accommodations.

The unique characteristics of the fan-in-wing designs are the tip driven fans mounted in the wing and in the nose of the fuselage. These fans govern the configuration geometry. Several constraints dictated the wing plan form which has essentially a constant chord. This configuration was arrived at by the following steps. First of all, the minimum fan/turbine diameter was determined. The second step was the determination of the routing of the fairly large diameter ducts for the hot gas in the wing. After analyzing many options, including routing in front of and in back of the wing beam, it was determined that the best possible routing was to keep the hot gas ducts between the front and rear box beams, thereby keeping the wing depth and structural weight penalty to a minimum since the ducts do not cut through the box beams. It is to be noted that the GE XV-5A uses this approach, but it has

single fans per wing making the problem simpler. This arrangement permits the shortest wing chord which was desired to provide the minimum DOC. The length of the chord of the wing is simply the fan diameter plus the front and rear box beam and the length of flap. To provide a taper would require adding area since the wing chord is already a minimum at each fan.

The outboard engines can be mounted in the conventional "underslung" nacelle below the wing. The proximity to the fuselage requires the inboard nacelles to be located above the wing. Several low wing designs of fan-in-wing airplanes were studied and these were found to have good features, such as more direct ducting paths for the hot gas which drives the nose fan. From further study of these low wing arrangements, it was concluded that the basic gas generators would have their performance severely penalized during hover due to the reingestion of the heated exhaust gases; therefore, the low wing arrangement was selected for the STOL airplanes only, and the high wing arrangement for the airplanes required to operate VTOL.

The front and rear box beams are designed to provide the same strength and stiffness as a conventional single wing box. This increases the weight of the box approximately 30 percent which corresponds to a 15-percent increase in wing weight.

Figure 8 is a schematic drawing of the hot gas ducting and engine locations. As can be seen, with all engines operating, the hot gas from each engine is divided so that each wing fan absorbs approximately two-thirds of the hot gas of one engine. The engine sizes are established by the requirements to provide a thrust-to-weight ratio of 1.15 with the airplane trimmed and no maneuvering control input on an 86° F day at sea level.

Figure 9 illustrates an engine-out condition (in this case, the outboard engine requires the most corrective action to meet the roll and trim and control requirements). In this situation the thrust-to-weight ratio is a minimum of 1.0 in conjunction with combined inputs of 50 percent roll, 20 percent pitch, and 20 percent directional control authority. For this condition all the hot gas of the operating engine adjacent to the failed engine is directed to the outboard fan. The two inboard fans are powered to their maximum capability. The nose fan is limited to the amount necessary to provide the required 20 percent of the pitching acceleration. The remainder of the hot gas is then ducted to the opposite outboard fan.

Note that with one engine out, the remaining five engines operate at an emergency rating of 110 percent of gas generator gas horsepower take-off rating. This, however, only increases fan thrust per engine approximately 6-1/2 percent.

The engine nacelles are located so that the engine hot gases are directed to the fans between the wing and trailing-edge box beams. This is in accord with previously noted philosophy of keeping the hot gas ducts from cutting through the beams.

The key to the propulsion system is the variable inlet turbine which is designed to operate through a range of hot gas flow of approximately ±47 percent from the nominal gas flow rate. This propulsion concept is known as "gas power exchange" or "power transfer." The principle involved is to have one gas generator supply hot gas to more than one power turbine. Each power turbine is mounted on the tip of a fan. Varying the turbine inlet area differentially from one power turbine to another, holding total turbine inlet area constant, makes more hot gas flow through one turbine than the other, thereby providing differential fan thrust.

Each engine is provided with a diverter valve so that its hot gas can be diverted from the fan-turbine system to a straight through nozzle providing conventional jet thrust for cruising flight. During cruising flight, pitch control is provided by the unit horizontal tail. During V/STOL operation pitch control is provided by differential thrust between the nose and wing fans. During cruise, directional control is provided by the rudder and lateral control is provided by the ailerons. During V/STOL flight, directional control is provided by differential movement of the vanes which direct the exhaust of each of the wing fans. Lateral control is provided by the "gas power exchange" system, previously described, which gives differential thrust between the left- and right-hand side wing fans. The lateral and directional control systems are connected by a roll-yaw integrator mechanical linkage to correctly phase ailerons, rudder, deflector vanes, turbine inlet, etc., for transition.

Propulsive Wing Concepts

The last concept to be discussed is the propulsive wing concept, and a representative propulsive wing general arrangement is shown in figure 10. The low wing STOL airplane is powered by six turbojets driving eight wing-mounted turbines which drive eight wing fans and two fuselage-mounted turbines which drive two nose fans. The relatively low aspect ratio wing is fixed at a 5° incidence. The fan air is deflected by a flap located at the wing trailing edge. The horizontal tails are located on the wing booms.

A conventional fin and rudder vertical tail is located on the fuselage. The fuselage and the crew passenger accommodations are essentially the same as for the other concepts.

Some of the unique features of the propulsive wing concept include:

- Twin forward facing nose fans which operate in the cruise as well as the STOL mode
- Outboard tails mounted on wing booms
- Efficient jet flaps
- High thrust-to-weight ratios in all flight regimes

- Efficient propulsion system for a wide range of conditions
- High cruise Mach number (0.90)

As can be seen in figure 11, the gas generators are mounted one in each boom and two on each side of the fuselage. The wing turbines are sized so that each absorbs half the gas generated by one engine; therefore, four engines drive the eight fans. The fuselage turbines are sized so that each absorbs all the gas power from one engine; therefore, each inboard engine drives a nose turbine-fan combination.

Figure 12 shows a section through one of the wing fans. As can be seen, the propulsive wing consists of a fan mounted vertically within the lifting surfaces of the wing behind a leading-edge inlet air duct. Each fan is driven directly by a turbine mounted in the aft section of the wing. The straight through fan air flow duct exits through a variable nozzle area to insure efficient fan operation under a wide range of power settings. The installation of the fuselage nose fans is similar in concept to the wing fans, with the turbines mounted in the midsection of the fuselage in order to eliminate routing the hot gas ducting the entire distance from the gas generators forward to the nose fans.

For safety in the event of an engine failure, each engine is connected to the corresponding engine on the opposite side by a hot gas duct with a shut-off valve. When an engine is started, the valve is closed permitting each engine to be started in turn. The valve also functions to maintain complete thrust symmetry in the event of an engine failure. The propulsive wing concept also uses the "gas power exchange" system. The thrust loss due to a failed engine is quite small, in the order of 8 to 10 percent with one engine out and the other five engines operated at 110 percent of take-off rating.

The wing structure is greatly influenced by the propulsive wing concept and represents a departure from conventional wing design. The main wing torque box is comprised of front and rear truss beams plus upper and lower stiffened and stressed skin panels. The beams occupy the full depth of the physically thick propulsive wing, providing an exceedingly stiff structure. Note that the wing torque box is located well forward of all the hot gas ducting; and a gas leak, should one occur, would not impair the integrity of primary structure.

In cruising flight, longitudinal control is provided by the two fully powered horizontal tail surfaces. During slow speed flight, pitch control is augmented by differential thrust between the nose and wing fans.

In cruising flight, lateral and directional control are provided by the flap and ailerons and the rudder, respectively. During slow speed flight, lateral and directional control are augmented by differentially deflecting the wing thrust vector as well as differentially varying the magnitude of the thrust vector by an exchange of gas power.

Design Integration Conclusions

It is apparent that the aircraft designer is faced with a challenge in his endeavor to successfully integrate all the requirements of V/STOL and to a somewhat lesser degree STOL aircraft. He must package an extremely complex propulsion and control system in an airframe, include all the other aircraft design requirements, and do it at a nominal cost and for a minimum weight. The designer of V/STOL aircraft soon comes to the conclusion that the airplane has to be considered as one completely integrated package. No single system or component can be changed without affecting another. The more integrated the packaging, the more efficient the concept. The most successful V/STOL airplane cannot be obtained by simply combining the "optimum" propulsion system with the "optimum" control system, etc. The success depends not only on how well each subsystem operates, but more important on how well all the systems are integrated to function as a unit - as a V/STOL airplane.

SUPPLEMENTAL STUDIES

Parametric Study Methodology

Figure 13 is a block diagram of the parametric study approach. Drag and weight information are generalized. Skin friction drag is based on the three major aircraft components of fuselage, engine nacelles, and combined wing plus tail surfaces. Drag rise or compressibility drag is based on predicted drag divergent Mach number and on test data. Drag due to lift uses a correlation method based on aspect ratio. Propulsion system performance is kept general by considering the basic gas generator to be either a turboshaft, turbojet, or turbofan engine. Propellers are sized to keep the wing fully immersed with variations in aspect ratio and wing loading. With these specific propeller sizes, the turboshaft engine is then sized to produce specified thrust-to-weight ratios. One propeller activity factor, integrated design lift coefficient, and design tip speed are used. Fans are sized to produce specified thrust-to-weight ratios.

Weights were estimated from statistical data by procedures developed by LTV. These generalized data were processed by digital computer programs to determine mission performance capabilities.

The Federal Aviation Regulations define the landing field length as 67 percent greater than the calculated or demonstrated distance over a 50-foot obstacle. The study ground rule limitations of 800 feet per minute maximum sink rate and 0.5 g deceleration rate on the ground are so specific that the approach speeds for the 1000 and 2000 foot field lengths automatically become 54 and 86 knots, respectively.

XC-142A experience has shown that the analytical approach of Cromwell and Payne (ref. 2) is sufficiently accurate for parametric performance studies of turboprop airplanes. In fact, the XC-142A descent capability as determined by flight tests is better than predicted using this method. This method assumes a mass flow for the stream tube defined by the wing filled with the

same velocity as the stream tubes defined by the props, and then adjusts power off aerodynamic data in proportion to the ratio of the actual mass flow to the assumed mass flow. Actual XC-142A flap effectiveness has been used for the present study of turboprop transition and field performance.

Goldsmith and Hickey's analytical method (ref. 3) has been used to estimate induced effects for fan-in-wing configurations. Checks against wind-tunnel data show that this method predicts the induced effects accurately enough for use in parametric studies.

The lack of data on propulsive wing concepts forces the use of test data obtained for a less efficient configuration. These data are considered sufficiently accurate for this study. With improved flap arrangements and configurations performance of propulsive wing designs may be even better than predicted.

Point Design Selection Process

The point design selection process was based on a DOC analysis of each aircraft capable of performing the mission. Figure 14 is an example of the point design selection process for the turboprop STOL configurations. The direct operating cost, corresponding design take-off weight, block times, and block fuel are plotted versus thrust-to-weight ratio. This example is for one wing loading, aspect ratio, and cruise altitude combination. The minimum direct operating cost then defines the point design aircraft unless field length requirements are not satisfied.

Critical Design Conditions

The critical design conditions for the 10 point designs of the 60 passenger aircraft are shown in figure 15. From this list it can be seen that take-off requirements predominate in sizing propulsion systems of aircraft having a VTOL capability, mainly because of VTOL thrust-to-weight ratio requirements. Cruise speeds for minimum DOC and landing conditions primarily influence STOL propulsion system sizing. The optimum cruise Mach number of the turboprops is approximately 0.6. Fan-in-wing configurations are limited to 0.8 cruise Mach number, and propulsive wing configurations to 0.9. It should be noted that high-speed wind-tunnel tests have substantiated the ability of the propulsive wing concept to cruise at a 0.9 Mach number.

Special Sensitivity Studies

A number of sensitivity studies were conducted to determine the influence of certain parameters on direct operating costs or aircraft sizing. The turboprop powered STOL point designs had their engines sized for cruise performance and their propellers sized for maximum static thrust. If the 100-percent free turbine speed is coupled with a take-off tip speed of 1000 feet per second (to produce maximum static thrust), a significant horsepower loss results in cruise because it is necessary to reduce tip speeds as low as

700 feet per second to reduce compressibility losses. Since the STOL designs had more static thrust than was required for the desired performance, a trade-off study was conducted in an attempt to increase cruise speed without increasing engine size. The effects of propeller tip speed (coupled with the 100-percent free turbine tip speed), activity factor, and design integrated lift coefficient on cruise speed were investigated. The results are summarized in figure 16. The initial design point for maximum static thrust is indicated by the circular symbol at a cruise speed of about 330 knots. It is seen that the cruise speed is increased about 45 knots by changing the take-off tip speed from 1000 to 700 or 800 feet per second, the activity factor from 140 to 100, and the integrated design lift coefficient from 0.5 to 0.3. It should be noted that the cruise tip speed was maintained between 700 and 750 feet per second. The effect of varying propeller tip speed on take-off performance is shown in figure 17. It can be seen that decreasing tip speed has little effect on take-off distance.

The sensitivity of the roll and yaw requirements to true airspeed for this same configuration was studied to determine the approximate minimum speed where cross shafting would no longer be needed. Figure 18 presents the net rolling moment available from a spoiler roll control system versus true airspeed. The rolling moment obtained with a spoiler deflection of 6-percent chord is shown and aircraft trim angles of attack of 5°, 10°, and 15° are indicated on the figure. For any speed above 65 knots the maneuvering roll control requirement can be met with reasonable angles of attack by this spoiler system. However, the yaw control requirement is more critical. In figure 19 the yawing moment from a rudder with a plain flap and boundary layer control and also from a double hinged rudder without boundary layer control is shown as a function of true airspeed. The maneuvering plus trim control requirement includes the required spoiler control input to trim the resulting rolling moment at a trim angle of attack of 10° and with the number one engine out and propeller feathered. These calculations show that control of the resulting yawing moments at maximum power require a relatively large vertical tail area or sophisticated rudder system to eliminate cross shafting below approximately 75 knots. Since the yaw control available is marginal for the 2000-foot STOL, cross shafting is used on all turboprop configurations.

Figure 20 shows that the weight of the fan-in-wing V/STOL point design configuration is sensitive to the fuel reserve required. For each percent reduction in reserve fuel which is over 30 percent of the total fuel weight, a reduction of approximately 0.15 percent in design empty weight and 0.17 percent in design take-off weight results.

The design take-off weight of the 2000-foot point design propulsive wing configuration is not sensitive to increased skin friction drag and decreased installed thrust (fig. 21). This study was made because only limited data are available to support this concept. The slopes for drag increases are relatively independent of thrust losses and thrust loss slopes are relatively independent of the drag levels. For each percent change in installed thrust, a change of 0.55 percent in design take-off weight is required. Approximately 0.4 percent change in design take-off weight is required for each percent change in drag.

The limited sensitivity studies conducted indicated the refinements of the point designs studied that could be made if more accurate data were available. Corresponding analyses of each configuration could affect the selection of most promising concepts if the sensitivity of each configuration to various design parameters were included in the selection process.

POINT DESIGN COMPARISON

Sixty Passenger Point Designs

Figures 22 and 23 show a comparison of the three-view drawings of the 60 passenger turboprop powered point designs. The similarity of the designs is evident. All are equipped with both leading- and trailing-edge high-lift devices. The VTOL and V/STOL airplanes have wings that tilt through 100°, and dual pitch engines in the rear of the fuselage. The 1000-foot STOL point design has a wing that tilts to an angle of 20° for landing, and it is equipped with one pitch augmentation engine. The 2000-foot STOL airplane does not have a tilt wing or any pitch augmentation engines.

Figures 24 and 25 show a comparison of the 60 passenger fan-in-wing point designs. All designs are equipped with six gas generators, four wing fans, and a fuselage nose fan. The airplanes having a VTOL capability have high wings and "Tee-tails"; whereas the STOL airplanes have low wings and more conventional tail configurations.

The propulsive wing point designs shown in figure 26 are geometrically similar, differing only in size because the 1000-foot STOL point design has a higher design thrust-to-weight ratio.

A comparison of the gross weights of these 10 point designs (fig. 27) shows that the weights range from approximately 53,000 pounds for the turboprop powered 2000-foot STOL airplane to approximately 95,000 pounds for the fan-in-wing VTOL airplane. The breakdown of gross weights into the four major categories of structure, propulsion, fixed equipment, fuel, and useful load less fuel (fig. 28) shows that all designs have comparable structural weight ratios which vary from 27 percent to 29 percent of the gross weight. The actual fixed equipment weight plus useful load less fuel is almost the same for all point designs; therefore, the percentage of gross weight assigned to these items varies inversely with the airplane's gross weight. The factors which are predominant in establishing the gross weight are then the sum of the propulsion system and the fuel weights. These factors vary from 23 percent for the turboprop powered 2000-foot STOL airplane to 40 percent for the fan-in-wing VTOL airplane.

The noise generated by V/STOL aircraft looms as one of the major stumbling blocks to community acceptance of V/STOL short-haul transport systems. As a result, the far field noise characteristics of the ten 60 passenger point designs have been estimated and are shown in figure 29. This figure shows the distance, from the airplane, at which the perceived noise level drops to 112 decibels, the maximum level considered acceptable around airports.

This figure shows that the levels of each of these designs are approximately the same except for the turboprop powered 2000-foot STOL airplane. This airplane has a lower noise level than the other turboprop powered designs because it does not have the pitch engines. Analyses showed that the noise generated by the pitch engines makes a major contribution in the 300 to 600 cycles per second octave band and predominates in the octave bands above 600 cycles per second.

Designs Warranting Additional Study

The fan-in-wing V/STOL, turboprop tilt wing VTOL, propulsive wing 2000-foot STOL, and turboprop powered 2000-foot STOL point designs were selected as designs which warranted additional study. The direct operating costs of these four point designs are presented in figure 30. It must be remembered that these airplanes are optimized for a design stage length of 500 miles, and it can be seen that the seat mile costs vary from approximately 2.0 cents for the propulsive wing 2000-foot STOL to nearly 3.1 cents for the fan-in-wing V/STOL at the design stage length. As the stage length reduces to 100 miles, the seat mile costs increase to a low of approximately 3 cents for the turboprop 2000-foot STOL to 5.5 cents per seat mile for the fan-in-wing V/STOL.

One facet of this study extension was to evaluate the performance of these designs on a hypothetical route shown in figure 31. The block time to complete a circuit of the entire route is shown in the bar chart of figure 32. Two assignments of nonproductive time were made. One was a nonproductive time assignment of 10-1/4 minutes for all route segments (as specified in reference 1). The other was as follows:

For a short take-off:

- Two minutes for taxi from the passenger loading area to the end of the runway
- One minute for the take-off and acceleration to the climb speed

For a vertical take-off:

- One minute for taxi from the passenger loading area to the take-off area
- One minute for the take-off and acceleration to the climb speed

For a short landing:

- Four and one-fourth minutes for getting into the traffic pattern and getting alined with the runway
- One minute for the landing itself
- Two minutes for taxi from the runway to the passenger area

For a vertical landing:

- One minute to descend and decelerate from the let-down speed at an altitude of 1000 feet to the landing touchdown; this is performed as a straight-in approach
- One minute for taxi from the touchdown point to the passenger loading area

For the variable nonproductive time analysis, the V/STOL airplane is operated with a short take-off and a vertical landing on segments A-B and D-E, VTOL on segments B-C, E-F, and F-A, and STOL on segment C-D. Figure 32 shows the power of nonproductive time on the route block time when nonproductive time has been computed as described. As an example, this analysis shows that, for the variable nonproductive time, the turboprop tilt-wing VTOL airplane with a normal rated power cruise speed of 350 knots has a route block speed almost equal to that of the propulsive wing 2000-foot STOL airplane which cruises at approximately 520 knots - nearly 50 percent faster. If the propulsive wing airplane could reduce its nonproductive time to such a level, its route block speed would increase from 313 mph to over 390 mph. Only a 6-percent improvement in route block speed, from 350 to 370 mph, can be realized by giving the fan-in-wing V/STOL airplane a VTOL nonproductive time.

In order to determine the sensitivity of V/STOL aircraft to the design passenger load, 90 and 120 passenger versions were developed for the four point designs considered to warrant additional study. Figure 33 shows the ratio of the gross weight of airplanes designed for other passenger loads to the gross weight of the airplane designed for 60 passengers. This figure shows that as the passenger load is doubled for the fan-in-wing V/STOL the design gross weight increases by approximately 65 percent. For the turboprop tilt-wing VTOL, a passenger load increase of 50 percent increases the design gross weight 45 percent; and a passenger load increase of 100 percent increases the design gross weight 80 percent. This change in slope occurs because a transition is made from four to six propellers in going from 60 to 90 passenger design loads; but the six propeller arrangement is still adequate for the 120 design passenger load. The design gross weight for the propulsive wing 2000-foot STOL increases approximately 65 percent when the passenger load is doubled, and the design gross weight for the turboprop 2000-foot STOL increases approximately 60 percent as the design passenger load is doubled.

As the design passenger load is increased above 60 passengers, the growth characteristics of the four designs are comparable except for the turboprop tilt-wing VTOL which has a noticeably higher growth factor.

Most Promising Concepts

From this feasibility study some of the fundamental requirements for the most promising V/STOL concepts for short-haul transports can be defined.

They are:

• A high subsonic speed cruise capability. While the passenger sees only a few minutes difference in travel time for the higher speed capability, the additional productivity these few minutes give to the operator are very important in minimizing direct operating costs.

• A low fuel plus propulsion system weight. It is seen from this study that a low fuel plus propulsion system weight is a key to the efficiency of a V/STOL short-haul transport aircraft concept. V/STOL aircraft use their propulsion systems to augment aerodynamic lift at low speeds as well as to provide power for cruise. The power requirements for low speed flight of V/STOL aircraft are usually considerably higher than the cruise and the loiter power requirements; therefore, it is essential for the propulsion system to be able to operate efficiently at off-design conditions. A rocket engine would represent the lightest propulsion system, but its fuel requirements would prohibit its use. A nuclear propulsion system would be the most efficient from the standpoint of fuel requirements, but the present state of the art makes the propulsion system weight (including shielding) too high. Hence, a compromise propulsion system, within the state of the art must be selected. For the time period of this study, a low speed lift to thrust augmentation system will minimize the size of the gas generators required and aid in providing a good compromise between the propulsion system and fuel weights. In addition, V/STOL airplanes will require that the propulsion system exhaust velocities be matched with the cruise velocities over a wide range of cruise conditions; therefore, a high bypass ratio cruise propulsion system will be appropriate for the 1970 time period.

Studies have also indicated that air traffic control may impose cruising altitude limits on short-haul transport airplanes; therefore, the most promising concept must not be severely penalized by such a cruise altitude limitation.

• Minimum nonproduction time. The nonproductive time as used for this study consists of: (a) the time spent in ground taxi between passenger loading areas and take-off and landing areas; (b) the time spend in actual take-off and acceleration to the climb speed; and (c) the time spent in declerating and descending from the let-down speed at an altitude of 1000 feet to the end point of the landing roll out. The nonproductive time can have a vital effect on the operational efficiency of a short-haul transport system, especially on a route structure that calls for numerous short flights. The most promising concept will be able to minimize the nonproductive time. Some of the possible effects this requirement can have on a design are to: (a) favor those concepts which will have the highest acceleration and deceleration rates; (b) favor those concepts which have a minimum preparation time for landing (i.e., time to start engines, time to change the configuration, etc.); and (c) favor those concepts which can take-off and land nearer to the passenger loading areas.

• All weather operational capability. The similarities between a V/STOL short-haul air transport system and conventional air transport systems lead to the conclusion that an all-weather operational capability is required, with the ability to operate under zero-zero weather conditions being desirable.

• Community acceptance of far field noise. Far field noise looms as a major problem in getting community acceptance of a V/STOL short-haul air transport system. The far field noise characteristics of the most promising V/STOL concept must meet community acceptance standards.

STUDY RESULTS

Specific Research Required

The specific research required to assure the timely development of the most promising V/STOL short-haul transport concepts can be broken into two categories. One category includes those items that are applicable to specific concepts and the other includes those items which are applicable to all concepts. For the first category, the following specific items of research required are identified:

1. For the fan-in-wing V/STOL concepts:

• Data are required which define changes that must be made to permit tip driven fans to operate efficiently at higher pressure ratios than the present limit of 1.3. This will permit the fan-in-wing designs to have higher disk loadings and hence lower direct operating costs.

• Data are required which will permit design of a producible fan louver system to turn exhuast air to high angles, efficiently. Such a capability will provide better take-off performance for the STOL fan-in-wing airplanes.

• Data are needed which will guide the design optimization of a gas power exchange system and its control. These data must be able to define design changes which will permit the required control response characteristics of a fan system to be developed.

• Data are needed which will guide the design of a hot gas interconnect system connecting several gas generators through a common plenum. This will also require research data which will permit the design of a multiple engine control system.

• Data are needed which will guide the design optimization of hot gas ducting system. In particular, specific research is needed which will guide the design of hot gas ducting joints, expansion provisions, insulation, shielding, supports and flow control devices.

• Data are required which will permit a more accurate assessment of the change in aerodynamic characteristics due to changes in configuration variables.

2. For the turboprop powered concepts:

- Data are required which will accurately identify the effects of propeller characteristics on static propeller performance.

- Data are required which will accurately define compressibility effects on airplane-propeller interference in cruise flight.

- Data are required which will accurately define the limits on the propeller-wing relationships for tilt-wing aircraft, that is, how far from the fuselage side can a propeller tip be and the airplane still have acceptable transition performance? What is the influence of propeller overlap or gap on transition performance? How far beyond the propeller tip can the wing tip extend and the airplane still have acceptable transition performance? What are the limits on the longitudinal positioning of the propeller plane with respect to the wing insofar as transition performance is concerned?

3. For the propulsive wing concepts:

- Data are required which will guide the design of the best method for deflecting the fan thrust downward for slow speed flight. These data should consider both the internal flow characteristics within the duct, and the external flow characteristics around the wing.

- Data are required which will guide the optimization of inlet design for propulsive wing inlets.

- Data are required which will guide the optimization and establishment of design requirements for exhaust systems in cruise flight and slow speed flight for propulsive wing concepts.

- Data are needed to guide the design optimization of a gas power exchange system, a common interconnecting plenum and a hot gas ducting system as has been mentioned for the fan-in-wing concept.

- Data are required to permit accurate assessment of the change in aerodynamic characteristics due to changes in configuration variables; for example, how does the induced lift vary as fan pressure ratio, inlet aspect ratio, exhaust aspect ratio and/or flap deflection vary.

For the second category - those items which are applicable to all concepts - the following specific items of research are identified:

- Data are required which will define the control power requirements for all flight regimes and size aircrafts.

- Data are required which will define the cockpit display requirements for a VTOL all-weather (zero/zero) landing system. This will include both the readout of data required by the pilot and the data accuracy.

- Data are required to guide the design of foreign object damage (FOD) protection devices on propulsion system installations and the determination of techniques to minimize the reingestion of hot exhaust gases by gas generators.

- Data are required which can be used to establish design criteria for VTOL and STOL airport surfacing.

- Data are required that will permit the noise generated by the propulsion system to be an optimization variable in the analysis process of optimizing a propulsion system.

- Data are needed which will better define the origin of noise for all concepts, and which will provide guidance on how noise might best be reduced at its source.

- Data are needed which will describe the noise attenuation characteristics of various structural fabrication techniques and materials.

- Research data are needed which will guide propulsion system manufacturers in the reduction of weight of propulsion systems and the reduction in specific fuel consumption especially for operations at low power settings.

- Data are required to better define the nonproductive times that should be used with each of the V/STOL concepts. A minimization of the nonproductive time will require an understanding of the operational limitations that contribute to nonproductive time for each concept.

- Data are required which will permit the engineer to make accurate estimates of the static and rotary stability derivatives for all configurations.

Airworthiness Requirements

In reviewing the capabilities of airworthiness requirements to cope with the novel flight capabilities of V/STOL aircraft, Federal Aviation Regulations Part 25, "Airworthiness Standards: Transport Category Airplanes," and Part 29, "Airworthiness Standards: Transport Category Rotorcraft," have been used. In Part 25, the stalling speed of the airplane is considered an operational limit, and many other flight characteristics are based on this speed, for example, the minimum allowable take-off and approach speeds are functions of the stall speed. Such requirements are not appropriate for V/STOL aircraft because they are designed to operate safely below the stall speed.

V/STOL aircraft will be influenced by ground effects more than will conventional aircraft, because the V/STOL aircraft are often able to fly in air disturbances that they are creating. Hence, Federal Aviation Regulations must take cognizance of this unique flight capability and assure that the airplane always operates in a safe flight regime.

Numerous V/STOL concepts use gas generators to drive thrust producing devices through interconnected transmission systems. The propulsive wing and

the fan-in-wing concepts have fans driven through an interconnected system of hot gas ducts, and the turboprop powered aircraft have propellers driven by turboshaft engines through an interconnecting system of gear cases and shafting. The existing Federal Aviation Regulations are concerned with engine failures where propellers are connected directly to the engine. The Federal Aviation Regulations must be modified to take cognizance of these interconnected transmission systems and establish regulations which assure safety after a failure occurs anywhere in the propulsion system.

In addition, design standards for components of the transmission system must be established. Special attention must be given to the installation requirements for hot gas ducting systems to assure sufficient fire protection and protection of surrounding structure from damage due to heat.

Where conventional aircraft can put fuel in their wings and thus keep it away from the passenger compartments, many V/STOL concepts will be prevented from putting fuel tanks in the wings, and hence forced to put it adjacent to the passenger compartments. The fan-in-wing concept, as an example, has its wing filled with propulsion system components. Federal Aviation Regulations must take cognizance of this potential safety hazard and define fuel system design standards that will maximize safety.

The requirements of FAR Part 29 could be used to cover some of the low flight speed modes that will encountered by V/STOL aircraft; but other requirements, such as those for autorotation probably cannot be met by many V/STOL concepts. Numerous modifications of wording would be required, and the areas where Part 25 and Part 29 are applicable would have to be explicitly defined.

GENERAL STUDY CONCLUSIONS

Considerable data are available to guide the design of turboprop powered V/STOL aircraft, and the feasibility of such concepts has been proven by the Ryan VZ-3RY, Boeing-Vertol VZ-2, the LTV-Hiller-Ryan XC-142A, the Brequet 941, and the Canadair CL-84. Even though the data are considerable, they are far from sufficiently complete to permit the characteristics of an optimum design to be defined. For this study, design limitations, found acceptable in tests, have been imposed.

Data are available to guide the design of fan-in-wing V/STOL aircraft and the feasibility of such concepts has been proven by the General Electric-Ryan XV-5A. Although the mass of data available to guide the designer of fan-in-wing aircraft is large, it is not nearly so complete as for the turboprop powered designs, and it is far from being sufficiently complete to support a design optimization study. Again, proven design limitations have been imposed.

Additional data are needed on both the turboprop powered and fan-in-wing V/STOL concepts. These data should permit the designer of a V/STOL airplane with one of these propulsion system concepts to optimize all major variables. With the data now available, the designer simply knows some of the combinations

of variables that will and will not work, and he has very little to tell him when he is reaching the acceptable limits on combinations of variables.

Only limited data are available to guide the design of propulsive wing V/STOL aircraft, and the feasibility of this concept has not been proven by any flying vehicles. Design studies based on the limited data available have indicated that a V/STOL aircraft using the propulsive wing concept is feasible, and this study has shown that a V/STOL short-haul transport version of propulsion wing aircraft would be promising. Extensive data are needed to better define the capabilities of this propulsion system concept.

Additional research data will permit the designer of V/STOL airplanes to reduce direct operating costs by permitting a better selection of configuration variables. Even more important, it will reduce the technical risk associated with the development of short-haul transport aircraft around the V/STOL propulsion system concepts evaluated in this study.

Since V/STOL aircraft are neither conventional nor are many of them rotorcraft, it appears that a new part of Federal Aviation Regulations should be established to define the airworthiness standards for V/STOL aircraft.

REFERENCES

1. Anon.: Study on the Feasibility of V/STOL Concepts for Short-Haul Transport Aircraft. Contract NAS2-3036, June 28, 1965.

2. Cromwell, C. H., III; and Payne, H. E., III: A Stability Analysis of Tilt-Wing Aircraft (Analytical). Rep. 477, Princeton Univ., May 1960.

3. Goldsmith, Robert H.; and Hickey, David H.: Characteristics of Aircraft With Lifting-Fan Propulsion Systems for V/STOL. IAS paper 63-27, Jan. 1963.

CONCEPTS STUDIED

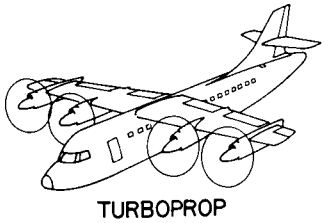

TURBOPROP

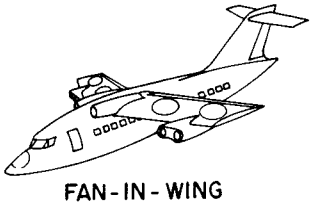

FAN-IN-WING

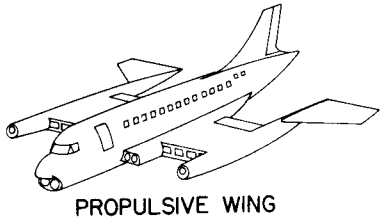

PROPULSIVE WING

Figure 1

POINT DESIGN DEVELOPED

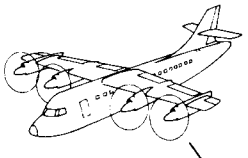

TURBOPROP

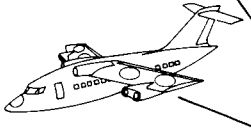

FAN-IN-WING

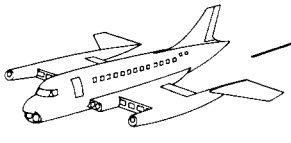

PROPULSIVE WING

VTOL	V/STOL	1000 FT STOL	2000 FT STOL
✓	✓	✓	✓
✓	✓	✓	✓
		✓	✓

Figure 2

LTV STUDY FLOW BLOCK DIAGRAM

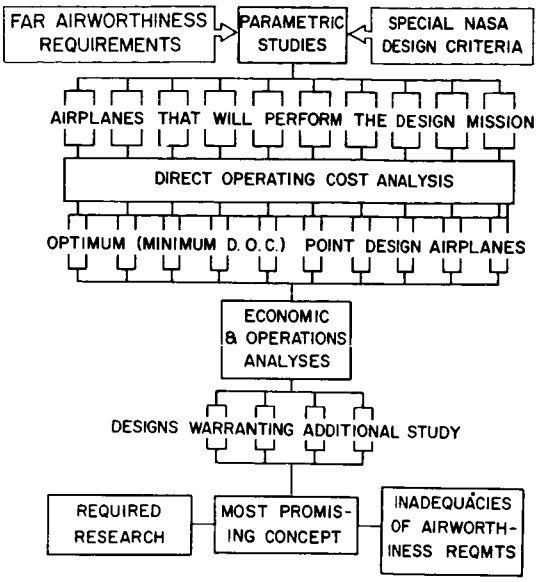

Figure 3

GAS GENERATOR TECHNOLOGY

TURBINE INLET TEMPERATURE	2200° F
TURBOJET ENGINE VERSIONS	
• THRUST PER POUND OF AIR	75-85
• THRUST PER POUND OF ENGINE WEIGHT	8
• THRUST PER UNIT ENGINE VOLUME	350 POUNDS/FT^3
TURBOSHAFT ENGINE VERSIONS	
• HORSEPOWER PER POUND OF AIR	140 - 150 HP/POUND
• HORSEPOWER PER POUND OF ENGINE WEIGHT	7 HP/POUND
• HORSEPOWER PER UNIT ENGINE VOLUME	215 HP/FT^3

Figure 4

TYPICAL TURBOPROP AIRPLANE

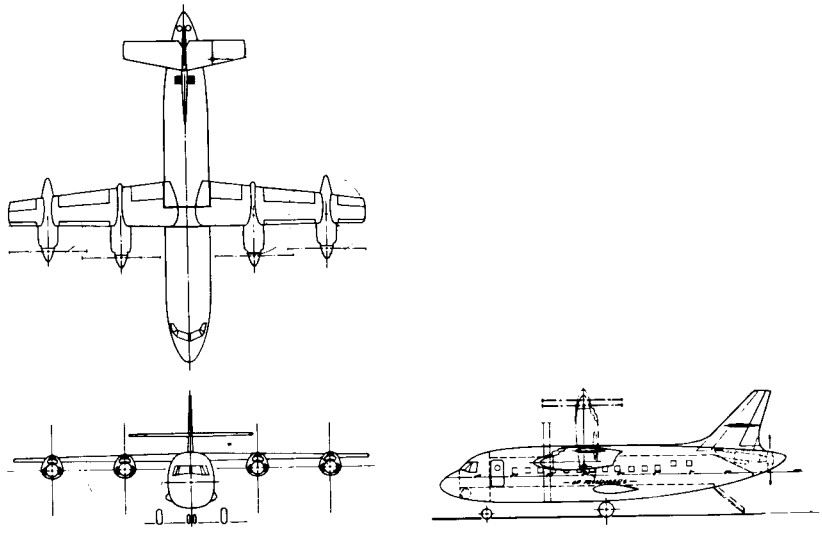

Figure 5

TURBOPROP AIRPLANE TRANSMISSION SYSTEM

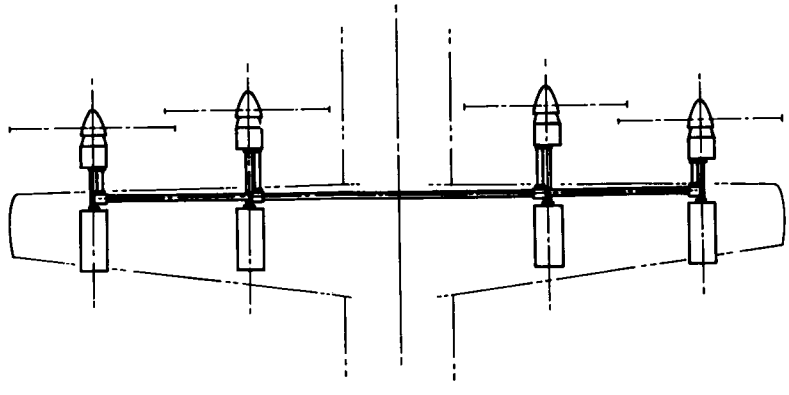

Figure 6

TYPICAL FAN-IN-WING AIRPLANE

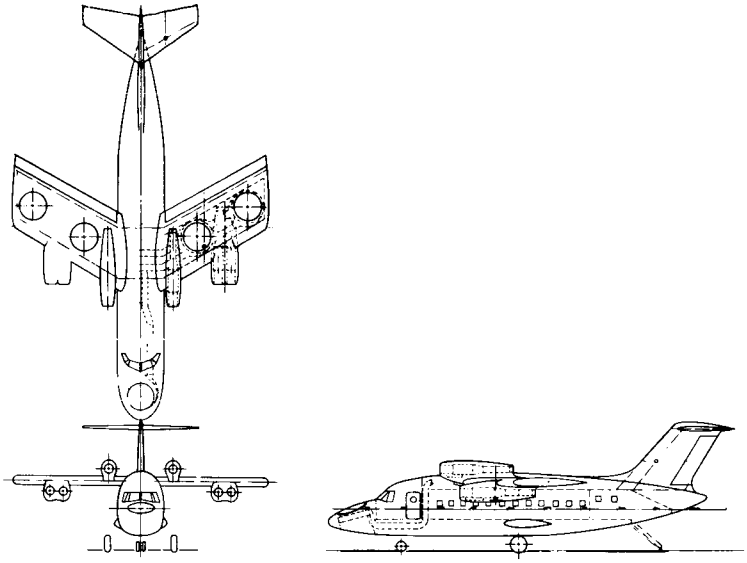

Figure 7

V/STOL POINT DESIGN
FAN-IN-WING -ALL ENGINES OPERATING

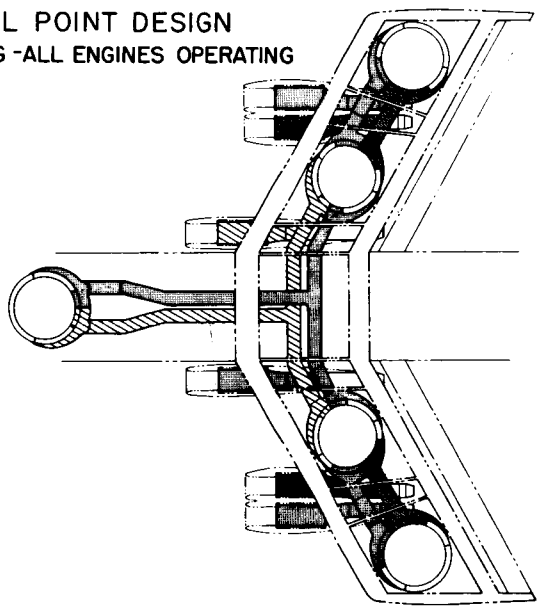

Figure 8

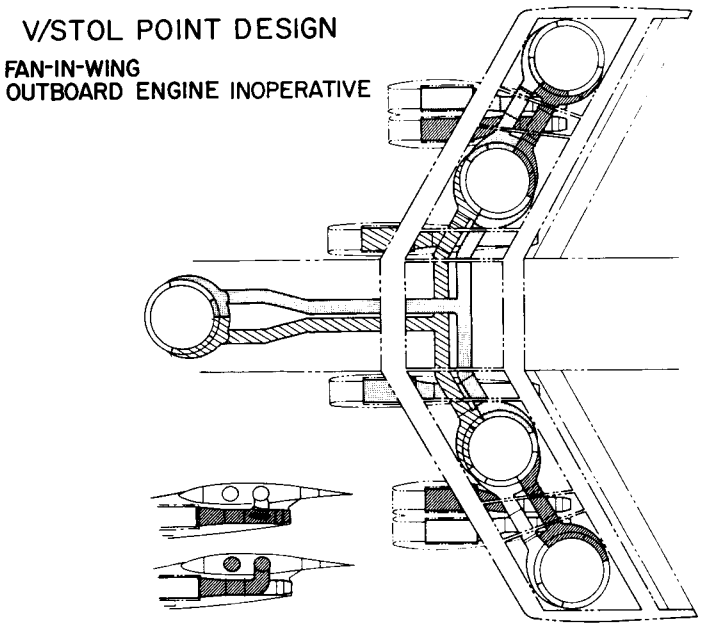

Figure 9

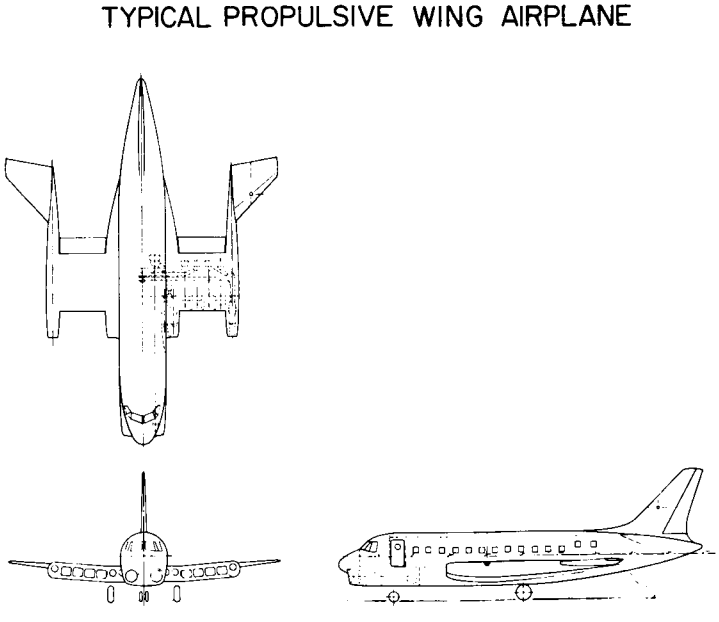

Figure 10

STOL POINT DESIGN PROPULSIVE WING, ALL ENGINES OPERATING

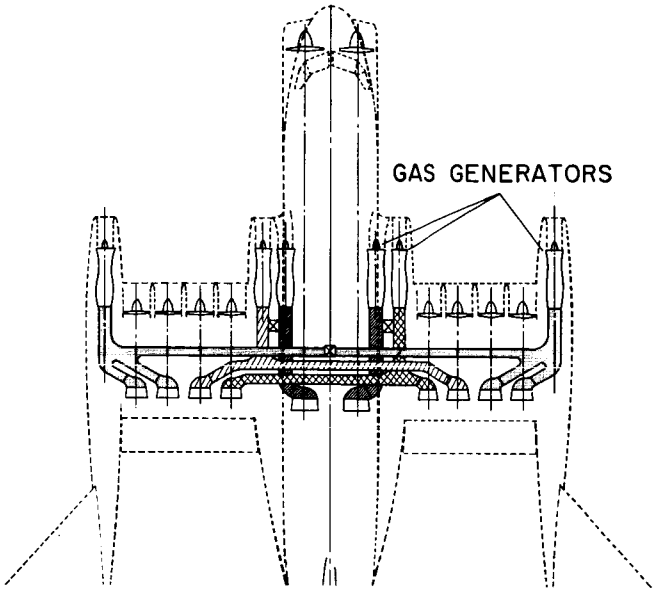

Figure 11

TYPICAL PROPULSIVE WING CROSS SECTION

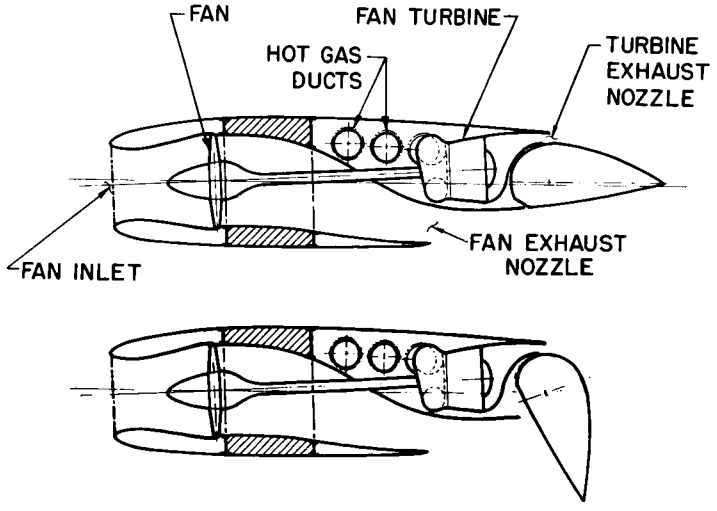

Figure 12

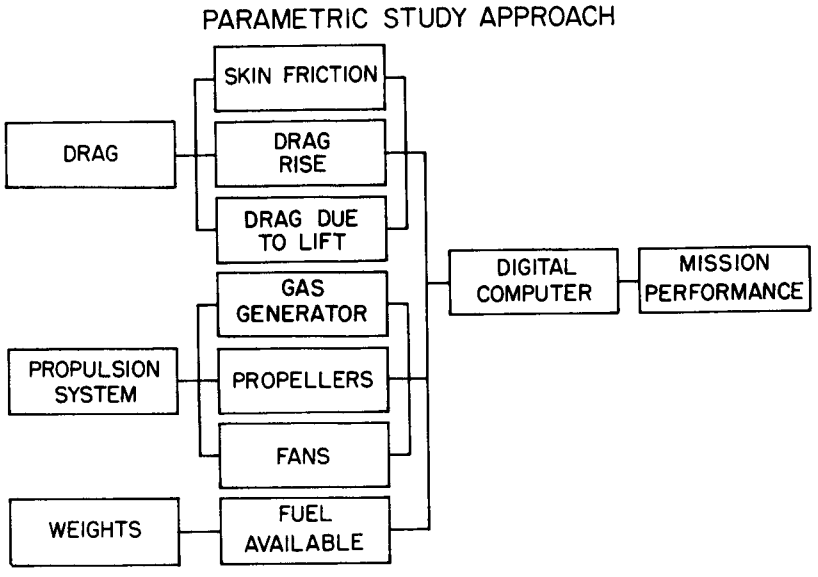

Figure 13

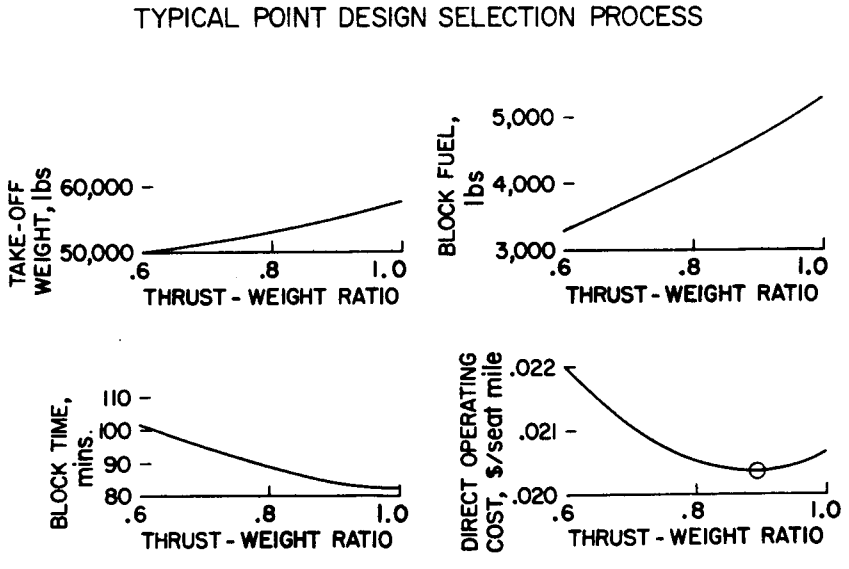

Figure 14

CRITICAL DESIGN CONDITIONS FOR POINT DESIGNS

CONCEPT	DESIGN FIELD LENGTH	CRUISE ALT, FT	CRUISE MACH NO.	CRITICAL DESIGN CRITERIA
TURBOPROP	VTOL	35,000	.59	TAKEOFF VTOL
	V/STOL	25,000	.65	TAKEOFF AS VTOL
	1000 FT STOL	25,000	.615	MIN DOC (CRUISE SPEED)
	2000 FT STOL	25,000	.615	MIN DOC (CRUISE SPEED)
FAN-IN-WING	VTOL	35,000	.8	TAKEOFF VTOL
	V/STOL	35,000	.8	TAKEOFF AS VTOL
	1000 FT STOL	35,000	.8	LANDING
	2000 FT STOL	35,000	.8	TAKEOFF (FAN SIZE), MIN DOC (CRUISE SPEED)
PROPULSIVE WING	1000 FT STOL	35,000	.9	LANDING
	2000 FT STOL	35,000	.9	MIN DOC (CRUISE SPEED)

Figure 15

EFFECT OF PROPELLER CHARACTERISTICS ON DESIGN CRUISE SPEED, TURBOPROP STOL

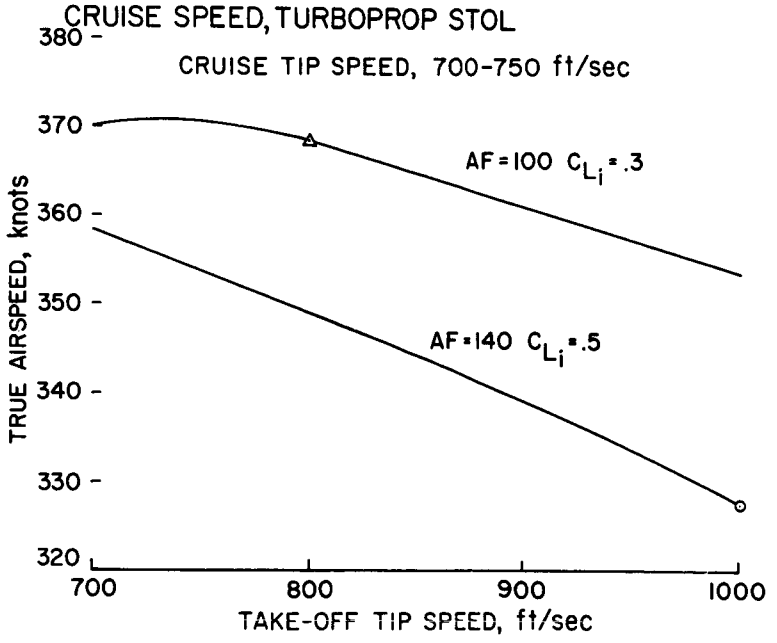

Figure 16

TAKE-OFF DISTANCE OVER 35 FOOT OBSTACLE
TURBOPROP 2000 FT STOL

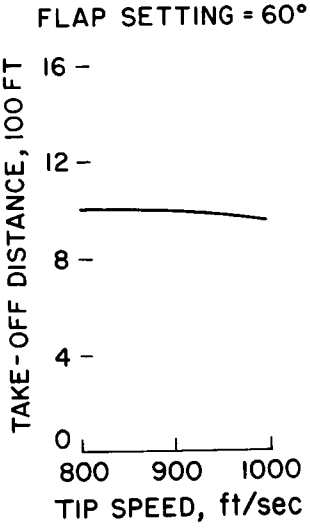

Figure 17

ABILITY OF SPOILERS TO PROVIDE ROLL CONTROL
TURBOPROP 2000 FOOT-NO CROSS SHAFTING
TAKEOFF POWER - OUTBOARD ENGINE FAILED

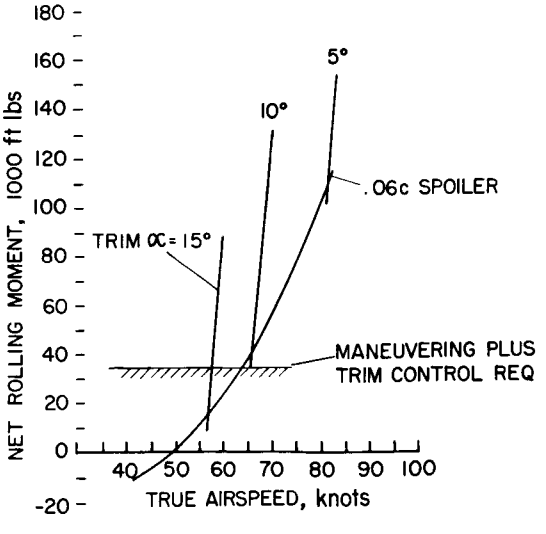

Figure 18

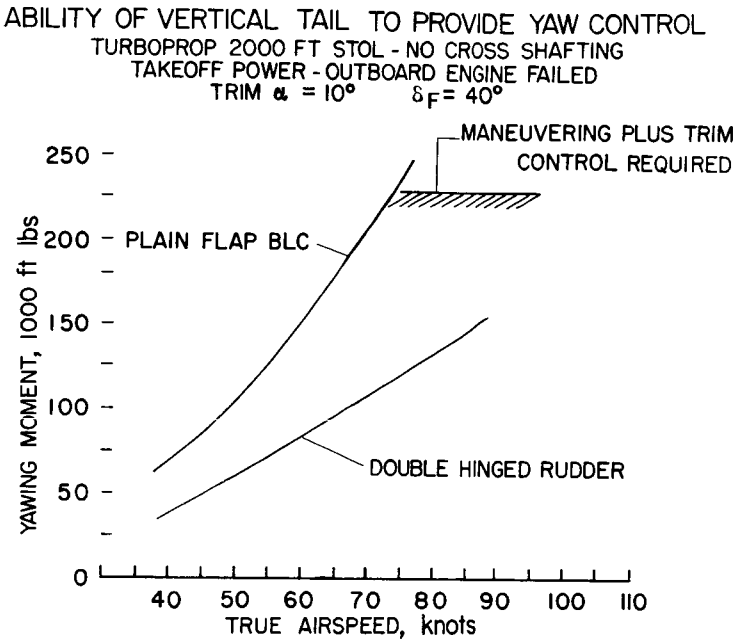

Figure 19

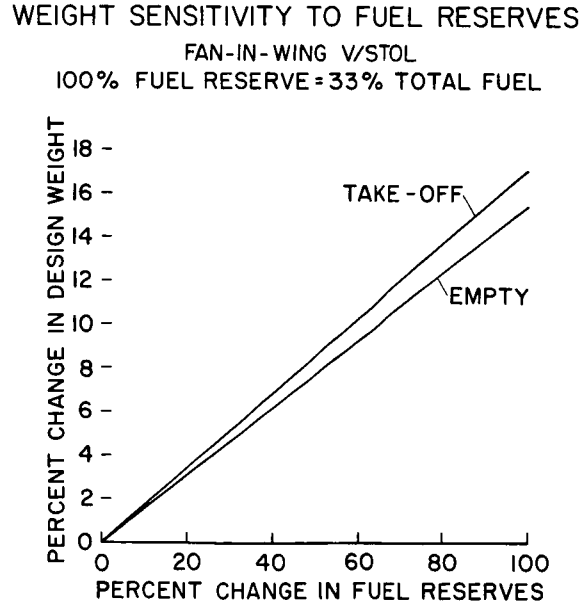

Figure 20

WEIGHT SENSITIVITY TO DRAG AND PROPULSION SYSTEM EFFICIENCY

PROPULSIVE WING 2000 FT

STOL

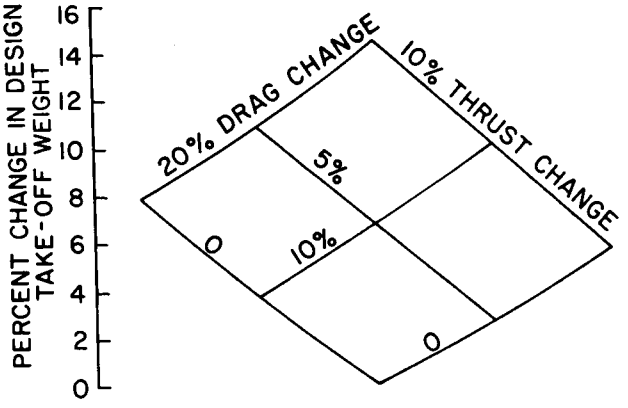

Figure 21

TURBOPROP POWERED POINT DESIGNS

TILT WING VTOL

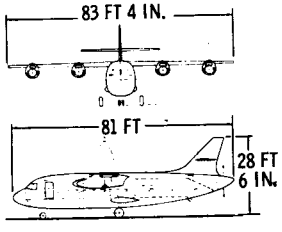

W = 62,300 LBS

AR = 10

W/S = 90 LBS/FT^2

SHP/ENG = 5960

TILT WING V/STOL

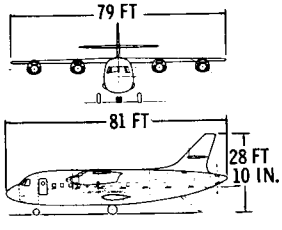

W = 62,115 LBS

AR = 9.23

W/S = 91.8 LBS/FT^2

SHP/ENG = 5540

Figure 22

TURBOPROP POWERED POINT DESIGNS

1000 FT STOL

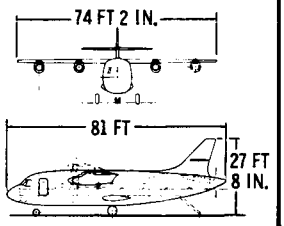

W = 53,783 LBS
$\mathcal{R}$ = 9
W/S = 88.2 LBS/FT^2
SHP/ENG = 3410

2000 FT STOL

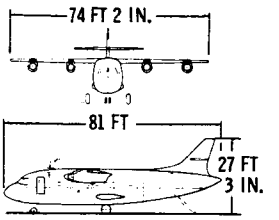

W = 52,758 LBS
$\mathcal{R}$ = 9
W/S = 86.6 LBS/FT^2
SHP/ENG = 3410

Figure 23

FAN-IN-WING POINT DESIGNS

VTOL

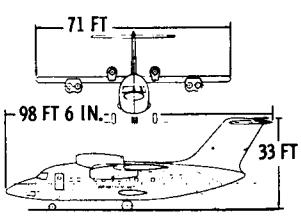

W = 95,327 LBS
$\mathcal{R}$ = 3.73
W/S = 70.6 LBS/FT^2
T/ENG = 7720 LBS

V/STOL

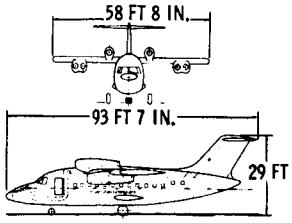

W = 79,587 LBS
$\mathcal{R}$ = 3.44
W/S = 79.6 LBS/FT^2
T/ENG = 6400 LBS

Figure 24

FAN-IN-WING POINT DESIGNS

1000 FT STOL

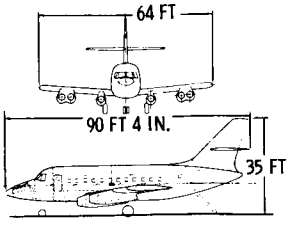

W = 78,919 LBS
$A\!R$ = 3.73
W/S = 71.7 LBS/FT^2
T/ENG = 5710 LBS

2000 FT STOL

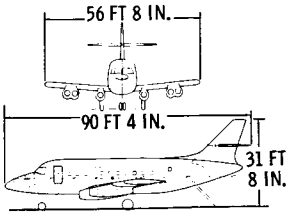

W = 72,110 LBS
$A\!R$ = 3.60
W/S = 80.5 LBS/FT^2
T/ENG = 4600 LBS

Figure 25

PROPULSIVE WING POINT DESIGNS

1000 FT STOL

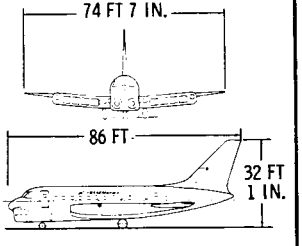

W = 67,451 LBS
$A\!R$ = 3.74
W/S = 87.8 LBS/FT^2
T/ENG = 4700 LBS

2000 FT STOL

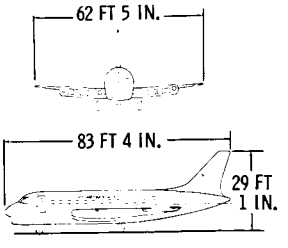

W = 54,963 LBS
$A\!R$ = 3.36
W/S = 95.5 LBS/FT^2
T/ENG = 2540 LBS

Figure 26

GROSS WEIGHT COMPARISONS

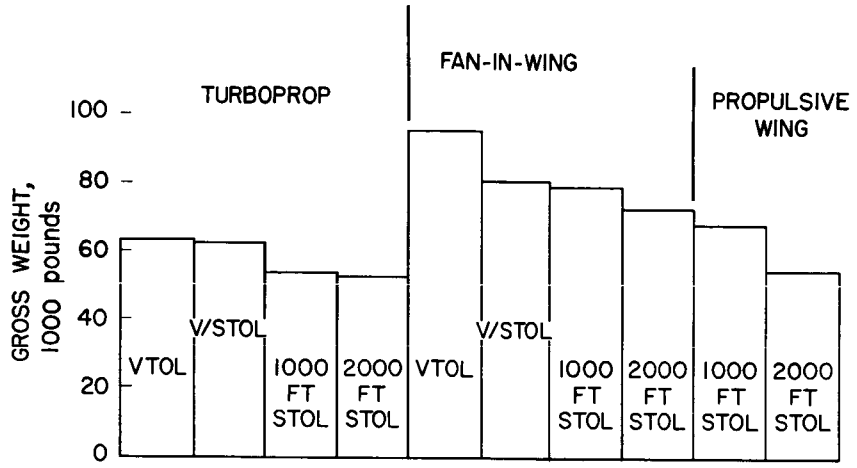

Figure 27

WEIGHT BREAKDOWN COMPARISONS

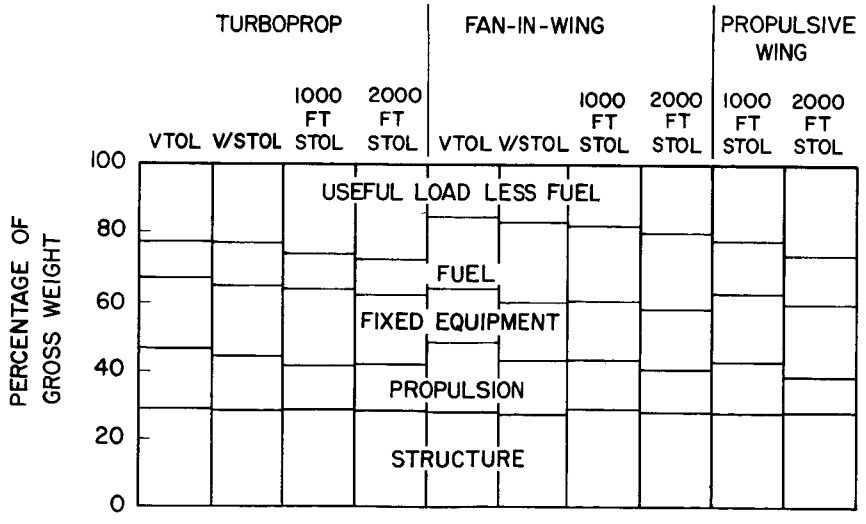

Figure 28

FAR FIELD NOISE CHARACTERISTICS

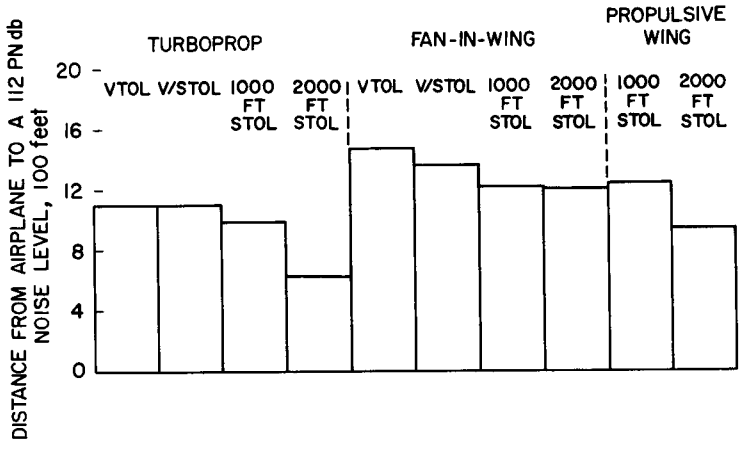

Figure 29

DIRECT OPERATING COSTS

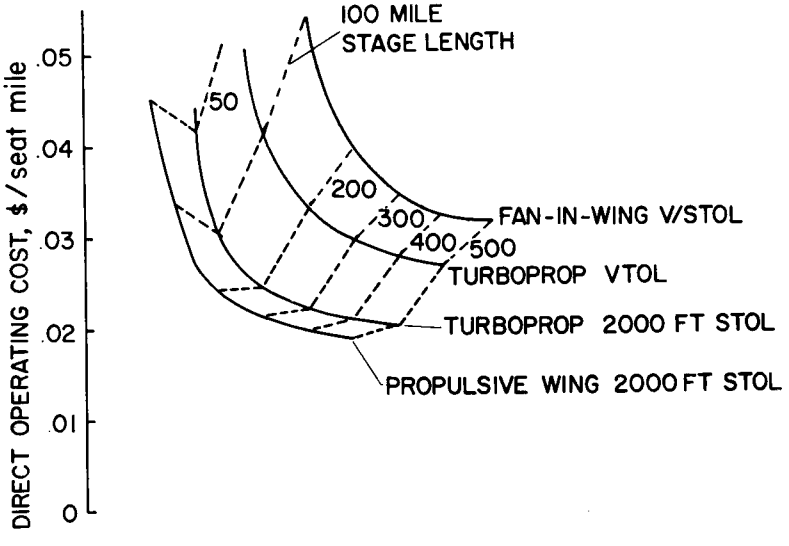

Figure 30

HYPOTHETICAL ROUTE

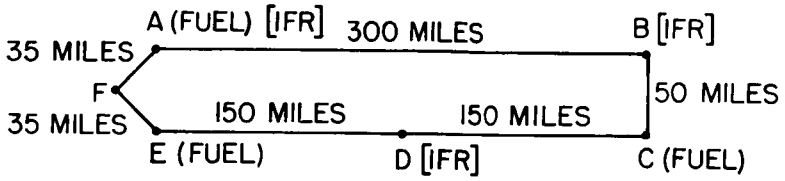

NON PRODUCTIVE TIME

① 10 1/4 MINUTES

② SHORT TAKEOFF 3 MINUTES
VERTICAL TAKEOFF 2 MINUTES
SHORT LANDING 7 1/4 MINUTES
VERTICAL LANDING 2 MINUTES

Figure 31

HYPOTHETICAL ROUTE BLOCK TIME

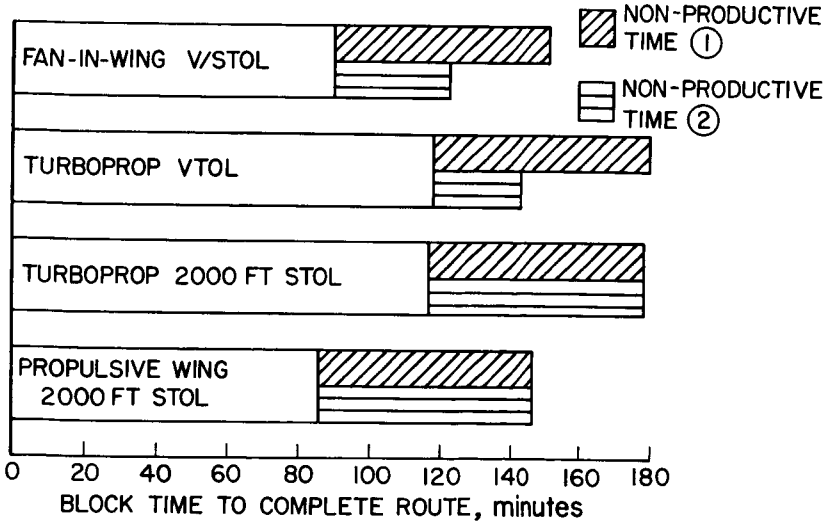

Figure 32

GROSS WEIGHT VARIATION WITH PASSENGER LOAD

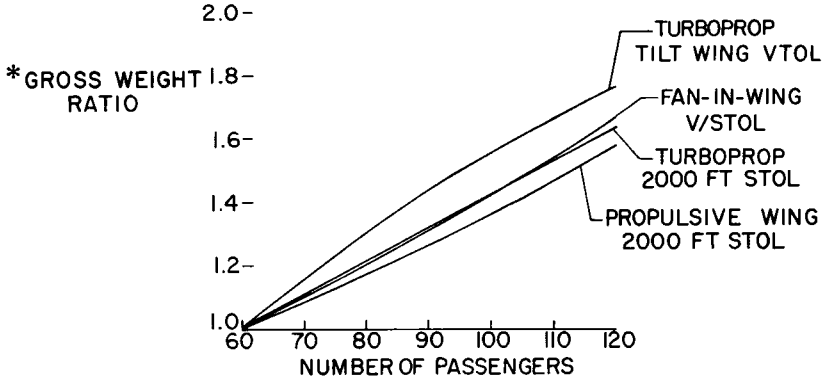

*THE RATIO OF THE GROSS WEIGHT OF AN AIRPLANE DESIGNED TO A PASSENGER LOAD TO THE GROSS WEIGHT OF AN AIRPLANE DESIGNED TO CARRY 60 PASSENGERS

Figure 33

23. NASA-LOCKHEED SHORT-HAUL TRANSPORT STUDY

By Richard Scherrer, Dr. W. C. J. Garrard, Edward M. Davis, and Wm. D. Morrison

INTRODUCTION

The present study was divided into two principal activities. The first was a highly integrated concept-development and vehicle-optimization study. The operational analysis that was conducted was included in this phase. The second phase consisted of the final design work and a series of concurrent sensitivity and trade-off studies.

CONCEPT DEVELOPMENT AND OPTIMIZATION

Each concept was examined in terms of the multitude of subconcepts that dictate vehicle and propulsion system configurations. This process was repeated several times during the study which allowed interim results to be fed back into the concept development process. The major steps in this process will be reviewed in the first two figures.

Turbofan Jet-Flap STOL Concepts

The major steps in developing the STOL concept for 60-passenger vehicles are shown in figure 1. The jet-flap concept initially evolved as a turbojet aircraft with engines located close to the fuselage and manifolded to the trailing-edge nozzles to provide high C_μ and high circulation lift. Tail surfaces were provided with blowing BLC, and a download on the large horizontal tail was used for pitch-trim control. This vehicle weighed about 90,000 pounds for a 1000-foot field, and the evaluation suggested that some method of glide-path control was required to offset the large thrust component from blowing. The evaluation also indicated that turbofan engines, with the fan flow directed downward at the flaps, would provide a more efficient vehicle. Jets were located forward underneath the fuselage to control pitch trim and glide path. The parametric programs resulted in a minimum DOC aircraft weighing 82,600 pounds that was obviously unacceptable; hence, the forward-ducting pitch and glide-path control system was replaced with rotatable nozzles on the engines and the engines were moved slightly further outboard to reduce drag. At the second review the STOL for a 2000-foot field was selected for further study.

Fan-In-Wing STOL Concepts

The major variables for the fan-in-wing STOL configuration were the number and arrangement of fans, and the method of control. To vary fan diameters logically as required in the parametric study and to minimize the wing

weights resulting from incorporating fans into the wing structure, a fixed ratio of fan diameter to wing chord and a fixed chordwise location of the fans was specified for the outboard fans. The number of fans was selected as 4, after consideration of an 8-fan design, and the method of control, after numerous iterations, was selected as reaction type about all axes. This concept remained essentially unchanged throughout the study, and the final design was optimized for the 1000-foot field length.

Deflected Slipstream STOL Concepts

For the deflected slipstream aircraft the task was mainly to select the flap geometry appropriate for a chosen field length. Various flap geometries were evaluated in terms of glide path and stall margin capability. For the parametric study the rather complicated double segment slotted flap of reference 1 was selected for both the 1,000- and 2,000-foot STOL. The 1,000-foot STOL optimized through the parametric study weighed 50,600 pounds. At the second review the 2,000-foot STOL was selected for further evaluation; hence, the flap system was re-evaluated and simplified to a single segment slotted Fowler flap.

Lift/Cruise Fan VTOL Concepts

The steps in the development of the VTOL concepts, corresponding to those of the STOL concepts, are shown in figure 2. Again the data shown are for 60-passenger aircraft optimized for a 500-mile stage length.

Developing the lift/cruise fan concept essentially entailed selection of lift and cruise fan locations. For the parametric study the lift fans were located at a fixed forward position on the fuselage ahead of the wings. The tiltable cruise fans were located on the aft fuselage. At the second review this concept was selected for further study to devise means of reducing the gross weight, improving safety and maintenance, and reducing cruise fuel requirements. This final design incorporated six engines and located the cruise and lift fans in pods at each wing tip. The resulting takeoff gross weight was 71,800 pounds.

Tilt-Wing Turboprop VTOL Concepts

The tilt-wing turboprop concept evolved into two separate concepts because of a desire to consider a range of disk loadings from 10 to 100 pounds per square foot. The extreme wing size that results from using light disk loadings with four nonoverlapped propellers produced the tilt-rotor family as a subcategory of the tilt-wing family. Both types of configurations were included in the optimization program with the result that the lightest and lowest cost four-propeller tilt wing had a gross weight of 73,000 pounds while the corresponding tilt-rotor vehicle had a gross weight of 60,900 pounds and a 17-percent lower direct operating cost. This result led Lockheed to recommend dropping the heavier vehicle from the study. With acceptance of this recommendation, all tilt-wing work was concentrated on the twin-rotor configuration.

The initial tilt-rotor configuration had a tilt wing as well. Later the disk loading was reduced from 25 to 15.5 pounds per square foot to match the final output of the optimization study. With this reduction in disk loading it became practical to fix the wing to the fuselage and only tilt the wing-tip-mounted nacelles.

Stopped Rotor VTOL Concepts

Various rotor and forward propulsion systems were evaluated during the development of the stopped rotor VTOL configuration. The configuration selected for the parametric study incorporated a single folding rotor to allow low disk loadings and incorporated a tail pusher propeller for conventional flight. The final configuration chosen redefined the forward propulsion system to two wing-mounted propellers since the pusher propeller diameter became excessively large for the larger vehicles. In addition, the rotor is folded and retracted down onto the top of the fuselage to minimize drag in cruising flight. The final design for the 60-passenger aircraft resulted in a take-off gross weight of 71,000 pounds.

The best stopped-rotor vehicle has a small wing, like the other VTOL vehicles, and has a disk loading of 10 pounds per square foot. The disk loading is set as the lowest value for which the blades do not require special stiffening provisions for stopping and starting. The blades, however, do have an optimized taper in planform, percent thickness, and in spartube wall thickness. Transition drag considerations determine the size of the propellers for this vehicle; consequently, there are few variables to be optimized. The optimization was relatively flat in terms of disk loading in that values as high as 15 pounds per square foot could have been used with less than 5-percent increase in direct operating cost.

Optimization Study

The optimization study was conducted with the rather extensive use of computers to map the performance characteristics of specific classes of vehicles. A typical set of maps for gross weight, cruise speed, and direct operating cost are shown in figures 3 and 4. For the 1000-foot field deflected slipstream turboprop airplane these maps use wing aspect ratio and propeller diameter as basic variables because a convenient design rule specified a relationship between propeller diameter and wing span.

Performance optimization maps were calculated for all the vehicles in the study and specific design points were chosen on the basis of minimum direct operating cost.

STOL VEHICLE DESCRIPTIONS AND TRADE-OFFS

The three basic STOL aircraft that resulted from the study will be described in terms of performance and operation. In addition, there were

several trade-off and sensitivity studies conducted relative to each vehicle after the final designs were selected. Results of these studies provide insight into the key problem areas of each vehicle and indicate methods for providing improvements.

Turbofan Jet-Flap 2,000-Foot STOL

The 60-passenger vehicle designed for operation from 2,000-foot fields is shown in figure 5. A high wing and wing-mounted nacelles were chosen to minimize aerodynamic ground interference effects, reingestion, and damage caused by foreign objects. The "T" tail configuration is used to minimize the destabilization due to downwash and to minimize jet effects. The gross weight is 63,200 pounds.

Blowing boundary layer control is used on the full span flaps, $C_\mu = 0.2$, rudder and elevator. A leading-edge slot is also provided.

The blowing flow is provided by the exhaust gas of the four scaled GE-1-type turbofan engines (bypass ratio 1.1:1) of 6800 pounds thrust each. The fan flow exhausts through two rotatable vectoring nozzles at the front of the nacelle. The gas generator exhaust duct contains two rotatable vectoring nozzles and a fixed aft nozzle. A valve in the rear duct can divert half the primary gas flow from each engine to a wing manifold. One duct in the wing is in the leading edge of the flap and aileron; the other is between the flap and aileron leading edge and the wing rear beam. A crossover duct in the center fuselage connects with a single duct running aft for tail surface blowing.

Located on the aft fuselage duct are two gas jettison valves, which jettison one-fourth of the manifold gas. Should an engine fail, the jettison valves and the diverter valve of the failed engine close so that the blowing gas flow is the same for three or four engine operation.

The vectoring fan and primary gas nozzles provide cruise thrust, thrust deflection for takeoff, and reverse thrust for descent and landing.

The outboard flaps are used as ailerons; they are deflected from a drooped position which corresponds to the inboard flap deflection, during takeoff and landing. Takeoff and landing speeds are both about 86 knots EAS, at which speed stability and control do not present severe problems.

The variation, with the turbofan bypass ratio, of gross weight, block speed, and DOC is shown in figure 6. The vehicle thrust-to-weight ratio and engine characteristics are maintained constant with the 1.1-to-1 and 6-to-1 bypass ratios. The selected jet-flap STOL aircraft is based on a 1.1-to-1 engine bypass ratio, hence does not represent a fully optimized configuration.

Fan-In-Wing 1000-Foot STOL

The 60-passenger fan-in-wing 1000-foot STOL design is shown in figure 7 and the propulsion system diagram for this vehicle is shown in figure 8.

A high wing is used to minimize reingestion and foreign object damage to the wing mounted lift fans and a T-tail was chosen to reduce destabilization on the horizontal tail due to downwash and to reduce jet effects on the horizontal tail.

The wing is a conventional two-spar torque box except at the lift-fan positions where wing loads are carried by stiffening rings which enclose the fan apertures.

The propulsion system consists of four GE1/J1 gas generators rated at 6488 pounds thrust each, which are used in the normal manner for cruising flight, and are diverted into a common manifold to drive GE variable-stator-area tip-turbine lift fans for takeoff and landing. The lift fans are equipped with inlet doors and vectoring exhaust louvers. The common manifold maintains symmetrical fan lift in case of gas generator failure. When a gas generator fails it is shut off from the system by the diverter valve and the total gas generator exit area is reduced by one quarter by partial closure of the tip turbine and reaction control jet nozzles. Reaction jets at the wing tips and in the fuselage tail, to augment aerodynamic control force about all three axes in low-speed flight, are manifolded into the fan duct system.

Takeoff and initial climb are made using vectored fan thrust from all four fans. The landing sequencing is the reverse of that used for takeoff.

A cruise speed trade-off study, figure 9, considered cruising at various percent powers with the wing thickness and sweep being adjusted to provide suitable critical Mach numbers. The only stage length considered was 500 miles. As the design cruise speed is increased beyond Mach 0.65, the gross weight increases, mainly because the wing thickness is decreased and the sweep increased, to provide higher critical Mach numbers. The increased weight increases DOC but the increased block speed has an opposite effect, so that the DOC decreases up to a cruising speed of Mach 0.75 and increases about this speed.

The sensitivity of direct operating cost to maximum lift coefficient, with fixed aspect ratio, is shown in figure 10.

Raising the $C_{L_{max}}$ 10 percent above the selected value reduces the DOC by 4 percent. This gain suggests that the use of blowing type flaps could possibly lead to significantly lower DOC.

The importance of $C_{L_{max}}$ for the fan-in-wing vehicle, and the importance of bypass ratio for the jet-flap vehicle suggests that, with further study, these two concepts might merge into one.

Deflected Slipstream 2,000-Foot STOL

The general arrangement of the 60-passenger 2,000-foot STOL, deflected slipstream design is shown on figure 11. The gross weight is 46,900 pounds.

The aircraft is a conventional high wing configuration with 4 interconnected, 4-bladed, 14-foot-diameter propellers driven by 4 turboshaft engines rated at 1275 shp each. The engine drive is transmitted through a clutch and the shafts, which are connected to each propeller by a clutch.

Full-span, constant-chord, Fowler flaps are utilized. The flap chord is 40 percent of the average wing chord. The location of the propellers relative to the wing is selected to optimize maximum lift.

The aircraft utilizes 50-percent-chord elevators and a movable stabilizer interconnected to the flap for pitch control and trim, and a 40-percent-chord rudder with blowing boundary layer control for yaw control. Constant-chord full-span wing spoilers are used differentially for roll control. The rudder blowing air is supplied by engine compressor bleed.

The takeoff speed is 68 knots EAS and the approach speed is 86 knots EAS. Preliminary analysis indicates that, as a minimum, sideslip rate damping is required to provide satisfactory low-speed handling qualities.

The first trade-off study results are shown in figure 12. A significant increase in block speed and hence a small reduction of DOC can be obtained by increasing the cruise power and flat rating the engines so that the takeoff distance is not changed. This study assumed that installed engine power to gross weight ratio is increased, to 1.5 and 2 times that of the basic vehicle level, without changing the takeoff power to gross weight ratio. This revision does not significantly change the takeoff performance or the transmission and gear-box weight but provides higher power for cruise at higher altitudes.

For a small increase in power the appreciable improvement in both cruise and block speeds more than compensates for the higher vehicle gross weight and fuel cost. Larger increases in power do not provide equivalent speed advantages.

The data in figure 13 show the variation of gross weight with field length for aircraft with and without cross shafting. The effect on the gross weight and takeoff distance of removing the cross shafting was determined for the three designs considered in the field length trade-off study. Each of these designs was reweighed without cross shafting, with the vertical tail increased to provide directional trim at the takeoff engine failure speed, with an outboard engine failed and the remaining engines at 110 percent of the normal takeoff power. Takeoff is the critical case, since the landing field length of all designs considered is equal to or less than that for takeoff at the design gross weight. The effect of cross shafting on lift is more significant than on directional or roll control.

VTOL VEHICLE DESCRIPTIONS AND TRADE-OFFS

Three VTOL vehicle concepts were considered in this analysis, a lift/cruise fan concept and two rotary wing types, a tilting rotor vehicle, and a stopped and folded rotor craft. All were sized to perform a 500-mile mission and optimized to realize minimum DOC.

Lift/Cruise Fan VTOL

Figure 14 shows the general arrangement of the 60-passenger, 6-engine lift/cruise fan VTOL. Figure 15 is a schematic drawing of the propulsion system for that aircraft.

To realize a reasonable balance between requirements for hovering with 1 engine out and efficient cruise for minimum DOC, 6 engines were selected, 3 in each wing-tip nacelle. Supplemental lift and cruise thrust is provided by a shaft-driven fan in each nacelle. Two tip-driven fans provide direct lift. The lift-fan design pressure ratio is 1.3 and the cruise-fan design pressure ratio is 1.4. Each cruise fan is driven by a four-stage turbine. The cruise fan discharges through two swivelling-type nozzles which are vectored down for lift and aft for cruise. The cruise-fan nozzles and lift-fan exit louvers are vectored to control lift, roll, and transition. In the hover mode the air flow from the two fans in each nacelle is converged to achieve lift differential for roll control. This convergence will reduce lift at one nacelle, for 50-percent control power, by 15 percent without changing power settings.

Pitch and yaw control are provided by jet nozzles at the tail cone from the coupled gas generators. Cruise is performed with but one gas generator per nacelle in operation driving the shaft-driven cruise fans.

The high power and fuel requirements for the lift/cruise fan concept result in significant effect on DOC when propulsion system characteristics are varied. Changes to unit engine costs will have an overwhelming effect on DOC as shown in figure 16 wherein a doubling of engine cost will reflect a 22-percent increase in DOC.

Control power requirements for the lift/cruise fan concept at approximately 20 percent of the total installed power affect the DOC as shown in figure 17. A 25-percent increase equals 8-1/2-percent increase in DOC. Gross weight effect is approximately at the same percentage as shown for DOC. Block speed effect is negligible.

The various levels of control power indicated were achieved by varying the thrust capability of jet reaction controls in all three axes. The amount of engine gas bleed-off and the total installed propulsion power requirements were adjusted to satisfy the new control conditions.

Tilt Rotor

In this concept (fig. 18) two rotors operating at a disk loading of 15 pounds per square foot for hover are mounted on tip nacelles each containing two turboshaft engines. The nacelles are rotated forward during transition to cruise flight. Each pair of engines is connected by cross shafting through overrunning clutches. The cross shaft is sized to accept one-half the power output of one engine to permit equal power distribution to the rotors during engine out operation. The engine nacelles are rotated by the action of high ratio harmonic drives powered by a hydraulically actuated drive shaft connecting the nacelles.

Rigid rotors with integral control gyros provide good handling qualities in hover and preclude whirl-mode aeroelastic interactions with the wing. Both normal and side forces on the rotors with angle of attack and sideslip are essentially eliminated.

In the helicopter mode, control in the roll, pitch, and yaw axes is provided, respectively, by collective pitch control, cyclic pitch control, and differential cyclic pitch control. Conventional control surfaces coupled with rotor controls are used in the airplane mode.

The rotor tip speed is 900 feet per second for hover, reducing to approximately 5/8 of that value at transition to keep advancing tip Mach numbers within acceptable values and to maintain high rotor efficiency in the cruise mode. Rotor speeds are varied with turbine RPM changes. Analysis has shown that the slight losses in turbine efficiency will result in weights approximately equal to those of the gear shift mechanism required if constant speed turbines were used.

On the ground the engine nacelles must be in the up position in order to provide the necessary rotor clearance with the ground. A safe emergency landing with the rotor disks located in the cruise position is questionable.

The tilt-rotor VTOL DOC is quite sensitive to engine rated shaft horsepower (flat rated) as shown in figure 19. The engine shaft horsepower has been increased up to two times the basic design vehicle horsepower level; however, the maximum horsepower output to the transmission and gear boxes was limited to its previous value. This revision did not modify the power available at takeoff but provided additional power to the propellers for cruise at higher altitudes. The block speed rises rapidly at first but is more than compensated by a 12-percent increase in gross weight attributable mainly to higher fuel weight increments.

Stopped Rotor VTOL

As shown in figure 20, hover lift for the stopped rotor VTOL aircraft is provided by the single three-bladed rotor operating in a helicopter mode. In cruising flight, the rotor is unloaded, folded, and stowed above the fuselage. Conventional winged flight and conventional controls are used in the cruising mode. The propulsion system consists of four free-turbine turboshaft engines

driving the two tractor propellers, the main rotor, and the antitorque rotor systems through individual overrunning clutches. The rotors are each connected to the systems by a brake and clutch which are operated when the rotor system is unloaded and folded for cruise. Full-span flaps are used to relieve wing downloads in hover and to improve wing $C_{L_{max}}$ during transition and during emergency wing-lift landings. The maximum rotor and propeller tip speeds are 800 and 900 feet per second, respectively. Hover disk loading is 10 pounds per square foot. The transition from rotary to fixed wing flight is performed at 130-140 knots at which time the propeller pitch is increased and the rotor collective is decreased to effect the transfer of power.

The rigid rotor principle with free gyro control phasing into an aerodynamic control as RPM is reduced permits stopping of the blades in flight during transition. The stopped rotor aircraft is capable of landing in an STOL mode with rotors folded as an emergency operation.

NOISE

In developing the common basis for comparison of noise for the vehicles, the propeller selection criteria, tip speed (900 fps), and blade loading coefficient ($C_T/\sigma = 0.12$) in effect became noise criteria for propeller and rotor type vehicles. There was no equivalent criteria for the jet type vehicles. All the noise data are given in perceived noise levels as specified in references 2 to 5.

The noise data for six 60-passenger vehicles are compared in figure 21. This comparison is based on selection of the radial noise distribution from the source along the peak intensity rays. For STOL aircraft these rays extended in the rear quadrants from the aircraft, whereas, for the VTOL aircraft the lateral rays are representative. All data are shown for maximum static thrust which is the noisiest operating condition. The jet flap has the highest noise level because of the low bypass ratio (1.1:1) for the example aircraft. The fact that noise decreases with increasing bypass ratio, and better vehicle performance has been shown at higher bypass ratios, indicates that quieter jet-flap aircraft can be provided. The deflected slipstream has a high noise level because of tip speed, but also because of the large amount of energy at low frequencies. (The perceived noise level computational technique contains weighting factors that penalize vehicles that create low frequency noise because such noises are more objectionable than those at higher frequencies.) The tilt-rotor vehicle produces even lower frequency noise than the deflected slipstream type but it has a significantly lower disk loading and thus a lower noise level. Significant reductions in noise could be provided by reducing the design tip speed to 800 feet per second. Lift fans such as used in the fan-in-wing and lift/cruise fan vehicles produce high frequency noise that is both favored by the definition of perceived noise level and attenuates rapidly with distance. As a result, the lift/cruise fan with many times the installed power of the tilt-rotor vehicle appears to have a similar noise level. The lowest noise level in the present study is

provided by the stopped rotor vehicle because of its light disk loading (10 lb/sq ft) and low tip speed (800 fps). Values only slightly above those for current helicopters are indicated.

The comparison shown in figure 21 was only for maximum static thrust; however, the noise in low altitude transit over populated areas is also of concern. At a speed of 200 knots at 1000 feet altitude, almost all the vehicle concepts will produce less noise than at takeoff but the quietest is expected to be the tilt rotor because of the 40-percent reduction in tip speed in cruise and the large reduction in blade loading that is a characteristic of this vehicle concept.

The operational analysis conducted as part of the present study disclosed that noise should be considered a primary design requirement for commercial V/STOL transport. Since none of the vehicles in the present study have completely acceptable noise characteristics some future study should probe the impact of requiring some low perceived noise level, such as 100 PNdb, on vehicle weights and direct operating costs.

PRIMARY RESEARCH PROBLEMS

All the vehicles that have been studied have numerous research problems. For the purpose of this paper only the most important research problem will be discussed for each vehicle (see fig. 22).

The jet flap STOL vehicle has been refined to a point where the 2000-foot field-length requirement can be met at a blowing momentum coefficient of 0.2. Since a C_μ of 0.04 is generally regarded as sufficient to prevent separation for a large flap deflection, more detailed investigations of blowing distributions, particularly over leading-edge devices, should raise lift coefficients and reduce pitching moments.

The fan-in-wing and lift/cruise fan vehicles share a common problem which is the operation of the complete engine and ducting system. Static performance of such systems is relatively simple to compute but the dynamics of such systems with relatively long pipes, multiple engine, and a multitude of control valves cannot be predicted or controlled with complete confidence.

Performance of the deflected slipstream vehicles in the present study could be improved by providing multiple slots at both hinge lines of such double-extension flaps. Such multislot designs appear to offer significantly reduced flap chords and weight for a given performance.

The tilt-rotor vehicle can have a potential problem called rotor-tip-path-plane instability. This instability is a strong function of disk loading, being extreme at a disk loading near 5 pounds per square foot and essentially nonexistent at a disk loading of 25 pounds per square foot.

The stopped rotor concept is important when high cruise speed and light disk loadings are required in a single vehicle. The primary problem for this

class of vehicle is rotor weight as affected by starting and stopping loads. Theoretical studies of loads on stabilized stopping rotors have shown that there is little weight increase due to providing stopping capability when the blades are provided with the optimum taper in planform, thickness, and structural gage. Additional experimental research is needed to provide the thorough comparisons that are needed for complete confidence in design procedures.

These typical programs indicate that NASA can make significant contributions to all the vehicles studied and, in fact, the success of these vehicles will depend significantly upon NASA Research.

VEHICLE COMPARISON

One of the objectives of the present study in each of the STOL and VTOL categories is to determine which concepts are most suitable for commercial transports. In support of this objective each of the vehicles has been judged on a variety of criteria on as consistent a basis as possible.

Considering STOL vehicles (fig. 23) the DOC includes effects of gross weight and block speeds but these are included on the figure because they have additional implications. The other selection criteria are more difficult to evaluate in that they include a cross section of opinions of a large number of people. A rating scale of 10 down to 1 is used for safety, service and maintenance, noise, and developability (or development risk). For the STOL vehicles there are small differences in these qualitative parameters. As a result, the order of preference is based largely on two factors; first, cruise speed as it affects passenger preference, and, second, direct operating costs. It should be noted that slight changes in design criteria, such as reduction of design range, could reverse the order of preference of the first and second place vehicles.

The VTOL vehicle comparison (fig. 24) has a somewhat wider spread in direct operating costs and in safety and service as well. The relative qualitative ratings happen to coincide with the DOC trend. Both the tilt-rotor and the stopped-rotor vehicles have definite advantages relative to each other.

The operation of the VTOL and STOL aircraft over a hypothetical route having a sequence of stage lengths of 35, 35, 150, 150, 50, and 300 statute miles results in relative-direct operating costs that are significantly different from those for a 500-mile stage length. In making a comparison, the VTOL aircraft were assigned a nonproductive time of 2 minutes at each stop and the STOL aircraft, because of taxi time, were assigned a 4-minute nonproductive time. The direct operating costs for 120-passenger aircraft, ratioed to that of the deflected slipstream airplane for both routes are shown below, in the order of increasing costs.

Cost ratios	
Hypothetical route	500-mile stage length
1.0	1.0
1.06	1.18
1.30	1.20
1.37	1.47
1.50	1.38
1.64	1.60

Deflected slipstream (2000 ft)
Tilt rotor (VTOL)
Turbofan jet flap (2000 ft)
Stopped rotor (VTOL)
Fan in wing (1000 ft)
Lift/cruise fan (VTOL)

The short stage lengths of the hypothetical route structure and the assigned nonproductive times favor the rotary wing VTOL vehicles. As can be seen in the above table, the tilt rotor VTOL cost is only 6 percent above that of the minimum cost vehicle in the study. The best conclusion that can be drawn is that rotor-type short-haul transports are the best of the VTOL types and are competitive with the best STOL-type short-haul transport.

CONCLUSIONS

The design, operational, and economic aspects of several V/STOL and STOL configurations have been evaluated to determine the suitability of the aircraft for use as commercial short-haul transports. Within the guidelines and scope of the study, several conclusions are drawn and these are listed in figure 25.

REFERENCES

1. Kuhn, Richard; and Hayes, William C.: Wind-Tunnel Investigation of Longitudinal Aerodynamic Characteristics of Three Propeller-Driven VTOL Configurations in the Transition Speed Range, Including Effects of Ground Proximity. NASA TN D-55, 1960.

2. White, Donald S.: General Procedures for Estimation of Noise Levels for New Turbine Engined Designs. Pratt and Whitney Aircraft Report PWA 2321.

3. Sowers, H. D.: Investigation of Methods of Prediction and Alleviation of Lift-Fan Noise. U.S. Army Trecom Tech. Rep. 65-4.

4. Harris, C. M.: Handbook of Noise Control. McGraw-Hill Book Company.

5. Maglieri, D. J.; and Hubbard, H. H.: Preliminary Measurements of Noise Characteristics of Some Jet Augmented Flap Configurations. NASA MEMO 12-4-58L, 1959.

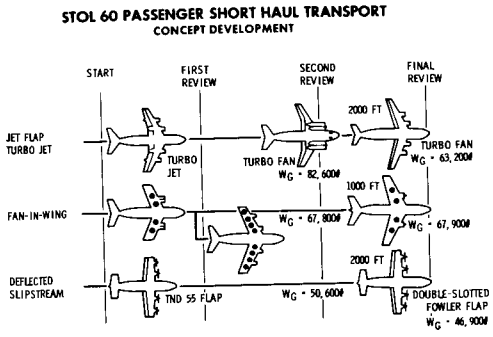

Figure 1

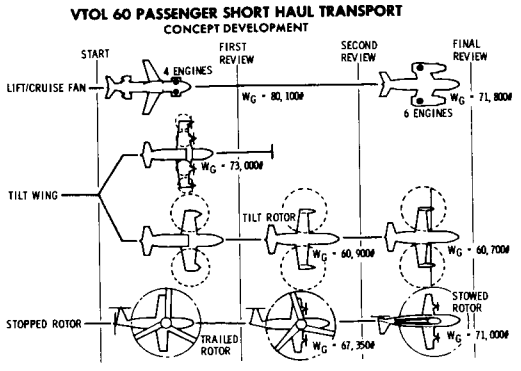

Figure 2

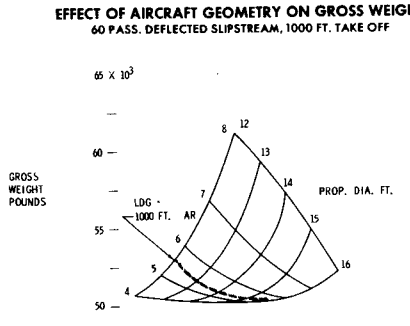

Figure 3

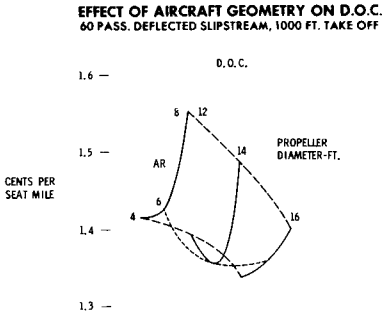

Figure 4

60 PASSENGER TURBOFAN JET FLAP STOL
GENERAL ARRANGEMENT

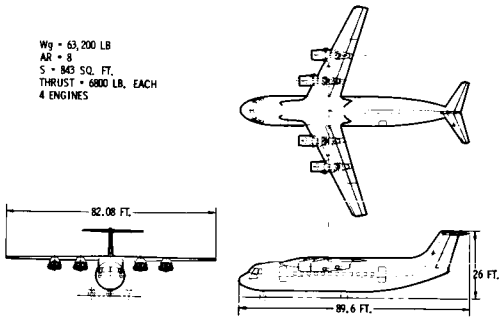

Figure 5

EFFECT OF ENGINE BY-PASS RATIO ON D.O.C.
2000 FT. T.O. JET FLAP AIRPLANE

BYPASS RATIO	% GROSS WT. CHANGE	V_{BLOCK}, KNOTS	% DOC CHANGE
1.1 TO 1	-	368	-
6.0 TO 1	-10.9	356	-5.5

Figure 6

60 PASSENGER FAN-IN-WING STOL
GENERAL ARRANGEMENT

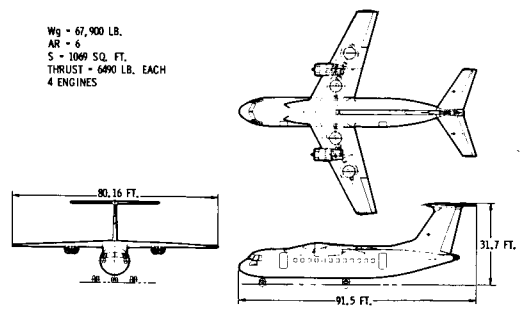

Figure 7

60 PASSENGER FAN-IN-WING STOL
PROPULSION SYSTEM DIAGRAM

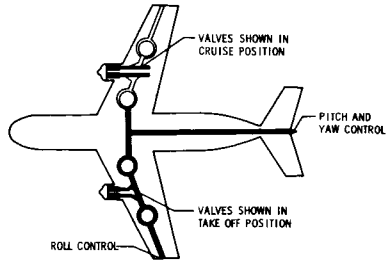

Figure 8

EFFECT OF CRUISE SPEED ON D.O.C.
1000 FT. T.O. FAN-IN-WING AIRPLANE

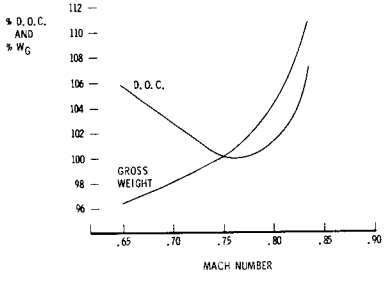

Figure 9

EFFECT OF C_L MAX. ON D.O.C.
1000 FT. T.O. FAN-IN-WING AIRPLANE

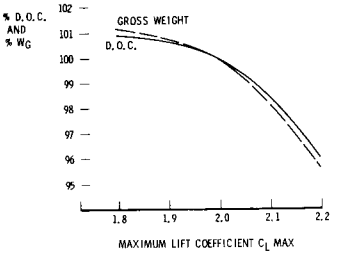

Figure 10

60 PASSENGER DEFLECTED SLIPSTREAM STOL
GENERAL ARRANGEMENT

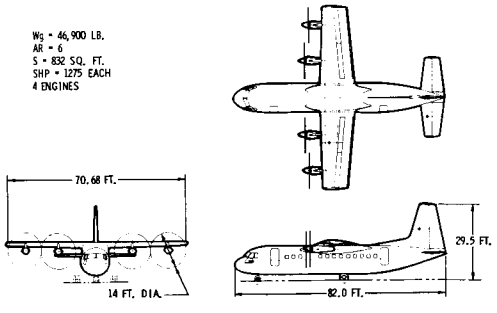

Figure 11

EFFECT OF INCREASED INSTALLED POWER ON D.O.C.
2000 FT. T.O. DEFLECTED SLIPSTREAM AIRCRAFT
WITH FLAT - RATED ENGINES

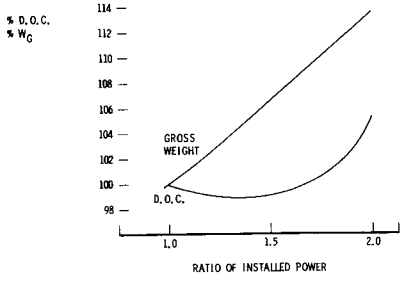

Figure 12

EFFECT OF CROSS SHAFTING ON TAKEOFF GROSS WT.
DEFLECTED SLIPSTREAM STOL AIRCRAFT

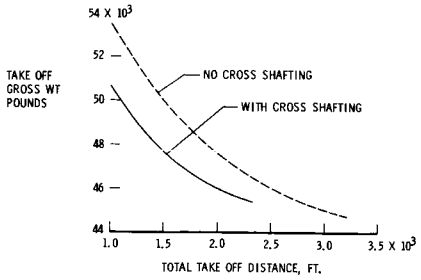

Figure 13

60 PASSENGER LIFT/CRUISE FAN VTOL
GENERAL ARRANGEMENT

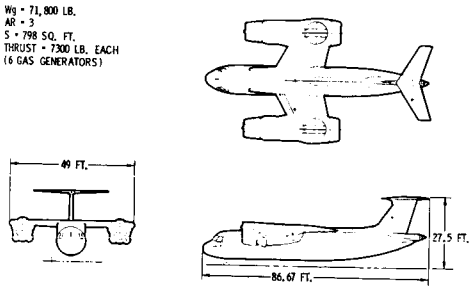

Figure 14

60 PASSENGER LIFT/CRUISE FAN VTOL
PROPULSION SYSTEM DIAGRAM

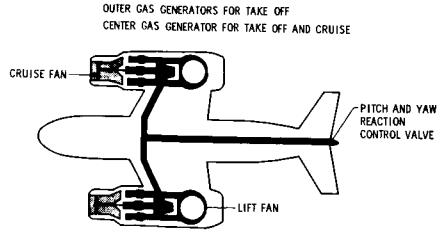

Figure 15

EFFECT OF ENGINE COST ON D.O.C.
LIFT/CRUISE FAN VTOL

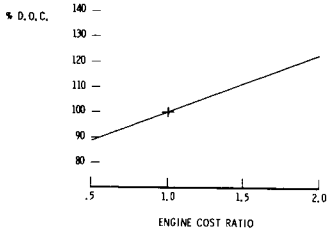

Figure 16

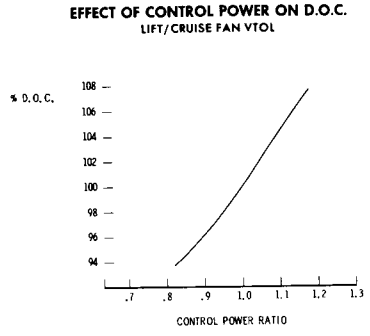

Figure 17

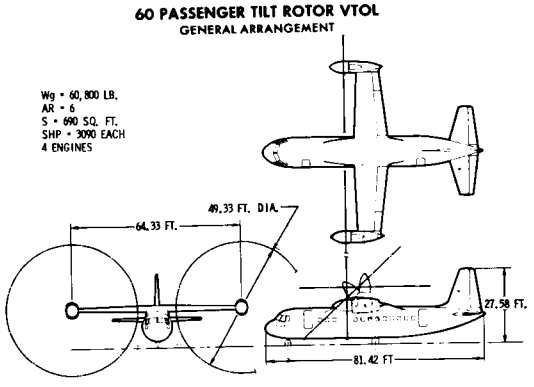

Figure 18

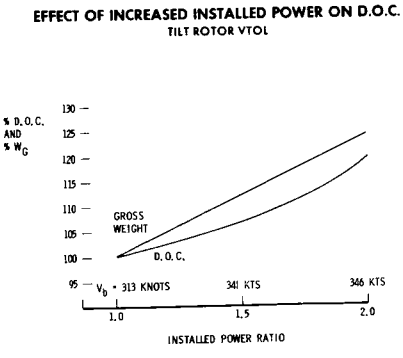

Figure 19

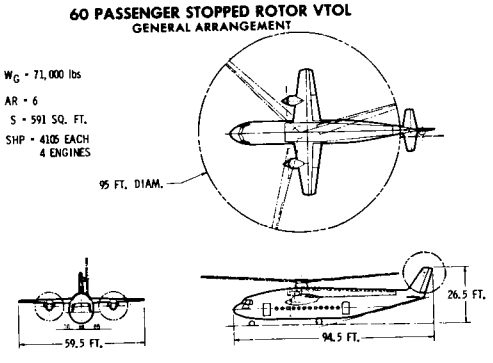

Figure 20

COMPARISON OF PEAK NOISE LEVELS - 60 PASS. AIRCRAFT
MAX. STATIC THRUST - S.L. STD. DAY

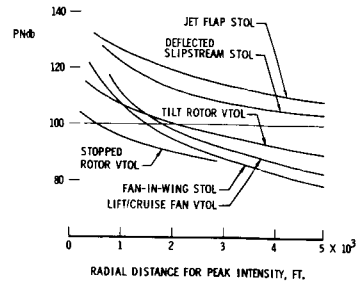

Figure 21

PRIMARY DESIGN-ORIENTED RESEARCH

VEHICLE	RESEARCH PROBLEM
JET FLAP, STOL	HIGHER LIFTS AT LOW C_μ AND REDUCED PITCHING MOMENTS
FAN-IN-WING, STOL	GAS DUCTING SYSTEM OPERATION FOR STARTING, LIFT AND CONTROL
DEFLECTED SLIPSTREAM, STOL	IMPROVED DOUBLE-EXTENSION FLAPS
LIFT-CRUISE FAN, VTOL	GAS DUCTING SYSTEM OPERATION FOR STARTING, LIFT AND CONTROL
TILT-ROTOR, VTOL	BASIC UNDERSTANDING AND CONTROL OF TIP-PATH-PLANE STABILITY
STOPPED-ROTOR, VTOL	EXPERIMENTAL VERIFICATION OF THEORETICAL STOPPING AND STARTING LOADS

Figure 22

COMPARISON OF STOL AIRCRAFT

	2000 FT. JET FLAP		1000 FT. FAN-IN-WING		2000 FT. DEFLECTED SLIPSTREAM	
NUMBER OF PASSENGERS	60	120	60	120	60	120
W_G, POUNDS	63,200	120,000	67,900	124,000	46,900	86,400
V_{BLOCK}, M.P.H.	424	425	440	444	281	279
D.O.C., ¢/SEAT MILE	2.26	1.77	2.67	2.04	1.96	1.47
FAIL SAFETY	10		9		10	
SERVICE/MAINTENANCE	10		9		10	
TAKE OFF NOISE	8		10		8	
DEVELOPMENT RISK	9		8		10	
PREFERENCE	FIRST		THIRD		SECOND	

Figure 23

COMPARISON OF VTOL AIRCRAFT

	LIFT/CRUISE FAN		TILT ROTOR		STOPPED ROTOR	
NUMBER OF PASSENGERS	60	120	60	120	60	120
W_G, POUNDS	71,800	141,600	60,800	113,500	71,000	134,000
V_{BLOCK}, M.P.H.	409	409	360	377	339	345
D.O.C., ¢/SEAT MI.	2.87	2.36	2.35	1.75	2.81	2.16
FAIL SAFETY	8		9		10	
SERVICE/MAINTENANCE	7		10		8	
TAKE OFF NOISE	8		9		10	
DEVELOPMENT RISK	9		9		10	
PREFERENCE	THIRD		FIRST/SECOND		FIRST/SECOND	

Figure 24

CONCLUSIONS

- FURTHER IMPROVEMENTS POSSIBLE IN REDUCED GROSS WEIGHT AND COMMERCIAL SUITABILITY
- ORDER OF PREFERENCE - STOL:
  1. JET FLAP
  2. DEFLECTED SLIPSTREAM
  3. FAN-IN-WING
- ORDER OF PREFERENCE - VTOL:
  1. ROTARY WING TYPES
  2. LIFT/CRUISE FAN
- SIGNIFICANT R AND D, DESIGN REFINEMENTS REQUIRED BEFORE COMMERCIAL USE ACCEPTABLE
- ACCEPTABLE COMMUNITY NOISE A MAJOR DESIGN CRITERION

Figure 25

Page intentionally left blank

24. WIND-TUNNEL BOUNDARY INTERFERENCE FOR V/STOL TESTING

By Harry H. Heyson and Kalman J. Grunwald

NASA Langley Research Center

SUMMARY

The wake skew angle used in applying the theory of NASA TR R-124 to data correction should be such that the angular deflection of the wake vorticity from the horizontal is one-half that calculated from momentum theory at the lifting element. This usage is in contrast to that of the original paper which used the angle of the mass flow. Because of large-scale recirculation effects, there is a finite lower limit to the test speed at which reliable and correctable data can be obtained in closed wind tunnels. Although a zero-correction wind tunnel for V/STOL testing has not yet been achieved, it is shown that the use of suitably mixed wind-tunnel boundaries can alleviate boundary effects on V/STOL data.

INTRODUCTION

The very slow speed regimes of flight give the aerodynamicist some of his most difficult problems. The small perturbation assumptions inherent in almost all configuration studies begin to break down, and extreme interferences appear to exist between the various aerodynamic components of the aircraft. As a result, the wind tunnel is almost the only means of determining, even approximately, the performance and stability of the entire aircraft.

Unfortunately, wind-tunnel results are not identical to the results obtained in flight because of the wind-tunnel boundaries in close proximity to the model. The purpose of the present paper is to examine experimentally the adequacy of current theory in predicting the effect of the wind-tunnel boundaries on the data from specific models. In addition, some information is presented on the degree of relief from corrections which can be obtained by appropriate slotting and opening of the wind-tunnel walls.

The present paper is limited to the effect of the wind-tunnel boundaries upon model data. In particular, no attempt is made to evaluate the problems of scaling or model detailing on the extrapolation of model data to full-scale Reynolds numbers.

SYMBOLS

A_M momentum area of lifting system

A_T cross-sectional area of wind-tunnel test section

B	semiwidth of wind-tunnel test section
C_L	lift coefficient, L/qS
$C_{N,t}$	tail normal-force coefficient, $\frac{\text{Tail normal force}}{qS}$
C_μ	jet momentum coefficient, $\frac{(\text{Jet mass flow})(V_j)}{qS}$
ΔC_μ	difference between corrected and uncorrected values of C_μ
$\bar{c}$	mean aerodynamic chord
H	semiheight of wind-tunnel test section
L	lift
M_Y	pitching moment, positive nose up
q	dynamic pressure
R	rotor radius
S	wing area
T_s	static thrust
V	tunnel velocity
V_j	jet velocity
$V_{j,s}$	jet velocity in static thrust
u_o	mean or momentum-theory value of longitudinal induced velocity at model, positive rearward
Δu_D	longitudinal interference velocity due to drag, positive rearward
Δu_L	longitudinal interference velocity due to lift, positive rearward
w_o	mean or momentum-theory value of vertical induced velocity at model, positive upward
Δw	vertical interference velocity (general), positive upward
Δw_D	vertical interference velocity due to drag, positive upward

Δw_L vertical interference velocity due to lift, positive upward

x distance rearward from center of lift

α angle of attack

$\Delta\alpha$ correction to angle of attack resulting from presence of wind-tunnel boundaries

γ ratio of wind-tunnel width to wind-tunnel height, B/H

δ jet-boundary correction factor, defined by equation $\Delta\alpha = \delta \frac{S}{A_T} C_L$; also, jet-boundary correction factor (general)

$\delta_{u,D}$ correction factor for longitudinal interference due to drag, defined by equation $\Delta u_D = \delta_{u,D} \frac{A_M}{A_T} u_o$

$\delta_{u,L}$ correction factor for longitudinal interference due to lift, defined by equation $\Delta u_L = \delta_{u,L} \frac{A_M}{A_T} w_o$

$\delta_{w,D}$ correction factor for vertical interference due to drag, defined by equation $\Delta w_D = \delta_{w,D} \frac{A_M}{A_T} u_o$

$\delta_{w,L}$ correction factor for vertical interference due to lift, defined by equation $\Delta w_L = \delta_{w,L} \frac{A_M}{A_T} w_o$

χ angle between vertical and angle of wake at model

χ_{eff} effective skew angle, $\frac{\chi + 90^o}{2}$

RESULTS AND DISCUSSION

Review of Theory

The classical corrections to wind-tunnel data (for example, ref. 1) are applied according to the equation

$$\Delta\alpha = \delta \frac{S}{A_T} C_L \tag{1}$$

Equation (1) appeared to present considerable difficulty when VTOL models were first tested in wind tunnels. The problem was that, as the wind-tunnel velocity was decreased at constant lift, the lift coefficient increased without bound, and the correction angle approached infinity. As a point of fact, the problem was never really quite this serious. Equation (1) was derived by obtaining the vertical interference velocity and then assuming that the correction angle was small enough so that the angle and its tangent were equal. Without this final assumption, equation (1) would have been

$$\tan \Delta\alpha = \frac{\Delta w}{V} = \delta \frac{S}{A_T} C_L \qquad (2)$$

In equation (2), as the wind-tunnel speed approaches zero, the lift coefficient at constant lift still approaches infinity; however, the correction angle only approaches 90°. In other words, if the tunnel velocity (V) is zero, a closed wind tunnel still produces an upwash (Δw) in the vicinity of a lifting model. Unfortunately, the assumption lying behind the calculation of the correction factor δ, namely that the wake passes directly downstream along the wind-tunnel axis, is severely violated at very low and zero wind-tunnel velocities. Thus, usable results cannot be anticipated from the application of either equation (1) or (2) to tests of VTOL models.

A more recent analysis made at the Langley Research Center (refs. 2 and 3) treats the case where the wake is deflected substantially downward from the model. This theory obtains corrections in the form of interference velocities that are functions of the wake skew angle. (See fig. 1.) It will be observed that, in general, both horizontal and vertical interference velocities are obtained as a result of both lift and drag. In actually applying corrections to data, these interference velocities are used to obtain a new corrected angle of attack and a new effective forward velocity.

The correction factors describing the interference velocities have been calculated and tabulated for a wide range of variables (refs. 4 to 7). A sample case for the center of lift in a closed wind tunnel having a width-height ratio of 1.5 is presented in figure 2. The correction factor that corresponds to the classical correction factor is $\delta_{w,L}$. At $\chi = 90°$, it differs from the classical correction factor only by a factor of -4, which occurs solely because of the difference in definition. Furthermore, at $\chi = 90°$, all the other correction factors are zero. Thus, the classical theory is contained as a subcase of the new theory. It will be observed, however, that when the wake is deflected substantially downward, the vertical interference due to lift increases substantially, and in addition, a smaller upwash due to drag is encountered. Furthermore, both lift and drag contribute, in general, to a reduction in effective forward velocity.

Earlier Experimental Studies

Over the past several years investigators at the Langley Research Center have conducted experimental studies of the adequacy of the new theory by testing tilt-wing (ref. 8) and fan-in-fuselage (ref. 9) models in different size wind tunnels. Other investigators have tested rotors in wind-tunnel inserts (ref. 10). The tunnels have ranged from about 15 to over 1600 square feet in area. In general, substantially improved agreement was obtained in all cases, with a tendency toward overcorrection at the most severe lift coefficients.

At this point a fan-in-wing model was tested in both a 7- by 10-foot wind tunnel and a 30- by 60-foot wind tunnel (ref. 11). This model was the first model with a tail to which this theory was applied. Once more the theory corrected the model lift and drag reasonably well; however, the calculated correction to the pitching moment was approximately equal, but opposite in sign, to that required to bring the two sets of data into agreement. Obviously, there was an unexplained factor in the application of the corrections.

Location of the Wake

Before proceeding further, it is well to inquire into the fundamental question of the actual location of the wake. Fortunately, some information on this subject already exists. For example, figure 3 shows the measured vorticity distribution in the wake of a helicopter rotor (ref. 12). The wake of a rotor is usually represented for purposes of calculation as a series of concentric vortex cylinders whose strength is proportional to the local disk-load distribution. Thus it would be expected that, in the survey plane of figure 3, the vorticity would be found to be concentrated within the intersection of these vortex cylinders and the survey plane. (This intersection is shown by the dashed ellipse in fig. 3.) The figure shows that the expected result is not obtained. The dominant feature of the vorticity distribution is the presence of two large, and already well rolled-up, vortices behind the outermost portions of the rotor. It is notable that these vortices are deflected downward only about one-half as far as indicated by momentum theory. This behavior is in contrast to that of the wake mass flow which behaves essentially as indicated by momentum theory.

Joppa (ref. 13), of the University of Washington, starting from the analysis of reference 14, has been able to show theoretically that for low-aspect-ratio wings the result is essentially identical to the previous observation. That is, the final wake vorticity is deflected through approximately one-half of the angle calculated at the wing, rather than through twice the angle as predicted (for the wake mass flow) by linearized theory.

Effective Wake Skew Angle

The calculation of wind-tunnel boundary corrections may be accomplished by the use of suitably arranged image systems around the real test section. It will be observed that these image systems are comprised of the wake vorticity

rather than the wake mass flow. Furthermore, when the effects of all the image wakes are added, it will be observed that the calculated results are largely produced by image wakes which are at a substantial distance from the model. Thus, the far portions of the wake have a proportionately larger effect on the model (insofar as wall interference is concerned) than does the small portion of the wake immediately near the model. Therefore, it is proposed that a skew angle yielding just one-half the downward angular displacement of momentum theory (such as ref. 15) be used in applying the corrections of reference 2 to wind-tunnel data. In terms of skew angle, the effective skew angle χ_{eff} is

$$\chi_{eff} = \frac{\chi + 90^{\circ}}{2} \tag{3}$$

It is recognized that equation (3) cannot be correct in hovering or at extremely low forward speeds. This is evident since in true hovering the skew angle, whether based on wake vorticity or on wake mass flow, is indeed 0° and not 45° as would be indicated by equation (3). On the other hand, there are limitations on the minimum speed at which tests can be made in a meaningful fashion in wind tunnels, and it is believed that these limitations will generally be encountered before the failure of equation (3). In any event, it appears that the effective skew angle is a superior approximation to the actual wake over the bulk of reasonable test conditions.

Jet-Flap Model

Recently, data have been obtained for a jet-flap model (fig. 4) in the Langley 300-MPH 7- by 10-foot tunnel as well as in a small wind tunnel 2.70 feet high and 1.88 feet wide. (These wind tunnels are designated 7' × 10' and 2.70' × 1.88' herein.) The model was equipped with a sensitive tail balance, which measured tail normal force, and also was equipped with the usual sting balance, which was arranged so as to measure only the forces on the wing. Roughness strips were applied to both the wing and the tail surfaces to minimize Reynolds number effects.

A sample of the data obtained with this model is shown in figure 5. Corrections have been applied to the data from both wind tunnels. (The corrections to the 7' × 10' wind-tunnel data are very small, on the order of several tenths of a degree; consequently, the uncorrected data are not shown.) The corrections used are those of reference 2 with finite-span effects (for uniform loading) on both wing and tail accounted for by the superposition methods outlined in that paper. Inclusion of the finite-span effects substantially improves the correlation. The small differences in C_{μ} resulting from the horizontal interference velocities have been removed from the lift data (fig. 5(a)) by finding dC_L/dC_{μ} from closely spaced test runs in the 7' × 10' wind tunnel and then subtracting an amount equal to $(dC_L/dC_{\mu})\Delta C_{\mu}$ from the lift coefficient. In the case of the tail normal force, the behavior of $dC_{N,t}/dC_{\mu}$ was very erratic with respect to both C_{μ} and α; consequently, no similar correction has been

applied to the tail-normal-force data. (See fig. 5(b).) The actual changes in C_μ as a result of the horizontal interference were small for this model.

In addition, no correction has been made to the data to account for the effective aerodynamic warpage of the model as a result of the nonuniformity of the wall-induced interference over the model. In particular, the tail location is aerodynamically equivalent to a tail location that is slightly different from the actual geometric location on the physical model. Also neglected is the vertical motion of the tail in the wind tunnel as the model angle of attack is changed by pivoting about the quarter-chord.

Despite the unaccounted-for features mentioned, it is evident that the application of corrections according to reference 2 has greatly improved the correlation between the data from the two wind tunnels. This trend is particularly evident in the stall angle of attack of the wing at $C_\mu = 1.5$. In the corrected data, the stall angle is reproduced faithfully in both wind tunnels, despite the fact that the wall-induced interference is about 10 percent greater at the wing tips than it is at the center of the model. The improved agreement is equally obvious in the fidelity with which the angle for reversal of tail normal force is reproduced in the corrected data at $C_\mu = 5.0$.

The trend of greatly improved agreement is evident throughout the study except for the highest momentum coefficient at which tests were made. Data for this case ($C_\mu = 10$) are shown in figure 6. The corrected lift coefficients obtained in the two wind tunnels are in reasonable agreement up to an angle of attack of about 10°, after which the two sets of data diverge. Since the tail normal-force data have substantial scatter and the corrections are large, these data are also in reasonable agreement up to an angle of attack of approximately 10°, after which these two sets of data also diverge. The physical reason for this divergence is discussed in a subsequent section of this paper.

Effect of Finite Span

As previously mentioned, inclusion of finite-span effects substantially improves the agreement between the two wind tunnels. In the 7' × 10' wind tunnel, of course, the 1-foot-span model is a reasonably good representation of a vanishingly small model in comparison to the 10-foot width of the tunnel. On the other hand, the 1-foot-span model in the 1.88-foot width of the small wind tunnel cannot be considered vanishingly small under any circumstances. It was for this reason that finite-span effects were included. The importance of including these effects can be seen by comparing figures 7 and 8 with figures 5 and 6. The data of figures 7 and 8 were corrected by using the correction factors for a zero-span model. It is evident from this comparison that it is necessary to include finite-span effects if complete correction of data is desired.

Jet Thrust

It will be observed that (depending on the value of C_μ) from 40 to over 70 percent of the lift of the jet-flap model is due to the direct thrust of the

compressible jet at the trailing edge of the wing. All the jet thrust was included in the lift coefficient when correcting the data. The close correlation between the two sets of data after correction indicates that, as assumed in references 2 and 3, the exact nature of the lifting system is inconsequential, whether it be propeller, rotor, wing, fan, or jet. The only feature of the configuration that is significant is the distribution of lift and drag within the wind tunnel.

The foregoing comments are reinforced by the information presented in paper no. 13 by Richard J. Margason. In that paper it is shown that even the wake of a direct, circular, compressible jet rapidly rolls up into a subsonic vortex pair when operated in transition. Thus, the application of corrections to such jets should require little or no change in procedure.

Fan-In-Wing Model

Pitching-moment data from a fan-in-wing model have been mentioned previously in this paper. The model is shown in figure 9. The pitching-moment data from both the 7' × 10' and 30' × 60' wind tunnels are shown in figure 10 as it was originally presented in reference 11. The curve labeled "7' × 10', corrected" was obtained by applying the corrections of reference 2 in accordance with X rather than X_{eff}. It will be observed that the correction displaces the pitching-moment data in a direction opposite to that required in order to correlate the data from the two wind tunnels.

The same data corrected according to reference 2, but with the use of the effective skew angle, are shown in figure 11. The corrections as applied in this case are extremely crude. It is assumed that the model is vanishingly small. Obviously, the 64.5-inch-span model is not small in the 7' × 10' wind tunnel. Examination of the results of reference 2 indicates that this assumption in the present case overestimates the required correction. The effect of the flow distortion over the rear portion of the fuselage (which has substantial area and moment compared with the relatively small tail plane) has also been neglected. This assumption would result in a smaller correction. In the absence of measurements of the load distribution between the fans and the wing, it has been assumed that the load is carried entirely upon the fans. In practice, of course, the wing does carry substantial lift, and two wakes, at different skew angles, exist in the wind tunnel. If the lift distribution between the two lifting systems was accounted for, the upwash at the tail would be reduced. In addition, the vertical displacement of the tail from the wing plane, as well as the large motion of the tail within the wind tunnel as a result of changes in angle of attack, has been neglected. Furthermore, no camber effects on the wing and no pitching-moment changes due to induced flow gradient on the fans were considered.

In addition to the foregoing assumptions, all the data shown herein for this model were obtained at speeds far below an apparently limiting lower speed for VTOL tests in closed wind tunnels. This limit will be discussed in a subsequent section of this paper.

As a result of the factors mentioned previously, the close correlation of the corrected pitching moments is fortuitous. Actually, unpublished tail-off data from both the 7' × 10' and 30' × 60' wind tunnels indicate that the effect of the walls on the pitching moment due to the tail is quite small. Examination of the circulatory flow discussed in a subsequent section indicates that the result of such flow should largely counteract the wall-induced upwash at the tail in this particular test. On the other hand, figure 11 does indicate, at least, that the correction is not in the wrong direction as it appeared to be when calculated with the use of χ instead of χ_{eff} (as in fig. 10).

The change in the correction by changing to the effective skew angle may be explained by examination of figure 12. This figure shows the variation of $\delta_{w,L}$ (which in this case is the most significant correction factor) along the longitudinal axis of the model. Note that in correcting pitching moments the problem is generally one of correcting the contribution of the tail to coincide with the tail moment that would be obtained at the conditions to which the lifting system has already been corrected. Thus, it is the relative difference between, rather than the absolute values of, the correction at the center of lift and the tail which is of interest. At $\chi = 0^{\circ}$, which approximates the original skew angles for the fan-in-wing model, it will be seen that there is a lesser upwash at the tail than at the wing. Thus the tail is working with less lift in the wind tunnel than if it were at the same condition as the wing. To correct for this situation, an appropriate amount of lift must be added to the tail to make the moment more negative as in figure 10. On the other hand, for $\chi = 45^{\circ}$, which approximates the effective skew angle for this case, the tunnel produces more upwash at the tail than at the center of lift. Consequently, correction makes the moment more positive (fig. 11).

Tilt-Wing Model

The earlier studies of wall effects on the tilt-wing model (ref. 8) indicated that the wind-tunnel interferences calculated in reference 2 overcorrected the data in extreme conditions. The use of the effective skew angle would have reduced the corrections somewhat for the tilt-wing model, too, and would have led to improved correlation.

Comparison With Flight

In view of scale effects and differences in model detailing and the differing accuracies and types of corrections required, comparison between flight tests and wind-tunnel tests can be a particularly difficult task. This comparison is unusually difficult when the comparison is attempted in order to evaluate only one of the many effects that are being considered. Paper no. 5 by Kenneth W. Goodson, for example, showed that a 0.09-scale model suffered from large Reynolds number effects (fig. 6 of paper no. 5), but that a 0.60-scale model did yield reasonable results in predicting the maximum rate of descent for a four-propeller tilt-wing configuration. As noted in paper no. 5, the data for the 0.60-scale model were corrected for wall effects. The corrections used the effective skew angle and considered the effect of finite span. The correction,

as obtained in this manner, resulted in a change of flight-path angle of several degrees and substantially improved the correlation between results from the large model and flight data.

Limit on Testing in Closed Wind Tunnels

Rae, of the University of Washington, by testing rotors in inserts in the UWAL 8- by 12-foot wind tunnel,[1] has shown that the wake, upon meeting the floor behind the model, spreads laterally on the floor, is turned upward by the sidewalls, and produces a flow pattern in the wind tunnel as indicated on the left-hand side of figure 13. Normally, this disturbance is too far behind the model to produce any discernible effect on the data. However, if the wake is deflected downward sharply enough, the recirculation pattern envelops the model and the data are severely affected. In the present case, the point of divergence occurs at an effective skew angle of 65° and produces a theoretical intersection of wake and floor about $2\frac{2}{3}$ spans behind the point of origin of the wake. This point agrees quite closely with the value obtained by Rae.

The close correlation between such widely divergent models (rotor and jet flap) and wind-tunnel configurations ($\gamma = 1.5$ and $\gamma = 0.7$) indicates two things. First, there is a finite lower limit to the test speed at which reliable and correctable data can be obtained in a closed wind tunnel; and, second, this limit is not seriously affected by model configuration but is largely determined only by the size of the vertical-lift elements of the model. This limiting effect is still relatively unexplored. It may be that certain wind-tunnel configurations will be affected differently from others. It further seems possible that if the model configuration were extremely long, or if the lifting elements were disposed over a large longitudinal distance, the limiting speed could be adversely affected. Substantial additional experimental work will be required in order to define these (and similar) effects.

Actually, the onset of this limiting lower speed follows a rule rather similar to that presented in paper no. 25 by Thomas R. Turner, in which it is noted that a moving belt is required in order to simulate ground effect when the combination of lift coefficient and height above the ground produces an intersection of effective wake and floor which is less than $2\frac{1}{2}$ spans behind the model. Thus, the boundary layer on the walls is probably a major causative factor in producing these recirculation effects. The study of a number of boundary-layer control features is indicated in the hope that significant gains could be obtained.

As stated previously, the study of limiting forward speeds for VTOL tests in wind tunnels is still in an early stage and, consequently, large uncertainties are present. In view of this uncertainty, a value of 3 spans is suggested

---

[1]Rae, William H., Jr.: An Experimental Investigation of the Maximum Size Rotor That Can be Tested in a Rectangular Wind Tunnel. Grant No. DA-ARO(D)-31-124-G481 (U.S. Army Res. Office, Durham, N.C.), Jan. 5, 1966.

as an adequately accurate number to use in deciding the speed above which full confidence in the data is justified. In considering the span of the model, it should be adequate to consider only the span of the vertical-lift elements of the configuration.

It might be noted that there could be two ways of locating this limit. In the present paper, the wake vorticity is assumed to be responsible for the circulatory flow around the wind-tunnel walls. An alternative viewpoint is that the circulatory flow is a result merely of the wake mass flow dividing at the tunnel floor. If so, the proper skew angle to use for the limit would be the original or momentum-value skew angle, and the corresponding limit would be an intersection of wake and floor just $1\frac{1}{4}$ spans behind the model. At the present time, insufficient experimental evidence exists and therefore a choice between the two concepts is difficult.

Size of Models

The real limitation on the allowable size of a model is not really the absolute size of the correction which will be engendered by testing a given size model in a given wind tunnel. Instead, the limitations on model size are defined largely by the variation of the wall-induced interference over the extent of the model. As pointed out previously, this variation can be considered in terms of effective aerodynamic distortion (such as twist and camber) of the model. The maximum size model that can be used, therefore, is determined by the extent to which the effect of such distortions can be determined. For simple isolated wings, as well as for isolated rotors and propellers, such effects can be determined with reasonable accuracy, and relatively large models may be accepted. For more exotic means of producing lift, as well as for many interacting combinations of simple elements, the prediction of the effect of these interference distortions is doubtful at best. In such cases, it may be necessary to limit the size of VTOL models to one-quarter to one-third of the wind-tunnel width if accurate, reliable results are desired.

On the other hand, scale effects and the physical size limitations in providing small powered models may override considerations of wall effects. Thus the eventual sizing of a particular model will be the result of many engineering compromises and the overall accuracy of predication of full-scale flight characteristics will be determined by the degree to which such compromises are optimized.

Application to Langley Data

The close correlation of data from different wind tunnels, both in this paper and in references 8 to 10, as a result of applying the corrections of reference 2 is quite encouraging. As a result, the decision has been made to incorporate these corrections into all new VTOL data from the Langley 300-MPH 7- by 10-foot tunnel at the earliest possible date.

Wind-Tunnel Configurations for Small Wall Effects

As indicated in the foregoing sections of this paper, wall effects can be large and troublesome in a closed wind tunnel; however, a large degree of relief can be obtained by the use of wind tunnels with mixed boundaries. An example, suggested by Ray H. Wright of the Langley Research Center, is shown in figure 14. In this example, the wind tunnel is 1.5 times as deep as it is wide, has an open lower boundary, a closed upper boundary, and slotted sidewalls.

The classical correction factor (eq. (1)) for a vanishingly small model in this wind tunnel has been calculated and is also presented in figure 14 as a function of the percentage of the sidewalls that is opened by the slots. The correction factor is observed to fall very rapidly for very small slot openings. The curve then becomes less sensitive to slot opening, and the correction factor becomes zero with a 5-percent slot opening.

This calculation was made for a wake which passes directly rearward without deflection. In order to determine the effect of deflecting the wake, the small (2.70' × 1.88') wind tunnel was built. Extensive tests have been conducted on the jet-flap model previously described. A sample of the results is shown in figure 15. At a momentum coefficient of 3.0, the wall effects on the model lift are essentially negligible (fig. 15(a)). However, wall effects at the tail are not zero (fig. 15(b)). Despite the large scatter, there seems to be some, but certainly not total, relief from wall effects at the tail.

At the highest momentum coefficient (C_μ = 10.0), the boundary effects on the tail are far more severe (fig. 16). Figure 16 shows that the wind tunnel with mixed boundaries leads to measurements less accurate than even those from the small closed wind tunnel. This effect is believed to be due to the gross disruption of the tunnel flow resulting from the large spillage of air from the lower open boundary of the tunnel.

Despite the fact that a zero-correction wind tunnel for VTOL testing has not been achieved as yet, the results obtained to date are sufficiently encouraging so that work on several slotted wind tunnels is continuing. This work is being expanded to include several other low-correction wind tunnels such as the closed-on-bottom-only configurations.

CONCLUSIONS

This study of the application of jet-boundary corrections to VTOL wind-tunnel data indicates the following conclusions:

1. The skew angle used in applying the corrections of NASA TR R-124 to VTOL data should be such that the angular deflection of the wake vorticity from the horizontal is essentially one-half of the wake deflection obtained from momentum theory at the lifting element.

2. When the effective skew angle is used, the corrections of NASA TR R-124 provide greatly improved agreement between the data obtained in different wind tunnels, not only for lift, but also for pitching moment and tail normal force.

3. For accurate corrections, it is necessary to include the effects of finite model span, at least when the model span is on the order of one-half the wind-tunnel width.

4. There appears to be a lower limit to the test speed at which reliable and correctable results can be obtained from closed wind tunnels. In view of present uncertainties, it is suggested that this limit be taken as an intersection of effective wake and floor that is three times the span of the vertical-lift system behind the wake origin.

5. Considerable alleviation of boundary effects may be obtained by the use of wind tunnels employing mixed boundaries.

REFERENCES

1. Theodorsen, Theodore: The Theory of Wind-Tunnel Wall Interference. NACA Rept. 410, 1931.

2. Heyson, Harry H.: Linearized Theory of Wind-Tunnel Jet-Boundary Corrections and Ground Effect for VTOL-STOL Aircraft. NASA TR R-124, 1962.

3. Heyson, Harry H.: Wind-Tunnel Wall Interference and Ground Effect for VTOL-STOL Aircraft. J. Am. Helicopter Soc., vol. 6, no. 1, Jan. 1961, pp. 1-9.

4. Heyson, Harry H.: Tables of Interference Factors for Use in Wind-Tunnel and Ground-Effect Calculations for VTOL-STOL Aircraft. Part I - Wind Tunnels Having Width-Height Ratio of 2.0. NASA TN D-933, 1962.

5. Heyson, Harry H.: Tables of Interference Factors for Use in Wind-Tunnel and Ground-Effect Calculations for VTOL-STOL Aircraft. Part II - Wind Tunnels Having Width-Height Ratio of 1.5. NASA TN D-934, 1962.

6. Heyson, Harry H.: Tables of Interference Factors for Use in Wind-Tunnel and Ground-Effect Calculations for VTOL-STOL Aircraft. Part III - Wind Tunnels Having Width-Height Ratio of 1.0. NASA TN D-935, 1962.

7. Heyson, Harry H.: Tables of Interference Factors for Use in Wind-Tunnel and Ground-Effect Calculations for VTOL-STOL Aircraft. Part IV - Wind Tunnels Having Width-Height Ratio of 0.5. NASA TN D-936, 1962.

8. Grunwald, Kalman J.: Experimental Study of Wind-Tunnel Wall Effects and Wall Corrections for a General-Research V/STOL Tilt-Wing Model With Flap. NASA TN D-2887, 1965.

9. Davenport, Edwin E.; and Kuhn, Richard E.: Wind-Tunnel-Wall Effects and Scale Effects on a VTOL Configuration With A Fan Mounted in the Fuselage. NASA TN D-2560, 1965.

10. Lee, Jerry Louis: An Experimental Investigation of the Use of Test Section Inserts as a Device To Verify Theoretical Wall Corrections for a Lifting Rotor Centered in a Closed Rectangular Test Section. M. S. Thesis, Univ. of Washington, Aug. 20, 1964.

11. Staff of Powered-Lift Aerodynamics Section, NASA Langley Res. Center: Wall Effects and Scale Effects in V/STOL Model Testing. AIAA Aerodynamic Testing Conf., Mar. 1964, pp. 8-16.

12. Heyson, Harry H.; and Katzoff, S.: Induced Velocities Near a Lifting Rotor With Nonuniform Disk Loading. NACA Rept. 1319, 1957. (Supersedes NACA TN 3690 by Heyson and Katzoff and TN 3691 by Heyson.)

13. Joppa, R. G.: Experimental and Theoretical Investigation of Wind Tunnel Geometry, Emphasizing Factors Pertinent to V/STOL Vehicles Testing. Progr. Rept. No. 2 (NASA Grant NGR-48-002-010), Univ. of Washington, Jan. 15, 1966.

14. Cone, Clarence D., Jr.: A Theoretical Investigation of Vortex-Sheet Deformation Behind a Highly Loaded Wing and Its Effect on Lift. NASA TN D-657, 1961.

15. Heyson, Harry H.: Nomographic Solution of the Momentum Equation for VTOL-STOL Aircraft. NASA TN D-814, 1961. (See also "V-STOL Momentum Equation," Space/Aeron., vol. 38, no. 2, July 1962, pp. B-18 — B-20.)

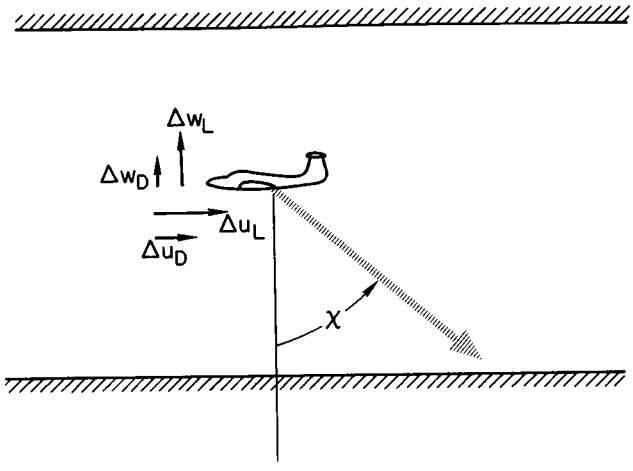

Figure 1.- Notation and positive direction of interference velocities and skew angle used in correction theory of NASA TR R-124.

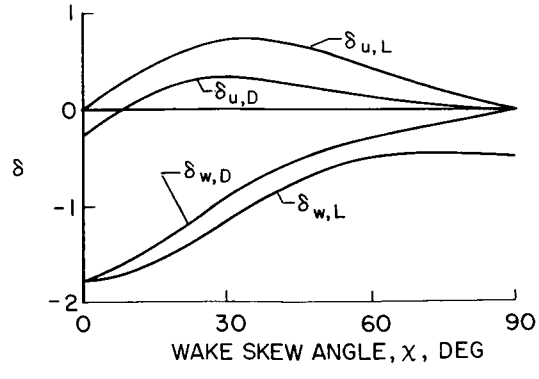

Figure 2.- Typical behavior of correction factors as a function of wake skew angle. Closed tunnel; $\frac{B}{H} = 1.5$.

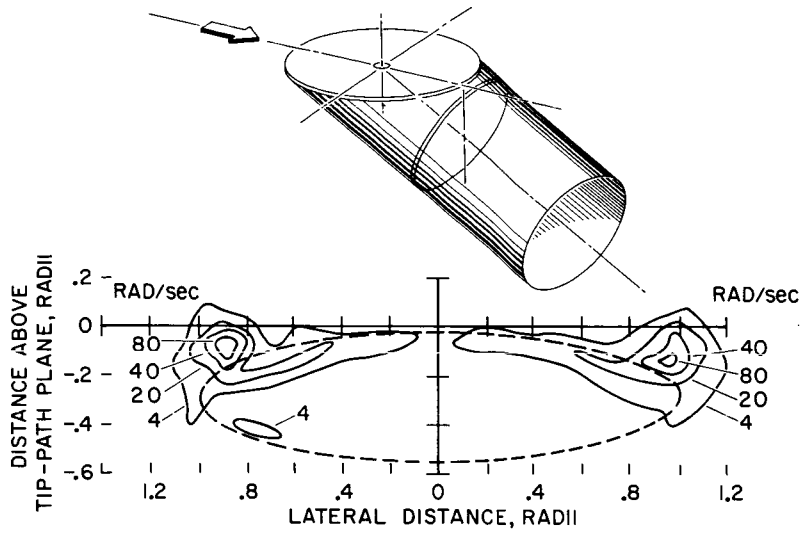

Figure 3.- Vorticity distribution measured at $x = 0.07R$ behind the trailing edge of a lifting rotor. $\chi = 75^{0}$.

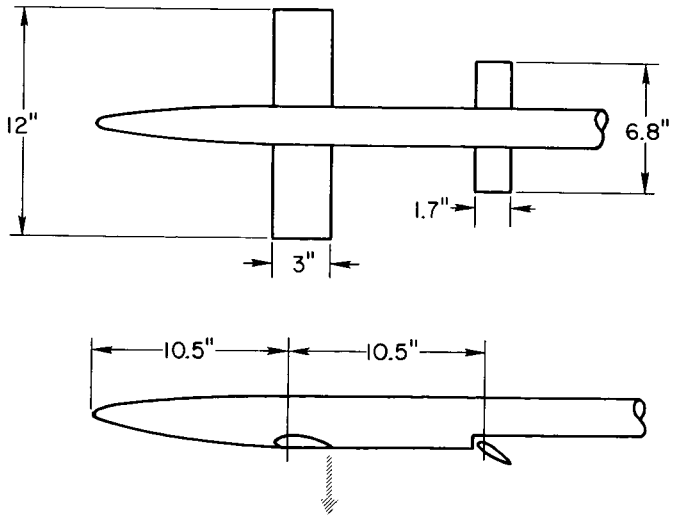

Figure 4.- Jet-flap model.

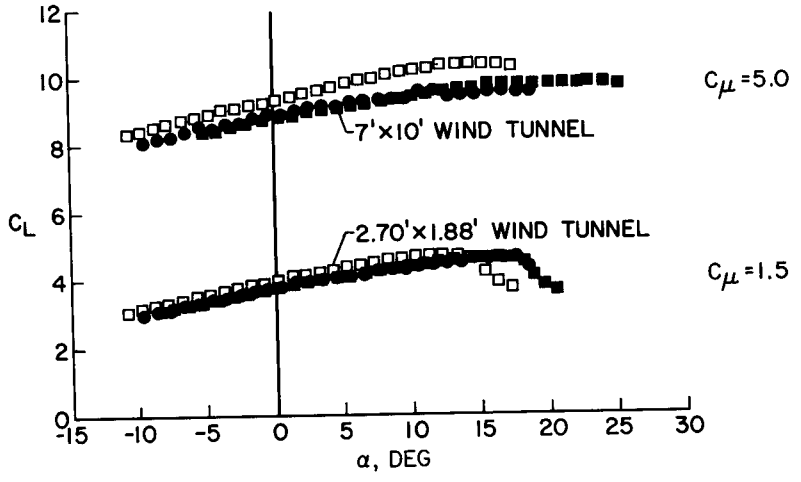

(a) Lift coefficient C_L.

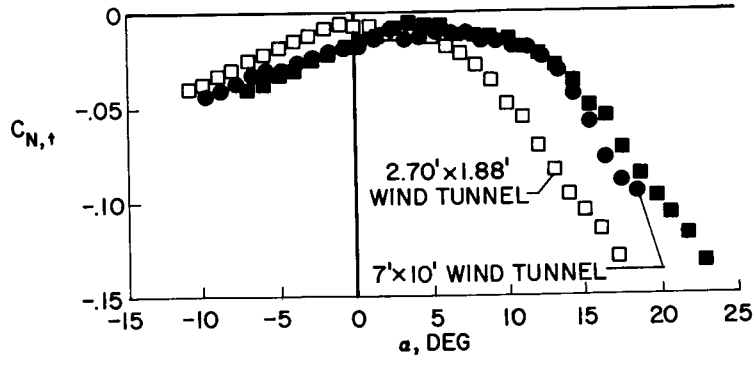

(b) Tail-normal-force coefficient $C_{N,t}$. C_μ = 5.0; tail incidence, 21.6°.

Figure 5.- Comparative data for jet-flap model tested in two different closed wind tunnels. Solid symbols denote values corrected by using X_{eff}; correction factors include effect of finite span of both wing and tail.

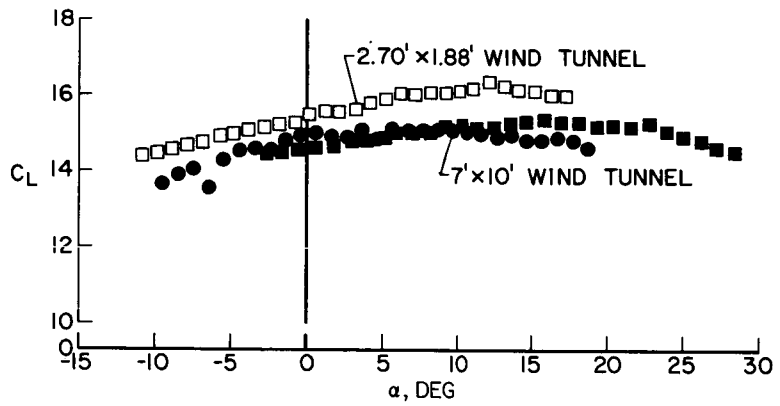

(a) Lift coefficient C_L.

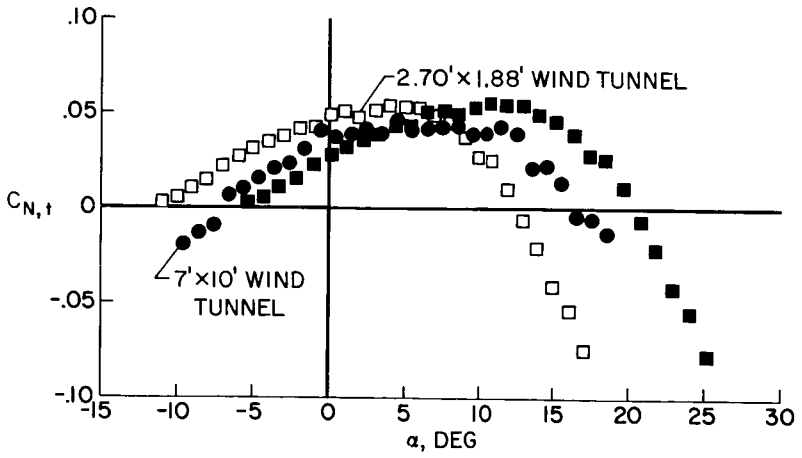

(b) Tail-normal-force coefficient $C_{N,t}$. Tail incidence, 29°.

Figure 6.- Comparative data for jet-flap model at $C_\mu = 10.0$ tested in two different closed wind tunnels. Solid symbols denote values corrected by using X_{eff}; correction factors include effect of finite span of both wing and tail.

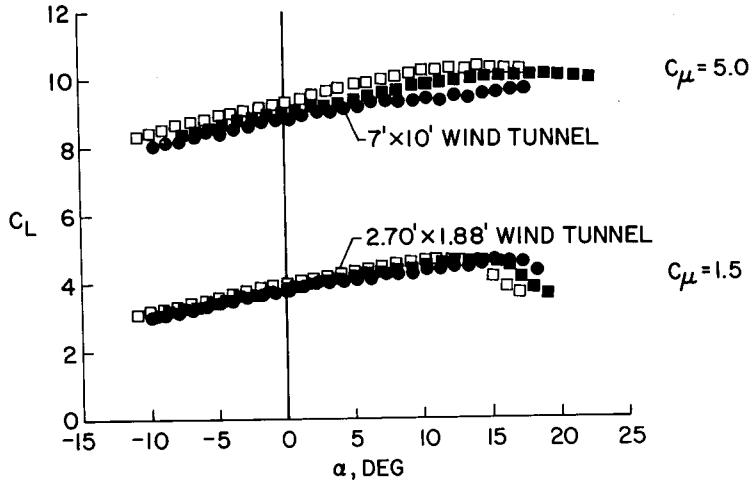

(a) Lift coefficient C_L.

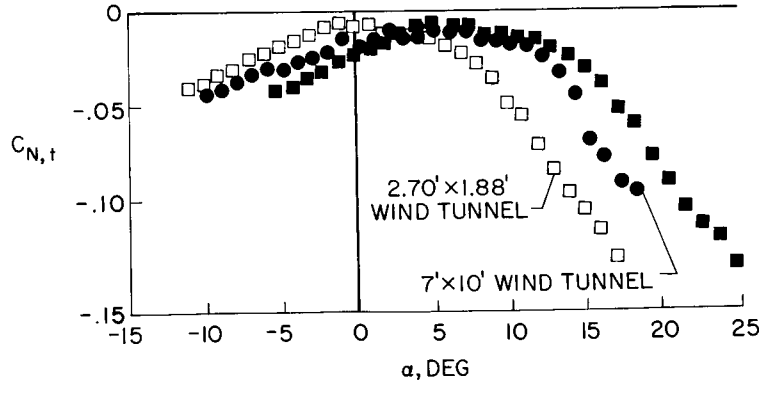

(b) Tail-normal-force coefficient $C_{N,t}$. C_μ = 5.0; tail incidence, 21.6°.

Figure 7.- Comparative data for the jet-flap model tested in two different closed wind tunnels. Solid symbols denote values corrected by using X_{eff}; correction factors for a zero-span model.

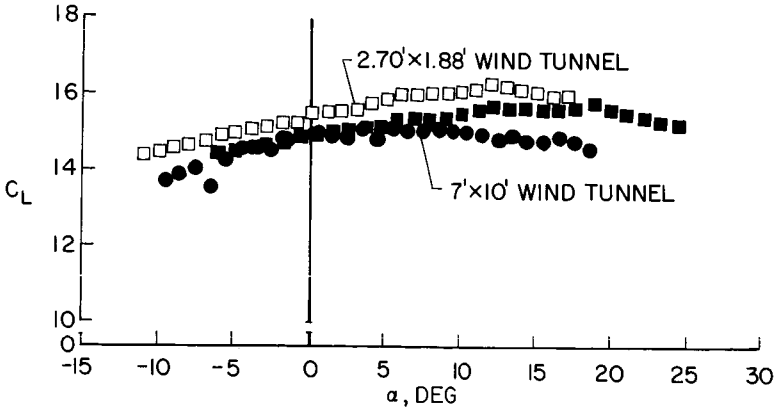

(a) Lift coefficient C_L.

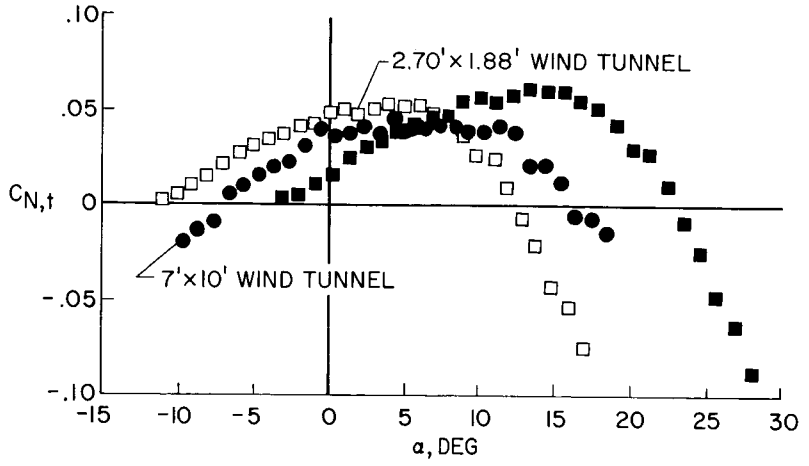

(b) Tail-normal-force coefficient $C_{N,t}$. Tail incidence, 29°.

Figure 8.- Comparative data for the jet-flap model at $C_\mu = 10.0$ in two different closed wind tunnels. Solid symbols denote values corrected by using χ_{eff}; correction factors for a zero-span model.

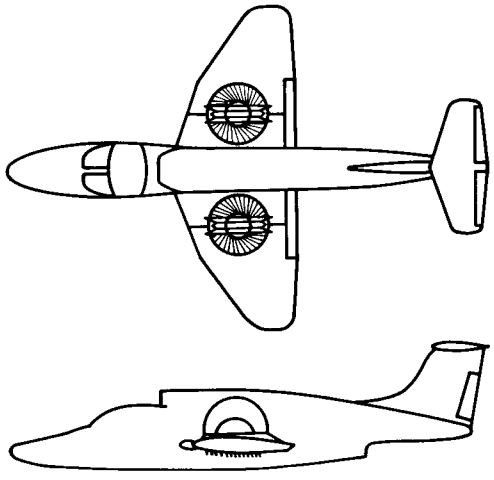

Figure 9.- Sketch of fan-in-wing model.

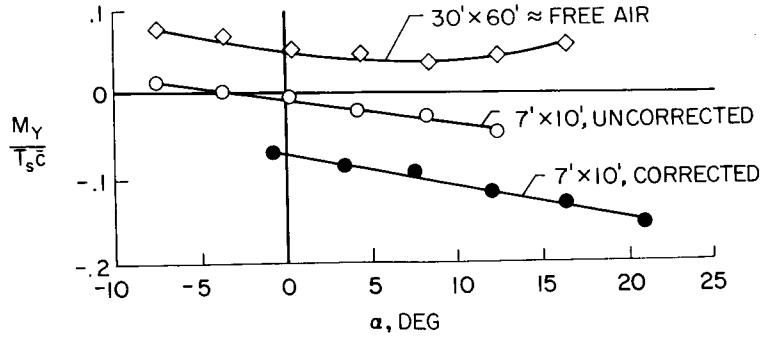

Figure 10.- Comparison of pitching-moment data obtained in two wind tunnels with fan-in-wing model. Corrections have been applied by using method of NASA TR R-124 with the original skew angle. $\frac{V}{V_{j,s}} = 0.48$; exit-louver angle, 0^0.

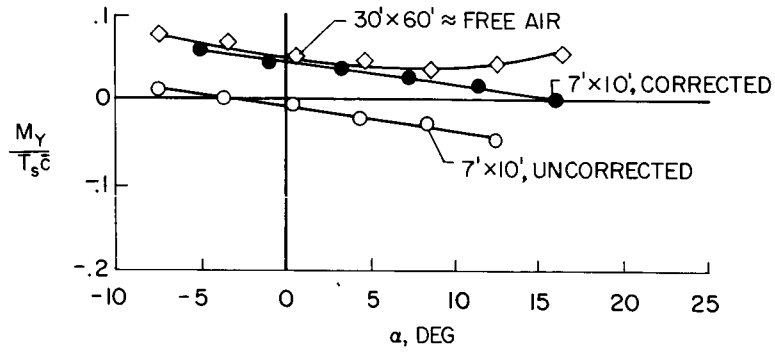

Figure 11.- Comparison of pitching-moment data obtained in two wind tunnels with fan-in-wing model. Corrections have been applied by using method of NASA TR R-124 with effective skew angle. $\frac{V}{V_{j,s}} = 0.48$; exit-louver angle, 0^0.

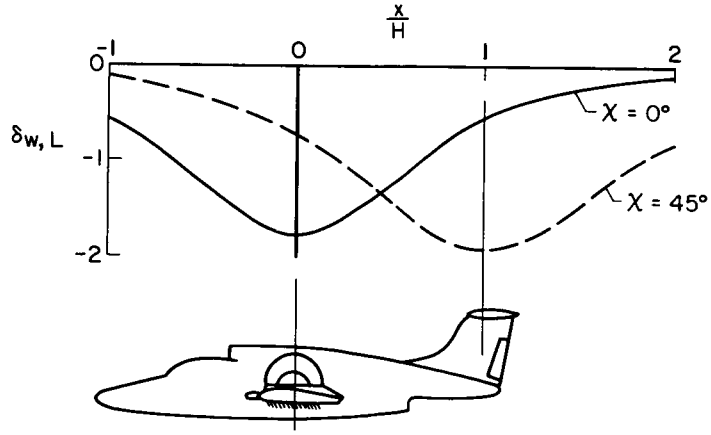

Figure 12.- Variation of vertical interference due to lift $(\delta_{w,L})$ along the longitudinal axis of fan-in-wing model.

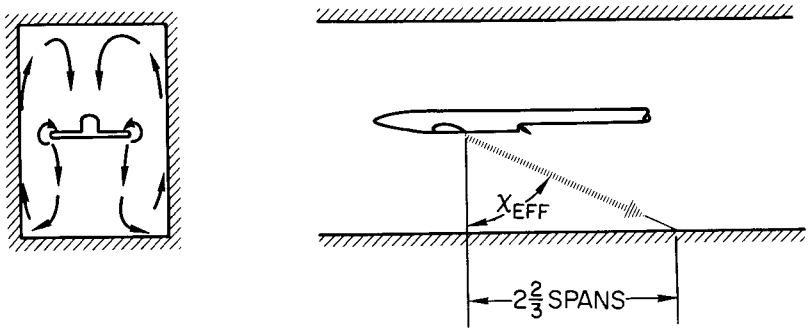

Figure 13.- Sketch of flow behind model in a closed wind tunnel, and limit found in tests of jet-flap model.

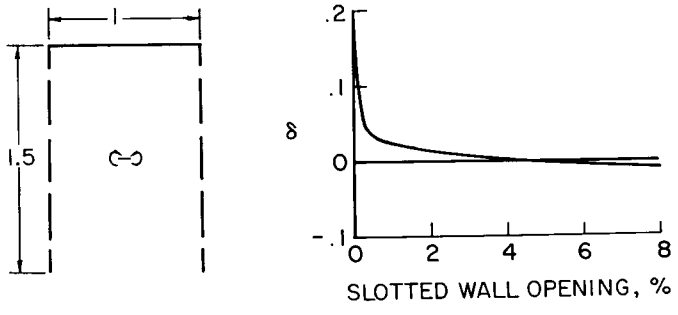

Figure 14.- Calculated classical correction factors for a wind tunnel with mixed boundaries. Model is assumed to be vanishingly small.

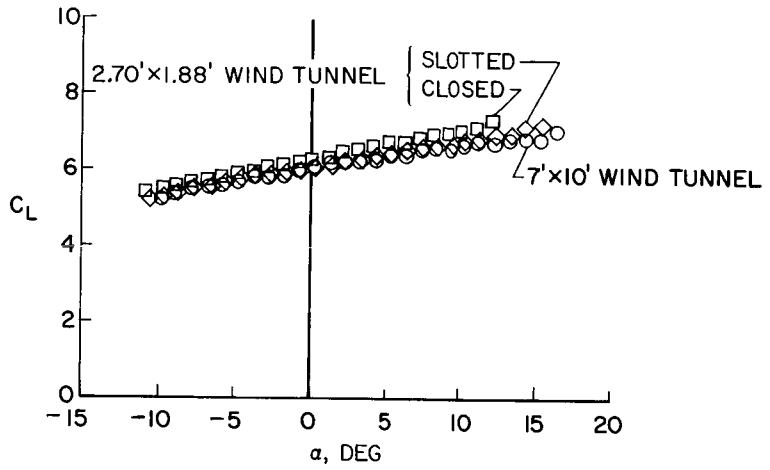

(a) Lift coefficient C_L.

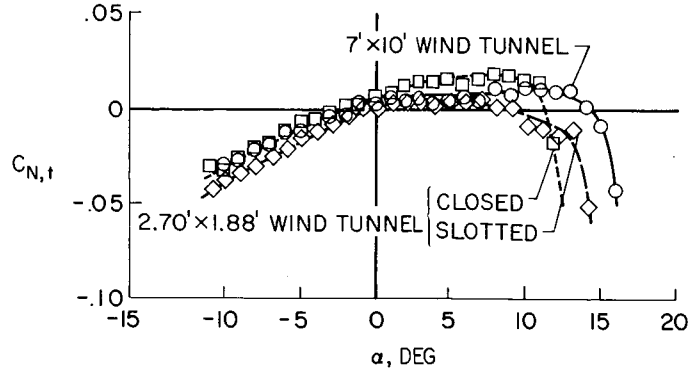

(b) Tail-normal-force coefficient $C_{N,t}$.

Figure 15.- Comparison of data obtained in three wind tunnels for jet-flap model at $C_\mu = 3.0$.

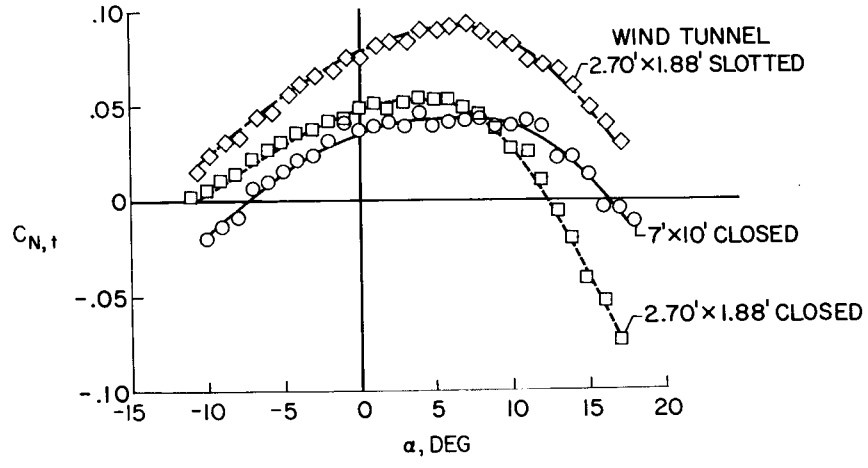

Figure 16.- Comparative data on tail-normal-force coefficient for jet-flap model at $C_\mu = 10.0$ in three different wind tunnels.

25. ENDLESS-BELT TECHNIQUE FOR GROUND SIMULATION

By Thomas R. Turner

NASA Langley Research Center

SUMMARY

The use of an endless-belt ground plane for ground simulation in wind-tunnel tests has been investigated. Results of the investigation presented herein indicate that the endless-belt ground plane correctly simulates the ground but that not all models require this technique of simulation. In general, those configurations in which the lift is carried primarily in discrete jets (tilting ducted and jet V/STOL) do not require the endless belt for ground simulation and those in which the lift is distributed over the span of the wing do require the endless-belt ground plane. However, the need is dependent upon the lift coefficient and height above the ground.

INTRODUCTION

Author

Normally in wind-tunnel investigations of ground effects the ground is simulated by placing a board in the airstream immediately below the model, as illustrated in figure 1. This simulation is not strictly correct because a boundary layer develops between the airstream and the ground board. This boundary layer has not been a serious problem in tests of conventional aircraft models. However, with the advent of V/STOL configurations in which a jet sheet or propeller slipstream is used to augment the lift, the question of possible interaction between the jet sheet or slipstream and this boundary layer arises. If an endless belt moving at the same velocity as the tunnel airstream instead of the conventional fixed ground board is used for ground simulation, the boundary layer can be eliminated. The present investigation was therefore made to study this method of ground simulation and to determine the conditions under which it would be preferable to the conventional method.

SYMBOLS

A	aspect ratio	
b	span, feet	
C_D	drag coefficient,	$\frac{\text{Drag}}{q_\infty S}$
C_L	lift coefficient,	$\frac{\text{Lift}}{q_\infty S}$

C_m pitching-moment coefficient, $\frac{\text{Pitching moment}}{q_\infty S \bar{c}}$

C_T thrust coefficient, $\frac{\text{Thrust}}{q_\infty S}$

$\bar{c}$ mean aerodynamic chord, feet

h height of wing chord above ground, feet

L_h lift at height h above ground, pounds

$L_{h=\infty}$ lift out of ground influence, pounds

$\Delta L_h = L_h - L_{h=\infty}$

q_∞ free-stream dynamic pressure, pounds/foot^2

S area, feet^2

V velocity, feet/second

α angle of attack, degrees

δ_{duct} duct deflection from horizontal, degrees

∞ free stream or infinity

BASIC CONSIDERATIONS

In order to investigate whether or not the boundary layer caused by the conventional ground board produced possible adverse effects, experiments were made a few years ago by using a carriage to move a model through still air over the ground in the same fashion as an airplane landing or taking off (ref. 1). This same model was then tested over a conventional fixed ground board in a wind tunnel. The lift results from these investigations are compared in figure 2. The increment of lift loss in ground effect divided by the lift out of ground effect is presented as a function of model height in spans. The full-span blowing-flap configuration of aspect ratio 6 developed a lift coefficient out of ground effect of 9.5. The lift loss over the fixed ground board was much greater than that experienced with the moving-model technique. The increment between the curve for the moving model and zero represents the true loss in lift that this type of configuration would experience in ground effect. The increment between the two curves is the additional lift loss caused by the boundary layer on the conventional fixed ground board.

Figure 3 shows schematically the type of flow that has been observed in tests over the endless-belt ground plane, to be described later, and in

O.N.E.R.A. water-tunnel flow visualization experiments (ref. 2). The top sketch shows the flow pattern around the model with the ground plane moving at stream velocity V with no boundary-layer loss, as illustrated on the left. The jet sheet from the model impinges on the ground board with some of the sheet attempting to flow forward under the model. This forward flow can penetrate the high-energy free-stream air only a short distance. The bottom sketch shows the flow field around the model over a fixed ground board with the velocity profile at the left showing the loss in energy in the boundary layer on the ground board. The jet sheet impinges as before but the part of the sheet that flows forward under the model can penetrate farther because of the low energy of the stream air near the board; this upstream penetration thus separates the boundary layer even upstream of the model. This boundary-layer separation results in an appreciable alteration of the flow field in the vicinity of the model, as indicated by the relocation of the stagnation streamline.

The flow visualization tests and the preceding test data indicate that, for this type of configuration, it is necessary to eliminate the boundary layer on the ground board for proper ground simulation. The moving-model technique was not used further because of the inherent problems associated with the technique and because the technique does not have the flexibility and adaptability normally associated with wind-tunnel testing. It was, therefore, decided to develop the endless-belt ground plane shown schematically in figure 4 for the 17-foot test section of the Langley 300-MPH 7- by 10-foot tunnel (ref. 3). A similar installation had been developed earlier by the R.A.E. in England (ref. 4).

ENDLESS-BELT GROUND PLANE

The endless belt used to simulate the ground plane in this testing technique is 10 feet long and 12 feet wide, and the belt upper surface is 10 inches above the tunnel floor. (See fig. 4.) A 1-inch suction slot extends the width of the belt at the leading edge to remove any boundary layer up to this point, and with the belt moving at stream velocity no boundary layer can build up downstream. The belt is made of 1/8-inch-thick plastic-impregenated woven wool and can be driven at velocities from 0 to 100 feet per second. The model is mounted on an internal strain-gage balance fitted to a sting that can be remotely driven to change model height and attitude. The photograph in figure 5 shows the endless-belt ground plane installed in the test section. The full-width boundary-layer-removal slot and the belt upper surface can be observed.

RESULTS AND DISCUSSION

Distributed-Lift Configurations

The first model investigated over the Langley endless-belt ground plane was the same model used in reference 1 to obtain the moving-model data presented in figure 2. Figure 6 presents the data of figure 2 along with data

from the endless-belt technique. The ratio of lift loss in ground influence to lift out of ground influence is plotted as a function of wing height in spans. With the belt velocity equal to air velocity the lift loss is in good agreement with the moving-model data. With the belt velocity equal to zero the lift loss is in good agreement with the conventional ground board results.

In theory the velocity of the belt must be the same as the airstream velocity. The data presented in figure 7 show the effect of varying the belt velocity from values less than to values greater than stream velocity. These results are for an out-of-ground-influence lift coefficient of 7.4. The lift loss is plotted as a function of the ratio of belt velocity to air velocity. The insets show the type of boundary layer existing over the belt at velocity ratios of 0, 1.0, and 1.4. The lift loss for the given conditions decreases almost linearly with increasing velocity ratio. The slope of the lift-loss curve is such that extreme precision is not required in setting belt speed. Normally the moving belt would be used to simulate take-off and landing in still air, that is, belt velocity equal to free-stream air velocity. However, with the belt operating below stream velocity, head wind conditions may be approximated if the boundary-layer profile on the runway is known.

All the ground influence effects presented up to this point have been based on blowing-flap configurations developing very high lift coefficients. However, various other models typical of existing or proposed aircraft configurations including delta-wing, double slotted flap, tilting ducted fan, propeller powered tilt-wing, and other configurations have been investigated over the endless-belt ground plane. The main factors influencing the ground flow conditions which determine the need for the endless-belt ground plane appear to be lift (including spanwise distribution) and height above the ground. In general, configurations which operate at high circulation lift coefficients, such as tilt-wing, jet-flap, and in some cases unpowered double slotted flap configurations, require the belt.

Other models, even without blowing flaps, show a need for the belt if the height of the model above the belt is low enough. Some ground influence results for a double slotted flap configuration very near the ground ($h/b = 0.033$) are presented in figure 8. There is a large loss in lift due to ground effect at $\alpha = 0$ with the belt stopped, but essentially zero loss with the belt running at stream velocity. The changes in drag and pitching moment are a reflection of the lift changes.

Ground effect data for a tilt-wing propeller-powered configuration (XC-142A) are presented in figure 9. The wing is tilted 20° and the flap is deflected 60°. This configuration develops lift coefficients from 6.0 to 8.0. A significant loss in lift occurs as the height decreases from infinity to 0.19 spans with the belt stopped, but with the belt running this loss is reduced. There is a large effect of the ground on the pitching-moment coefficients, due primarily to the change in downwash caused by the ground, but a negligible effect on the endless belt for this moderately high tail configuration.

A correlation in terms of lift coefficient and ground height for full-span high-lift configurations, which shows conditions that require the moving belt, is shown in figure 10. The plotted points are the lift values for a given height at which the lift curves for belt velocity equal to air velocity and belt velocity equal to zero noticeably diverge, as illustrated in the inset. The solid line in figure 10 is the height above the ground computed for a given lift coefficient by assuming that the effective deflection angle θ_{eff} for the stream tube impinges on the ground a distance of 2.5 spans downstream from the model. It should be noted that θ_{eff} is equal to one-half the deflection calculated from momentum theory, as explained in paper no. 24 by Heyson and Grunwald. (The stream-tube deflection angle of the present paper is the complement of the wake skew angle used in paper no. 24.) The agreement between the plotted points and the solid (boundary) line is interesting. It is also interesting to note that the downstream distance of 2.5 spans is almost the same as the impingement distance at which recirculation effects in the wind tunnel begin to produce noticeable effects on the data (paper no. 24). However, elimination of the boundary layer on the ground by means of the endless-belt technique may alleviate the circulation effects to some degree. The conventional ground board is adequate for those combinations of lift and height falling above the boundary shown by the solid line. For those combinations falling below the boundary shown, the moving belt is required.

Direct-Lift Configurations

In general, configurations in which the lift is concentrated in discrete jets, such as direct-jet VTOL and tilting ducted models, do not require the belt, as is illustrated in figure 11. Although there is clearly an effect of the ground on all components, there is no measurable effect of the moving belt.

CONCLUDING REMARKS

Results of an investigation of an endless-belt ground plane for ground simulation indicate that the endless-belt ground plane correctly simulates the ground but that not all models require this technique of simulation. In general, those configurations in which the lift is carried primarily in discrete jets (tilting ducted and jet V/STOL) do not require the endless belt for ground simulation and those in which the lift is distributed over the span of the wing do require the endless-belt ground plane. However, the need is dependent upon the lift coefficient and height above the ground.

REFERENCES

1. Turner, Thomas R.: Ground Influence on a Model Airfoil With a Jet-Augmented Flap as Determined by Two Techniques. NASA TN D-658, 1961.

2. Werlé, Henri: Simulation de L'Effet de Sol au Tunnel Hydrodynamique (Ground-Effect Simulation at the Water-Tunnel). La Rech. Aérospatiale, no. 95, July-Aug. 1963, pp. 7-15.

3. Vogler, Raymond D.: Ground Effects on Single- and Multiple-Jet VTOL Models at Transition Speeds Over Stationary and Moving Ground Planes. NASA TN D-3213, 1966.

4. Williams, John; and Butler, Sidney F. J.: Further Developments in Low-Speed Wind-Tunnel Techniques for VSTOL and High-Lift Model Testing. AIAA Aerodynamic Testing Conf., Mar. 1964, pp. 17-32.

CONVENTIONAL WIND-TUNNEL GROUND BOARD

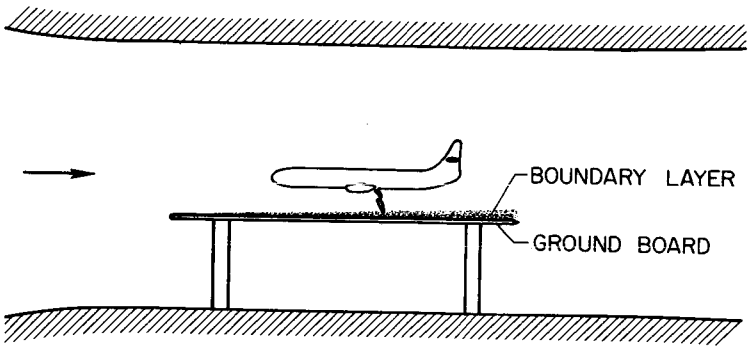

Figure 1

LIFT LOSS FOR MOVING MODEL AND CONVENTIONAL GROUND BOARD

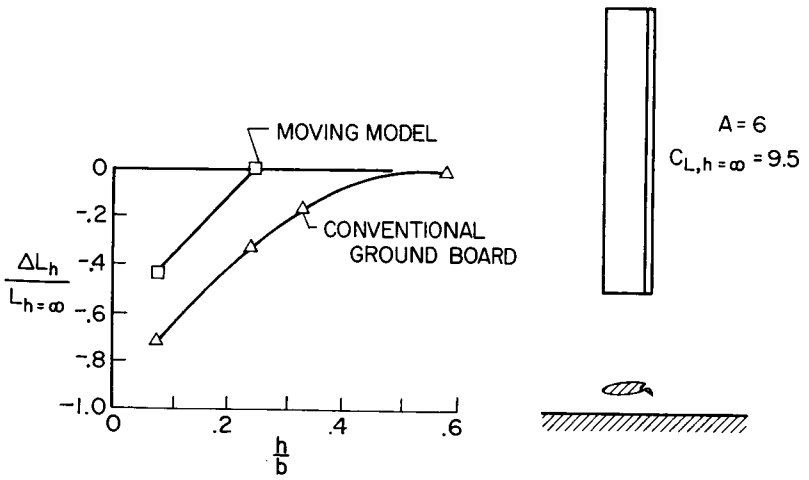

Figure 2

FLOW STUDIES OVER FIXED AND MOVING GROUND PLANES

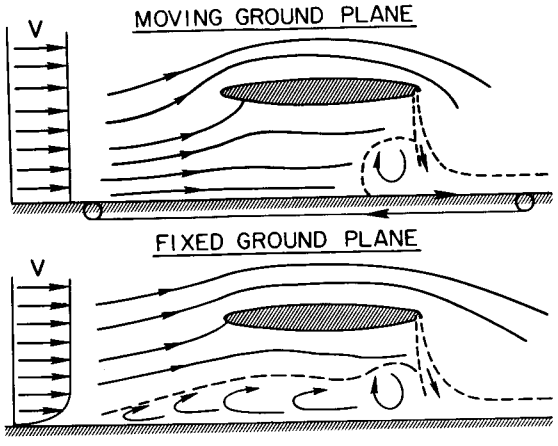

Figure 3

ENDLESS-BELT GROUND PLANE IN 17-FOOT TEST SECTION

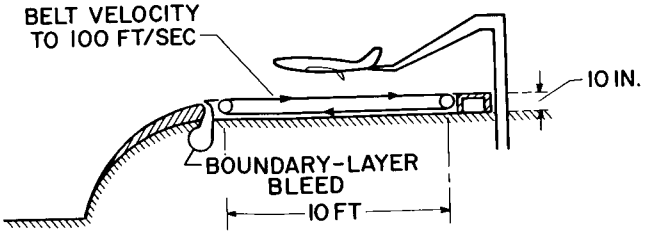

Figure 4

PHOTOGRAPH OF ENDLESS-BELT GROUND PLANE

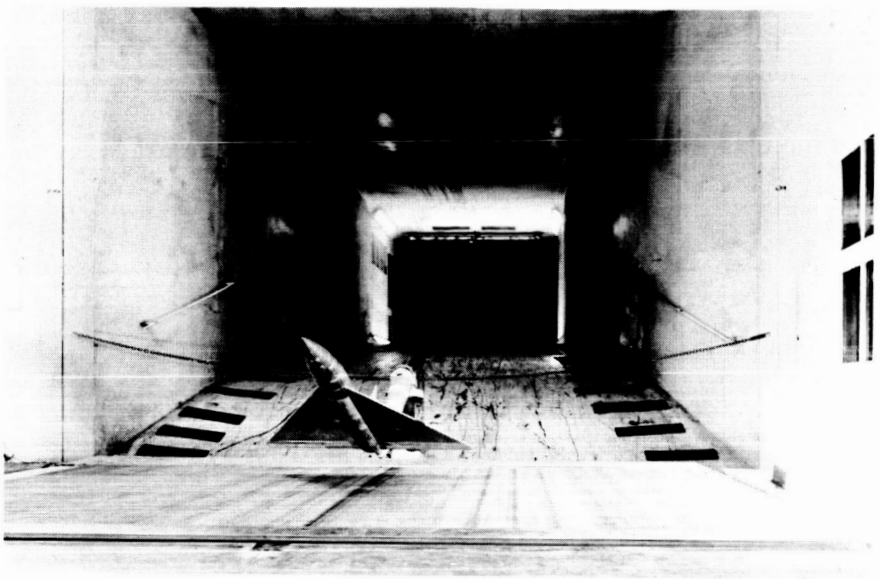

Figure 5

L-2653-6

LIFT LOSS FOR MOVING MODEL AND ENDLESS-BELT GROUND PLANE

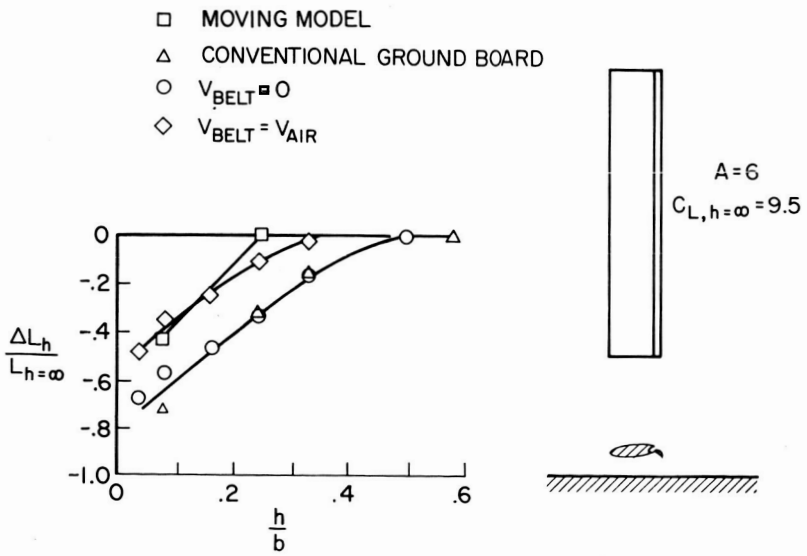

Figure 6

EFFECT OF BELT VELOCITY

$A = 7.0;\ \frac{h}{b} = 0.166;\ C_{L,h=\infty} = 7.4$

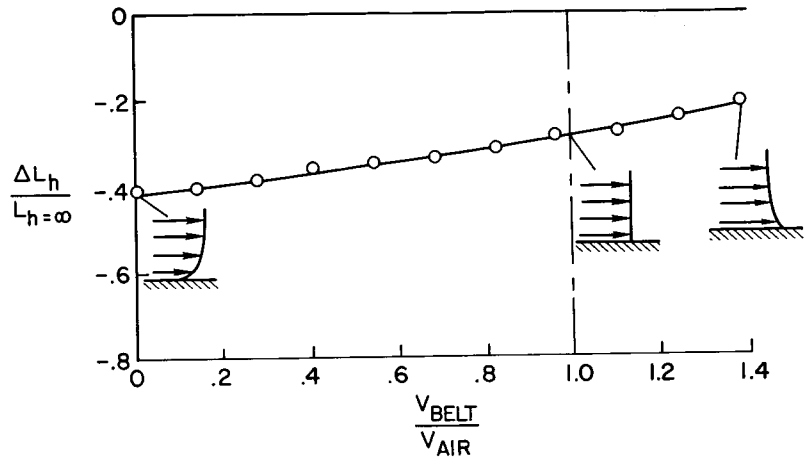

Figure 7

GROUND EFFECT ON UNPOWERED MODEL

A = 10; TAIL OFF

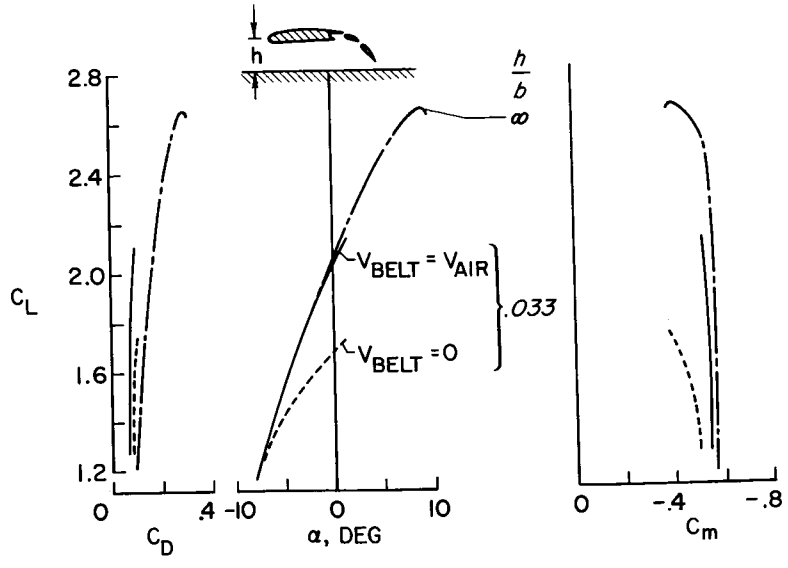

Figure 8

GROUND EFFECT ON TILT-WING CONFIGURATION

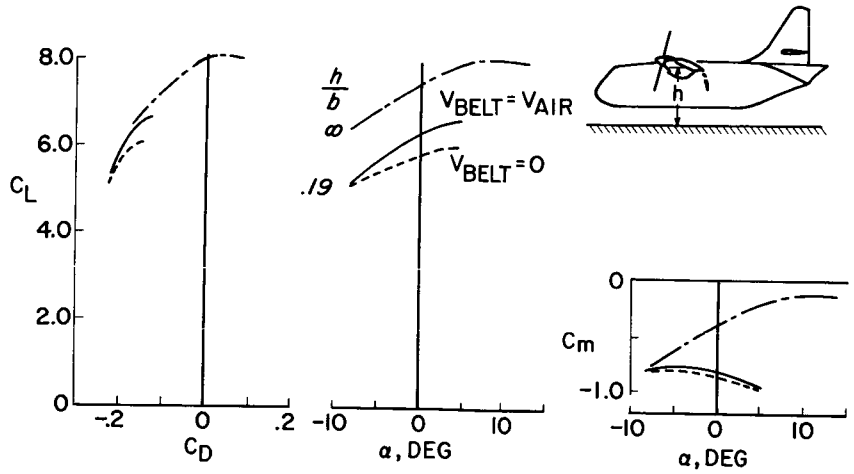

Figure 9

CONDITIONS REQUIRING ENDLESS-BELT GROUND PLANE

FULL-SPAN HIGH-LIFT CONFIGURATIONS

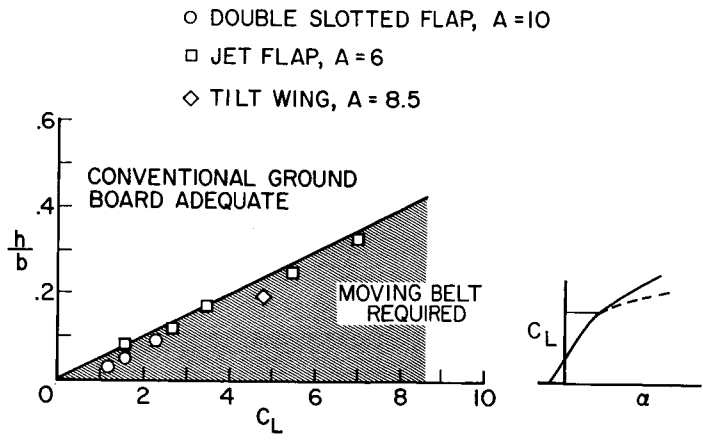

Figure 10

GROUND EFFECTS ON A TILTING DUCTED PROPELLER MODEL

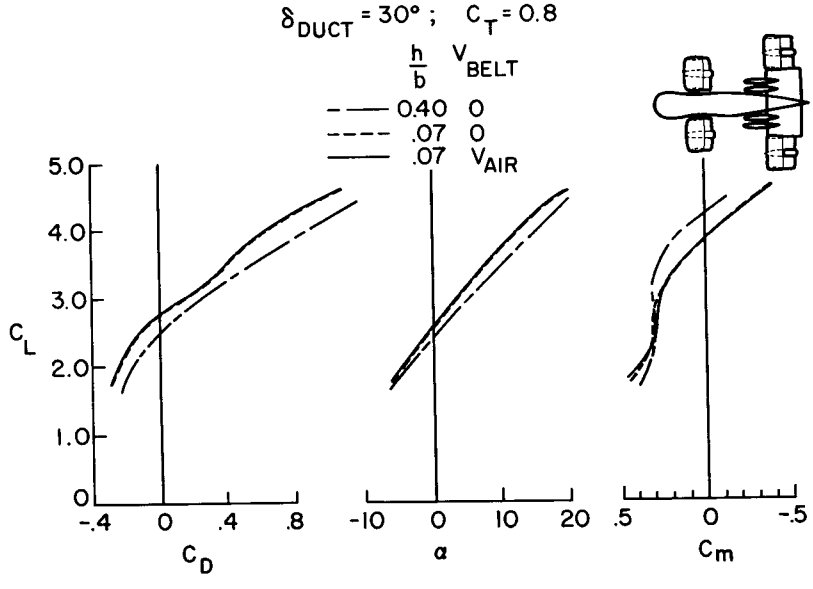

Figure 11

26. COMPARISON OF WIND-TUNNEL AND FLIGHT-TEST AERODYNAMIC DATA IN THE TRANSITION-FLIGHT SPEED RANGE FOR FIVE V/STOL AIRCRAFT*

By Woodrow L. Cook and David H. Hickey
Ames Research Center

SUMMARY

Four aircraft and one large-scale model which represent the V/STOL spectrum from low-disk-loading rotocraft to high-disk-loading lift-fan systems have been studied in the Ames Research Center's 40- by 80-Foot Wind Tunnel. In general, the aircraft were tested in the wind tunnel near trimmed, level-flight conditions. The power required, angle of attack, and control positions for the appropriate flight conditions as measured in the wind tunnel are compared with flight-test results. Agreement between wind-tunnel and flight-test measurements was generally good when wind-tunnel wall corrections were omitted. The aircraft and wind-tunnel geometry is related to wind-tunnel model sizing parameters and a VTOL lift parameter in order to establish tentative sizing criteria for V/STOL wind-tunnel testing with small wall effects.

INTRODUCTION

Author

For the advancement of the V/STOL state of the art and the development of useful V/STOL concepts and configurations, it is essential to have correct wind-tunnel test data. Very little experimental information is available for defining acceptable geometric relationships between models and wind tunnels or the momentum relationships between the propulsive and lift forces and the wind-tunnel air flow necessary for keeping wall effects small in wind-tunnel test data for the transition speed range of V/STOL type aircraft. The jet-boundary effects for V/STOL wind-tunnel tests are complex, and although the theoretical treatment of reference 1 represents an advancement in determining these effects, more accurate methods are being developed. The theory of reference 1 has been verified experimentally for helicopter rotors with low disk loadings (ref. 2). To determine wall effects of V/STOL concepts with higher disk loadings, a single model was tested in various sized wind tunnels (refs. 3-5) and the measured wall corrections were correlated with those calculated by the method of reference 1.

26

In order to predict the aerodynamic characteristics of V/STOL aircraft, it is often necessary to compromise the ideal ratio of model size to tunnel size required for data with small wall effects for a number of reasons, including the Reynolds number of the model and the propulsion system components, the

*Presented at AGARD Flight Mechanics Panel, Rome, Italy, Oct. 12, 1965.

requirement for tests of full-scale airplane hardware in large wind tunnels, and difficulties involved in designing and constructing of propulsion system hardware for small wind tunnels.

In this report the effect of wall constraints are examined by correlating the aerodynamic characteristics of wind-tunnel and flight investigations for four aircraft and one large-scale model representing several V/STOL concepts. In an attempt to provide some insight into the order of magnitude of model size to wind-tunnel size ratio, tentative boundaries for three sizing parameters are also presented, based on the correlation of flight results to wind-tunnel data.

NOMENCLATURE

A_L area of VTOL lifting element, $n(\pi D_L^2/4)$, sq ft

A_M momentum area of aircraft, $\pi b^2/4$, sq ft

A_T wind-tunnel cross-section area, sq ft

b wing span, ft

b_T tunnel width, ft

D_L diameter of lifting element, ft

h_T tunnel height, ft

i_w wing incidence angle, deg

L lift, lb

n number of propellers, fans, or rotors

T_F fan thrust, lb

V airspeed, knots

V_j jet velocity, knots

δ_f flap deflection angle, deg

DESCRIPTION OF TEST AIRCRAFT

Aircraft dimensions pertinent to the calculation of wind-tunnel wall corrections are presented in table I. Further details of the individual aircraft follow.

Bell XV-3

The XV-3 shown in figure 1 has a 23-foot-diameter helicopter rotor mounted on a mast at each wing tip. While hovering, the aircraft functions as a helicopter with helicopter-type controls. In order to attain wing-supported flight speed, the rotor masts are tilted forward until the rotor axes are alined with the flight path. Further details of this aircraft are given in reference 6.

Ryan VZ-3

The VZ-3 (fig. 2) uses an extensive flap system to deflect the propeller slipstream downward to attain VTOL capability. The VTOL controls consist of a combination of propeller-pitch controls, wing-mounted controls in the propeller slipstream, and reaction control from the thrust of the turboshaft engine. The transition from hover to conventional flight is accomplished by decreasing the flap deflection (and thus the propeller slipstream deflection) to provide thrust for acceleration. Further details of this aircraft are presented in reference 7.

Chance Vought-Ryan-Hiller XC-142

The XC-142 (the 0.6-scale model tested in the wind tunnel is shown in fig. 3) is a tilt-wing aircraft with four engines and four propellers. The aircraft uses full-span flaps to help deflect the propeller slipstream and reduce the wing tilt required. Hover controls consist of variable-pitch propeller controls, controls mounted on the wing in the propeller slipstream, and a tail-mounted rotor for pitch control. Speed for wing-supported flight is obtained by reducing wing tilt and flap deflection. Wind-tunnel data presented herein are from the 0.6-scale model (ref. 8). Model power limitations caused the test airspeed to be reduced to about one-half of the full-scale value.

Lockheed XV-4A

The XV-4A (fig. 4) is powered by two jet engines which exhaust vertically through an ejector in the fuselage for VTOL lift and exhaust normally for cruise thrust. Hover, pitch, and yaw control are supplied by the reaction from tail-pipe bleed, and roll control from compressor bleed. Blowing boundary-layer control is used to increase tail and elevator effectiveness during transition. Acceleration to wing-supported flight is achieved by tilting the aircraft. Further details of the aircraft are presented in reference 9.

Ryan XV-5A

The XV-5A (fig. 5) is powered by two jet engines which drive two fans in the wing and one in the nose for VTOL lift. These engines provide direct thrust for cruise. VTOL roll control is provided by lift-fan thrust modulation, yaw control by differential operation of wing-fan exit louvers, and pitch control by nose-fan thrust modulation. Acceleration to wing-supported

flight is provided by deflecting the main fan flow aft with the fan exit louvers. Further details of the aircraft are presented in reference 10.

TESTING

The wind-tunnel tests were all performed in the Ames 40- by 80-Foot Wind Tunnel with similar test setups (e.g., see figs. 1-5) and procedures. However, the flight tests were carried out by various agencies which had various specific objectives. In none of the wind-tunnel or flight tests was the prime objective to correlate wind-tunnel and flight-test results; thus the amount of data available for this correlation is limited.

Wind-Tunnel Testing

Aerodynamic and static-stability and control characteristics were all explored near balanced flight conditions. At discrete airspeeds, from 0 to wing-supported flight speed, data were obtained with lift equal to weight, drag equal to thrust, and pitching moment equal to zero. Then angle of attack, angle of sideslip, power setting, and the various control settings were varied to determine the effect of each variable on aircraft characteristics. This type of wind-tunnel testing is the fastest way of obtaining pertinent data on flying characteristics.

Flight Testing

Unless otherwise noted, the flight-test results were obtained with steady-state conditions for approximately level flight or hovering and were further limited to avoid deep penetration into known problem areas. Flight work with the XV-3 and VZ-3 was done at Ames, and an Ames representative was on hand during XV-5A flight tests, so the problems of coordinating and interpreting data were easily solved. The contractors supplied the applicable flight-test data that had been reduced for the XC-142 and the XV-4A, which resulted in a smaller amount of data being available for correlation because the major interests of the contractors were not wind-tunnel and flight-test correlations.

RESULTS AND DISCUSSION

Correlation of Wind-Tunnel and Flight-Test Results

Representative aerodynamic data from wind-tunnel and flight tests for the five aircraft are compared in this section. Unless otherwise noted, none of the wind-tunnel data are corrected for wall effects. In most cases the comparison is made at steady-state level-flight or hovering conditions (lift equal to weight, thrust equal to drag).

XV-3.- Power required for level flight, fuselage angle, and longitudinal control position for trim both in flight and in the wind tunnel are shown as functions of airspeed in figure 6. Power required as a function of airspeed shows excellent agreement, but angle-of-attack and longitudinal-control data show scatter. Since accuracy in setting longitudinal control was $\pm 1^{\circ}$ in the wind tunnel, and angle of attack is difficult to measure accurately in slow-speed flight, the agreement between the two sets of data is considered good. Although the aircraft span was large with respect to the tunnel width (table I), the disk loading was low (about 5 psf) so that the wake deflection angle due to airspeed was large and the adverse effects of model size on wind-tunnel wall effects were small.

VZ-3.- Similar results (power required, angle of attack, and longitudinal control) are presented in figure 7 for this deflected slipstream aircraft. Again, power required for level flight showed excellent agreement between wind tunnel and flight. A 23-percent increase in horizontal-tail area, added after the wind-tunnel tests, may have contributed to the fuselage angle of attack for trim being about 1° greater in flight and the nose-down elevator for trim being about 2° less in flight than in the wind tunnel. This aircraft was small with respect to the wind tunnel and the disk loading was moderate (20 psf) so that wind-tunnel wall effects were small.

The small discrepancies noted between wind-tunnel and flight-test results did not prevent adequate assessment of the aircraft performance, stability, and control.

XC-142.- Wing incidence angle for trimmed, level flight is presented in figure 8 as a function of airspeed. Wind-tunnel and flight-test results agree within 5° for the wing-tilt angle required for 30-knots airspeed and within 2° for 55-knots airspeed.

Descent rates obtained in flight and predicted from wind-tunnel data are presented in figure 9 as a function of airspeed for several aircraft configurations. The flight-test data fall into two curves, one is the descent rate for buffet onset, and the other is the maximum descent rate as defined by small lateral-directional oscillations. The descent rates for buffet onset seem to agree with wind-tunnel data up to 45-knots airspeed at the higher wing-tilt angles. At higher airspeeds and lower wing-tilt angles the maximum descent rates obtained in flight are much greater than those estimated from the wind-tunnel data. The descent rates estimated from the wind-tunnel data are based on when $C_{l_{max}}$ was first attained, or, in the cases noted, on the maximum angle of attack for which data are available. It is unlikely that wind-tunnel wall effects are responsible for the discrepancy because of the better correlation of flight and wind-tunnel results at low speed. A more likely cause of the difference is either the low maximum lift of the model, or the aircraft's flying beyond $C_{l_{max}}$ with no adverse effects. Model scale and the reduction in test airspeed caused by the low installed power combined to reduce Reynolds number to one-third of the full-scale value for a given value of thrust coefficient; this caused model Reynolds number to be in the region where maximum lift can be significantly affected, and can thus affect the correlation.

Based on present knowledge, agreement is fair for trimmed level flight but poor for allowable descent angles.

XV-4A.- Flight-test data were limited for this aircraft. Data are available only for transitions during which the aircraft was decelerating. Figure 10 shows the longitudinal acceleration, angle of attack, and elevator position as functions of airspeed during a transition. The angle of attack and elevator position for trim estimated from the wind-tunnel data to produce the equivalent deceleration in level flight are included on the figure. Angle of attack generally agreed to within 1°, but elevator position differed by 4° to 7° (12 percent of maximum travel). The reason for the relatively poor correlation of elevator angle is not clear. The aircraft tested in the wind tunnel was not the same aircraft that supplied the flight-test data, so some of the difference could be based on differences in rigging or effectiveness of horizontal-tail boundary-layer control.

Both conventional wind-tunnel wall corrections and Heyson's corrections were applied to the XV-4A wind-tunnel data in an attempt to improve correlation with flight. Figure 11 shows the XV-4A angle of attack for the same deceleration as in figure 10, as calculated from uncorrected wind-tunnel data (level flight was assumed), and from wind-tunnel data with conventional corrections and with Heyson's corrections (including the effects of finite span). Conventional corrections increased the angle-of-attack discrepancy from 1° to about 1.5°. Heyson's corrections increased the discrepancy slightly.

XV-5A.- Relative power, angle of attack, fan exit louver angle, and longitudinal stick position required for balanced flight are presented as functions of airspeed in figure 12. The power required for level flight decreased as airspeed increased, indicating that, rather than a "suckdown" effect, lift for a constant power setting increased with airspeed. Based on the results in reference 11, a reduction of lift with airspeed would be expected for constant power. Although the flight-test data show considerable scatter due to small accelerations, the agreement between wind tunnel and flight is good. It should be noted that this aircraft was nearly twice the size of the XV-4A, and lifting-element loading was about the same. The largest discrepancy between flight and wind-tunnel tests is in longitudinal stick position; this discrepancy is about 1°, or 3 percent of the total stick travel.

Subsequent to these flights, the fairings at the wing-fan hub between the rotor blades were removed, changing fan performance so that more power and larger fan-exit louver angles were required for a given flight speed. Flight-test data with the revised fan configuration were obtained at constant airspeed and several angles of attack. The longitudinal stick position for trim as a function of angle of attack is presented in figure 13 for three airspeeds. Good correlation is evident at 36 and 50 knots. Agreement is poor at 70 knots, indicating the static stability in the wind tunnel was different from that measured in flight; the discrepancy would be further increased by wall corrections. At least a part of the failure to correlate at 70 knots is due to the sensitivity of pitching moment to exit louver angle at this airspeed. Because the fairings had been removed, the louver angles in flight were 1.5° to 7° greater than for the wind-tunnel results shown in figure 13.

The XV-5A wind-tunnel tests showed an instability with angle of attack over part of the angle-of-attack range, the particular angle of attack for instability being a function of the nose-fan thrust-modulator position. Tests with and without nose-fan thrust modulation indicated that the instability was caused by a reduction of tail effectiveness due to the flow from the nose fan with the thrust modulated to give a large nose-down control moment. In the flight tests, aircraft angle of attack was increased until the tail angle-of-attack indicator registered turbulent flow; the test was then terminated. The consequent flight-test angle-of-attack boundary and the wind-tunnel angle of attack for instability are presented in figure 14. Considering the qualitative nature of the flight-test data, agreement is good, and it appears that flow conditions at the tail were adequately simulated in the wind tunnel.

The effect of wind-tunnel wall corrections on the XV-5A wind-tunnel and flight correlation is shown in figure 15. The effect of both finite span and side-by-side lifting elements were included for Heyson's corrections. In this case conventional wall corrections were nearly as large as Heyson's corrections, but they did not improve the correlation; however, the effect on exit louver angle required for trimmed flight was small. The most significant effect was on power required; wall-effect corrections amounted to a 10-percent increase over that measured in flight.

Summary of test results.- The correlation between flight-test and wind-tunnel results for these five aircraft demonstrates the accuracy achieved in V/STOL wind-tunnel testing with aircraft-tunnel size ratios approaching those used for wind-tunnel tests of conventional aircraft. Correlation with uncorrected wind-tunnel data was good, with the exception of the XC-142 model. It was also shown that for the two cases examined, applying wind-tunnel wall corrections calculated by the available methods degraded the correlation, indicating a need for more theoretical work on wind-tunnel wall corrections for aircraft with localized, high-disk-loading lifting elements. For the majority of correlations of wind tunnel with flight, the conditions considered were for lift equal to weight, and thrust equal to drag. Wall effects were smaller for these flight conditions than when aircraft drag was unbalanced, because the lifting-element wake is deflected downstream.

Wall-Effect Parameters

Present test results.- The preceding section examined the accuracy of uncorrected wind-tunnel data for several aircraft of widely differing characteristics and sizes with respect to the wind tunnel. Model-tunnel sizing parameters for the aircraft that demonstrated acceptable correlation can be related to aerodynamic parameters in order to indicate acceptable V/STOL model sizing. According to reference 3, the pertinent model-tunnel sizing parameters are the ratio of the area of the VTOL lift generators to wind-tunnel cross-sectional area, A_L/A_T, for VTOL concepts where the majority of the lift is supplied by the lifting elements, and the ratio of momentum area to tunnel cross-sectional area, A_M/A_T, for concepts where the lift is distributed across the wing span. Study of reference 1 also shows that lifting-element wake-deflection angle, which is a function of disk loading at a given airspeed (wake deflection angle = $f(V/V_j) = f(V/\sqrt{T_F})$), is another important parameter.

Disk loading is an important parameter for all V/STOL aircraft and provides a common basis for comparison. Accordingly, both lifting-element and momentum area ratios are plotted versus disk loading in figure 16 for the five test aircraft.[1] Both suggested area ratios are included for all five aircraft. The XV-3 and XV-5A represent extremes of the ratio of model size to wind-tunnel size that have small wall effects. Narrow shaded areas have been drawn connecting their data points to indicate a possible size-ratio boundary for small wall effects. Ratios of model to wind-tunnel size that fall below these areas indicate acceptable model sizing. The point for the XC-142, which appears above the shaded area, leaves unresolved questions concerning the correlation, and it may be that this model is too large for the wind tunnel. The wind-tunnel and flight correlation was acceptable for the VZ-3 and XV-4A, and the data points for these aircraft fall below the shaded area. The tentative nature of the location and shape of the shaded areas on figure 16 should be emphasized.

The narrow shaded areas shown in figure 16 connect points for two aircraft tested in the wind tunnel at different minimum speeds; the aircraft with the lower disk loadings showed good agreement to speeds as low as 20 knots; whereas for those with higher disk loadings it was difficult to get reliable data below 30 knots because blockage and recirculation made it difficult to achieve steady test conditions. Additional data may show that separate 20- and 30-knot boundaries should be drawn on the figure, rather than the single boundary for the two airspeeds. The boundaries drawn on figure 16 probably approximate a practical test boundary because the need for wind-tunnel data between 0 and 30 knots depends on disk loading; aircraft with low disk loadings will fly a larger percentage of the time at low speeds and will be more sensitive to gusts or small maneuver velocities than aircraft with higher disk loadings at the lower forward speeds.

Comparison of boundaries with other results.- Small-scale results, from testing the same model in different wind-tunnel test sections (refs. 2 and 5), were analyzed in an attempt to document further the boundaries in figure 16. For all models, the ratio of model to tunnel size in the smallest test section approached conventional values, and test conditions were near the shaded boundary areas of figure 16. Discrepancies in lift of 6 percent or less (when evaluated with thrust equal to drag), caused by differing test-section size, are considered to be small wall effects and of the same order as the accuracy of the data in the preceding wind-tunnel flight-test correlation. The uncorrected tilt-wing data from the 7- by 10-foot wind tunnel (ref. 5) were well within the 6-percent margin for balanced flight at low speed. Uncorrected lift data from a helicopter rotor in large and small test sections (ref. 2) also agreed within 6 percent for balanced flight at low speed. Reference 5 did not present balanced flight data for the lift-fan configurations, so it was necessary to use data that correspond to large aircraft decelerations. Unlike the other two models, the two lift-fan configurations in the smallest

[1]Other common parameters, such as the ratio of disk loading to dynamic pressure, velocity ratio V/V_j, or wake deflection angle, were considered but were not used because of the assumptions required for their calculation. Furthermore, these parameters obscure the wide range of disk loading represented by the composite data from the several aircraft.

test sections showed sizable lift errors. It was thus necessary to plot both the fan-in-fuselage and fan-in-wing lift errors in the various wind-tunnel test sections as functions of ratio of model to wind-tunnel size in order to determine the area ratio for a 6-percent lift discrepancy. This method introduced a further uncertainty because the wind tunnels had different width-to-height ratios. The appropriate ratios of model to wind-tunnel size for these four models are compared with the wind-tunnel flight-test correlation boundaries on figure 17. The two model tests with the lower disk loadings indicate no conflict between the full-scale results (the shaded areas on fig. 17) and the model tests; however, for the models with the higher disk loadings a decided discrepancy is evident. At least a partial explanation is failure to balance model drag, so that the wake deflection angle was less for these models than for the similar aircraft. If Heyson's corrections are taken as an indication of the importance of wake deflection angle, balancing the drag can reduce the calculated wall corrections to as little as 50 percent of the values with the drag unbalanced. A change in this direction would tend to reduce the discrepancy between the small-scale results with high disk loading and the correlation of wind-tunnel and flight-test data. Another possible cause of the discrepancy is the large span relative to wind-tunnel width; this subject is discussed in the next section.

Although some of the results presented in reference 5 disagree with the results presented here for model-tunnel sizing parameters, adequate reasons for the disagreement exist. For the conditions considered in the present report (i.e., realistic flight conditions and allowable errors no larger than data-measurement errors), the ratios of model to wind-tunnel size, as indicated by the boundary lines on figure 16, which are larger than previously considered usable, should give acceptable wind-tunnel results for V/STOL model testing.

Test-section geometry.- The correlation of wind-tunnel and flight-test results is based on tests in a wind tunnel with a 2-to-1 width-height ratio, which is larger than that in any of the small-scale tests. This test-section geometric parameter has a direct bearing on span-to-tunnel width ratios, which is an important parameter in conventional wind-tunnel wall corrections and may also be important for V/STOL model testing. This ratio is presented in figure 18 as a function of disk loading for the aircraft in the correlation of wind-tunnel and flight-test data (solid symbols) and for the models in references 2 and 5 installed in their smallest test section (open symbols). The aircraft and models that indicated insignificant corrections have conventional ratios of span to wind-tunnel width at low disk loadings and relatively small span-to-width ratios at high disk loadings. The two small-scale lift-fan models that indicated large wind-tunnel wall corrections had larger span-to-width ratios than the comparable aircraft. These results suggest that another boundary area in addition to those in figure 16, indicating acceptable ratios of span-to-tunnel width, may be appropriate to specify the effects of test-section geometry when sizing a V/STOL model. For certain V/STOL concepts where the propulsive system span extends considerably beyond the span of the wing, as on compound helicopters or tilt rotor aircraft or where the propulsive system extends only over a small part of the wing span, as on fan-in-wing systems, the lifting element span may be a factor along with wing span for determining the magnitude of wall effects or model size. The effects

of wind-tunnel cross-section geometry on wall effects should be studied experimentally since they may significantly influence V/STOL wind-tunnel data.

CONCLUDING REMARKS

In order to obtain satisfactory data from V/STOL wind-tunnel testing in the low-speed flight range, it is necessary to resolve the conflict in model sizing caused by the need to minimize both wall effects and scale effects. In reference 5, scale effects were shown to be larger than the effect of Heyson's corrections in some cases, but in other cases (the XV-4A, 0.18 scale, $A_L/A_T = 0.01$) were shown to be negligible. Thus careful planning of test programs is required in order to minimize the possibility of obtaining erroneous or misleading test data.

The results of correlating the aerodynamic data obtained in wind-tunnel and flight investigations of several V/STOL concepts have given an indication of gross tentative boundaries that should be observed for three sizing parameters of model geometry to wind-tunnel geometry. Experience may indicate that these boundaries are optimistic in model size in other width-to-height ratio wind-tunnels or apply only to the specific type of aircraft considered in the correlation. Observation of the indicated boundaries should yield data of reasonable accuracy and prove to be useful for predicting aerodynamic characteristics and trends related to changes in configuration. However, the data may be lacking in absolute precision with regard to angle of attack and effects of distortion, particularly at velocities below 20 to 30 knots, depending on the disk loading of the propulsive system. For testing at lower airspeeds or at higher disk loadings than considered herein, smaller ratios of model to wind-tunnel size will be necessary; whereas for STOL testing larger values of the sizing ratios should be acceptable. The models should be as large as permissible because Reynolds number effects can be critical for inlets, high-lift devices, and the characteristics of propellers, fans, and compressors. The flow distribution of the lifting elements should approximate full-scale characteristics to match secondary flow effects, and disk loading should approximate full-scale disk loading in order to obtain adequate data over the airspeed range of interest and provide an acceptable Reynolds number when matching full-scale thrust coefficients. For a given wing loading, conditions closely corresponding to realistic flight values of acceleration and deceleration reduce wind-tunnel wall effects and enable use of larger models in wind tunnels. Instrumentation sufficient for determining the performance of the various model components, including the lifting elements, is useful in detecting substandard performance of the components due to low Reynolds number or failure to realistically simulate the aircraft or lifting-element disk loading.

REFERENCES

1. Heyson, Harry H.: Linearized Theory of Wind-Tunnel Jet-Boundary Corrections and Ground Effect for VTOL-STOL Aircraft. NASA TR R-124, 1962.

2. Lee, Jerry Louis: An Experimental Investigation of the Use of Test Section Inserts as a Device to Verify Theoretical Wall Corrections for a Lifting Rotor Centered in a Closed Rectangular Test Section. Thesis for Masters Degree, University of Washington, 1964.

3. Davenport, Edwin E.; and Kuhn, Richard E.: Wind-Tunnel Wall Effects and Scale Effects on a VTOL Configuration With a Fan Mounted in the Fuselage. NASA TN D-2560, 1965.

4. Grunwald, Kalman J.: Experimental Study of Wind-Tunnel Wall Effects and Wall Corrections for a General-Research V/STOL Tilt-Wing Model With Flap. NASA TN D-2887, 1965.

5. Powered-Lift Aerodynamics Section Staff: Wall Effects and Scale Effects in V/STOL Model Testing. Paper at AIAA-Navy Aerodynamic Testing Conference, 1964.

6. Koenig, David G.; Greif, Richard K.; and Kelly, Mark W.: Full-Scale Wind-Tunnel Investigation of the Longitudinal Characteristics of a Tilting-Rotor Convertiplane. NASA TN D-35, 1959.

7. James, Harry A.; Wingrove, Rodney C.; Holzhauser, Curt A.; and Drinkwater, Fred J., III: Wind-Tunnel and Piloted Flight Simulator Investigation of a Deflected-Slipstream VTOL Airplane, the Ryan VZ-3RY. NASA TN D-89, 1959.

8. Deckert, Wallace H.; Page, V. Robert; and Dickinson, Stanley O.: Large-Scale Wind-Tunnel Tests of Descent Performance of an Airplane Model With a Tilt Wing and Differential Propeller Thrust. NASA TN D-1857, 1964.

9. Anon.: Lockheed Hummingbird Preliminary Aircraft Specification. Lockheed Document ER-5180M, May 1961.

10. Anon.: Lift-Fan Flight Research Aircraft Program, Airplane Detail Specification. Specification 118A, General Electric Company, Flight Prop. Lab. Dept., Cincinnati, Ohio, April 1963.

11. Spreemann, Kenneth P.: Induced Interference Effects on Jet and Buried-Fan VTOL Configurations in Transition. NASA Conference on V/STOL Aircraft, 1960.

TABLE I.- AIRCRAFT GEOMETRY WITH RESPECT TO THE WIND TUNNEL

Aircraft	Type	$\frac{A_L}{A_T}$	$\frac{A_M}{A_T}$	$\frac{b}{b_T}$	$\frac{T}{A_L}$	Applicable figures
XV-3	Tilt rotor	0.291	0.758	0.656	5.6	1, 6
VZ-3	Vectored slipstream	.046	.151	.292	19.9	2, 7
XC-142	Tilt wing	.095	.451	.506	50*	3, 8, 9
XV-4A	Jet ejector	.0077	.186	.325	300	4, 10, 11
XV-5A	Lift fan	.0149	.244	.372	275	5, 12, 13, 14, 15

*Full-scale disk loading only; model disk loading was 15 lb/sq ft.

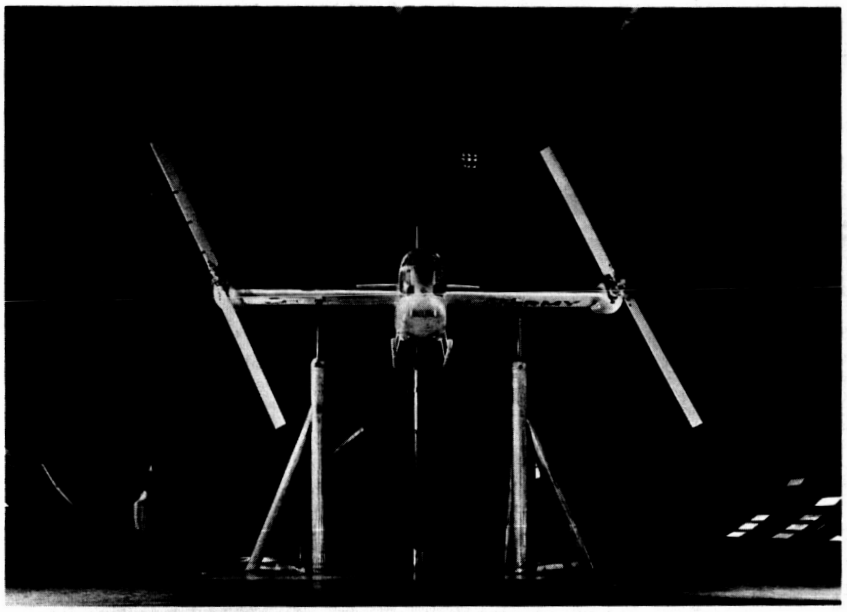

A-23164

Figure 1.- The Bell XV-3 mounted in the Ames 40- by 80-Foot Wind Tunnel (aircraft wind-tunnel geometry in table I).

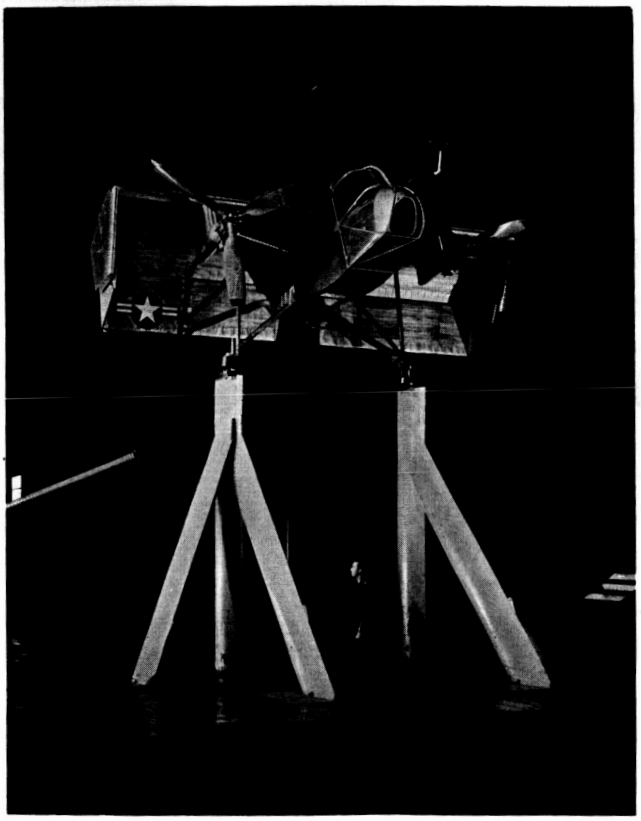

A-23991

Figure 2.- The Ryan VZ-3 mounted in the Ames 40- by 80-Foot Wind Tunnel (aircraft wind-tunnel geometry in table I).

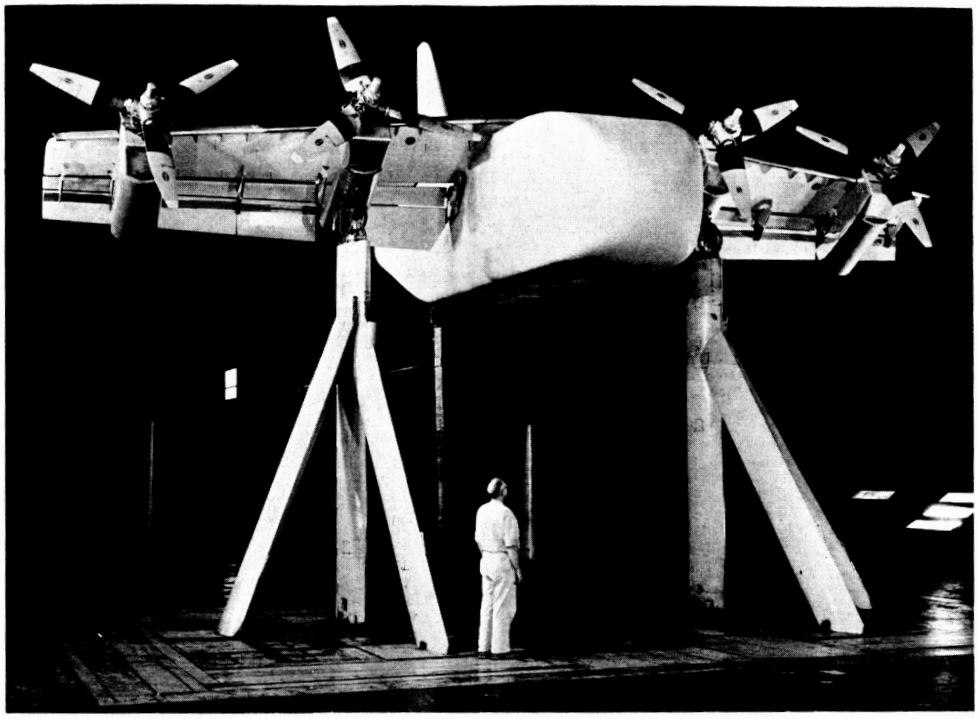

A-29909

Figure 3.- The LTV XC-142 model mounted in the Ames 40- by 80-Foot Wind Tunnel (model wind-tunnel geometry in table I).

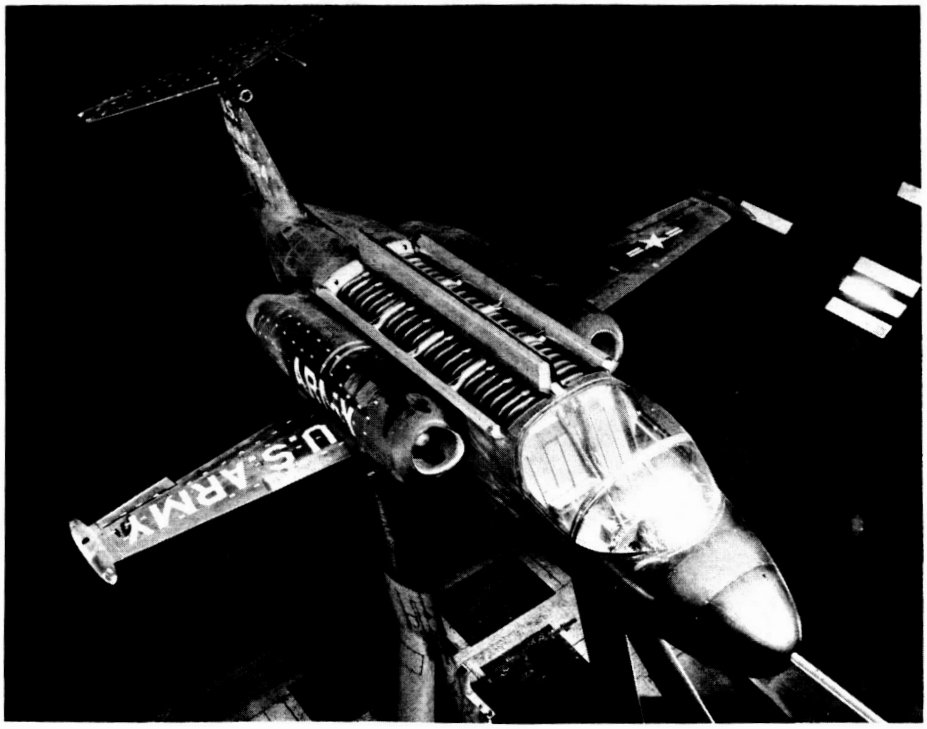

A-33193

Figure 4.- The Lockheed XV-4A mounted in the Ames 40- by 80-Foot Wind Tunnel (aircraft wind-tunnel geometry in table I).

A-35394-11

Figure 5.- The Ryan XV-5A mounted in the Ames 40- by 80-Foot Wind Tunnel (aircraft wind-tunnel geometry in table I).

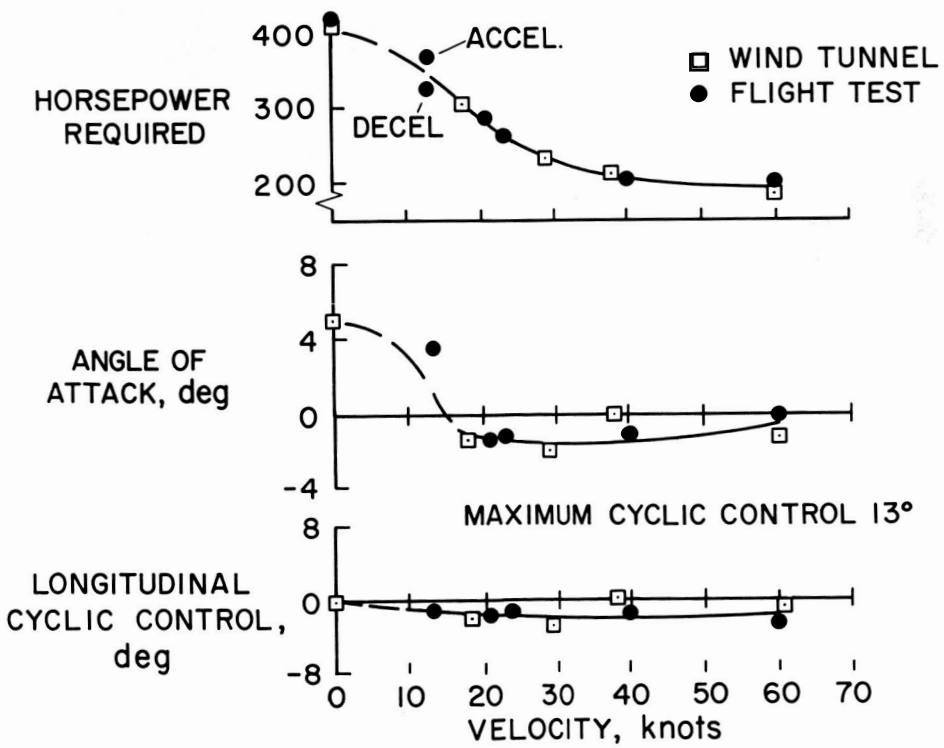

Figure 6.- Balanced, level-flight characteristics of the XV-3 convertiplane as measured in the wind tunnel and in flight.

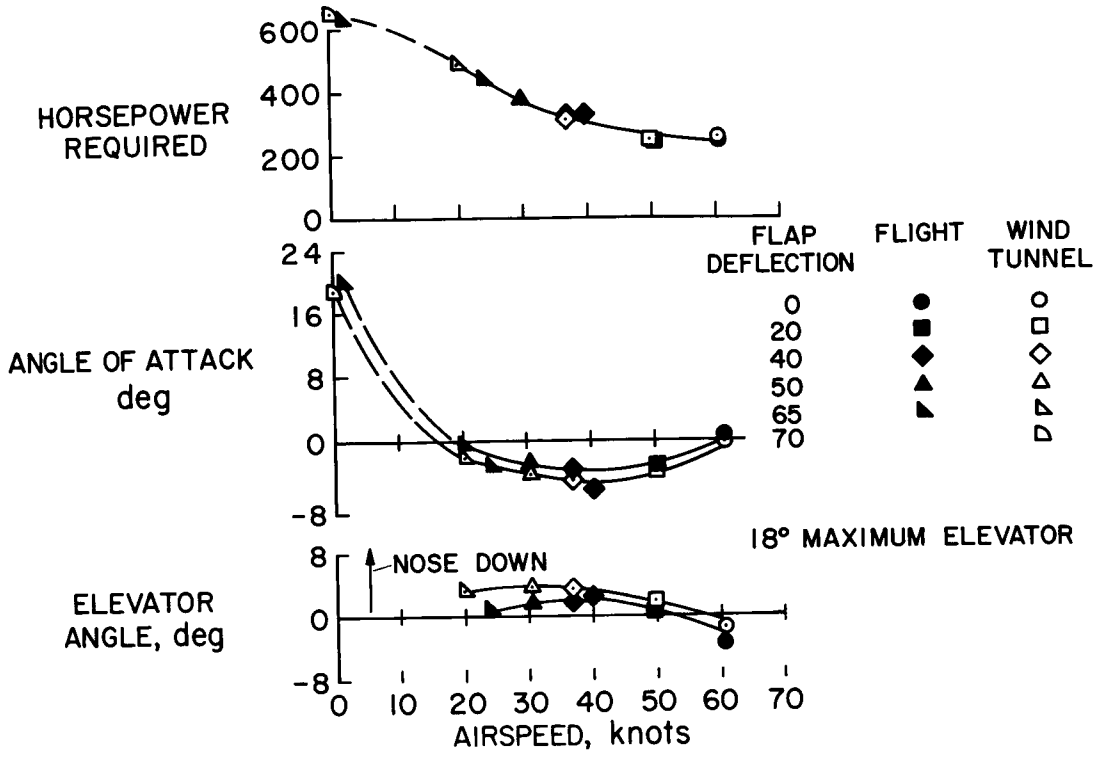

Figure 7.- Balanced, level-flight characteristics of the VZ-3 aircraft as measured in the wind tunnel and in flight.

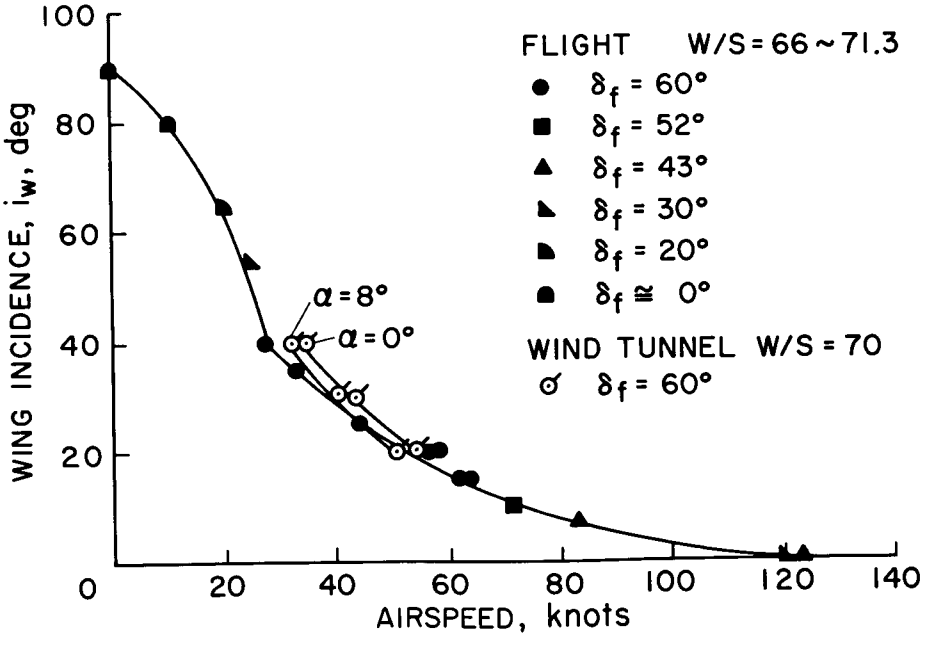

Figure 8.- Wing-tilt angle for balanced, level flight of the XC-142.

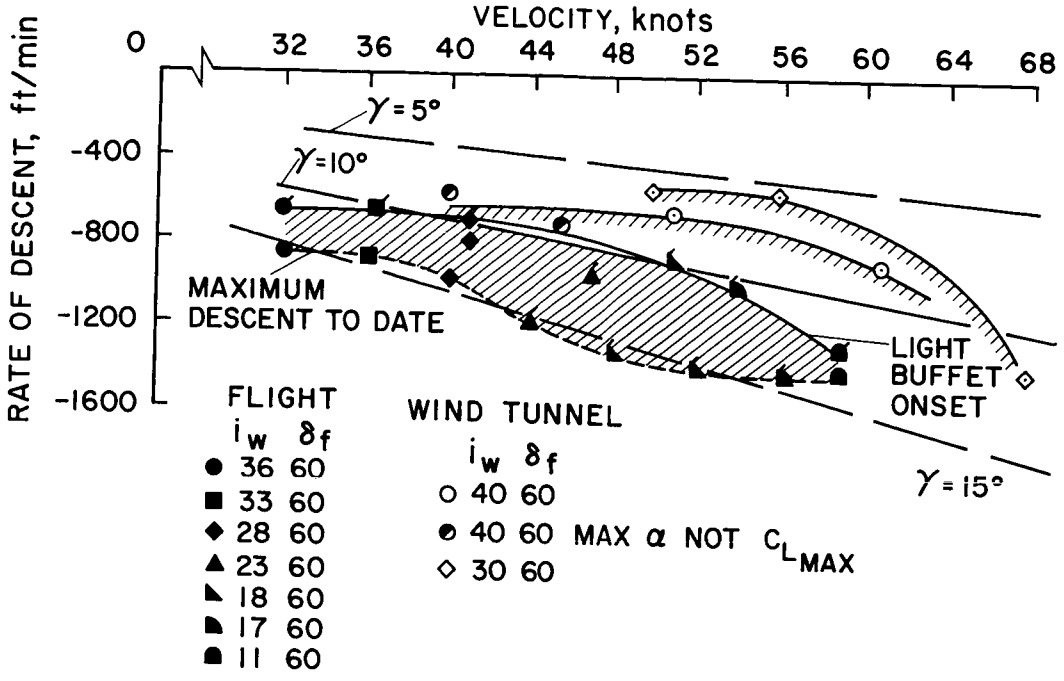

Figure 9.- Descent boundaries for the XC-142.

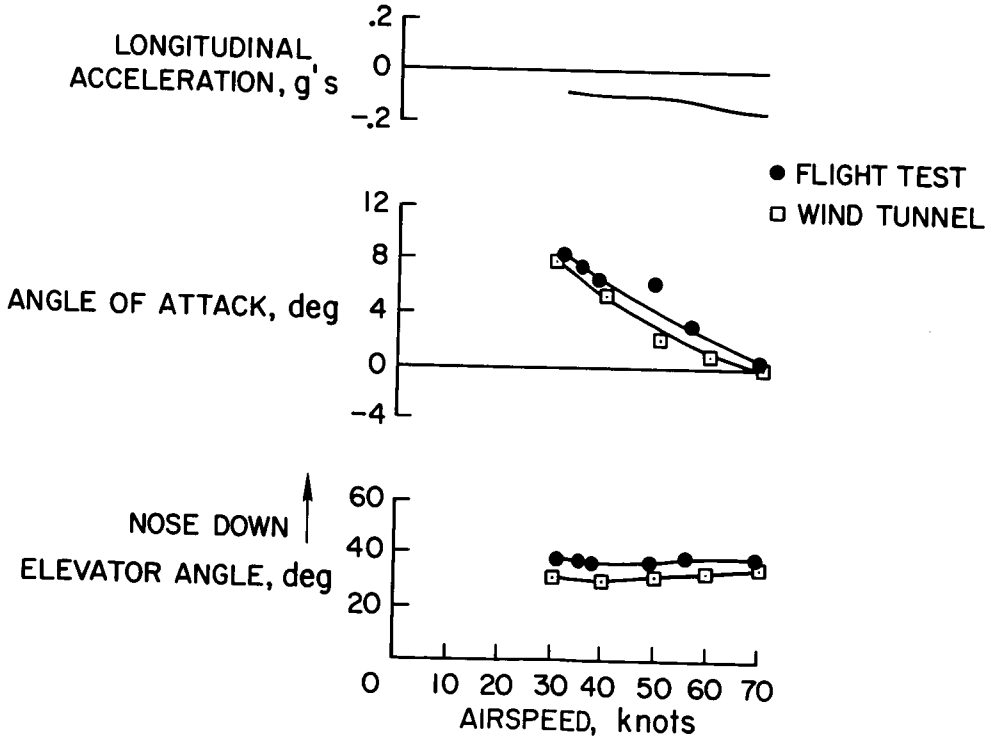

Figure 10.- Characteristics of the XV-4A.

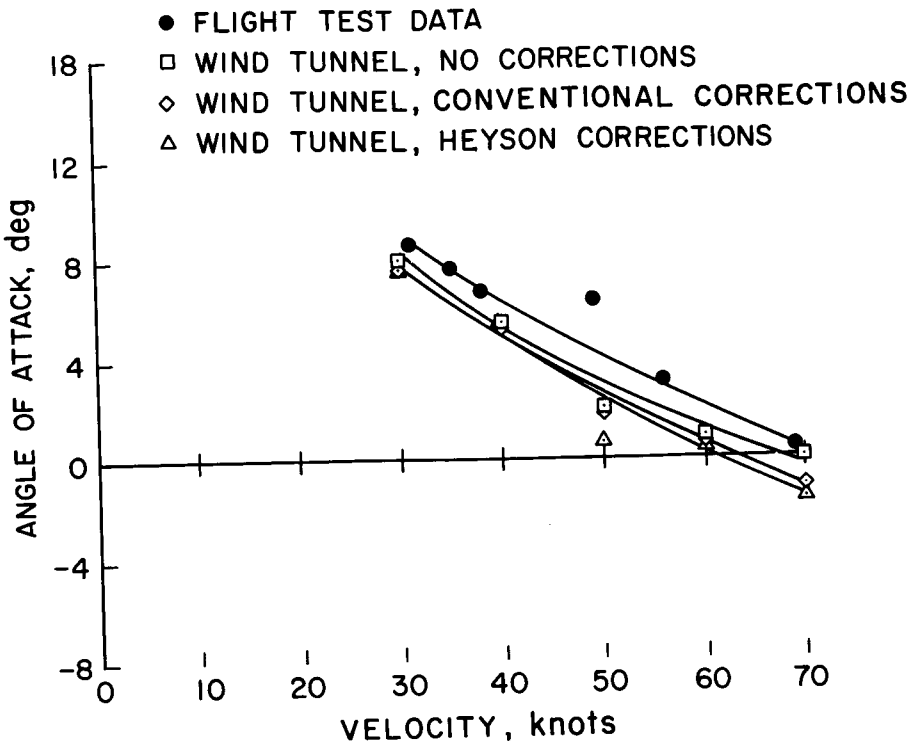

Figure 11.- The effect of wind-tunnel wall corrections on the correlation between wind-tunnel and flight-test results for the XV-4A.

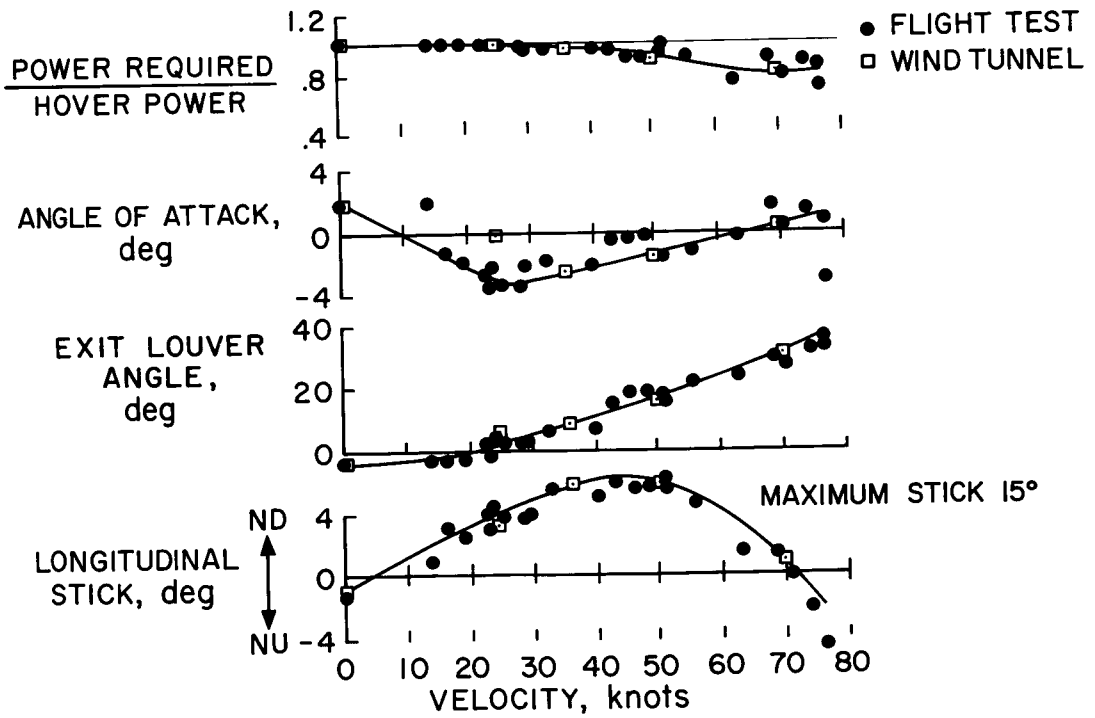

Figure 12.- Balanced, level flight characteristics of the XV-5A as measured in the wind tunnel and in flight.

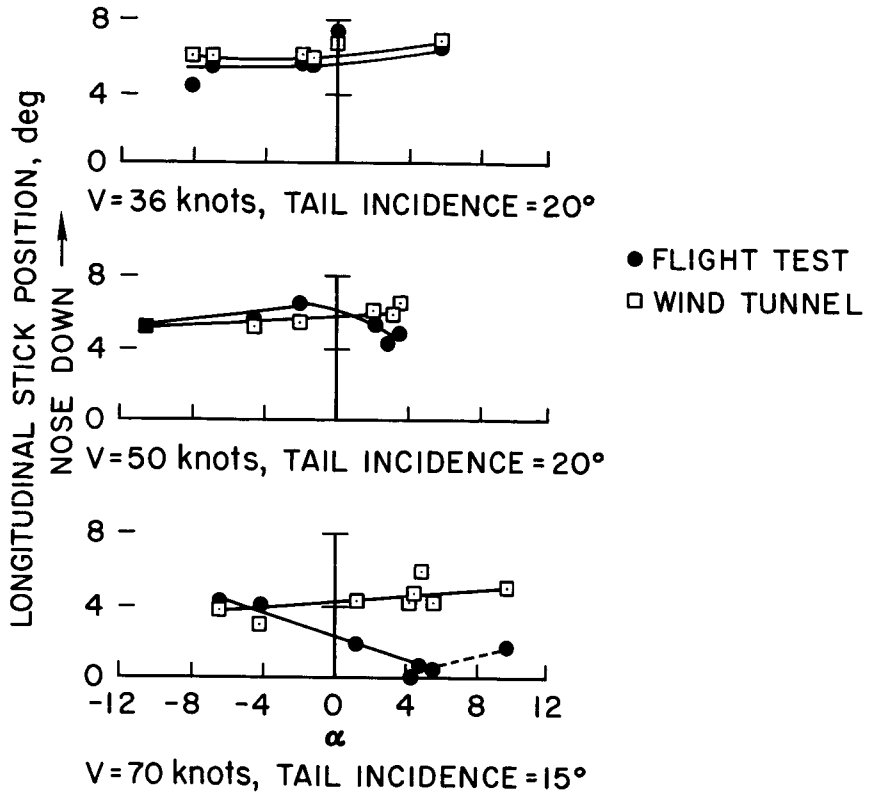

Figure 13.- The variation with angle of attack of longitudinal stick position for trim for the XV-5A aircraft in flight and in the wind tunnel.

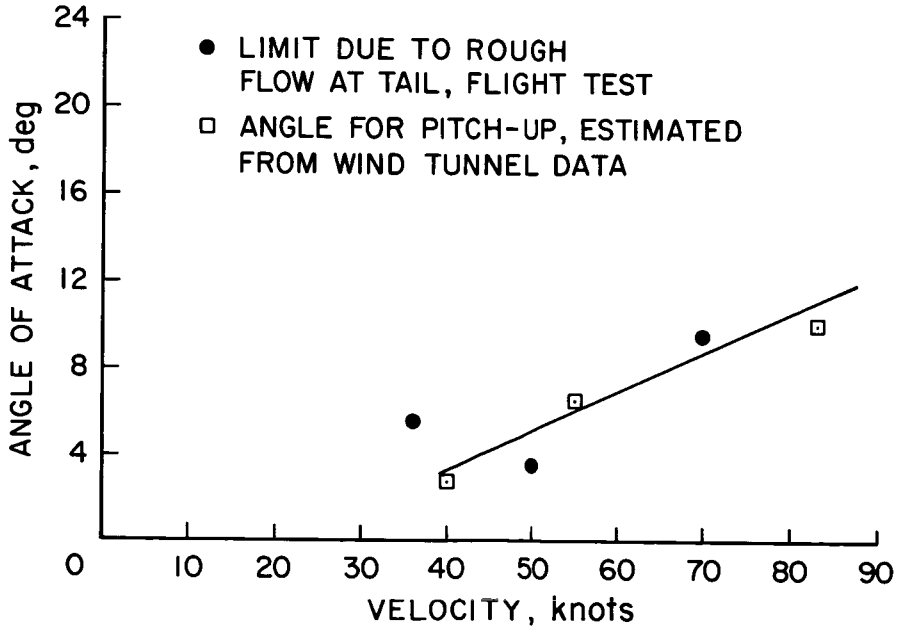

Figure 14.- Angle of attack for instability or rough flow at the tail of the XV-5A in flight and in the wind tunnel.

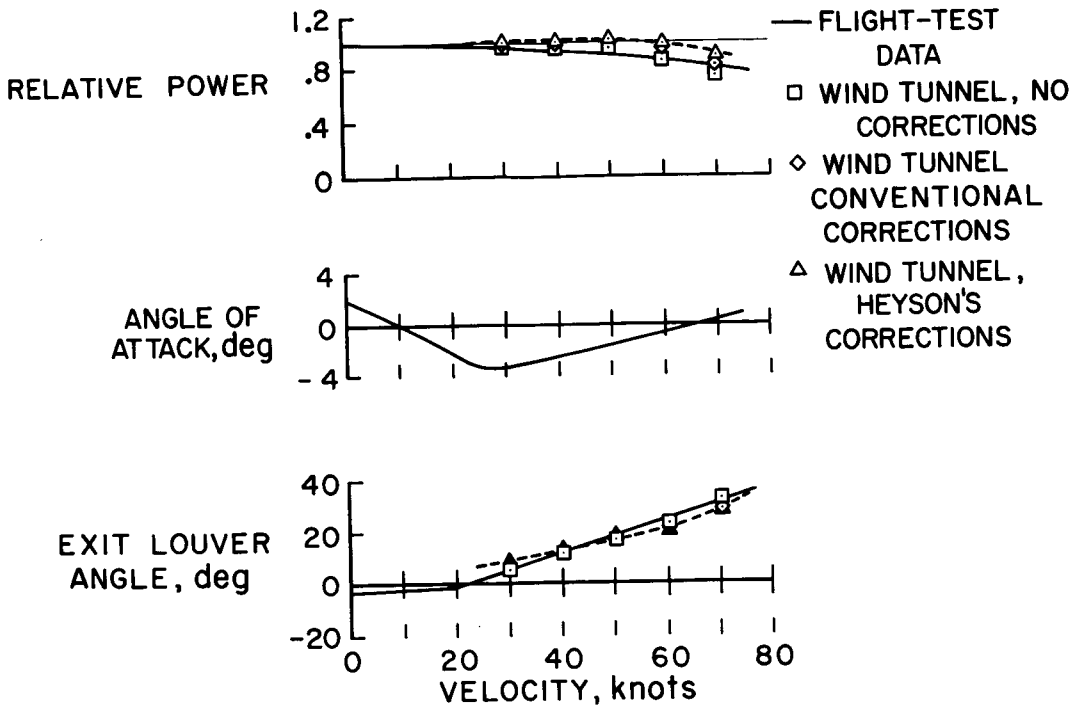

Figure 15.- Effect of wind-tunnel wall corrections on correlation between wind-tunnel and flight-test results for the XV-5A aircraft.

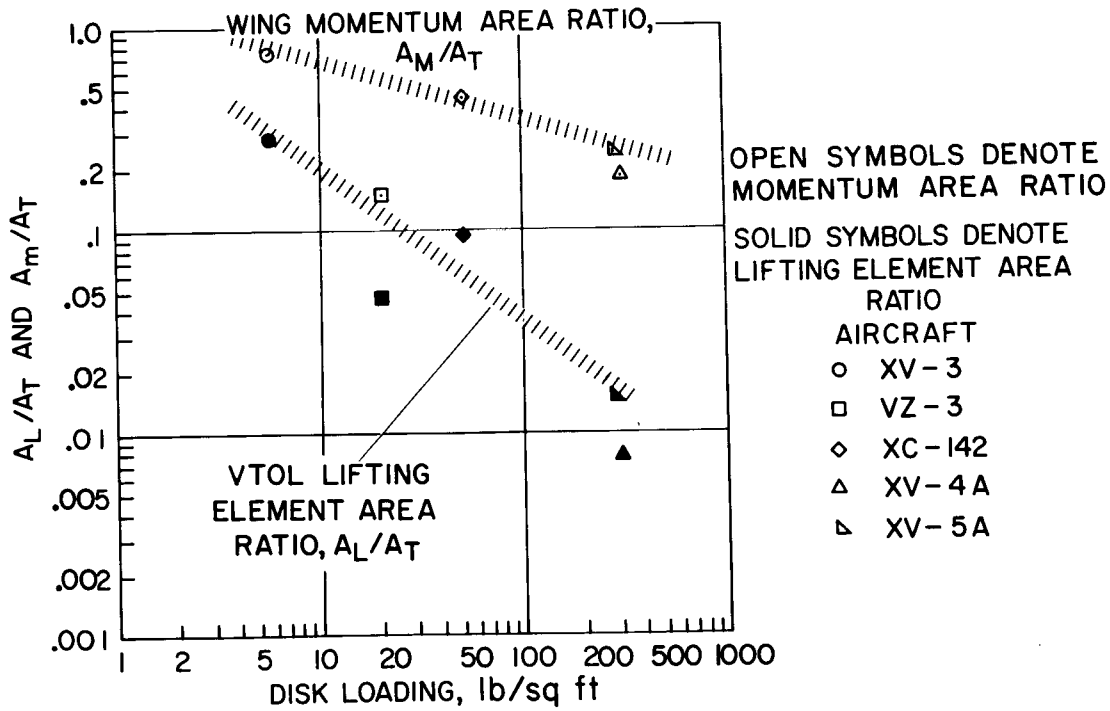

Figure 16.- The variation of the ratio of aircraft to wind-tunnel size with disk loading for aircraft tested in the wind tunnel at 20 to 30 knots airspeed.

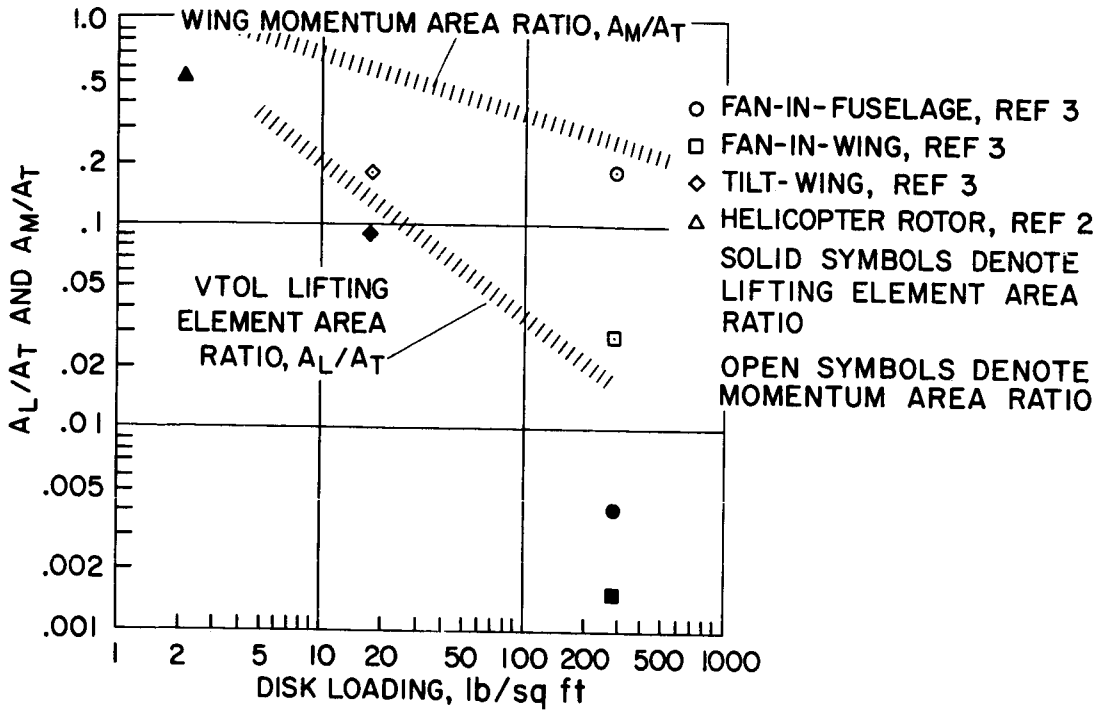

Figure 17.- The variation of the ratio of small-scale model to wind-tunnel size with disk loading.

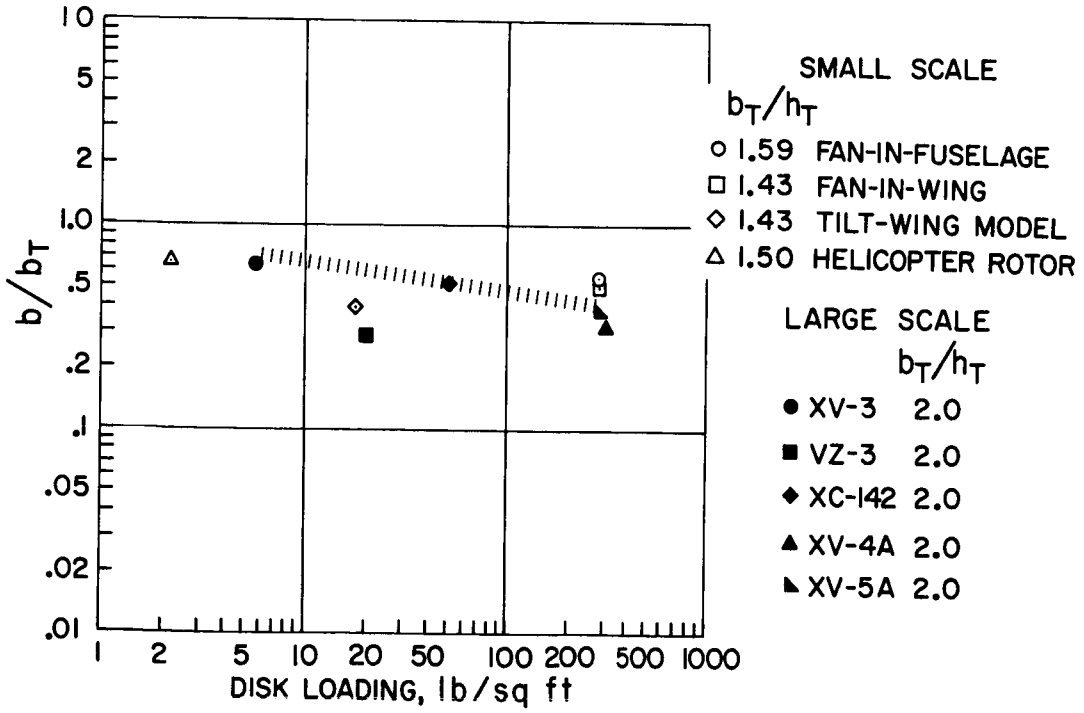

Figure 18.- The ratio of aircraft and model span to wind-tunnel width.